Adaptation of *Listeria monocytogenes* to food processing environments

Oleksii Omelchenko

100351362

A thesis submitted in fulfilment of the requirements of the University of East Anglia for the degree of Doctor of Philosophy

Quadram Institute Bioscience

Norwich Medical School, University of East Anglia

Word count: 71328

September 2025

© This copy of the thesis has been supplied on condition that anyone who consults it is understood to recognise that its copyright rests with the author and that use of any information derived therefrom must be in accordance with current UK Copyright Law. In addition, any quotation or extract must include full attribution.

Acknowledgements

First and foremost, I would like to thank my supervisors, Mathew Gilmour and Mark Webber, for their invaluable guidance. They not only kept me on the right scientific track but also offered life advice whenever it was needed. I appreciated their laissez-faire style of supervision, which gave me the independence to grow as a scientist rather than simply follow instructions.

I am deeply grateful to my postdoctoral researchers, Maria Diaz and Ana Victoria Gutiérrez. This project would not have reached completion without their constant support. Over the years, they became not just colleagues, but lifelong friends, whose company I will miss, especially the countless lunch breaks we shared together.

I am also grateful to my friends at the Quadram Institute, Gab, Ho Yu and Elin who shared the struggles of PhD life with me. I wish them the very best in their academic journeys and beyond. I thank my friend George, my long-time travel companion, who reminded me that there is life outside the lab and took me on adventures.

I would also like to thank my fiancée, Marnie, to whom I became engaged during this PhD. She not only supported me through the daily challenges of life and the writing process but also pushed me forward when motivation waned. From keeping me focused to even taking the occasional gel image, her presence has been invaluable. As well as to our two little dogs Aggie and Lilly.

A big thanks as well to my niece and nephew, Tobias and Emelia, who have absolutely no idea what a PhD is, but brought me joy and helped take my mind off science. I hope they grow up to be kind, loving people who pursue their dreams wholeheartedly.

Most of all, I would like to thank my family: my mother Olha, my father Serhii, and my grandfather Anatolii. For the past 28 years, they have given me unwavering love and support. During the preparation and writing of this thesis, they endured their own hardships yet always stood by me as though their own struggles did not exist. Their resilience has been my greatest inspiration to pursue an academic path.

I dedicate this work to my country, which has endured unimaginable suffering over the last decade, and to all the young souls who lost their lives defending it - so that others may live in freedom and have a home.

Finally, I would like to dedicate this work to my cousin Ivan, who tragically passed away during my PhD, far too soon. He lived life to the fullest, always seeking adventure and adrenaline. May he rest in peace.

Access Condition and Agreement

Each deposit in UEA Digital Repository is protected by copyright and other intellectual property rights, and duplication or sale of all or part of any of the Data Collections is not permitted, except that material may be duplicated by you for your research use or for educational purposes in electronic or print form. You must obtain permission from the copyright holder, usually the author, for any other use. Exceptions only apply where a deposit may be explicitly provided under a stated licence, such as a Creative Commons licence or Open Government licence.

Electronic or print copies may not be offered, whether for sale or otherwise to anyone, unless explicitly stated under a Creative Commons or Open Government license. Unauthorised reproduction, editing or reformatting for resale purposes is explicitly prohibited (except where approved by the copyright holder themselves) and UEA reserves the right to take immediate ‘take down’ action on behalf of the copyright and/or rights holder if this Access condition of the UEA Digital Repository is breached. Any material in this database has been supplied on the understanding that it is copyright material and that no quotation from the material may be published without proper acknowledgement.

Abstract

Despite rigorous cleaning and disinfection regimes, food production environments (FPE) can still harbour *Listeria monocytogenes,* a significant concern to food manufacturers and health authorities due to the high mortality rate associated with invasive listeriosis. Mechanisms contributing to *L. monocytogenes* persistence in FPE are proposed to include biofilm formation and reduced susceptibility to biocides, such as benzalkonium chloride (BC). We hypothesised that prolonged exposure to these disinfectants and other FPE-associated stressors would drive *L. monocytogenes* adaptation, resulting in the accumulation of genetic mutations linked to biofilm formation and reduced biocide susceptibility. To test this, I developed a biofilm persistence model and conducted 30 sequential passages of biofilm-associated cells under subinhibitory BC concentrations. Whole-genome sequencing of evolved populations, observed fixed concurrent mutations across independent experimental lineages, identifying mechanisms associated with persistence and niche adaptation. Reduced BC susceptibility arose through multiple independent mutations in the *fepRA* operon, encoding the FepR transcriptional repressor and the FepA MATE efflux pump. These mutations conferred comparable levels of reduced BC susceptibility in both planktonic and biofilm lifestyles. Fixed mutations associated with biofilm growth mapped to several loci, including the *ykoK* riboswitch and downstream *mgtA* metal transporter, the pyrimidine biosynthesis operon, and the stress response-related *rsb* operon. For the loci most affected by mutations, I constructed a panel of deletion mutants, and phenotypic analyses revealed that Δ*rsbU* (stress response), exhibited reduced biofilm thickness, with biovolume significantly decreased in Δ*rsbU* and Δ*pyrD* (nucleotide synthesis) mutants. In addition, distinct biofilm morphologies were observed in Δ*rsbU* and Δ*mgtA* (metal homeostasis) mutants, which displayed web-like filaments and a porous extracellular matrix, respectively. Collectively, these findings provide new insights into the mechanisms underlying *L. monocytogenes* biofilm persistence and reduced biocide susceptibility in the context of FPE, and reveal novel targets potentially exploited by *L. monocytogenes* to establish and maintain niches in unfavourable environments.

List of Abbreviations

a.u.	Arbitrary units
AU	Absorbance unit
AFM	Atomic force microscopy
AIP	Autoinducing peptide
ALOA	Agar *Listeria* according to Ottaviani and Agosti
ANOVA	Analysis of Variance
API	Analytical profile index
ATP	Adenosine triphosphate
AUC	Area under curve
BBB	Blood-brain barrier
BC	Benzalkonium chloride
BHI	Brain heart infusion
BPM	Biofilm persistence model
BPR	Biocidal products regulation
C&D	Cleaning and disinfection
CC	Clonal Complex
CDC	U.S. Centers for Disease Control and Prevention
c-di-GMP	Cyclic-di-GMP
CFU	Colony forming unit
cgMLST	core genome Multilocus sequence typing
CLSI	Clinical and laboratory standards Institute

CTAB	Cetyltrimethylammonium bromide
DBD	DNA binding domain
DFR	Drip flow reactor
EB	Elution buffer
ECM	Extracellular matrix
EPS	Extracellular polymeric substances
EU	European Union
FAO	Food and agriculture Organization
FMN	Flavin mononucleotide co-factor
FPE	Food processing environment
FSA	Food Standards Agency
Fwd	Forward
HACCP	Hazard Analysis and Critical Control Point
HMW	High molecular weight
HSE	Health and safety executive
HTH	Helix-turn-helix
HU	Histone-like protein
IHF	Integration host factor
LB	Lysogeny broth
LIPI	*Listeria* pathogenicity island
LPXTG	Leucine-proline-X-threonine-glycine
LTA	Lipoteichoic acid

MATE	Multi-antimicrobial extrusion protein
MBC	Minimum bactericidal concentration
MCS	Multiple cloning site
MIC	Minimum inhibitory concentration
MLST	Multilocus sequence typing
MRD	Modified Robbins device
MWB	Welshimers broth, modified
OD	Optical density
ORF	Open reading frame
PBS	Phosphate-buffered saline
PDB	Protein Data Bank
PFA	Paraformaldehyde
Ppm	Parts per million
PTS	Phosphotransferase System
QAC	Quaternary ammonium cations
QS	Quorum sensing
Rev	Reverse
RPM	Rates per minute
RTE	Ready-to-eat
SD	Standard deviation
SEM	Scanning electron microscopy
SFB	Short fragment buffer

SMR	Small multidrug resistance
SNP	Single-nucleotide polymorphism
SOEing	Splicing by overlap extension
SS	Stainless steel
SSI	Stress survival islet
ST	Sequence type
TBE	Tris-Borate-EDTA
TSB	Tryptic Soy Broth
UKHSA	United Kingdom Health Security Agency
UMP	Uridine monophosphate
UTR	Untranslated region
WGS	Whole genome sequencing
WHO	World health organization
WT	Wild-type

Contents

Adaptation of *Listeria monocytogenes* to food processing environments.....1

Acknowledgements.....2

Abstract.....4

List of Abbreviations.....5

Table of Tables.....16

Chapter 1: Introduction.....18

1.1. Contributions.....19

1.2. Publications.....19

1.3 Microbial Evolution and the Food Safety Context.....19

1.4. Listeria monocytogenes, a Foodborne Pathogen.....19
1.4.1. Clinical Presentation.....20
1.4.3. Treatment.....21

1.5. L. monocytogenes Subtyping.....22

1.6. Food Processing Environments (FPEs).....24
1.6.1. Microbial Communities and Regulatory Control in FPEs.....24
1.6.2. *L. monocytogenes* in FPEs.....25
1.6.3. Control Measures.....26
1.6.4. Challenges with controlling *L. monocytogenes* in FPE.....32
1.6.5. Surfaces in FPEs.....33

1.7. Biofilms.....34
1.7.1. Biofilms - the Preferred Form of Microbial Life.....34
1.7.2. Extracellular Polymeric Matrix of Biofilms (ECM).....35
1.7.3. Biofilm Lifestyle.....36
1.7.4. Conceptual Change of Biofilm Lifestyle.....40
1.7.5. Heterogeneity within Biofilms.....41
1.7.6. *L. monocytogenes* Biofilms.....42
1.7.7. Genes and Pathways Involved in Biofilm Formation in *L. monocytogenes*.....42
1.7.8. Metabolic Shift During Biofilm Formation.....46
1.7.9. Biofilm Associated Persister Cells.....47
1.7.10. Multi-species Communities.....48
1.7.11. Novel Methods for *L. monocytogenes* Biofilm Biocontrol.....49
1.7.12. Established Methods to Study Biofilm Formation.....50

1.8. Project overview.....53
1.8.1. Detection of Genetic Traits Associated with Biofilm Lifestyle and Reduced Susceptibility to Benzalkonium Chloride.....53
1.8.2. A Deeper Understanding of How the Loci Identified in the Biofilm Persistence Model Influence Biofilm Formation and Architecture.....55

Chapter 2: Materials and Methods.....56

2.1. Bacterial strains.....56

2.2. Plasmids.....59

2.3. Cryopreservation of strains and plasmids.....59

2.4. DNA extraction.....59

2.4.1. DNA extraction for generation of hybrid assemblies....59
2.4.2. DNA Extraction from the Biofilm Persistence Model Isolates....60
2.4.3. Quantification of Genomic DNA....60

2.5. Sequencing....61
2.5.1. Illumina Short-Read Sequencing....61
2.5.2. Oxford Nanopore Long-Read Sequencing for Hybrid Assembly Generation....61
2.5.3. Whole Plasmid Sequencing....62

2.6. Bioinformatic Analysis....62
2.6.1. Bioinformatic Analysis for Hybrid Assembly Generation....62
2.6.2. Bioinformatic Analysis for Whole Plasmid Sequencing Data....64
2.6.3. Phylogenetic Reconstruction and Population Structure....64
2.6.4. Quality Control and Base Calling Analysis for Processing Biofilm Persistence Model Data....66
2.6.5. Functional Categorisation of Mutations Identified Through Biofilm Persistence Model....66
2.6.6. Analysis of the genome structure and genes related to BC survival and biofilm formation...67
2.6.7. Conservation Analysis of Mutated Residues....67
2.6.8. Domain and Structure Predictions....67

2.7. Layout of in vitro Bead-based Biofilm Persistence Model (BPM)....68

2.8. Phenotypic Assays....71
2.8.1. BC Sensitivity Testing by Agar Dilution Method....71
2.8.2. Crystal Violet Assay for Biomass Formation....72
2.8.3. Cell Attachment Capacity....73
2.8.4. Short Term Cell Attachment Capacity....73
2.8.5. Macrocolony Morphology Assessment....74
2.8.6. Growth Kinetics Assay....74

2.9. Molecular Techniques....75
2.9.1. Construction of Deletion Vectors....75
2.9.2. Preparation of Competent Cells....83
2.9.3. Transformation and Mutant Generation in *L. monocytogenes*....84

2.10. Microscopy....86
2.10.1. Brightfield Microscopy....87
2.10.2. Widefield Fluorescence Microscopy....88
2.10.3. Scanning Electron Microscopy (SEM)....91

2.11. Figures....91

2.12. Statistical analysis....91

Chapter 3: Establishing the Experimental Basis for Biofilm Persistence Studies: Expansion of *L. monocytogenes* Culture Collection and Optimisation for Food Processing Environment Conditions....92

3.1. Contributions....93

3.2. Publications....93

3.3. Introduction....93

3.4. Aims....95

3.5. Results....95
3.5.1. Expansion and Characterisation of the *L. monocytogenes* Culture Collection....95
3.5.2. Population Structure of the Expanded *L. monocytogenes* Culture Collection....108
3.5.3. Establishment of a biofilm persistence model for *L. monocytogenes*....120

3.6. Discussion....126

3.7. Conclusions....130

Chapter 4: A Continuous Biofilm Persistence Model Identified Mechanisms of Niche Adaptation in *Listeria monocytogenes*.....132

4.1. Contributions:.....133

4.2. Publications.....133

4.3. Introduction.....133

4.4. Aims.....135

4.5. Methodology Specific to Chapter 4.....135

4.5.1. Execution of the BPM and Complexity of the Evolved Isolate Collection.....135

4.6.1. Exposure of *L. monocytogenes* to BC Leads to the Emergence of Planktonic and Biofilm Lineages Exhibiting Reduced Susceptibility.....138

4.6.2. Grouping Mutations by Selective Pressure.....144

4.6.3. Functional Distribution of Mutations Associated with Reduced Susceptibility to BC.....147

4.6.4. Mutations in *fepRA* Operon Related to Efflux Activity Become Fixed in the Populations Evolved Under BC Exposure.....150

4.6.5. Mutations in Pathways Involved in Inorganic Ion Transport (*corA*), Transcription (*bglG*) and Nucleotide Transport and Metabolism (*mtnN*) Become Fixed in the Populations Evolved Under BC Exposure.....152

4.6.6. Stepwise BC Escalation Does Not Affect BC Susceptibility but Selects for *fepA* Mutations Potentially Counteracting *fepR* Effects.....155

4.6.7. Distribution of Mutations Associated with Biofilm Persistence.....156

4.6.8. Mutations in Genes Related to Inorganic Ion Transport and Metabolism (*mgtA*), Nucleotide/Amino Acid Transport and Metabolism (*pyr* operon) and Transcription/Signal Transduction (*rsb* operon) Became Fixed in the Biofilm Condition.....160

4.6.9. Biofilm Persistence Did Not Elicit an Increase in Biomass/Population Generation, Nor Had an Effect on the Fitness of the Evolved Isolates.....168

4.7. Discussion.....172

4.8. Conclusion.....177

Chapter 5: Generation of nonpolar in-frame deletion mutants in *Listeria monocytogenes* for target genes detected in biofilm persistence model.....178

5.1. Contributions.....179

5.2. Aknowledgments.....179

5.3. Introduction.....179

5.4. Aims.....181

5.5. Results.....181

5.5.1. Construction of pKSV7 Vectors for Deletion of Target Genes.....181

5.5.1. Step 1 - Creation of Homologous Arms.....182

5.5.2. Step 2 - Creation of the Inserts.....185

5.5.3. Step 3 - Cloning of the Final Constructs.....185

5.5.4. Steps 4 - 6 - Successful Deletion Mutants for *corA, bglG, mgtA, ykoK, carB, rsbU* and *pyrD* Were Obtained in the Second Recombination Event.....189

5.6. Discussion.....194

5.7. Conclusions.....196

Chapter 6: Functional and Phenotypic Analysis of the Loci Associated with Biofilm Persistence and Reduced Susceptibility to Disinfectant Detected Through the In vitro Biofilm Persistence Model.....197

6.1. Contributions.....198

6.2. Publication.....198

6.3. Introduction....198
6.4. Aims....202
6.5. Results....203
6.5.1. Phenotypic Analysis of Biofilm-Related Mutants....203
6.5.2. Susceptibility Against BC Remained Unchanged in Mutant Strains....204
6.5.3. Assessing Biofilm-Forming Properties of Mutant Strains....205
6.5.3.1 Long-term Cell Attachment Not Affected in Mutant Strains....206
6.5.4. Influence of Mg^{2+} Supplementation on Cell Length of Natural Mutants....212
6.5.5. Mg^{2+} Influence on Surface Attachment in Δ*mgtA* and Δ*ykoK* Mutants....213
6.5.6. Mg^{2+} Ions have Concentration Dependent Effect on Biofilm Base Area, but not Thickness or Volume....215
6.6. Discussion....218
6.7. Conclusion....221
Chapter 7: General Discussion....223
Emergence of Reduced Disinfectant Susceptibility in FPE Settings....224
Adaptation to Biofilm Lifestyle Under FPE Pressures....225
rsb Operon....225
Magnesium Homeostasis....226
Metabolic Shift Under Sessile Lifestyle and Reduced Disinfectant Susceptibility....229
The Strength of the Adaptive Evolution Bead Model....229
Captures a Complex Selective Landscape of Adaptation....229
Captures Convergent Evolution and Reproducibility....229
Captures Emergence of Compensatory Mechanisms....230
Limitations of the Study....230
Future Work....231
The Future of the Bead Model....232
Conclusion....232
References....233
Appendices....284

Table of Figures

Figure 1. Schematic representation of a food production environment.25
Figure 2. Schematic overview of the biofilm lifecycle according to the updated biofilm formation model.42
Figure 3. Schematic overview of the thesis structure and chapter content.56
Figure 4. Overview of the experimental design of the biofilm persistence model (BPM).71
Figure 5. Alluvial diagram of the Food Standards Agency (FSA) food surveys conducted in Northern Ireland.97
Figure 6. Assessment of benzalkonium chloride tolerance in FSA panel isolates.100
Figure 7. Biofilm-forming capacity of the FSA panel isolates measured using the crystal violet assay.101
Figure 8. Genotypic and phenotypic analysis of benzalkonium chloride tolerance and biofilm-associated traits in selected *L. monocytogenes* isolates.105
Figure 9. Phylogenetic Analysis of *L. monocytogenes* ST121.112
Figure 10. Phylogenetic Analysis of *L. monocytogenes* ST7.114
Figure 11. Phylogenetic Analysis of *L. monocytogenes* ST9.116
Figure 12. Phylogenetic Analysis of *L. monocytogenes* ST204.117
Figure 13. Selection of the suitable media for biofilm microscopy.119
Figure 14. Optimisation of incubation time for biofilm biomass accumulation.121
Figure 15. Optimisation and validation of the conditions for the biofilm persistence model experiment.122
Figure 16. Widefield fluorescence microscopy of morphological differences in the biofilm of *L. monocytogenes* strain BL87-028 on stainless steel grade 316.124
Figure 17. Schematic overview of the Biofilm Persistence Model (BPM) experimental timeline.134
Figure 18. Alluvial plot illustrating the complexity of the Biofilm Persistence Model (BPM) and the diversity of evolved lineages and experimental conditions135
Figure 19. Exposure of *L. monocytogenes* to BC results in emergence of tolerant planktonic and biofilm lineages in steady model.137
Figure 20. Exposure of *L. monocytogenes* to BC results in emergence of tolerant planktonic and biofilm lineages in ladder model.137
Figure 21. Types of single nucleotide polymorphisms (SNPs).138
Figure 22. Venn diagram illustrating genes with detected mutations in BPM, grouped by experimental condition and timepoint.139
Figure 23. Bump chart visualising the number of loci affected by non-synonymous or intergenic mutations per functional subgroup under exposure to BC in the steady model. 142
Figure 24. Bump chart visualising the number of individual SNPs per functional subgroup under exposure to BC in the steady model.144
Figure 25. Mutations in *fepRA* operon promote BC tolerance in *L. monocytogenes* under steady and escalating exposure.145
Figure 26. Graphical overview of substitutions in (A) CorA, (B) MtnN, (C) BglG, (D) FepA, (E) MenH, (F) FliG.148
Figure 27. Bump chart visualising the number of loci affected by non-synonymous and intergenic mutations grouped by functional subgroup under biofilm lifestyle (on beads).

151
Figure 28. Bump chart visualising the number of individual SNPs by functional subgroup under biofilm lifestyle (on beads).153
Figure 29. Mutations associated with metal homeostasis, pyrimidine synthesis and stress response were affected in biofilm lineages.156
Figure 30. Graphical overview of substitutions in pyrimidine synthesis operon.159
Figure 31. Biomass production of evolved lineages (populations), measured with crystal violet assay, remained unchanged across conditions.162
Figure 32. Assessment of surface attachment capacity (CFU/bead) by evolved lineages (populations).164
Figure 33. Fitness of evolved lineages, measured as area under the curve (AUC) from growth curves, remained unchanged across conditions.165
Figure 34. An overview of the method for the construction of nonpolar in-frame gene deletion mutants (Rychli et al., 2021).175
Figure 35. Schematic representation of pKSV7 plasmid constructs used for the generation of nonpolar knockout mutants.177
Figure 36. Generation of homologous arms for deletion mutants.178
Figure 37. Generation of overlapping fragments for deletion mutants.179
Figure 38. Virtual gel electrophoresis of pKSV7 plasmid reads containing inserts for each mutant.180
Figure 39. pKSV7 construct for *pitA* deletion182
Figure 40. Predicted secondary structure of the *pitA* deletion construct insert.183
Figure 41. Confirmation of successful mutant generation by PCR product size visualised on the agarose gel.185
Figure 42. Schematic representation of the SigB activation cascade.194
Figure 43. Schematic representation of the *de novo* pyrimidine biosynthetic (pyr) operon. 195
Figure 44. Phenotypic characterisation of mutant strains compared to the parental strain. 197
Figure 45. Tolerance of mutant and parental strains to BC199
Figure 46. Biofilm-forming capacity of the mutant strains compared to the parental strain. 202
Figure 47. Global biofilm parameters of mutant strains compared to the parental strain, extracted from widefield fluorescence z-stacks imaged on stainless steel grade 316.202
Figure 48. Comparison of biofilm structure between the ΔmgtA and ΔrsbU mutant strains and the parental strain under SEM.205
Figure 49. Violin plot demonstrating the cell length of natural mutants obtained from BPM, under no Mg^{2+} supplementation and at 50 mM of Mg^{2+}.207
Figure 50. Cell attachment of mutant strains involved in Mg^{2+} homeostasis (*ykoK, mgtA*) compared to the parental strain.208
Figure 51. Global biofilm parameters of ΔykoK and ΔmgtA mutants, alongside parental strain, exposed to increasing concentrations of Mg^{2+} ions on stainless steel grade 316.211
Figure 52. Schematic representation of the experimental design and key scientific findings related to adaptive evolution under biofilm persistence and disinfectant exposure……...……. 211

Table of Tables

Table 1. Strains of bacteria used in this work.....57
Table 2. Plasmids used in this work.....59
Table 3. List of primers designed for generation of in-frame deletion mutants.....77
Table 4. Reaction setup for colony PCR using GoTaq® Green Master Mix.....79
Table 5. Cycling conditions for colony PCR.....80
Table 6. Reaction setup for colony PCR using Q5 High-Fidelity 2X Master Mix.....80
Table 7. Cycling conditions for high fidelity polymerase PCR.....81
Table 8. Primers used for screening second homologous recombination event to distinguish between WT reversion and successful gene deletion.....86
Table 9. Isolates selected from the larger FSA collection to make up the 'FSA panel' of 23 *L. monocytogenes* isolates that underwent genomic and phenotypic characterisation. 97
Table 10. Quality metrics of the hybrid assembled genomes of the FSA panel isolates. 106
Table 11. Indicating the size of loci selected for deletion.....182
Table 12. Summary of whole-plasmid sequencing results for pKSV7-based deletion constructs.....187
Table 13. Summary of non-synonymous and intergenic background mutations in *L. monocytogenes* deletion mutant strains.....193

‘Bacteria had the planet to themselves for around three billion years, and they were busy. They made the oxygen we breathe, the soils we till, the food webs that support our oceans…’

Dr. Martin J. Blaser

Chapter 1: Introduction.

1.1. Contributions

Oleksii Omelchenko, Ana Victoria Gutiérrez, Maria Diaz, Erin Lewis, Mark Webber, Matthew Gilmour.

1.2. Publications

Material presented in sections 1.6. '**Food Processing Environments (FPEs)**' and 1.7. **'Biofilms'** has contributed to the following publication:

Oleksii Omelchenko, Maria Diaz, Ana Victoria Gutiérrez, Mark Webber, Nicola Wilson, Matthew Gilmour. **The influence of disinfectants on controlling and selecting microbial communities in food production settings.** *npj Antimicrobials and Resistance*, *under review*

1.3 Microbial Evolution and the Food Safety Context

Bacteria evolved more than three billion years ago, long before the industrial age, and have since dominated the biosphere, shaping ecosystems into the ones we recognise today (Walter et al., 1980; Mojzsis et al., 1996; Grotzinger and Knoll 1999; Rosing, 1999; Kaiser, 2001; Allwood et al., 2007). Yet in food safety, we often adopt a narrow view, focusing on a handful of pathogens as if they exist in isolation. In reality, every food production environment is a dynamic microbial ecosystem, echoing three billion years of evolution. Microbial species are continually introduced through ingredients, water, people, and equipment. They are selected for, or against, by interventions such as cleaning regimes, temperature control, and nutrient availability. These pressures don't just suppress microbes but steer their adaptation influencing the genetic traits that persist within microbial populations and enabling them to thrive in the niches we create. By studying microbes and their evolutionary traits within this broader ecological context, we aim to better anticipate microbial behaviour and design more effective, long-term strategies for food safety and quality.

1.4. *Listeria monocytogenes*, a Foodborne Pathogen

Listeria monocytogenes was initially detected in 1926 in rabbit and guinea pigs and was first named - *Bacterium monocytogenes* (Murray et al., 1926). It was later assigned to a novel genus *Listerella* in 1935 (Burn, 1935) and was thought to cause human meningitis. The genus was then renamed to *Listeria* in 1940 (Pirie, 1940). In 1980's, awareness of *L. monocytogenes* as a food safety and public health threat emerged as the first well

documented *L. monocytogenes* outbreak occurred in Nova Scotia, Canada in 1981. During the Nova Scotia outbreak, the foodborne transmission of *L. monocytogenes* was determined for the first time (Schlech, 1983). This was followed by two large-scale outbreaks in Massachusetts and California, US in 1983 and 1985 leading to 14 and 48 deaths respectively (Fleming et al., 1985; Linnan et al., 1988). In the UK, there was also a notable outbreak towards the end of the 1980's linked to pâté, with more than 300 reported cases (McLauchlin et al., 1991), highlighting the outbreak-associated public health concern posed by *L. monocytogenes*. Today, *L. monocytogenes* is a nationally notifiable foodborne pathogen in the UK, and of concern to both food manufacturers and health authorities (Scobie *et al*., 2019). It is a psychrotolerant, Gram-positive, facultative anaerobic rod found in soil, water, sewage, and vegetation and is the main etiological agent for listeriosis (Queiroz et al., 2018).

Invasive listeriosis is a rare but deadly infection. Although the incidence of listeriosis remains relatively low, ranging from 0.13 to 0.38 cases per 100,000 people in England and Wales in 2023 (UK Health Security Agency, 2023), it has the highest case to fatality ratio of all foodborne pathogens, with mortality rates of up to 30% and hospitalisation rates reaching 93% (Center for Veterinary Medicine (FDA), 2019). *L. monocytogenes* is infective to all humans, however it mainly affects immunocompromised patients, neonates and pregnant women, resulting in bloodstream, brain infections and abortions (GOV.UK, 2021; Liu, 2006). In 2024 up to 21% of England and Wales *L. monocytogenes* cases involved pregnant women with 43.7% of those leading to stillbirth or miscarriage (GOV.UK, 2024). *L. monocytogenes* infections are on the rise and in 2022 the highest number of cases has been reported in EU since 2007 (0.62 per 100,000 population), with EU fatality rate of 18.1% and even higher rate in England and Wales at 19.9% reported in 2024. (EFSA, 2023; UK Health Security Agency, 2024).

1.4.1. Clinical Presentation

The most common forms of clinical presentation of listeriosis are bacteraemia, neurolisteriosis and pregnancy-related listeriosis which represent 52%, 31% and 14% of cases respectively (Popovic, Heron and Covacin, 2014; Feng et al., 2013; Charlier et al., 2017). However, the proportion of clinical representation varies with WHO reporting that up to 43% of total listeriosis cases occurred during pregnancy, with reports from China suggesting up to 52% pregnancy-related cases (Fan et al., 2019; Feng et al., 2013; Southwick and Purich, 1996).

1.4.3. Treatment

Due to the rarity of listeriosis in humans, a controlled trial has not been possible to identify the most effective therapy and majority of data have been collected retrospectively on clinical observation studies. (Dickstein et al., 2019). In pregnancy-related listeriosis two weeks of intravenous amoxicillin (> 6 g/day) are prescribed, which has been shown to be safe for the fetus (Wang et al., 2021). Gentamicin can be added to amoxicillin treatment if required, which has synergistic effect, however there is potential toxicity of gentamicin to the fetus. Gentamicin has been shown to increase patient survival rates of invasive *L. monocytogenes* infection, however, has limited efficacy against intracellular *L. monocytogenes* (Charlier et al, 2017). In case of patient's allergy to amoxycillin, the treatment is complicated, and trimethoprim/sulfamethoxazole is administered (Temple and Nahata, 2000). Ttrimethoprim is however toxic to the fetus and might result in complication with development of the nervous system and heart (Andersen et al., 2012). Another option is erythromycin, which is safe to the fetus, however the concentration of the drug reduces once passed the placenta thus higher doses must be administered (Mylonakis, Hohmann and Calderwood, 1998). Normally, two to three-week treatment is sufficient in pregnancy related listeriosis, however in case of the nervous system involvement in pregnant patient, longer treatment is required. In severe cases of aggravation of listeriosis symptoms in both patient and the fetus, termination of the pregnancy is considered to save mothers life, especially in case of cardiovascular involvement, liver or kidney failure and placental function decrease (Mylonakis et al., 2002; McLauchlin, 1990).

For treatment of non-pregnancy related cases of listeriosis, β-lactams (penicillin, ampicillin, amoxicillin, and gentamicin) are commonly prescribed (Hof, Nichterlein and Kretschmar, 1997). Recently, new fluoroquinolones have been reported to be effective against non-pregnancy related cases of listeriosis, including oral use of levofloxacin (500 mg/day) (Ishihara and Akazawa, 2023). Previously combination therapy has been recommended, including amoxicillin together with gentamicin, however, there has been conflicting reports with some suggesting lack of benefit and even harm from combination therapy (Amaya-Villar et al., 2010, Mitja et al., 2009; Mercedes Suárez et al., 2007; Fernández et al., 2012).

In cases of neurolisteriosis, treatment with amoxicillin-trimethoprim is the most appropriate regimen with amoxicillin being substituted by rifampicin in case of patient

allergy towards beta-lactams. Amoxicillin-trimethoprim have shown to be highly effective in countering *L. monocytogenes* in brainstem, with both drugs readily penetrating blood-brain barrier (BBB) (Merle-Melet et al, 1996). Additionally, there has been conflicting reports regarding administration of dexamethasone, with initial report of MONALISA study suggesting that adjunctive dexamethasone is associated with increased mortality (Charlier et al, 2017). However, later studies including a prospective cohort study by Brouwer and van de Beek in 2023, demonstrated the opposite, where adjunctive dexamethasone was associated with a reduced risk of unfavourable outcome and death in adults with community-acquired *L. monocytogenes* meningitis.

There have been reports on the problem of antibiotic resistance occurring during treatment of listeriosis. High resistance has been reported for clindamycin (66.7%), penicillin G (66.7%), amoxicillin (50%), and vancomycin (50%) (Welikidan et al., 2019). Additionally, intrinsic resistance of *L. monocytogenes* to broad-spectrum cephalosporins has been reported, which is especially significant in clinical settings, where *β*-lactam antibiotics including cephalosporins are frequently administered for treatment of sepsis of unknown cause but fail to protect against *L. monocytogenes* (Krawczyk-Balska and Markiewicz, 2015). On the other hand, food survey study in Poland demonstrated susceptibility of *L. monocytogenes* to ciprofloxacin, chloramphenicol, and trimethoprim/sulfamethoxazole (Sosnowski et al., 2019). Similarly, isolates from a food survey in China exhibited high sensitivity to ciprofloxacin (90.5%) and trimethoprim/sulfamethoxazole (57.1%) (Zhang et al., 2019). Overall, currently antibiotic resistance in *L. monocytogenes* is not as concerning as of other foodborne pathogens (Luque-Sastre et al., 2018). There has been limited research investigating the potential of the *Listeria* vaccines, however injection of the patients with attenuated *L. monocytogenes* strains before or during pregnancy have not demonstrated reduction in abortions or stillbirths (Clark et al., 2014).

1.5. *L. monocytogenes* Subtyping

There are several laboratory methods to differentiate between *L. monocytogenes* strains. Serotyping used to be the gold standard method (Borucki and Call, 2003; Doumith et al., 2004) and is still widely used. There are 13 described serotypes based on a unique combination of flagellar (H) and somatic (O) antigens, which are comprised of 4 and 15 subtypes, respectively (Ranjbar and Halaji, 2018; Orsi, Bakker and Wiedmann, 2011). In humans up to 98% of cases are reported to be caused by serotypes 1/2a, 1/2b, 4b (Sullivan,

Diggle and Clarke, 2005; Jacquet et al., 2002). In addition, strains belonging to serotype 1/2a are the most common food isolates, while 4b strains are most commonly isolated from *L. monocytogenes* outbreaks (Liu, 2006). Together, all *L. monocytogenes* serotypes can be grouped into four evolutionary lineages (I, II, III, IV). Serotypes linked to human listeriosis (1/2a, 1/2b, 4b) belong to lineages I and II, while lineages III and IV are rare and associated with animals (Kuenne et al., 2013). Additionally, strains from lineage II are commonly isolated from foods and food manufacturing environments (Orsi, Bakker and Wiedmann, 2011).

In 1998, multi locus sequence typing (MLST) was introduced for strain differentiation (Maiden et al., 1998), allowing for higher resolution when compared to traditional typing methods (Larsen et al., 2012). MLST is based on the detection of single nucleotide polymorphisms in the sequence of seven housekeeping genes: *abcZ, bglA, cat, dapE, dat, ldh* and *lhkA* (Wu et al., 2016). MLST groups strains into sequence types (ST) and clonal complexes (CC) (Chen et al., 2016). If isolates have six alleles in common out of the seven previously mentioned housekeeping genes, then they are grouped into the same CC. With the cost reduction and improved feasibility of whole genome sequencing (WGS) technologies this methodology became commonly used in public health and food safety investigations to link human listeriosis infections to the cause of the outbreak (Hyden et al., 2016). WGS advances allowed the extension of MLST to a larger set of loci, which allows whole genome or core genome strain differentiation (Ruppitsch et al., 2015). Several distinct core genome multi locus sequence typing (cgMLST) schemes have been developed for *L. monocytogenes*, encompassing between 1,013 and 1,827 loci (Ruppitsch et al., 2015; Pightling, Petronella and Pagotto, 2015). Among these, a widely used open-source reference scheme comprising 1,748 gene loci is curated in the Bacterial Isolate Genome Sequence database (BIGSdb; Jolley and Maiden, 2010; Moura et al., 2017) and has been adopted internationally for standardised surveillance and comparative analyses of *L. monocytogenes* isolates.

Previous research has shown that strains belonging to certain STs are associated with foods and food factories. ST121 is regarded as the most common ST found in food manufacturing environments, while ST9 dominates meat production lines (Fox et al., 2016; Fagerlund, Langsrud and Møretrø, 2020). Furthermore, there are several studies that have demonstrated how ST121 strains have been persistently contaminating food processing plants (Knudsen et al. 2017; Holch et al., 2013; McLauchlin 2021), highlighting that ST121 is potentially well suited to survive in niches that exist in food

processing environments (FPEs). As such, ST121 isolates contain stress survival islets (SSI-1, SSI-2) with genes responsible for better survival under stress conditions (Schmitz-Esser et al., 2015; Harter et al., 2017). Additional STs that are important in the context of foodborne diseases in the UK include ST8 that caused the 2019 UK NHS outbreak and ST6 that caused the multi-national sweetcorn outbreak in 2015 (Public health England, 2020; McLauchlin et al., 2021).

1.6. Food Processing Environments (FPEs)

FPEs are the settings where raw food materials are transformed into edible products. FPEs include a range of facilities like factories, kitchens, and storage areas and vary significantly in terms of raw materials and foods handled as well as processes involved (**Figure 1**). In the UK alone there are around 9,400 businesses involved in food product manufacturing, with sales from food manufacturing reaching £82.3 billion and employing up to 456,000 people, making it a nationally important sector (Nils-Gerrit Wunsch, 2025).

1.6.1. Microbial Communities and Regulatory Control in FPEs

In FPEs, material surfaces can harbour microbial communities that persist over time, even with measures in place to control microbial risks. (Diaz et al., 2024). Most of these microbes are commensal and not considered harmful to food producers. However, a small proportion of the microbiota may consist of foodborne pathogens capable of contaminating food products and subsequently infecting consumers (Møretrø and Langsrud, 2017; Fagerlund et al., 2021; Diaz et al., 2024).

The primary goal of food producers is to minimise the presence of these pathogens within facilities. However, rigorous cleaning, disinfection routines, and controlled temperatures are not always sufficient to ensure that FPEs remain pathogen-free (Omelchenko et al., 2025, *under review;* **Figure 1**). In many countries, the responsibility for controlling pathogenic biota lies with the food business operator, who must design and implement procedures tailored to their specific facility. In the UK, food manufacturers are required to comply with regulations that mandate food safety management systems based on Hazard Analysis and Critical Control Point (HACCP) principles (FSA, 2024). These include guidance on risk reduction and corrective actions if contamination occurs, with responsibility resting on the food producer (Omelchenko et al., 2025, *under review*).

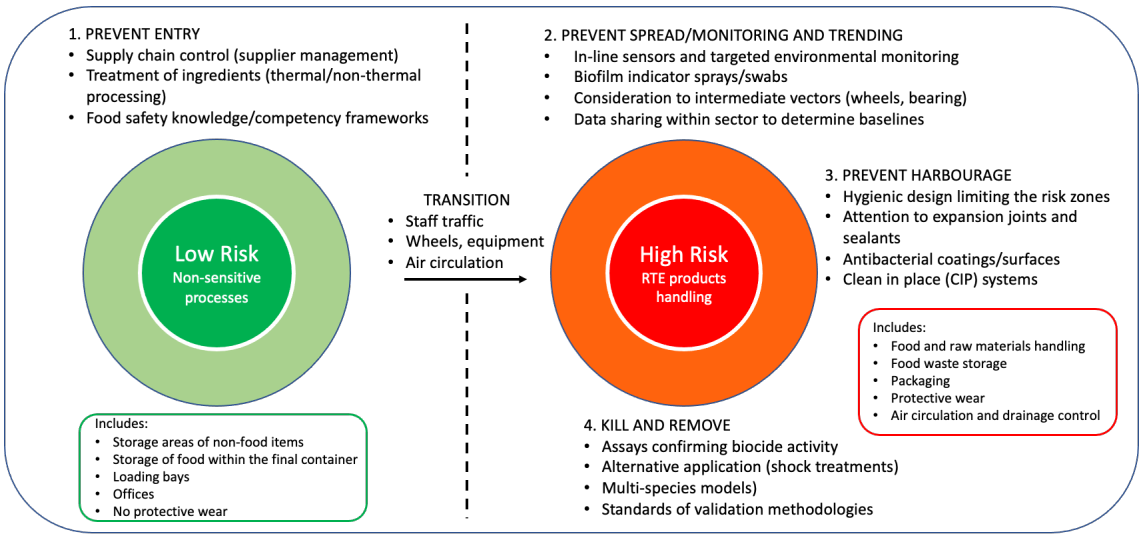


Figure 1. Diagram highlighting the key zones of the food production environment (FPE), including the high risk area (for handling ready-to-eat (RTE) foods and raw materials) and the low risk area (for packaging and non-sensitive processes). The diagram illustrates the critical cleaning, disinfection and monitoring steps implemented by food producers to minimise the risk of pathogen contamination. These steps are designed to: (**1**) prevent the entry of pathogens into high care areas, (**2**) prevent the spread of contaminants between the zones, (**3**) prevent harbourage by eliminating niches where pathogens could persist and (**4**) effectively kill and remove microorganisms from surfaces and equipment. Adapted from Omelchenko et al., 2025, *under review*.

1.6.2. *L. monocytogenes* in FPEs

When focusing specifically on *L. monocytogenes*, up to 99% of listeriosis cases are foodborne, with common sources including ready-to-eat (RTE) products, dairy, and vegetables (Orsi, Bakker, and Wiedmann, 2011). RTE chilled products that do not require heating before consumption are of particular concern, as unlike most foodborne pathogens, *L. monocytogenes* can proliferate at refrigeration temperatures (Walker, Archer, and Banks, 1990). If contamination occurs, the pathogen may grow during cold storage and reach infectious doses over shelf life, posing a significant risk to consumers (Rosso et al., 1996; Koutsoumanis et al., 2010). Reflecting this, up to 90% of invasive listeriosis cases in Europe are linked to RTE foods (Ricci et al., 2018). In the UK, two in five people consume RTE products weekly, highlighting the ongoing risk of exposure (Pilkington, 2022). A notable example is the 2019 *L. monocytogenes* outbreak in the UK, linked to RTE sandwiches and salads served in hospitals, which resulted in five deaths (Public Health England, 2020). According to Pérez-Rodríguez et al., 2008, the most likely point of food contamination by *L. monocytogenes* is the food production facility itself. Some *L. monocytogenes* strains have been shown to persist in food manufacturing sites for years, or even decades (Holch et al., 2013; McLauchlin et al., 2021). The ability of *L.*

monocytogenes to persist is largely due to its capacity to adapt to stress conditions through intrinsic and acquired genetic traits that enable survival under refrigeration, high salt concentrations, low pH, and biocide exposure (Xayarath and Freitag, 2012; Ferreira et al., 2014; Sibanda and Buys, 2022; Ribeiro et al., 2006; NicAogáin and O'Byrne, 2016; Mazaheri et al., 2021). Once established, biofilms formed by *L. monocytogenes* are notoriously difficult to eradicate, leading to recurrent contamination (Fagerlund et al., 2022; Holch et al., 2013; Ferreira et al., 2014; McLauchlin et al., 2021). Furthermore, foods not traditionally associated with *L. monocytogenes* contamination have emerged as sources of infection. Recent outbreaks have implicated caramel apples, fresh fruit, mushrooms, and notably, the 2016 US multistate and 2018 European outbreaks linked to frozen vegetables (sweetcorn and peas), which resulted in 3 and 10 deaths respectively and were both linked to the manufacturing facilities (CDC, 2016, Madad et al., 2023; Carstens et al., 2018; O'Mahony, 2020; McLauchlin et al., 2021; Fay et al., 2024).

1.6.3. Control Measures

Effective control of *L. monocytogenes* and other pathogens in FPEs involves a combination of strategies aimed at addressing contamination from multiple angles. While cleaning and disinfection (C&D) are often the primary focus, preventing the initial harbourage and spread of microbes is equally important (Omelchenko et al., 2025, *under review;* **Figure 1**). Sources of contamination include staff movement (footwear not changed between sections), equipment (wheels, bearings, conveyor belts), air ventilation, and drainage systems. Facility design also plays a crucial role with cracks, crevices, and poorly sealed joints creating high-risk zones for microbial colonisation (Berrang and Frank, 2012; Food Standards Scotland, 2020).

1.6.3.1. Monitoring Strategies

An essential component of C&D protocols is the implementation of monitoring strategies, which help identify contamination hotspots requiring additional attention. Food producers are typically required to establish monitoring programmes to detect bacterial species of concern, including *L. monocytogenes* (EU Regulation No 2073, article 3 and 5, 2005). These programmes often involve swabbing food contact and non-contact surfaces, followed by culture-based pathogen detection in private or reference laboratories, which in the United Kingdom is designated by the Food Standards Agency (outlined by National Control Plan, as required by Official Feed and Food Control Regulations 2017/625; FSA, 2024). When biofilms do form, peroxide-based commercial detection solutions have

gained popularity due to their ease of use and effectiveness (Ripolles-Avila, Ríos-Castillo and Rodríguez-Jerez, 2018) (**Figure 1**). If the presence of pathogenic bacteria exceeds acceptable limits, food businesses must follow a set of prescribed actions, which may include root cause analyses and intensified monitoring and corrective measures to identify and eliminate the contamination source (EU Regulation No 2073, article 7, 2005; FSA, 2023).

1.6.3.2. Cleaning

The first step is the design and execution of effective cleaning protocols, which are critical yet often overlooked. Cleaning removes organic matter and debris that would otherwise inhibit disinfectants. It is estimated that proper cleaning alone can remove up to 99.8% of microbes from FPE surfaces (Dunsmore et al., 1981). The choice of cleaning agent depends on the type of soil. Alkaline-based detergents (e.g., sodium hydroxide, potassium hydroxide, sodium carbonate) are effective against proteins and fats, while acidic agents (e.g., phosphoric acid, nitric acid, citric acid) are used to remove mineral deposits. Solvent-based cleaners target oil and grease (Gottschalk et al., 2022). Mechanical energy such as manual brushing, scraping, automated scrubbing, or pressure-jet washing is typically employed alongside chemical cleaning, although, certain methods, such as pressure washing, are discouraged as they can create aerosols that spread contaminants (Gibson et al., 1999).

1.6.3.3. Disinfection Methods Against L. monocytogenes

After cleaning, disinfection targets the remaining microbial population. Disinfectants are selected based on their spectrum of activity, surface compatibility, and regulatory compliance. In the EU, disinfectants used in FPEs are regulated under the Biocidal Products Regulation (Regulation No 528, 2012), while in the UK, the Health and Safety Executive (HSE) oversees equivalent frameworks (Regulation No 352, 2024).

In addition to the chemical and mechanical components of C&D programs, both time and temperature play significant roles (CDC, 2024). Elevated temperatures can aid in the removal of oils and grease and help denature proteins, improving cleaning efficiency. Prolonged contact time, achieved with soak tanks, foams, or gels, further enhances the action of C&D agents (Kakurinov, 2014).

1.6.3.4. Commonly Used Disinfectants in FPEs

Common disinfectants include chlorine derivatives, hydrogen peroxide, peracetic acid, iodophors, and alcohols (Dawan, Zhang and Ahn, 2025). Chlorine-based compounds provide broad coverage but are prone to inactivation by organic matter and may corrode metal surfaces (Iqbal et al., 2016; Gallandat et al., 2021). Oxidizing agents like hydrogen peroxide and peracetic acid are effective against biofilms and are often preferred for closed-system applications (Goetz et al., 2021). Iodophors offer broad-spectrum efficacy with low toxicity, while alcohol-based sanitizers act quickly but are limited by short contact time and material compatibility (Lio and Kaye, 2011; Rutala and Weber, 2015).

Current food safety trends are moving toward the use of biocides that are effective, but less chemically aggressive and more environmentally sustainable (Omelchenko et al., 2025, *under review*). Hypochlorous acid (HOCl; oxidising agent) is gaining popularity due to its non-toxic, non-corrosive, biodegradable and relatively inexpensive nature, as well as demonstrated efficacy across various food safety applications (Block and Rowan, 2020).

1.6.3.5. Quaternary Ammonium Compounds (QACs)

One of the widely used classes of disinfectants in the FPEs are quaternary ammonium compounds (QACs) (Kim et al., 2018). QACs are a large class of chemicals that have been used for decades due to their broad-spectrum antimicrobial activity, although less effective against spores and mature biofilms (Pereira et al., 2023; Buffet-Bataillon et al., 2016). QACs are made of two components - a central nitrogen atom, surrounded by four clusters of atoms. In commercial formulations they consist of mixtures with varying alkyl chain lengths (C8-C18), with C12 and C14 chains showing the highest bactericidal activity (European Commission EURL-SRM, 2012). QACs have a multi-factorial mode of action (Lambert and Hammond, 1973; Piovesan Pereira and Tagkopoulos, 2019) including inactivation of metabolic enzymes, denaturation of proteins, and disruption of membrane bilayers by binding to negatively charged bacterial membranes and causing leakage of cellular contents (Wessels and Ingmer, 2013; McDonnell & Russell, 1999).

1.6.3.6. Challenges with QAC Use

QACs are applied at concentrations significantly higher than the minimum bactericidal concentration (MBC) to ensure efficacy. However, due to factors like condensation or inadequate rinsing, certain areas within the facilities may be exposed to sub-inhibitory

concentrations, allowing *L. monocytogenes* to adapt (Martínez-Suárez, Ortiz, and López-Alonso, 2016).

Adaptation to QACs, especially benzalkonium chloride (BC), has been linked to cross-resistance to antibiotics such as cefotaxime, cephalothin and ciprofloxacin, as well as to ethidium bromide (Rakic-Martinez et al., 2011; Yu et al., 2018; Kode et al., 2021; Bland et al., 2022). BC has been linked to misuse or improper diluting, resulting in several outbreaks throughout last 4 decades (Weber, 2007). Therefore, QACs are regulated, with the guidelines being frequently updated based on recent scientific findings.

1.6.3.7. L. monocytogenes Tolerance/Reduced Susceptibility to BC

Firstly, it is essential to establish the terminology that will be applied throughout this thesis when discussing the interaction between *L. monocytogenes* and disinfectants. The scientific literature shows a lack of consensus in this area, with the term 'resistance' often used loosely (Maillard, 2022), which complicates comparison between the studies. For the purposes of this work, the following definitions will be adopted:

- **Tolerance**: the ability of bacteria to grow in the presence of a low (below MIC) concentration of a biocide (Gerba, 2015).
- **Reduced susceptibility**: an upward shift in the MIC or MBC of a biocide compared to wild-type (WT) or reference strains (Maillard, 2022).
- **Resistance**: the ability of bacteria to survive exposure to an in-use concentration of a biocidal product (Maillard, 2022).

Several mechanisms conferring reduced susceptibility to BC have been described and include changes in composition of the membrane, porin downregulation, efflux pump upregulation, transposon elements and biofilm formation (Piovesan Pereira and Tagkopoulos, 2019). All together there has been more than 200 efflux pumps predicted for *L. monocytogenes* reference strain EGD-e, but only some of them have been associated with reduced susceptibility to BC including *bcrABC* cassette, *qacH*, *fepR/fepA*, *emrE/C, mrdL* genes and *sug* operon (Dutta, Elhanafi and Kathariou, 2013; Müller et al., 2013; Jiang et al., 2018). These efflux pumps are responsible for the transport of BC and other toxic substances outside of the cell through protein transporters in the cytoplasmic membrane. The first efflux pumps associated with reduced susceptibility to BC was MdrL, described in 2000, and belongs to the major facilitator superfamily (MFS)

and is also involved in adaptation of *L. monocytogenes* to ethidium bromide (EtBr) (Mata, Baquero and Pérez-Díaz, 2000). Latter studies have described that expression of *mdrL* increased in the presence of QACs, and MdrL knockout strain has resulted in growth defect in QACs presence (Jiang et al., 2018). However, the role of MdrL could not be confirmed for tolerance against cefotaxime and ethidium bromide in laboratory strains and therefore there is no consensus on MdrL's involvement in antimicrobial tolerance (Yu et al., 2018). In 2010, in *L. monocytogenes* strain H7550 responsible for 1998-1999 hotdog outbreak of listeriosis in the United States, *bcrABC* cassette was described, which has been harboured on a IS*1216* composite transposon (Elhanafi et al., 2010). The *bcrABC* cassette is a mobile plasmid-borne efflux system, providing reduced susceptibility to BC due to *bcrA* TetR-family transcription regulator with helix-turn-helix (HTH) DNA binding motif and two SMRs (*bcrB* and *bcrC*). All three genes of the cassette are essential for imparting reduced susceptibility to BC. Transcription levels of *bcrABC* cassette have been shown to be elevated in the presence of BC and in low temperature (4, 8, and 25°C) compared to 37 °C (Elhanafi et al., 2010). In addition, *sug* operon has been recognised as a counterpart to *bcrABC* cassette and is responsible for reduced susceptibility against QACs. *sug* operon includes TetR-family transcription regulator SugR and two SMRs SugE1 and SugE2. In the absence of QACs, *sugR* has been repressed and in presence of QACs both *sugE1* and *sugRE2* have been overexpressed. In 2013, *qacH* was described, which is encoded on Tn*6188* transposon and belongs to small multidrug resistance transporter family (SMR) of efflux pumps. Strains containing Tn*6188* demonstrated reduced susceptibility to BC (MIC of 28.5 ± 4.7 mg/L) compared to *qacH* knockout mutants (MIC of 14 ± 3.2 mg/L) (Müller et al., 2013). In addition to *qacH*, EmrE SMR located on genomic island LGI1 has been associated with reduced susceptibility to BC in EmrE positive strains, with both mechanisms being specific to CC121 and CC8 strains respectively (Gilmour et al., 2010; Kovacevic et al., 2016; Ortiz et al., 2016; Müller et al., 2013). In 2014, chromosomally encoded novel MATE Fluoroquinolone Efflux Pump FepA has been described as resistance mechanism against fluoroquinolones in *L. monocytogenes,* with its overexpression being driven by inactivation of transcription regulator of TetR family - *fepR* (Guérin et al., 2014). Recently, it has been demonstrated that defects in *fepRA* system were adaptation response to BC, leading to *fepA* upregulation and reduced susceptibility against BC, CTAB, ciprofloxacin, and gentamycin (Douarre et al., 2022). Notably, as has been demonstrated by Bolten et al., 2022, nonsynonymous mutations in *fepR* are associated with adaptation to low concentration of BC, however, do not result in increased survival following

exposure to recommended concentrations of BC (300 mg/L). Additionally, Bolten et al., has demonstrated similar outcomes for *bcrABC* and *qacH*, concluding that both of these genetic traits confer reduced susceptibility to low concentrations of BC, but do not result in resistance to recommended BC concentrations. Finally, it was suggested that none of the described genetic traits *(fepR, qacH, bcrABC*) are a plausible indicator of *L. monocytogenes* persistence in FPEs (Bolten et al., 2022). In 2019, Hurley et al., demonstrated that up to 62% of *L. monocytogenes* isolates contained BC-tolerance genes, with *emrC* being the most prevalent gene followed by *bcrABC* and Tn*6188* transposon *qacH* and *qacC* genes. In 2023, Schulz et al., further evolved susceptible *fepA*-free strain in presence of CTAB, which resulted in a strain with reduced susceptibility to BC and CTAB and contained mutations in *sugR*. Further adaptation study revealed that strains lacking both FepA and SugE1/E2 efflux pump systems could develop reduced susceptibility to BC and CTAB through overexpression of the remaining efflux pump systems, with all isolated strains containing mutations in diacylglycerol kinase-encoding gene *lmo1753* (*dgkB*). DgkB is involved in conversion of diacylglycerol to phosphatidic acid, which is subsequently utilised in synthesis of phospholipids, suggesting that *dgkB* could be implicated in changes in the membrane composition. Similar membrane composition alterations have previously been associated with BC tolerance in other genus, but never in *Listeria* (Schulz et al., 2023). The genetic traits associated with reduced susceptibility to BC that were described above can be acquired through the horizontal gene transfer. Successful horizontal gene transfer of genes associated with reduced susceptibility to BC has been described from non-pathogenic *Listeria innocua* and *Listeria welshimeri* to *L. monocytogenes*. This means that non-pathogenic and less concerning *Listeria* strains possessing mechanisms that confer reduced susceptibility may support the persistence of pathogenic *Listeria* in food manufacturing (Katharios-Lanwermeyer et al., 2012).

Recently, a study by Bechtel et al., 2024, performing transcriptome analysis in the presence of BC revealed that genes related to the phosphotransferase system (PTS) (including *bglG*, *dhaL*, *dhaM*, *ulaA*, *fruA*, *manZ*, and *licABC*) and internalins were up-regulated in designed mutants, suggesting their significance in the BC stress response and provide deeper insights into alternative mechanisms for reduced susceptibility to BC, which may involve broader metabolic shift in addition to previously described efflux pump upregulation. In addition, in clones with reduced susceptibility to BC, the group detected non-synonymous mutations in *dagK* (a diacylglycerol kinase), *lmo2768* (a

permease-encoding gene), and *lmo0186* (resuscitation promoting factor), which also are likely to play role in response to QACs. In other bacteria genus, including *Pseudomonas,* more mechanisms have been described for BC tolerance and reduced susceptibility including downregulation of porins to reduce BC intake which have not yet been described in *L. monocytogenes* (Loughlin, Jones and Lambert, 2002).

1.6.4. Challenges with controlling *L. monocytogenes* in FPE

The majority of the studies focusing on disinfectants against *L. monocytogenes* solely examine planktonic lifestyle, not considering that biofilms are the preferred mode of microbial life and therefore the disinfectants in FPEs environments are applied directly against biofilm embedded cells (O'Toole, Kaplan and Kolter, 2000). A study by Luque-Sastre et al, 2018, determined the most effective disinfectant against both planktonic and biofilm *L. monocytogenes* strains out of ethanol, ethanol-propanol mix, BC, Triclosan and Triquart. Disinfectants were tested on 48-hour pre-formed biofilms, demonstrating that BC was the most effective disinfectant against planktonic bacteria, with the least effective being ethanol. However, for the biofilm communities only effective disinfectant able to significantly reduce the biomass was Triclosan-5-chloro-2-(2,4-dichlorophenoxy) phenol-based disinfectant, which has been banned in the UK due to health concerns to the users (GOV.UK, 2016). Another study by Fagerlund et al., 2017, focusing on FPEs biofilms have demonstrated that recommended C&D programs are not sufficient to remove biofilms formed on conveyor belts, with *L. monocytogenes* biofilms developing tolerance over time not just to BC, but also to peracetic acid, with *L. monocytogenes* being trapped and protected in the fibres of the conveyor belt. Later study by Fagerlund et al., 2020, has also demonstrated that 7-day old *L. monocytogenes* biofilms were harder to remove than 4-day old biofilms. Similar conclusion was reached by Chaturongkasumrit et al., 2010, demonstrating difficulty to eradicate *L. monocytogenes* biofilm formed on conveyor belts with a combination of detergent (alkaline foam) and Tego-51 disinfectant (an amphoteric disinfectant), with lower efficacy on worn out belts.

The majority of studies conclude that removal of both industrial and laboratory biofilms requires shear-stress, increased temperatures or prolonged exposure to antimicrobial compounds. Some of the recommended strategies such as heat-treatment are impractical in FPE settings, whilst strategies of increasing the concentrations of antimicrobial compounds puts workers at risk and may result in transfer of disinfectants into the food produce, as well as facilitate surface corrosion (Fagerlund et al. 2016).

1.6.5. Surfaces in FPEs

There are sanitary requirements that must be adhered by food manufacturers when choosing surface materials (Regulation 1935, 2004; FSA, 2025). Food surfaces should be smooth, non-porous, free of cracks and crevices, non-absorbent, non-contaminating, non-reactive, durable and cleanable. Stainless steel (SS) is regarded as the preferred surface material for FPEs as stated by FSA's 'Materials and Articles in Contact with Food (England) Regulations 2012' and '3-A sanitary standards' in the US. SS is the Fe-C alloy with additional alloying elements. The most used SS types in food processing and manufacturing are Fe-C-Cr and Fe-C-Cr-Ni alloys, such as SS grade 304 (American Iron and Steel Institute (AISI) grading). To improve the non-corrosion properties of SS grade 304, grade 316 has been designed which contains 2 – 3 % of molybdenum and extra 4 % of nickel compared to grade 304. Molybdenum creates molybdenum oxide which enhances the passivation layer preventing pitting corrosion. Addition of molybdenum makes SS grade 316 less prone to oxidation by disinfectants used in FPEs and therefore food producers can apply higher concentrations of disinfectants. Grade 316 can withstand concentration of chlorine up to 4 ppm, whilst grade 304 demonstrates signs of corrosion at 2 ppm. Similarly, behaviour is observed with food preservatives commonly used in FPEs such as sodium chloride. Grade 316 can withstand concentrations of up to 2000 ppm whilst grade 304 demonstrates localised sings of corrosion at 100 ppm (British Stainless Steel Association, 2001).

Recent advancements have been made in the development of antibacterial surface materials. One such innovation involves the creation of antibacterial metal alloys that inhibit bacterial adhesion, growth, and proliferation. Alloys incorporating elements such as copper (Cu), in particular copper-bearing stainless steels (e.g., 304-Cu SS, 430-Cu SS), demonstrated over 99% bacterial reduction. The antimicrobial effect is attributed to slow-release copper ions and reactive oxygen species (ROS) generation, which inhibit microbial adhesion and growth (Zhang et al., 2021; Tripathi et al., 2024; Huang et al., 2023). However, these have not been widely introduced into the FPEs to evaluate their effectiveness on industrial scale.

Despite the selection of materials with lower corrosion properties, the food manufacturers are still concerned about the interaction of food-contact surfaces and disinfectant. Even though the disinfectants are relatively effective, hypochlorite-based agents can pose a risk to stainless steel surfaces, particularly under certain pH conditions (FAO/WHO, 2008).

These chemicals may release free chlorine, which can damage the surface by initiating pitting corrosion where the metal's protective oxide layer deteriorates, forming small but deep cavities (Frankel, 1998). These imperfections provide ideal niches for bacterial attachment and biofilm development in FPEs. A study by Verran and Whitehead (2005) revealed that in cases where bacteria cells are similar size to the cracks in the stainless surface, the cells are more protected compared to when the cells are significantly smaller than the cracks. Several studies have concluded that the roughness of the surface plays an important role in colonisation of the surface by bacteria, however there is no consensus on the matter as several studies demonstrated conflicting data suggesting no correlation between surface roughness and colonisation potential (Hilbert et al., 2003; Singh et al., 2011). Additionally, investigation into electro-polished stainless steel revealed lower cell attachment rate compared to standard stainless steel, and therefore the biofilm formation was slower (Arnold and Bailey, 2000).

1.7. Biofilms

1.7.1. Biofilms - the Preferred Form of Microbial Life

One of the mechanisms responsible for persistence of *L. monocytogenes* strains in FPEs could be its biofilm forming ability (Møretrø and Langsrud, 2004). Biofilms have classically been defined as complex communities of microorganisms able to produce an extracellular matrix (ECM) consisting of exopolysaccharides, nucleic acids (eDNA and eRNA), proteins, lipids, and other biomolecules (Whitchurch et al., 2002; Sugimoto et al., 2018). Biofilms have been recognised as a prominent growth strategy of microorganisms in freshwater and marine environments since their first observations in the 18th century by Antonie van Leeuwenhoek (van Leeuwenhoek, 1712) and later in the early 20th century by Claude ZoBell (ZoBell and Allen, 1935). Biofilms weren't well studied all the way until Costerton et al., popularised the idea of studying adhered communities in 1987.

In the environment, biofilms are the prevalent mode of microbial existence with up to 90% of bacteria living within biofilm communities (O'Toole, Kaplan and Kolter, 2000). Biofilms help embedded bacteria survive harsh environmental conditions including high salt, pH, nutrient deficiency, and presence of antimicrobial compounds. Biofilms can contain microorganisms from different kingdoms including protozoa, fungi and algae, while also containing multiple bacteria species simultaneously. In addition, multi-species biofilms have been shown to possess higher antimicrobial resistance properties including

to quaternary ammonium compounds (QACs) (Giaouris et al., 2015). A key finding in 1985 (Nickel et al., 1985) was the heightened resistance of microorganisms within biofilm communities when compared to planktonic populations.

These structures have been shown to successfully form on hard surfaces commonly used in food manufacturing environments including stainless steel, food grade plastics, glass, and resin and can also proliferate on biological structures including vegetables, meat and bones (Colagiorgi et al., 2017; Flemming et al., 2016). In food manufacturing environments biofilms provide embedded bacteria with physical resistance against desiccation, mechanical resistance against liquid streams in production chains and chemical protection against antimicrobial compounds (Flemming et al., 2016).

1.7.2. Extracellular Polymeric Matrix of Biofilms (ECM)

ECM was initially described by Costerton et al., in 1987 as "glycocalyx", which is known to play a critical role in the biofilm formation. ECM makes up more than 90% of biofilms dry mass with microbial count only representing the remaining 10%, where matrix fills up the gaps between the cells (Mishra et al. 2023). ECM contains water channels for nutrient transfer and creates gradients for nutrient and oxygen diffusion. ECM can isolate unwanted substances from the rest of the cells and store desired nutrients due to its compartmentalised architecture. Moreover, components of lysed cells can be stored in ECM and used by embedded cells when required in a process known as sorption (Flemming et al., 2016).

A breakthrough in the understanding of biofilm ECM came when Whitchurch et al., 2002, discovered the presence of eDNA in the ECM of *Pseudomonas aeruginosa* biofilms. eDNA was later shown to serve not only as a structural component but also as a reservoir facilitating horizontal gene transfer within biofilms (Flemming and Wingender, 2010). Until recently, it was assumed that eDNA exists predominantly in its canonical right-handed B-DNA form. However, recent findings demonstrated that eDNA can adopt non-canonical structures, including extracellular G-quadruplexes (Seviour et al., 2021) and Z-DNA (Buzzo et al., 2021). With Z-DNA identified as the predominant eDNA structure in mature biofilms of several bacterial species (Buzzo et al., 2021). These structures deviate from the standard double helix and provide additional structural reinforcement to the biofilm. Their formation is influenced by the mechanical stresses of the extracellular environment, with salts playing a key role in stabilising these conformations (Minero et al., 2024). Despite these findings, the presence of G-quadruplexes and Z-DNA structures

has not yet been reported in *L. monocytogenes* biofilms. Although, it is known that the biofilm matrix of *L. monocytogenes* also incorporates eDNA (Harmsen et al., 2010; Renier, Hébraud and Desvaux, 2010). Harmsen et al., demonstrated that treating biofilms with DNase effectively disrupted biofilms formed by 41 *L. monocytogenes* isolates collected from diverse environments and food products. It is possible that these recently discovered DNA conformations are undiscovered due to limited research.

In addition to eNA-based structures, ECM polysaccharides play a vital role in biofilm architecture, promoting surface attachment and overall stability. In *L. monocytogenes*, teichoic acids represent the main polysaccharide component of the ECM (Colagiorgi et al. 2016). However, unlike many Gram-negative bacteria where polysaccharides dominate, *L. monocytogenes* biofilms are primarily composed of proteins, with DNA and polysaccharides present in comparable amounts (Combrouse et al., 2013). Proteolytic enzyme treatment significantly disrupts biofilm formation, reinforcing the importance of proteinaceous components in *L. monocytogenes* (Flemming and Wingender, 2010). In *Salmonella* and other Gram-negative foodborne pathogens, cellulose (Zogaj et al., 2001) combined with curli fimbriae (Barnhart and Chapman, 2006) forms a significant part of the ECM. Notably, although *L. monocytogenes* does not naturally produce amyloid-like proteins akin to curli, a cellulose synthase machinery has been recently reported as part of a tentative prophage. This machinery contains partial cellulose synthase operon elements, presumably acquired by horizontal gene transfer through transduction from *Enterococcus faecalis* (Gutiérrez et al., 2025), and has been hypothesised to contribute to persistence in FPEs. Although research into the ECM composition of *L. monocytogenes* remains limited, surfactome analyses of *L. monocytogenes* biofilms grown on abiotic surfaces revealed the presence of peptidoglycan, teichoic acids, and cell wall-associated proteins (Janež et al., 2021).

1.7.3. Biofilm Lifestyle

The concept of biofilm formation was first described for *P. aeruginosa* and involves several distinct steps including initial attachment, proliferation and detachment/dispersal (Sauer et al., 2022; Stoodley et al., 2002).

1.7.3.1. Initial Attachment

Initially, primary colonising cells reversibly bind to the surface (Palmer, Flint and Brooks, 2007). There are two generally accepted theories for bacterial attachment to the surface:

two-step and three-step processes. In the two-step process the first step is for the cell to be transported close to the surface where initial attachment would happen with van der Waals forces, electrostatic forces and hydrophobic interactions. Initial attachment depends on properties of the surface, including factors such as texture, charge, hydrophobicity, pH and temperature (Stoodley et al., 2002). At this stage the cells may detach, returning to the planktonic state with fluid shear force. Then, attachment becomes irreversible, which involves production of polysaccharides and ligands to lock cells onto the surface and much stronger force must be applied to detach them (Stoodley et al., 2002).

An alternative theory is the three-step attachment process, which involves Lifshitz–van der Waals forces, facilitating first step attachment at several hundred nanometres from the surface (Bos, van der Mei and Busscher, 1999). The second step occurs 20 nanometres from the surface, involving a combination of Lifshitz–van der Waals forces and electrostatic interactions, while in the third step at around 5 nanometres from the surface, adhesion receptors facilitate strong attachment (Van Oss, Good and Chaudhury, 1986).

When the binding becomes irreversible, it requires strong shear force or chemical treatment to remove biofilm from the surface. The time required for the cells to go from reversible to irreversible attachment varies, and the topic has not been deeply researched. A study by Butler et al., carried out on biotic surfaces reported that the highest attachment to the surface happens in the first minute of the contact, with only small increase in the number of cells attached over time (Butler et al., 2002), while a study by Cadillo-Rodríguez et al., 2008, using atomic force microscopy (AFM) suggested that over time, the force required to separate the cell from the surface increased.

One of the important factors in cell attachment is the surface (see section 1.6.5. '**Surfaces in FPEs**'). In FPEs stainless-steel is the most common surface. Examination of stainless steel with AFM and scanning electron microscopy (SEM) has revealed cracks and crevices, which are used by bacteria to evade C&D treatments. Another contributing factor is hydrophobicity, which depending on the parameters of the surface can increase the likelihood of adhesion. The generally accepted rule is that hydrophobic cells adhere more strongly to hydrophobic surfaces and vice versa (Kochkodan et al., 2008; Giaouris et al., 2009). However, in environmental settings, communities contain several microorganisms at a time which demonstrate hydrophobic and hydrophilic properties hence only proportion of the cells would participate in surface attachment (Krasowska

and Sigler, 2014). Several studies have been performed to better understand hydrophobicity phenomenon in cell attachment. An investigation by Rogers, Gustavo Espinoza Garcia and Geissler, 2021 concluded that hydrophobicity of the cell is determined by proteins and lipids of the cell membrane, while another study by Paul and Jeffrey, 1985 revealed that the exposure of *Vibrio proteolytica* to proteolytic enzymes reduced its hydrophobicity and as a result decreased its attachment to hydrophobic surfaces like polystyrene. Similarly, treatment of hydrophobic *Streptococcus sanguis* by trypsin resulted in reduced adhesion to hydrophobic liquid, presumably due to degradation of hydrophobic proteins from the cell membrane (Oakley, Taylor and Doyle, 1985). Another principal feature involved in cell attachment to the surface is motility, which has been demonstrated in *L. monocytogenes*. Motile cells have an advantage over non-motile counterparts due to ability to overcome repulsive and hydrodynamic forces in route to the surface (Lemon et al. 2007).

1.7.3.2. Proliferation

Attachment is followed by proliferation and recruitment of additional planktonic cells, with biofilm growing into a mature, complex, multicellular form. Contact with the surface leads to changes in gene expression, upregulating machinery required for ECM production, associated with the proliferation step (Prigent-Combaret and Lejeune 1999; Otto and Silhavy 2002; Inagaki et al., 2005; Morici et al., 2007; Beloin et al., 2008; Bhomkar et al., 2010). At the proliferation step, subpopulations of cells within the biofilm emerge. Cells embedded deep within a biofilm, close to the attachment surface, are positioned far from the liquid interface and therefore encounter nutrient and oxygen limitations as well as increased competition for the resources, driving formation of micro-environments and eventually distinct sub-populations. Consistent with this, cells within the biofilms been reported to express genes linked to oxygen deprivation, general stress and stationary phase conditions, nutrient stress, and slow growth (Stewart and Franklin, 2008; Serra and Hengge, 2014; Williamson et al., 2012; Heacock-Kang et al., 2017). Further details are provided in section 1.7.2. '**Extracellular Polymeric Matrix of Biofilms (ECM)**' and 1.7.5. '**Heterogeneity within Biofilms**'.

1.7.3.3. Detachment/Dispersal

The final stage of biofilm development is detachment, where the cells can return to the planktonic lifestyle and colonise new areas. Biofilms can detach as individual cells or as aggregates, which retain against disinfectants (Purevdorj-Gage, 2005; Stoodley, Hall-

Stoodley and Lappin-Scott, 2001). Detachment is a complex process involving multiple signal transduction pathways and there is no universal dispersal system utilised by all bacteria (Karatan and Watnick, 2009). Currently, three known dispersal mechanisms have been described: erosion, central hollowing and sloughing. Erosion is a continuous process happening throughout the biofilm formation when individual cells and small aggregates separate from the main body of the biofilm at low rate. Central hollowing is an active process that involves a rapid detachment of cells and clusters from hollow cavities inside the colony (Boles, Thoendel and Singh, 2005; Sauer et al., 2002), whilst sloughing is a sudden detachment that can be either active or passive and happens during late biofilm development stages (Lappin-Scott and Bass, 2001; Stoodley et al., 2001; Wilson et al., 2004).

As the ECM engulfs the cells within, its structure first needs to be digested for the cells to detach. Therefore, one of the mechanisms of dispersal is enzymatic degradation of the ECM by a range of extracellular enzymes that bacteria produce to degrade their own matrix. Among these, dispersin B produced by *Aggregatibacter actinomycetemcomitans* is the most researched of biofilm-matrix degrading enzymes (Kaplan et al., 2003). In multi-species communities, biofilm-matrix degrading enzyme produced by one species may produce enzymes to degrade ECM of other organisms, which can act as a defensive strategy to displace competitors (Zhang and Bishop, 2003).

Factors affecting dispersal in biofilms have been extensively studied and it is accepted that dispersal is a selective advantage under unfavourable environmental conditions as allows a search for a more favourable environment. Factors such as low nutrient and oxygen availability, pH and temperature have all been shown to result in dispersal (Karatan and Watnick, 2009). Several studies on nutrient availability effect on dispersal have been carried out on *P. aeruginosa*, demonstrating that both, increase and decrease of carbon sources results in dispersal. Studies on *Aeromonas hydrophila* supported the theory that starvation increases biofilm dispersal whilst alternatively a study on *Acinetobacter* spp. demonstrated that high nutrient availability leads to dispersal (Sawyer, 1998; James et al., 1995). Overall, detachment of *L. monocytogenes* biofilms is not thoroughly investigated, and general biofilm dispersal model is extrapolated on *L. monocytogenes.*

1.7.4. Conceptual Change of Biofilm Lifestyle

Recently, the biofilm concept has been reviewed as it became evident not all biofilms develop in the same way and the definition did not describe the complexity of the biofilm formation in natural settings (**Figure 2**). The model did not include diversity of attachment, aggregation and detachment mechanisms that are currently known. In contrary with the original model, the new model suggests that biofilm formation does not require attachment surface for a colonising cell to bind, and the planktonic cell aggregates can be considered free-floating biofilms (Sauer et al., 2022).

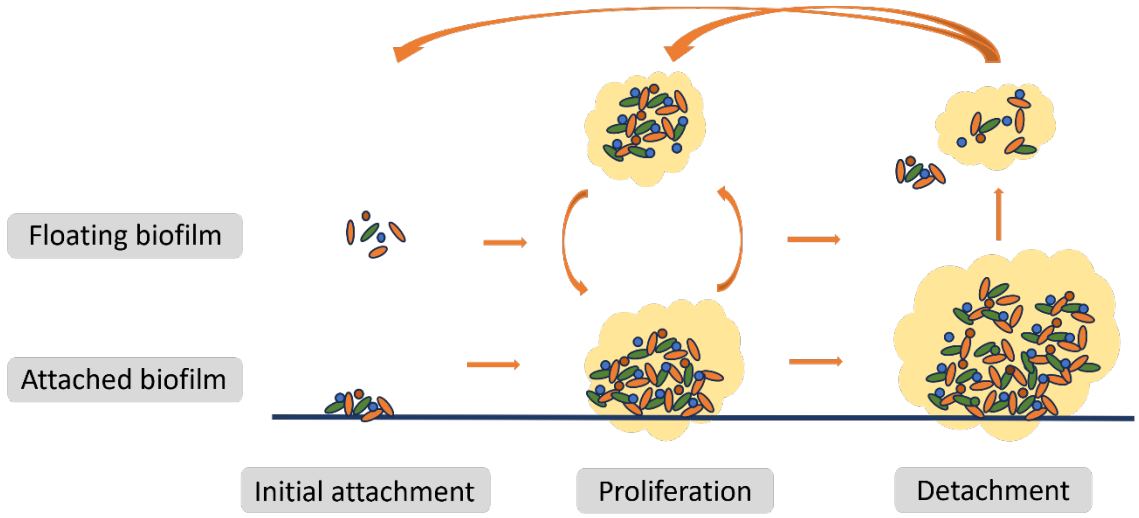


Figure 2. Schematic overview of the biofilm lifecycle according to the updated biofilm formation model. This model expands upon the traditional understanding of biofilm formation by incorporating both surface-attached biofilms and floating biofilm aggregates (also known as non-attached or planktonic biofilm structures). The schematic illustrates key stages of the biofilm lifecycle: initial attachment to a surface, proliferation of cells and matrix production, and detachment of biofilm components. Notably, the updated model emphasises on the dynamic and reversible nature of biofilm states, highlighting that bacteria can transition between surface-attached and free-floating biofilm forms throughout the lifecycle. Expanded biofilm formation concept adapted from Sauer et al., 2022.

1.7.5. Heterogeneity within Biofilms

In many biological multicellular systems, the gradients of oxygen are known to influence activity of regulatory cascades that modulate metabolism and/or morphogenesis, including tumour development or tissue differentiation in plants (Jo, Price-Whelan and Dietrich, 2022). In bacteria, the importance of gradients was demonstrated by the fathers of environmental microbiology, Winogradsky, Beijerinck and ZoBell, and has recently gained more attention in biofilm research, which have been shown to exhibit heterogeneity as they are not uniform structures (Jo, Price-Whelan and Dietrich, 2022).

EPS is a contributing factor to the heterogeneity in biofilms as the matrix restricts exchange of molecules for the cells that are further away from its surface, and embedded into the deeper layers of the biofilm structure, establishing microenvironments (Karygianni et al., 2020). This leads to a rise of subpopulations with different phenotypes and unique expression patterns, altered for its role within the community. As an example, in biofilms of *P. aeruginosa* the subpopulations use different metabolic pathways and even catalyse subsequent steps in metabolic pathways such as denitrification (Williamson et al., 2012; Chiang et al., 2012). When measured the redox potential of certain

compounds like phenazine, its pool became more reduced towards the bottom of the biofilm indicating that the subpopulations at the hypoxic and anoxic zones in the bottom are reducing it (Jo et al., 2017; Evans et al., 2023), suggesting that such population distribution is driven by oxygen availability.

Phenotypic heterogeneity has also been reported in other species. As such, in *Bacillus subtilis* there has been three distinct phenotypes detected specialising in motility, matrix production and sporulation (Yannarell et al., 2022; Srinivasan et al., 2018).

Heterogeneity within *L. monocytogenes* biofilms remains understudied. In multispecies environmental biofilms, *L. monocytogenes* is likely to adapt to spatial gradients of nutrients, oxygen, and other factors. However, whether *L. monocytogenes* can exhibit similar heterogeneity within its own monospecies biofilms is less clear. This uncertainty arises partly because *L. monocytogenes* produces relatively little extracellular matrix, which lacks polysaccharides, compared to organisms like *P. aeruginosa*, where substantial matrix production creates pronounced oxygen and nutrient gradients (Harmsen et al., 2010).

1.7.6. *L. monocytogenes* Biofilms

L. monocytogenes biofilms have been extensively studied, however the molecular mechanism of their formation has not been completely elucidated.

Three structures have been revealed including monolayer, unstructured multilayer and a network of knitted chains (Borucki et al., 2003; Rieu et al., 2008). A more recent study by Guilbaud et al., 2015 used high-throughput confocal imaging to study biofilms in 96 *L. monocytogenes* isolates. The group was able to demonstrate complex honeycomb-like structures containing hollow voids formed by dead cells and ECM. Such voids have been previously described in staphylococcal species (Bridier et al., 2010). In addition, the group demonstrated the importance of flagellum in the creation of these honeycomb-like structures. Finally, it was shown that there is only a weak correlation between the lineage of the strains and the structure of the biofilms they produce (Guilbaud et al., 2015).

1.7.7. Genes and Pathways Involved in Biofilm Formation in *L. monocytogenes*

Several pathways have been associated with biofilm production in *L. monocytogenes*.

1.7.7.1 Global Regulators

Previous research has shown that the key transcriptional activator PrfA, which is required for transcription of a *Listeria* pathogenicity island 1 (LIPI1) comprising of six virulence genes (*prfA, plcA, hly, mpl, actA, plcB*), has an important role in biofilm formation (Poimenidou et al., 2018). *prfA* deficient strains were still able to colonise the surface, however further cell proliferation was significantly reduced (Vázquez-Boland et al., 2001; Lemon, Freitag and Kolter, 2010). The gene encoding for internalin L (*inlL*), which is under regulation of PrfA, has also been described as crucial for surface adherence and biofilm formation in *L. monocytogenes* (Popowska et al., 2017).

Another global regulator of stress response genes in *L. monocytogenes,* SigB, has been shown to have importance for the formation of both static and continuous-flow biofilms (Van der Veen and Abee, 2010). Later, it was demonstrated that the upstream regulator of SigB, RsbU, was also involved in biofilm formation (Hsu et al., 2020) by increasing the number of cells and overall biomass as was visualised with scanning electron microscopy (SEM). Although not directly demonstrated in *L. monocytogenes*, *rsbW* and *rsbV* have also been demonstrated to be involved in biofilm formation in other species, which are part of the same *rsb* operon as *rsbU* (Jeffrey et al., 2023; He et al., 2025).

1.7.7.1. Other Genes/Motifs Involved in Biofilm Formation

Other genes that were involved in biofilm formation included genes encoding for sortase A and FlaA, as well as genes encoding for various proteins carrying LPXTG motif, which have been identified in several studies under different conditions, indicating importance of these traits regardless of the environment (Nowak et al., 2021). The importance of LPXTG motifs on biofilm formation has later been emphasised by Shi et al., 2024, identifying a new LPXTG motif and demonstrating its importance for both biofilm formation and eukaryotic virulence.

Additionally, a study by Di Ciccio et al., analysed biofilm forming capacity of 57 *L. monocytogenes* isolates and revealed that isolates from meat products exhibited higher biofilm forming capacity than isolates from dairy products. The study identified three genetic traits associated with significant increase in biofilm production: *arsD* stress response gene, truncated *inlA* and SS-I (Di Ciccio et al., 2022). Alternatively, a study that looked at the importance of surface proteins on biofilm formation in *L. monocytogenes* revealed eight proteins linked to a decrease in biofilm formation regardless of the

screening temperature or background strain serotype. They are functionally involved in peptidoglycan assembly (Lmo2229), lipoteichoic acid (LTA) synthesis (DltB, Lmo2554, Lmo0644) the flagellar apparatus (FlaA, FliP, Lmo0707), or have an unknown function (Lmo2056) (Abachin et al., 2002; Bigot et al., 2005; Zawadzka-Skomiał et al., 2006; Webb et al., 2009). Studies mentioned above mostly focus on screening for impaired biofilm formation, whereas Piercey et al., 2016, reported transposon mutants that exhibit enhanced biofilm phenotypes; these included surface proteins (muramidase MurA and flagellin A) and virulence factors (amidase Ami and internalins A, B and H).

In 2019, the first pan-genome-wide association study was performed to link genomic data with biofilm phenotypes in *L. monocytogenes*. As part of the study the biofilm formation by persistent, prevalent, and rarely detected genotypes from FPEs was compared. Notably, in several conditions there was significantly more biofilm produced by genotypes rarely detected in FPEs, suggesting that for *L. monocytogenes* increased biomass production may not be beneficial in factory settings. (Lee et al., 2019).

1.7.7.2. Signal Molecules and Quorum Sensing Involved in Biofilm Formation of L. monocytogenes

Quorum sensing (QS) refers to a process by which bacteria detect their population density and regulate gene expression in response. This system enables bacteria to modify cellular processes based on changes in environmental conditions (Miller and Bassler, 2001; Otto, Dickey and Wolz, 2023). In Gram-positive bacteria, the best characterised QS system is encoded by the accessory gene regulator (*agr*) locus, first described in *Staphylococcus aureus* (Recsei et al., 1986) and known for over 20 years. A homologous system has also been identified in *L. monocytogenes* and is encoded by the *agr* locus (*lmo0048–lmo0051*, *agrBDCA*), with its expression controlled by the P2 promoter located upstream of *agrB* (Autret et al., 2003). The precursor peptide AgrD is processed by AgrB into the mature signalling molecule, an autoinducing peptide (AIP), which is secreted into the extracellular environment. When the concentration of AIP reaches a threshold, it binds to the receptor histidine kinase AgrC, triggering its autophosphorylation. The phosphate group is subsequently transferred to the response regulator AgrA, which then binds to promoter regions to regulate downstream gene expression. In *L. monocytogenes*, the Agr system positively regulates biofilm formation. Deletion of either *agrA* or *agrD* in the reference strain EGD-e leads to reduced adhesion to solid surfaces (Rieu et al., 2007; Garmyn et al., 2009; Zetzmann et al., 2019). In contrast, in *S. aureus*, the Agr system has the opposite effect, inhibiting biofilm formation by reducing cell adhesion and promoting

protease production. This regulation is mediated by the dual-functional regulatory RNA, RNAIII (Bronesky et al., 2016; Lauderdale et al., 2009), which has not been identified in *L. monocytogenes*. This difference illustrates how the same QS system can produce distinct regulatory outcomes depending on the presence of additional regulatory components. Despite its classification as a QS system, it remains debated whether the Agr system in *L. monocytogenes* functions as a traditional QS mechanism. Recent evidence suggests it does not operate as a classical population-density sensing system that triggers a coordinated response across the bacterial community (Bejder et al., 2024).

A second QS system reported in *L. monocytogenes* is the LuxS/AI-2 system, which negatively regulates biofilm formation. Disruption of the *luxS* gene results in increased cell attachment to surfaces (Challan Belval et al., 2006; Sela et al., 2006). However, since the receptor for the AI-2 signal has not been identified in *L. monocytogenes*, the functional role of this system as a QS mechanism remains controversial.

In addition to QS systems, intracellular second messengers play a critical role in regulating biofilm formation. One such molecule is cyclic-di-GMP (c-di-GMP), a well-established regulator of the transition between motile and sessile lifestyles (Valentini and Filloux, 2016). This signalling molecule has been extensively studied in various bacterial species, including *Escherichia coli*, *P. aeruginosa*, and *Salmonella enterica* serovar Typhimurium. In 2011, it was reported that c-di-GMP binding protein BdcA has an involvement in reduction of c-di-GMP in biofilm and subsequent reduction in ECM generation, leading to increased motility and dispersal of *Pseudomonas* species and *Rhizobium mellioti* biofilms (Ma, Zhang and Wood, 2011). In *L. monocytogenes*, c-di-GMP promotes biofilm formation by upregulating the expression of the *pssA*-E and *pssZ* operons (Chen et al., 2014), which are involved in the production of exopolysaccharides (Koseoglu et al., 2015).

1.7.7.3. Effect of Magnesium Cations on Biofilm Formation

Magnesium (Mg^{2+}) uptake systems are present in all domains of life, due to its importance as a co-factor in diverse enzymatic reactions as well as for membrane stabilisation in both eukaryotic and prokaryotic life forms (Zeinert et al., 2025). Previous studies have demonstrated that Mg^{2+} deprivation is an environmental trigger for biofilm formation in *P. aeruginosa* (Mulcahy and Lewenza, 2011). Similarly, Mg^{2+} has been shown to play a critical role in the biofilm architecture of *P. mendocina* and enhance biofilm formation in *P. fluorescens* (Song and Leff, 2006; Mangwani et al., 2014). In contrast,

in *Bacillus* species, Mg^{2+} concentrations of up to 10 mM enhanced biofilm bundling of cells; however, concentrations above 25 mM reduced bundling through the regulation of matrix gene expression and extracellular polymeric substance (EPS) production (Oknin, Steinberg and Shemesh, 2015). Moreover, Mg^{2+} significantly reduced biomass in *Acidithiobacillus ferrooxidans* and *Vibrio parahaemolyticus* in a dose-dependent manner and had a comprehensive impact on physiology and gene expression (Tang et al., 2018; Li et al., 2024).

In *L. monocytogenes* the effect of Mg^{2+} on biofilm formation is less studied. Chalke et al., 2022, reported that exposure to 50 mM Mg^{2+} enhanced *L. monocytogenes* biofilm formation and influenced later stages of biofilm development. Similarly, Nowak et al., 2021, found that inactivation of *mgtB*, led to the formation of a unique biofilm with a sandwich-like structure, likely due to the stabilisation of the extracellular polymeric matrix. Although the effects of Mg^{2+} on biofilms vary across bacterial species, either promoting or inhibiting biofilm formation depending on concentrations and environmental context (Mulcahy and Lewenza, 2011, Song and Leff, 2006; Mangwani et al., 2014, Oknin et al., 2015, Tang et al., 2018; Li et al., 2024).

1.7.8. Metabolic Shift During Biofilm Formation

Bacteria residing in biofilms are thought to be metabolically different to their planktonic counterparts (Sauer et al., 2002). When transitioning from the planktonic to the biofilm state, bacteria undergo significant metabolic remodelling to adapt to a lifestyle that is critically different from the planktonic form (Kragh et al., 2014; Poulsen et al., 1993; Sternberg et al., 1999; Corte et al., 2019).

Studies on *B. subtilis* have demonstrated widespread remodelling affecting central carbon metabolism, primary biosynthetic pathways, fermentation pathways, and secondary metabolism. This remodelling is hypothesised to be driven by the limited availability of specific nutrients and shaped by microbial competition (Pisithkul et al., 2019). Other studies on *B. subtilis* suggest that the initial stages of biofilm formation are associated with a rapid increase in metabolism, driven by the need to produce large amounts of ECM to embed the cells. However, this elevated ECM production is associated with trade-offs that lead to a reduction in overall metabolic activity and cellular growth rate (Niederdorfer et al., 2017), resulting in cells that are slow-growing but metabolically efficient. Findings from studies on *P. aeruginosa* support these observations. Using a microcalorimetric approach, Lichtenberg et al., 2022, have demonstrated that c-di-GMP signalling plays a

major role in determining the metabolic activity of *P. aeruginosa*, both in planktonic cultures and in two different biofilm models. A high intracellular c-di-GMP concentration in biofilm-associated cells leads to the rapid expenditure of energy on exopolysaccharide production, ultimately resulting in a low metabolic state. In a study by Lu et al., 38 differential metabolites were detected, and three metabolic pathways including glycerolipid metabolism, amino acid metabolism, and carbohydrate metabolism, were found to be significantly altered during biofilm formation in uropathogenic *E. coli* (Lu et al., 2019). Gene deletion approaches have been used to explore how metabolic changes affect biofilm formation. For instance, disruption of several central metabolic pathways, including glycolysis (Δ*pgi*), the Entner–Doudoroff pathway (Δ*edd*), and the pentose phosphate pathway (Δ*gnd*), (Ranson, Barton and McLean, 2023), surprisingly increased biofilm formation.

Some of the investigated metabolic shifts are also linked to the metal homeostasis, (discussed in section 1.7.7.3. '**Effect of Magnesium Cations on Biofilm Formation**') with a reorganisation of iron metabolism and transport being reported (Pisithkul et al., 2019). The topic of metabolic shift during biofilm formation remains underexplored in *L. monocytogenes.*

1.7.9. Biofilm Associated Persister Cells

Biofilms often contain persister cells, a dormant subpopulation with increased capacity to withstand antimicrobial exposure, presenting a challenge to effective disinfection (Brooun, Liu and Lewis, 2000; Singh et al., 2009). Persister cells can be pre-existing in the population or their formation can be promoted by environmental changes (Balaban et al. 2004; Dorr et al. 2010). When a disinfectant is applied, susceptible non-persister cells that make up the majority of the community quickly become eliminated whilst the proportion of persister cells within the community increases, allowing re-establishment of the population once the disinfectant is removed. (Lewis, 2010). *L. monocytogenes* persister cells may form at the FPEs as has been demonstrated by Li et al., 2023 in a study mimicking leafy green packaging facility. However, *L. monocytogenes* persisters behaved unusually, demonstrating higher susceptibility to chlorine than normal cells (Li et al., 2023). Overall, in *L. monocytogenes* persister cells and their role within communities is understudied.

1.7.10. Multi-species Communities

In recent years, there has been a growing focus on studying multi-species biofilm communities involving *L. monocytogenes*, particularly due to increasing evidence that such communities exhibit reduced susceptibility to disinfectants commonly used in C&D protocols, compared to single-species biofilms.

An example is a 2015 study by da Silva Fernandez et al., that examined a multi-species biofilm community composed of *Enterococcus faecium*, *Enterococcus faecalis*, and *L. monocytogenes*, pre-grown over an eight-day period. The study demonstrated that peracetic acid was the most effective disinfectant, successfully eliminating the multi-species biofilm. In contrast, other disinfectants such as biguanide failed to eradicate the biofilm, highlighting the selective efficacy of biocidal agents against complex microbial communities (da Silva Fernandes et al., 2015). More recently, Lake et al., 2024, investigated the efficacy of C&D treatments on multi-species biofilms resembling those found in mushroom processing environments, grown on PVC surfaces. There was significantly lower reduction of *L. monocytogenes* in multi-species biofilms compared to single-species counterparts. Furthermore, post-treatment analyses revealed regrowth of *L. monocytogenes* and persistent dominance of *Enterobacteriaceae* and *Pseudomonas*. Supporting these findings, Voloshchuk et al., 2025, reported that the presence of *Pseudomonadaceae* within multi-species biofilms increased the tolerance of *L. monocytogenes* to both peracetic acid and benzalkonium chloride, further emphasizing the protective role of certain cohabiting species in biofilm communities. In addition, a recent study by Voglauer et al., 2025, demonstrated the rapid colonisation capability of *L. monocytogenes* in pre-formed multi-species biofilms. The pathogen was able to integrate into a pre-formed multi-species community within just two hours of exposure, without significantly altering the biofilm's community composition or matrix structure. This study used a model biofilm composed of three bacterial species including *Pseudomonas fragi*, *Brochothrix thermosphacta*, and *Carnobacterium maltaromaticum*, which were originally isolated from a meat processing facility. These findings collectively underscore the complexity and resilience of multi-species biofilms, and the critical need for tailored C&D strategies when targeting pathogens like *L. monocytogenes* in FPEs.

1.7.11. Novel Methods for *L. monocytogenes* Biofilm Biocontrol

Recently, there has been an increased focus on novel biocontrol measures for *L. monocytogenes.* One of the alternative methods for biofilm removal are the enzymatic

solutions, which can be applied prior to the disinfectant treatment. The biofilm with EPS containing a range of proteins, polysaccharides and eDNA acts as a shield for embedded bacteria, limiting the contact between bacteria and the antimicrobial compounds. Enzymatic cocktails digest the biofilm matrix prior to disinfectant treatment, creating disruption of the ECM and exposing the embedded cells. The cocktails can be designed specifically against the ECM of the targeted strain as there is variation in composition of ECM between *L. monocytogenes* strains (Colagiorgi et al., 2016; Fagerlund et al., 2020; Hua and Zhu, 2024). A commercially available example (EnzyJet), containing ethoxylated sodium lauryl ether glycolate, *N*-oxide *N*,*N*-dimethyl-C12-C14-alkylamine, anionic surfactants (<5%), non-ionic surfactants (<5%), enzymes including proteases (<5%), and phenoxyethanol was tested for removal of mature biofilm pre-formed for 7 days. EnzyJet solution was applied for 20 minutes resulting in maximum of 6.9 log reduction with strain specificity being a challenge as there was reduced removal of biofilms in strains with robust matrix (Mazaheri et al, 2020). Another study by Rodríguez-López et al., 2017, demonstrated high effectiveness of combining enzymatic treatments with BC to target dual-species biofilms. The highest effectiveness was obtained using DNaseI followed by pronase and cellulase, however high number of viable cells was observed following the enzyme/BC treatment and more research has to be carried out to assess the effectiveness of enzymatic control measures.

Another alternative option for biocontrol of *L. monocytogenes* biofilms are the bacteriophages with lytic phages (Grigore-Gurgu et al., 2024). With successful applications of phages in therapeutics, more research is carried into phage application in FPEs, however factors such as organic matter, low temperatures, variability of biofilm components and treatment time make such application challenging. Several commercially available phage solutions have been designed to specifically target *L. monocytogenes* in FPEs including ListShieldTM and ListexTM P100. Several studies have achieved 5-log reduction in *L. monocytogenes* counts when applying ListexTM P100 on stainless steel biofilms (Soni, Nannapaneni and Hagens, 2010; Montañez-Izquierdo et al., 2012), while another study has shown complete elimination of *L. monocytogenes* biofilms following 24-hour treatment. In FPEs, however, such prolonged treatment is not feasible and a study with shorter treatment period have demonstrated limited efficacy of ListShield, resulting in 2-log reduction of *L. monocytogenes* biofilm on stainless steel following 2-hour exposure (Sadekuzzaman et al., 2017). While a study by (Gutiérrez et al., 2017) demonstrated even lower efficacy of 1-log reduction following 4-hour exposure to

ListShield. An additional challenge associated with the use of bacteriophages is strain-specific activity, with ListexTM P100 being able to infect 7 out 11 tested *L. monocytogenes* strains. Recently a study by Voloshchuk et al., (2025) revealed that commercially available biofilm remover significantly reduced the concentration of *L. monocytogenes* in multi-species biofilm containing *Pseudomonadaceae, Xanthomonadaceae, Flavobacteriaceae, Microbacteriaceae* and *L. monocytogenes* representing fruit-tree packaging facility.

1.7.12. Established Methods to Study Biofilm Formation

Over the last decades, as focus on biofilm research has increased, several well-established methods for studying biofilms have been developed, varying in their complexity.

1.7.12.1. Static High-Throughput Models

The most well-known and widely used approach is the static model (Merritt, Kadouri and O'Toole, 2005), which utilises microtiter plates of various well capacities. In this model, bacterial adhesion to the polystyrene surface occurs during incubation. Biomass is quantified by staining with crystal violet or safranin (Christensen et al., 1985). While this assay is relatively simple, providing only a general indication of biofilm-forming capacity, it offers the advantage of being a high-throughput method. Static microtiter models are often used as an initial screening tool before employing more time-consuming and complex techniques.

An advanced version of the static model is the Calgary Biofilm Device (Ceri et al., 1999), which requires bacterial motility to form biofilms on pegs suspended in the culture medium. Despite their convenience, the main drawback of static models is the lack of standardisation across laboratories.

1.7.12.2. Flow Cells

The flow cell biofilm system is a widely used in vitro method for studying bacterial biofilms under hydrodynamic conditions. These systems facilitate the development of mature biofilms while continuously removing planktonic cells through the constant medium flow (Crusz et al., 2012). The current gold standard setup, as described by Wolfaardt et al., 1994, consists of a polystyrene flow cell mounted with a microscope slide, connected via tubing to a medium inlet and waste outlet. A multichannel pump placed upstream of the flow cell, delivers the liquid medium and allows precise control

over nutrient composition, incubation temperature, and flow rate. This setup also supports real-time imaging, as flow cells can be directly mounted onto microscopes.

Despite its advantages, this system has notable limitations. Air bubble formation is a significant issue, particularly at incubation temperatures of 37 °C. These bubbles can disrupt biofilm integrity or cause biomass detachment, affecting approximately one in three experiments and often making results unusable (Crusz et al., 2012). Additionally, traditional flow cells are relatively low throughput, limiting their scalability for large studies. To overcome this, commercial platforms such as BioFlux have been developed (Benoit et al., 2010). These systems enable simultaneous fluid flow through up to 96 individual biofilms, enhancing throughput. More complex flow systems are also available, including flow reactors such as the Modified Robbins Device (MRD) and the Drip Flow Reactor (DFR) (Yang et al., 2024).

1.7.12.3. Rotating Biofilm Reactors

A widely used approach for studying biofilms under dynamic conditions is the use of rotary biofilm devices, particularly the well-established CDC Biofilm Reactor (Goeres et al., 2005). This system consists of a stirred media reservoir with eight removable coupon holders. The coupons allow biofilm formation under constant shear stress and a steady nutrient supply, simulating conditions found in natural settings (Williams et al., 2019).

A key advantage of this method is its high reproducibility, making it widely adopted. The CDC reactor also accommodates a variety of coupon materials, including those that mimic surfaces commonly found in FPEs. Coupons can undergo direct microscopic examination. This approach has been successfully applied to study biofilm formation by *L. monocytogenes*, including within multi-species and multi-strain communities representative of the dairy farm environments (Mendez et al., 2020).

1.7.12.4. Microfluidic-Based Biofilm Models

Microfluidic-based biofilm models have gained popularity in the last decade. One example is the BiofilmChip, a sensor that allows attachment of clinically derived bacterial cells, even directly from patient samples (Blanco-Cabra et al., 2021). Biofilm development on this device can be monitored in real time using confocal microscopy or electrical impedance spectroscopy. Microfluidic models have become valuable in research on extracellular eDNA and the streamer-like structures it forms (Secchi et al., 2022).

1.7.12.5. Biofilm Adaptive Models

There are several proposed models designed to study how single- or multi-species biofilms adapt to changing environmental conditions. The most well-known is the adaptive in vitro biofilm bead model, introduced by Poltak and Cooper in 2010. This model is particularly effective for studying bacterial adaptation to antimicrobials and has been used to monitor longitudinal changes in biofilm formation and biomass accumulation (Poltak and Cooper, 2010; Trampari et al., 2021). The system was initially described for *Burkholderia cenocepacia* as the model organism within a rotating test tube setup (Poltak and Cooper, 2010). Bacteria attached to the beads can be transferred to fresh beads on a daily or multi-day cycle, enabling biofilm attachment, propagation, and dispersal. This approach simulates every stage of the biofilm lifecycle, unlike many other models that only represent biomass accumulation. A key strength of this model is its adaptability to a wide range of conditions, including those relevant to *L. monocytogenes* in FPEs.

1.7.12.6. Limitations Across Models

A persistent challenge across these models is the lack of standardisation. Certain assays, such as the crystal violet assay are performed differently across laboratories, including variations in stain concentration, incubation time, number of washing steps, presence or absence of biofilm fixation, and the method of fixation, making these assays less reproducible (Allkja et al., 2021).

1.8. Project overview

1.8.1. Detection of Genetic Traits Associated with Biofilm Lifestyle and Reduced Susceptibility to Benzalkonium Chloride

With this project we were aiming to deepen our understanding of the mechanisms behind *L. monocytogenes* adaptation and long-term persistence in the FPEs, especially in the context of the biofilms. **We hypothesised that *L. monocytogenes* adapts to FPE-associated stressors through acquisition of genetic mutations that enhance biofilm formation and confer reduced susceptibility to biocide.** However, the specific genetic changes driving this persistence, especially in the context of biofilm-associated cells, remain unknown. To address this, we developed a longitudinal in vitro biofilm model that resembles key conditions in FPE and allows to study the long-term evolution of *L. monocytogenes* under subinhibitory concentrations of BC. We selected a biocide-susceptible, 1980s-era, chicken-derived *L. monocytogenes* ST121 isolate as a naïve baseline strain. As an older susceptible isolate, it was less likely to have undergone contemporary FPE bottlenecks, thus providing an opportunity to observe adaptation under experimentally imposed stresses. After 30 consecutive passages of evolution, followed by whole-genome sequencing of the evolved populations, we identified adaptive mutations that became fixed over time and uncovered novel genetic mechanisms that may be associated with persistence of *L. monocytogenes* in FPEs.

In **Chapter 3**, I prepared for the biofilm persistence model (BPM) experiment which forms the central part of the project, where we defined persistence as the ability of a microbial population to maintain long-term colonisation of a surface through successive cycles of biofilm attachment and dispersal, under recurrent antimicrobial or environmental stress. I expanded the *L. monocytogenes* strain collection by incorporating additional isolates, which were subsequently sequenced and phenotyped (**Figure 3**). I then performed a phylogenetic analysis of the relevant sequence types (ST9, ST204, ST121, and ST7) within the UK context to understand how our isolates fit into the broader population structure. Based on this analysis, we selected a representative isolate to be used in the biofilm evolution experiment. The isolate was susceptible and did not contain previously described tolerance/reduced susceptibility mechanisms against BC as well as having strong biofilm forming ability. Additionally, this chapter includes the development of a methodology for widefield fluorescence microscopy, which was later applied in **Chapter 6** to visualise biofilm architecture (**Figure 3**).

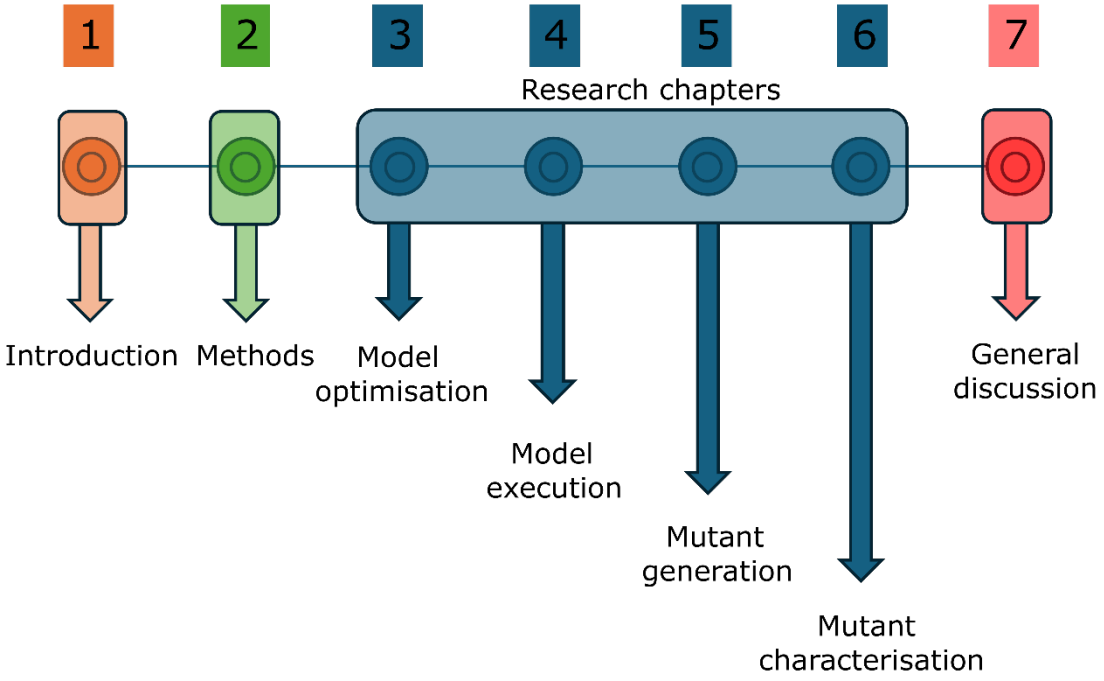


Figure 3. Schematic overview of the thesis structure and chapter content. The thesis is organised into seven chapters: an Introduction (**1**) and Materials and Methods (**2**), followed by four research chapters, which focus on optimisation of the biofilm persistence model (BPM) (**3**), execution of the model (**4**), generation of a mutant panel based on genomic findings (**5**), and characterisation of the mutant panel and the biofilm forming ability of the mutant strains (**6**). The thesis concludes with a General Discussion (**7**).

In **Chapter 3**, I adapted an existing biofilm persistence model (Poltak and Cooper, 2010; Trampari et al., 2021) to *L. monocytogenes* within the context of FPEs (**Figure 3**). Using the isolate selected in **Chapter 3**, the model was executed over 30 subsequent passages of biofilm and planktonic cells in the presence of BC. Biofilm lineages undergone approximately 500 generations. The evolved strains were stored for subsequent phenotypic and genotypic analyses, which were described in **Chapter 4**. Non-synonymous mutations were identified in genes and pathways involved in metal homeostasis, stress response and pyrimidine biosynthesis. In addition, reduced susceptibility to BC arose through multiple independent mutations within the *fepRA* operon, encoding FepR transcriptional repressor and FepA MATE efflux pump. These mutations were observed across both planktonic and biofilm lifestyles, resulting in a comparable level of reduced susceptibility to BC in both states. Fixed mutations associated with biofilm lineages aided identification of several loci involved in adaptation, including the *ykoK* riboswitch leader, the pyrimidine synthesis operon, and the stress response-related gene *rsbU*.

1.8.2. A Deeper Understanding of How the Loci Identified in the Biofilm Persistence Model Influence Biofilm Formation and Architecture

In **Chapter 5**, I constructed a panel of in-frame knockout mutants targeting loci identified as candidates in **Chapter 4**. We successfully generated seven knockout mutants, for the genes putatively involved in biofilm formation. In **Chapter 6**, I conducted a detailed phenotypic characterisation of the knockout mutants. This included assessments of biofilm-forming ability, biofilm architecture, and potential fitness trade-offs associated with the loss of each target region (**Figure 3**).

Chapter 2: Materials and Methods

2.1. Bacterial strains

Isolates from three separate Quadram Institute Biosciences *L. monocytogenes* culture collections were used in this thesis: the Quadram Institute Biosciences 'Historic collection', which contains 190 *L. monocytogenes* isolates collected between 1986 and 1991; the United Kingdom Health and Security Agency (UKHSA) collection, with 25 isolates of *L. monocytogenes* collected between 2010 and 2020 and the Food Standards Agency (FSA)-sponsored food surveys collection containing 198 *Listeria* isolates of which 115 are *L. monocytogenes* isolates collected in 2012 (**Appendix 1**).

The primary bacterial strains used in the work was *L. monocytogenes* BL87-028 (hereafter referred to as the 'parental' strain) and its derivative mutants (**Table 1**), originating from the historic *Listeria* collection. BL87-028 strain was isolated in 1987 from chicken in the UK. Based on the analysis of the complete hybrid genome assembly (BioSample: SAMN28229363), we previously identified it as belonging to ST121 and as a non-carrier of the *qacH* and *bcrABC* cassettes. This strain was selected for biofilm persistence experiment (see section 3.5.3.1 '**Strain Selection for Biofilm Evolution Experiment**') primarily due to its susceptibility to BC, exhibiting a minimum inhibitory concentration (MIC) of 3.12 µg/mL - significantly lower than that of closely related strains (Gutiérrez et al., 2025), as well as for its ability to form biofilms.

Additionally, we included 23 *L. monocytogenes* strains from the FSA-sponsored food surveys (**Table 1**), which hereafter will be referred to as the 'FSA panel'. The isolates were collected from RTE meats in Northern Ireland in 2012.

The isolates were recovered by streaking on 'Agar *Listeria* according to Ottaviani and Agosti' (ALOA) selective differential medium and incubated at 30 °C for 72 hours under aerobic conditions. Plates were examined after 72 hours for colony colour, halo formation and colony size. Blue colonies with a distinctive halo were incubated at 30 °C for 24 hours in Brain Heart Infusion (BHI) broth (Sigma-Aldrich, United States) on a shaking incubator (180 rpm). Subsequently, 20% glycerol stocks were prepared for storage at - 80 °C.

Table 1. Strains of bacteria used in this work.

Strain	**Source**
L. monocytogenes BL87-028	Quadram Institute Bioscience collection (Historic)
BL87-028-T10-No-BC-Biofilm1-3	Natural mutant generated in this study
BL87-028-T10-No-BC-Biofilm2-P	Natural mutant generated in this study
BL87-028-T30-No-BC-Biofilm1-1	Natural mutant generated in this study
BL87-028-T30-No-BC-Biofilm1-3	Natural mutant generated in this study
BL87-028-T30-No-BC-Biofilm3-3	Natural mutant generated in this study
BL87-028 Δ*ykoK*	Generated in this study
BL87-028 Δ*mgtA*	Generated in this study
BL87-028 Δ*rsbU*	Generated in this study
BL87-028 Δ*pyrD*	Generated in this study
BL87-028 Δ*carB*	Generated in this study
BL87-028 Δ*corA*	Generated in this study
BL87-028 Δ*bglG*	Generated in this study
L. monocytogenes LS12/71	RTE sliced meat survey (FSA Panel)
L. monocytogenes LS12/142	RTE sliced meat survey (FSA Panel)
L. monocytogenes LS12/177	RTE sliced meat survey (FSA Panel)
L. monocytogenes LS12/211	RTE sliced meat survey (FSA Panel)
L. monocytogenes LS12/257	RTE sliced meat survey (FSA Panel)
L. monocytogenes LS12/426	RTE sliced meat survey (FSA Panel)
L. monocytogenes LS12/453	RTE sliced meat survey (FSA Panel)
L. monocytogenes LS12/495	RTE sliced meat survey (FSA Panel)
L. monocytogenes LS12/519	RTE sliced meat survey (FSA Panel)
L. monocytogenes LS12/521	RTE sliced meat survey (FSA Panel)
L. monocytogenes LS12/522	RTE sliced meat survey (FSA Panel)
L. monocytogenes LS12/570	RTE sliced meat survey (FSA Panel)
L. monocytogenes LS12/579	RTE sliced meat survey (FSA Panel)
L. monocytogenes LS12/646	RTE sliced meat survey (FSA Panel)
L. monocytogenes LS12/685	RTE sliced meat survey (FSA Panel)
L. monocytogenes LS12/741	RTE sliced meat survey (FSA Panel)
L. monocytogenes LS12/808	RTE sliced meat survey (FSA Panel)
L. monocytogenes LS12/847	RTE sliced meat survey (FSA Panel)
L. monocytogenes LS12/859	RTE sliced meat survey (FSA Panel)
L. monocytogenes LS12/964	RTE sliced meat survey (FSA Panel)
L. monocytogenes LS12/970	RTE sliced meat survey (FSA Panel)
L. monocytogenes 08-5578	(Kovacevic et al., 2016)
L. monocytogenes 81-0861	(Kovacevic et al., 2016)
Escherichia coli DH5-Alpha	Quadram Institute Bioscience collection

2.2. Plasmids

The plasmids used in this study are listed in **Table 2**. Plasmids carrying fluorescent tag were used for visualising biofilms (see section 2.10.2. '**Widefield Fluorescence Microscopy**'). pKSV7 vector was used to generate in-frame targeted gene deletions (see section 2.9.1. '**Construction of Deletion Vectors**').

Table 2. Plasmids used in this work.

Plasmid	**Source**
pHPL3-mCherry	(Mitchell et al., 2017)
pHPL3-GFP	(Mitchell et al., 2017)
pKSV7	Shared by Martin Loessner (ETH Zurich)
pKSV7-Δ*ykoK*	Generated in this study
pKSV7-Δ*mgtA*	Generated in this study
pKSV7-Δ*rsbU*	Generated in this study
pKSV7-Δ*pyrD*	Generated in this study
pKSV7-Δ*carB*	Generated in this study
pKSV7-Δ*corA*	Generated in this study
pKSV7-Δ*bglG*	Generated in this study

2.3. Cryopreservation of strains and plasmids

E. coli and *L. monocytogenes* strains were first grown on Lysogeny broth (LB) or BHI plates respectively at 30 °C overnight. A single colony was then used to inoculate LB or BHI broth and was incubated with shaking at 30 °C for 18 hours. 800 µL of the culture was aliquoted into a cryovial and mixed with 40% (v/v) glycerol in a ratio of 1:1. Cryovials were stored at -70 °C.

Regarding cryopreservation of isolates from the BPM, see section 2.7 '**Layout of *in-vitro* Bead-based Biofilm Persistence Model (BPM)**'.

2.4. DNA extraction

2.4.1. DNA extraction for generation of hybrid assemblies

The FireMonkey High Molecular Weight DNA (HMW-DNA) extraction kit (RevoluGen, United Kingdom) was used to extract HMW-DNA for short- and long-read sequencing.

The isolates were incubated on a rotational platform (180 rpm) at 37 °C for 18 hours in BHI broth and 1 mL was used for DNA extraction.

First, the cells were harvested by centrifugation (4722 x g; 5 min) and washed with 1x volume of phosphate-buffered saline (PBS). The cells were lysed by resuspending the pellet in 180 µL of custom lysis solution (containing 20 mg/mL lysozyme (Roche, Switzerland) and 1.2% Triton X-100 (Sigma-Aldrich, United States) in H_2O) and incubated at 37 °C for 60 minutes. Subsequently, 10 µL of 20 mg/mL RNase A solution (Promega, United States) was added and mixed. Then 20 µL of 20 mg/mL Proteinase K was added and thoroughly mixed, followed by incubation at 56 °C for 20 minutes.

Following the addition of 350 µL of binding solution (BS) and 400 µL of 75% isopropanol, the sample was mixed by vortexing and transferred to the spin column provided in the DNA purification kit. DNA washing was then carried out according to the manufacturer's protocol.

Following the wash steps, the column was placed into a new 1.5 mL Eppendorf tube, and 100 µL of elution buffer (EB) was added. The column was incubated at 80 °C for 1 minute and centrifuged at 1180 x g for 1 minute to collect Fraction A, which typically yields a higher total DNA mass.

The column was then transferred to a second fresh 1.5 mL Eppendorf tube, and 80 µL of EB were added. After 1-minute incubation at 80 °C and centrifugation at 1180 x g for 1 minute, Fraction B was collected, typically enriched in longer average DNA fragment lengths.

2.4.2. DNA Extraction from the Biofilm Persistence Model Isolates

For samples derived from the biofilm persistence model (BPM), DNA extraction for short-read sequencing was performed using the Maxwell RSC Cultured Cells DNA Kit (Promega, United States) on the Maxwell RSC 48 automated extraction system, following the manufacturer's instructions. (For lysis solution see section 2.4.1. '**DNA extraction for generation of hybrid assemblies**').

2.4.3. Quantification of Genomic DNA

For batches of more than 25 samples, DNA quantification was performed using the QuantiFluor dsDNA System (Promega, United States) in microtiter 96-well plates using GloMax Discover Microplate Reader (Promega, United States) according to the manufacturer's instructions.

For smaller batches (< 25 samples), DNA was quantified using the Qubit™ dsDNA High Sensitivity Quantification Assay Kit (ThermoFisher Scientific, United States) on a Qubit Fluorometer (ThermoFisher Scientific, United States) where 1 µL of DNA sample was loaded for measurement.

2.5. Sequencing

2.5.1. Illumina Short-Read Sequencing

For high-accuracy short-read sequencing, including isolates derived from the BPM experiment and the FSA panel, genomic DNA was normalised to 5 ng/µL and 10 µL were submitted to the QIB core sequencing team (Quadram Institute Biosciences, United Kingdom).

Library preparation was performed using the Illumina DNA Prep Kit (Illumina, United States), and sequencing was conducted on the NextSeq 500 platform (Illumina, United States). The generated reads were 150 bp paired-end and run on a Mid Output Flowcell using NSQ 500 Mid Output KT v2 (300 cycles). Short-read sequencing data have been made publicly available (BioProject: PRJNA1276474).

2.5.2. Oxford Nanopore Long-Read Sequencing for Hybrid Assembly Generation

For long-read sequencing, genomic DNA was prepared using a modified protocol based on the ligation sequencing kit SQK-LSK109 (Oxford Nanopore Technologies, United Kingdom).

A total of 1.1 µg of DNA was concentrated in 6.25 µL using AMPure XP beads (Beckman Coulter, United States), mixed on a HulaMixer (ThermoFisher Scientific, United States), and washed twice with 80% ethanol. The DNA was eluted in 7 µL of nuclease-free water, mixed again, and 6.25 µL of the supernatant was recovered.

End-prep was performed with 0.875 µL Ultra II end-prep buffer and 0.375 µL end-prep enzyme mix (New England Biolabs, United States), followed by incubation at 20 °C for 5 minutes and 65 °C for 20 minutes. Barcoding was done by adding 1.25 µL of native barcode (EXP-NBD196) and 5 µL of BluntITA ligase master mix, incubated at 20 °C for 20 minutes and 65 °C for 10 minutes; barcoded samples were pooled.

The pooled library was cleaned using 0.6X AMPure XP beads (Beckman Coulter, United States) and washed with 700 µL of Short Fragment Buffer (SFB) followed by 70% ethanol. DNA was eluted in 35 µL nuclease-free water, and 34 µL was used for adapter ligation with 5 µL Adapter Mix II and 10 µL NEBNext Quick Ligation Buffer (New England Biolabs, United States), incubated at room temperature for 20 minutes.

A final bead clean-up was performed as above, and the DNA was eluted in 15 µL of EB. 14 µL of the final library was loaded onto a SpotON flow cell (R9.4.1) and sequenced on a MinION device (Oxford Nanopore Technologies, United Kingdom). Data acquisition was performed using MinKNOW v3.1.8, and basecalling was done in high-accuracy mode with Guppy v5.0.12 (Oxford Nanopore Technologies, United Kingdom).

2.5.3. Whole Plasmid Sequencing

Whole plasmid sequencing was performed by PlasmidsNG (United Kingdom). Genomic DNA libraries were prepared with the Rapid Barcoding Kit 96 V14 (SQK-RBK114.96) and sequenced using an R10.4.1 flow cell (FLO-MIN114) on GridION (Oxford Nanopore Technologies, United Kingdom). Raw signal data was basecalled using the GridION deployment for Guppy (ont-guppy-for-gridion v6.3.9) using model number r1041_e82_400bps_hac_v4.2.0. Barcode trimming was enabled. Reads under 200 bp were discarded.

2.6. Bioinformatic Analysis

Once the reads were sequenced the data was stored on IRIDA genome sequence data management platform (Matthews et al., 2018). Sequencing data in FASTQ format was then downloaded from IRIDA and uploaded into the Galaxy platform (Afgan et al., 2018).

2.6.1. Bioinformatic Analysis for Hybrid Assembly Generation

Hybrid assemblies were generated using both Illumina short-read and Oxford Nanopore long-read sequencing data.

Short-read data were first quality-checked using fastp (Chen et al., 2018). Quality reports in JSON format were compiled into a unified summary using MultiQC (Ewels et al., 2016). Reads were filtered based on default criteria: minimum length (15 bp), base quality (<Q15), and proportion of ambiguous bases (N's ≤5%). The remaining reads were

trimmed to a minimum Phred score of Q20 using Trim Galore! (GitHub - FelixKrueger/TrimGalore) (**Appendix 2**).

Long-read data were filtered using Filtlong (GitHub - rrwick/Filtlong). The top 95% of reads longer than 6,000 bp were retained for downstream analysis. Both short and long reads were screened for contamination using Kraken2 (Wood, Lu, and Langmead, 2019) with the kraken2_benlangmead_standard database. A species-level threshold of > 90% Kraken2-assigned reads was used to confirm *L. monocytogenes* identity.

For short-read assembly, high-quality trimmed reads from Trim Galore! were used to perform *de novo* genome assembly using Shovill (GitHub - codeworkscn/shovel) with the default assembler SPAdes (Prjibelski et al., 2020). Assemblies were annotated using Bakta (Schwengers et al., 2021), and sequence types were assigned via PubMLST (Jolley, Bray, and Maiden, 2018).

Long-read assemblies were generated using filtered reads in Flye (Kolmogorov et al., 2019) with the nano-raw setting. After assembly, reads were further filtered with a minimum length of 1,000 bp, retaining the top 95%. Assemblies were polished with Medaka (Oxford Nanopore Technologies, United Kingdom) to improve consensus accuracy. To further refine the assemblies, Pilon (Walker et al., 2014) was used to polish long-read assemblies with Illumina short reads.

The order and orientation of complete bacterial genomes was calculated with Socru v2.2.4 (Page, Ainsworth and Langridge, 2020).

Detection, reconstruction, and typing of plasmids were performed using the MOB-suite modular toolkit v3.0.3 (Robertson and Nash, 2018). Plasmid reconstruction and initial classification were conducted using MOB-recon, run with default parameters. Circular contigs were identified using Unicycler-generated contig headers (--unicycler_contigs) and by detecting assembly overhangs (--run_overhang). Mash distances were used for plasmid clustering, with thresholds of 0.002 for filtering valid closed genomes, 0.06 for primary plasmid cluster assignment, and 0.025 for secondary cluster assignment. Maximum contig and reconstructed plasmid sizes were set to 450 kb. BLAST-based detection thresholds included minimum e-values of 1e-05 for replicons, relaxases, contigs, and repetitive elements. Minimum sequence identity thresholds were set to 80% for all features, with minimum coverage thresholds of 80% for replicon and relaxase queries, 60% for contig coverage against the plasmid reference database, and 80% for

repetitive elements. Only contigs ≥1,000 bp were considered for plasmid classification. Plasmid typing was additionally performed using MOB-typer independently with default parameters to annotate plasmid mobility, relaxase families, and replicon types. For this analysis, minimum identity thresholds were set to 80% for replicons, relaxases, and contigs, with minimum coverage thresholds of 80% for replicons and relaxases and 70% for contigs. A minimum fragment overlap of 10 bp was required.

2.6.2. Bioinformatic Analysis for Whole Plasmid Sequencing Data

Bioinformatic analysis of plasmid data was performed by PlasmidsNG (United Kingdom). Oxford Nanopore long-reads were processed with Rasusa v0.7.0 (Hall, 2022) and SeqKit v2.2.0 (Shen et al., 2016) and assembled with Canu v2.2.0 (Koren et al., 2017) and Trycycler v0.5.3 (Wick et al., 2021). Assemblies were annotated by pLannotate v1.2.0 (McGuffie and Barrick, 2021). Polishing was performed using Medaka v1.7.0 (Oxford Nanopore Technologies, United Kingdom).

Virtual gels were prepared to visualise the most frequent peaks within the reads, based on log weighted distribution of long read sizes. The peaks were displayed as bands on a simulated gel with brighter bands corresponding to the higher-frequency read lengths.

pKSV7 plasmid was annotated with PlasMapper 3.0 (Wishart et al., 2023).

2.6.3. Phylogenetic Reconstruction and Population Structure

Phylogenetic reconstruction was performed following Gutiérrez et al., 2025.

For ST121, a total of 870 *L. monocytogenes* genomes were analysed comprising 30 human isolates, 551 food isolates, 279 environmental and one isolate from unknown source. Of these, 869 were isolated in the UK and one was from an unknown location. This dataset included 16 complete genomes from Quadram Institute Biosciences' collection (4 - Historic collection, 11 - UKHSA collection and 1 from the FSA panel, isolated between 1987 and 2022) (Gutiérrez et al., 2025), along publicly available genomes gathered through UKHSA surveillance between 2008 and 2022 (accessed 18 June 2022).

For ST9 a total of 341 *L. monocytogenes* genomes were analysed: 55 human, 216 food, 67 environmental and two from unknown sources). This set comprised of 336 UK, 3 Canadian samples, 1 from the USA, and one from an unknown location. This dataset included 29 complete genomes from the Quadram Institute Biosciences collection (13

from the Historic collection, 8 from the UKHSA collection and 8 from the FSA panel, isolated between 1936 and 2019).

For ST7 a total of 103 *L. monocytogenes* genomes were included in the phylogenetic analysis: 47 human, 45 food, 5 environmental and 5 from unknown sources, with all samples isolated in the UK. This dataset included 6 complete genomes from the Quadram Institute Biosciences collection (3 from the Historic collection and 3 from the FSA panel, isolated between 1941 and 2012).

For ST204, a total of 146 *L. monocytogenes* genomes were included in the phylogenetic analysis: 15 human, 109 food and 13 environmental, with all isolated in the UK. This dataset included 3 complete genomes from the FSA panel collection, isolated in 2012.

Along the Quadram Institute Biosciences' in-house collection, we included publicly available genomes for each ST, gathered through UKHSA surveillance between 2008 and 2022 (accessed 18 June 2022) from private and public collections.

Assemblies of the ST121 genomes were aligned to the reference genome CFSAN054109 (GCA_003030165.1) using Snippy v3.2 (Seemann, 2015). For other STs, *L. monocytogenes* EGD-e (GCF_000196035.1) was used as the reference genome. Repeat regions in the reference genome were masked using BEDTools v2.29.0 (Quinlan and Hall, 2010). Variant calling was performed with the following criteria: a minimum base quality of 20, read coverage of at least 10×, and a minimum of 90% read concordance. Single nucleotide polymorphisms (SNPs) within the core genome were identified by aligning sequence reads to the reference genome. Both monomorphic and polymorphic sites were included to calculate the total size of the core genome using snp-sites v2.5.1 (Page et al., 2016).

To account for homologous recombination, Gubbins v2.4.1 (Croucher et al., 2014) was used to detect recombinant regions, which were subsequently masked from the alignments. Recombination-purged variant sites were retained by selecting only positions containing A, C, G, or T, again using snp-sites v2.5.1 (Page et al., 2016).

Phylogenetic reconstruction was carried out using RAxML v8.2.4 (Kozlov et al., 2019) with the GTRCAT model on the filtered alignment. The rooting was placed at the midpoint of the longest path between genomes.

2.6.4. Quality Control and Base Calling Analysis for Processing Biofilm Persistence Model Data

Paired-end Illumina reads were quality filtered using Trimmomatic v0.38.0 (GitHub - usadellab/Trimmomatic) with default parameters, applying a sliding window of 4 bp and a minimum base quality threshold of 20. Filtered reads were screened for potential contamination using Kraken2 v2.1.1 (Wood, Lu, and Langmead, 2019).

Single nucleotide polymorphisms (SNPs) between evolved lineages and the parental strain BL87-028 (BioSample: SAMN28229363) were identified using Snippy v4.4.3 (Seemann, 2015), aligning trimmed reads to the annotated reference genome with default settings. Output variant tables were manually curated in Excel (Microsoft Corporation, United States), and synonymous mutations were excluded from downstream analyses. To detect SNPs specific to the biocide (BC) or biofilm conditions, SNP sets were compared using an online Venn diagram tool (Heberle et al., 2015). Genes affected by SNPs, as well as SNP frequencies across experimental conditions, were visualised using RAWGraphs v2.0 (Mauri et al., 2017). SNP locations were annotated and visualised on the BL87-028 genome using SnapGene Viewer v6.2.2.

2.6.5. Functional Categorisation of Mutations Identified Through Biofilm Persistence Model

Genes containing non-synonymous mutations were grouped by function according to the *ListiWiki* database (Elfmann et al., 2023), which consists of four major functional groups including cellular processes, metabolism, information processing and lifestyles. Each of the major functional groups were further divided into functional subgroups.

Two ways of characterising functional distribution were used. First, we characterised mutations by the number of affected loci in each functional subgroup and how it changed over timepoints. Then, to not only capture the number of loci affected in each functional subgroup but also to represent the frequency of SNPs within mutated loci, we grouped individual SNPs identified in the steady model based on their functional roles. Functional distribution was visualised with bump charts using RAWGraphs v2.0 (Mauri et al., 2017).

2.6.6. Analysis of the genome structure and genes related to BC survival and biofilm formation

Analysis of the genes related to BC survival and biofilm formation was performed using ABRicate at default parameters (GitHub - tseemann/abricate) with an in-house gene database **(Appendix 3**) curated from published sources (Doumith et al., 2004; Hingston et al., 2017; Maury et al., 2019; Moura et al., 2016; Pasquali et al., 2018), where we solely focused on the genes associated with BC survival and biofilm formation. Hybrid assemblies were used for ABRicate analysis.

The presence and absence of Tn*6188* elements were assessed using the Pasteur *Listeria* database in conjunction with the Gene Presence Analysis tool (https://bigsdb.readthedocs.io/en/latest/data_analysis/gene_presence.html). The analysis included the genes Tn*6188-qac*, Tn*6188-tetR*, Tn*6188-tnpA*, Tn*6188-tnpB*, and Tn*6188-tnpC*, using the default minimum identity threshold of 70%. To specifically evaluate the *qac* gene, an additional analysis was performed using a 100% identity cutoff for Tn*6188-qac*. Hybrid assembled genome sequences in FASTA format were used as input for these analyses.

2.6.7. Conservation Analysis of Mutated Residues

To evaluate conservation of nucleotide changes within the *ykoK* leader region, homologous sequences of this region were retrieved from NCBI BLAST (Altschul et al., 1990). For intra-genus analysis, *L. monocytogenes* sequences (taxid: 1639) were excluded, focusing on conservation within other *Listeria* species (**Appendix 4(I)**). For inter-genus comparisons, homologous sequences from related non-*Listeria* species were used (**Appendix 4(II)**). A multiple sequence alignment of 50 representative sequences was conducted using ClustalW v2.1 (Sievers et al., 2011) at the default parameters, and a visual consensus logo was generated with WebLogo v2.8.2 (Schneider and Stephens, 1990; Crooks et al., 2004).

Alignment of the mutated *ykoK* leader sequence against the *Bacillus subtilis* IA40 *ykoK* leader (PDB: 2QBZ) was performed using the Sequence Alignment Tool from VectorBuilder.

2.6.8. Domain and Structure Predictions

Protein domains in affected genes were predicted with InterPro (Blum et al., 2020), using default search settings across integrated member databases. Predicted structures were

obtained from the AlphaFold Protein Structure Database Database (Jumper et al., 2021; Varadi et al., 2021; Varadi et al., 2023), while experimentally determined structures were sourced from the Protein Data Bank (PDB) (Berman, 2000). Accession numbers for all structures used are provided in the results.

2.7. Layout of in vitro Bead-based Biofilm Persistence Model (BPM)

An in vitro bead-based biofilm persistence model (Adapted from Poltak and Cooper, 2010; Trampari et al., 2021) was established to investigate the effects of exposure of *L. monocytogenes* to steady and ascending BC concentrations as well as to biofilm persistence (**Figure 4**). In the context of this experiment, we defined biofilm persistence as the ability of a microbial population to maintain long-term colonisation of a surface through successive cycles of biofilm attachment and dispersal, under recurrent antimicrobial or environmental stress.

Four experimental conditions (biofilm steady-exposed, biofilm ladder-exposed, planktonic steady-exposed and planktonic ladder-exposed lineages) and two control conditions (biofilm non-exposed and planktonic non-exposed lineages) were performed, with 4 biologically independent lineages each (**Figure 4; Appendix 5**). For all conditions, the inoculum was prepared by growing *L. monocytogenes* in BHI broth for 18 hours at 37 °C, followed by dilution to an optical density of 0.05 AU ($OD600_{nm}$) in 1/10 diluted BHI. Each independent lineage was established from a different colony.

For the development of biofilm-evolved lineages, a single stainless-steel bead (grade 316, 6 mm diameter, surface area = 113.1 mm^2; Simply Bearings Ltd, United Kingdom) was placed in each well of Costar 12-well microtiter plate (Corning, United States), containing 2 mL of diluted culture in 1/10 BHI broth. Cultures were incubated for 48 hours at 20 °C under mild agitation (60 rpm). After incubation, beads were individually washed by submerging twice in sterile PBS to remove loosely attached cells. Each washed bead was then transferred into fresh sterile 1/10 BHI broth containing a new sterile bead. This transfer process was repeated for 30 consecutive passages, corresponding to approximately 562 generations, calculated according to the method described by Poltak and Cooper (2010).

To distinguish between successive beads during transfers, alternating beads were marked with a strip of lacquer (covering ~5% of the bead surface), leaving the majority of the

stainless-steel surface available for biofilm formation. Beads were prepared by rinsing with water, autoclaving, and submerging in 70% ethanol prior to use. All beads were used once.

In parallel, planktonic lineages (without beads) were propagated under the same conditions, acting as planktonic control. Each passage consisted of 2 mL of diluted culture (0.05 AU ($OD600_{nm}$)) in 1/10 BHI broth incubated at 20 °C with mild agitation (60 rpm) for 48 hours, followed by a 1:100 dilution into fresh medium for the next passage.

To investigate adaptation under biocide stress, benzalkonium chloride (BC, C8H17 – C18H37 alkyl distribution; Merck, United States) was introduced under two separate exposure models:

1. In the 'steady' model, cultures were continuously passaged in 1/10 diluted BHI broth containing 0.625 µg/mL BC.

2. In the 'ladder' model, BC concentrations were progressively increased:

- 1-step ladder: 0.625 µg/mL from passage 1 to 11 (part of the steady model), then 1.3 µg/mL from passage 11 to 30 (separated from the steady model).
- 2-step ladder: 0.625 µg/mL from passage 1 to 11 (part of the steady model), then 1.3 µg/mL from passage 11 to 22 (separated from the steady model), with an additional increase to 1.75 µg/mL that was introduced at passage 22 and continued to passage 30.

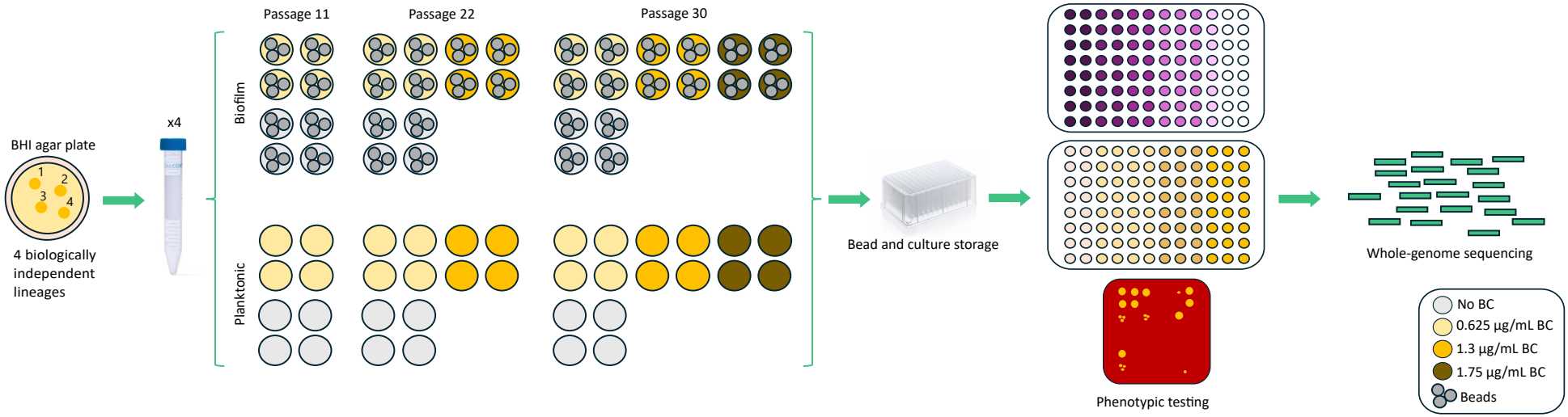


Figure 4. Overview of the experimental design of the biofilm persistence model (BPM). The evolution experiment started with four biologically independent colonies of the parental strain (BL87-028) under experimental (BC-exposed biofilm and planktonic) and control (non-exposed biofilm and planktonic) conditions, which were passaged 30 times, with a 48-hour incubation period between the passages. Beads and cultures were stored and cryopreserved after 11 (early), 22 (mid) and 30 (late) passages. Samples were analysed with a range of phenotypic tests (biocide sensitivity testing, cell attachment capacity, and biomass production). Evolved lineages underwent whole-genome sequencing, followed by identification of genetic changes compared to the hybrid genome assembly of the parental strain, with the rapid haploid variant calling tool - Snippy.

Glycerol stocks were prepared from selected timepoints: ‘early’ (passage 11), ‘mid’ (passage 22), and ‘late’ (passage 30). Biofilm beads were preserved in 1.5 mL of 20% glycerol prepared in 1/10 BHI broth, while 750 µL of planktonic cultures were directly mixed with 50% glycerol in 1:1 ratio, and both were stored at -70 °C in 96-well deep well plates (Merck, United States).

At each of the three timepoints, isolated populations were sampled from both biofilm and planktonic populations. For biofilm lineages, bead-attached cells were detached (see section 2.8.3. ‘**Cell Attachment Capacity**’), and both detached and planktonic cultures were plated onto BHI agar and incubated at 37 °C for 18 hours. For both planktonic and biofilm-derived lineages, three random colonies were selected from each lineage and preserved in 20% glycerol at -70 °C. These stocks were used for phenotypic characterisation of the populations as well as individual colonies derived from respective populations.

Populations: refers to the entire culture derived from evolved biofilm and planktonic lineages (one per lineage). These contain a mixture of genetic or phenotypic variants.

Individual colonies: refer to three individual colonies randomly selected from each population. Each individual colony represents a clonal subpopulation rather than the full diversity present in the whole population.

2.8. Phenotypic Assays

2.8.1. BC Sensitivity Testing by Agar Dilution Method

The minimum inhibitory concentration (MIC) of BC was determined using a modified agar dilution method based on CLSI guidelines (Clinical and Laboratory Standards Institute, 2018). A 96-well pin replicator (Boekel Scientific, United States) was used to inoculate approximately 10^4 CFU/mL onto lysed horse blood–Mueller Hinton agar (LHB-MHA) plates containing increasing concentrations of BC (0, 2.5, 5, 7.5, 10, 12.5, 15, and 20 µg/mL). Growth control plates (0 µg/mL BC) were inoculated at both the beginning and end of each run to monitor for contamination and biocide carryover. Strain 08-5578 was used as a control of reduced susceptibility (Kovacevic et al., 2016). Strain 81-0861 was used as a sensitive control (Kovacevic et al., 2016).

The MIC was defined as the lowest concentration of BC that completely inhibited visible bacterial growth. MIC values were averaged from three biological replicates, and results

were reported for both evolved populations and individual colonies randomly isolated from these populations, in terms of fold change against the mean MIC value of the parental strain (BL87-028).

Sensitivity against BC was assessed as either exhibiting reduced susceptibility (>5 μg/mL) or susceptible (<5 μg/mL) based on the Gaussian distribution analysis (Gutierrez et al., 2025).

2.8.2. Crystal Violet Assay for Biomass Formation

Biofilm biomass production was quantified using a crystal violet staining assay, adapted from Di Bonaventura et al, 2008. The assay was used to assess biomass production of FSA-panel isolates, evolved lineages from biofilm persistence model as well as mutant strains with specific gene deletions.

Overnight cultures were grown in BHI broth and diluted in fresh BHI to an absorbance of 0.05 AU ($OD600_{nm}$). Subsequently, 200 μL of the diluted culture was transferred into wells of a 96-well microtiter plate (Greiner, Austria). Plates were sealed with a gas-permeable adhesive membrane (Starlab, United Kingdom) and incubated statically at 37 °C for 48 hours.

After incubation, cultures were discarded, and wells were gently washed three times with deionised water and air-dried. Wells were stained with 1% (w/v) crystal violet (Sigma-Aldrich, United States) for 15 minutes at room temperature. Excess stain was removed with water and air dried. Then, 70% ethanol was added to solubilize the bound dye. Biofilm biomass was quantified by measuring absorbance at OD_{590} using a FLUOstar OMEGA plate reader (BMG Labtech, Germany) in spiral averaging mode.

Strain 08-5578 was used as a high biofilm producing control (Kovacevic et al., 2016). Strain 81-0861 was used as a low biofilm producing control (Kovacevic et al., 2016).

Each assay included three biological replicates and three technical replicates per isolate. Sterile media-only controls were included in all experiments to account for background absorbance.

For measuring biomass production by the FSA-panel isolates, the optical density ($OD600_{nm}$) values were normalised against the high biofilm forming control strain (08-

5578). For normalisation, the $OD600_{nm}$ values of each test sample was divided by the mean $OD600_{nm}$ value of the high biofilm producing control.

2.8.3. Cell Attachment Capacity

Cell attachment capacity assay was used to measure population of parental strain on beads during BPM optimisation, as well as to measure surface attaching capacity of evolved lineages from biofilm persistence model.

One bead per well was placed in a 12-well microtiter plate containing 2 mL of the diluted culture (0.05 AU ($OD600_{nm}$) in 1/10 BHI broth) and incubated for 48 hours at 20 °C under mild agitation (60 rpm). Following incubation, the beads were submerged twice into 1 mL of sterile PBS contained in a 24-deep well plate (Axygen, United States) to remove loosely attached cells.

Following washing step, the beads were transferred into 1 mL PBS and sonicated at 50 Hz for 5 minutes to remove loosely attached cells from the surface of the bead. Plate counts of the detached cell suspensions were performed on BHI agar plates, incubated at 37 °C for 24 hours, and the CFUs per bead were calculated using the following formula: [(Number of colonies*dilution factor) / volume of culture plated] / volume used to sonicate 1 bead. CFU/bead values were $\log_{10}$-transformed prior to plotting and statistical analysis.

Three biological and three technical replicates were included for each tested isolate.

Cell attachment capacity under varying Mg^{2+} concentrations was also performed for mutant and parental strain. The culture was prepared in 1/10 diluted BHI broth supplemented with different concentrations of magnesium chloride ($MgCl_2$): 0 mM (control), 1 mM, 10 mM, and 50 mM. The rest of the steps followed the method for the cell attachment capacity assay without Mg^{2+} supplementation.

2.8.4. Short Term Cell Attachment Capacity

Short term cell attachment capacity assay was used to assess the population of mutant and parental strains on stainless steel beads after 30-minute exposure to stainless steel.

Overnight cultures of mutant and parental strains were incubated in 1/10 diluted BHI broth at 20 °C and inoculum was diluted to 0.45 AU ($OD600_{nm}$).

One bead per well was placed in a 12-well microtiter plate containing 2 mL of the diluted culture (0.45 AU ($OD600_{nm}$) in 1/10 BHI broth) and incubated for 30 minutes at 20 °C under mild agitation (60 rpm).

For the washing steps and CFU calculations see section 2.8.3. '**Cell Attachment Capacity**'.

2.8.5. Macrocolony Morphology Assessment

Methodology for assessment of macrocolony morphology was adapted from Quendera et al. (2023).

Macrocolony morphology was observed for mutant and parental strains.

Overnight cultures were grown in BHI at 37 °C. The cultures were diluted to 1.0 AU ($OD600_{nm}$) and 5 µL were spotted on BHI agar. The morphology was then observed and imaged following 2 and 6 days of incubation at 25 °C statically. Imaging was performed using a Stereo Research Macro Zoom Fluorescence Microscope (Olympus, Japan) with a numerical aperture of 0.3.

Three biological and three technical replicates were imaged for each tested isolate.

2.8.6. Growth Kinetics Assay

Bacterial fitness was assessed through growth kinetic experiments by measuring the area under the curve (AUC) of growth curves. This method was used to evaluate the fitness of evolved lineages from the biofilm persistence model as well as mutant strains with gene deletions.

Overnight cultures were grown in BHI at 37 °C. The cultures were diluted to absorbance of 0.05 AU ($OD600_{nm}$) in BHI. Subsequently, 200 µL of the diluted culture was transferred into wells of a 96-well microtiter plate (Greiner, Austria). Plates were sealed with a gas-permeable adhesive membrane (Starlab, United Kingdom) and incubated statically at 37 °C.

Absorbance at $OD600_{nm}$ was measured every 60 minutes, starting at time point 0, using a FLUOstar OMEGA plate reader (BMG Labtech, Germany) in spiral averaging mode. Measurements continued for approximately 12 hours, until the growth curve plateaued.

Wells containing only media served as sterility controls. The average absorbance value of these control wells was subtracted from the readings of experimental wells to correct for background. The AUC was calculated and plotted using GraphPad Prism v5.4 (GraphPad Software, United States).

2.9. Molecular Techniques

2.9.1. Construction of Deletion Vectors

The method employed to generate nonpolar in-frame deletion mutants was a modified version of the original and updated protocols for the use of the pKSV7 vector with SOEing-PCR as described by Rychli et al., 2021, and was further adapted from an unpublished protocol of Martin Wiedmann group (Bolten and Roberts).

2.9.1.1. Primer design

The primer design was performed in accordance with Rychli et al., 2021. The '*Left Homologous Arm Forward'* primer was designed to bind 300-500 bp upstream of the gene of interest and included a 5′-terminal restriction endonuclease site for subsequent cloning into the pKSV7 vector, along with an additional 4-6 bp overhang to enhance restriction enzyme digestion efficiency (**Table 3**). The '*Left Homologous Arm Reverse'* primer was designed to flank the upstream boundary of the gene, beginning at the first base pair outside the open reading frame (ORF). Similarly, the *'Right Homologous Arm Forward'* primer was positioned immediately downstream of the ORF and incorporated a 5′-terminal 20 bp sequence that is the reverse complement of the *'Left Homologous Arm Reverse'* primer, to enable overlap extension during PCR. The '*Right Homologous Arm Reverse'* primer was designed 300-500 bp downstream of the target gene and included a 5′-terminal restriction site for cloning along with an overhang.

To facilitate screening of correct insertions into the vector, two additional primers were used: the *'Forward Screen'* primer, located at least 50 bp upstream of the *'Left Homologous Arm Forward'* primer, and the *'Reverse Screen'* primer, located at least 50 bp downstream of the *'Right Homologous Arm Reverse'* primer.

All primers were synthesized by Sigma-Aldrich at a 0.025 µmole scale, with desalting purification, and supplied in dry format. Upon receipt, primers were resuspended in molecular-grade water to a stock concentration of 100 µM and stored at −20 °C. For use

in PCR reactions, working aliquots were diluted to 10 μM in molecular water and stored at room temperature.

Table 3. List of primers designed for generation of in-frame deletion mutants. Includes the primer sequence, melting temperature (T_m), restriction sites, size in WT and expected size following deletion. LHA – left homologous arm. RHA – right homologous arm, frw – forward, rev – reverse.

Gene	Primer direction	Primer sequence	Tm	Size of amplicon (bp)	Restriction site	Size in WT (bp)	Size after deletion
ykoK	LHA frw	TAAGCACTGCAGGGATCATTAAACGCCCGAATAAAG	65	497	PstI	1155	988
	LHA rev	TTTAGTATGCGTATAAACTCAGAAGTCCT	65				
	RHA frw	CTGAGTTTATACGCATACTAAA	60	491			
	RHA rev	GCATAGGATCCGTATGAAGGCCGAAATCAATCA	63		BamHI		
mgtA	LHA frw	TAAGCACTGCAGCGAACACCGCAACCCTTT	67	401	PstI	3367	796
	LHA rev	ATGCGTGCTGGACGC	68				
	RHA frw	GCGTCCAGCACGCAT TTTCCTTGCCTCCAATTCTTTC	64	395			
	RHA rev	GCCTGGTACCCAAAGACGCCAATGGGTAGA	66		BamHI		
rsbU	LHA frw	CTGCAGCGGGAGTTCCTGTTGTTGAT	59	1024	PstI	2358	1353
	LHA rev	TTTTTTCTAGCTCTCCTTACCGAA	58				
	RHA frw	CGGTAAGGAGAGCTAGAAAAAA	59	996			
	RHA rev	GGATCCTGGTAAGCGGCAATCCAAATA	59		BamHI		
pyrD	LHA frw	CTGCAGTCCCTTTGCCGTGTTCTTTA	58	1010	PstI	2921	2006
	LHA rev	ATGAATAAACCAATTATCGCGCTAG	58				
	RHA frw	GCGCGATAATTGGTTTATTCAT	59	996			
	RHA rev	GGATCCGGACAAGTTACGCTCGTAGTAAA	59		BamHI		

carB	LHA frw	TAAGCAAAGCTTCTTTGCCGAGCTGGTACAT	66	398	HindIII	4014	800
	LHA rev	ATAGAAGAAACGGGGTGGAAC	65				
	RHA frw	GGTTCCACCCCGTTTCTTCTAT	65	402			
	RHA rev	GCAGAGGATCCTTAGAAATGATTCGCGGCATTC	64		BamHI		
corA	LHA frw	TAAGCACTGCAGATGTCTATACAGCGATGGGAAT	64	425	PstI	1804	859
	LHA rev	AAATAAACAAAAAGCGATTGTATTACCTAA	62				
	RHA frw	TACAATCGCTTTTTGTTTATTT	64	434			
	RHA rev	GCCAAGGATCCCCGGACAACTTTGCTATTTCC	65		BamHI		
bglG	LHA frw	AAACTGCAGGTTACGCGACCTGCATATCT	66	414	PstI	2856	825
	LHA rev	CTCTATCACCTCTTTATACTAGTTGCG	65				
	RHA frw	CTAGTATAAAGAGGTGATAGAG	64	411			
	RHA rev	CGGGGTACCGCGATGTCGTCTAACTCACTT	65		KpnI		
pitA	LHA frw	CGCGGATCCTAACCGCTTAGACGACGTAATG	62	392	BamHI	1789	790
	LHA rev	CTATCTAGGCCCCTTACGC	62				
	RHA frw	GCGTAAGGGGCCTAGATAG	63	398			
	RHA rev	CCGGAATTCACGACTTTATCTTTACCGTCGATT	61		EcoRI		

2.9.1.2. Polymerase Chain Reaction

All components of the PCR reaction were thawed on ice prior to use. GoTaq® 2X Green Master Mix (Promega, United States), containing 400 µM each of dATP, dGTP, dCTP, and dTTP, 3 mM $MgCl_2$, and adjusted to pH 8.5, was used for colony PCR reactions (**Table 4**). The master mix was vortexed briefly to ensure homogeneity and then centrifuged briefly to collect contents at the bottom of the tube.

The PCR reaction mixture was prepared as follows:

Table 4. Reaction setup for colony PCR using GoTaq® Green Master Mix.

Component	**Final Concentration**	**Volume for 12.5 µL**	**Volume for 25 µL**
GoTaq® Green Master Mix (2X)	1X	6.25 µL	12.5 µL
Upstream primer (10 µM)	0.2 µM	0.25 µL	0.5 µL
Downstream primer (10 µM)	0.2 µM	0.25 µL	0.5 µL
DNA template	<250 ng (1 colony)	1 colony equivalent	1 colony equivalent
Nuclease-Free Water	N/A	To 12.5 µL	To 25 µL

For overlap PCR, instead of using colony lysate as the DNA template, 200 ng of each homologous arm was added to the reaction. All reactions were assembled in PCR strip tubes, thoroughly mixed, and then loaded into a Mastercycler PRO S 6325 Thermal Cycler (Eppendorf, Germany) for amplification.

The following PCR conditions were set:

Table 5. Cycling conditions for colony PCR.

Step	Conditions
Initial Denaturation	95°C for 2 minutes
Denaturation	95 °C for 30 seconds
Annealing	55 °C for 30 seconds
Extension	72 °C for 45 seconds
Final Extension	72 °C for 2 minutes
Hold	4 °C (refrigeration)
Cycle Number	25–30 cycles

For generation of homologous arms and an overlap extension PCR a Q5 High-Fidelity 2X Master Mix (New England Biolabs, United States) was used.

Table 6. Reaction setup for colony PCR using Q5 High-Fidelity 2X Master Mix.

Component	Final Concentration	Volume for 50 µL
Q5 High-Fidelity Master Mix (2X)	1X	25.0 µL
Upstream primer (10 µM)	0.25 µM	1.25 µL
Downstream primer (10 µM)	0.25 µM	1.25 µL
DNA template	≈200 ng	200 ng of each arm
Nuclease-Free Water	N/A	To 50 µL

The following cycling conditions were set at the thermal cycler when using high fidelity polymerase:

Table 7. Cycling conditions for high fidelity polymerase PCR.

Step	Conditions
Initial Denaturation	98 °C for 30 seconds
Denaturation	98 °C for 10 seconds
Annealing	58 °C
Extension	72 °C for 30 seconds
Final Extension	72 °C for 2 minutes
Hold	4°C (refrigeration)
Cycle Number	25 cycles

2.9.1.3. Gel Electrophoresis

Gel Electrophoresis was performed using 1% agarose gels prepared with molecular biology-grade agarose (Melford Biolaboratories Ltd, United Kingdom). Gels were prepared and run in 1X Tris-Borate-EDTA (TBE) buffer (0.089 M Tris base, 0.089 M boric acid (pH 8.3), and 2 mM Na_2EDTA), prepared from a 10X stock solution (National Diagnostics, United States) in deionised water. To visualise DNA on agarose gels, SYBR Safe DNA Gel Stain (Invitrogen, United States; 10,000X concentrate in DMSO) was added to the molten agarose to a final concentration of 1X. Electrophoresis was carried out at a constant voltage of 100 V on PowerPac (Bio-Rad, United States) for 30 - 60 minutes.

For molecular weight reference, 1 kb DNA ladder (New England Biolabs, United States) ranging from 500 bp to 10,000 bp and HyperLadder (Bioline, United States) ranging from 200 bp to 10,037 bp were used.

2.9.1.4. Gel Extraction and DNA Purification

The gel was visualised on a blue light transilluminator and the target bands containing the product were cut out with a scalpel (Slaughter Ltd, United Kingdom) and transferred into

a 1.5 mL microcentrifuge tube. The product was purified using the NucleoSpin Gel and PCR Clean-up Kit (MACHEREY-NAGEL, Germany) according to the manufacturer's instructions and eluted from affinity column with milli-Q water. Purified products were stored at -20 °C.

2.9.1.5. Plasmid Isolation

Plasmid DNA was isolated with NucleoSpin Plasmid DNA Kit (MACHEREY-NAGEL, Germany) from *E. coli* strains. Strains were incubated on the LB agar supplemented with 100 µg/mL carbenicillin (LB-Carb100) and a single colony was incubated in 250 mL of LB-Carb100 broth at 30 °C with shaking. The cells were pelleted by centrifuging at 4,000 rpm for 10 minutes. The cell pellet was processed according to the manufacturer's instructions. The plasmids were eluted from the affinity column using milli-Q water and stored tat -20 °C. The plasmids used in this project are indicated in section 2.2 '**Plasmids**'.

2.9.1.6. Quantification of Plasmid DNA and PCR Products

The concentration of PCR products and plasmids was measured with NanoDrop ND-1000 UV/Vis Spectrophotometer (Thermo Scientific, United States) and the absorbance at the wavelengths of 230, 260, and 280 nm was recorded. The concentration was calculated based on A_{260}. The 260/280 and 260/230 ratios were used to assess the purity. The ratio of 260/280 of pure DNA was in the range of 1.8 to 2.0, and the 260/230 was above 1.8.

2.9.1.7. Cloning of the Insert into Vector pKSV7 (Ligation)

PCR-amplified inserts and the pKSV7 vector were digested with appropriate restriction enzymes (**Table 3**) in the presence of NEB CutSmart Buffer (New England Biolabs, United States). Digestion reactions (25 µL total volume) contained 20 µL of DNA (insert or vector), 2.75 µL of CutSmart Buffer, 1 µL of each restriction enzyme, and 1.25 µL of molecular-grade water (Sigma-Aldrich, United Sates). Reactions were incubated at 37 °C for 20 minutes. The digestion products were then separated by agarose gel electrophoresis and purified using the NucleoSpin Gel and PCR Clean-up Kit (MACHEREY-NAGEL, Germany) according to the manufacturer's instructions (see section 2.9.1.4 '**Gel Extraction and DNA Purification**').

Purified insert and vector fragments were combined at molar ratios of 3:1, 5:1, and 7:1 (insert : vector), calculated using NEBioCalculator v1.16.23. For each ligation reaction, 1 µL of T4 DNA ligase (New England Biolabs, United States) was added, and the mixture was incubated at room temperature for 2 hours.

The ligated plasmids were transformed into chemically competent *E. coli* DH5α cells and plated onto LB-Carb100 plates. Plates were incubated at 37 °C for 24 hours. A negative control ligation lacking insert DNA was included to assess background colony formation. Following incubation, a marked reduction in colony number on the control plate relative to insert-containing reactions was used as an initial indication of successful ligation.

Several colonies were subjected to colony PCR using MCS primers (see section 2.9.2.2 '**Heat-shock Transformation of *E. coli* DH5α**'). In parallel, colonies were streaked onto fresh LB-Carb100 plates for storage. Colonies producing amplicons of the expected size were selected for plasmid extraction with Plasmid Maxi Kit (QIAGEN, Germany) and underwent whole plasmid sequencing at PlasmidNG (United Kingdom).

2.9.2. Preparation of Competent Cells

2.9.2.1. Preparation of Chemically Competent DH5α Cells

Overnight cultures of *E. coli* DH5α were grown in LB broth at 37 °C with shaking at 180 rpm. Next day, 1 mL of the overnight culture was used to inoculate fresh LB broth and grown at 37 °C with shaking to an absorbance of 0.6 AU ($OD600_{nm}$).

The cells were harvested by centrifugation at 4,000 rpm for 10 minutes at 4 °C. The supernatant was decanted out, and the pellet was resuspended in 50 mL of cold 0.1 M calcium chloride ($CaCl_2$) followed by incubation on ice for 30 minutes.

The cells were once again pelleted and resuspended in 10 mL of cold 0.1 M $CaCl_2$ containing 15% glycerol and the suspension was stored in 100 µL aliquots in pre-chilled microcentrifuge tubes at -70 °C.

2.9.2.2. Heat-shock Transformation of E. coli DH5α

For transformation, chemically competent DH5α cells were thawed on ice for 10 minutes or until crystals were no longer visible. Then, 50 ng of plasmid DNA (volume <5 µL) was added to the competent cells and left to incubate on ice for 30 minutes. Following incubation, the cells were subjected to the heat shock at 42 °C for 45 seconds. The cells were then immediately placed on ice and incubated for 5 minutes.

For recovery, 900 µL of LB broth warmed to 37 °C was added to the cells and the mixture was incubated at 37 °C with 400 rpm shaking for 1 hour. Following recovery, culture was LB-Carb100 plates and dried with the L-shape spreader.

The remaining cells were centrifuged at 11,000 rpm for 2 minutes. Supernatant was removed and the cells were resuspended in 100 µL of LB broth and plated on LB-Carb100 plate. The plates were incubated overnight at 37 °C.

Transformants were identified based on their ability to grow on selective media. Potential transformants were tested with colony PCR using plasmid specific multiple cloning site (MCS) primers: (pKSV7 fwd 5′- **ATGTGCTGCAAGGCGATTA**, pKSV7 rev: 5′- **CCAGGCTTTACACTTTATG**.

2.9.2.3. Preparation of Electrocompetent Cells

Methodology for preparation of electrocompetent cells in *L. monocytogenes* was adapted from Monk, Gahan and Hill (2008).

Overnight cultures of *L. monocytogenes* BL87-028 were prepared in BHI supplemented with 500 mM sucrose and grown at 37 °C. Then, a new 500 mL culture was inoculated from the overnight cultures and grown to mid-log phase reaching an absorbance of 0.18 - 0.22 AU ($OD600_{nm}$). Ampicillin was added to a final concentration of 10 µg/mL, and cells were incubated for two hours.

The cells were chilled on ice for 10 minutes, harvested by centrifugation at 5,000 rpm for 10 minutes at 4 °C, and resuspended in 250 mL of cold wash buffer. After two additional washes, the cells were pelleted and resuspended in decreasing volumes of wash buffer (150 mL and 50 mL).

Lysozyme was added to a final concentration of 40,000-45,000 U/mg, and the suspension was incubated for 20 minutes at 37 °C. The cells were pelleted again, resuspended in 20 mL of wash buffer, and pelleted for a final time.

The resulting pellet was resuspended in 2.5 mL of wash buffer, distributed into 50 µL aliquots, and stored at -70 °C. Freshly prepared cells yielded significantly better transformation efficiencies.

2.9.3. Transformation and Mutant Generation in *L. monocytogenes*

2.9.3.1. Transformation of L. monocytogenes by Electroporation

For pKSV7 construct plasmids that were confirmed by sequencing to carry the overlapping arms for gene deletion, transformation was performed using

electrocompetent BL87-028 cells. The process was also performed for transforming electrocompetent BL87-028 cells with fluorescent plasmids for biofilm visualisation.

Aliquots of electrocompetent cells were thawed on ice or used from fresh. Geneflow Electroporation 2 mm Cuvettes (Geneflow, United Kingdom) were incubated on ice for 5 minutes. 2 µg of plasmid DNA and 50 µL of electrocompetent cells were added into a chilled cuvette, followed by addition of cAMP to make up 32 mM in final volume. Cuvettes were immediately electroporated using Gene Pulser II electroporator (Bio-Rad, United Sates) with the following settings: 400 **Ω**, 2.2 kV, 25 µF. The cuvettes were immediately placed back on ice and 300 µL of BHI broth supplemented with 0.3 % sucrose were added into the cuvettes, followed by 90-minute incubation at 37 °C.

The inoculum was then distributed on BHI supplemented with 100 µg/mL carbenicillin (BHI-Carb100) plates and incubated at 37 °C for 48 - 72 hours. Following incubation, successful transformation was confirmed with pKSV7 MCS primers (see section 2.9.2.2 '**Heat-shock Transformation of *E. coli* DH5α**').

2.9.3.2. Chromosomal Integration and Plasmid Excision

Three individual colonies that had successfully undergone transformation with the pKSV7 vector (confirmed by PCR) were each used to inoculate 10 mL of pre-warmed BHI supplemented with 10 µg/mL chloramphenicol (BHI-Cm10) broth. Cultures were incubated statically at 42 °C until visible growth was observed. The first passage requires up to 72 hours incubation. If no growth occurred within this timeframe, subculturing was reinitiated at a lower temperature above 39 °C. Once growth was established, a 1:1000 dilution was prepared in fresh pre-warmed BHI-Cm10 and incubated statically for 24 hours. Passaging was repeated for a total of five times.

Following the fifth passage, cultures were streaked onto BHI-Cm10 agar and incubated at 42 °C for 24 hours. Several colonies were used to inoculate BHI broth (antibiotic-free) and incubated at 30 °C and incubated for 18 hours. Cultures were passaged up to 20 times with a 1:1000 dilution every 12-18 hours. Starting from passage 8, aliquots were plated onto BHI agar and incubated for 24 hours at 30 °C without antibiotic selection. Following incubation, between 250 and 500 colonies were replica-streaked onto both BHI agar and BHI-Cm10 agar and incubated again for 24 hours at 30 °C.

Colonies that grew on the antibiotic-free medium but failed to grow on chloramphenicol-supplemented plates were considered candidates for successful plasmid excision. These colonies were screened by colony PCR using the '*Forward Screen'* and '*Reverse Screen'* primers (**Table 8**). PCR products were resolved by agarose gel electrophoresis, and mutants were identified by the presence of a band smaller than the parental control by a size corresponding to the deleted gene.

Table 8. Primers used for screening second homologous recombination event to distinguish between WT reversion and successful gene deletion.

Gene	Primer direction	Primer Sequence
ykoK	Forward Screen	GCGATGGACAATGAACCAAAG
	Reverse Screen	GAGAAATGGGCAGCAAAGATATG
mgtA	Forward Screen	CGAGCAAACGAGTAGTCCTAAA
	Reverse Screen	CCATCAGGGAGAGGAAGTAGA
rsbU	Forward Screen	GCCTTGACGAACAGAGAGATAG
	Reverse Screen	GCTTGGCAGGAAGTTGTAATG
pyrD	Forward Screen	TGCCACTTGGAGAACCTATTT
	Reverse Screen	ACAGGGTTTCGTCACAGATATT
carB	Forward Screen	GCGCGGGAGTAGTATCAATATC
	Reverse Screen	CTATGTGACGGTCGTTCCTTAC
corA	Forward Screen	AGCGATGGGAATACAACATAGTC
	Reverse Screen	GAAGGAGTTGAGGAACGTGAAA
bglG	Forward Screen	GTTACGCGACCTGCATATCT
	Reverse Screen	GTCCACTTCACAGGCTTACTT

Mutants that passed the PCR size screen were sequenced with Illumina short-read WGS at the Quadram Institute Bioscience sequencing facility to confirm precise gene deletion and assess potential background mutations.

Short-read data processing and SNP identification were carried out as described in section 2.6.4. '**Quality Control and Base Calling Analysis for Processing Biofilm Persistence Model Data**'.

2.10. Microscopy

All microscopy imaging was conducted at the Quadram Institute Advanced Microscopy Facility (United Kingdom).

All image data were stored in Quadram Institute Biosciences OMERO storage server.

2.10.1. Brightfield Microscopy

2.10.1.1. Sample Fixation

Desired bacterial strains were grown overnight in liquid cultures (25 mL of 1/10 BHI broth), statically at 20 °C. For experiments where the effect of Mg^{2+} on cell length was assessed, the initial inoculum was grown in 1/10 BHI broth supplemented with 50 mM of magnesium chloride hexahydrate ($MgCl_2 \cdot 6H_2O$) (MilliporeSigma, United States).

The inoculum was then centrifuged for 10 minutes at 4000 rpm at 4 °C and the supernatant was decanted out. The cell pellet was resuspended in 1 mL of 4% Paraformaldehyde (PAF) and incubated at room temperature for 15 minutes to fix the cells. Next, the cells were centrifuged for 10 minutes at 4000 rpm and the supernatant was decanted out. The pellet was resuspended in 200 µL of PBS and stored at 4 °C until further use.

For experiment where effect of Mg^{2+} on cell length was assessed, five natural mutant strains from the BPM were used (**Appendix 5**) including BL87-028-T10-No-BC-Biofilm1-3; BL87-028-T10-No-BC-Biofilm2-P; BL87-028-T30-No-BC-Biofilm1-1; BL87-028-T30-No-BC-Biofilm1-3, BL87-028-T30-No-BC-Biofilm3-3. In the results section, the names of these strains were shortened for the ease of interpretation to T10-No-BC-Biofilm1-3; T10-No-BC-Biofilm2-P; T30-No-BC-Biofilm1-1; T30-No-BC-Biofilm1-3, T30-No-BC-Biofilm3-3, removing the indicator of BL87-028 strain which these strains had evolved from.

2.10.1.2. Sample Preparation

A 1% agarose solution was prepared in PBS, melted until fully transparent, and maintained at 55 °C. Two pads were assembled by placing four 1.5 mm glass coverslips (Corning, United States), previously washed in 70% ethanol, 5 mm apart on a clean glass slide. Another coverslip was positioned on top of the pads to form a mold. Subsequently, 100 µL of the molten agarose was pipetted into the space beneath the top coverslip and allowed to solidify at room temperature for 10 minutes.

After solidification, the top coverslip was gently removed using forceps, ensuring the integrity of the agarose layer remained intact. A 10 µL aliquot of fixed cells was then applied directly onto the agarose surface and covered with a sterile 1.5 mm coverslip, previously sterilised by immersion in 70% ethanol and wiped with a microscopy wipe

(Kimtech Science, United States). The coverslip was secured in place using clear adhesive tape to prevent any displacement during imaging.

2.10.1.3. Imaging

Brightfield imaging was conducted using Axio Imager M2 microscope (Zeiss, Germany) equipped with a 63× objective lens. Prior to imaging, Immersol immersion oil (Zeiss, Germany) was applied to the coverslip. Image acquisition was performed using Zen v3.9 software (Zeiss, Germany).

2.10.1.4. Cell Length Assessment

Cell length was measured for a randomly selected set of 100 cells per technical replicate with Fiji v1.54i. Measurements were conducted in a blinded manner, ensuring that I was unaware of the sample identity to minimise bias.

2.10.2. Widefield Fluorescence Microscopy

2.10.2.1. Biofilm Growth on Coupons

Desired bacterial strains were grown overnight in BHI broth (Sigma-Aldrich, United States), at 37 °C on a rotational platform (180 rpm). The overnight cultures were diluted to an absorbance of 0.05 AU ($OD600_{nm}$) in 1/10 BHI and 2 mL were transferred into each well of 12-well polystyrene plate (Corning, United States) containing one stainless-steel grade 316, 10 mm diameter, 3 mm thickness, milled finish coupons (LaserMaster, United Kingdom). Coupons were incubated at 20 °C under mild agitation (60 rpm) for 48 hours.

During biofilm growth on coupons under varying Mg^{2+} concentrations, the same method was followed but the overnight cultures were diluted to an absorbance of 0.05 AU ($OD600_{nm}$) in 1/10 BHI broth supplemented with different concentrations of $MgCl_2 \cdot 6H_2O$: 0 mM (control), 10 mM, and 50 mM.

When performing biofilm growth for 10 days as part of the BPM incubation timepoint optimisation, the media was replenished every 48 hours of incubation, by removing 2 mL of inoculum and replacing it with 2 mL of sterile 1/10 strength BHI.

2.10.2.2. Biofilm Fixation and Coupon Mounting

Following incubation, the coupons were carefully transferred into a sterile Petri dish using sterile forceps. To remove non-attached cells and residual media, each coupon was gently washed by pipetting PBS on top.

The coupons were submerged into 4% PFA, ensuring the entire surface was fully covered. Following overnight incubation at 4 °C, the PFA was pipetted out and PBS was gently added on top of the coupon until fully submerged.

Using forceps, the washed coupon was flipped and transferred into 35 mm, high, glass bottom µ-Dish (ibidi, Germany) containing an adhesive gene frame (25 µL, 1.0 x 1.0 cm; ThermoFisher Scientific, United States) fixed to the bottom. The dish was then filled with PBS until the coupon was fully submerged to prevent desiccation of the biofilm. The dishes were sealed, wrapped in aluminium foil, and stored at 4 °C until further use.

2.10.2.3. Imaging

For staining, a 100 µL aliquot of SYTO 9 Green Fluorescent Nucleic Acid Stain (5 µM in PBS; ThermoFisher Scientific, United States) was applied to each coupon. The samples were incubated in the dark for 15 minutes to allow staining, after which excess dye was removed by a single PBS wash. When fluorescent plasmid-labelled cells were used, the coupons were not stained.

The stained coupons or coupons containing fluorescent plasmid labelled bacteria, were then mounted in µ-Dishes (35 mm, high, glass-bottom; ibidi, Germany) fitted with adhesive gene frames (25 µL volume, 1.0 × 1.0 cm; ThermoFisher Scientific, United States). Fluorescence imaging was performed using a DeltaVision Elite Deconvolution Microscope (General Electric, United States) equipped with a UPlanFLN Semi Apochromat 10× objective (numerical aperture: 0.3) (Olympus, Japan). Images were acquired in the FITC channel (excitation: 470/24 nm; emission: 525/36 nm) at a resolution of 512 × 512 pixels. Z-stacks were collected at 0.2 µm intervals.

Four biological replicates were analysed, with ten fields of view captured per replicate.

2.10.2.4. 3D Image Processing

Z-stack images were exported in digital video format (.dv). For 3D reconstruction of biofilms, these files were converted to Imaris format (.ims) using Imaris v10. To facilitate

analysis with BiofilmQ image processing software (Hartmann et al., 2021), the Z-stack images were further converted to Open Microscopy Environment Tagged Image File Format (OME-TIFF) using Imaris v10 and then imported into BiofilmQ.

During image preprocessing with BiofilmQ, out-of-focus stacks were removed using the "Find out-of-focus stacks" function. In the segmentation section, images were corrected for potential coverslip tilt by aligning to the brightest focal plane. Denoising by convolution was applied using the built-in algorithm with default parameters, followed by Top-Hat filtering to enhance feature contrast. For thresholding, the Otsu method was applied using 2-class segmentation, and the sensitivity value was set to 0.15. Post-processing involved the removal of small voxel clusters with a volume below 0.17 μm^3.

2.10.2.5. Biofilm Quantification

Based on the segmentation, various global (calculated for the whole image of the biofilm rather than individual segments) biofilm parameters were calculated:

- Biofilm_MeanThickness: Mean of the local thickness values across the entire biofilm volume.
- Biofilm_BaseArea: Area of the fitted ellipse at the biofilm base, or convex hull if fewer than five cubes are detected.
- Biofilm_Volume: Total segmented biovolume in cubic micrometers (μm^3).

The representative biofilm image in the top view was selected as the field of view with a Biofilm_Volume value closest to the median. The representative biofilm image in the side view was selected as the field of view with a Biofilm_MeanThickness value closest to the median.

Global biofilm parameters were visualised with GraphPad Prism v5.4 using box and whisker plots, demonstrating the minimum value, the first quartile (Q1), the median (Q2), the third quartile (Q3), and the maximum value.

In experiment investigating the impact of Mg^{2+} on biofilm formation, we used the previously acquired values for Δ*mgtA*, Δ*ykoK* and parental strain from section 6.5.3.4 '**Disruption of Stress Response and Pyrimidine Metabolism Pathways Impacts Global Biofilm Architecture**', as reference values.

2.10.3. Scanning Electron Microscopy (SEM)

Biofilm-coated coupons were fixed by immersion in 2.5% glutaraldehyde prepared in 0.1 M sodium cacodylate buffer for 1 hour at room temperature. A blank (sterile) coupon was processed in parallel to distinguish surface morphology from biofilm structures. After fixation, the glutaraldehyde solution was removed, and the coupons were washed three times with 0.1 M sodium cacodylate buffer to remove residual fixative. Samples were then post-fixed in 1% osmium tetroxide for 1 hour.

Following post-fixation, samples were washed three times with distilled water, then subjected to a graded ethanol dehydration series: 30%, 50%, 70%, 80%, 90%, and three changes of 100% ethanol, including a final step in dry 100% ethanol. Each step lasted a minimum of 15 minutes.

Samples were then critical point dried using an EM CPD300 (Leica, Germany), with liquid carbon dioxide serving as the transitional fluid. Dried coupons were mounted onto aluminium SEM stubs using silver paint, then coated with an 8.5 nm layer of gold using an ACE 600 (Leica, Germany) sputter coater. Imaging was performed immediately using a Nova NanoSEM (FEI, United States) scanning electron microscope operated at 3 kV.

2.11. Figures

All figures were prepared in Inkscape v1.3.

2.12. Statistical analysis

All data were analysed using GraphPad Prism v5.4, and results are expressed as mean ± standard deviation (SD), unless stated otherwise.

For experiments assessing short- and long-term cell attachment to beads, the crystal violet assay, and growth kinetics, all individual data points are shown. Each experiment was initiated from three independent mother cultures (biological replicates). Inoculum from each mother culture was transferred into multiple individual wells of microtitre plates, as detailed in the methodology sections corresponding to each specific technique. Following inoculation, each well constituted an independent experimental unit and experienced independent growth and attachment conditions. Individual wells were therefore analysed as replicates, and all measured values are presented to reflect the full distribution of the

data. Statistical comparisons between multiple groups were performed using one-way ANOVA, followed by Tukey's post-hoc test for pairwise comparisons. Statistical significance was set at $p < 0.05$, with significance levels indicated as follows: $p < 0.05$ (*), $p < 0.01$ (**), $p < 0.001$ (***), and $p < 0.0001$ (****).

Chapter 3: Establishing the Experimental Basis for Biofilm Persistence Studies: Expansion of *L. monocytogenes* Culture Collection and Optimisation for Food Processing Environment Conditions

3.1. Contributions

Oleksii Omelchenko, Ana Victoria Gutiérrez, Maria Diaz, Erin Lewis, Mark Webber, Matthew Gilmour.

3.2. Publications

Data in section 3.5.1.1 '**Phenotypic Testing of Persistence Determinants: Tolerance to BC and Biofilm-forming Capacity**' was used for publication (Microbial Genomics):

Gutiérrez, A.V., Matthews, M., Diaz, M., Viet, T.L., Leonardo, Jørgensen, F., Aird, H., Anaïs Painset, Som, N., Oleksii Omelchenko, Adriaenssens, E.M., Kingsley, R.A. and Gilmour, M.W. (2025). **Population structure and gene flux of *Listeria monocytogenes* ST121 reveal prophages as a candidate driver of adaptation and persistence in food production environments**. *Microbial Genomics*, 11(4). doi:https://doi.org/10.1099/mgen.0.001397.

Data in section 3.5.3 '**Establishment of a biofilm persistence model for *L. monocytogenes***' was used for publication (Microbial Genomics):

Oleksii Omelchenko, Ana Victoria Gutiérrez, Maria Diaz, Erin Lewis, Maria Solsona Gaya, Mark Webber, Matthew Gilmour. **A continuous biofilm evolution model of *Listeria monocytogenes* identified mechanisms of persistence and niche adaptation.** *Microbial genomics, under review*.

3.3. Introduction

L. monocytogenes is one of the most persistent foodborne pathogens in FPEs, where it can withstand C&D regimes and cause recurrent contamination events (Møretrø and Langsrud, 2004; Ortiz et al., 2016; Méndez Acevedo et al., 2024). Persistence in FPEs contributes to cross-contamination of RTE foods and increases the risk of outbreaks. Understanding how *L. monocytogenes* adapts to these conditions requires experimental systems that reflect both the diversity of strains encountered in food production and the selective pressures shaping their evolution.

Increasing use of advanced genomic analysis techniques has significantly enhanced our understanding of the population structure of *L. monocytogenes* (Fox et al., 2016; Haase

et al., 2014). In particular, MLST has proven valuable in tracing the evolutionary history of the species and revealing associations between specific subgroups and environmental niches (Fox et al., 2016).

In the first part of this chapter, I sought to create a comprehensive *L. monocytogenes* culture collection, representing diverse sequence types, sources, and time periods of isolation, to understand how our isolates fit into the broader population of *L. monocytogenes* in the UK. Expanding the collection with strains from FPEs and RTE food sources ensured that our work captured the diversity circulating in food production settings. This was also a learning opportunity to develop the fundamental microbiology and genomic skillsets to then characterise, sequence and analyse the resulting data sets from the BPM.

We recived a collection of *Listeria* spp. isolates from FSA-sponsored food surveys and generated hybrid assemblies of 23 *L. monocytogenes* isolates from this collection (FSA panel). The strains were genotypically and phenotypically characterised and traits associated with FPE persistence, including reduced susceptibility to BC and biofilm formation were investigated. These isolates were used to expand Quadram Institute Biosciences' collection of *L. monocytogenes* (see section 2.1. '**Bacterial Strains**') (Gutiérrez et al., 2025).

The enriched collection was used to select a representative baseline isolate to go through adaptive BPM (executed in **Chapter 4**), and study the acquisition of genetic traits associated with FPE persistence. It was crucial to select a strain representative of sequence types commonly associated with FPEs, yet sufficiently naïve in both phenotype and genetic adaptations to retain the capacity to evolve under FPE-associated stress. Our focus primarily centered on *L. monocytogenes* sequence types associated with FPEs, specifically ST121 (Holch et al., 2013; Schmitz-Esser et al., 2015; Knudsen et al., 2017; McLauchlin 2021), ST204 (Palma et al., 2020), ST7 (Brown et al., 2021) and ST9 (Morganti et al., 2016; Palma et al., 2020), which were all present in the FSA panel (more on *L. monocytogenes* subtyping can be found in section 1.5. '***L. monocytogenes* subtyping**').

As a secondary focus of this chapter, we aimed to optimise the BPM to suit *L. monocytogenes* and mimic FPEs. To establish a robust and reproducible BPM, we had to first optimise several parameters including: 1) suitable media, 2) incubation time for

consistent biofilm formation, 3) subinhibitory concentration of BC, 4) long-term stability of bacterial populations in presence of BC and 5) differentiation method between the beads from alternating passages.

This chapter outlines the rationale behind our choice of method and details the experimental optimisation of conditions most suitable for representing FPEs.

3.4. Aims

1. To carry out a genotypic and phenotypic characterisation of the FSA panel.
2. To create a comprehensive *L. monocytogenes* culture collection representing diverse sequence types, sources, and time periods of isolation.
3. To select a naïve, baseline strain of *L. monocytogenes* capable of acquiring FPE stress-relevant genetic traits over time that will be subjected to a biofilm persistence model.
4. To establish a robust biofilm persistence model (BPM) that mimics FPEs and accomodates for *L. monocytogenes* through a series of optimisation steps.

3.5. Results

3.5.1. Expansion and Characterisation of the *L. monocytogenes* Culture Collection

The rationale for enriching the isolate collection with the strains from FPEs and RTE food sources, as well as performing a phylogenetic analysis of their sequence types, was to facilitate the selection of a suitable strain for use in the BPM (see section 3.5.3.1 '**Strain Selection for Biofilm Evolution Experiment**').

A total of 198 *Listeria* spp. isolates were obtained from FSA-sponsored food surveys conducted in Northern Ireland between September 2007 and February 2013. These included 115 *L. monocytogenes*, 36 *Listeria welshimeri*, 32 *Listeria innocua,* 14 *Listeria seeligeri*, and 1 *Listeria ivanovii* isolates (**Figure 5; Appendix 1**).

From this larger FSA collection, we focused on a comprehensive survey of RTE sliced meats conducted between June and December 2012, during which 78 *Listeria* spp. isolates were collected. Isolates belonging to other *Listeria* spp. than *L. monocytogenes* were excluded from the analysis and to ensure a representative dataset, only one *L. monocytogenes* isolate was chosen per sampling timepoint. Together, 23 *L.*

monocytogenes isolates (FSA panel) were selected for phenotypic and genotypic characterisation (**Table 9; Figure 5**).

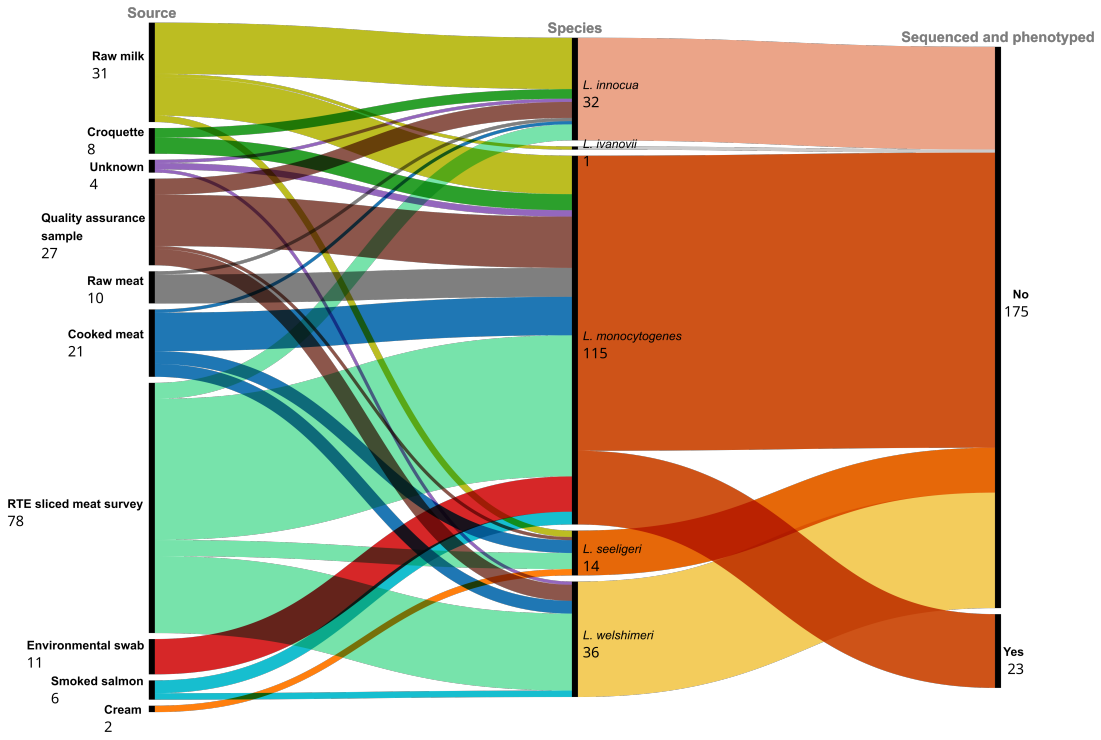


Figure 5. Alluvial diagram of the *Listeria* species isolates from the Food Standards Agency (FSA) collection (198 isolates). The diagram illustrates the flow of isolates from the source of isolation to the identified *Listeria* species, and finally to the characterisation approach (phenotyping; whole-genome sequencing; Yes - No) applied to each isolate. Food sources include raw milk, croquette, quality assurance samples, raw meat, cooked meat, environmental swabs, smoked salmon, cream, and RTE sliced meat survey samples. Identified species, determined based on Analytical Profile Index (API) scores, include *L. monocytogenes, Listeria innocua, Listeria welshimeri, Listeria seeligeri* and *Listeria ivanovii*. The width of each stream is proportional to the number of isolates moving between categories, providing a visual representation of the distribution across sources, species, and characterisation pathways.

Upon receipt, the isolates had not undergone WGS. Species allocation was initially performed using biochemical profiling with Analytical Profile Index (API) testing, which consistently yielded a score of 6510, indicating their identification as *L. monocytogenes*.

Once WGS was performed, MLST analysis revealed that eight strains belonged to ST9, four to ST2, three to ST7, three to ST204, two to ST121, and one to ST20 (See 3.5.1.2. '**Genomic Determinants of Persistence: Reduced Susceptibility to BC and Biofilm-associated Gene Detection section for detailed genomic analysis**').

3.5.1.1. Phenotypic Testing of Persistence Determinants: Reduced Susceptibility to BC and Biofilm-forming Capacity

Sensitivity to BC was evaluated for the FSA panel using the agar dilution method and was assessed as either exhibiting reduced susceptibility (>5 μg/mL) or susceptible (<5 μg/mL) based on the Gaussian distribution analysis (Gutierrez et al., 2025). Among the test strains, 2 of 23 isolates had an MIC of 5 μg/mL, 7 isolates had an MIC of 15 μg/mL, and 14 isolates had an MIC of 20 μg/mL (**Figure 6A-B;** For experimental layout see **Appendix 6**). These results indicate a broad range of reduced susceptibility levels among *L. monocytogenes* isolates from RTE foods.

Table 9. Isolates selected from the larger FSA collection to make up the 'FSA panel' of 23 *L. monocytogenes* isolates that underwent genomic and phenotypic characterisation. Includes metadata for each selected isolate, detailing the source of isolation (RTE sliced meat survey), country of origin (Northern Ireland), date of isolation, the Analytical Profile Index (API) score (6510 – *L. monocytogenes*) and sequence type (ST) based on the whole-genome sequencing data.

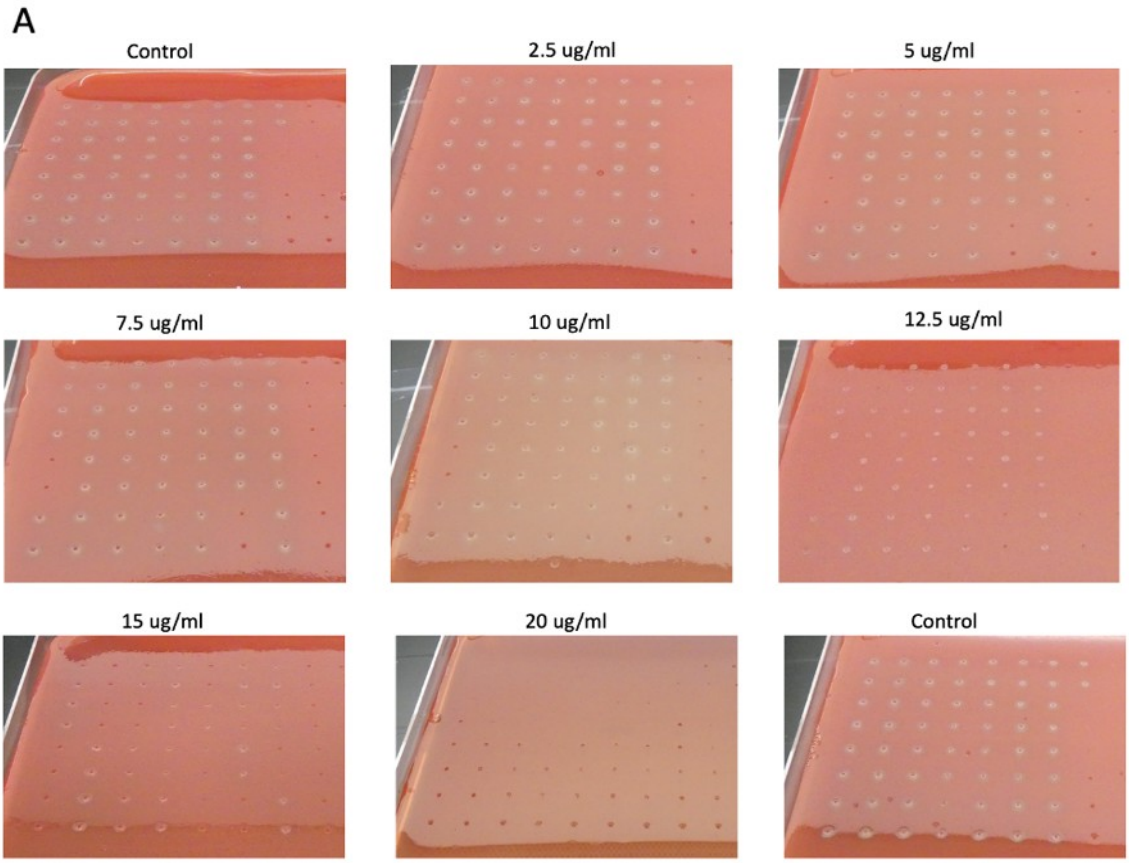
Isolate	Source	Country	Year	API score	Sequence Type
LS12/71	RTE sliced meat survey	Northern Ireland	22.05.2012	6510	ST9
LS12/142	RTE sliced meat survey	Northern Ireland	12.06.2012	6510	ST9
LS12/177	RTE sliced meat survey	Northern Ireland	12.06.2012	6510	ST9
LS12/211	RTE sliced meat survey	Northern Ireland	28.06.2012	6510	ST7
LS12/257	RTE sliced meat survey	Northern Ireland	28.06.2012	6510	ST9
LS12/426	RTE sliced meat survey	Northern Ireland	17.08.2012	6510	ST20
LS12/453	RTE sliced meat survey	Northern Ireland	22.08.2012	6510	ST9
LS12/495	RTE sliced meat survey	Northern Ireland	30.08.2012	6510	ST20
LS12/505	RTE sliced meat survey	Northern Ireland	12.09.2011	6510	ST9
LS12/519	RTE sliced meat survey	Northern Ireland	12.09.2012	6510	ST7
LS12/521	RTE sliced meat survey	Northern Ireland	12.09.2012	6510	ST204
LS12/522	RTE sliced meat survey	Northern Ireland	12.09.2012	6510	ST204
LS12/570	RTE sliced meat survey	Northern Ireland	14.09.2012	6010	ST9
LS12/579	RTE sliced meat survey	Northern Ireland	13.09.2012	6510	ST9
LS12/580	RTE sliced meat survey	Northern Ireland	13.09.2013	6510	ST9
LS12/646	RTE sliced meat survey	Northern Ireland	20.09.2012	6510	ST9
LS12/685	RTE sliced meat survey	Northern Ireland	05.10.2012	6510	ST7
LS12/741	RTE sliced meat survey	Northern	19.10.2012	6510	ST204

		Ireland			
LS12/808	RTE sliced meat survey	Northern Ireland	09.11.2012	6510	ST121
LS12/847	RTE sliced meat survey	Northern Ireland	16.11.2012	6510	ST2
LS12/859	RTE sliced meat survey	Northern Ireland	16.11.2012	6510	ST121
LS12/964	RTE sliced meat survey	Northern Ireland	19.12.2012	6510	ST2
LS12/970	RTE sliced meat survey	Northern Ireland	19.12.12	6510	ST2

When comparing the MICs of BC across sequence types, variability was observed. In ST9, the majority of isolates (7/10) exhibited an MIC of 20 µg/mL, while 2 isolates showed 5 µg/mL and 1 - 15 µg/mL BC. Within ST2, 2 of 4 isolates displayed an MIC of 20 µg/mL, whereas 1 isolate each exhibited MIC of 15 µg/mL and 5 µg/mL. Isolates from ST204, ST7, ST121, and ST20 consistently exhibited reduced susceptibility. Specifically, ST204 included 2 isolates with an MIC of 20 µg/mL and 1 with an MIC of 15 µg/mL; ST7 comprised 2 isolates with MIC of 15 µg/mL and 1 with MIC of 20 µg/mL. Both isolates from ST121 exhibited MIC of 20 µg/mL; and a single ST20 isolate displayed an MIC of 15 µg/mL (**Figure 6B**).

All isolates grew on control plates lacking BC, confirming inoculum viability and ruling out cross-transfer of disinfectant between the plates (**Figure 6A**).

Control strains displayed expected results, with the susceptible control (81-0861) showing a MIC of 5 µg/mL and control exhibiting reduced susceptibility (08-5578) with an MIC of 20 µg/mL (Kovacevic et al., 2016).


A
Control
2.5 ug/ml
5 ug/ml
7.5 ug/ml
10 ug/ml
12.5 ug/ml
15 ug/ml
20 ug/ml
Control

B

Sequence type	Strain	MIC (µg/mL)
ST9	LS12/177	5
	LS12/257	15
	LS12/646	15
	LS12/71	20
	LS12/142	20
	LS12/453	20
	LS12/505	20
	LS12/570	20
	LS12/579	20
	LS12/580	20
ST2	LS12/970	5
	LS12/847	15
	LS12/495	20
	LS12/964	20
ST204	LS12/741	15
	LS12/521	20
	LS12/522	20
ST7	LS12/211	15
	LS12/519	15
	LS12/685	20
ST121	Ls12/808	20
	LS12/859	20
ST20	LS12/426	15

Figure 6. Assessment of Reduced Susceptibility to BC in FSA panel isolates with MIC by agar dilution method. (A) Representative LHB-MHA plates with increasing concentrations of BC (0, 2.5, 5, 7.5, 10, 12.5, 15, and 20 µg/mL) from MIC experiment, visualising growth or no growth of FSA panel isolates. Isolates were inoculated onto control plates containing 0 µg/mL BC both prior to and following inoculation onto BC-supplemented plates, in order to control for potential disinfectant carryover. Layout for MIC experiment in panel (**A**) is demonstrated in **Appendix 6**. (**B**) Table summarising the MIC values of BC (ranging from 5 to 20 µg/mL) observed in the FSA panel, grouped by sequence type. FSA panel includes the following sequence types: ST9, ST2, ST204, ST7, ST121, and ST20.

As part of the phenotypic analysis of persistence determinants of the FSA panel, the isolates were tested for biofilm-forming capacity using the crystal violet assay (**Figure 7; Appendix 7**). Results were compared and normalised to the strong biofilm-forming control strain (08-5578) to account for batch variation.

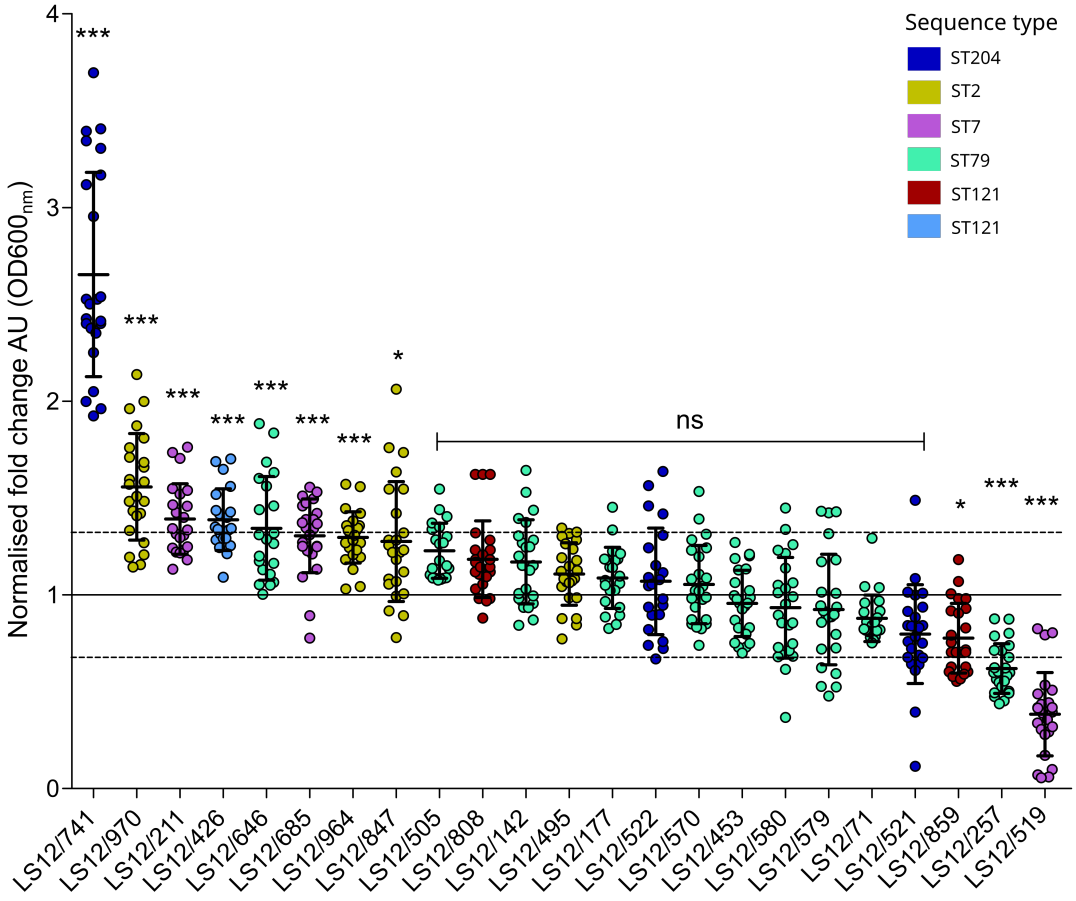


Figure 7. Biofilm-forming capacity of the FSA panel isolates, as measured by the crystal violet assay, is presented as normalised fold change relative to the strong biofilm-forming control. The solid line at 1 represents the mean fold change of the strong biofilm control (08-5578), while the dashed lines denote the standard deviation. Error bars indicate standard deviation of the samples. Colour coding is based on sequence type, as indicated in the legend. A one-way ANOVA followed by Tukey's test was performed to compare the groups: $p < 0.01$ (*), $p < 0.01$ (**), $p < 0.0001$ (***), ns – not significant). Full list of multiple comparison and statistical analyses attached in **Appendix 7**. Statistical significance is indicated in relation to the high biofilm forming control strain. Three biological replicates were performed, each with eight technical replicates. The optical density ($OD600_{nm}$) values obtained from the crystal violet assay were normalised against the high biofilm-forming control strain. For normalisation, the $OD600_{nm}$ values of each test sample was divided by the mean $OD600_{nm}$ value of the strong biofilm control.

The highest biofilm-forming capacity was observed for strain LS12/741, belonging to ST204 (**Figure 7**). The amount of biomass was significantly higher than that of the strong biofilm-forming control.

In contrast, the lowest biofilm formation was recorded for strain LS12/519 (ST7), which produced significantly less biomass than the strong biofilm-forming control (**Figure 7**). Notably, the other two ST7 strains produced significantly more biomass than the strong biofilm control, highlighting variation within the sequence type.

All ST2 isolates had mean biomass values above the mean of the strong biofilm-forming control, and all but one strain (LS12/495) produced significantly more biomass than the control (**Figure 7**).

Among the ST9 group, 8 out of 10 strains showed no significant difference in biofilm production relative to the strong biofilm control, while one strain produced significantly more and one significantly less biomass.

3.5.1.2. Genomic Features and Plasmid Content or Overview of Genome Assemblies

Hybrid genome assemblies were generated for the 23 selected isolates using both short-read and long-read sequencing data (**Table 10; Appendix 2**). Genome size ranged from 2,917,402 bp (LS12/580) to 3,073,696 bp (LS12/741). For comparison, the reference *L. monocytogenes* EGD-e genome is 2.9 Mb. GC content ranged between 36.8% and 39.5%, with *L. monocytogenes* EGD-e exhibits GC content of around 38% (NCBI RefSeq assembly: GCF_000196035.1).

Hybrid assemblies resulted in genome circularisation for all 23 isolates (**Table 10; Appendix 2**). Structural assessment using Socru, a tool for evaluating the orientation of genome fragments between ribosomal operons, indicated that 22 out of 23 isolates exhibited a green result, suggesting previously known structural genotypes. Isolates with green Socru result exhibited the same genome structure - GS1.0 (**Figure 8**). One isolate, LS12/580, yielded a red result, indicating a structural inconsistency and wasn't involved in further analysis.

Plasmid content was assessed using MOB-suite, which identified circularised plasmids in 20 of the 23 isolates. One isolate (LS12/970) lacked plasmids, while plasmid data could not be resolved for two isolates (LS12/505; LS12/580) (**Figure 8**). Notably, two isolates (LS12/964; LS12/211) harboured two plasmids each (**Table 10**). Among the 21 isolates with complete plasmid data, 7 contained conjugative plasmids, 8 contained non-mobilisable plasmids, and 6 had mobilisable plasmids, suggesting a possibility of the

gene transfer for dissimination of reduced susceptibility to disinfectants or other adaptation traits (**Figure 8**).

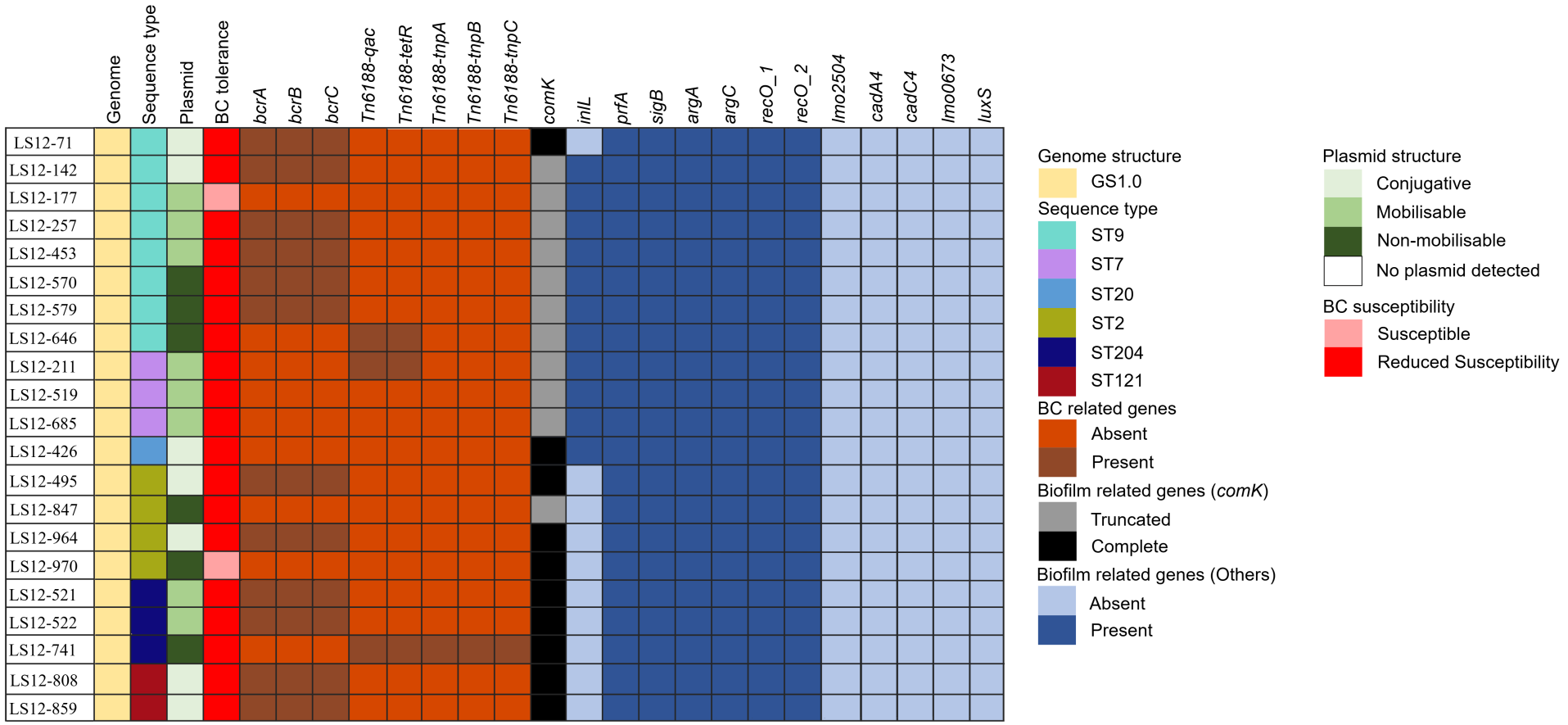

Genome
Sequence type
Plasmid
BC tolerance
bcrA
bcrB
bcrC
Tn6188-qac
Tn6188-tetR
Tn6188-tnpA
Tn6188-tnpB
Tn6188-tnpC
comK
inlL
prfA
sigB
argA
argC
recO_1
recO_2
lmo2504
cadA4
cadC4
lmo0673
luxS
LS12-71
LS12-142
LS12-177
LS12-257
LS12-453
LS12-570
LS12-579
LS12-646
LS12-211
LS12-519
LS12-685
LS12-426
LS12-495
LS12-847
LS12-964
LS12-970
LS12-521
LS12-522
LS12-741
LS12-808
LS12-859
Genome structure
GS1.0
Sequence type
ST9
ST7
ST20
ST2
ST204
ST121
BC related genes
Absent
Present
Biofilm related genes (comK)
Truncated
Complete
Biofilm related genes (Others)
Absent
Present
Plasmid structure
Conjugative
Mobilisable
Non-mobilisable
No plasmid detected
BC susceptibility
Susceptible
Reduced Susceptibility

Figure 8. Genotypic and phenotypic analysis of reduced susceptibility to benzalkonium chloride (BC) and biofilm-associated traits in FSA panel isolates. The categorical heatmap includes MIC data of BC, with isolates ranked according to the level of their susceptibility (susceptible, reduced susceptibility), presence/absence of genes previously associated with reduced susceptibility to BC (*bcrABC* casette and Tn*6188* (Tn*6188-qac,* Tn*6188-tetR,* Tn*6188-tnpA,* Tn*6188-tnpB,* Tn*6188-tnpC*)) and genes associated with biofilm formation analysed with ABRicate and Institut Pasteur gene presence tool, including *comK* in complete and truncated forms. Genome structure, sequence types (STs: 2; 7; 9; 20; 121, 204), and plasmid types (conjugative, mobilisable, non-mobilisable) (derived from hybrid-assembled genomes) are also included. Colour coding is explained in the figure. The gene database used for ABRicate analysis is provided in **Appendix 3**. Continuous data for MIC of BC of the FSA panel is indicated in **Figure 6**.

Table 10. Quality metrics of the hybrid assembled genomes of the FSA panel isolates. Includes GC content, chromosome size in base pairs, circularisation status (Y – circularised), plasmid presence and size in base pairs and Socru analysis outcome (Green – valid order and orientation; Red – invalid structure). In beige - data obtained from short-read sequecing with Illumina, in blue - data obtained from hybrid assembled genomes. Additional quality metrics data is provided in **Appendix 2.**

Order	Strain	GC content (%)	Chromosome size (bp)	Circular (Y/N)	Plasmid size (bp)	Socru result
1	LS12/71	39.40%	3056349	Y	80441	Green
2	LS12/142	39.10%	2972598	Y	90964	Green
3	LS12/177	39.30%	2970201	Y	62777	Green
4	LS12/211	39.30%	2975809	Y	58464; 21283	Green
5	LS12/257	39.50%	3062255	Y	63117	Green
6	LS12/426	39.30%	2926419	Y	82636	Green
7	LS12/453	39.10%	3056175	Y	80468	Green
8	LS12/495	39.40%	3031093	Y	95969	Green
9	LS12/505	39.20%	-	Y	-	Green
10	LS12/519	39.10%	2975934	Y	58464	Green
11	LS12/521	39.30%	2959521	Y	91319	Green
12	LS12/522	39.20%	2959227	Y	91305	Green
13	LS12/570	37.00%	3056951	Y	8465	Green
14	LS12/579	39.20%	3006108	Y	59632	Green
15	LS12/580	36.10%	2917402	Y	-	Red
16	LS12/646	36.80%	2971803	Y	8515	Green
17	LS12/685	36.90%	2976087	Y	58479	Green
18	LS12/741	38.90%	3073696	Y	62223	Green
19	LS12/808	39.10%	3031060	Y	95965	Green
20	LS12/847	39.00%	3026770	Y	60936	Green
21	LS12/859	39.10%	3030718	Y	95970	Green
22	LS12/964	39.00%	3030683	Y	95987; 6044	Green
23	LS12/970	39.10%	3031053	Y	None	Green

3.5.1.3. Genomic Determinants of Reduced Susceptibility to BC

To identify the genomic basis of reduced suscpetibility to BC, hybrid assemblies of FSA panel genomes were analysed using ABRicate to detect genes previously associated with reduced susceptibility (**Figure 8;** gene database included in **Appendix 3**). In our dataset, we focused on two genomic determinants associated with reduced susceptibility to BC: the *bcrABC* cassette and the Tn*6188-qac* system (Tn*6188-qac*, Tn*6188-tetR*, Tn*6188-tnpA*, Tn*6188-tnpB*, and Tn*6188-tnpC*), and gene profiles varied among the isolates.

The *bcrABC* cassette was present in 12 of 21 isolates and was absent in the remaining 9 (**Figure 8**). All three genes of the *bcrABC* cassette were either detected together or not at all. The presence of the *bcrABC* cassette was generally associated with an MIC of ≥15 µg/mL, with the exception of isolate LS12/257 (carried *emrE*). All isolates exhibiting reduced susceptibility carried the *bcrABC* cassette, except for one (LS12/685; carried *emrE*).

The Tn*6188-qac*, another contributor to reduced susceptibility to BC, was detected in 3 of 21 isolates (**Figure 8**). All three isolates containing Tn*6188-qac* gene exhibited reduced susceptibility to BC, with MIC values of 15 µg/mL. Notably, two isolates (LS12-211; LS12-646) harboring Tn*6188-qac* contained only the efflux pump gene (*qac*) and the transcriptional regulator (*tetR*), likely representing remnants of the Tn*6188* system that may have lost the transposases and become non-mobile. Both Tn*6188*-related *qac* efflux pumps exhibited 100% identity to the reference sequences in the Institut Pasteur MLST database. In contrast, strain LS12-741 carried a complete Tn*6188* element, including the efflux pump, transcriptional regulator, and all three transposase genes (*tnpA*, *tnpB*, *tnpC*).

The *bcrABC* cassette and Tn*6188-qac* gene were never co-occuring in the same isolate, suggesting a possibility of a trade-off in presence of both.

Notably, isolate LS12/685 exhibited an MIC of 20 µg/mL despite lacking *bcrABC* casette and Tn*6188-qac* mechanisms, and on closer inspection contained *emrE*, encoding a SMR pump. Similarly, LS12/426 had an MIC of 12.5 µg/mL without either genes, which also contained *emrE* gene.

3.5.1.5. Biofilm-Related Genes

To assess genetic determinants of biofilm formation, hybrid assemblies were analysed using ABRicate to detect genes associated with biofilm formation (**Figure 8**; gene database included as **Appendix 3**).

21 analysed strains harbored core regulatory genes *prfA*, *sigB*, *agrA*, and *agrC*, that are known to play a role in biofilm formation (Rieu et al., 2007; Lemon, Freitag and Kolter, 2010; van der Veen and Abee, 2010).

comK was detected in all isolates. Notably, in 10 isolates it was present in a complete form, whereas the remaining isolates carried a truncated version, likely resulting from the insertion of a prophage. The *inlL* genes were present in 11 isolates and co-occurred with complete *comK* in only one strain (LS12/426). This strain lacked both the *bcrABC* cassette and the Tn*6188-qac* mechanisms, yet still displayed a phenotype with reduced susceptibility to BC, suggesting that such phenotype may be influenced by biofilm formation.

Notably, strain LS12/847 lacked both *inlL* and a complete *comK*, a unique profile among the dataset, but was able to form more biomass than a strong biofilm control strain, likely compensated by other biofilm associated mechanisms.

Other biofilm-associated genes, including *bapL*, *lmo1460_1*, *lmo1460_2*, *lmo2504*, *cadA4*, *cadC4*, *lmo0673*, and *luxS*, were absent across all isolates.

3.5.2. Population Structure of the Expanded *L. monocytogenes* Culture Collection

To understand how our isolates fit within the broader population structure of *L. monocytogenes* in the UK, we analysed genomes from the Quadram Institute Biosciences collection (Historic, UKHSA, FSA panel; see section 2.1. '**Bacterial Strains**'), comprising previously sequenced isolates and those sequenced in this study, alongside publicly available genomes from the UKHSA. We constructed maximum likelihood phylogenetic trees for sequence types ST121, ST7, ST9, and ST204, as these are commonly associated with FPEs, and were present within the FSA panel isolates (further information on *L. monocytogenes* subtyping is provided in section 1.5. '***L. monocytogenes* subtyping**'). The phylogenies were annotated with relevant metadata, including source, year of isolation, and BC susceptibility. Data on reduced susceptibility

to BC were obtained either from previous studies conducted by our group (Quadram Institute Biosciences Historic and UKHSA collections) or were determined in this study (FSA panel).

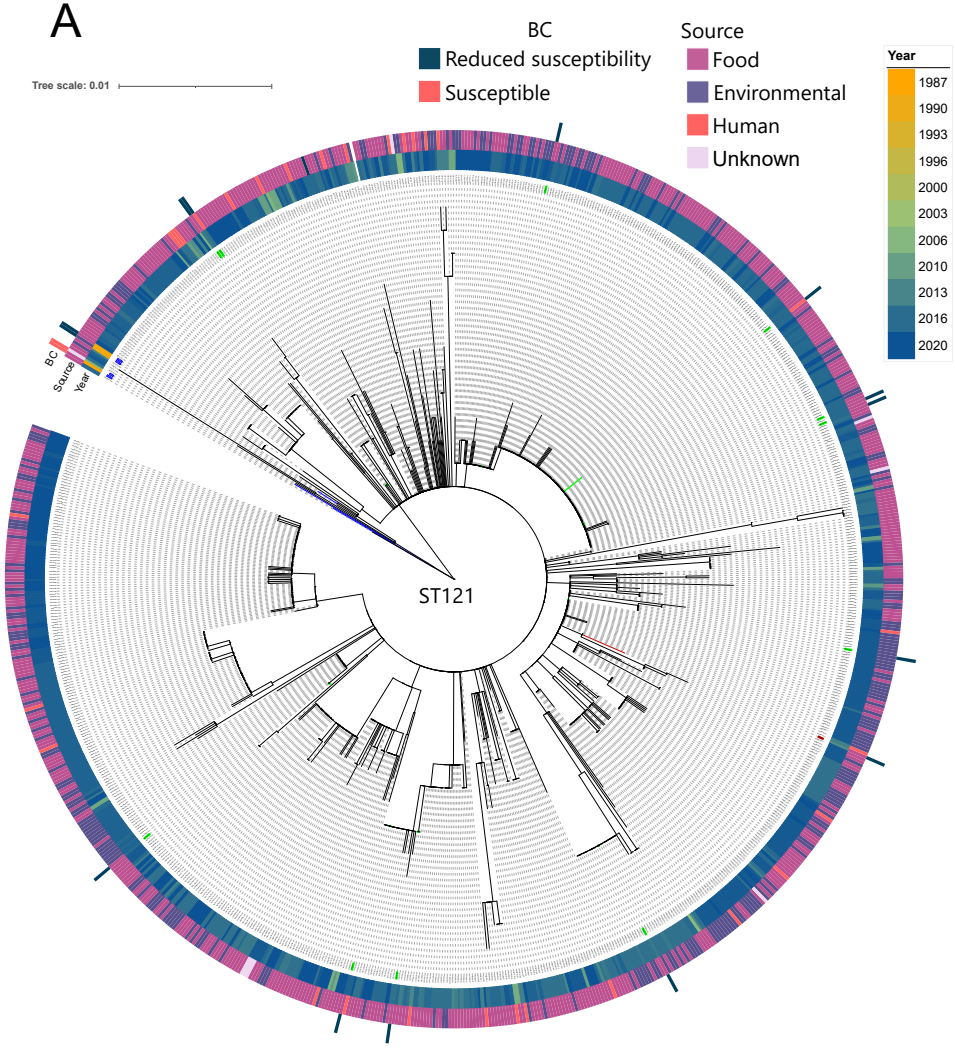
3.5.2.1. Population Structure of L. monocytogenes ST121 Collection

The phylogeny of *L. monocytogenes* ST121 (**Figure 9**) was built with a panel of 870 ST121 genomes isolated between 1987 and 2022 (30 human isolates, 551 isolates from food, 279 environmental and 1 isolate from unknown sources), including 1 isolated at unknown location and 869 UK-isolated samples. From 870 genomes - 16 were hybrid assemblies from the collections at Quadram Institute Biosciences (4 from the Historic collection, 11 from the UKHSA and 1 from the FSA panel). The included UKHSA isolates were part of the UK listeriosis outbreak caused by RTE sandwiches and salads in 2017 (McLauchlin et al., 2021). 11 isolates were isolated from food sources, 2 environmental, 2 human and 1 of unknown source.

Overall, 92.32% of the collection contained transposon Tn*6188* with *qacH* gene, which is known for conferring reduced susceptibility to quaternary ammonium compounds (Gutierrez et al., 2025).

From the 16 isolates tested, 2 were susceptible to BC (MIC < 5 μg/mL), while the rest exhibited phenotype with reduced BC susceptibility. Notably, both BC susceptible isolates were localised on a separate branch of the phylogenetic tree (**Figure 9**). Additionally, ST121 isolates from the collection were distributed across different branches of the ST121 phylogeny, indicating they are not clonal but represent diverse subgroups (**Figure 9**).

A



B

Historic collection
UKHSA collection
FSA panel

Isolate	Year	Source	BC susceptibility
BL87 -028	1987	Food	Susceptible
BL07 -032	2007	Unknown	Susceptible
BL89 -019	1989	Environmental	Reduced susceptibility
BL89 -020	1989	Food	Reduced susceptibility
SRR7873592	2015	Food	Reduced susceptibility
SRR7167591	2020	Human	Reduced susceptibility
SRR9298670	2019	Food	Reduced susceptibility
SRR7163869	2017	Human	Reduced susceptibility
SRR7841399	2017	Food	Reduced susceptibility
SRR7866629	2017	Food	Reduced susceptibility
SRR9226492	2019	Environmental	Reduced susceptibility
LS12 -868	2019	Food	Reduced susceptibility
SRR7850130	2015	Food	Reduced susceptibility
SRR7873684	2016	Food	Reduced susceptibility
SRR7866357	2018	Food	Reduced susceptibility
SRR7827106	2017	Food	Reduced susceptibility

Figure 9. Phylogenetic Analysis of *L. monocytogenes* ST121. (**A**) A rooted maximum-likelihood phylogenetic tree constructed from a recombination-purged SNP core alignment of 870 *L. monocytogenes* isolates, using CFSAN054109 as the reference genome. Tree scale at 0.01. For a high-resolution figure download through the link. (**B**) A list of ST121 isolates from the Quadram Institute Biosciences' *L. monocytogenes* collection that were part of the analysis, including details on the original collection source (Historic (in blue), UKHSA (in green), FSA panel (in red)), isolation source (food, environment, human, unknown), year of isolation (1987 –2022), and susceptibility level to BC (reduced susceptibility or susceptible). All but one (unknown location) isolate were obtained in the UK.

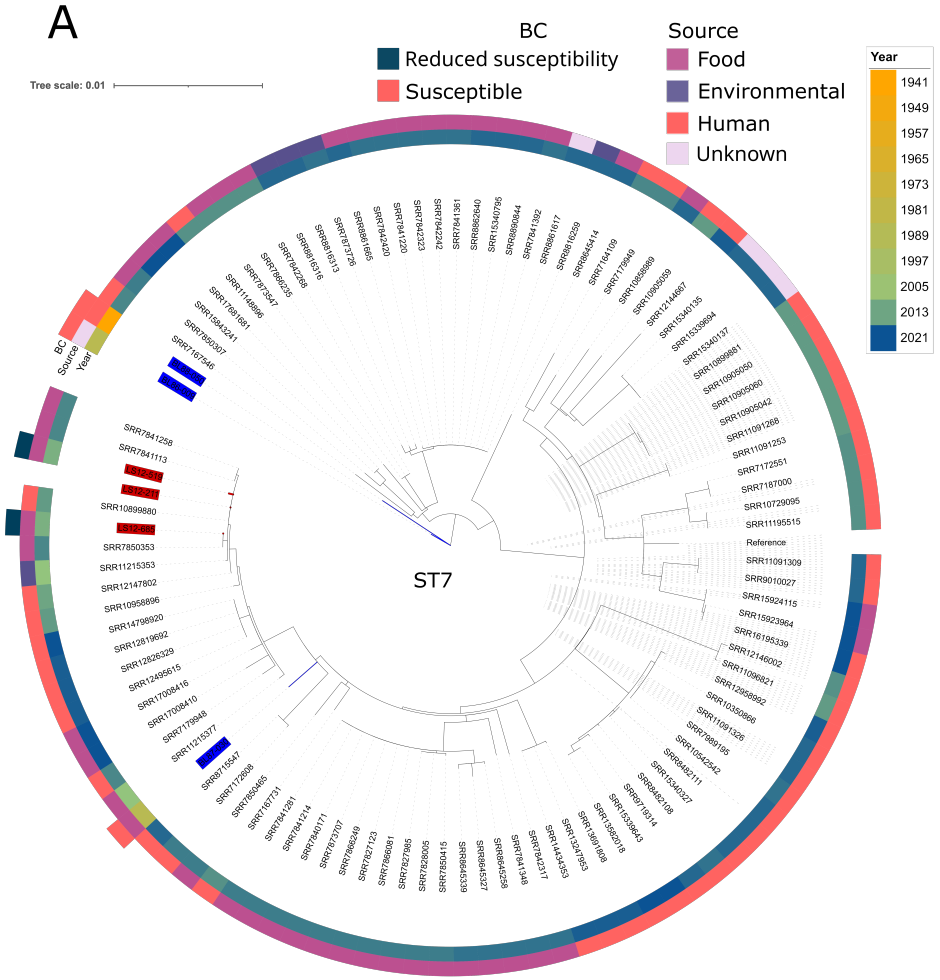
3.5.2.2. Population Structure of ST7 Collection

A total of 103 ST7 *L. monocytogenes* genomes collected between 1941 and 2021 were subjected to phylogenetic analysis (**Figure 10**) (47 human isolates, 45 isolates from food, 5 environmental and 6 isolates from unknown sources), with all samples isolated in the UK. We included 6 complete genomes from the collections at the Quadram Institute Biosciences (3 from Historic collection; 3 from FSA Panel).

Three out of 6 isolates tested were susceptible to BC, while three exhibited reduced susceptibility.

Notably, two isolates from the Historic collection were located on separate clades of the phylogenetic tree, distinct from each other and from all other ST7 isolates analysed (**Figure 10**). Both of these isolates were susceptible to BC.

A



B

Historic collection
FSA panel

Isolate	Year	Source	BC susceptibility
BL86-009	1986	Unknown	Susceptible
BL88-050	1941	Human	Susceptible
BL86-009	1987	Food	Susceptible
LS12-685	2012	Food	Reduced susceptibility
LS12-211	2012	Food	Reduced susceptibility
LS12-519	2012	Food	Reduced susceptibility

Figure 10. Phylogenetic Analysis of *L. monocytogenes* ST7. (**A**) A rooted maximum-likelihood phylogenetic tree constructed from a recombination-purged SNP core alignment of 102 *L. monocytogenes* isolates, using *L. monocytogenes* EGD-e as the reference genome. Tree scale at 0.01. For a high-resolution figure download through the link. (**B**) A list of ST7 isolates from the Quadram Institute Biosciences' *L. monocytogenes* collection, including details on the original collection source (Historic (in blue), FSA panel (in red)), isolation source (food, human, unknown), year of isolation (1941–2012), and susceptibility level to BC (reduced susceptibility or susceptible). All isolates were obtained in the UK.

3.5.2.3. Population Structure of ST9 Collection

The phylogeny of *L. monocytogenes* ST9 (**Figure 11**) was built with a panel of 341 *L. monocytogenes* genomes isolated between 1936 and 2019 (55 human isolates, 216 isolates from food, 67 environment and 2 isolates from unknown sources), including 336 UK samples, 3 Canadian samples1 from the USA and 1 unknown.

This dataset included 29 complete genomes from the Quadram Institute Biosciences' collections (13 from Historic collection, 8 from FSA Panel and 8 from UKHSA collection).

14 out of the 29 isolates tested were susceptible to BC, the rest exhibited reduced susceptibility.

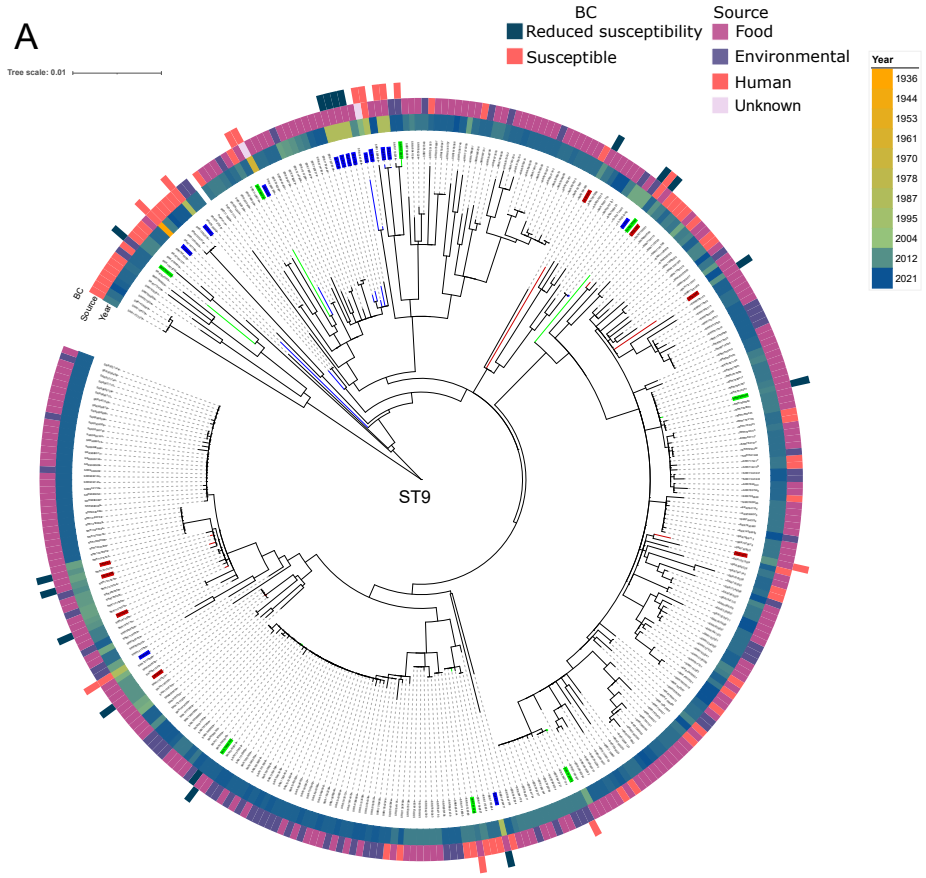
A single isolate from the UKHSA collection was located on a separate clade from the rest of the isolates. There were several clonal isolates from the FSA collection that clustered together. In addition, the distribution of ST9 isolates across different branches of the phylogeny shows that they are not clonal but instead encompass a range of diverse subgroups (**Figure 11**).

3.5.2.4. Population Structure of ST204 Collection

For analysis of ST204 a total of 146 *L. monocytogenes* genomes, isolated between 2006 and 2021, were included in the phylogenetic analysis (**Figure 12**) (15 human isolates, 109 isolates from food, 13 environmental), all isolated in the UK. This collection was enriched with 3 isolates from the FSA collection, which underwent BC tolerance testing. All three tested isolates were tolerant to BC (MIC > 12.5 μg/mL).

Notably, all three isolates clustered on a clade of 5 isolates that was separate from the rest of the phylogenetic tree.

A



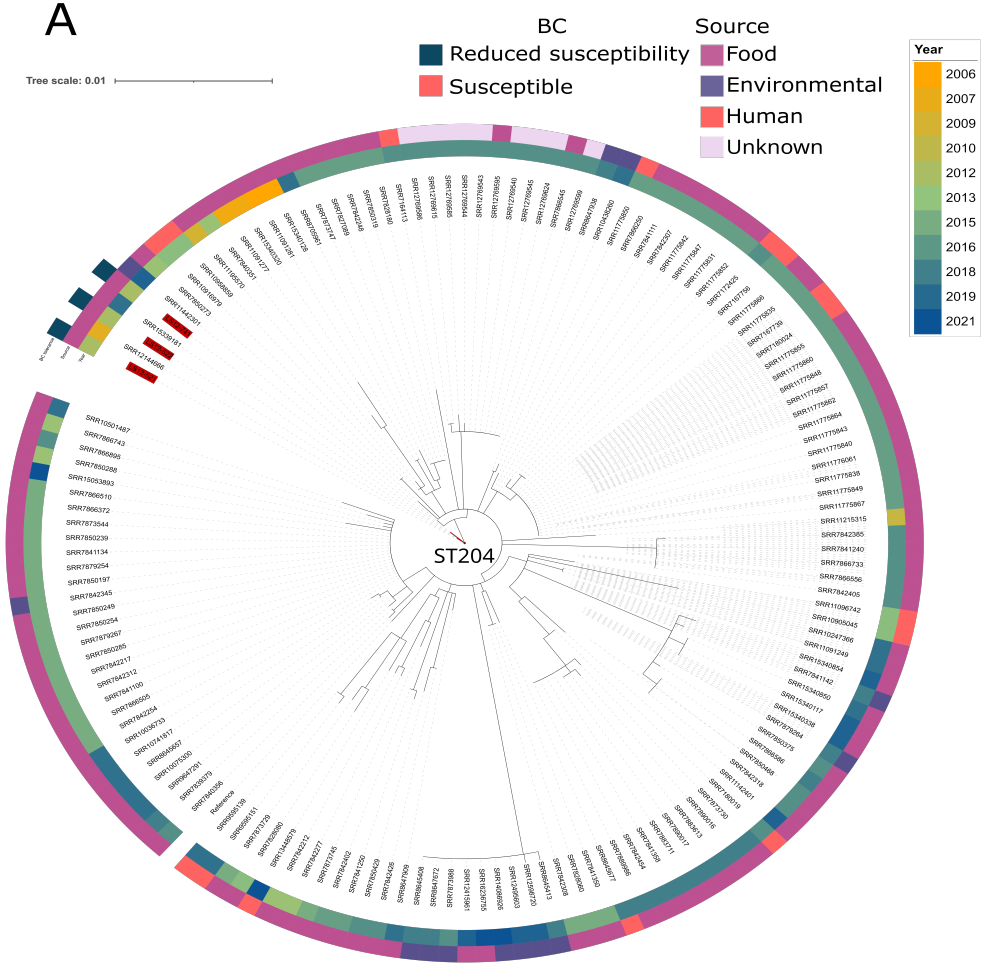
B

Historic collection
UKHSA collection
FSA panel

Isolate	Year	Source	BC susceptibility
BL88-049	1936	Human	Sensitive
BL88-052	1988	Human	Sensitive
BL89-007	1966	Unknown	Sensitive
BL87-038	1987	Food	Reduced susceptibility
BL87-019	1987	Food	Reduced susceptibility
BL87-032	1987	Food	Reduced susceptibility
BL87-020	1987	Food	Reduced susceptibility
BL07-039	1987	Unknown	Sensitive
BL88-051	2007	Unknown	Sensitive
BL88-008	1988	Food	Sensitive
BL88-007	1988	Food	Sensitive
BL89-003	1989	Food	Reduced susceptibility
BL88-047	2010	Human	Sensitive
LS12-579	2012	Food	Reduced susceptibility
LS12-142	2012	Food	Reduced susceptibility
LS12-646	2012	Food	Reduced susceptibility
LS12-177	2012	Food	Sensitive
LS12-257	2012	Food	Reduced susceptibility
LS12-570	2012	Food	Reduced susceptibility
LS12-453	2012	Food	Reduced susceptibility
LS12-71	2012	Food	Reduced susceptibility
SRR7866314	2012	Environmental	Reduced susceptibility
SRR7866290	2018	Food	Sensitive
SRR11102097	2020	Environmental	Sensitive
SRR8645387	2018	Human	Sensitive
SRR7866563	2014	Food	Reduced susceptibility
SRR7828198	2015	Environmental	Sensitive
SRR7879266	2016	Food	Sensitive
SRR10666945	2019	Food	Reduced susceptibility

Figure 11. Phylogenetic Analysis of *L. monocytogenes* ST9. (**A**) A rooted maximum-likelihood phylogenetic tree constructed from a recombination-purged SNP core alignment of 341 *L. monocytogenes* isolates, using *L. monocytogenes* EGD-e as the reference genome. Tree scale at 0.01. For a high-resolution figure download through the link. (**B**) A list of ST9 isolates from the Quadram Institute Biosciences' *L. monocytogenes* collection, including details on the original collection source (Historic (in blue), UKHSA (in green), FSA panel (in red)), isolation source (food, environment, human, unknown), year of isolation (1936–2019), and susceptibility level to BC (reduced susceptibility or susceptible). Included 3 Canadian samples, 1 USA, 1 Unknown and 336 UK samples.

A



B

FSA panel

Isolate	Year	Source	BC susceptibility
LS12-521	2012	Food	Reduced susceptibility
LS12-522	2012	Food	Reduced susceptibility
LS12-741	2012	Food	Reduced susceptibility

Figure 12. Phylogenetic Analysis of *L. monocytogenes* ST204. (**A**) A rooted maximum-likelihood phylogenetic tree constructed from a recombination-purged SNP core alignment of 146 *L. monocytogenes* isolates, using *L. monocytogenes* EGD-e as the reference genome. Tree scale at 0.01. For a high-resolution figure download through the link. (**B**) A list of ST204 isolates from the Quadram Institute Biosciences' *L. monocytogenes* collection, including details on the original collection source (FSA panel (in red)), isolation source (food), year of isolation (2012), and susceptibility level to BC (reduced susceptibility). All isolates were obtained in the UK.

3.5.3. Establishment of a biofilm persistence model for *L. monocytogenes*

The purpose of my work was to investigate the mechanisms underlying adaptation of *L. monocytogenes* to FPE by developing a BPM that resembles the conditions in FPE and would allow for in vitro genetic evolution. The model involves biofilm formation on a solid substrate (bead) suspended in liquid culture media, followed by biofilm detachment and re-establishment of the biofilm through sequential bead passaging. This cycle is repeated under selective pressure (i.e., exposure to subinhibitory concentration of a biocide), enabling the characterisation of evolving *L. monocytogenes* populations using whole-genome sequencing.

3.5.3.1 Strain Selection for Biofilm Evolution Experiment

The goal was to identify a strain with the potential to adapt both to BC exposure and to a biofilm-associated lifestyle. Out of the analysed STs (ST121, ST7, ST9, ST204), we decided to focus on ST121, one of the most prevalent STs in the food production environments (Holch et al., 2013; Schmitz-Esser et al., 2015; Knudsen et al., 2017; McLauchlin et al., 2021). From our ST121 collection, we prioritised the selection of an isolate with a relatively low initial tolerance to BC (**Figure 9**), under the assumption that this would increase the likelihood of observing adaptive responses. Additionally, we aimed to select a strain capable of sustaining a stable biofilm population over an extended period. In our ST121 collection, two isolates exhibited susceptibility to BC (BL87-028 and BL07-032) (**Figure 9**). Both of the BC-susceptible *L. monocytogenes* isolates did not carry reduced BC susceptibility mechanisms, including the Tn*6188-qac* gene or the *bcrABC* cassette. With BL87-028 isolated from chicken in the UK in 1987, we hypothesised that this isolate was less likely to pass through the bottlenecks associated with modern FPE practices in comparison to BL07-032 isolate from 2007. We propose that BL87-028 represents a suitable baseline strain that could be used to study the acquisition of genetic traits associated with FPE persistence when subjected to FPE-like selective pressures.

3.5.3.2. Establishment of the conditions of the biofilm persistence model

To establish a robust and reproducible BPM, we first optimised several parameters including: 1) suitable media, 2) incubation time for consistent biofilm formation, 3) subinhibitory concentration of BC, 3) long-term stability of bacterial populations in

presence of BC and 4) differentiation method between the beads from alternating passages.

3.5.3.2.1 Selection of the Media for BPM

Several media have been successfully used to grow *L. monocytogenes* biofilms in vitro. Among the most commonly employed are Tryptic Soy Broth (TSB) and BHI broth. In previous studies, *L. monocytogenes* demonstrated a strong capacity for biofilm formation in both media, including the formation of complex three-dimensional structures (Blackman and Frank, 1996).

In our study, the goal was to replicate conditions similar to those found in FPE. As such, the use of full-strength BHI or TSB would not realistically mimic the nutrient-limited nature of FPE surfaces. Therefore, we tested 1/10-strength BHI as a more approximating medium with previously demonstrated capacity for *L. monocytogenes* biofilm formation (Lee et al., 2019). Additionally, we evaluated 1/10-strength BHI supplemented with sodium chloride (NaCl), based on previous findings that salt supplementation can enhance biofilm formation by *L. monocytogenes*.

TSB was used as a control condition, given its well-documented support of biofilm formation (Blackman and Frank, 1996). This allowed for a comparative assessment against the nutrient-limited conditions of 1/10-strenght BHI.

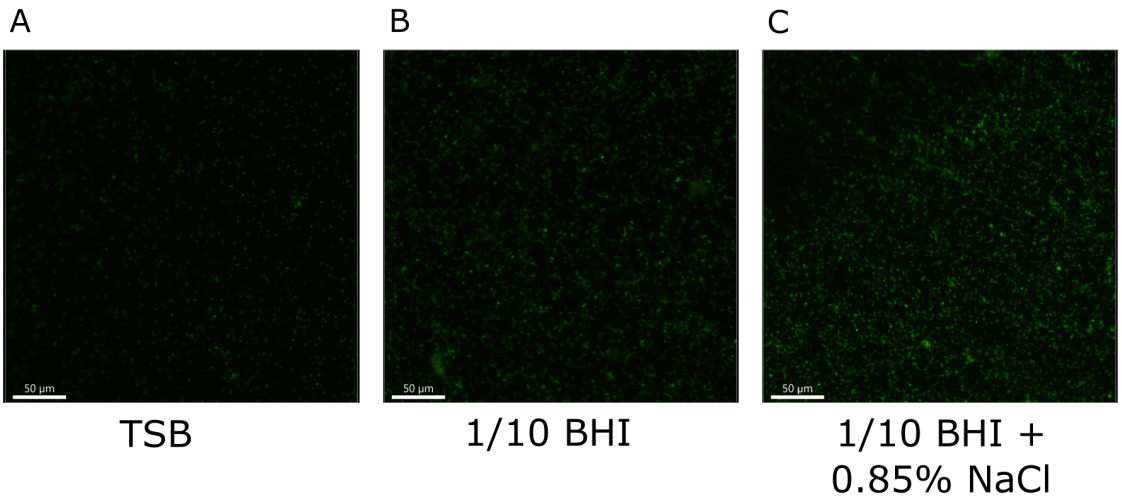


Figure 13. Selection of the media for BPM to best represent FPEs and support biofilm formation. Widefield fluorescence micrographs of *L. monocytogenes* strain BL87-028 transformed with the GFP-expressing plasmid (pHPL3-GFP) and grown in (**A**) TSB, (**B**) 1/10 diluted BHI, and (**C**) 1/10 diluted BHI supplemented with 0.85% sodium chloride. Scale bars

represent 50 µm. Images were acquired using a DeltaVision Elite microscope with a 10× objective and processed using Imaris 10 software.

In preliminary experiments (**Figure 13**), greatest visual attachment was observed in 1/10-strength BHI supplemented with NaCl. Surprisingly, TSB resulted in the least attachment. Based on these findings, 1/10-strength BHI was selected for BPM and microscopy experiments. It offered sufficient biofilm development while better approximating nutrient conditions of real-world FPE scenario than 1/10 BHI supplemented with sodium chloride.

3.5.3.2.2. Optimising Incubation Time for Biofilm Biomass Accumulation

The next objective was to determine the optimal time point for maximal biomass production. We tested multiple incubation durations in 1/10-strength BHI broth. Time points included 2, 4, 6, 8, and 10 days, with replenishing of media at those timepoints.

Based on visual assessment (**Figure 14**), the greatest biofilm attachment was observed at the 48-hour (2-day) time point. At later time points, a noticeable reduction in biomass was detected, likely due to biofilm detachment or dispersal.

In addition to visualising cell attachment, we aimed to compare the viable attached population to those observed in previous bead adaptation models (Trampari et al., 2021), to ensure sufficient cell carry-over.

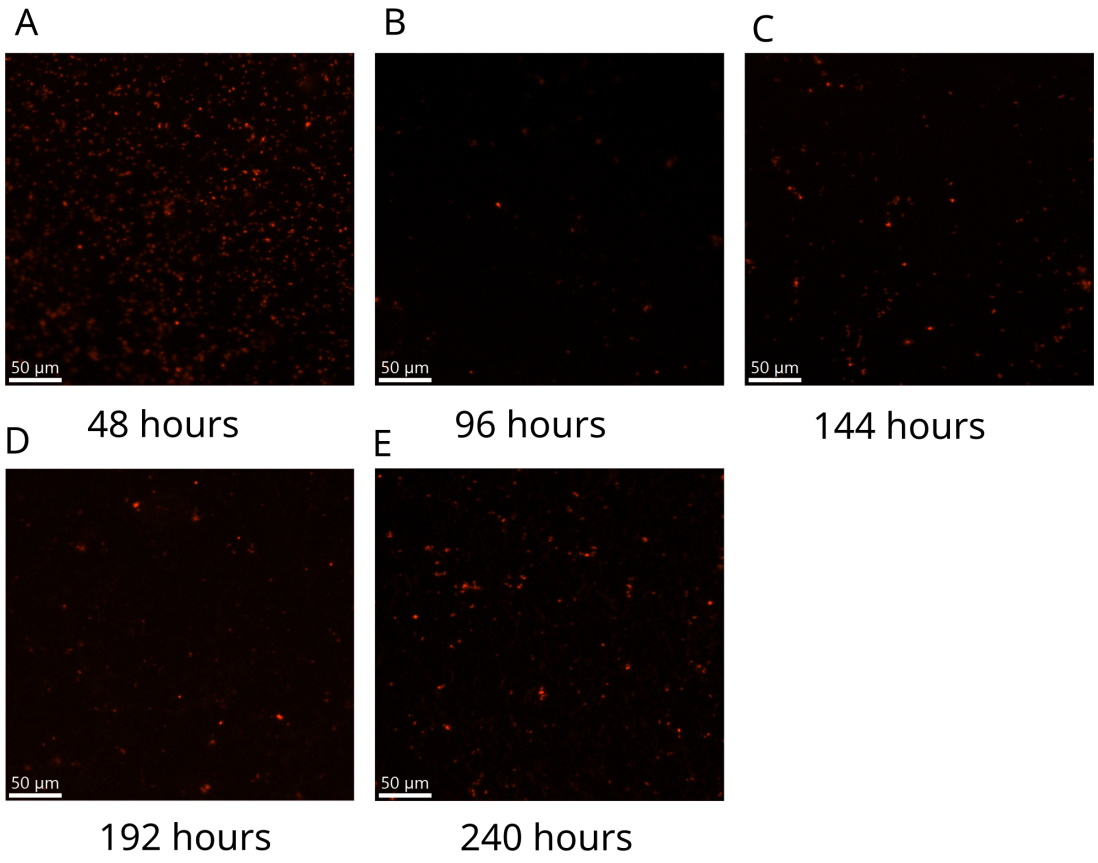


Figure 14. Optimisation of incubation time for biofilm biomass accumulation. Widefield fluorescence micrographs of L. monocyogenes strain BL87-028 transformed with the mCherry-expressing plasmid (pHPL3-mCherry) and grown in 1/10 diluted BHI for (**A**) 48, (**B**) 96, (**C**) 144, (**D**) 192, and (**E**) 240 hours. Scale bars represent 50 µm. Images were acquired using a DeltaVision Elite microscope with a 10× objective and processed using Imaris 10 software.

Microscopy enabled us to narrow down the range of relevant time points, allowing for more precise adjustment of the incubation period. To determine the optimal incubation time for cell attachment, we quantified the total population of the *L. monocytogenes* parental strain supported on a 6 mm bead in 1/10-strength BHI broth at three time points (24, 48, and 72 hours), selected based on the previous microscopy experiment. (**Figure 14A**).

With the CFU-based method, the largest population was observed after 72 hours (**Figure 15A**), however, all time points consistently yielded 10^5 - 10^6 CFU/bead, a range previously described to be sufficient for stable biofilm carry-over (Trampari et al., 2021). To facilitate experimental progression, a 48-hour incubation period between passages was selected.

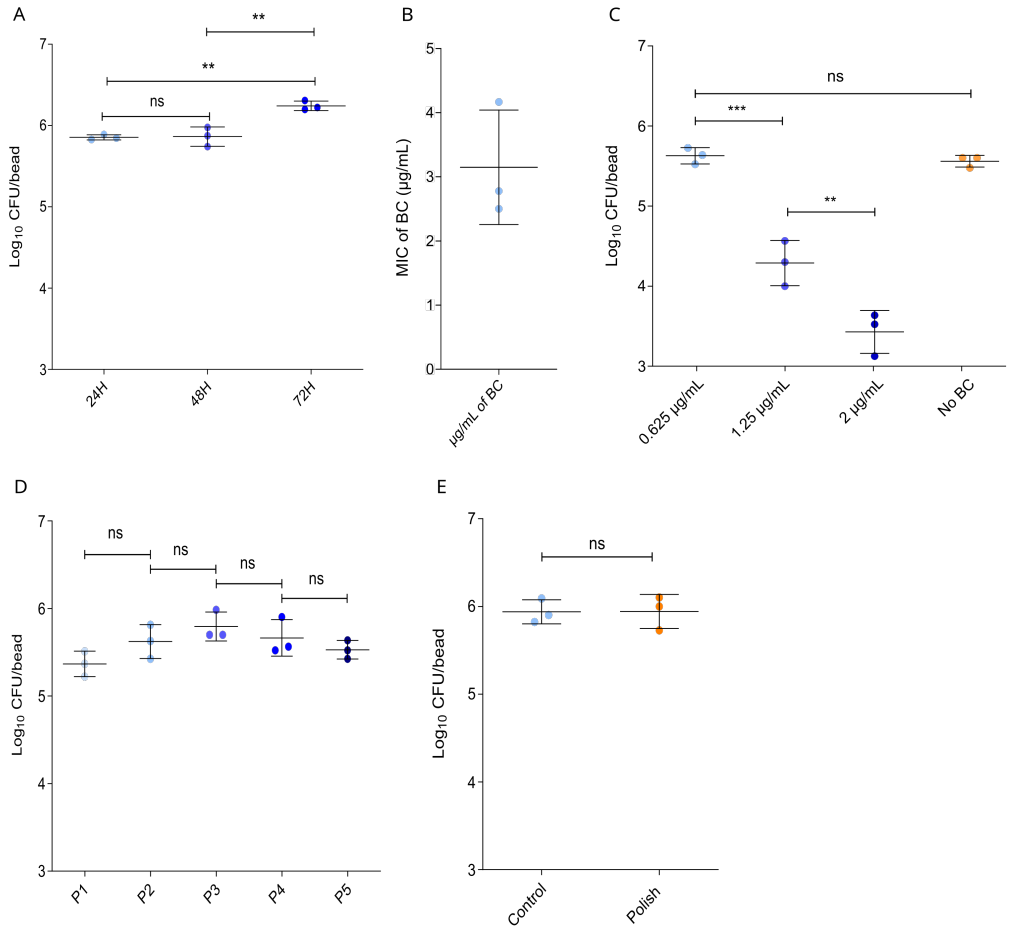


Figure 15. Optimisation and validation of the conditions for the biofilm persistence model experiment. (**A**) **Selection of incubation period.** Suitable incubation period of 48 hours was selected at 1/10-strength BHI broth at 20 °C. (**B**) **The MIC of BC against the parental strain** was measured (3.12 µg/mL). (**C**) **Selection of suitable disinfectant concentration for the model.** Sub-inhibitory concentration of BC (0.625 µg/mL) maintained the population size of the parental strain on the bead surface in desired 10^5-10^6 CFU/bead range. (**D**) **Confirmed stability of the model.** Obtained stable population in presence of 0.625 µg/mL of BC over the course of 5 passages (P1 – P5), with 48-hour incubation period between the passages. (**E**) Confirmed that the marking used for **differentiation of the beads from different timepoints** did not impact the capacity of the parental strain to attach to the surface of the bead. A one-way ANOVA followed by Tukey's test was performed to compare the groups: $p < 0.01$ (*), $p < 0.01$ (**), $p < 0.0001$ (***), ns - not significant). CFU/bead data were $\log_{10}$-transformed prior to plotting, and statistical analyses were performed on the transformed values. Dots represent mean values of 3 technical replicates. Horizontal bars represent the mean of 3 biological replicates ± standard deviation. An increase in colour intensity corresponds to higher values of the tested variable, while orange indicates the control condition. All experiments were performed in triplicates.

3.5.3.2.3. Determination of the sub-inhibitory concentration of BC

We then identified a BC concentration that could support a population density on the beads comparable to non-exposed control. The mean MIC value for planktonic cells was determined to be 3.12 µg/mL (**Figure 15B**). We tested the effect of subinhibitory BC

concentrations below the MIC level (2, 1.25, 0.625 µg/mL) on biofilm forming capacity on beads. A concentration of 0.625 µg/mL BC was selected, as it did not significantly reduce the number of viable cells attaching to the bead surface compared to non-exposed control (**Figure 15C**). This concentration was further validated to consistently support the bacterial populations over the course of five passages, with a 48-hour incubation between each passage (**Figure 15D**).

3.5.3.2.4. Determination of the Bead Differentiation Method

We also confirmed that the lacquer marking for differentiation between alternating beads from subsequent passages did not significantly impact bacterial attachment to the surface of stainless-steel bead (**Figure 15E**).

3.5.3.3. Variability in Biofilm Architecture on Stainless Steel under Biofilm Model Conditions

Biofilms of *L. monocytogenes* strain BL87-028 formed on stainless steel surface, mimicking FPE (grade 316), were visualised using fluorescent dye (SYTO 9).

Upon closer examination of the biofilm architecture, defined here as the reproducible spatial organisation of attached cells (e.g., density, clustering, surface coverage, roughness, distribution patterns, layering) within otherwise monolayer biofilms - two distinct spatial patterns were observed (**Figure 16**). The first exhibited a more uniform yet sporadic distribution, marked by disorganised attachment and scattered microcolony formation (**Figure 16A**). The second exhibited a hexagonal, honeycomb-like arrangement characterised by organised and interconnected structures (**Figure 16B**).

Notably, both structural patterns could be observed within a single sample, indicating that the variation was not driven by batch-to-batch differences.

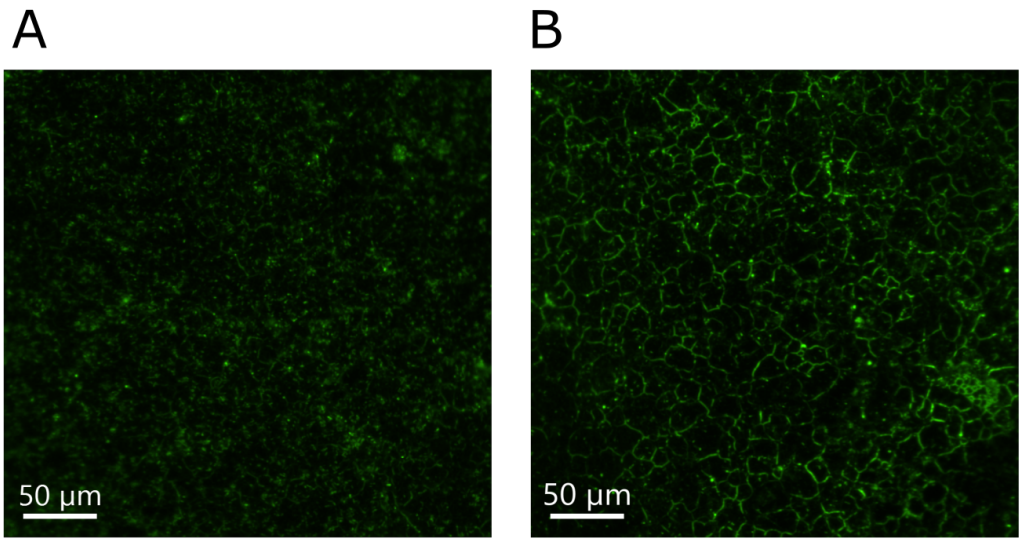


Figure 16. Widefield fluorescence microscopy of morphological differences in the biofilm of *L. monocytogenes* strain BL87-028 on stainless steel grade 316. (**A**) **Sporadic biofilm** showing uniformly scattered attachment. (**B**) **Organised biofilm** with a honeycomb-like, hexagonal arrangement. Images were captured using DV Elite microscope at 10× magnification with SYTO 9 nucleic acid fluorescent dye. Images were viewed with Imaris v10.0.1. Scale bars represent 50 µm. Experiment was performed in quadruplicate, with 10 fields of view analysed per biological replicate.

Further investigation of the stainless-steel surface using SEM revealed the presence of cracks and crevices that resembled the spatial organisation of the biofilm (**Appendix 9**). This observation suggests that the organised biofilm pattern may be influenced by the topographical features of the surface rather than driven by intercellular communication mechanisms.

3.6. Discussion

In **Chapter 3**, my objective was to expand and characterise the culture collection of *L. monocytogenes*, increasing the representation of UK-derived strains. The phenotypic and genotypic characterisation was intended to inform the selection of a suitable isolate for the subsequent BPM experiment, leading to the selection of isolate BL87-028 for further study. Following the selection, we optimised the conditions for the BPM that mimics key aspects of FPE.

The culture collection acted as a strong representation of the UK population within each of sequence types studied. Notably, we enriched our collection of ST121 isolates through inclusion of UKHSA isolates linked to the 2017 listeriosis outbreak associated with RTE sandwiches and salads (McLauchlin et al., 2021). This enrichment increases the relevance

of the collection by incorporating isolates that are not only persistent in FPEs and RTE foods but also able to lead to clinical cases.

There was, however, a selection bias in the overall collection between the sequence types, as the isolates have not been systemically collected over decades and relied on local efforts of the governmental agencies UKHSA, FSA, as well as previous and current efforts at the Quadram Institute Biosciences and its predecessor The Institute of Food Research (IFR).

We selected a single *L. monocytogenes* isolate from ST121, BL87-028, to undergo adaptive evolution with the BPM experiment. This isolate was susceptible to BC and phylogenetically distinct from the majority of ST121 isolates in our collection (**Figure 9**). While this means that BL87-028 isolate is not fully representative of the contemporary ST121 population, where most of the isolates carry BC tolerance mechanisms (Gutierrez et al., 2025), it offers important advantages for studying adaptation. Using a tolerant isolate as the starting point would likely reduce our ability to observe phenotypic shifts, as it would already possess mechanisms that may mitigate the selective pressure from the disinfectant.

The historical context further supports my choice: BL87-028 was isolated in 1987, and we hypothesise that it is less likely to have undergone the selective bottlenecks imposed by modern FPEs. Although the use of BC in the UK was likely widespread by that time, having gained popularity following the implementation of the Food Hygiene (General) Regulations in 1970 (UK Statutory Instruments, 1970). The strain's susceptibility to BC and absence of BC-associated tolerance mechanisms suggest that selected strain was unlikely to have been exposed to the disinfectant.

The BPM was designed to mimic real-world FPE conditions, including growth on stainless steel grade 316, low nutrient availability, and exposure to sub-inhibitory BC concentrations. These parameters ensured that the model captured core selective pressures relevant to persistence in the processing facilities. However, several simplifications were necessary to maintain experimental feasibility. We maintained the temperature at 20 °C throughout, whereas in real-world FPEs, the temperature fluctuates from around 5 °C in cold storage rooms to 8 °C in food preparation areas (FSA, 2024). The temperature we selected is higher than typical temperature maintained in FPEs, and

we acknowledge that *L. monocytogenes* may respond differently to the same stressors at lower temperatures.

Another important parameter is simplification of the C&D practices that take place in FPEs. C&D include not just the disinfection phase but also cleaning step where detergents are aimed at removal of biological matter and create an extra selective pressure for *L. monocytogenes* (FSA, 2025). Additionally, in many factories, frequent disinfectant rotation strategy is implemented with a change in selective pressure, which is not represented in our model (Rahman, Sahoo and Yemmireddy, 2022). Our experimental model is meant to represent the key moment of bacterial attachment and initial biofilm formation to a solid FPE substrate, under selective pressures that are commonly found in the same environments.

Regarding the optimisation of incubation times, we detected the highest biofilm formation at a 48-hour time point, which reduced at later time points and might have been associated with limited nutrient availability. Even though we replenished the nutrients every 48 hours, we did so with addition of 1/10-strength BHI, which is scarce in nutrients and may not compensate dispersal mechanisms driving the cells back to planktonic lifestyle (Gjermansen et al., 2005; Nair et al., 2021).

Microscopy revealed highly organised honeycomb-like structures, which are consistent with the earlier findings. In 2015, Guilbaud et al., explored the architectural diversity of *L. monocytogenes* biofilms and reported a predominance of honeycomb-like arrangements, characterised by the presence of hollow voids. Similarly, Ripollés-Avila et al., 2020, described mature biofilm structures featuring interstitial voids. Notably, honeycomb-like architectures are not exclusive to *L. monocytogenes* and have also been observed in other bacterial species. These structures were first described in *P. aeruginosa* biofilms, where cell differentiation within the biofilm leads to the formation of voids composed of dead cells (Sauer et al., 2002). In our study, however, we favour the hypothesis that surface topography (cracks and crevices; plateaus) plays a key role in driving the formation of voids and the hexagonal arrangements, rather than mechanisms involving cell differentiation or intercellular communication. Supporting our hypothesis, other studies acknowledged the effect of cracks and crevices in the surface of stainless steel and showed that that modification of surface topography by polishing inhibits development of biofilms on stainless steel grade 316L and 304 (Kumar et al., 2024).

The concentration of BC selected for BPM is sub-inhibitory to the selected strain of *L. monocytogenes*, meaning it does not inhibit bacterial growth but is sufficient to exert selective pressure, allowing the detection of adaptive response over time. Although this concentration is approximately 480 times lower than those typically used in food processing facilities (Bolten et al., 2022), it remains relevant when considering in-use conditions at FPEs. In real-world settings, several factors contribute to localised reductions in disinfectant concentration, including dilution due to moisture and condensation, human error during preparation or application, presence of organic matter, and the inaccessibility of certain areas where bacteria may reside (van Dijk et al., 2022; CDC, 2024). Additionally, biofilms that commonly present in these environments exhibit an inherent tolerance to disinfectants and can withstand higher concentrations than planktonic cells (Fagerlund et al., 2017; Thomassen et al., 2023). These factors contribute to the formation of tolerant sub-populations within factories, which may continuously reseed adapted clones. Therefore, considering that a gradient of disinfectant concentrations is frequently encountered at FPEs, investigating the effect of sub-inhibitory concentrations is highly relevant.

When biofilm formation was assessed across isolates, considerable variation in biomass production was observed within some sequence types. Although previous research has reported associations between biofilm formation and specific clonal complexes of *L. monocytogenes,* evidence for a consistent genetic basis remains inconclusive. The strength of such associations may be influenced by the methodologies employed and the number of isolates included in the studies (most studies including under 150 isolates) (Myintzaw et al., 2023; Lee et al., 2019). A larger study that tested biofilm formation in 725 isolates, determined that isolates origin, temperature, and sublethal acidic stress were influencing the biofilm forming ability to a higher extent than phylogenetic subgroups alone (Barbosa et al., 2013). Guilbaud et al., in 2015, further demonstrated only a weak correlation between phylogenetic lineage and biofilm structure, supporting the idea that environmental adaptation plays a critical role in the development of *L. monocytogenes* biofilms.

Within the FSA Panel, we found that the *bcrABC* cassette and Tn*6188*-associated efflux pump were never present simultaneously in the same genome. This likely reflects functional redundancy, which is selectively disadvantageous, as bacteria under selective pressure tend to streamline their genomes to minimise the resources required for

replication (Hunter, 2022). From an evolutionary perspective, once bacteria acquire one of the tolerance mechanisms, the selective pressure to acquire a second is reduced (Durão, Balbontín and Gordo, 2018). Alternatively, efflux machinery is associated with fitness costs, as in addition to removing toxic compounds, they may also export essential cytoplasmic components, limiting the availability of cellular resources. Finally, the presence of both efflux pumps simultaneously could lead to competition for membrane space, or the energy sources required for their operation (Zgurskaya, 2009; Liu et al., 2024).

Notably, we detected a range of tolerance levels against BC amongst the isolates within the same sequence types. As an example, within ST9 and ST2, MICs ranged from 5 to 20 μg/mL of BC, encompassing both susceptible and tolerant isolates. However, these represent only a minority of the samples within the sequence types, where the majority of the isolates exhibited tolerance. Certain sequence types may also be predisposed to carrying BC tolerance mechanisms. For example, studies on *S.* Typhimurium ST34 demonstrated higher likelihood of developing tolerance to BC through *ramR* mutations, which did not occur in other tested STs (ST19, ST36) (Wu-Chen et al., 2023).

3.7. Conclusions

In this chapter, we expanded and characterised an extensive *L. monocytogenes* culture collection, encompassing a diverse range of sequence types, sources, and isolation time periods, providing a robust foundation for investigating *L. monocytogenes* persistence in FPEs.

Based on phylogenetic analysis of STs commonly associated with FPEs, combined with BC tolerance testing, we selected a suitable strain for use in the BPM experiment. The isolate, collected in 1987, predates many of the selective bottlenecks imposed by modern FPEs, making it less likely to carry adaptations specific to contemporary industrial pressures. We hypothesised that this historical isolate would serve as a suitable baseline strain for studying the acquisition of genetic traits linked to FPE persistence when exposed to FPE-like selective pressures.

Using this isolate, we developed and optimised a BPM experiment that mimics key aspects of FPE conditions. By adjusting culture parameters and selective pressures, we established a model capable of supporting long-term biofilm development and enabling

the monitoring of *L. monocytogenes* evolutionary dynamics over time, as executed in **Chapter 4**.

Chapter 4: A Continuous Biofilm Persistence Model Identified Mechanisms of Niche Adaptation in *Listeria monocytogenes*

4.1. Contributions:

Oleksii Omelchenko, Ana Victoria Gutiérrez, Maria Diaz, Erin Lewis, Maria Solsona Gaya, Mark Webber, Matthew Gilmour.

4.2. Publications

The work described in this chapter was submitted for publication (Microbial Genomics):

Oleksii Omelchenko, Ana Victoria Gutiérrez, Maria Diaz, Erin Lewis, Maria Solsona Gaya, Mark Webber, Matthew Gilmour. **A continuous biofilm evolution model of *Listeria monocytogenes* identified mechanisms of persistence and niche adaptation.** *Microbial Genomics, Under review.*

4.3. Introduction

Evolution experiments have interested microbial ecologists since the early 20th century, but it was not until Jacques Monod described the construction, operation, and kinetics of bacterial growth in a continuously growing culture in 1940 that the new field of experimental microbial evolution was established (Adams and Rosenzweig, 2014). One notable example is the ongoing evolution experiment by Lenski et al., which began in 1988 with 12 independent lineages of *E. coli*. This experiment has been in execution for over three decades and has surpassed 75,000 generations, making it a remarkable case study in adaptive evolution. A spike in the popularity of evolution experiments has begun with the discovery and subsequent cost reduction of sequencing techniques, which enabled the detection of large-scale genomic changes (Adams and Rosenzweig, 2014).

Several mechanisms against a broad range of antimicrobials have been identified using adaptive evolution models. For example, prolonged exposure to QAC biocides has led to the selection of persister cells in *E. coli* (Nordholt et al., 2021). While mutants of *Staphylococcus aureus* evolved to withstand higher concentrations of chlorhexidine following extended exposure, by inducing rapid cell wall self-repair mechanisms (Van de Lagemaat et al., 2022).

Adaptive evolution experiments have also been used to investigate bacterial adaptation within biofilms. In this chapter, we used an in vitro bead-based BPM. This model was initially introduced by Poltak and Cooper in 2010 to study *Burkholderia cenocepacia* biofilms and was later adapted by the Webber group (Quadram Institute Bioscience) to

study the adaptation of biofilms in *S.* Typhimurium, *P. aeruginosa*, *S. aureus*, and *E. coli* to a range of antimicrobial compounds and preservatives (Poltak and Cooper, 2010; Trampari et al., 2021; Abi Assaf et al., 2024).

Compared to other models used to study biofilms (see section 1.7.12. '**Established Methods to Study Biofilm Formation**'), the bead transfer model enables the full cycle of biofilm formation to occur within each passage. The cells colonise the bead and begin to proliferate, eventually forming a mature biofilm. The cells then detach from the original bead and colonise a new one, effectively replicating the natural biofilm development process. Another advantage of the bead-based system is its flexibility. The model is easily adaptable to specific scientific questions by modifying variables such as the substrate surface, growth media, or disinfectant/antibiotic exposure. The BPM has not yet been used to study *L. monocytogenes* in the context of FPEs, and overall, it has not been widely applied to adaptation of study Gram-positive species.

The persistence of ST121 in FPEs poses a critical food safety challenge with notable incidents that occurred in the United Kingdom (McLauchlin et al., 2021) and Norway (Løvdal et al., 2021), where *L. monocytogenes* contaminated RTE foods were consumed by immunocompromised individuals. Such persistence is facilitated by intrinsic and acquired genetic traits that enhance *L. monocytogenes* survival and niche establishment within larger microbial communities (Xayarath and Freitag, 2012; Ferreira et al., 2014; Sibanda and Buys, 2022), under refrigeration temperatures, high salt concentrations, low pH and exposure to biocides (Ribeiro et al., 2006; Ferreira et al., 2014; NicAogáin and O'Byrne, 2016; Mazaheri et al., 2021). However, the specific genetic changes driving this persistence of *L. monocytogenes*, particularly in biofilm-associated cells, remain poorly understood. We hypothesised that *L. monocytogenes* adapts to FPE-associated disinfectant stress through the acquisition of mutations that enhance biofilm formation and confer reduced susceptibility to disinfectant. To investigate this, we executed a continuous in vitro BPM that mimics key FPE conditions and enables the study of long-term evolution under subinhibitory exposure to BC. To achieve this objective, we selected a biocide-susceptible *L. monocytogenes* ST121 isolate from the 1980s, derived from chicken (see section 3.5.3.1 '**Strain Selection for Biofilm Evolution Experiment**').

After 30 consecutive passages of evolution, followed by WGS of the evolved populations, we identified adaptive mutations that became fixed over time and described in this chapter genetic mechanisms that may be driving *L. monocytogenes* persistence in FPE.

4.4. Aims

1. To execute an adaptive biofilm persistence experiment; prepare and store a collection of evolved samples for further analysis.
2. To perform phenotypic and genotypic characterisation of populations evolved in biofilm-associated cells under disinfectant stress.
3. To integrate phenotypic and genotypic data to identify mechanisms underlying reduced disinfectant susceptibility and adaptation to the biofilm lifestyle.

4.5. Methodology Specific to Chapter 4

4.5.1. Execution of the BPM and Complexity of the Evolved Isolate Collection

After the optimisation and establishment step, as detailed in **Chapter 3**, the model was executed (**Figure 17**). We exposed the parental strain to a constant concentration of 0.625 µg/mL BC across eight independent lineages (four biologically independent planktonic lineages; four biologically independent biofilm lineages). Additionally, we included four non-exposed control lineages under both planktonic and biofilm lifestyles. The steady model underwent an evolutionary period of 30 subsequent passages, and three timepoints were selected to store evolved lineages for subsequent phenotypic and genotypic analyses: early (passage 11, P11), mid (passage 22, P22), and late (passage 30, P30) (**Figure 1; 17**).

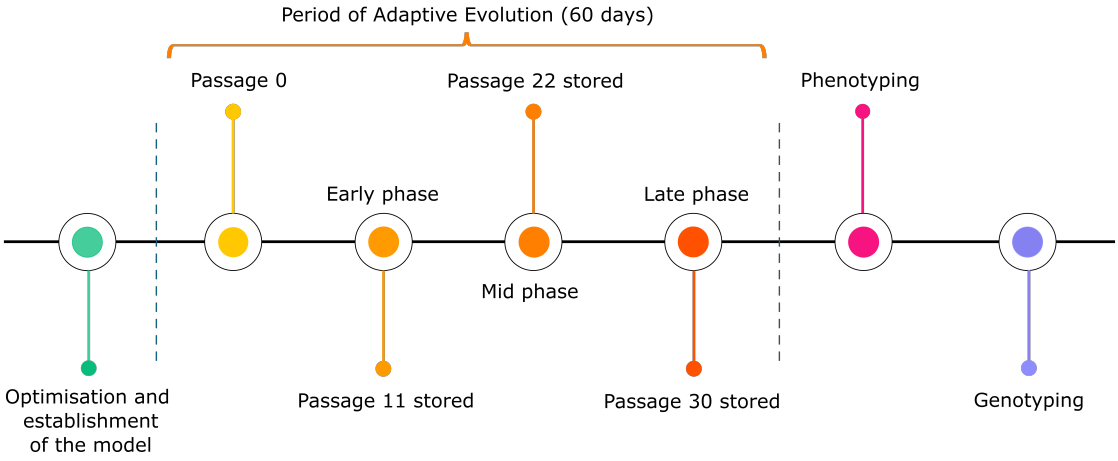


Figure 17. Schematic overview of the Biofilm Persistence Model (BPM) experimental timeline, illustrating the initial optimisation phase, the 60-day adaptive evolution period with key milestones at early, mid and late timepoints (passages 11, 22, and 30), followed by phenotypic and genotypic analyses.

We have also executed a ladder model, where lineages that were initially exposed to 0.625 µg/mL BC during the first 11 passages of the steady model, had undergone an increase to 1.3 µg/mL BC and further evolved until the late passages (P30) in a one-step ladder model. Additionally, a two-step ladder model was employed, where lineages exposed to 1.3 µg/mL BC between early (P11) and mid (P22) passages from the one-step model were exposed to 1.75 µg/mL BC from mid (P22) to late (P30) passages.

At each timepoint, collected evolved lineages were subdivided into populations (whole culture) and randomly selected individual colonies (three colonies per population), hereafter referred to as '*isolates*'. This sampling approach yielded a comprehensive collection of 272 evolved isolates across three timepoints, comprising of 68 populations and 204 individual colonies (**Appendix 5**). Of the 272 evolved isolates, 144 were derived from the biofilm model, and 128 from the planktonic model (**Figure 4**; **Figure 18)**.

Based on the sampling timepoints, 64 isolates were collected at the early timepoint, 96 at the middle timepoint, and 112 at the late timepoint. The increase in evolved isolates across timepoints reflects the addition of extra isolates during implementation of the ladder models. Regarding exposure to BC, 96 isolates were exposed to 0.625 µg/mL, 64 isolates to 1.3 µg/mL, and 16 isolates to 1.75 µg/mL of BC. A total of 96 isolates served as control and were not exposed to BC. Out of the 272 isolates collected, 191 underwent both WGS and phenotypic characterisation (**Figure 4; Figure 18**). The remaining 81 isolates

underwent phenotypic characterisation only and were not sequenced. With this approach three of the four independent lineages per condition were sequenced, while the fourth was retained as a backup.

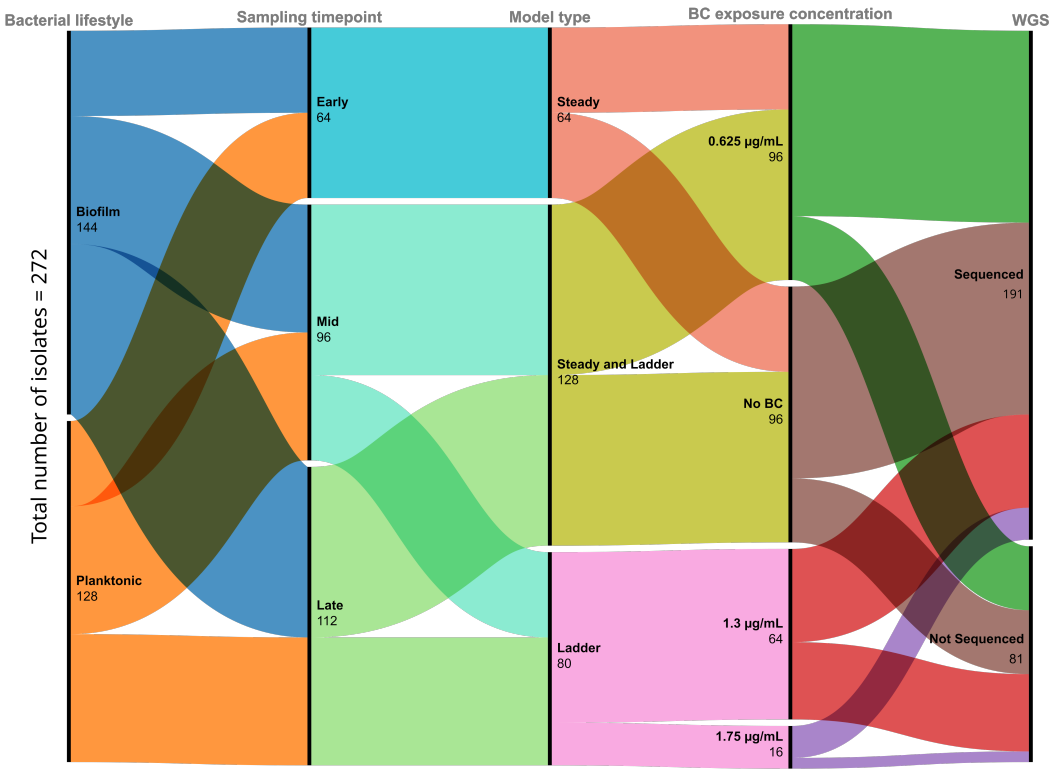


Figure 18. Alluvial plot illustrating the complexity of the Biofilm Persistence Model (BPM), as well as diversity of evolved lineages and experimental conditions. The plot includes information on bacterial lifestyle (biofilm or planktonic), sampling timepoint (early, mid, late), model type (steady, ladder or both), BC exposure concentration (0.625 µg/mL, 1.3 µg/mL, 1.75 µg/mL, no BC), and whether isolates underwent whole-genome sequencing. At each timepoint, evolved lineages were split into populations (whole culture) and randomly selected individual colonies (three per population), yielding 272 evolved isolates across three timepoints. Of these, 144 isolates came from the biofilm model and 128 from the planktonic model. Sampling yielded 64 isolates at the early, 96 at the middle, and 112 at the late timepoint. Regarding BC exposure, 96 isolates were exposed to 0.625 µg/mL, 64 isolates to 1.3 µg/mL, 16 isolates to 1.75 µg/mL, and 96 served as controls. In total, 191 isolate underwent both whole genome sequencing and phenotypic characterisation, while 81 were only phenotypically characterised. Visualisation created using RawGraphs v2.0.

4.6. Results

4.6.1. Exposure of *L. monocytogenes* to BC Leads to the Emergence of Planktonic and Biofilm Lineages Exhibiting Reduced Susceptibility

In order to evaluate the adaptive response of *L. monocytogenes* to BC, we first analysed how exposure of the parental strain to the steady model supported bacterial adaptation. Exposure of the parental strain to BC in the steady model led to the emergence of evolved planktonic and biofilm isolates that exhibited reduced susceptibility to BC (**Figure 19A-D; Appendix 10**). MIC values were analysed for both evolved populations as well as for individual colonies derived from respective populations.

When comparing the level of susceptibility against BC between isolates from different timepoints, no significant change in MIC values was observed among biofilm populations and individual colonies (**Figure 19A, C; Appendix 10**). In contrast, planktonic populations exhibited susceptibility dynamics, with a significant reduction in the mean MIC values from early (P11) to mid (P22), followed by an increase from mid (P22) to late (P30) passages (**Figure 19C-D**). In planktonic individual colonies, no significant change was observed in the mean MIC values from early (P11) to mid (P22), but there was a significant increase going from mid (P22) to late (P30) passages. BC susceptibility level of non-exposed control populations remained consistently comparable to that of the parental strain across timepoints (**Figure 19A-D**).

Next, in order to evaluate the adaptive response of *L. monocytogenes* to escalating concentrations of BC, we utilised the ladder model (**Figure 20A-D; Appendix 10**). Populations that were initially exposed to 0.625 μg/mL BC during the first 11 passages of the steady model, had undergone an increase to 1.3 μg/mL BC and further evolved until the late passages (P30) in a one-step ladder model. All isolates that have been exposed to increased concentrations of BC exhibited significantly higher mean MIC values compared to the non-exposed controls. Although we did not detect any further increase in mean MIC values in either biofilm (**Figure 20A; C**) or planktonic (**Figure 20B; D**) isolates compared to those from the steady model exposed to 0.625 μg/mL BC.

We also deployed a two-step ladder model, where isolates exposed to 1.3 μg/mL BC between early (P11) and mid (P22) passages from the one-step model were exposed to 1.75 μg/mL BC from mid (P22) to late (P30) passages. We were only able to retain biofilm isolates from the two-step ladder model, while planktonic isolates were not

recoverable (**Figure 20B; D**). Biofilm isolates from the two-step ladder model exhibited significantly higher mean MIC values (for populations and individual colonies) compared to the non-exposed controls and maintained BC tolerance at comparable levels to isolates exposed to 1.3 μg/mL BC.

BC susceptibility level of non-exposed control isolates remained consistently comparable to that of the parental strain throughout both ladder experiments. (**Figure 20A-D**).

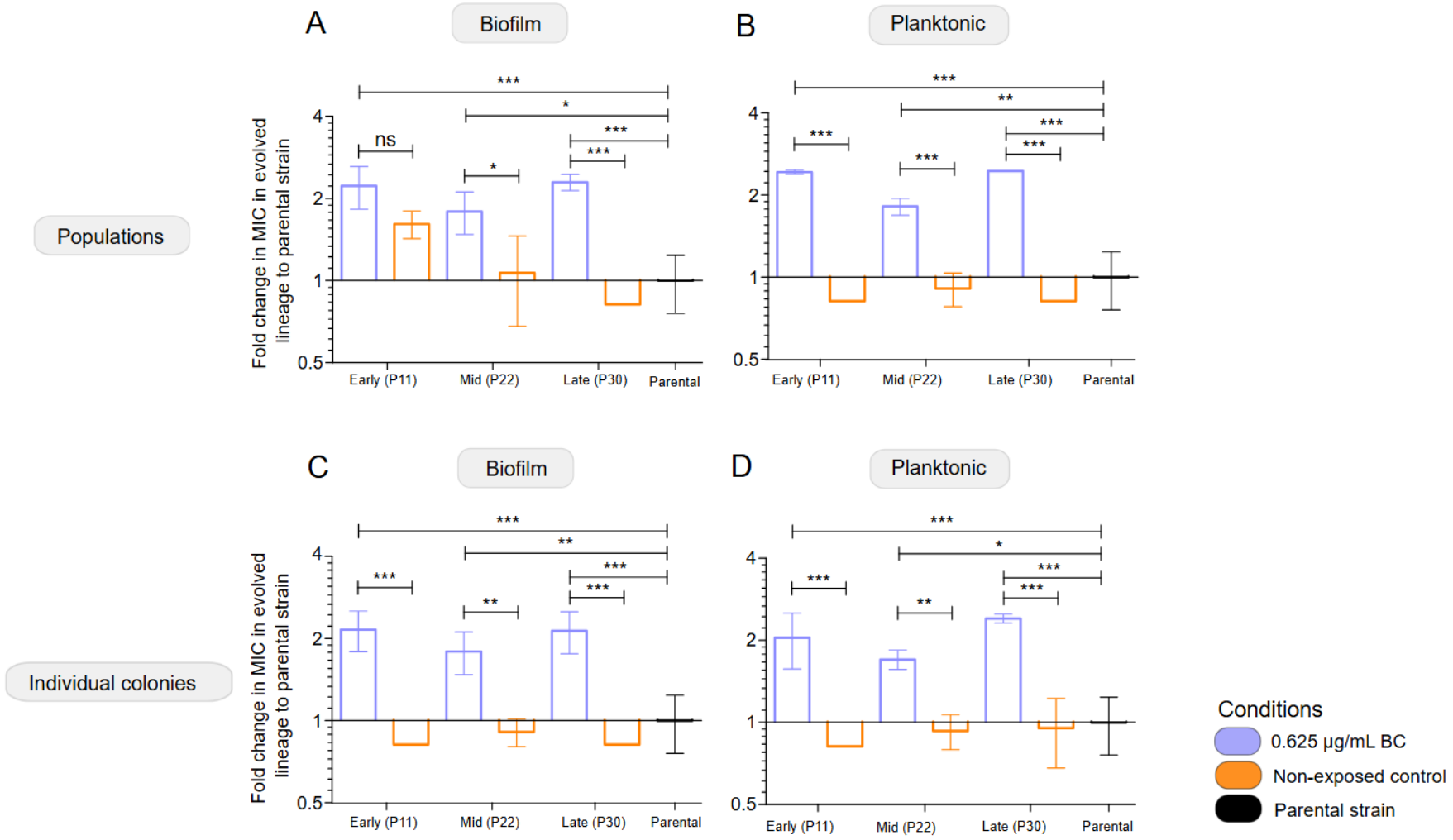

Populations
Individual colonies
A
Biofilm
B
Planktonic
C
Biofilm
D
Planktonic
Fold change in MIC in evolved lineage to parental strain
ns
*
**
***
Early (P11)
Mid (P22)
Late (P30)
Parental
Conditions
0.625 µg/mL BC
Non-exposed control
Parental strain

Figure 19. Exposure of *L. monocytogenes* to BC results in emergence of planktonic and biofilm lineages exhibiting reduced susceptibility to BC in the steady model. Fold change in mean MICs of BC in exposed and non-exposed lineages, relative to the parental strain, across early (P11), mid (P20), and late (P30) evolutionary passages, under the steady model. Data are presented for both populations **(A–B)** and individual colonies (**C**–**D)**. MIC values were measured in triplicate for each lineage. For populations, results from four independent lineages were averaged. **Populations**: refers to the entire culture derived from evolved biofilm and planktonic lineages (one per lineage). These contain a mixture of genetic or phenotypic variants. For individual colonies, the mean MIC from individual representative colony is shown. **Individual colonies**: refer to three individual colonies randomly selected from each population. Each individual colony represents a clonal subpopulation rather than the full diversity present in the whole population. Error bars represent standard deviation. Statistical comparisons between BC-exposed lineages and non-exposed controls were performed using one-way ANOVA followed by Tukey's post hoc test (*$p < 0.05$, **$p < 0.01$, ***$p < 0.001$, ns = not statistically significant). Extended statistical results are provided in **Appendix 10.**

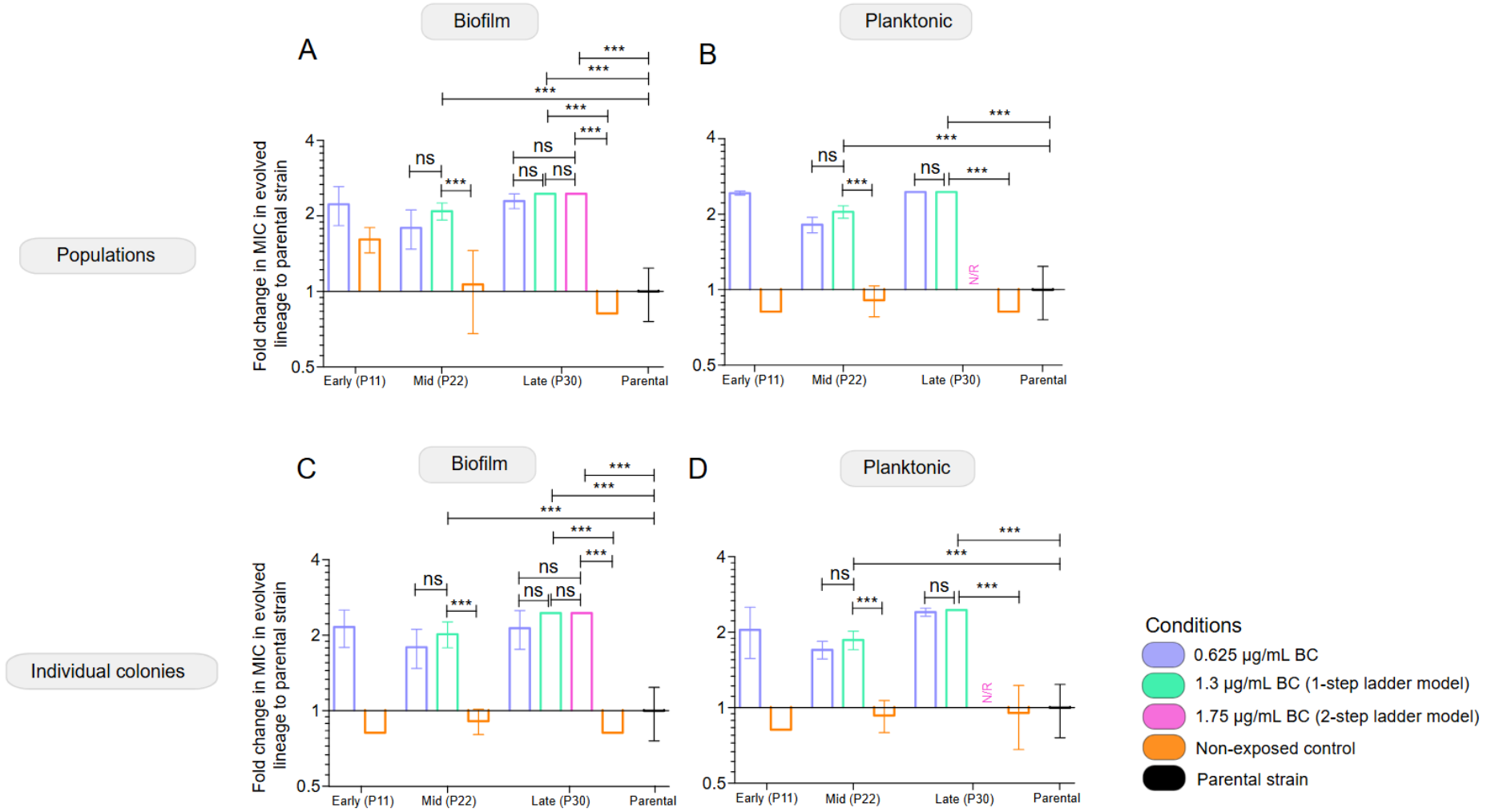

Biofilm
Planktonic
A
B
C
D
Populations
Individual colonies
Fold change in MIC in evolved lineage to parental strain
Early (P11)
Mid (P22)
Late (P30)
Parental
ns
***
N/R
Conditions
0.625 µg/mL BC
1.3 µg/mL BC (1-step ladder model)
1.75 µg/mL BC (2-step ladder model)
Non-exposed control
Parental strain

Figure 20. Exposure of *L. monocytogenes* to BC results in emergence of planktonic and biofilm lineages exhibiting reduced susceptibility to BC in the ladder model. Fold change in mean MICs of BC in exposed and non-exposed lineages, relative to the parental strain, across early (P11), mid (P20), and late (P30) evolutionary passages, under the steady model. Data are presented for both populations **(A–B)** and individual colonies (**C**–**D)**. MIC values were measured in triplicate for each lineage. For populations, results from four independent lineages were averaged. **Populations**: refers to the entire culture derived from evolved biofilm and planktonic lineages (one per lineage). These contain a mixture of genetic or phenotypic variants. For individual colonies, the mean MIC from individual representative colony is shown. **Individual colonies**: refer to three individual colonies randomly selected from each population. Each individual colony represents a clonal subpopulation rather than the full diversity present in the whole population. Error bars represent standard deviation. Statistical comparisons between BC-exposed lineages and non-exposed controls were performed using one-way ANOVA followed by Tukey's post hoc test (*$p < 0.05$, **$p < 0.01$, ***$p < 0.001$, ns = not statistically significant). N/R indicates non-recovered planktonic lineages exposed to 1.75 μg/mL BC. Extended statistical results are provided in **Appendix 10.**

4.6.2. Grouping Mutations by Selective Pressure

To further investigate the genetic changes associated with the development of reduced susceptibility to BC and adaptations to biofilm lifestyle, three lineages (one population and three individual colonies per lineage) from each timepoint (**Appendix 5**) were subjected to WGS under planktonic and biofilm conditions. Mutations were detected by aligning short-read data from evolved isolates against the hybrid assembled genome of the annotated parental strain (Gutierrez et al., 2025). We focused on non-synonymous and intergenic mutations and reported if the mutation resulted in a premature stop codon (nonsense) or led to a change in amino acid (missense) (**Figure 21**).

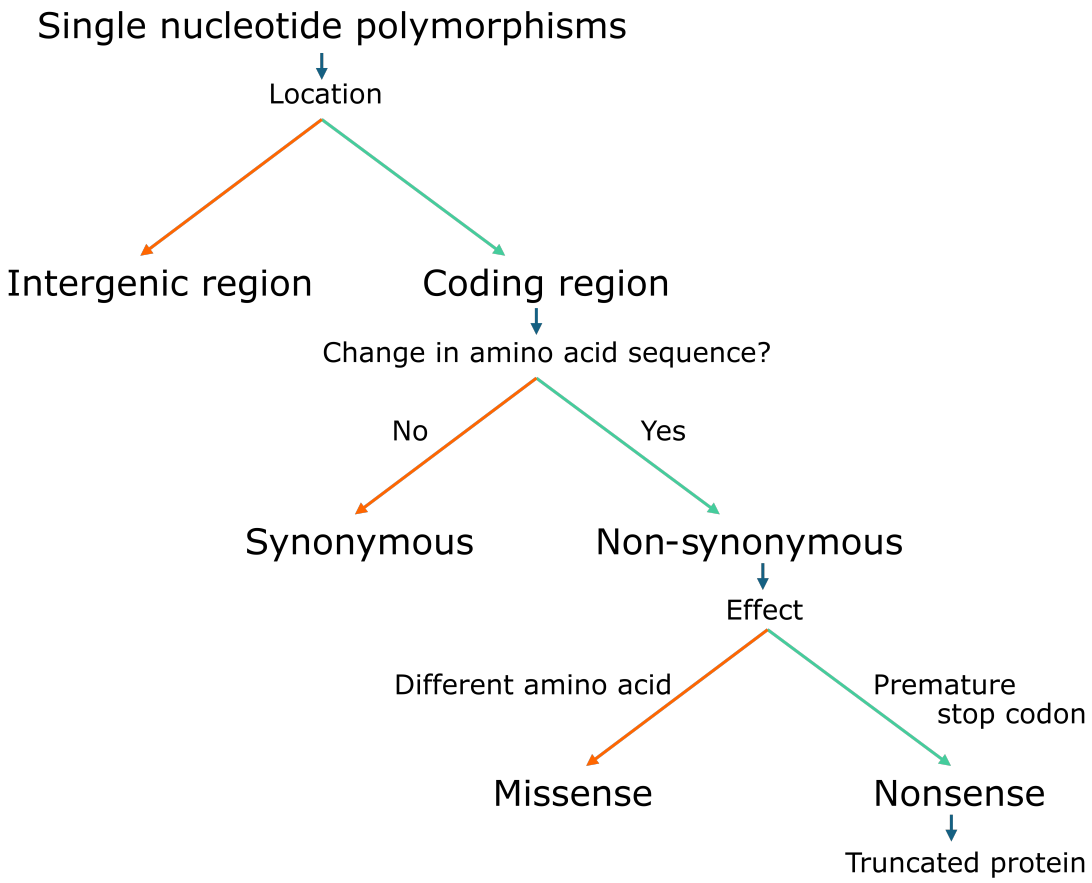


Figure 9. Types of single nucleotide polymorphisms (SNPs). Schematic overview of SNPs types and their consequences, including changes based on genomic location (intergenic, coding region), amino acid substitutions (synonymous, non-synonymous), and premature stop codons. Adapted from Hsu, C.-Y. Doctoral thesis (2019).

Non-synonymous and intergenic mutations were grouped according to the condition in which they occurred and were visualised using Venn diagrams (**Figure 22**). Synonymous mutations were disregarded from these analyses.

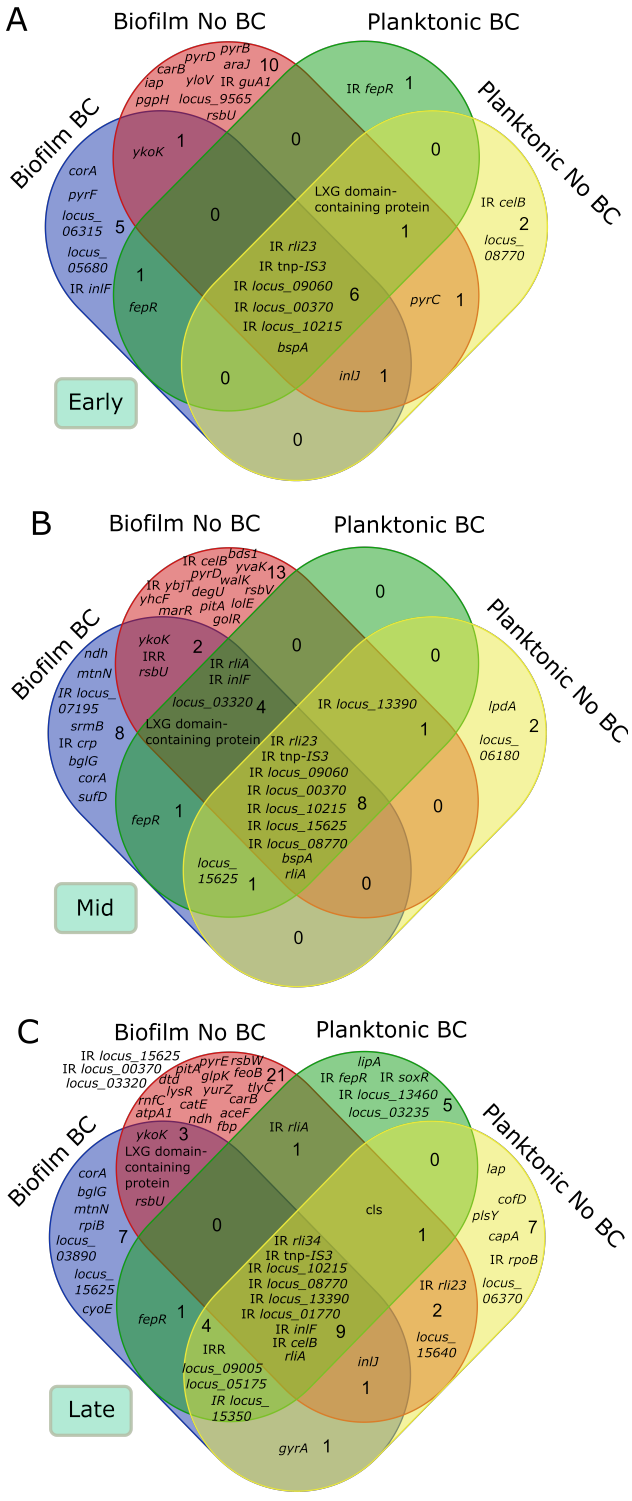


Figure 10. Venn diagrams illustrating loci where mutations were detected throughout the BPM experiment, grouped by experimental condition and timepoint (early (passage 11), mid (passage 22), and late (passage 30)). Each segment contains loci names and the number of mutated loci per particular condition. Conditions include biofilm BC-exposed, biofilm non-exposed, planktonic BC-exposed, and planktonic non-exposed. Analysis was performed using

steady model isolates. Was generated with an online Venn diagram tool (Heberle et al., 2015). Intergenic region mutations were labelled as IR, followed by the name of the downstream gene.

At the early timepoint, mutations in six loci were detected across all experimental conditions. These were considered adaptive to the general experimental environment (i.e., medium, temperature, surface, rotation rate). Notably, five of these six loci were located in the intergenic regions, with only one occurring within a coding region. The highest number of affected loci occurred in the biofilm, non-exposed group (ten loci), followed by the biofilm, BC-exposed group (five loci). The planktonic, non-exposed group contained mutations in two loci, while the planktonic, BC-exposed group exhibited mutations only at intergenic region upstream of *fepR*.

At the mid timepoint, eight mutated loci were shared across all conditions. Mutations in four loci were shared amongst the biofilm BC-exposed**,** biofilm non-exposed, and planktonic BC-exposed groups which was not detected at an early timepoint. These mutations are likely to be representation of adaptations to the general experimental environment. Similar to the early timepoint, the biofilm, non-exposed group exhibited the highest number of affected loci (thirteen), followed by the biofilm, BC-exposed group (eight). The planktonic, BC-exposed group did not accumulate mutations, whereas the planktonic, non-exposed group exhibited mutations in two loci.

By the late timepoint, one additional mutation was present across all conditions, bringing the total number of affected loci to nine. As observed at the earlier timepoints, the biofilm, non-exposed group exhibited the highest number of affected loci (twenty-one). The biofilm, BC-exposed group exhibited mutations in seven loci. Unexpectedly, the planktonic BC-exposed group, which contained mutations only in the intergenic region upstream of *fepR* at the early timepoint and none at the mid timepoint, displayed mutations in five coding regions at the late timepoint. Additionally, the planktonic**,** non-exposed group showed an increase in the number of mutated loci, from two at the mid timepoint to seven at the late timepoint.

This analysis, although informative in what selective pressure leads to the highest number of loci and intergenic regions affected by mutations, is limited in terms of the frequency of the mutations in each region and their functional roles. This limitation will be approached in the following sections.

4.6.3. Functional Distribution of Mutations Associated with Reduced Susceptibility to BC

Next, we sought to increase our understanding about the functional role of the mutations reported in BC-exposed lineages. To achieve this objective, we categorised the mutated loci that were detected in condition exposed to BC by their functional subgroups. We solely included non-synonymous mutations and mutations occurring in intergenic regions detected in the steady model, under both biofilm and planktonic conditions. This analysis followed previously generated Venn diagrams (see section 4.5.4. '**Grouping mutations by selective pressure**') but avoided the noise from the genes that were associated with adaptation to the general experimental environment, as such mutations were disregarded.

Mutations were grouped by function according to the *ListiWiki* database (Elfmann et al., 2023). As such, we detected mutations in loci belonging to four major functional groups: cellular processes, metabolism, information processing and lifestyles. Each of the major functional groups were further divided into 12 functional subgroups (Elfmann et al., 2023), including: transcription; translation; replication, recombination, and repair; nucleotide transport and metabolism; energy production and conversion; carbohydrate transport and metabolism; secondary metabolite biosynthesis, transport, and catabolism; inorganic ion transport and metabolism; signal transduction mechanisms; defense/virulence mechanisms; cell wall/membrane biogenesis; posttranslational modification, protein turnover, and chaperones; and a group with unknown function (**Appendix 11(I)**). Next, we created bump charts to visualise how the number of affected loci in each functional subgroup changed over timepoints (**Figure 23**).

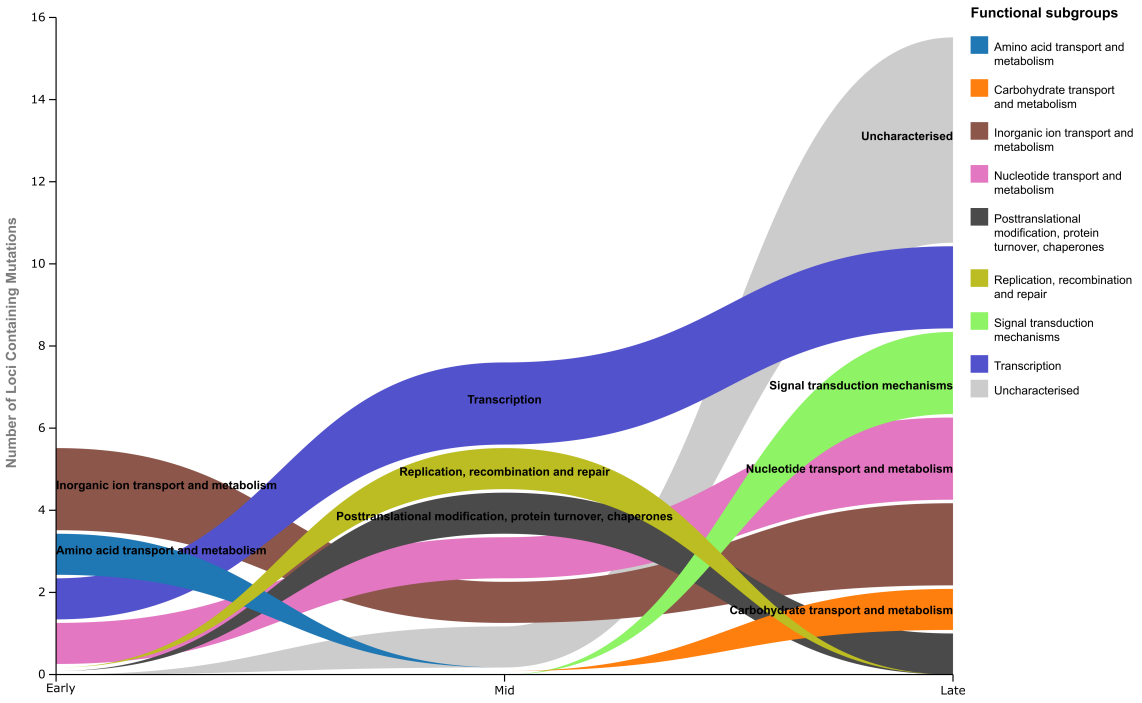


Figure 11. Bump chart visualising the number of loci affected by non-synonymous or intergenic region mutations per functional subgroup under exposure to BC in the steady model. Functional subgroups are colour-coded and include: transcription; translation; replication, recombination, and repair; nucleotide transport and metabolism; energy production and conversion; carbohydrate transport and metabolism; secondary metabolite biosynthesis, transport, and catabolism; inorganic ion transport and metabolism; signal transduction mechanisms; defence/virulence mechanisms; cell wall/membrane biogenesis; posttranslational modification, protein turnover, and chaperones and an uncharacterised group. Functional subgroups were determined using *ListiWiki*. Visualisation created using RawGraphs v2.0. The genes that were included into each functional subgroup are listed in the **Appendix 11(I).**

At the early timepoint, the functional group associated with inorganic ion transport and metabolism contained the highest number of affected loci (three). In contrast, only one locus was affected in each of the amino acid transport and metabolism; transcription; nucleotide transport and metabolism subgroups.

By the mid timepoint, the number of mutated loci in the functional group associated with transcription has increased to two, while in the group related to inorganic transport and metabolism decreased to one mutated locus. Additionally, mutations in loci related to replication, recombination and repair; posttranslational modification, protein turnover, and chaperones appeared at mid timepoint.

At the late timepoint, the unknown group contained the most mutated loci, with five. Groups associated with transcription; signal transduction; nucleotide transport and metabolism; inorganic ion transport and metabolism, contained two mutated loci each. Mutations were also harboured by loci associated with carbohydrate transport and

metabolism; signal transduction mechanisms, indicating that these functional adaptations may be advantageous only during later stages of the BPM progression. Notably, no mutated loci were observed in functional subgroups associated with replication, recombination and repair; posttranslational modification, protein turnover and chaperones.

Overall, these results suggest that there may be a general metabolic shift as well as fine-tuning of transcription regulation to modify the cellular response to BC exposure.

Next, to not only capture the number of loci affected in each functional subgroup but also to represent the frequency of SNPs within mutated loci, we grouped individual SNPs identified in the steady model based on their functional roles (**Figure 24**).

Across all timepoints, the functional subgroup involved in transcription harboured the highest number of individual SNPs, with 7, 8, and 11 SNPs at the early, mid, and late timepoints, respectively. This was primarily driven by mutations in *fepR* (*lmo2088*) and 5` untranslated region (5` UTR) of *fepR*, encoding a repressor of the MATE fluoroquinolone efflux pump FepA (Guérin et al., 2014).

At the early timepoint, two SNPs were also detected in loci associated with inorganic ion transport and metabolism, which reduced to one SNP by middle timepoint and increased to two at the late timepoint.

Another subgroup that was affected through all timepoints was nucleotide transport and metabolism group that contained one SNP each at early and mid-timepoints, increasing to two SNPs at the late timepoint.

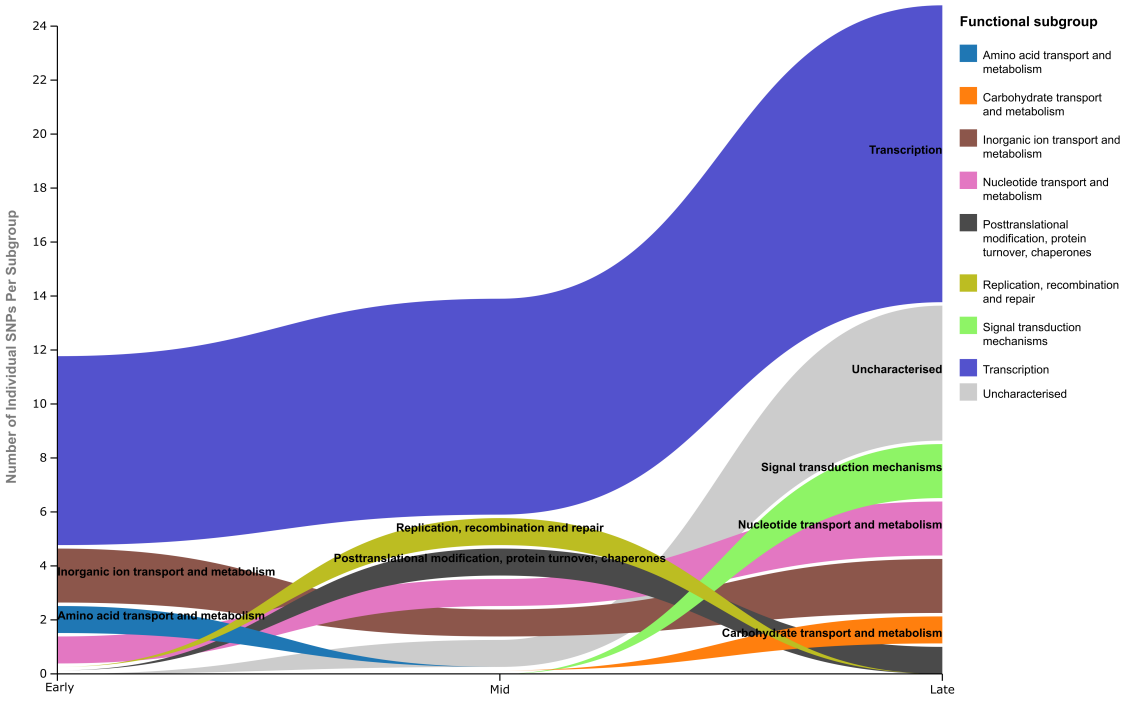


Figure 12. Bump chart visualising the number of individual SNPs per functional subgroup under exposure to BC in the steady model. Functional subgroups are colour-coded and include transcription; translation; replication, recombination, and repair; nucleotide transport and metabolism; energy production and conversion; carbohydrate transport and metabolism; secondary metabolite biosynthesis, transport, and catabolism; inorganic ion transport and metabolism; signal transduction mechanisms; defence/virulence mechanisms; cell wall/membrane biogenesis; posttranslational modification, protein turnover, and chaperones and an uncharacterised group. Functional subgroup classifications were determined using *ListiWiki*. Visualisation created using RawGraphs v2.0.

4.6.4. Mutations in *fepRA* Operon Related to Efflux Activity Become Fixed in the Populations Evolved Under BC Exposure

From functional analysis we revealed that the highest number of individual SNPs in isolates evolving under BC-exposure was occurring within *fepR*, which we sought to investigate in more details. Non-synonymous and intergenic mutations detected in the genomes of BC-exposed lineages from both biofilm and planktonic conditions were merged, encompassing six independent lineages (one population and three individual colonies per lineage). In the steady model, all six BC-exposed lineages, contained mutations in *fepR,* which were consistently detected across early, mid and late timepoints (**Figure 25A**).

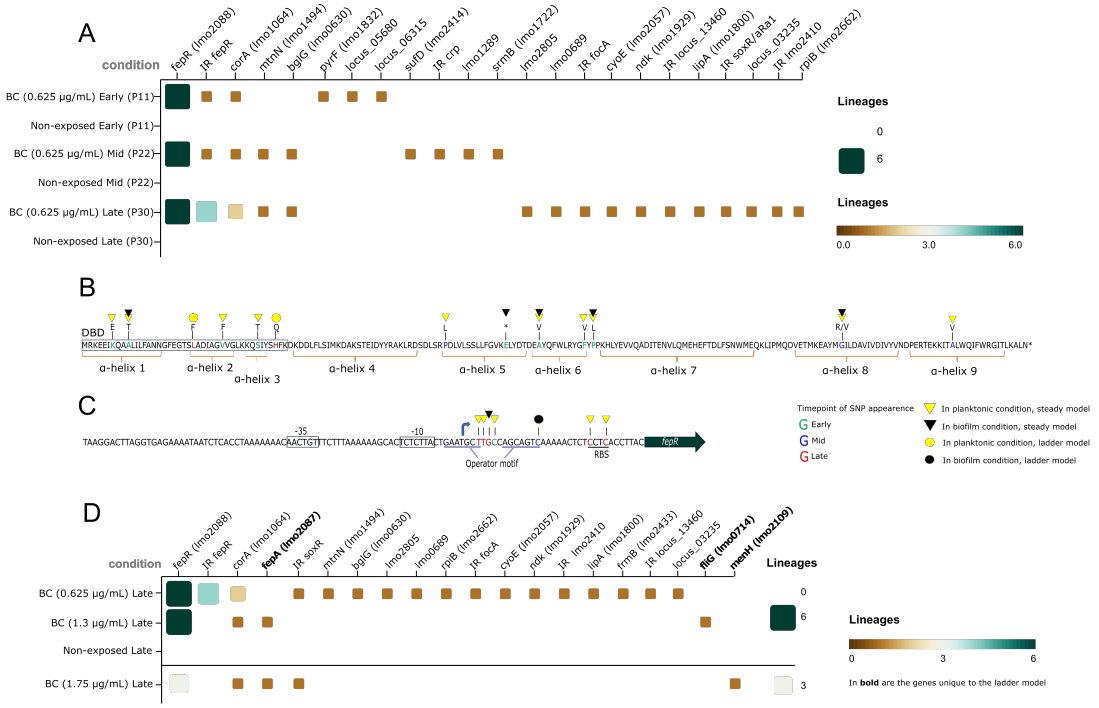


Figure 13. Mutations in *fepRA* operon promote reduced susceptibility to BC in *L. monocytogenes* under steady and escalating exposure to BC. (**A**) **Mutation frequency scheme** for SNPs acquired under steady exposure to BC (0.625 µg/mL) compared to non-exposed control at different timepoints: early (Passage 11), mid (Passage 22) and late (Passage 30). Data for each condition represents 6 biologically independent lineages. (**B**) **Distribution and predicted domain location of non-synonymous mutations (14 mutations at 13 positions)** within *fepR* under steady and ladder BC exposure. Gained residues are indicated above the sequence (amino acid map). Amino acids are colour coded according to the timepoint in which the mutations were first detected: green - early phase, blue – mid phase and red - late phase. * Indicates a gain of an early stop codon. Yellow triangle represents mutations that occurred in planktonic lineages, black triangle - in biofilm lineage, yellow and black circles – in the ladder model. N-terminal DNA binding domain (DBD) is indicated by a rectangle (residues 1 – 42). Structural elements (α-helices) are highlighted below the sequence. (**C**) **Map of base pair substitutions within 5` UTR of *fepR*** occurring in the steady and ladder models under BC exposure. Several functional elements were colour coded: blue arrow indicates transcription start site (TSS), promoter regions -35 and -10 indicated by rectangle, putative FepR operator motif underscored in light-blue and ribosome binding site (RBS) underscored in black. (**D**) **Mutation frequency scheme** for SNPs acquired under **ladder model** (0.625 - 1.3 - 1.75 µg/mL) at late evolutionary timepoint. Includes 6 biologically independent lineages for lineages exposed to 0.625 and 1.3 µg/mL BC and 3 lineages for 1.75 µg/mL BC, as planktonic lineages were non-recoverable at 1.75 µg/mL BC. Mutations exclusive to the ladder model were highlighted in bold. High-resolution figure can be downloaded through the link.

Overall, we detected 12 non-synonymous mutations (at 11 positions) within *fepR* in response to a steady concentration of BC (14 non-synonymous mutations at 13 positions in total for steady and ladder models) (**Figure 25B**), with mutations never co-occurring within the same isolate. Planktonic isolates exhibited a greater diversity of mutations,

with ten, compared to biofilm isolates with five mutations. Seven mutations appeared during the early timepoint (K7E, A10T, V30F, S37T, A96V, F105V, P107L), four emerged at mid timepoint (L76P, G157R, G157V, A181V), with G157R also detectable until the late timepoint (**Figure 25B**). Three mutations from an early timepoint (A10T, A96V, P107L) and one in mid timepoint (G157V) were shared between evolved isolates from planktonic and biofilm conditions. Notably, we detected a single premature stop codon mutation (E89*), which was exclusively present in one biofilm lineage. Mutations were distributed throughout the *fepR* and from the 12 identified mutations, five (K7E, A10T, L24F, V30F, S37T) were located within the N-terminal DNA-binding domain (DBD) (residues 1 - 42) (Samad et al., 2019), including two (V30F, S37T) within the HTH motif (residues 23 - 42). One notable substitution (A10T) resulted in the gain of a hydrogen bond forming ability by the side chain (**Appendix 12**) due to a change from a non-hydrogen forming methyl to a hydrogen forming hydroxyl group.

The rest (9/12) of the *fepR* mutations were located outside the DBD, spanning α-helices four to nine (**Figure 25B**). Mutations at position 157 (G157R/V) resulted in 2 independent substitutions. Structural mapping revealed that 11/12 *fepR* mutations that occurred under exposure to the steady model were located within α-helices (Samad et al., 2019).

In addition to the coding region mutations, we detected seven mutations in the *fepR* 5`UTR (**Figure 25C**). One mutation arose in a single planktonic lineage during the early timepoint and was situated within the intra-operator spacer, while another was detected in a single biofilm lineage at mid timepoint and was located within *fepR* operator. Five mutations were also detected at the late timepoint, with four observed in planktonic and one in a biofilm lineage and were distributed across the putative ribosome-binding site (RBS) (Guerin et al., 2014), the intra-operator spacer and the operator (**Figure 25C**). Two of these mutations were also predicted to overlap the transcription start site (TSS) (Guerin et al., 2014) occurring at the 3rd and 14th base pairs downstream of the TSS.

4.6.5. Mutations in Pathways Involved in Inorganic Ion Transport (*corA*), Transcription (*bglG*) and Nucleotide Transport and Metabolism (*mtnN*) Become Fixed in the Populations Evolved Under BC Exposure

Another candidate that may be associated with reduced susceptibility to BC is *corA* gene (*lmo1064;* inorganic ion transport and metabolism), encoding a metal cation transporter (Kehres, Lawyer and Maguire, 1998). We detected four non-synonymous

mutations within *corA* in two independent BC-exposed biofilm lineages. The S166P mutation arose at the early timepoint, while two mutations, T127K and L292F, emerged at the mid timepoint. A single mutation, P268Q, appeared at the late timepoint. Notably, mutation L292F was predicted to reside within a membrane-embedded region of CorA (InterPro) (**Figure 25A; Figure 26A**).

A single mutation (A180T) within the *mtnN* gene (*lmo1494;* nucleotide transport and metabolism), encoding 5'-methylthioadenosine nucleosidase (UniProt: Q9R4A1) was observed in a single biofilm lineage during mid and late timepoints (**Figure 25A; Figure 26B**). Likewise, mutation (E29V) in the *bglG* gene (*lmo0630;* transcription), encoding transcriptional regulator of the *bgl* operon (phosphotransferase system) (Amster-Choder and Wright, 1993) was observed in a single lineage at mid and late timepoints (**Figure 25A; Figure 26C**).

We detected additional mutations exclusively associated with BC-exposed condition, though these were only present at a single timepoint. In early timepoint we detected mutations in *pyrF* (*lmo1832;* nucleotide transport and metabolism), *lmo1040* (inorganic ion transport and metabolism), and *lmo1183* (unknown function). At the mid timepoint, mutations were observed in *sufD* (*lmo2414;* posttranslational modification), *srmB* (*lmo1722;* replication, recombination and repair), *lmo1289* (unknown function) and the intergenic region upstream of *crp*. In late timepoint, mutations emerged in *lmo2805* (unknown function), *lmo0689* (cell motility), *rpiB (lmo2662;* carbohydrate transport and metabolism*)*, *cyoE (lmo2057;* posttranslational modification*)*, *ndk (lmo1929*; nucleotide transport and metabolism*)*, *lipA (lmo1800;* signal transduction*)*, and *fliG* (*lmo0714;* cell motility) as well as in the intergenic regions upstream of *lmo2410*, *soxR* (*lmo2722;* transcription) and *focA* (*lmo0593;* inorganic ion transport and metabolism) (**Figure 25A**).

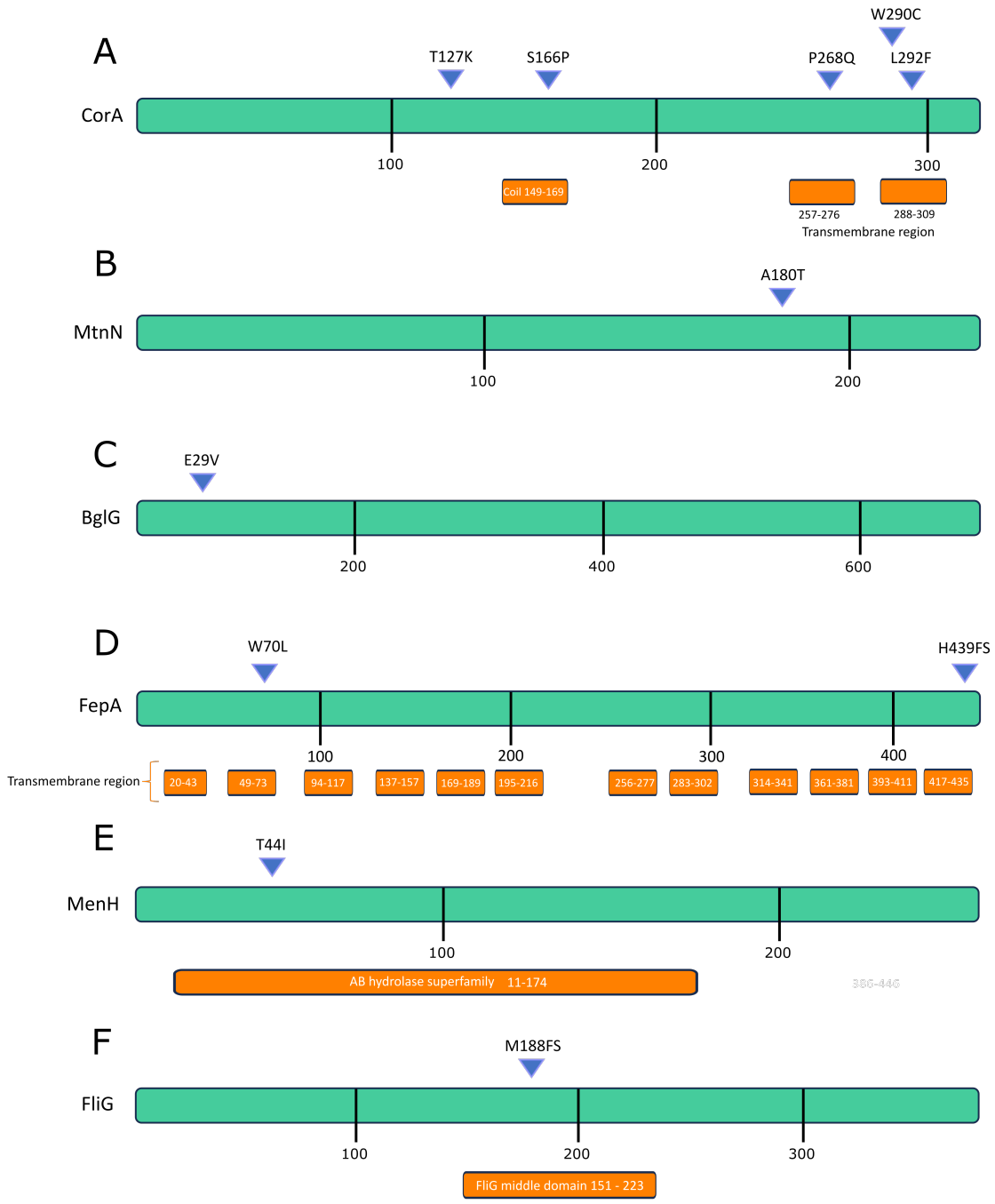


Figure 14. Graphical overview of substitutions in (A) CorA, (B) MtnN, (C) BglG, (D) FepA, (E) MenH, (F) FliG. Non-synonymous mutations are indicated by triangle. Affected domains are demonstrated.

4.6.6. Stepwise BC Escalation Does Not Affect BC Susceptibility but Selects for *fepA* Mutations Potentially Counteracting *fepR* Effects

To further evaluate genetic adaptations associated with reduced susceptibility to BC, we examined mutations that appeared under escalating BC concentration of the one-step and two-step ladder models. As with the steady model, we merged mutations occurring in BC-exposed condition from both biofilm and planktonic conditions, encompassing six independent evolved lineages. Overall, six regions contained mutations associated with escalating BC concentrations, which included three regions (*fepA* (*lmo2087;* defense/virulence mechanisms), *fliG* (*lmo0714;* cell motility), *menH* (*lmo2109*; unknown function)) that were not previously affected by mutations in the steady model. Mutations that were identified in early and late timepoints of the steady model were used as a reference to compare mutation profiles with the ladder model.

When assessing the one-step ladder model (0.625 µg/mL to 1.3 µg/mL), only mutations accumulated at the late timepoint were described. Similar to the steady model, all six evolved lineages exhibited mutations in *fepR* (**Figure 25B; D**). We detected two additional SNPs (L24F, H41Q), which were not previously identified in the steady model (**Figure 25B**). Both of these mutations appeared within the HTH motif of the DBD (amino acid residues 23-42). Conversely, three SNPs found in *fepR* in the steady model (A96V, P107L, G157R/V) were no longer observed in the one-step ladder model. Likewise, a mutation detected in the intra-operator spacer of *fepR* 5`UTR in a single lineage of the one-step ladder model was not detected in the two-step model (**Figure 25D**).

In addition to mutations within *fepR* that were identified in the one-step model, we also detected two SNPs in *fepA (*defense/virulence mechanisms), which encodes a MATE efflux pump downstream of *fepR* (Guérin et al., 2014) (**Figure 26D**). Both mutations within *fepA* co-occurred in the same biofilm lineage. One of these mutations (H439FS) resulted in a frameshift, while another (W70L) was part of an α-helix within a membrane region of FepA (amino acid residues 49-73) (InterPro) (**Figure 26D**). Notably, both mutations in *fepA* co-occurred with a mutation (E89*) in *fepR* that resulted in the gain of a premature stop codon. The above suggests a detection of a potential compensatory relationship between *fepR* and *fepA*.

Additional mutations were uniquely observed in the ladder model, including a T44I substitution in *menH*, encoding 2-succinyl-6-hydroxy-2,4-cyclohexadiene-1-carboxylate

(SHCHC) synthase (Jiang et al., 2008) **(Figure 26E**). In *fliG*, which is involved in cell motility (UniProt: P0ABZ1), we detected a frameshift mutation (M188FS) (**Figure 26F**).

The S166P mutation in *corA*, initially detected in a single biofilm lineage of the steady model, was absent at the ladder model. On the other hand, a new substitution, W290C, was detected in a biofilm lineage following the first BC escalation to 1.3 µg/mL, which was predicted to be harboured within a membrane-embedded region (InterPro) (**Figure 25D; Figure 26A**).

For isolates that underwent the second BC escalation in a two-step ladder model (1.3 µg/mL to 1.75 µg/mL), we were only able to evaluate mutations occurring in three biofilm lineages of the late timepoint, as three planktonic lineages exposed to 1.75 µg/mL BC could not be recovered.

The W290C and T44I substitutions in the *corA* and *menH* genes, respectively, which appeared during the one-step ladder model, were also present in isolates exposed to 1.75 µg/mL of BC, suggesting their emergence prior to the execution of the two-step ladder.

An additional mutation detected in the intergenic region upstream of *soxR* appeared at the late timepoint during the steady model and on escalation to 1.75 µg/mL of BC in the two-step model, however, was not detected in the one-step ladder at 1.3 µg/mL of BC.

4.6.7. Distribution of Mutations Associated with Biofilm Persistence

To investigate genetic traits associated with biofilm persistence (defined in section 2.7. '**Layout of in vitro Bead-based Biofilm Persistence Model (BPM)**'), we first categorised the mutations that accumulated in biofilm condition by functional roles. We followed the strategy previously employed in section: 4.5.5. '**Functional Distribution of Mutations Associated with Reduced Susceptibility to BC**. Non-synonymous and intergenic region mutations from BC-exposed and non-exposed biofilm lineages were grouped by their function according to *ListiWiki*. Mutations co-occurring in biofilm and planktonic condition were disregarded from this analysis. As such, we detected mutations in loci belonging to four major functional groups: cellular processes, metabolism, information processing and lifestyles. The loci were further divided into 15 functional subgroups, including: transcription; nucleotide transport and metabolism; energy production and conversion; inorganic ion transport and metabolism; signal transduction mechanisms; defence/virulence mechanisms; cell wall/membrane biogenesis;

carbohydrate transport and metabolism; posttranslational modification, protein turnover and chaperones; translation; replication/recombination and repair; secondary metabolite biosynthesis, transport and catabolism; amino acid transport and metabolism and a subgroup containing genes of unknown function. (**Appendix 11(II)**). Next, we created bump charts to visualise how the number of loci affected by mutations in each functional group changed over the timepoints (**Figure 27**).

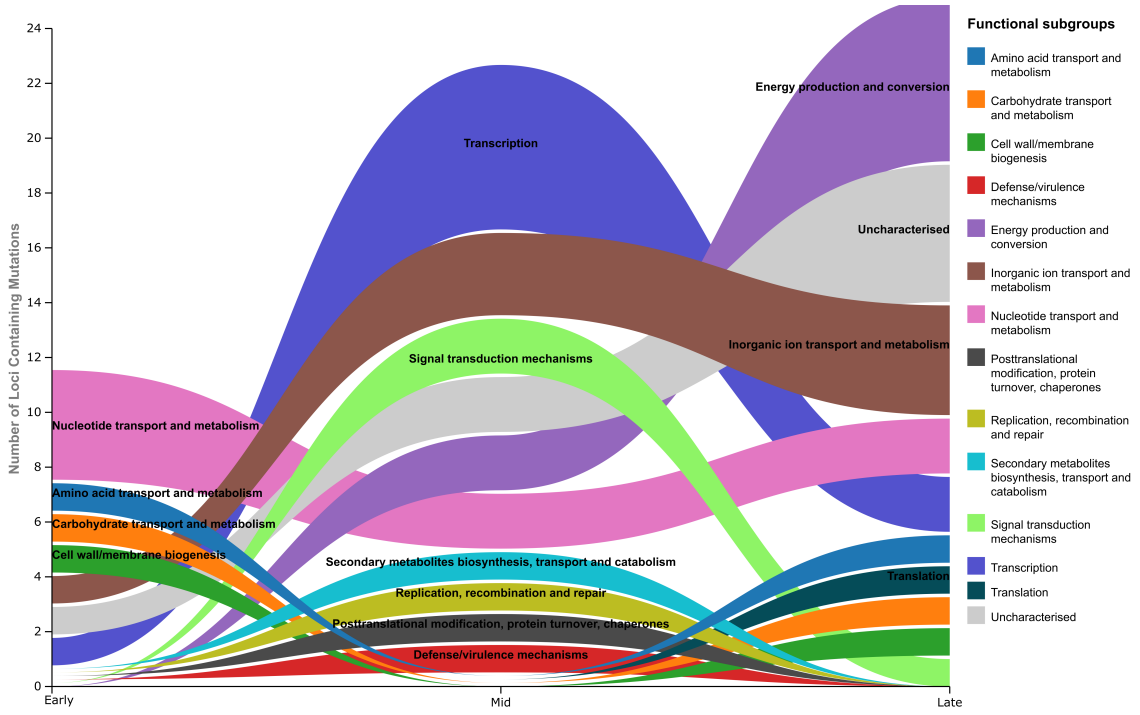


Figure 15. Bump chart visualising the number of loci affected by non-synonymous and intergenic region mutations grouped by functional subgroup, under biofilm lifestyle (on beads). Functional subgroups are colour-coded and include: transcription; nucleotide transport and metabolism; energy production and conversion; inorganic ion transport and metabolism; signal transduction mechanisms; defence/virulence mechanisms; cell wall/membrane biogenesis; carbohydrate transport and metabolism; posttranslational modification, protein turnover and chaperones; translation; replication/recombination and repair; secondary metabolite biosynthesis, transport and catabolism; amino acid transport and metabolism and an uncharacterised group. Functional subgroups were determined using *ListiWiki*. Visualisation created using RawGraphs v2.0. The genes that were included into each functional subgroup are listed in the **Appendix 11(II)**.

At the early timepoint, the nucleotide transport and metabolism subgroup harboured the most mutated loci (four). Functional groups associated with amino acid transport and metabolism; carbohydrate transport and metabolism; cell wall/membrane biogenesis; inorganic ion transport and metabolism; transcription, contained one mutated locus each.

At the mid timepoint, there was a pronounced increase in the number of mutated loci in transcription-associated subgroup (six). There was also an increase in the number of mutated loci in inorganic ion transport and metabolism subgroup (three). Notably, for the nucleotide transport and metabolism group, the number of affected loci decreased to two, after being the group with the most mutated loci at the early timepoint. Two mutated loci were also detected in the signal transduction and energy production and conversion subgroups. Finally, one mutated locus each was identified in subgroups associated with defence/virulence; posttranslational modifications, protein turnover and chaperones; secondary metabolite biosynthesis, transport and catabolism; and replication, which were solely affected by mutations in mid timepoint.

At the late timepoint, there was an increase in mutated loci associated with energy production and conversion, suggesting a fine-tuning of energy associated pathways may be beneficial solely at the later stages of the BPM. There was also an increase in mutated loci associated with inorganic ion transport and metabolism (four). We detected a notable reduction in a number of mutated loci involved in transcription, reducing to two. Finally, one mutated locus each was detected in translation; carbohydrate transport and metabolism; cell wall/membrane synthesis; amino acid transport and metabolism subgroups, which were initially present at the early timepoint but were not detected at the mid timepoint.

In addition to the number of loci affected in each functional category we aimed to demonstrate the variability in SNP frequency within those loci. To achieve this objective, we analysed individual SNPs that were only detected in biofilm condition, based on their functional roles (**Figure 28**).

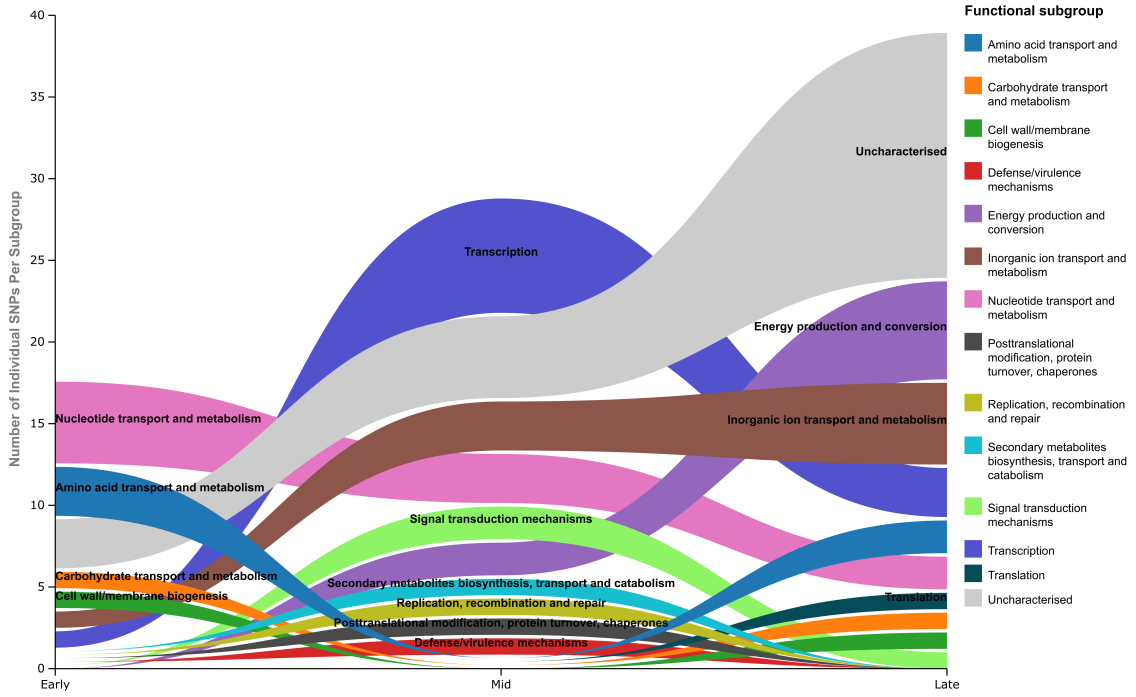


Figure 16. Bump chart visualising the number of individual SNPs by functional subgroup under biofilm lifestyle (on beads). Functional subgroups are colour-coded and include: transcription; nucleotide transport and metabolism; energy production and conversion; inorganic ion transport and metabolism; signal transduction mechanisms; defence/virulence mechanisms; cell wall/membrane biogenesis; carbohydrate transport and metabolism; posttranslational modification, protein turnover and chaperones; translation; replication/recombination and repair; secondary metabolite biosynthesis, transport and catabolism; amino acid transport and metabolism and an uncharacterised group. Functional subgroups were determined using *ListiWiki*. Visualisation created using RawGraphs v2.0.

At the early timepoint, loci associated with the nucleotide transport and metabolism subgroup exhibited the most SNPs with five, followed by the amino acid transport and metabolism subgroup with three SNPs. For the rest of the functional groups, including carbohydrate transport and metabolism; cell wall/membrane synthesis; inorganic ion transport and metabolism and transcription there was one SNP detected per group.

At the mid timepoint, the ratio shifted, with the transcription associated subgroup containing the most SNPs with seven, followed by the unknown group with five, inorganic ion and nucleotide transport and metabolism containing three SNPs each, signal transduction and energy production and conversion containing two SNPs each.

At the late timepoint, the group with the loci of unknown function contained the most SNPs with 15. This was primarily driven by mutations in *ykoK*, which encodes the M-Box riboswitch RNA. Although the function of *ykoK* is not listed on *ListiWiki*, M-Box

riboswitch has been previously reported to control expression of downstream metal transporters (Ramesh and Winkler, 2010).

Additionally, there was a pronounced increase in the number of SNPs associated with energy production and conversion, containing six individual SNPs. For SNPs in loci associated with transcription there was a continued reduction to three individual SNPs. SNPs in loci associated with nucleotide transport and metabolism reduced to two SNPs at the late timepoint.

Overall, these results indicate a broad evolutionary response to the biofilm lifestyle, with 15 functional subgroups affected, suggesting importance of fine-tuning of pathways related to metabolism, energy production, and transcriptional regulation over the BPM timeline.

4.6.8. Mutations in Genes Related to Inorganic Ion Transport and Metabolism (*mgtA*), Nucleotide/Amino Acid Transport and Metabolism (*pyr* operon) and Transcription/Signal Transduction (*rsb* operon) Became Fixed in the Biofilm Condition

Once we investigated the functional profile of mutations associated with adaptation to biofilm lifestyle, we sought to describe the mutations that recurrently occurred in several independent lineages or affected more than one gene in the same operon, in more details. We reanalysed the steady model dataset by focusing on mutations that have exclusively occurred under the biofilm condition.

One of the loci where mutations exclusively accumulated in biofilm condition was *ykoK* leader (M-box riboswitch RNA element). Five mutations were detected within *ykoK*, at residues 20, 33, 39, 63 and 97 (**Figure 29A-B**). Occurrence of these mutations was distributed throughout the timepoints, with three mutations observed in three independent lineages of the early timepoint, one mutation emerged in a fourth lineage during the mid timepoint, and another mutation was detected in a fifth lineage during the late timepoint.

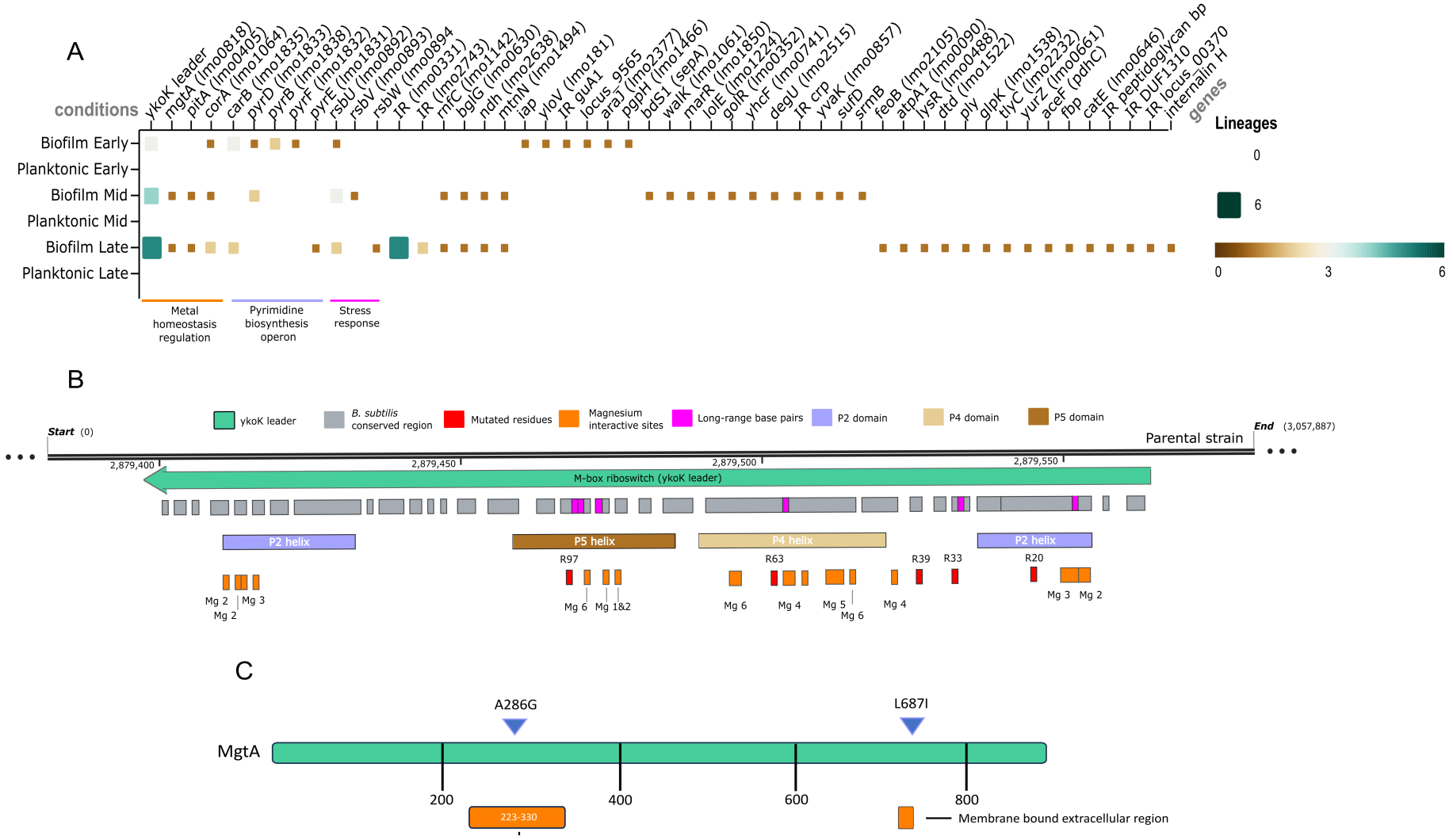

A
conditions
genes
ykoK leader
mgtA (lmo0818)
pitA (lmo0405)
corA (lmo1064)
carB (lmo1835)
pyrD (lmo1833)
pyrB (lmo1838)
pyrF (lmo1832)
pyrE (lmo1831)
rsbU (lmo0892)
rsbV (lmo0893)
rsbW (lmo0894
IR (lmo0331)
IR (lmo2743)
rnfC (lmo1142)
bglG (lmo0630)
ndh (lmo2638)
mtnN (lmo1494)
iap
yloV (lmo181)
IR guA1
locus_9565
araJ (lmo2377)
pgpH (lmo1466)
bdS1 (sepA)
walK (lmo1061)
marR (lmo1850)
lolE (lmo1224)
golR (lmo0352)
yhcF (lmo0741)
degU (lmo2515)
IR crp
yvaK (lmo0857)
sufD
srmB
feoB (lmo2105)
atpA1 (lmo0090)
lysR (lmo0488)
dtd (lmo1522)
plY
glpK (lmo1538)
tlyC (lmo2232)
yurZ (lmo0661)
aceF (pdhC)
fbp
catE (lmo0646)
IR peptidoglycan bp
IR DUF1310
IR locus_00370
internalin H
Biofilm Early
Planktonic Early
Biofilm Mid
Planktonic Mid
Biofilm Late
Planktonic Late
Metal homeostasis regulation
Pyrimidine biosynthesis operon
Stress response
Lineages
0
6
0
3
6
B
ykoK leader
B. subtilis conserved region
Mutated residues
Magnesium interactive sites
Long-range base pairs
P2 domain
P4 domain
P5 domain
Start (0)
End (3,057,887)
Parental strain
2,879,400
2,879,450
2,879,500
2,879,550
M-box riboswitch (ykoK leader)
P2 helix
P5 helix
P4 helix
P2 helix
R97
R63
R39
R33
R20
Mg 2
Mg 2
Mg 3
Mg 6
Mg 1&2
Mg 6
Mg 4
Mg 5
Mg 6
Mg 4
Mg 3
Mg 2
C
A286G
L687I
MgtA
200
400
600
800
223-330
Membrane bound extracellular region

Figure 17. Mutations associated with inorganic ion transport and metabolism (*mgtA*), nucleotide/amino acid transport and metabolism (*pyr* operon) and transcription/signal transduction (*rsb* operon) were affected in biofilm lineages. (**A**) **Mutation frequency scheme for SNPs acquired exclusively in biofilm lineages**. The number of lineages carrying genetic traits associated with biofilm persistence compared to planktonic control are shown. Six biologically independent lineages were included. Evolutionary timepoints include early, mid and late timepoints. (**B**) **Structural mapping of YkoK leader and mutated residues detected through the biofilm persistence model.** Conserved nucleotide regions between the parental strain and *B. subtilis* are shown in grey. Structurally important domains and putative Mg^{2+} interactive sites derived from *B. subtilis* are also presented. Ykok predicted structure in *B. subtilis* was extracted from NACB: 2QBZ and from previous work (Ramesh, Wakeman, Winkler, 2011). (**C**) **Graphical overview of substitutions in MgtA.** Substitutions are indicated by a triangle. Predicted structural and functional domains are indicated. Domains were predicted with InterPro. High-resolution figure can be downloaded through the link.

Due to the absence of a resolved structure of the *ykoK* leader in *L. monocytogenes*, we based our analysis on the complete structure of the *ykoK* leader from *B. subtilis* IA40 (PDB: 2QBZ). All five mutations in *ykoK*, mapped to conserved regions between *B. subtilis* IA40 and the *L. monocytogenes* parental strain (**Figure 29B**). Notably, residues 20, 63 and 97 mapped near Mg^{2+}-interacting sites, which are involved in structural conformation of the riboswitch (Ramesh et al., 2011), while residues 33, 63 and 97 mapped near long-range base pairs involved in termination loop stabilisation. In a comparative analysis of *ykoK* sequences from Gram-positive species outside of the *Listeria* genus (**Appendix 4(I); Appendix 13**), residues 20 and 63 were fully conserved, whereas residues 33, 39 and 97 contained substitutions (**Appendix 13B**). When comparing *ykoK* leader within the *Listeria* genus, excluding *L. monocytogenes*, residues 20 and 97 exhibited a high degree of conservation, while substitutions occurred at positions 33, 39 and 63 (**Appendix 4(II); Appendix 13A**). The residue at position 20 was conserved both within and outside the *Listeria* genus, suggesting that substitutions at this site are likely to have a critical impact on the structure and function of the M-box riboswitch.

We have also detected two non-synonymous mutations (A286G, L687I) in *mgtA (lmo0818;* inorganic ion transport and metabolism*)*, which encodes a metal transporter (Maguire, 1992), located downstream of *ykoK* leader. Both of the mutations were observed in a single biofilm lineage (**Figure 29A**) and were situated within the transmembrane domain (residues 223-330 and 634-810) (**Figure 29C**). Notably, mutation L687I co-occurred with mutations in *ykoK* at residue 37*,* suggesting a putative compensatory mechanism fine-tuning metal homeostasis. The same substitution leads to a loss of the hydrogen bond forming ability by the side chain (**Appendix 14**).

Another transporter that exhibited non-synonymous mutations in biofilm lineages was *pitA (lmo0405;* inorganic ion transport and metabolism), encoding a low-affinity inorganic phosphate transporter (Harris et al., 2001; Jackson et al., 2008). Notably, mutation I58M co-occurred with a mutation at residue 33 in *ykoK* and was detected in a single biofilm lineage during mid and late timepoints (**Appendix 16A**).

Several genes involved in pyrimidine biosynthesis (*pyrB* (*lmo1838*), *carB* (*lmo1835*), *pyrF* (*lmo1832*), *pyrD* (*lmo1833*) and *pyrE* (*lmo1831*); nucleotide/amino acid transport and metabolism) also exhibited non-synonymous mutations in biofilm lineages (**Figure**

29A, 30A-D). In *pyrB,* which encodes the catalytic subunit of aspartate carbamoyltransferase responsible for converting carbamoyl phosphate and aspartate into carbamoyl aspartate (Lipscomb and Kantrowitz, 2012), two mutations (A22E, G153R) were detected in the early timepoint. The A22E substitution, residing within a helical region of the carbamoyl-P binding domain (**Figure 30A**), likely leads to improved hydrogen bonding as a small hydrophobic alanine is replaced with a bulkier, negatively charged glutamic acid. While substitution (G153R), situated in the Asp/Orn binding domain, replaces a small glycine for a larger arginine, suggesting alteration in substrate binding.

Another gene of the pyrimidine biosynthesis operon associated with biofilm persistence, *carB*, encodes the large subunit of glutamine-dependent carbamoyl phosphate synthetase (CPSase) (Saeed-Kothe and Powers-Lee, 2002). In biofilm lineages, five mutations were identified in *carB*, with three detected during the early timepoint (G175V, Q262*, S599M) and two during the late timepoint (G781E, G969FS). Notably, the Q262* mutation resulted in a premature stop codon, while G969FS substitution resulted in a frameshift (**Figure 30B**). The remaining three mutations were predicted to be located in CPSase enzymatic domains (InterPro). The G175V substitution likely disrupts the ATP-binding region, as it occurs within both the carboxyphosphate synthetase domain (amino acid residues 1-401) and the ATP-grasp 1 motif (residues 133-327) (InterPro). Meanwhile, S599M and G781E are situated in the carbamoyl phosphate synthetase domain (amino acid residues 547-929), with G781E also located in the ATP-grasp 2 motif. These latter substitutions may affect the local chemical environment by altering side chain polarity and interfering with hydrogen bonding networks (**Figure 30B; Appendix 14**).

A single substitution in *pyrF* (D63H) was also detected in biofilm lineages of the early timepoint. *pyrF* encodes the orotidine 5'-phosphate decarboxylase, which facilitates conversion of orotidine 5'-monophosphate (OMP) to uridine 5'-monophosphate (UMP) (Tokuoka et al., 2007). Notably, D63H substitution was predicted to be situated at a dimer interface (amino acid residues 62-63; UniProt: P58641), suggesting a potential interruption of *pyrF* dimer formation (**Figure 30C**).

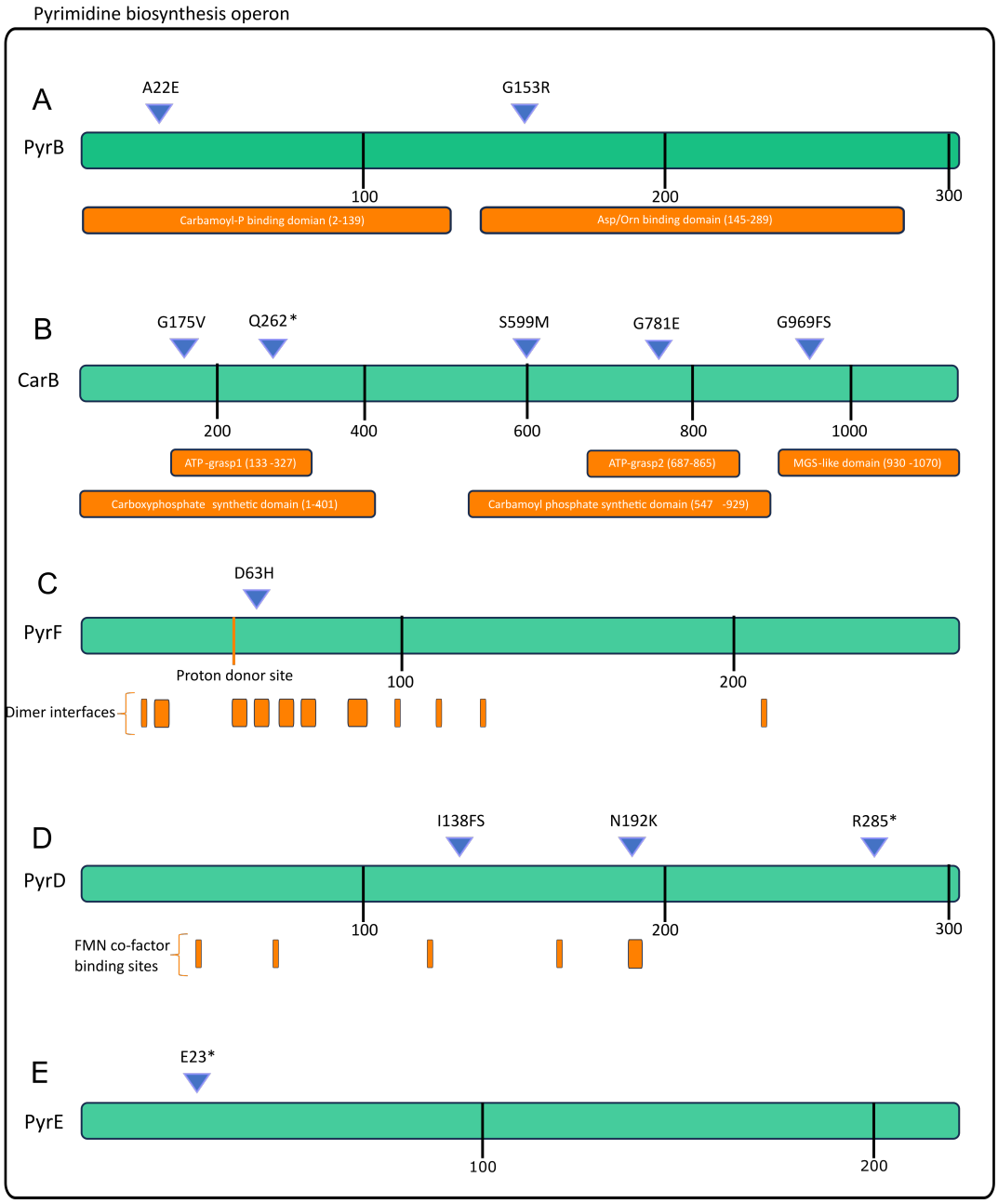


Figure 18. Graphical overview of substitutions detected in the pyrimidine synthesis operon under biofilm condition. Structural mapping of mutations occurring in (**A**) PyrB, (**B**) CarB, (**C**) PyrF, (**D**) PyrD and (**E**) PyrE indicated by orange boxes. Substitutions are indicated by triangles. * Indicates an early stop codon, FS – frameshift mutation. Domains were predicted with InterPro.

Mutations in *pyrD*, encoding the flavin mononucleotide co-factor (FMN)-containing dihydroorotate dehydrogenase (DHODH) that catalyses the conversion of dihydroorotate to orotate during *de novo* pyrimidine synthesis (Sykes, 2018), were detected in one biofilm lineage at the early passages and in two lineages at the mid passages, with no

mutations observed in the late passages. Notably, the I138FS mutation resulted in a frameshift, and the R285* mutation introduced a premature stop codon. Additionally, the N192K substitution, which replaces asparagine with lysine at the redox-active FMN binding site (residues 192-193) (InterPro) (**Figure 30D**), is predicted to impair FMN binding, which is critical for electron transfer during oxidation of dihydroorotate to orotate (Kow et al., 2009).

Finally, in *pyrE*, which encodes orotate phosphoribosyl transferase (the enzyme that catalyses the formation of OMP), we detected a premature stop codon (E23*). This mutation appeared only at the late timepoint.

Among the traits associated with biofilm persistence, accumulation of mutations also occurred in an operon regulating SigB (*rsbU, rsbV, rsbW*), which has been associated with general stress response in *L. monocytogenes* (Guerreiro et al., 2020) (**Appendix 15**). We detected a total of six non-synonymous mutations within *rsbU (lmo0892;* transcription) with one frameshift mutation (E94FS) at an early timepoint, three mutations (E22G, T204M, L60FS) including another frameshift mutation emerged during the mid timepoint, and two mutations including a premature stop codon emerged at the late timepoint (Y9H, S41*). The T204M substitution was predicted to occur within the metal-dependent protein phosphatase (PPM) domain (AlphaFold: Q8Y8K7), potentially disrupting metal coordination and catalytic function. Furthermore, the Y9H and E22G substitutions, located within the phosphoserine phosphatase domain, were predicted to alter the conformation of the *rsbU* active site. Y9H substitution may disrupt local hydrophobic interactions and substrate recognition, while the E22G removes a critical negative charge, potentially destabilising electrostatic interactions required for substrate binding. In addition to mutations within *rsbU*, we also detected non-synonymous mutations in other *rsb* operon genes. A single substitution (S58R) was detected in *rsbV* (*lmo0893;* signal transduction mechanisms), encoding a positive regulator of sigB activity. Non-phosphorylated RsbV binds to RsbW, thereby preventing it from sequestering sigB and allowing its activation. Notably, the S58R substitution occurs at the sole described regulatory phosphorylation site of RsbV (InterPro), potentially disrupting *rsb* stress response cascade. In addition, a mutation in *rsbW* (*lmo0893;* signal transduction mechanisms), which encodes a negative regulator of sigB activity, introduced a premature stop codon (Q22*). Such truncation was observed in the same

lineage as the S41* nonsense mutation in *rsbU*, suggesting a potential co-evolution of regulatory components to fine-tune the stress response pathway.

In *rnfC* (*lmo1142;* energy production and conversion), which encodes an oxidoreductase complex subunit involved in ion transport (UniProt: Q7VNT4), we detected a single frameshift mutation (V410FS) in a single biofilm lineage of the mid and late timepoints (**Appendix 16B**). While in *ndh* (*lmo2638;* energy production and conversion), which encodes NADH dehydrogenase, two mutations (A274T; A259P) were detected in a single biofilm lineage during the mid and late timepoints.

There was also a notable accumulation of intergenic mutations upstream of the hypothetical protein encoded by *lmo0331* (39% sequence identity with InlJ (PDB: 3BZ5)), with a total of eight mutations detected during the late timepoint.

Mutations in *corA*, *bglG*, *mtnN*, and the intergenic region upstream of *crp*, were previously associated with reduced susceptibility to BC in section 4.5.6. '**Mutations in *fepRA* Operon Related to Efflux Activity Become Fixed in the Populations Evolved Under BC Exposure**', however were also detected in the biofilm-adapted lineages (**Figure 29**), suggesting simultaneous adaptation to both selective pressures.

Finally, several mutations exclusive to biofilm-associated lineages were detected at single timepoints (**Figure 29A**). Regions affected during the early timepoint included *iap*, *yloV* (*lmo1814;* unknown function), *araJ (lmo2377;* carbohydrate transport and metabolism), *pgpH* (*lmo1466;* control of c-di-AMP homeostasis), locus_9565, and the intergenic region upstream of *guA1*. In the mid timepoint, mutations occurred in *bdS1* (*lmo2157;* secondary metabolites biosynthesis, transport and catabolism), *walK (lmo1061;* signal transduction mechanisms), *marR (lmo1850;* transcription), *lolE (lmo1224;* defence/virulence mechanisms), *golR (lmo0352;* transcription*)*, *yhcF (lmo0741;* transcription*)*, *degU (lmo2515;* orphan response regulator*)*, *yvaK (lmo0857*; unknown function), *sufD (lmo2414;* posttranslational modification, protein turnover, chaperones), *srmB* (unknown function). In the late timepoint, mutations were detected in *feoB (lmo2105;* inorganic ion transport and metabolism), *atpA1* (*lmo0090;* energy production and conversion), *lysR* (*lmo0488;* transcription), *dtd* (*lmo1522;* translation*)*, locus_12680 (L-alanoyl-D-glutamate peptidase), *glpK* (*lmo1538*; energy production and conversion), *tlyC (lmo2232*; unknown function), *yurZ* (*lmo0661*; unknown function), *aceF* (*lmo1054*; energy production and conversion), *fbp* (*lmo0830;* carbohydrate transport and

metabolism), *catE* (*lmo0646*; unknown function), *inlH* (*lmo0263*; cell wall/membrane biogenesis) and the intergenic regions upstream of *lmo2743* (carbohydrate transport and metabolism), peptidoglycan bound protein (locus_15625*),* DUF1310*,* locus_00370.

4.6.9. Biofilm Persistence Did Not Elicit an Increase in Biomass/Population Generation, Nor Had an Effect on the Fitness of the Evolved Isolates

We evaluated the phenotypic characteristics of the evolved isolates derived from the BPM, by measuring their biomass production, fitness, and capacity for surface attachment. These parameters were compared with those of the parental strain, and between BC-exposed and non-exposed isolates, in both biofilm and planktonic groups.

Evaluation of early and late passages of biofilm and planktonic lineages revealed no increase in biomass production, as determined by the crystal violet assay. Additionally, no significant differences were observed between BC-exposed and non-exposed lineages (**Figure 31**).

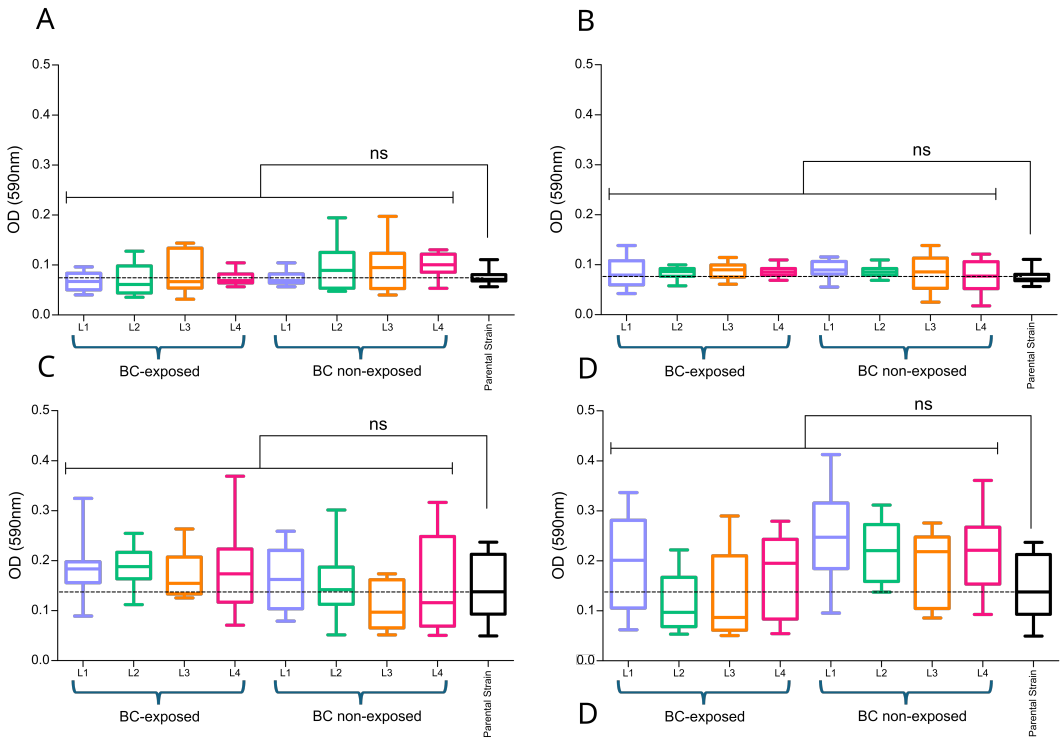


Figure 19. Biomass production of evolved populations, measured with crystal violet assay. (**A**) Biomass production of biofilm-evolved lineages at the early timepoint. (**B**) Biomass production of planktonic-evolved lineages at the early timepoint. (**C**) Biomass production of biofilm-evolved lineages at the late timepoint. (**D**) Biomass production of planktonic-evolved lineages at the late timepoint. Each panel includes data from both BC-exposed and non-exposed lineages. Dashed line indicates the mean of the parental strain. One-way ANOVA followed by

Tukey's test was performed to compare the groups. Statistical significance: ns - not significant. All experiments were performed in triplicates; whiskers represent minimum to maximum values.

Measurements of cell attachment to the bead in populations from the early biofilm passages revealed a significant reduction in attachment capacity in three quarters of independent lineages (*p* value ranging from 0.0036 to 0.0003), likely a response to the initial stress from the conditions of the model (**Figure 32A**). Notably, at the late timepoint, the cell attachment capacity was comparable to that of the parental strain, with gained mutations likely compensating for the initial loss of the cell attachment capacity (**Figure 32C**). In contrary, populations from the early planktonic passages exhibited cell attachment capacity comparable to the parental strain (**Figure 32B**), which was also consistent with the cell attachment capacity of the late planktonic populations (**Figure 32D**).

Assessment of fitness, based on the area under the curve (AUC) from growth curve experiments, revealed no detectable changes in fitness across early or late passages. Additionally, there were no significant differences in fitness observed between BC-exposed and non-exposed lineages (**Figure 33**).

Overall, these results suggest that the phenotypic changes enabling evolved cells to persist across the passages of the BPM may be subtle and not detectable by the low-resolution assays employed in this study. These limitations will be approached in **Chapter 6** where we will aim to describe the mechanisms detected in this chapter in more details.

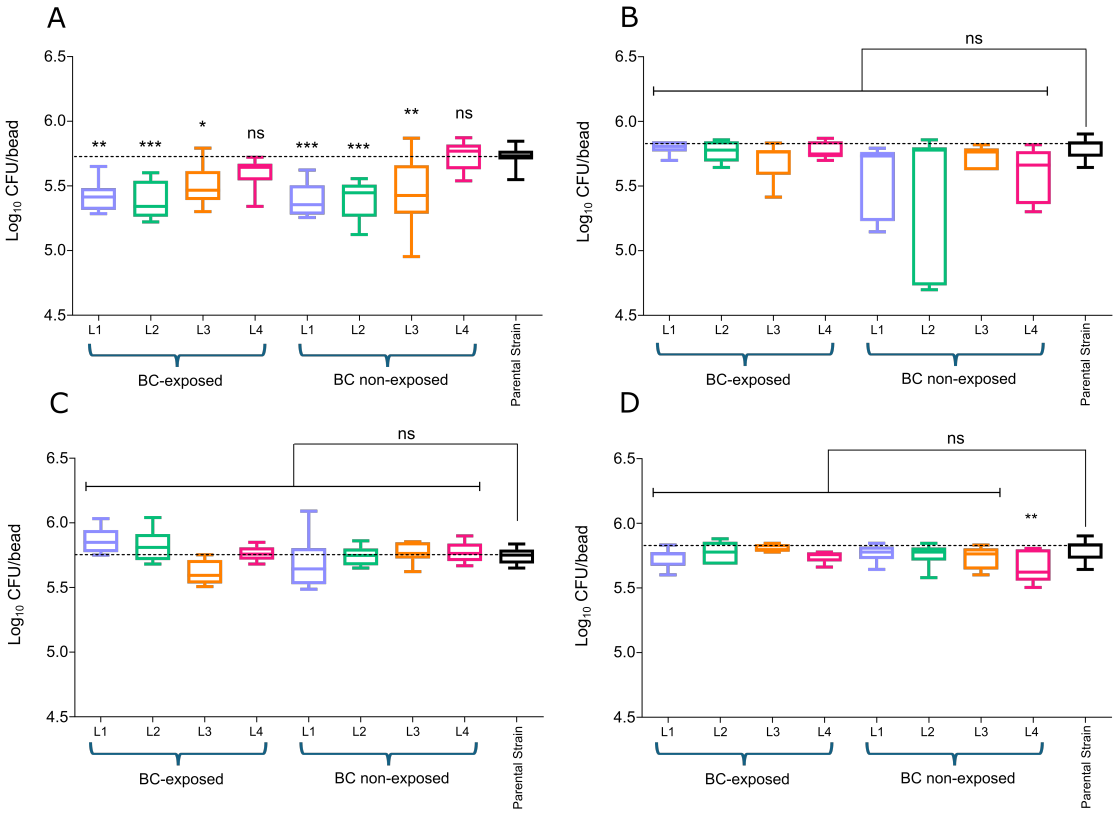


Figure 20. Assessment of surface attachment capacity (CFU/bead) by evolved lineages (populations). (**A**) Cell surface attachment capacity of evolved biofilm lineages from the early timepoint. (**B**) Cell surface attachment capacity of evolved planktonic lineages from the early timepoint. (**C**) Cell surface attachment capacity of evolved biofilm lineages from the late timepoint. (**D**) Cell surface attachment capacity of evolved planktonic lineages from the late timepoint. Includes data for BC-exposed and non-exposed groups**.** Dashed line indicates the median of the parental strain. CFU/bead data were $\log_{10}$-transformed prior to plotting, and statistical analyses were performed on the transformed values. One-way ANOVA followed by Tukey's test was performed to compare the groups. Statistical significance: $p < 0.05$ (*), $p < 0.01$ (**), $p < 0.0001$ (***), ns - not significant. All experiments were performed in triplicates. Whiskers indicate the range from the minimum to the maximum observed values. Median value indicated within the interquartile range.

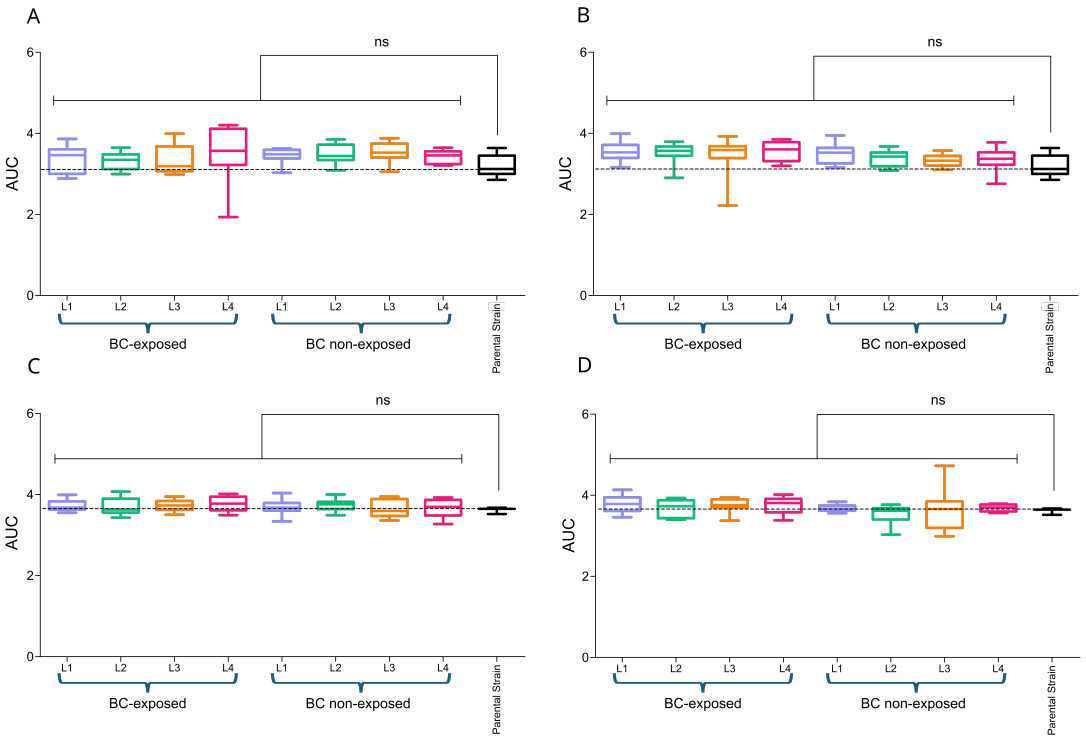


Figure 21. Fitness of evolved biofilm and planktonic lineages, measured as the area under the curve (AUC). (**A**) AUC of biofilm-evolved lineages at the early timepoint. (**B**) AUC of planktonic-evolved lineages at the early timepoint. (**C**) AUC of biofilm-evolved lineages at the late timepoint. (**D**) AUC of planktonic-evolved lineages at the late timepoint. Each panel includes data from both benzalkonium chloride (BC)-exposed and non-exposed lineages. Dashed line indicates the median of the parental strain. One-way ANOVA followed by Tukey's test was performed to compare the groups. Statistical significance: ns – not significant. All experiments were performed in triplicates. Whiskers indicate the range from the minimum to the maximum observed values. Median value indicated within the interquartile range.

4.7. Discussion

By evaluating the results of the steady model where the constant sub-inhibitory concentration of BC was applied on evolving isolates, we detected that the central genetic determinant of reduced susceptibility to BC was *fepR,* a transcriptional repressor of the MATE efflux pump. Our results are complementary to previous findings by Guerin et al., 2014 and Bolten et al., 2022, suggesting that non-synonymous mutations within *fepR* can lead to a 2-fold increase in MIC levels. This supports the validity of the methodology employed in our study. While our results align with the previous work investigating the role of the *fepRA* operon in reduced susceptibility to BC, our study differs in both the focus and the experimental design. Specifically, we explored long-term adaptation to BC, rather than short-term responses, which enabled us to identify putative compensatory mechanisms that had not been previously reported. Furthermore, our model was designed to simulate the biofilm lifestyle, a critical yet often overlooked factor influencing adaptive trajectories. By incorporating these elements, our approach allowed us to capture a broad and dynamic view of the evolutionary response to FPE stress, moving beyond a single determinant of tolerance/reduced susceptibility.

Previous studies suggest that non-synonymous mutations within *fepR* disrupt the interaction between FepR and DNA. Some of these mutations, located within the DNA-binding domain (DBD), are predicted to alter polarity and hydrogen bonding, potentially allowing water molecules to interfere with the DBD–DNA interface and thereby reducing FepR's binding affinity to the *fepRA* operator (Bolten et al., 2022). This reduced binding affinity may lead to overexpression of the efflux pump, facilitating the removal of toxic substances such as BC from the cell. Supporting this hypothesis, Douarre et al., 2022, reported that approximately 75% of detected *fepR* mutations occurred in the N-terminal region, within the helix-turn-helix (HTH) motif of the DBD, the region responsible for DNA binding. In our study, although mutations were also identified within the DBD, majority of the *fepR* mutations (8/13) were located outside of it, between -helices 4 and 9.

In addition to mutations within the coding region of *fepR*, we also detected mutations in the 5′ UTR upstream of *fepR*. This finding aligns with previous work by Schulz et al., 2023, which suggested that such mutations may lead to *fepA* derepression, resulting in a similar outcome to that caused by mutations within the *fepR* coding sequence.

Furthermore, we identified several previously unreported intergenic region mutations, including two located within the ribosome binding site, which may interfere with ribosomal binding and thus represent an alternative mechanism of FepA regulation.

Notably, the use of the ladder model allowed us to identify a putative compensatory mechanism, an insight that is only possible through longitudinal approaches such as adaptive evolution. We identified previously unreported mutations in *fepA* that co-occurred with a premature stop codon in *fepR* (E89*), with both becoming fixed in the later passages. We hypothesise that in cases where *fepR* is non-functional, leading to overexpression of *fepA*, the increased efflux activity may impose a significant metabolic burden on the cell, especially considering that in case of *fepR* inactivation there may be 6- to 64-fold increase in *fepA* expression (Guerin et al., 2014). In addition to removing toxic compounds, the overexpressed pump could potentially deplete essential nutrients or metabolites. Therefore, a loss-of-function mutation in *fepA* may reduce efflux activity to alleviate the fitness cost while still maintaining a phenotype with reduced susceptibility to BC.

Another notable observation related to adaptation to BC occurred in the *bglG* gene, transcriptional antiterminator of the phosphotransferase system (PTS) (Abdelhamed et al., 2019). Mutations in *bglG* were exclusively detected in BC-evolved biofilm lineages, suggesting that this gene may be linked not only to reduced susceptibility to BC but also to a sessile lifestyle. These findings are supported by the work of Bechtel et al., 2024, who demonstrated the upregulation of *bglG* and other PTS system genes following exposure to BC in tolerant mutants.

When focusing on metal transporters, a recurring theme throughout this chapter and those to follow, it is noteworthy that recent studies have implicated some of the metal transporters in the export of toxic substances beyond metals. For instance, in *Mycobacterium smegmatis* and *E. coli*, CorA has been suggested to mediate the export of a broad range of antibiotics and antitubercular medications, enhancing cellular tolerance to these agents (Chatterjee et al., 2024). Therefore, we hypothesise that the accumulation of mutations in *corA* may complement the role of *fepA* in antimicrobial efflux. However, this hypothesis requires further experimental validation.

As the scope of this research extended beyond adaptation to BC alone, we also directed efforts toward deciphering the mechanisms underlying adaptation to a sessile lifestyle.

Through this analysis, we identified several consistently affected functional subgroups, including transcription, energy production and conversion, nucleotide transport and metabolism as well as inorganic ion transport and metabolism. Among the most notable loci affected by mutations under biofilm lifestyle were the *ykoK* riboswitch leader, *mgtA*, and *pitA*.

A notable accumulation of mutations was detected within the *ykoK* leader (also known as the M-box riboswitch), which is located upstream of *mgtA* and is known to regulate its transcription in response to intracellular Mg^{2+} levels (as well as other divalent metal cations). While the structure of the M-box riboswitch in *L. monocytogenes* remains unresolved, structural models from *B. subtilis* have identified Mg^{2+}-binding sites essential for conformational control (Ramesh et al., 2011). We detected mutations in regions proximal to these structural elements, within sequences conserved between *L. monocytogenes* and *B. subtilis*. We hypothesise that these mutations may interfere with proper riboswitch folding and thus affect its ability to undergo Mg^{2+}-dependent conformational changes, potentially resulting in altered expression of *mgtA*.

It is worth noting that, in addition to mutations within the *ykoK* leader, we also detected co-occurring mutations in other metal transport-related genes, including *pitA* and *mgtA* itself. This pattern suggests a broader mechanism of fine-tuning of metal ion homeostasis as initial mutations in the *ykoK* leader may result in overactivation of Mg^{2+} transport, potentially triggering compensatory mutations in downstream or parallel mechanisms. *mgtA* encodes an ATP-dependent Mg^{2+} transporter that facilitates the uptake of Mg^{2+} into the cell (Maguire., 1992). Although *pitA* is not a Mg^{2+}-specific transporter, it is involved in the transport of soluble, neutral metal-phosphate ($MeHPO_4$) complexes (Harris et al., 2001). Given that Mg^{2+} readily forms salts with phosphate, alteration in transport of phosphates may lead to a change in availability of intracellular Mg^{2+}, acting as indirect Mg^{2+} regulator (Jackson et al., 2008).

Such coordinated changes likely reflect an adaptative strategy to balance Mg^{2+} acquisition with energy cost, a balance especially important in biofilms, where ionic gradients, nutrient limitations, and metabolic stress differ significantly from planktonic conditions (Booth et al., 2011).

Although the role of Mg^{2+} ions in biofilm formation by *L. monocytogenes* has not been extensively studied, our findings align with previous observations. For instance, Chalke

et al., 2022 reported that exposure to 50 mM Mg^{2+} enhanced *L. monocytogenes* biofilm formation and influenced later stages of biofilm development. Similarly, Nowak et al., 2021, showed that inactivation of *mgtB,* a gene encoding a metal transporter belonging to the same family as *mgtA*, led to reduced biofilm formation and altered architecture, resulting in distinctive sandwich-like structures. Despite these insights, a comprehensive understanding of magnesium's role in *L. monocytogenes* biofilm regulation remains lacking. Existing data across different studies are often condition-dependent, with Mg^{2+} reported to both promote and inhibit biofilm formation under varying circumstances (Mulcahy and Lewenza, 2011, Song and Leff, 2006; Mangwani et al., 2014, Oknin et al., 2015, Tang et al., 2018; Li et al., 2024). Nevertheless, taken together with our results, these studies contribute to growing evidence suggesting that Mg^{2+} ions play a role in regulation of the sessile lifestyle.

We also detected mutations in nucleotide transport and metabolism subgroup, specifically involved in biosynthesis of purines and pyrimidines, essential components for generation of nucleic acids. Three of the five primary nucleobases: cytosine (C), thymine (T), and uracil (U), are pyrimidine derivatives, and disruption of pyrimidine biosynthesis pathway is likely to limit the synthesis of these nucleobases. In our work, mutations were detected in several genes of the *pyr* operon, including *carB, pyrD, pyrF, pyrB*, and *pyrE*, all of which acquired mutations exclusively in biofilm-adapted lineages. Previous studies have linked pyrimidine biosynthesis disruption to biofilm formation. In *E. coli*, for example, inactivation of *pyrD* reduced flagellar motility and biofilm formation by downregulating the expression of type 1 fimbriae and curli subunit genes (Rossi et al., 2022). Likewise, in *Xanthomonas citri* subsp. *citri*, *carB* was required for swimming motility and biofilm development (Zhuo et al., 2015), while in *P. aeruginosa*, *de novo* UMP biosynthesis was essential for biofilm formation (Ueda et al., 2009). Involvement of *pyr* operon in biofilm formation, however, represents a novel finding in the biology of *L. monocytogenes*. Notably, pyrimidine analogues have been trialled as biofilm inhibitors with compounds like 5-fluorouracil, 5-fluorocytosine and 5-fluorouridine which demonstrated antivirulence and antibiofilm properties in different bacteria (Ravishankar et al., 2024). We hypothesise that disruption of pyrimidine biosynthesis in *L. monocytogenes* may act as a cellular stress signal, as impaired nucleotide production would directly affect DNA and RNA synthesis. Such stress could lead to the downregulation of biofilm-associated genes and potentially trigger biofilm dispersal or a shift to planktonic growth. This would

be consistent with stress-response mechanisms previously observed in *P. aeruginosa* (Nair et al., 2021).

We also identified biofilm-associated mutations in *rsbU*, a positive regulator of the alternative sigma factor SigB, which controls approximately 300 genes involved in stress tolerance and survival (Chaturongakul et al., 2011). Supporting the link between *rsbU* and biofilm lifestyle, *rsbU* deletion has been previously implicated in increased extracellular matrix production of *L. monocytogenes* (Hsu et al., 2020).

Notably, a longitudinal approach of adaptive evolution allowed us to detect a putative compensatory mechanism within the *rsb* operon. As such, a premature stop codon in *rsbW* co-occurred within the same lineage as the S41* premature stop codon in *rsbU* and only became fixed in the later passages. Such an evolutionary trajectory may select for a compensatory mechanism in which the *rsbW* loss-of-function mutation mitigates the exaggerated stress response caused by a dysfunctional *rsbU*.

Conflicting with the findings by Douarre et al., 2022, who detected association between mutations in *rsbU* and reduced susceptibility to BC, in our study *rsb* operon mutations were exclusively associated with the biofilm lineages.

Finally, we did not detect a response of accumulated mutations on biofilm formation, likely due to the sensitivity of the assays employed being insufficient to detect subtle phenotypic changes. From an adaptive evolution perspective, even subtle phenotypic shifts can confer enough selective advantage for mutations to become fixed within evolving populations. The convergence of mutations within specific pathways in independently evolving lineages supports this hypothesis. In the following chapters, we will explore in greater depth the connection between phenotype and genotype of BPM detected pathways, employing a targeted gene deletion approach.

It is worth noting that previous bead-based adaptive evolution models have reported mixed outcomes: some studies observed increased biofilm production in evolved lineages, which was interpreted as advantageous (Trampari et al., 2021), while others found no effect on total biomass generation (Wickham, 2021). Together with our findings, this variability suggests that changes in biofilm forming capacity are species- and model-specific. Moreover, increased bacterial biomass alone may not confer a survival advantage under FPE-like conditions. Instead, long-term adaptation in nutrient-

limited environments may favour traits that optimise persistence, likely due to the sustained energetic demands of biofilm-associated lifestyles and the continual requirement for population recovery across serial passages.

4.8. Conclusion

In **Chapter 4,** we established and executed a BPM experiment over 30 consecutive passages of adaptive evolution. WGS of evolved isolates revealed mechanisms that may be associated with persistence and niche adaptation of *L. monocytogenes* in FPE. Non-synonymous mutations were identified in genes and pathways related to efflux, metal homeostasis, stress response, and nucleotide biosynthesis. Reduced susceptibility to BC emerged through multiple independent mutations in the *fepRA* operon, which encodes the FepR transcriptional repressor and the FepA MATE family efflux pump. These mutations occurred in both planktonic and biofilm-associated populations, leading to comparable levels of reduced susceptibility to BC across both lifestyles. Fixed mutations specific to biofilm lineages highlighted several loci involved in long-term adaptation, including the *ykoK* leader region, the pyrimidine biosynthesis operon, and the stress response gene *rsbU*.

Collectively, we demonstrated that *L. monocytogenes* biofilms are highly sensitive to low concentrations of FPE disinfectants such as BC, and rapidly develop a phenotype exhibiting reduced susceptibility. Our findings also provide new insights into the genetic mechanisms underlying biofilm persistence within FPEs and identify potential targets exploited by *L. monocytogenes* to establish and maintain niches under otherwise unfavourable conditions. Importantly, the use of an evolutionary model enabled us to capture compensatory mechanisms and broad evolutionary trajectories that are not detectable through single time-point analyses or short-term stress exposures, highlighting the value of longitudinal approaches. Future investigations (**Chapter 5 - 6**) will focus on characterising the mechanisms associated with these targets and their roles in biofilm formation and persistence.

Chapter 5: Generation of nonpolar in-frame deletion mutants in *Listeria monocytogenes* for target genes detected in biofilm persistence model

5.1. Contributions

Oleksii Omelchenko, Ana Victoria Gutiérrez, Mark Webber, Matthew Gilmour.

5.2. Aknowledgments

The pKSV7 shuttle plasmid was kindly provided by Professor Martin Loessner (ETH Zürich).

5.3. Introduction

Generating targeted gene deletions is a fundamental molecular biology approach for the characterisation of gene function in bacteria (Ishikawa and Hori, 2013). In contrast to transposon insertions or other insertion-based mutagenesis methods, which may cause polar effects on downstream genes (Hutchison et al., 2019; Mateus et al., 2021), targeted deletions enable a more precise evaluation of the gene function.

One of the first and widely-used plasmids developed for constructing in-frame deletions in *L. monocytogenes* was described by Camilli et al., 1993. This system utilised the temperature-sensitive shuttle plasmid pKSV7, which carries genes conferring ampicillin tolerance for selection in *E. coli* and chloramphenicol tolerance for expression in *L. monocytogenes*. Initial transformations in *L. monocytogenes* were carried out by electroporation method of penicillin-treated cells (Park and Stewart, 1990) and using protoplast methods (Camilli et al., 1993). In 1999, Promadej et al., introduced a more efficient electroporation-based method, significantly improving genetic manipulation in *L. monocytogenes*. Another method was published in 2008 by Monk et al., which described electroporation method with 125-fold increased transformation efficiency compared with the widely used protocol of Park and Stewart.

In 2014, a new approach for generating in-frame deletion mutants in *L. monocytogenes* was developed, utilising the splicing by overlap extension PCR (SOEing-PCR) technique (Rychli et al., 2014; Rychli et al., 2021; Horton et al., 1990). In SOEing-PCR, two DNA fragments flanking the target gene are initially amplified using primers that incorporate an overlapping sequence. An overlap allows the fragments flanking the target gene to fuse into a single continuous amplicon, which can be introduced into pKSV7 vector through cloning. pKSV7 plasmid with a desired construct can be then transformed into homologous regions of the *L. monocytogenes* chromosome by cultivating the bacteria at

a restrictive temperature (42 °C) in the presence of chloramphenicol, conditions where plasmid cannot replicate independently. Plasmid excision and the second crossover allelic exchange resulting in deletion of the target gene is then identified by a loss of chloramphenicol tolerance at permissive temperature (30 °C) following multiple passages in the absence of selective pressure (chloramphenicol). Since its introduction, the SOEing-PCR method has been extensively used to create deletions and other allelic exchange mutants in *L. monocytogenes* (Schmid et al., 2009; Kovacevic et al., 2016; Shi et al., 2024; Ma et al., 2024).

A number of other plasmids have been developed for introducing mutations in *L. monocytogenes* including pAUL-A, pLSV1, pMAD, pGF-EM and (Wuenscher et al., 1991; Li and Kathariou, 2003; Arnaud, Chastanet and Debarbouille, 2004; Abdelhamed, Lawrence and Karsi, 2015; Schneewind and Missiakas, 2014; Schuster, Howard and Gründling, 2019). These plasmids have been successfully used for introduction of gene deletions in *L. monocytogenes*, but similarly to pKSV7 system, they lack selection markers for the second recombination event. Vectors employing antisense *secY* expression for positive selection of the second allelic exchange have been developed for Gram-positive species, including pKOR1 and pIMAY (Bae and Schneewind, 2006, Monk et al., 2012), but there have been reports of unsuccessful transformation of *L. monocytogenes* (Abdelhamed, Lawrence and Karsi, 2015).

Based on previous successes and the reported efficiency of the pKSV7 system facilitated by the SOEing-PCR method, we chose to adopt the protocol described by Rychli et al., 2021. With this approach, we aimed to generate nonpolar, in-frame deletions of the genes *pyrD, carB, rsbU, mgtA, corA, bglG*, *pitA* and genetic region *ykoK*, which were identified through the BPM in **Chapter 4** to play a role in biofilm formation and reduced susceptibility to disinfectant. Although mutations in *fepR* were clearly associated with reduced susceptibility to BC throughout the BPM experiment, we did not generate a *fepR* deletion strain, as the role of *fepR* in adaptation to BC has already been thoroughly investigated (Guerin et al., 2014; Bolten et al., 2022; Douarre et al., 2022). Functional characterisation of targeted genes will be evaluated in **Chapter 6**.

5.4. Aims

1. To construct nonpolar in-frame deletion mutants in the parental strain BL87-028 for genes associated with reduced susceptibility to BC and adaptation to biofilm lifestyle.

5.5. Results

5.5.1. Construction of pKSV7 Vectors for Deletion of Target Genes

For the generation of deletion mutants, we selected a homologous recombination-based approach (**Figure 34**), facilitated by SOEing-PCR (Rychli et al., 2021) with the thermosensitive 7.1 kbp shuttle vector pKSV7 (**Appendix 17**), which confers tolerance to both ampicillin and chloramphenicol.

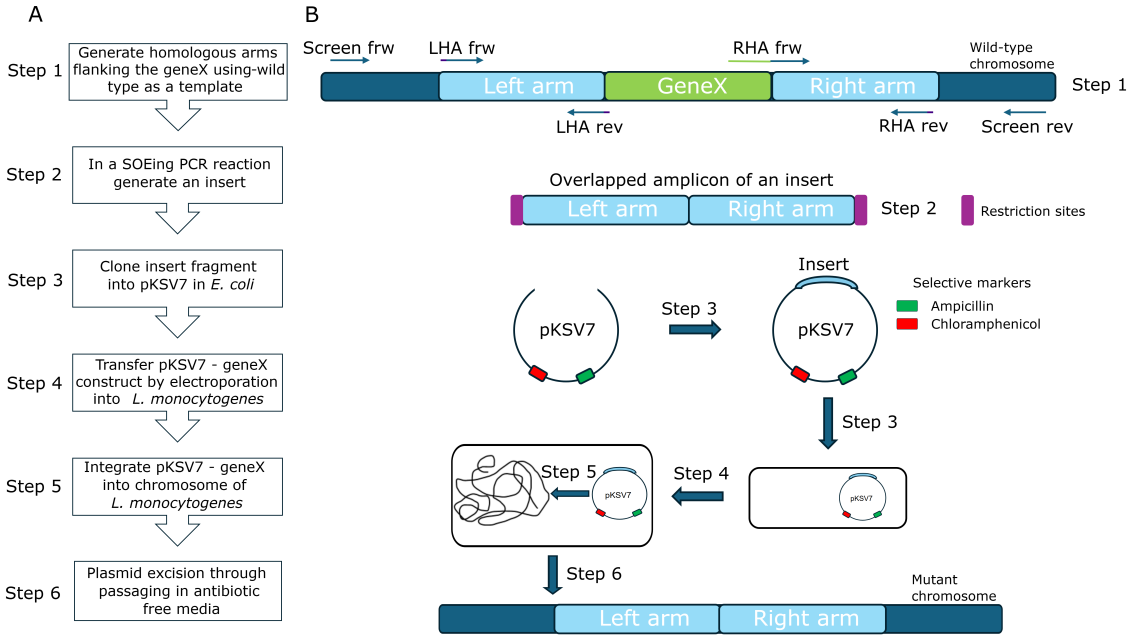


Figure 22. An overview of the method for the construction of nonpolar in-frame gene deletion mutants (Rychli et al., 2021). (**A**) A flow diagram illustrates the six key steps of the method, from generation of homologous arms (step 1) to plasmid excision (step 6). (**B**) Schematic workflow outlining the construction of nonpolar in-frame gene deletion mutants using the pKSV7 vector and SOEing-PCR. Abbreviations: LHA – Left Homologous Arm, RHA – Right Homologous Arm, frw – Forward, rev – Reverse.

The genetic features for deletion varied in size with the largest gene to be deleted was *carB* at 3213 bp and the smallest region - *ykoK* at 167 bp (**Table 11**).

Table 11. Indicating the size of loci selected for deletion. Sizes indicated in base pairs.

Loci	Size (bp)
ykoK	167
mgtA	2571
rsbU	1005
pyrD	915
carB	3213
corA	945
bglG	2031
pitA	999

5.5.1. Step 1 - Creation of Homologous Arms

In the first step (**Figure 34**), sequences flanking the gene of interest were amplified to produce left and right homologous arms. These homologous arms were generated by PCR using genomic DNA from the parental strain *L. monocytogenes* BL87-028 as a template and the gene-specific primers (see section 2.9.1.1 '**Primer Design**'; **Table 2**). For deletion constructs targeting *rsbU* and *pyrD*, homologous regions were used ranging from 996 to 1024 bp to account for recombination efficiency.

However, amplification of similarly long fragments was not successful for other target genes. Therefore, for *corA*, *bglG*, *mgtA*, *ykoK*, *carB*, and *pitA*, we reduced the size of each homologous arms to the range of 395 – 497 bp per amplicon (**Table 2; Figure 35**).

Successful amplification of all homologous arms was confirmed by PCR (**Figure 36**).

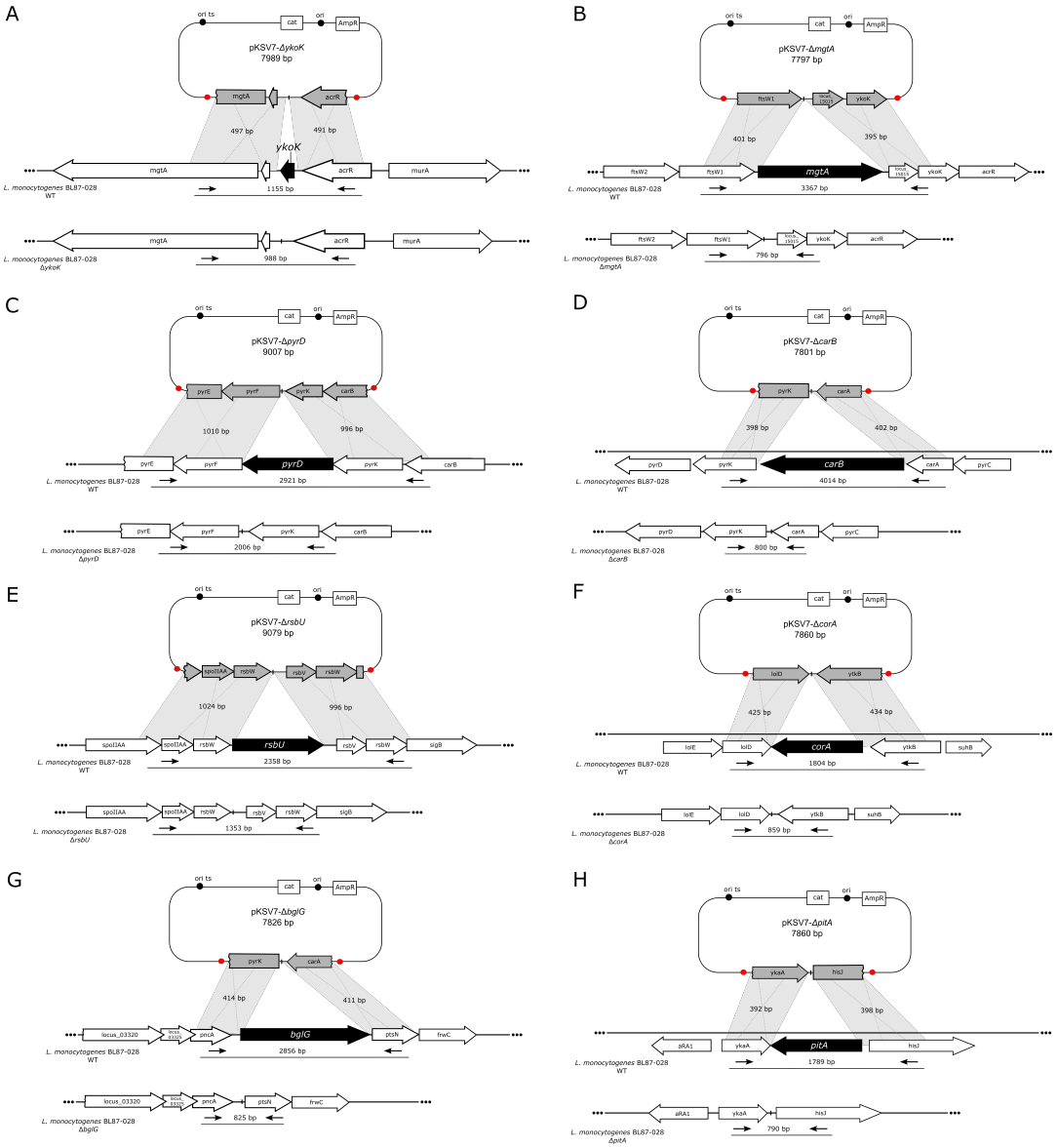
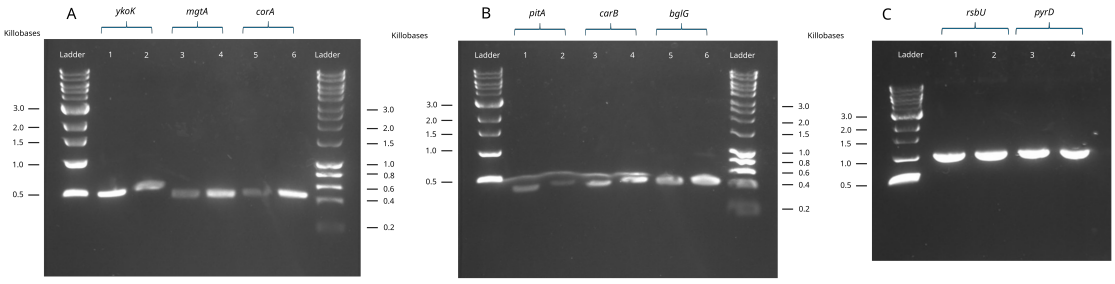


Figure 23. Schematic representation of pKSV7 plasmid constructs used for the generation of nonpolar knockout mutants. The diagram illustrates the wild-type gene arrangement in the parental strain alongside the expected configuration following successful knockout, with corresponding sizes indicated in base pairs. Red circles indicate primers flanking the multiple cloning site (MCS). Constructs are shown for the targeted deletion of (**A**) *ykoK,* (**B**) *mgtA,* (**C**) *pyrD,* (**D**) *carB,* (**E**) *rsbU,* (**F**) *corA,* (**G**) *bglG* and (**H**) *pitA*. Plasmid maps were generated using Inkscape.



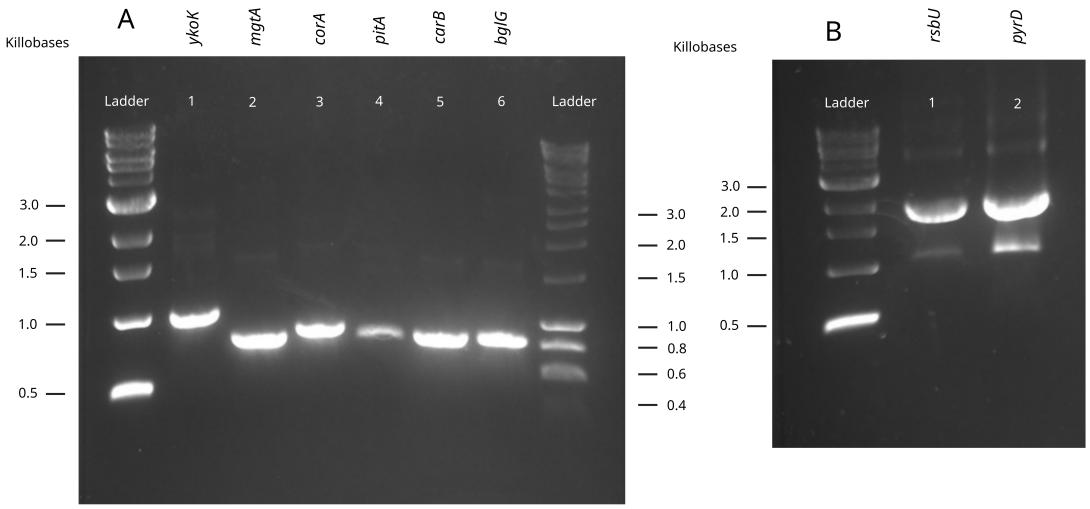
D

Loci	Amplicon	Size(bp)
ykoK	Left homologous arm	497
	Right homologous arm	491
mgtA	Left homologous arm	401
	Right homologous arm	395
corA	Left homologous arm	425
	Right homologous arm	434
pitA	Left homologous arm	392
	Right homologous arm	398
carB	Left homologous arm	398
	Right homologous arm	402
bglG	Left homologous arm	414
	Right homologous arm	411
rsbU	Left homologous arm	1024
	Right homologous arm	996
pyrD	Left homologous arm	1010
	Right homologous arm	996

Figure 24. Generation of homologous arms for deletion mutants. Left and right homologous arms were generated for each deletion mutant using the parental strain as a template. In panel (**A**), the following homologous arms are included: Lane 1 – *ykoK* left arm, Lane 2 – *ykoK* right arm, Lane 3 – *mgtA* left arm, Lane 4 – *mgtA* right arm, Lane 5 – *corA* left arm, Lane 6 – *corA* right arm. In panel (**B**): Lane 1 – *pitA* left arm, Lane 2 – *pitA* right arm, Lane 3 – *carB* left arm, Lane 4 – *carB* right arm, Lane 5 – *bglG* left arm, Lane 6 – *bglG* right arm. In panel (**C**): Lane 1 – *pyrD* left arm, Lane 2 – *pyrD* right arm, Lane 3 – *rsbU* left arm, Lane 4 – *rsbU* right arm. Predicted sizes are indicated in kilobases. A 1 kb DNA ladder was used as a molecular weight marker in all panels; panels **A** and **B** included the 1 kb DNA ladder, and HyperLadder. (**D**) The exact sizes of the amplified fragments are listed in base pairs. Bands corresponding to the expected sizes were excised and purified for further processing.

5.5.2. Step 2 - Creation of the Inserts

In the second step (**Figure 34**), homologous arms were fused in an overlap PCR reaction to form a single amplicon of an insert (see section 2.9.1.2 '**Polymerase chain reaction**'), which subsequently was confirmed by PCR (**Figure 37**).



C

Loci	Amplicon	Size(bp)
ykoK	Overlap	988
mgtA	Overlap	796
corA	Overlap	859
pitA	Overlap	790
carB	Overlap	800
bglG	Overlap	825
rsbU	Overlap	1353
pyrD	Overlap	2006

Figure 25. Generation of the overlapping fragments for deletion mutants. Overlapping fragments of the following loci were amplified and are shown in Panel (**A**): Lane 1 – *ykoK*, Lane 2 – *mgtA*, Lane 3 – *corA*, Lane 4 – *pitA*, Lane 5 – *carB*, Lane 6 – *bglG*; and Panel (**B**): Lane 1 – *rsbU*, Lane 2 – *pyrD*. Predicted fragment sizes are indicated in kilobases. A 1 kb DNA ladder and HyperLadder were used as molecular weight markers. (**C**) The exact sizes of the amplified fragments are listed in base pairs**.** Bands corresponding to the expected sizes were excised and purified for further processing.

5.5.3. Step 3 - Cloning of the Final Constructs

The insert fragment and the empty pKSV7 vector were digested with the appropriate restriction enzymes (**Table 2**). The insert was subsequently ligated into the pKSV7 plasmid and introduced into *E. coli* (step 3 **Figure 34;** see section 2.9.1.7 '**Cloning of the Insert into Vector pKSV7 (Ligation)**'). Transformants were screened for growth on carbenicillin-supplemented media, and several randomly selected colonies were subjected to colony PCR using primers flanking the multiple cloning site (MCS) (**Figure**

35). The expected PCR product size corresponded to the predicted size of the overlap fragment, confirming successful ligation.

5.5.3.1. Whole Plasmid Sequencing Confirmed Correct Integration of the Inserts Into pKSV7 Vector

Colonies with expected PCR product sizes were processed to extract plasmid DNA which then undergone whole plasmid sequencing. The sequencing reads were first analysed on a virtual gel electrophoresis, organised by read length frequency (**Figure 38; Appendix 18(I – VII)**).

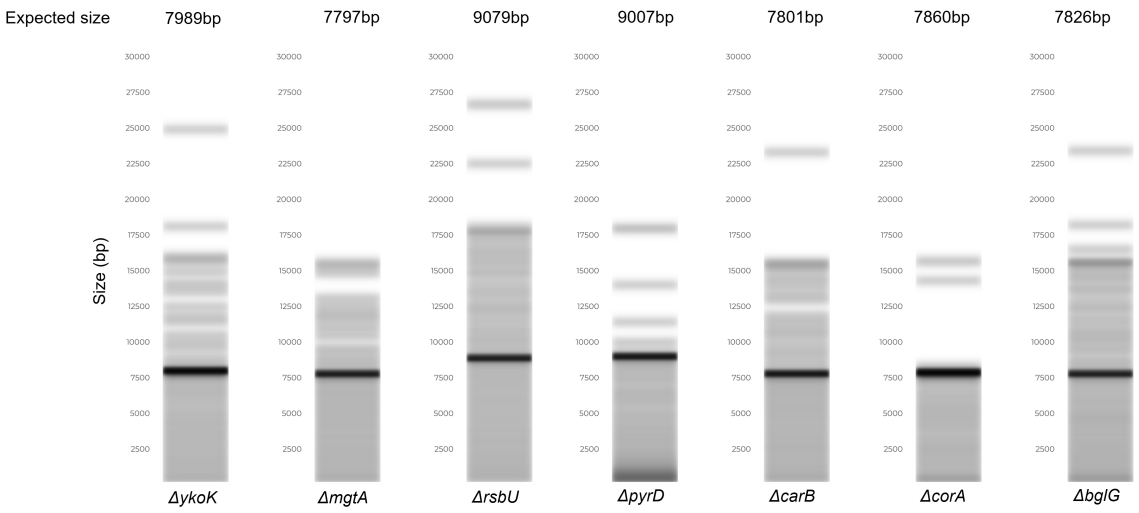


Figure 26. Virtual gel electrophoresis of pKSV7 plasmid reads containing inserts for generation of each mutant strain (Δ*ykoK*, Δ*mgtA*, Δ*rsbU*, Δ*pyrD*, Δ*carB*, Δ*corA*, Δ*bglG*). The image shows the bands of read counts at particular fragment sizes. A single bright band at the expected plasmid size corresponds to an intact plasmid, with the expected plasmid sizes indicated at the top. Each lane corresponds to a different mutant construct (bottom).

Sequencing data for the seven pKSV7-based plasmids (**Table 12**) revealed dominant read length peaks corresponding closely to the expected sizes of the plasmids. Although larger DNA fragments were detected in all samples, likely representing sheared *E. coli* chromosomal DNA, these appeared as faint smear, suggesting minimal contamination. The proportion of reads corresponding to the dominant peak (i.e., the expected plasmid size) ranged from 25.0% for Δ*bglG* to 40.4% for Δ*ykoK*.

Table 12. Summary of whole-plasmid sequencing results for pKSV7-based deletion constructs. The table presents the expected plasmid size, the most abundant read length peak, the proportion of reads corresponding to the most abundant peak, and the percentage of reads falling within ±1,000 bp of the expected size.

Plasmid	Expected Size (bp)	Most Abundant Peak (bp)	% of Reads at Peak	% Within ±1,000 bp
pKSV7 - Δ*ykoK*	7,989	~8,000	40.40%	49.00%
pKSV7 - Δ*mgtA*	7,797	~7,800	37.30%	47.00%
pKSV7 - Δ*rsbU*	9,079	~8,900	42.60%	48.20%
pKSV7 - Δ*pyrD*	9,007	~8,700	26.40%	40.30%
pKSV7 - Δ*carB*	7,797	~7,800	33.30%	42.40%
pKSV7 - Δ*corA*	7,860	~7,900	34.20%	59.30%
pKSV7 - Δ*bglG*	7,826	~7,800	25.00%	29.60%

Next, the insert regions in each pKSV7 construct apart from pKSV7-Δ*pitA* construct (failed at ligation phase; see section 5.5.3.2. '**Deletion of a Base Pair Within the pKSV7-Δ*pitA* Construct**') were aligned against the corresponding reference insert sequences to confirm construct integrity. Generated insert fragments for all gene deletions (apart from pKSV7-Δ*pitA*) had 100% identity match when aligned against the reference fragments (**Appendix 19(I – VI)**).

5.5.3.2. Deletion of a Base Pair Within the pKSV7-ΔpitA Construct

For the Δ*pitA* construct, we successfully generated the desired overlapping fragment, as confirmed by PCR (**Figure 37**). However, despite multiple attempts, ligation of the fragment into the pKSV7 vector consistently failed. Repeated trials using standard ligation protocols did not yield successful transformants, indicating a possible incompatibility with *E. coli* host.

To overcome these challenges, we outsourced the synthesis of a 790 bp Δ*pitA* insert and its subsequent cloning into pKSV7 vector. The insert was generated via oligonucleotide synthesis and assembled into an overlapping fragment without PCR amplification. The synthesised fragment was subsequently cloned into the pKSV7 vector. Successful insertion was confirmed by restriction digestion with HpaI and EcoRI enzymes, which yielded the expected band sizes (~2559 bp and ~5220 bp) on gel electrophoresis (**Figure 39**).

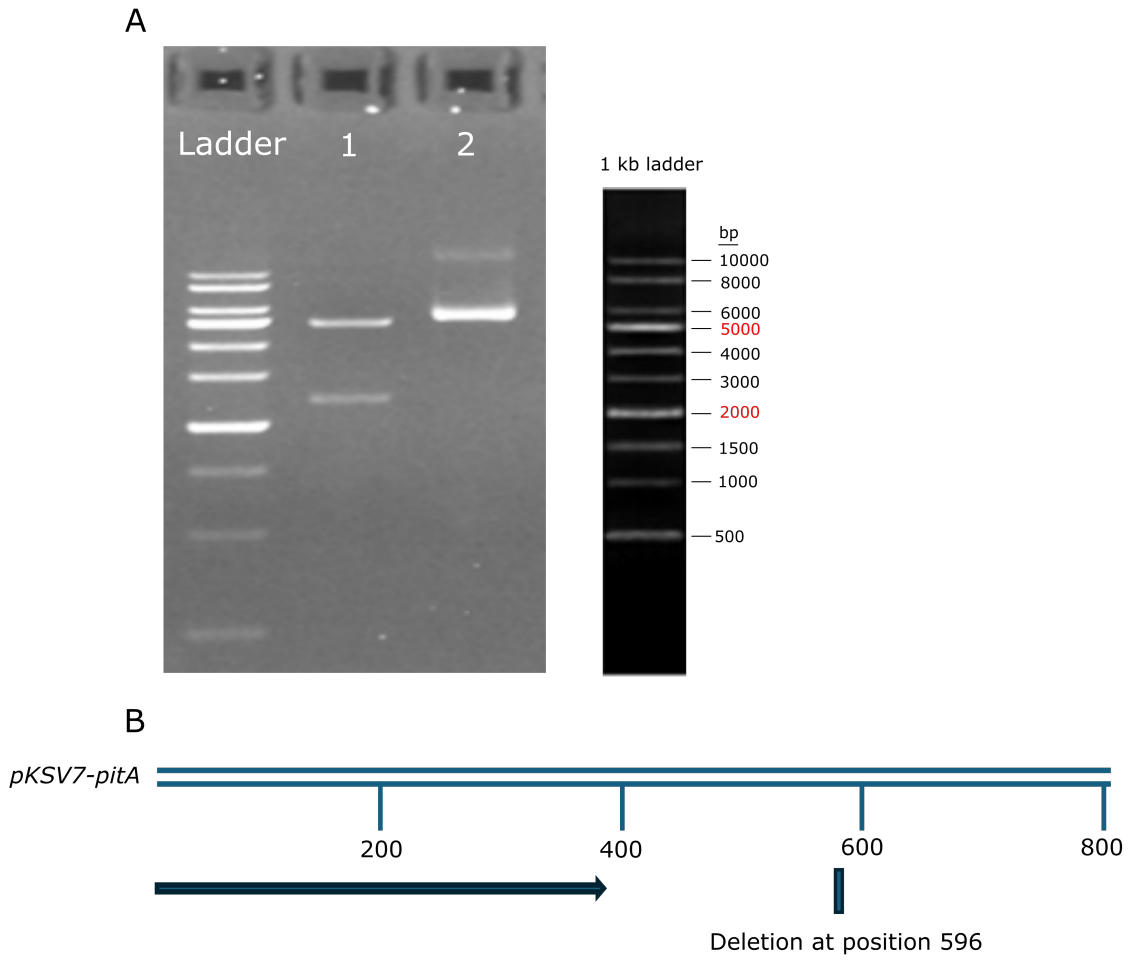


Figure 27. pKSV7 construct for *pitA* deletion. (**A**) **Agarose gel electrophoresis of candidate pKSV7-Δ*pitA* plasmid**. Lane 1: pKSV7-Δ*pitA* digested with HpaI and EcoRI, showing expected fragment sizes of 5220 bp and 2559 bp. Lane 3: Undigested pKSV7-Δ*pitA* plasmid. (**B) Sequence verification of pKSV7-Δ*pitA***, indicating a deletion at position 596 within the insert. Visualised with SnapGene Viewer. A 1 kb DNA ladder was used as molecular weight marker.

However, Sanger sequencing revealed a deletion at position 596 within the insert (**Figure 39B**). Multiple attempts, including re-synthesis and transformation into alternative *E. coli* strains (i.e. DH5α, TOP10F', EPI300) at different incubation temperatures, repeatedly resulted in constructs containing deletions.

When we predicted secondary structure of the *pitA* insert, we obtained a complex, highly branched structure with multiple long stem-loops, internal bulges and free energy ΔG = −165.20 kcal/mol, reflecting strong intramolecular base pairing (**Figure 40**). Such structures are likely to interfere with the cloning steps. Given the recurring issues and project time constraints, we discontinued efforts to generate the *pitA* deletion mutant.

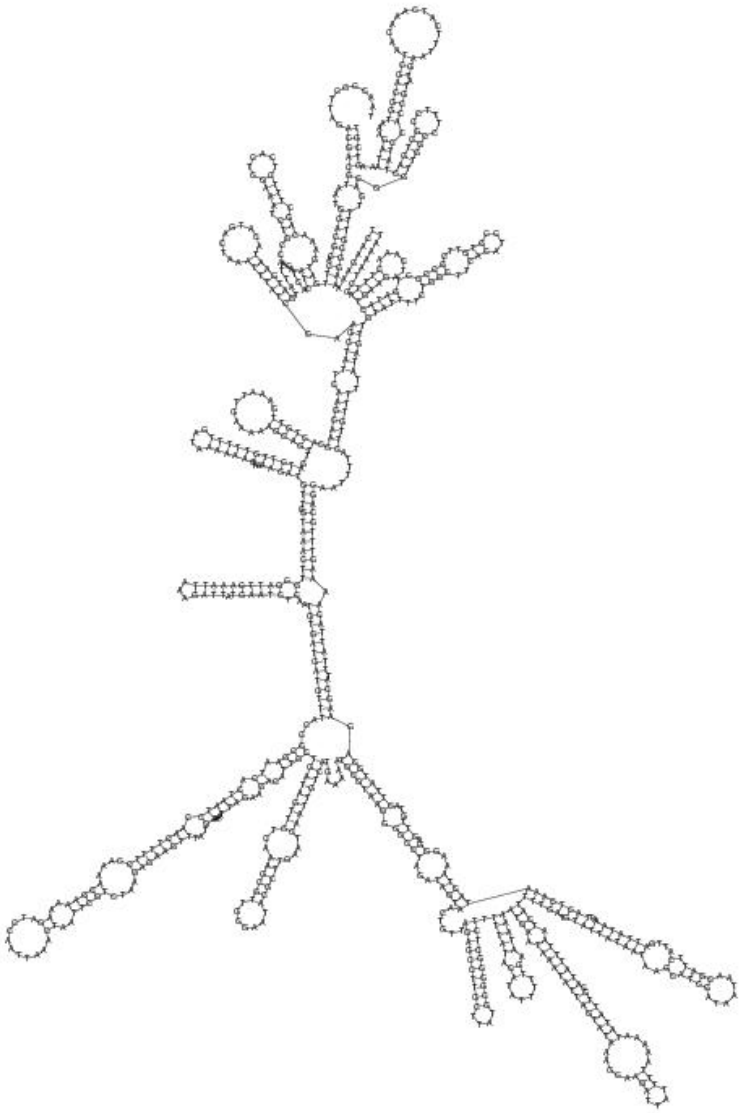


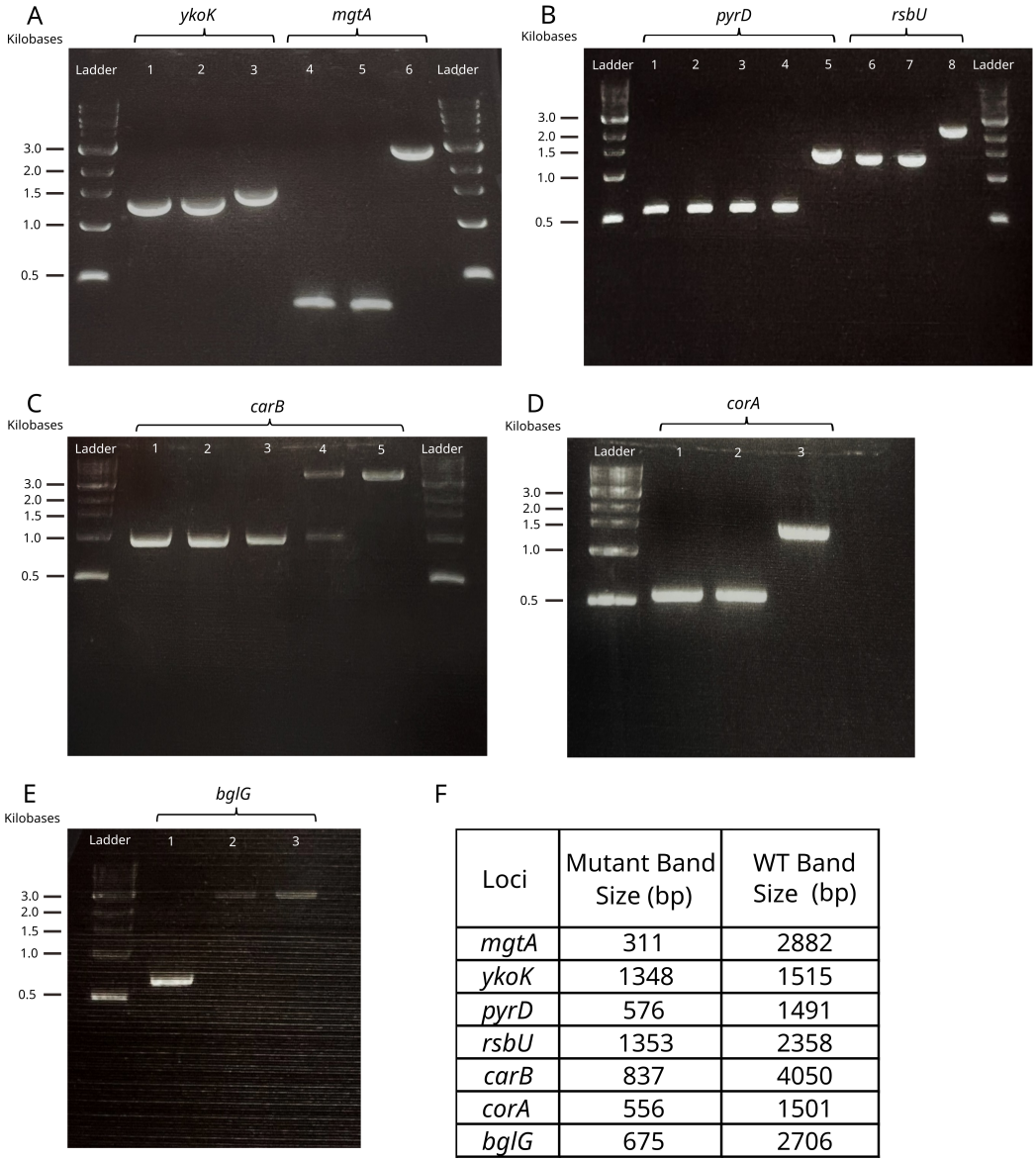
Figure 28. Predicted secondary structure of the *pitA* deletion construct insert. The 790 bp fragment was generated from overlapping homologous arms flanking the *pitA* gene. Secondary structure prediction, using the VectorBuilder online tool, indicates the presence of multiple stable stem-loops and hairpins, with a calculated free energy ΔG = −165.20 kcal/mol, suggesting strong secondary structure formation, which may interfere with downstream molecular cloning steps.

5.5.4. Steps 4 - 6 - Successful Deletion Mutants for *corA, bglG, mgtA, ykoK, carB, rsbU* and *pyrD* Were Obtained in the Second Recombination Event

In steps 4 and 5 (**Figure 34**) we transformed *L. monocytogenes* with the pKSV7 constructs which were then integrated into the chromosome of BL87-028 strain (see section 2.9.3.2 '**Chromosomal Integration and Plasmid Excision**'). In the final step 6 (**Figure 34**), sequential subculturing at lower temperatures (permitting plasmid replication) induced a second crossover event, leading to plasmid excision. This resulted in subpopulations that

either revert to the WT or incorporate the SOEing fragment in place of the target gene, consequently generating the desired deletion mutant.

To confirm successful gene deletions, 'Screen' primers (see section 2.9.3.2 '**Chromosomal Integration and Plasmid Excision**') were used to perform colony PCR on candidate mutant isolates. The size of the PCR fragments in putative mutant isolates was expected to be smaller than in the parental strain, with the size difference corresponding to the length of the deleted gene. For all deletion mutants (Δ*ykoK,* Δ*mgtA,* Δ*pyrD,* Δ*rsbU,* Δ*carB,* Δ*corA*, Δ*bglG*), colony PCR confirmed the generation of the desired deletion genotypes (**Figure 41**).



F

Loci	Mutant Band Size (bp)	WT Band Size (bp)
mgtA	311	2882
ykoK	1348	1515
pyrD	576	1491
rsbU	1353	2358
carB	837	4050
corA	556	1501
bglG	675	2706

Figure 29. Confirmation of successful mutant generation by PCR product size visualised on the agarose gel. (**A**) Lane 1: Δ*ykoK1*, Lane 2: Δ*ykoK2*, Lane 3: WT (*ykoK*), Lane 4: Δ*mgtA1*, Lane 5: Δ*mgtA2*, Lane 6: WT (*mgtA*); (**B**) Lane 1: Δ*pyrD1*, Lane 2: Δ*pyrD2*, Lane 3: Δ*pyrD3*, Lane 4: Δ*pyrD4*, Lane 5: WT (*pyrD*), Lane 6: Δ*rsbU1*, Lane 7: Δ*rsbU2*, Lane 8: WT (*rsbU*); (**C**) Lane 1: Δ*carB1*, Lane 2: Δ*carB2*, Lane 3: Δ*carB3*, Lane 4: Mixed community (Δ*carB* + WT), Lane 5: WT (*carB*); (**D**) Lane 1: Δ*corA1*, Lane 2: Δ*corA2*, Lane 3: WT (*corA*); (**E**) Lane 1: Δ*bglG1*, Lane 2: WT (*bglG*), Lane 3: WT (*bglG*). (**F**) The table summarises the predicted band sizes (bp) obtained by PCR screening of knockout mutants and their corresponding WT strains for each targeted gene. Successful deletion is indicated by a smaller amplicon corresponding to the size of the recombined fragment lacking the open reading frame (ORF), while the WT strain yields a larger product containing the intact gene. DNA size marker: Quick-Load 1 kb; molecular weight in kilobases (kb) indicated alongside gel.

5.5.4.1. Whole Genome Sequencing Assessment of Mutant Strain Following Gene Deletion

Once the *L. monocytogenes* colonies suspected of gene deletion undergone PCR screening, they were also validated for gene deletion using WGS. This confirmed the deletion of the target gene and overall genomic integrity of the mutant strains. No mutations were detected in the genes flanking the deleted regions.

Resulting genomes were aligned to the hybrid assembly of the parental strain to screen if other background mutations outside the target loci accumulated over the course of plasmid integration and excision (**Appendix 20(I – VII)**).

Sequence variations were detected across all mutants. The majority of these mutations were synonymous and therefore presumed to have minimal phenotypic impact and as such, they were not further analysed.

A number of non-synonymous mutations were detected in coding regions, and additional variants were found in intergenic regions, which may exert regulatory or functional effects, and therefore were examined in more detail.

The Δ*carB* mutant contained the highest number of non-synonymous mutations compared to other mutant strains, with 8 mutations, in addition to 2 mutations in the intergenic regions. This may be associated with the longer plasmid excision period of 20 passages to obtain Δ*carB* strain, compared to 12 passages required to generate a mutant on average, giving more time for mutations to accumulate.

Several non-synonymous and intergenic mutations were found to recur independently across multiple mutant strains, suggesting these regions may hold adaptive significance under stress conditions (**Table 13**; **Appendix 20**).

One such example is the gene encoding the LPXTG cell wall anchor domain-containing protein, where an in-frame deletion was identified in the Δ*mgtA*, Δ*ykoK*, Δ*bglG*, Δ*carB* and Δ*corA* strains. Mutations in this region were also frequently observed in the BPM experiment under various conditions (see section 4.5.4. '**Grouping Mutations by Selective Pressure**'), supporting the hypothesis that the gene encoding the LPXTG cell wall anchor domain, exhibits an increased mutation rate when the cells are exposed to mild stress. Alternatively, the mutation may not be related to the knockout creation and instead occurred following generation of the hybrid assembly.

Another recurrently mutated locus encoded for the exonuclease, where missense variants were detected in Δ*carB,* Δ*pyrD* and Δ*ykoK* strains, while mutations in *Lin2401* were found in the Δ*bglG* and Δ*ykoK* strains (**Table 13**).

Table 13. Summary of non-synonymous and intergenic background mutations in *L. monocytogenes* deletion mutant strains. Mutations were identified using Snippy by aligning each mutant genome to the hybrid assembly of the parental strain. Only non-synonymous mutations in ORFs are shown. Genes mentioned with intergenic region mutations correspond to the mutations located upstream of the mentioned genes. In green mutations that were present, in white - absent.

Location of mutation	Mutated region	Δ*ykoK*	Δ*mgtA*	Δ*rsbU*	Δ*pyrD*	Δ*carB*	Δ*corA*	Δ*bglG*
ORF	LPXTG domain							
	Exonuclease							
	Lin2401 protein							
	sulP							
	lap							
	Hypothetical protein							
	inlJ							
	TIVSS DNA transfer protein							
	nfnB							
	rliA							
	rli117							
	rli38							
	rli48							
	rnja							
	Leucine-rich repeat protein							
Intergenic regions	IR *rli34*							
	IR class I internalin							
	IR glycosyltransferase							
	IR IS3 transposase							
	IR *yokD*							
	IR *inlF*							
	IR *aroD*							

Notably, a single hypothetical protein carried non-synonymous mutations in multiple strains, including Δ*bglG*, Δ*corA*, Δ*mgtA*, Δ*carB* and Δ*pyrD*, pointing to potential adaptive significance in the context of the BPM. Prediction of the functional domains of the hypothetical protein yielded no reportable results (InterPro).

Additionally, two missense mutations were found in a plasmid-borne gene of Δ*mgtA* encoding a type IV secretory system conjugative DNA transfer family protein which also co-occurred in Δ*ykoK,* Δ*carB* strains (**Table 13**).

In the Δ*rsbU* strain, missense mutations were identified in *sulP* and *lap*, which encode an inorganic anion transporter (Saier, 2000; Zolotarev et al., 2008) and an adhesion-

mediating acetaldehyde dehydrogenase (Jagadeesan et al., 2010), respectively (**Table 13**).

In the Δ*pyrD* strain mutation affected *inlJ*, which encodes internalin J (Sabet et al., 2005).

The Δ*corA* strain exhibited mutations in *nfnB*, which encodes a nitroreductase family protein (Liochev et al., 1999; Pomposiello et al., 2001), and in *rli117*, a gene encoding the *Listeria* small RNA *rli117* (**Table 13**).

Notably, mutations in small RNAs such as *rli117* were commonly observed across different conditions in the BPM experiment, suggesting their potential role in general stress adaptation.

Similarly, in the Δ*bglG* strain, a mutation was identified in another small RNA gene, *rliA*, and in Δ*carB* mutant strain mutations were detected in 3 *rli* regions including *rliA*, *rli38* and *rli48* (**Table 13**).

5.6. Discussion

In this chapter, we aimed to construct nonpolar in-frame deletion mutants in the parental strain, for genes associated with reduced susceptibility to BC and adaptation to biofilm lifestyle, for their subsequent phenotypic characterisation.

We encountered persistent issues in generating a *pitA* deletion mutant. The pKSV7-Δ*pitA* constructs consistently contained a single-nucleotide deletion, and despite multiple attempts, we were unable to obtain a construct with the correct sequence. This persistent instability suggested a possible incompatibility of the Δ*pitA* fragment with *E. coli*, potentially due to unintended recombination or toxic effects. Various competent *E. coli* strains were tested under different environmental conditions, however, these efforts did not resolve the issue. To investigate potential sequence-related causes, we predicted the secondary structure of the Δ*pitA* insert. The analysis revealed a complex and highly branched conformation, characterised by multiple stem-loops and internal bulges, suggesting a stable structure that could interfere with molecular cloning. In particular, folding at the insert ends may obstruct ligase access or prevent proper alignment, as a result reducing ligation efficiency. Additionally, stable intramolecular structures can promote replication slippage and may negatively impact plasmid propagation (Gacy and McMurray, 1998). As a long-term strategy to improve cloning efficiency, we could

consider using *E. coli* ER1821R competent cells, which are deficient in methylcytosine and methyladenine restriction systems ($McrA^-$, $McrCB^-$, $McrF^-$, Mrr^-, $HsdR^-$), endonuclease I ($endA^-$), and recombination pathways ($recB^-$, $recJ^-$) (Jobling, Raleigh and Frank, 2016).

Several aspects of the protocol described by Rychli et al., 2021, required optimisation to suit our laboratory settings. During chromosomal integration of the plasmid under selective pressure with chloramphenicol at 42 °C, we observed inefficient initial growth, which in multiple cases did not let to continue with plasmid integration. Notably, an unpublished protocol by Bolten and Roberts (2012) recommends initiating chromosomal integration at 40 °C or below to facilitate the process. We adopted a gradual temperature reduction strategy, beginning at 41 °C and lowering the temperature by 1 °C increments, but not going below 39 °C. With the temperature reduction approach, efficiency of chromosomal integration improved. Alternatively, extending the duration of the initial growth phase (passage 1) beyond the standard 24 hours, during the chromosomal integration of pKSV7, may also be beneficial, with growth sometimes requiring up to 72 hours.

For plasmid excision, the unpublished protocol by Bolten and Roberts recommends initiating replica plating after three passages in antibiotic-free media, typically obtaining mutants by passage 10. In contrast, Rychli et al., 2021 protocols suggest beginning replica plating after 10 passages, with mutants appearing between passages 12 and 15. In our experiments, the majority of mutants were obtained by passage 15, with some cases requiring up to 20 passages. Initiating replica plating from passage 3 did not appear to detect earlier recombination events and proved to be labour-intensive without clear benefit.

Regarding the length of homologous arms used for recombination, Rychli et al., 2021, recommend arms of approximately 300 bp, whereas the protocol by Bolten and Roberts suggests a range of 300-500 bp. Traditional protocols employing homologous recombination typically recommend longer arms, around 1000 bp (Kung et al., 2013), to enhance recombination efficiency. In our study, we utilised homologous arms ranging from 300-500 bp as well as arms of up to 1000 bp in length. All tested configurations resulted in successful knockout deletions, indicating flexibility in the effective length of homologous regions for pKSV7 system.

Background mutations arising during plasmid integration and excision may be a consequence of these manipulations, due to stress of the culturing environment. While most detected mutations were synonymous and likely benign, a few non-synonymous mutations were observed that may have phenotypic relevance. Some mutations observed during plasmid excision occurred in the same genomic regions where mutations accumulated during the BPM experiment, including genes encoding LPXTG domain-containing cell wall proteins and leucine-rich repeat proteins, which are often involved in protein-protein interactions. Since both the plasmid excision and BPM experiments used BHI media, it is likely that these mutations represent a response to BHI or that the growth conditions themselves induce mild stress, sufficient for their fixation.

5.7. Conclusions

In **Chapter 5**, the mutants were constructed using a SOEing PCR strategy in parental *L. monocytogenes* strain BL87-028.

To deliver the deletion constructs, we used the thermosensitive shuttle plasmid pKSV7, which carries antibiotic tolerance markers for *E. coli* (ampicillin) and *L. monocytogenes* (chloramphenicol).

Successful mutant generation was confirmed by colony PCR, based on the expected size reduction corresponding to the size of the deleted gene. To verify the genomic integrity of the mutant strains and to screen for background mutations introduced during plasmid excision, WGS was performed. Although missense mutations were detected in all mutants, they were located in genomic regions unlikely to impact the phenotypes under investigation.

Notably, we encountered persistent difficulties in generating the *pitA* deletion mutant. The insert generated in-house failed to ligate into pKSV7. Repeated attempts resulted in constructs with partial deletions, despite extensive troubleshooting.

To conclude, we successfully generated deletion mutants for seven genes and genetic regions previously identified through a BPM experiment as being associated with reduced susceptibility to disinfectant and biofilm lifestyle adaptations (Δ*ykoK,* Δ*mgtA,* Δ*rsbU,* Δ*pyrD,* Δ*carB,* Δ*corA,* Δ*bglG*). The next step involves functional characterisation of these genes which is presented in **Chapter 6**.

Chapter 6: Functional and Phenotypic Analysis of the Loci Associated with Biofilm Persistence and Reduced Susceptibility to Disinfectant Detected Through the In vitro Biofilm Persistence Model

6.1. Contributions

Oleksii Omelchenko, Ana Victoria Gutiérrez, James Lazenby, Kathryn Gotts, Catherine Booth, Mark Webber, Matthew Gilmour.

6.2. Publication

In preparation:

Oleksii Omelchenko, Ana Victoria Gutiérrez, James Lazenby, Kathryn Gotts, Catherine Booth, Mark Webber, Matthew Gilmour. **Functional and Phenotypic Analysis of Pathways Associated with Biofilm Persistence and Reduced Susceptibility to Disinfectant in *Listeria monocytogenes.*** *In preparation.*

6.3. Introduction

Phenotypic characterisation of mutants has long been a central approach to understand function of genes and pathways (Pineda et al., 2010). This strategy typically involves perturbing a gene, either through a targeted mutation or chemical treatment, and then assessing the resulting effects using a range of phenotypic assays (Hue, Sahin and Andrews, 2022).

In this chapter, we characterised a panel of deletion mutants previously generated in **Chapter 5** (Δ*ykoK*, Δ*mgtA*, Δ*rsbU*, Δ*pyrD*, Δ*carB*, Δ*corA*, Δ*bglG*) to examine the functional roles of these loci in biofilm formation and reduced susceptibility to disinfectant. We hypothesised that deletion of loci identified through the BPM would influence phenotypes under selective pressure, leading either to reduced disinfectant susceptibility or to changes in biofilm architecture and formation capacity.

One gene previously associated with response to BC exposure is *bglG*, encoding a transcriptional regulator of the phosphotransferase system (PTS) operon (*bgl*) (Abdelhamed et al., 2019). The PTS is responsible for the transport and phosphorylation of monosaccharides, disaccharides, amino sugars, polyols, and other sugar derivatives (Deutscher, Francke and Postma, 2006). Previously, upregulation of PTS genes, including *bglG*, was reported in *L. monocytogenes* mutants with reduced BC susceptibility (Bechtel et al., 2024). However, this association was identified only at the level of differential gene expression and has not yet been examined in detail.

Another candidate gene associated with reduced disinfectant susceptibility is *corA*, encoding the CorA Mg^{2+} and cobalt transport protein (Kersey, Agyemang and Dumenyo, 2011). Recent research has suggested that CorA in *Mycobacterium smegmatis* and *E. coli* may facilitate extrusion of structurally diverse antimicrobial compounds including fluoroquinolones, aminoglycosides, ansamycin antibiotics and antimycobacterial drugs such as isoniazid, reducing susceptibility of host cells to these agents (Chatterjee et al., 2024). However, this potential role of CorA has not yet been demonstrated in *L. monocytogenes.*

Among the loci associated with biofilm formation, one key candidate was *rsbU*, encoding a positive regulator of the alternative sigma factor SigB, which governs the expression of approximately 300 genes involved in stress tolerance and survival (Becker et al., 1998; Nadon et al., 2002; Chaturongakul et al., 2011). SigB regulates responses to several stress cues, such as osmotic stress (Becker et al., 1998), light (Dorey et al., 2019), acid stress (Wiedmann et al., 1998), virulence (Nadon et al., 2002) and central metabolism (Marinho et al., 2019). SigB activation is regulated by a cascade of interacting proteins from the *rsb* operon (**Figure 42**). The anti-sigma factor RsbW inhibits SigB by direct binding. Upon exposure to stress, the RsbU phosphatase is activated by the stressosome complex (RsbR, RsbS, and RsbT) and dephosphorylates RsbV, enabling it to bind RsbW. This interaction sequesters RsbW, as a result releasing and activating SigB (Oliveira et al., 2022). Notably, deletion of *rsbU* has been associated with increased biomass and extracellular matrix production in *L. monocytogenes* biofilms (Hsu et al., 2020). In this chapter, we further investigated this potential link.

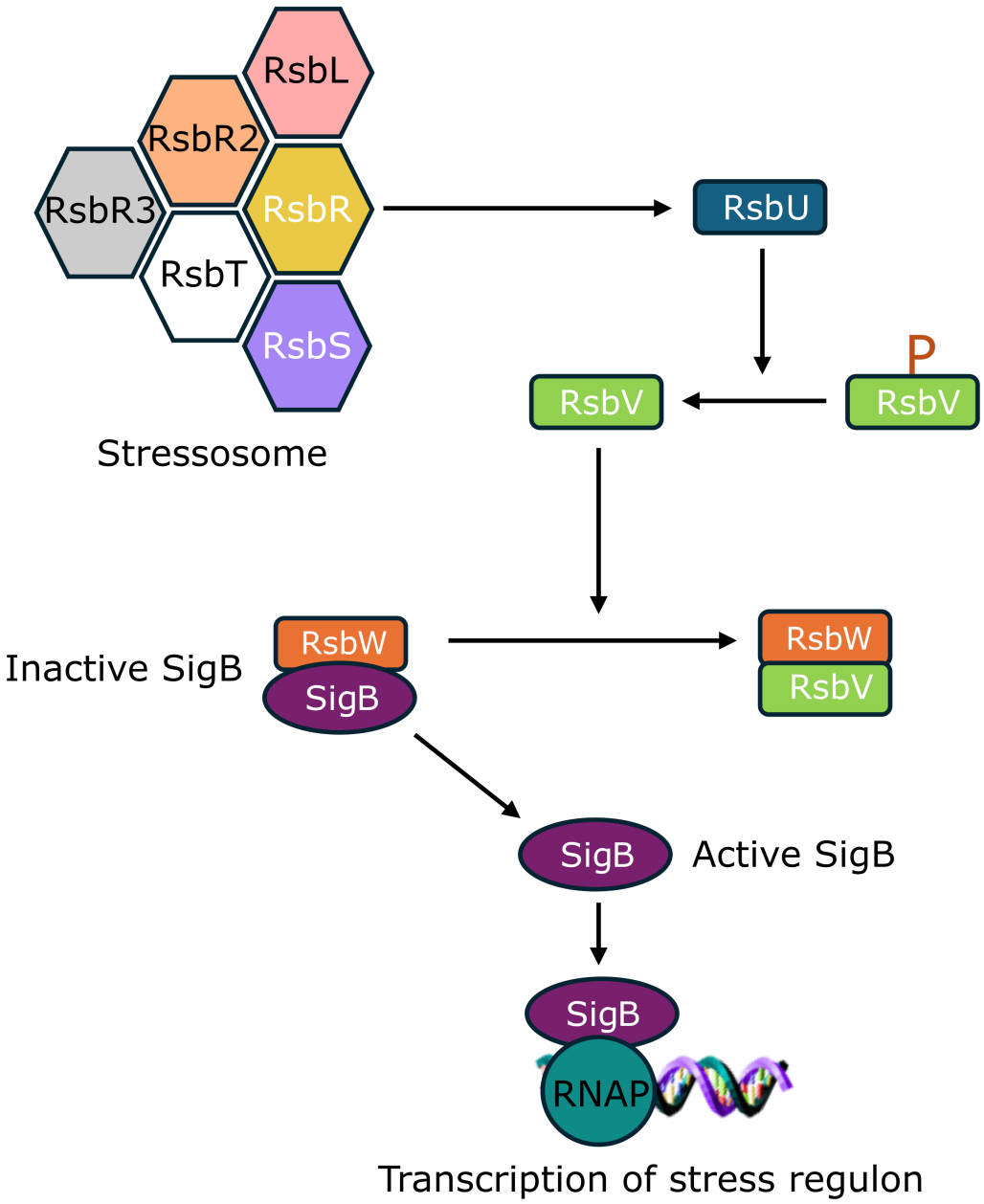


Figure 30. Schematic representation of the SigB activation cascade. Under stress conditions, the stressosome complex, composed of RsbT, RsbR (RsbR1, RsbR2), RsbL and RsbS, becomes activated and promotes the release of RsbT, which subsequently activates the RsbU phosphatase. Activated RsbU dephosphorylates RsbV, allowing RsbV to bind the anti-sigma factor RsbW. This interaction frees SigB from inhibition by RsbW, enabling it to initiate the transcription of the stress regulon (Adapted from Pathak et al., 2020 and Guerreiro et al., 2020).

The involvement of pyrimidine synthesis in biofilm formation has been established in several bacterial species, although it has not yet been investigated in *L. monocytogenes*. For instance, inactivation of *pyrD* in *E. coli* reduces motility and biofilm formation by downregulating genes encoding type 1 fimbriae and curli subunits (Rossi et al., 2022). Similarly, in *Xanthomonas citri* subsp. *citri*, *carB* is essential for both motility and biofilm

development (Zhuo et al., 2015), while in *P. aeruginosa*, *de novo* uridine monophosphate (UMP) biosynthesis is required for biofilm formation (Ueda et al., 2009). In **Chapter 5**, we generated mutant strains deficient in *pyrD* and *carB,* two genes of the *pyr* operon (**Figure 43**). We hypothesised that deletion of these genes would disrupt the conversion of dihydroorotate to orotate and of bicarbonate to carbamoyl-phosphate (**Figure 43**), consequently impairing downstream synthesis of UMP and as a result interfering with biofilm-formation.

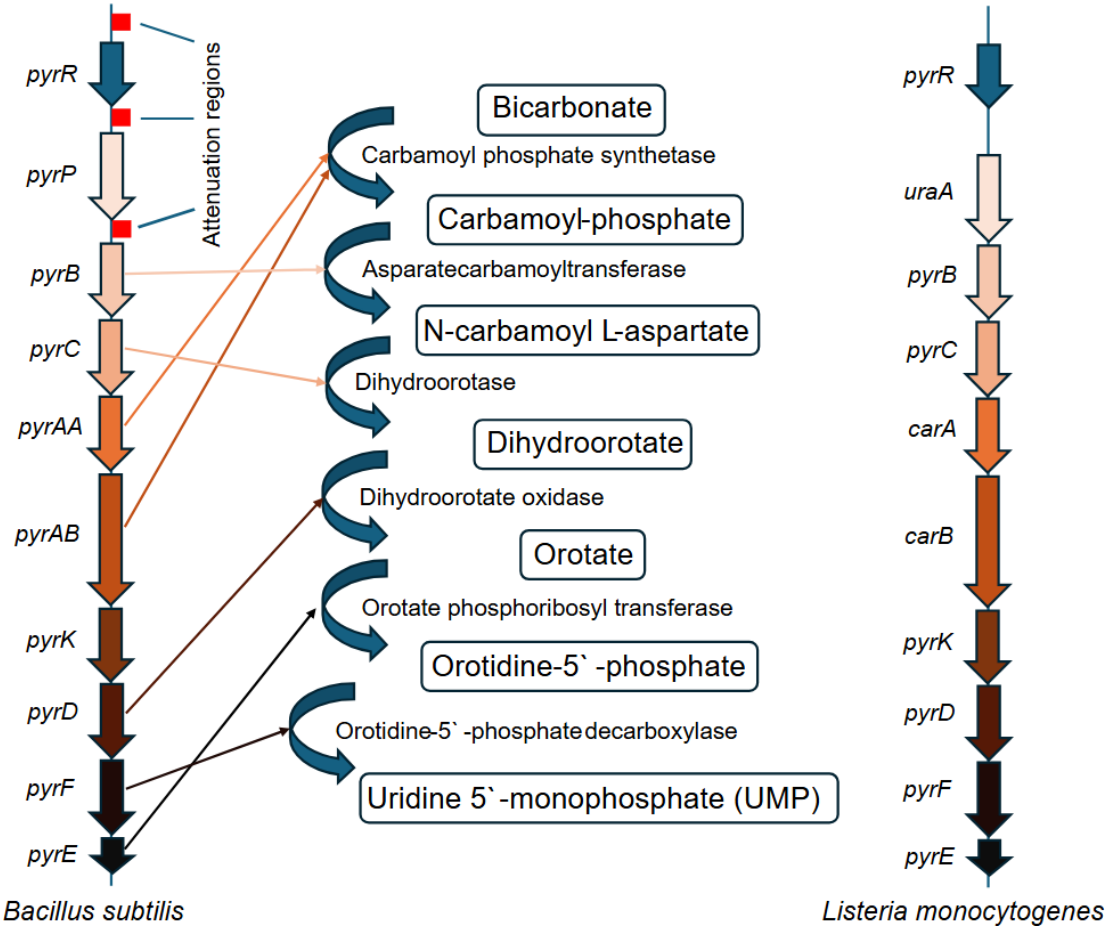


Figure 31. Schematic representation of the *de novo* pyrimidine biosynthetic (*pyr*) operon, demonstrating the products and the enzymes required for each step of the cascade. The operon arrangement in *B. subtilis* adapted from Turnbough and Switzer, 2008, with attenuating regions demonstrated. The operon arrangement of *L. monocytogenes* is based on the complete genome sequence of the parental strain (BL87-028). The enzymatic conversions in the UMP cascade were illustrated according to the *E. coli* model (Turnbough and Switzer, 2008). *pyrAA*, glutamine-utilising subunit of carbamylphosphate synthetase equivalent to *carA*; *pyrAB*, catalytic subunit of carbamylphosphate synthetase equivalent to *carB*. Not drawn to scale.

Mg^{2+} have also been shown to influence biofilm dynamics in a concentration-dependent manner. Moderate levels enhance biofilm development by reducing electrostatic repulsion and stabilising the matrix through cation bridging, whereas higher

concentrations (Chalke et al., 2022; Nowak et al., 2021), or Mg^{2+} in nanoparticle form (Dehkordi, Moshtaghi and Abbasvali, 2022), can inhibit biofilm formation. Intracellular Mg^{2+} regulation is partially mediated by the *ykoK* leader (M-box riboswitch), located upstream of the *mgtA* gene, which encodes a P-type ATPase responsible for Mg^{2+} uptake (Cromie et al., 2006; Maguire, 1992). Under low Mg^{2+} conditions, the M-box adopts an anti-terminator conformation, allowing transcription of *mgtA*. When Mg^{2+} concentrations are elevated, ions bind to specific aptamer regions of the M-box, triggering a conformational shift to a terminator structure that halts transcription (Ramesh and Winkler, 2010). To further explore this connection, we investigated the effect of Mg^{2+} supplementation on biofilm formation in Mg^{2+} homeostasis-related mutants (Δ*ykoK*, Δ*mgtA*) and natural mutants from the BPM.

In this chapter, we combined growth kinetics analysis with colony and cell morphology assessment to evaluate the fitness impact of these mutations. Biofilm phenotypes were first examined using conventional assays, including crystal violet staining to quantify total biomass and CFU-based surface attachment assays to assess viable cell adherence. However, these conventional approached have limited sensitivity for analysing biofilm structure. To address this limitation, we applied advanced microscopy coupled with BiofilmQ software, which enabled quantification of key architectural parameters such as mean thickness, total volume, and base area (Hartmann et al., 2021). In addition, SEM was used to visualise biofilm architecture and to investigate the interaction of mutant strains with stainless steel surfaces.

6.4. Aims

1. To evaluate fitness trade-offs and morphological consequences of gene deletions by assessing growth kinetics, cell and colony morphology of mutant strains.
2. To assess the biofilm forming capacity of mutant strains using conventional phenotypic assays, widefield fluorescence microscopy, and scanning electron microscopy.
3. To quantify global biofilm architecture parameters, including mean thickness, total volume, and base area for mutant strains.
4. To investigate the influence of Mg^{2+} on substrate attachment and biofilm formation in mutants associated with metal homeostasis.

6.5. Results

6.5.1. Phenotypic Analysis of Biofilm-Related Mutants

Deletion mutant strains were generated for seven loci of interest including *ykoK, mgtA, rsbU, pyrD, carB, corA, bglG*.

Phenotypic testing was conducted to evaluate fitness trade-offs and morphological consequences of these mutants, including growth kinetics, macrocolony morphology, cellular morphology, and reduced disinfectant susceptibility.

6.5.1.1 Fitness trade-off detected in mutants with disrupted metal ion homeostasis (ΔcorA), stress response (ΔrsbU) and pyrimidine synthesis (ΔpyrD) pathways

First, we compared the fitness of the mutant strains by calculating the area under the curve (AUC) from growth kinetics data. Several mutants exhibited significantly reduced AUC, including those deficient in metal ion homeostasis loci - *corA* ($p = 0.0282$); the general stress response gene *rsbU* ($p < 0.0001$); and the pyrimidine biosynthesis gene *pyrD* ($p = 0.0153$) (**Figure 44A**).

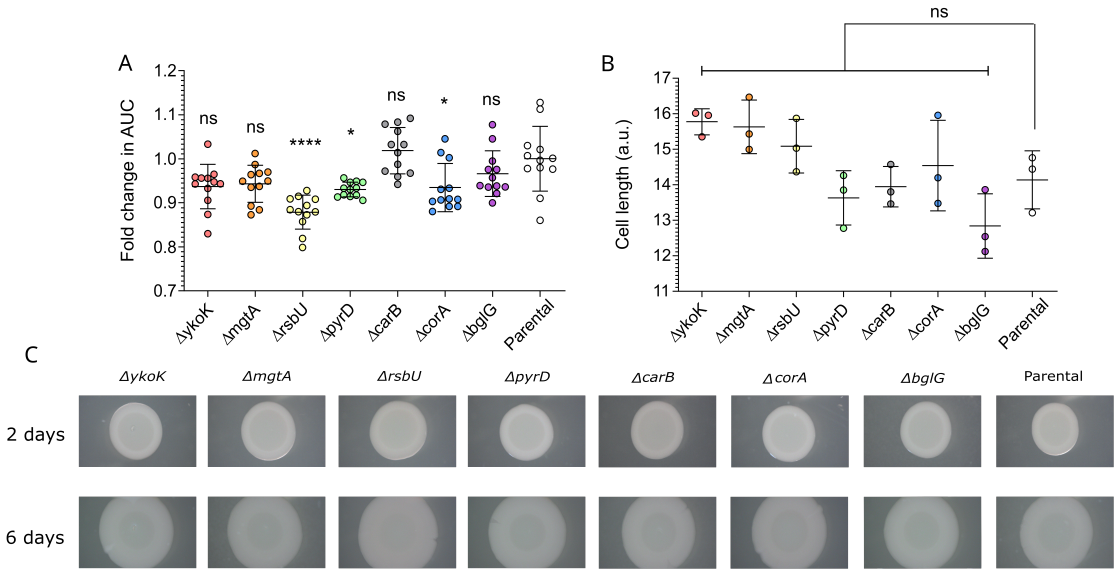


Figure 32. Phenotypic characterisation of mutant strains compared to the parental strain. (**A)** Area under the curve (AUC) derived from the growth curve experiments, indicating relative fitness of mutant strains compared to the parental strain. (**B**) Cell length measurements obtained via brightfield microscopy and quantified using Fiji. a.u. - arbitrary units. (**C)** Macrocolony morphology of mutant strains on BHI agar after 2 and 6 days of incubation. All experiments were performed in triplicates. In panel **A**, every datapoint was illustrated. A one-way ANOVA followed by Tukey's test was performed to compare the groups in panels **A** and **B**: $p < 0.05$ (*), $p < 0.01$ (**), $p < 0.001$ (***), $p < 0.0001$ (****), ns – not significant. Significance was indicated against the parental strain. Error bars represent standard deviation.

In contrast, deletion of other loci did not significantly affect growth, indicating that these mutants maintained fitness comparable to the parental strain under the tested conditions.

6.5.1.2. Subtle Trends in Cell Length Observed in Mutants Affecting Mg^{2+} Homeostasis and β-Glucoside Metabolism

Although not statistically significant, microscopic examination of cellular morphology indicated subtle trends in cell length associated with disruption of metal ion homeostasis pathways. The Δ*ykoK* and Δ*mgtA* mutants showed a putative trend for an increase in average cell length relative to the parental strain, whereas Δ*bglG* cells indicated a putative trend on decrease of cell length. There were no differences observed in cell length for the remaining mutants compared to the parental strain (**Figure 44B**).

6.5.1.3. Visual Characterisation of Macrocolony Morphology

Changes in macrocolony morphology are often associated with altered cell surface properties that can influence attachment and biofilm formation (Webb, Lau and Kjelleberg, 2004). To evaluate potential morphological consequences of the gene deletions, we examined the macrocolony morphology of mutant and parental strains after 2 and 6 days of incubation. Across all strains, macrocolonies exhibited a consistent appearance: round, smooth, and convex, featuring a translucent central core, a concentric ring, and a smooth peripheral edge (**Figure 44C**). There were no visible differences between mutant and parental strains at either time point.

6.5.2. Susceptibility Against BC Remained Unchanged in Mutant Strains

Next, we assessed the susceptibility of mutant strains to BC. There was no significant difference observed in MIC values between any of the mutant strains and the parental control (**Figure 45**). Notably, mutants lacking genes that displayed an association with reduced susceptibility to BC (*corA*, *bglG*) also exhibited MICs comparable to the parental strain.

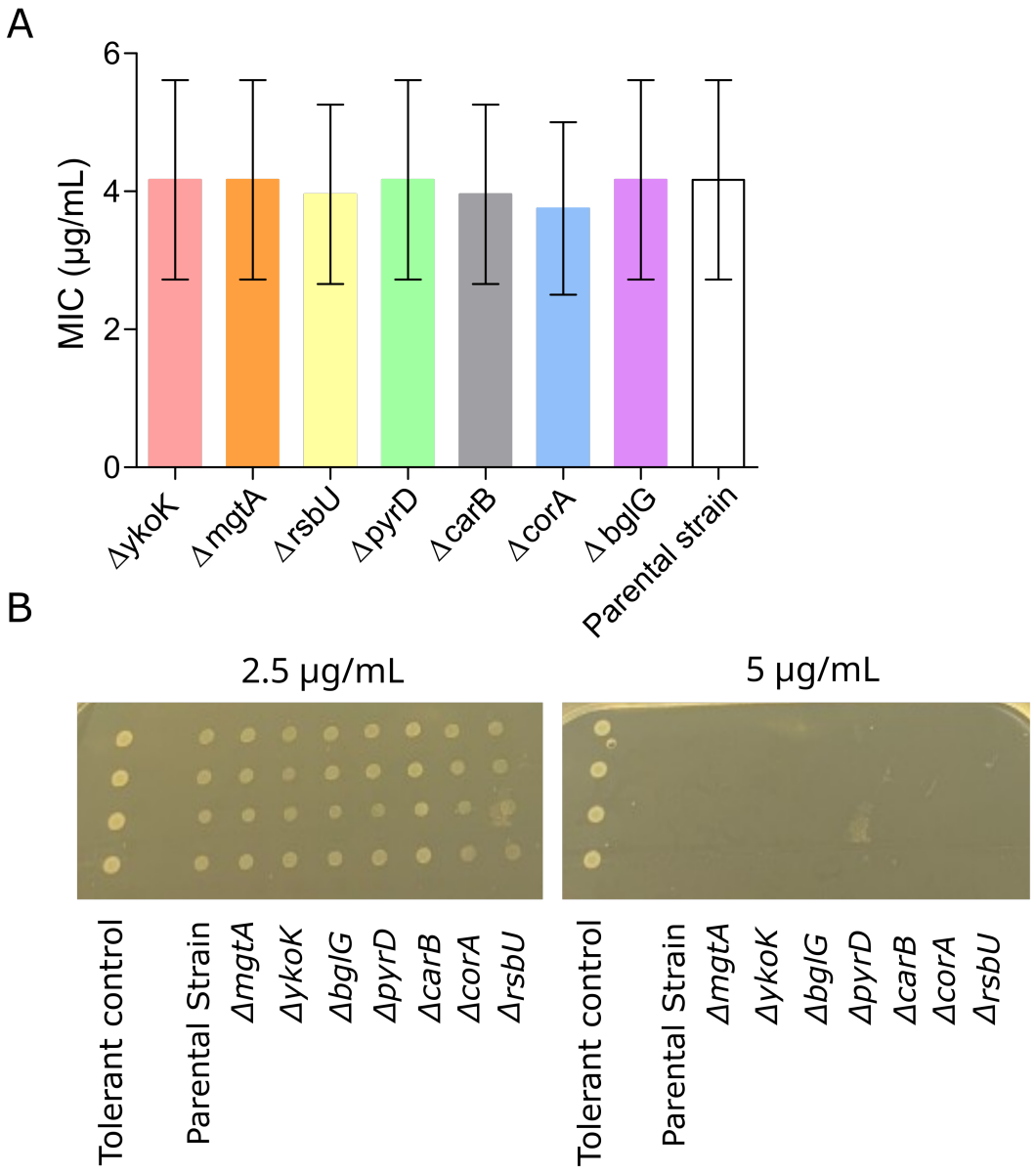


Figure 33. Susceptibility of mutant and parental strains to BC. (**A**) Minimum inhibitory concentration (MIC) of BC against each mutant strain compared to the parental strain, based on the agar dilution antimicrobial susceptibility method. (**B**) Visual representation of MIC results on BHI agar plates at 2.5 µg/mL (left panel) and 5 µg/mL (right panel) BC exposure. A known control strain exhibiting reduced susceptibility to BC (08-5578; MIC of 20 µg/mL) is included for comparison. All experiments were conducted in triplicate, with four technical replicates per experiment. Error bars represent standard deviation.

6.5.3. Assessing Biofilm-Forming Properties of Mutant Strains

Next, we assessed the biofilm-forming capacity of mutant strains employing a combination of complementary assays. A bead-based attachment assay was used to evaluate long-term adherence to stainless steel, while a short-term attachment assay measured initial cell-surface interactions within the first 30 minutes of exposure. In addition, total biomass was quantified using the crystal violet staining assay.

6.5.3.1 Long-term Cell Attachment Not Affected in Mutant Strains

When assessing long-term cell attachment, we found that after a 48-hour incubation period, none of the mutant strains exhibited a change in cell attachment capacity, (**Figure 46A**).

6.5.3.2. Assessment of Short-term Cell Attachment to Stainless Steel Revealed Reduced Adherence in Mutant Strains Associated with Stress Response, Metal Homeostasis, Pyrimidine Synthesis and β-glucoside Synthesis

Next, we assessed short-term cell attachment by quantifying the number of viable cells adhering to stainless-steel surfaces within the first 30 minutes of exposure. Initial attachment was significantly reduced in several mutant strains, including Δ*ykoK* (p = 0.0102), Δ*rsbU* (p = 0.0004), Δ*pyrD* (p = 0.0161), Δ*corA* (p = 0.0083), and Δ*bglG* (p < 0.0001) (**Figure 46B**). Notably, the number of cells adhering in the first 30 minutes of exposure to stainless steel (10^5–10^6 CFU/bead) was comparable to that observed in the long-term attachment assays, highlighting the role of initial adhesion in biofilm development.

6.5.3.3. Disruption of Stress Response and Pyrimidine Synthesis Pathways Result in Significant Reduction in Biomass Production

When comparing biomass production between the parental and mutant strains, we detected a significant reduction in the amount of biomass produced by the Δ*rsbU* mutant, with a 52.5% decrease (p < 0.0001) (**Figure 46C**). A significant reduction was also observed in the amount of biomass produced by the Δ*pyrD* mutant (p < 0.0001), indicating that both the general stress response regulation and pyrimidine biosynthesis contribute to biofilm formation. In contrast, the biomass produced by other mutant strains was comparable to that of the parental strain.

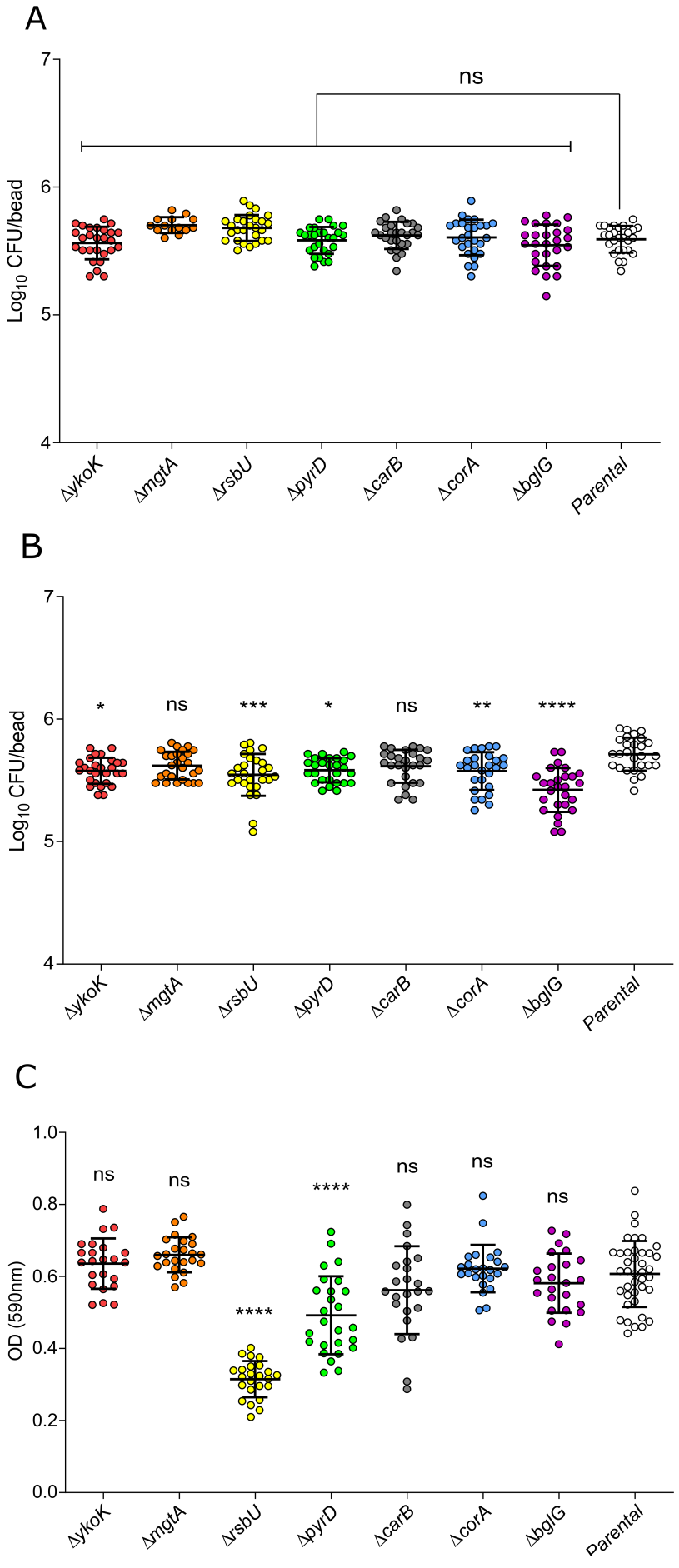

A
ns
Log10 CFU/bead
7
6
5
4
ΔykoK
ΔmgtA
ΔrsbU
ΔpyrD
ΔcarB
ΔcorA
ΔbglG
Parental
B
*
ns
***
*
ns
**
****
Log10 CFU/bead
7
6
5
4
ΔykoK
ΔmgtA
ΔrsbU
ΔpyrD
ΔcarB
ΔcorA
ΔbglG
Parental
C
ns
ns
****
****
ns
ns
ns
OD (590nm)
1.0
0.8
0.6
0.4
0.2
0.0
ΔykoK
ΔmgtA
ΔrsbU
ΔpyrD
ΔcarB
ΔcorA
ΔbglG
Parental

Figure 34. Biofilm-forming capacity of the mutant strains compared to the parental strain. (**A**) Long-term cell attachment to stainless steel beads over a 48-hour incubation period. (**B**) Short-term cell attachment of mutant strains to stainless steel over 30 minutes of exposure to a culture. (**C**) Biofilm biomass quantification using the crystal violet assay. Every datapoint is illustrated. CFU/bead data were $\log_{10}$-transformed prior to plotting, and statistical analyses were performed on the transformed values. A one-way ANOVA followed by Tukey's test was performed to compare the groups: $p < 0.05$ (*), $p < 0.01$ (**), $p < 0.001$ (***), $p < 0.0001$ (****), ns – not significant. Significance was indicated against the parental strain. Error bars represent standard deviation. All assays were performed in 1/10-strength BHI medium and were conducted in triplicate.

6.5.3.4 Disruption of Stress Response and Pyrimidine Metabolism Pathways Impacts Biofilm Architecture

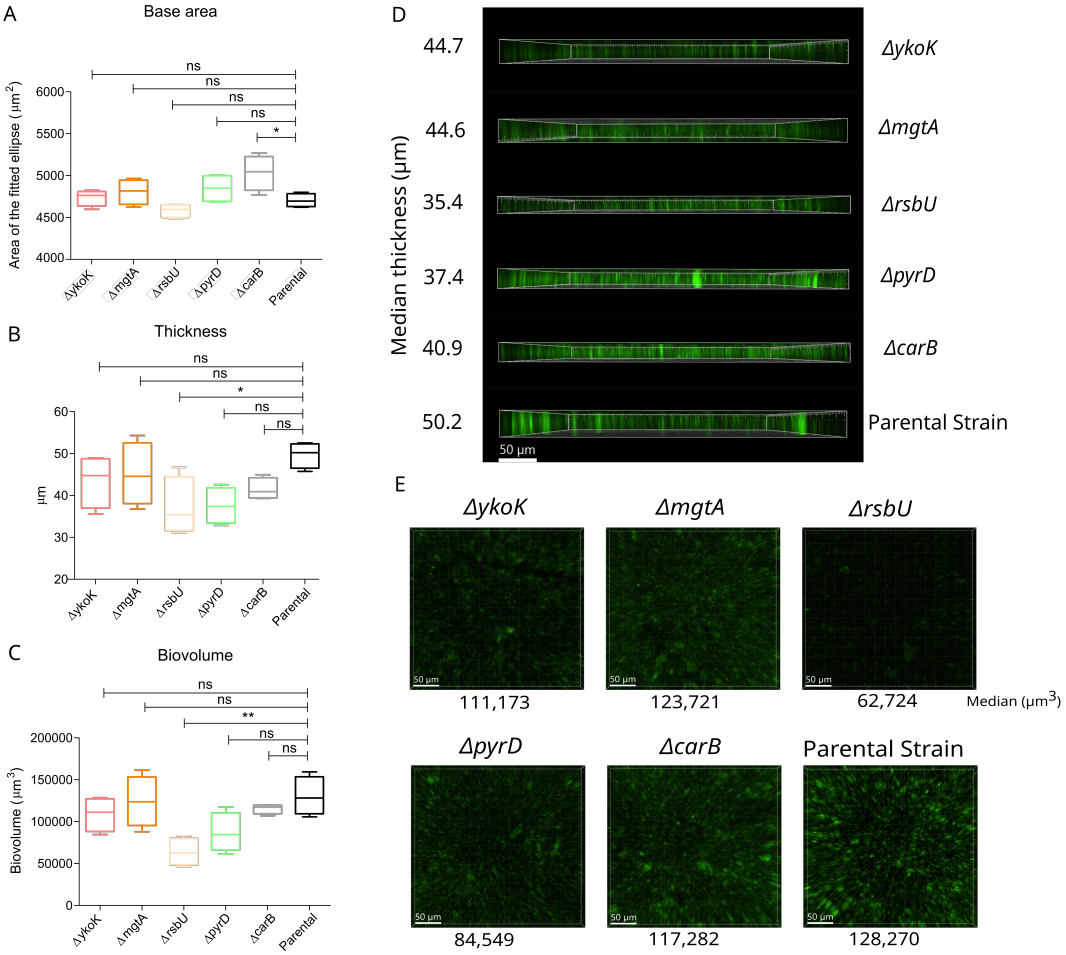


Figure 35. Global biofilm parameters of mutant strains compared to the parental strain, extracted from widefield fluorescence microscopy imaging on stainless steel grade 316. The following global biofilm parameters are included: (**A**) Biofilm base area, (**B**) Thickness, (**C**) Biovolume. A one-way ANOVA followed by Tukey's test was performed to compare the groups: $p < 0.05$ (*), $p < 0.01$ (**), ns – not significant. Whiskers indicate the range from the minimum to the maximum observed values. Median value indicated within the interquartile range. Parameters were calculated using BiofilmQ v1.0.2 with Otsu thresholding sensitivity of 0.15. Widefield fluorescent microscopy visualisation of mutant panel strains (*ykoK, mgtA, rsbU, pyrD, carB*) demonstrating (**D**) side-view and (**E**) top-view on the stainless-steel surface. Images were

visualised using the fluorescent nucleic acid stain SYTO 9. Representative images with median biofilm Thickness (**D**) and median biofilm Volume (**E**) were selected for each condition. 3D biofilm reconstructions were generated in Imaris v10.0.1. The median base area (in μm^3) and mean thickness (in µm) was indicated for each image. A scale bar indicates 50 µm. Experiments were performed in quadruplicate, with 10 fields of view analysed per biological replicate.

Following the detection of alterations in biofilm formation using conventional assays, we next assessed global biofilm properties to reveal subtle differences not captured by conventional methods. For this analysis, we focused on mutants corresponding to loci specifically affected under biofilm conditions in the BPM (*ykoK*, *mgtA*, *rsbU*, *pyrD*, *carB)*. Biofilms were stained with a nucleic acid dye and imaged by widefield fluorescence microscopy, and global parameters, including base area, biovolume, and mean thickness, were extracted using BiofilmQ. This analysis revealed significant differences in several parameters between mutant and parental strains (**Figure 47**).

When comparing base area (**Figure 47A**), only the Δ*carB* mutant exhibited a significant increase ($p = 0.036$) when compared to the base area of the parental strain, while for the other mutants there was no significant difference observed.

In contrast, mean biofilm thickness (**Figure 47B**) was significantly reduced in Δ*rsbU* ($p = 0.048$) mutant. There was also a visible reduction in thickness of Δ*pyrD* mutant, but it didn't pass the significance level ($p = 0.053$).

Biovolume measurements (**Figure 47C**) showed significant reduction detected in Δ*rsbU* ($p = 0.0036$), consistent with the decrease in biomass detected by the crystal violet assay (**Figures 46C; 47C**). There was also a notable reduction in biovolume of Δ*pyrD* mutant strain, but it did not pass the significance threshold.

Visual assessment of fluorescence microscopy images representing median biovolume and thickness values supported these trends, with the Δ*rsbU* mutant showing marked reduction in biomass with Δ*pyrD* and Δ*rsbU* also exhibiting thinner biofilms compared to the parental control (**Figures 47**).

*6.5.3.5. Scanning Electron Microscopy Revealed a Porous Matrix Structure in the Δ*mgtA* Biofilm, and the Presence of Web-like Filaments in the Δ*rsbU* Biofilm*

We next examined the biofilm architecture of the Δ*rsbU* and Δ*mgtA* mutants in more detail using SEM (**Figures 48**), which provides superior resolution compared to optical

microscopy (Liu, 2012). The rationale for selecting two of the mutant strains to undergo SEM from the larger panel of mutants was as follows: the Δ*mgtA* mutant, no significant differences were observed in any of the performed biofilm assays, so we decided to increase resolution to be able to detect subtle architectural differences with SEM. In contrast, the Δ*rsbU* mutant was selected due to its pronounced biofilm-deficient phenotype, with more than 50% reduction in biomass and altered architecture in quantitative analyses.

SEM analysis revealed distinct biofilm structures in both mutants that were absent in the parental control. A porous extracellular matrix was detected in the Δ*mgtA* biofilms (**Figure 48A**), which was consistently absent in the parental strain (**Figure 48B**) and in Δ*rsbU* biofilms. Although not uniformly distributed across all fields of view, the porous material was a recurring feature in Δ*mgtA* samples, suggesting a potential involvement of Mg^{2+} homeostasis in regulating extracellular matrix secretion.

When examining Δ*rsbU* biofilm under SEM, we detected thin, web-like filaments spanning between the cells (**Figure 48A**), structures not observed in the parental strain (**Figure 48B**). Notably, similar but less abundant filaments were also observed in the biofilms of Δ*mgtA* mutant strain (**Figure 48A**). We suggest that the observed web-like filaments may play a role in cell entrapment to promote aggregation.

Notably, both mutants and the parental strain exhibited cell-sized voids within the matrix (**Figure 48**, indicated by red arrows). These may represent areas where the cells were detached from the surface or, alternatively, where the matrix components were degraded and utilised as a source of nutrients.

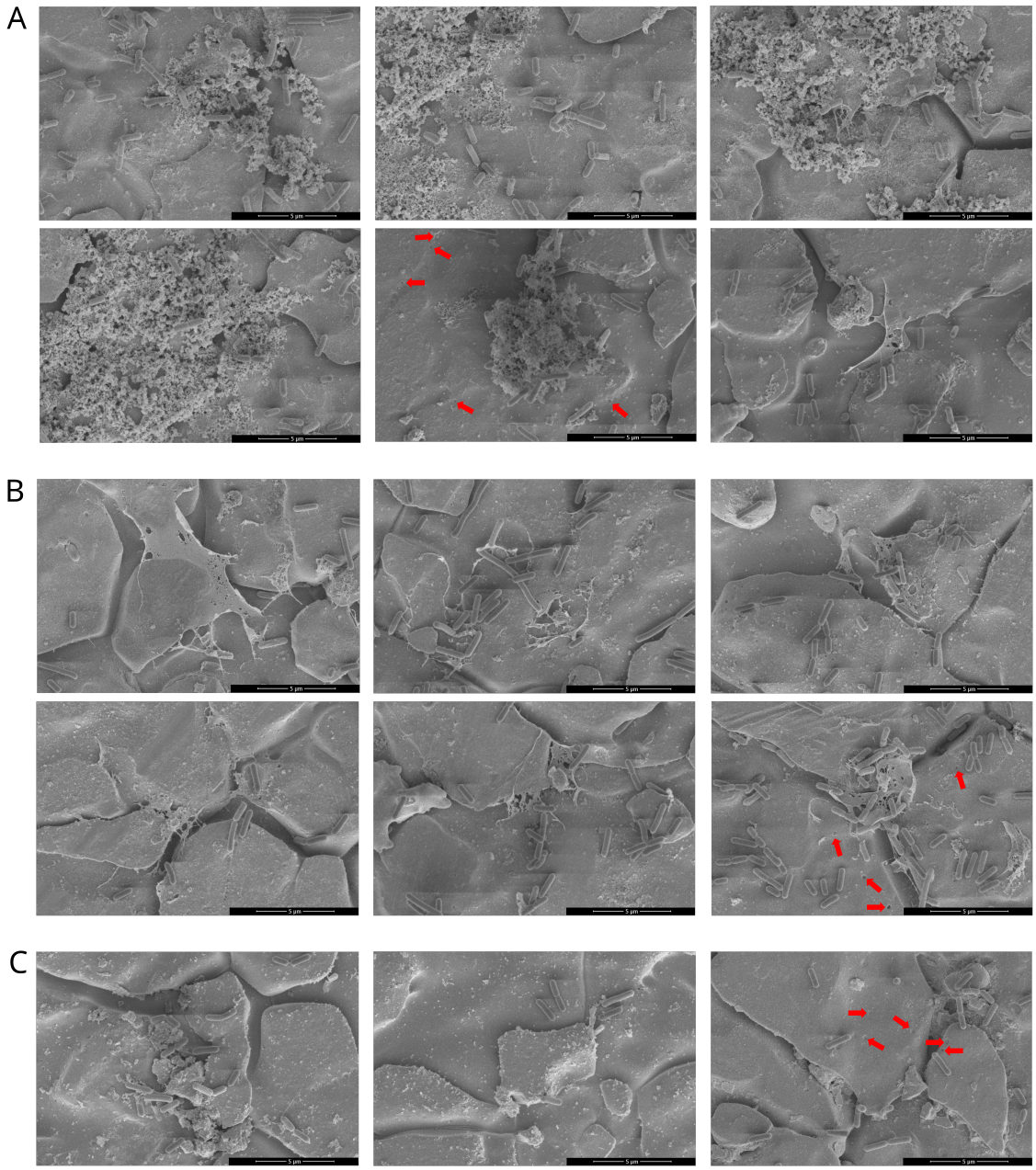


Figure 36. Comparison of biofilm structure between the Δ*mgtA* and Δ*rsbU* mutants and the parental strain under SEM. SEM micrographs of the Δ*mgtA* (**A**) and Δ*rsbU* (**B**) mutant strain on stainless steel grade 316 after 48-hour incubation, demonstrating (**A**) porous matrix for Δ*mgtA* and (**B**) presence of web-like filaments for Δ*rsbU* mutant. (**C**) SEM micrograph of the parental strain under the same conditions, with the absent matrix compared to the Δ*mgtA* and Δ*rsbU* mutants. Red arrows were drawn post-imaging and indicate cell-sized voids detected on micrographs. Experiments were performed in duplicate, with at least five fields of view analysed per sample.

6.5.4. Influence of Mg^{2+} Supplementation on Cell Length of Natural Mutants

As several metal homeostasis-related genes have been impacted by mutations during the BPM, we sought to further investigate the influence of Mg^{2+} supplementation on biofilm phenotypes (**Figure 49**). First, we compared the response of naturally evolved mutants obtained from the BPM to two Mg^{2+} concentrations (no supplementation; 50 mM Mg^{2+}).

Five isolates evolved under biofilm lifestyle were selected: two from an early timepoint (T10-No-BC-Biofilm1-3; T10-No-BC-Biofilm2-P), where the later served as a control mutant strain due to its intact metal homeostasis systems, and three from the late timepoint (T30-No-BC-Biofilm1-1, T30-No-BC-Biofilm1-3, T30-No-BC-Biofilm3-3) (**Appendix 5**). Among the late timepoint mutants, three contained mutations in *mgtA* and *ykoK*, while one carried a mutation in *pitA,* metal transport-related loci. Notably, all natural mutants harboured additional background mutations unrelated to metal regulation (**Appendix 5; Appendix 21**).

Selected Mg^{2+} supplementation level (50 mM) was considerably higher than typical intracellular Mg^{2+} concentrations, which in *E. coli* and B. *subtilis* range between 1-2 mM (Dávid Szatmári et al., 2020; not reported for *L. monocytogenes*). We hypothesised that under these *supra*-physiological conditions, phenotypic differences in mutants with disrupted metal homeostasis may be more pronounced. Indeed, three tested natural mutants (T10-No-BC-Biofilm1-3; T10-No-BC-Biofilm2-P; T30-No-BC-Biofilm1-1) exhibited significantly shorter cells when grown with Mg^{2+} supplementation compared to the same strains grown without Mg^{2+} supplementation. In contrast, for the other two late timepoint mutants (T30-No-BC-Biofilm1-3, T30-No-BC-Biofilm3-3) and the parental strain, cell length remained unaffected by Mg^{2+} supplementation. Notably, when comparing length of the cells under non-supplemented conditions, no significant differences were observed between any of the natural mutants and the control strains (**Figure 49**).

Obtained results were contradicting, with the parental strain and the control natural mutant (both possessing intact *ykok* and *mgtA* genes) exhibiting opposite behaviours under Mg^{2+} supplementation (**Figure 49**). This discrepancy is likely attributable to the additional background mutations that arisen during the BPM, confounding phenotypic interpretation. Therefore, for subsequent experiments, we focused on deletion mutants of

metal homeostasis loci, which provided a more controlled system for assessing the role of Mg^{2+} in biofilm formation.

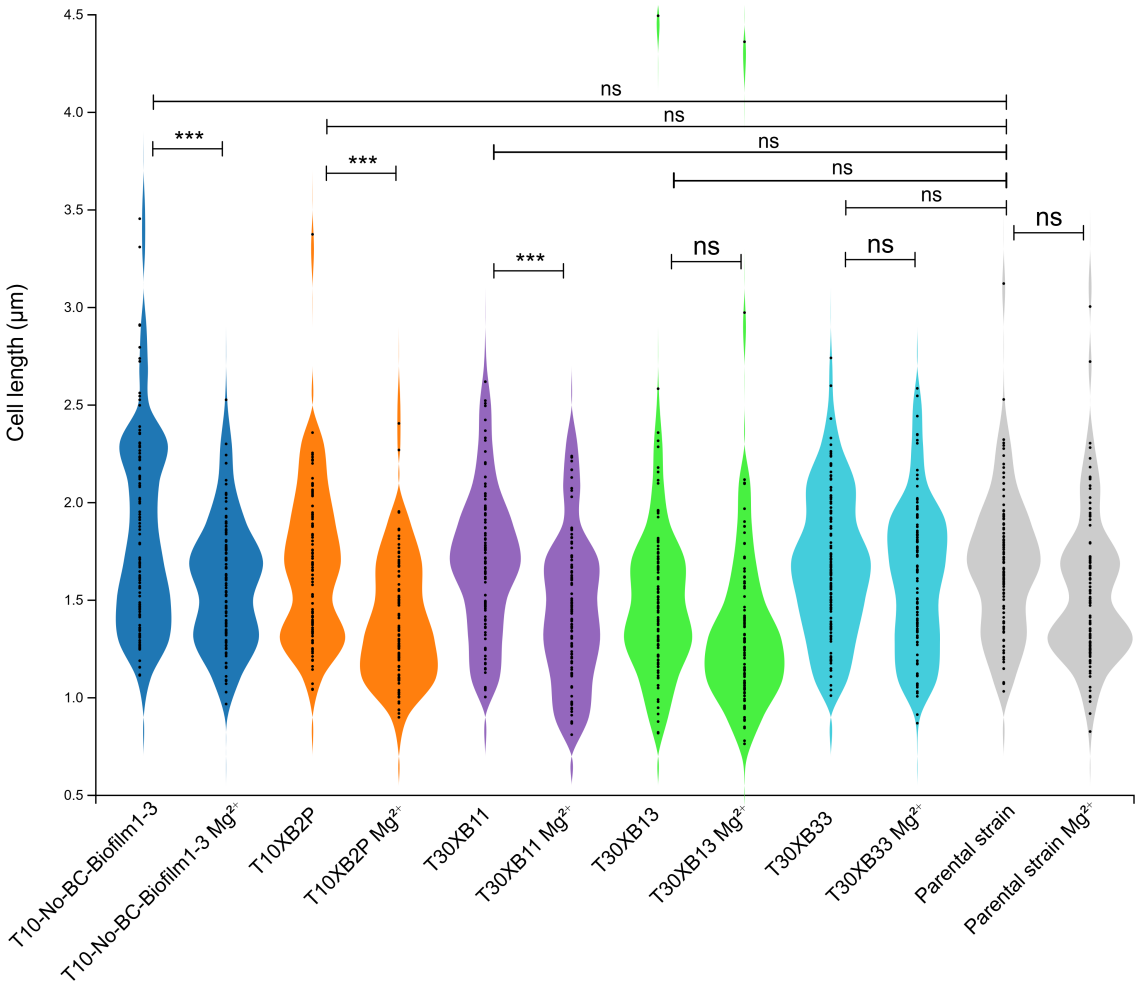


Figure 37. Violin plot demonstrating the cell length of natural mutants obtained from BPM, under no Mg^{2+} supplementation and at 50 mM of Mg^{2+}. Individual data points are indicated by black dots. Colour coded by strain, as indicated on the x-axis labels. Mg^{2+} supplementation status indicated on x-axis labels. A one-way ANOVA followed by Tukey's test was performed to compare the groups: $p < 0.001$ (***), ns – not significant. Plotted with RawGraph v2.0.

6.5.5. Mg^{2+} Influence on Surface Attachment in Δ*mgtA* and Δ*ykoK* Mutants

Next, we explored the effect of Mg^{2+} supplementation on cell attachment to stainless steel employing deletion mutants of Mg^{2+} homeostasis loci (Δ*mgtA*, Δ*ykoK*). Both Δ*mgtA* and Δ*ykoK* mutants were investigated for attachment capacity under a gradient of Mg^{2+} concentrations (0, 1, 10 and 50 mM) to capture physiologically relevant as well as *supra*-physiological concentrations (**Figure 50; Appendix 22**).

In the parental strain, a significant increase in cell attachment was observed as Mg^{2+} concentration increased from 0 to 1 mM (p = 0.0335). No further enhancement was detected at 10 mM; however, a significant reduction in attachment occurred between 10 and 50 mM (p < 0.0001), indicating a potential threshold beyond which elevated Mg^{2+} concentrations may exert an inhibitory effect on adhesion.

In the Δ*ykoK* mutant, there was no notable difference in attachment capacity between 0, 1, and 10 mM, but attachment was significantly reduced between 10 and 50 mM (p = 0.0211). This trend mirrors the parental strain, indicating a significant decrease in cell attachment when concentration increases above 10 mM level, suggestive of a threshold-dependent pattern.

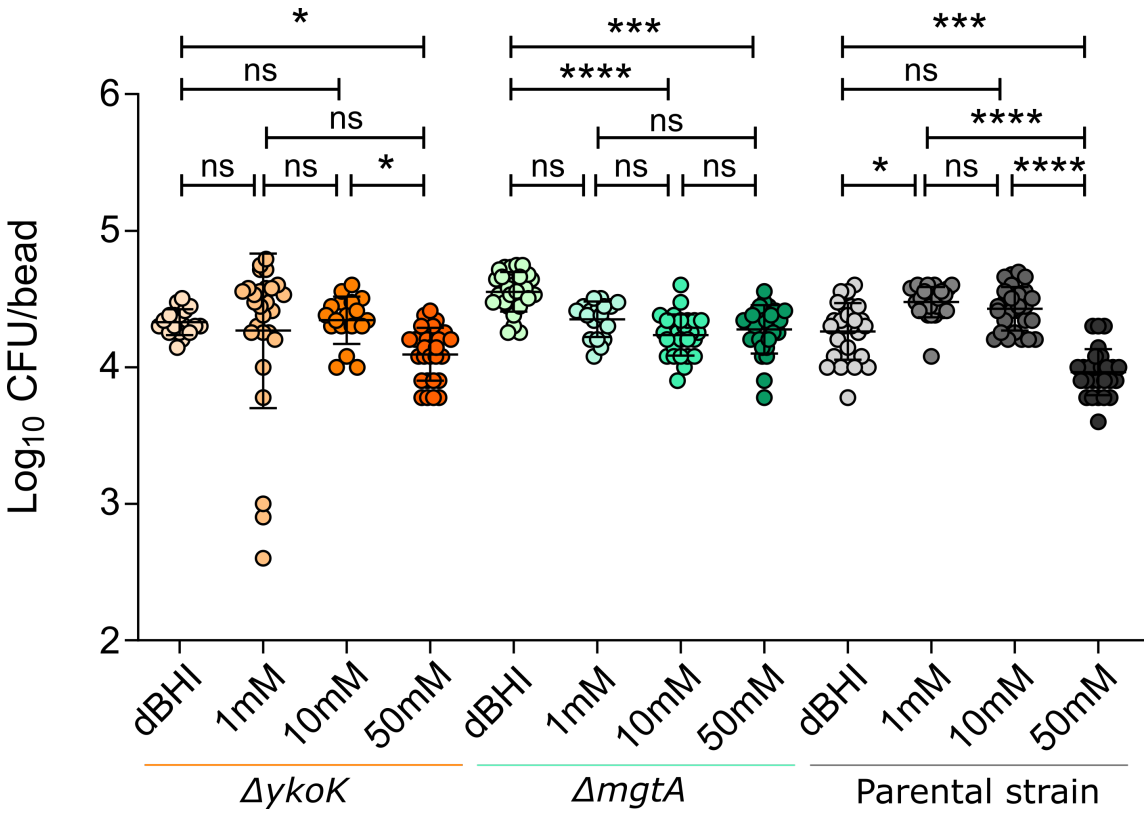


Figure 38. Cell attachment of mutant strains involved in Mg^{2+} homeostasis (Δ*ykoK*, Δ*mgtA*) compared to the parental strain. Bacterial cultures were grown in 1/10-strength BHI supplemented with 0-, 1-, 10-, and 50-mM Mg^{2+}, and colony-forming units (CFU) were quantified after 48-hours of incubation. Each experiment was performed in triplicate, with all individual values plotted. A one-way ANOVA followed by Tukey's test was performed to compare the groups: p < 0.05 (*), p < 0.01 (**), p < 0.001 (***), p < 0.0001 (****). Full set of statistical analysis demonstrated in **Appendix 22**. Error bars represent standard deviation.

For the Δ*mgtA* mutant, the detected pattern of cell attachment change was different. No change in cell attachment was detected in subsequent steps between 0, 1, 10 and 50 mM of Mg^{2+}. However, when comparing 0 to 10 mM (p < 0.0001) and 0 to 50 mM (p = 0.0009)

there was significant reduction in cell attachment. The threshold beyond which the cell attachment decreases is observably lower for Δ*mgtA* mutant than for the parental strain and Δ*ykoK* mutant. This response may suggest that the absence of the MgtA Mg^{2+} transporter disrupts normal regulation of metal cation homeostasis, leading to altered response of surface adhesion.

Overall, in both mutants and parental strain, cell attachment was significantly higher with no Mg^{2+} supplementation compared to condition with 50 mM Mg^{2+}.

6.5.6. Mg^{2+} Ions have Concentration Dependent Effect on Biofilm Base Area, but not Thickness or Volume

Once the effect of Mg^{2+} supplementation on cell attachment capacity was established, we next investigated how Mg^{2+} affects biofilm architecture. To achieve this objective, we analysed structural parameters in biofilms of the Δ*mgtA* and Δ*ykoK* mutants, alongside the parental strain, under varying supplementation of Mg^{2+} (0, 10, and 50 mM). Given the labour-intensive nature of the widefield microscopy experiments, we did not carry forward with 1 mM concentration, only testing 0, 10, and 50 mM of Mg^{2+} in subsequent experiments.

Widefield fluorescence microscopy combined with nucleic acid staining was used to assess biofilm architecture. We performed visual inspection of representative biofilms formed by Δ*ykoK,* Δ*mgtA* and the parental strain under increasing Mg^{2+} supplementation (**Figure 51 A - C**). Representative images were selected from fields of view with biofilm volume closest to the median value. In the parental strain, a visual increase in biofilm formation was detected at 10 mM of Mg^{2+} supplementation compared to condition with no supplementation, followed by a reduction at 50 mM. This pattern is consistent with the threshold-dependent regulation of biofilm formation by Mg^{2+} ions previously proposed by Oknin et al., in 2015, where Mg^{2+} enhances biofilm development only up to a concentration-associated threshold after which biofilm formation is significantly reduced. A similar pattern was detected in the Δ*mgtA* mutant strain, where growth of biofilms was enhanced at 10 mM but reduced again at 50 mM Mg^{2+}. By contrast, the Δ*ykoK* mutant strain did not exhibit a similar pattern and the biofilm formation at 50 mM was comparable to that at 10 mM of Mg^{2+} supplementation.

For the visual assessment of biofilm thickness, representative images were selected from fields of view with biofilm thickness closest to the median value. Visual assessment of

median-thickness (**Figure 51A, right side**) revealed a noticeable reduction in thickness for the parental strain grown at 50 mM Mg^{2+} compared to 10 mM and non-supplemented condition. In the Δ*mgtA* and Δ*ykok* mutants, however, the difference in thickness appeared more subtle and could not be visually determined.

In addition to visual inspection, we also quantified global biofilm parameters of Δ*ykoK,* Δ*mgtA* mutants and the parental strain under increasing Mg^{2+} supplementation. For the condition without supplemented Mg^{2+}, we used the previously acquired values for Δ*mgtA*, Δ*ykoK* and parental strain from section 6.5.3.4 '**Disruption of Stress Response and Pyrimidine Metabolism Pathways Impacts Global Biofilm Architecture**', as the reference values.

Biofilm base area was significantly increased by Mg^{2+} supplementation in both mutants and the parental strain (**Figure 51D**). In the Δ*ykoK* mutant strain, there was significantly higher base area at both 10 ($p = 0.015$) and 50 mM ($p = 0.0011$) compared to the condition without Mg^{2+}. In the Δ*mgtA* mutant, a similar pattern was observed, with significantly increased base area displayed at 50 mM ($p = 0.0042$) Mg^{2+} supplementation relative to the non-supplemented condition. In the parental strain, we also detected significantly increased base area in both Mg^{2+}-supplemented conditions compared to the non-supplemented control (10 mM ($p = 0.012$); 50 mM ($p = 0.016$)). Notably, in both mutants and parental strain there was no significant difference detected between base areas at 10 and 50 mM Mg^{2+} (**Figure 51D**).

In contrast, assessment of biofilm thickness and biovolume revealed no significant differences between mutant strains and the parental control when grown under different Mg^{2+} concentrations (**Figure 51E - F**).

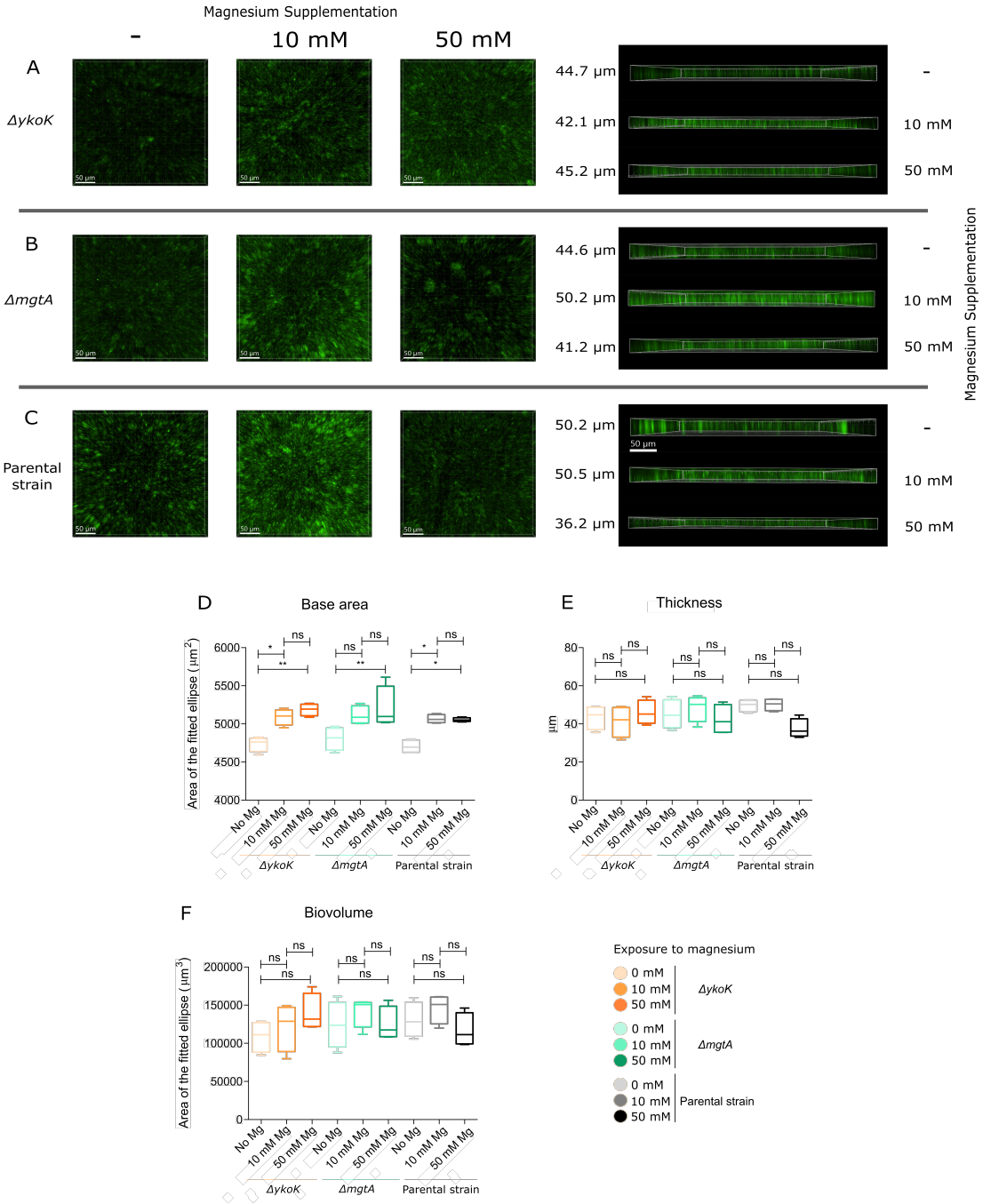


Figure 39. Global biofilm parameters of Δ*ykoK* and Δ*mgtA* mutants, alongside parental strain, exposed to increasing concentrations of Mg^{2+} ions on stainless steel grade 316. (**A, B, C**) Top-view (left side) and side-view (right side) widefield fluorescent microscopy representation of biofilms in (**A**) Δ*ykoK*, (**B**) Δ*mgtA* and (**C**) parental strain under 0, 10 and 50 mM of Mg^{2+} supplementation. Images were visualised using the fluorescent nucleic acid stain SYTO 9. Numbers indicate median biofilm thickness of the side-view images in µm. Representative images with median biofilm biovolume (left side) and median biofilm thickness (right side) were selected for each condition. 3D biofilm reconstructions were generated in Imaris v10.0.1. A scale bar indicates 50 µm. The global biofilm parameters were included in quantitative analysis of biofilm architecture: (**D**) Biofilm base area, (**E**) Thickness, (**F**) Biovolume. A one-way ANOVA followed by Tukey's test was performed to compare the groups: $p < 0.05$ (*), $p < 0.01$ (**), ns - not significant. Whiskers indicate the range from the minimum to the maximum observed values. Median value indicated within the interquartile range. Parameters were

calculated using BiofilmQ v1.0.2 with Otsu thresholding sensitivity of 0.15. Experiments were performed in quadruplicate, with 10 fields of view analysed per biological replicate.

6.6. Discussion

We have demonstrated in previous chapters that *L. monocytogenes* does not adapt to FPE-like conditions by increasing the amount of biomass or viable cells attaching to the surface. In context of *L. monocytogenes* in FPEs, biomass hyperproduction may not be of benefit, as there is presence of biota able to produce large volumes of biomass (e.g. *Pseudomonas fluorescens*) and offer 'sheltering' to less abundant species, similarly to the process described by Puga et al., 2018. Instead, in *L. monocytogenes,* mutations accumulate in pathways associated with stress response, nucleotide synthesis and inorganic ions transport and metabolism, indicating a complex fine tuning of intracellular processes in response to constant rounds of surface attachment, population generation and dispersal that the cells go through in each passage of the BPM. In this chapter, we aimed to understand a potential role of the mutations accumulated in BPM under FPE-like stress, by looking deeper into the genes and pathways where such mutations have been detected. We phenotypically characterised mutant strains generated for loci that were associated through BPM with biofilm persistence (*ykoK*, *mgtA*, *rsbU*, *pyrD*, and *carB*) and reduced BC susceptibility (*corA* and *bglG*) which we previously generated in **Chapter 5**.

Although, previous work in *M. smegmatis* and *E. coli* suggests that CorA contributes to antimicrobial extrusion (Chatterjee et al., 2024), our Δ*corA* mutant did not display altered BC phenotype. One possible explanation is the already low susceptibility of the parental ST121 strain, which may obscure subtle contributions of efflux systems. Another is the limited resolution of the agar-based MIC assay, which progresses in two-fold increments and may miss small shifts in MICs. The fixation of *corA* mutations in BC-exposed lineages during our BPM experiments, suggests that under selective pressure, *corA* disruption may confer context-dependent advantages not captured in our assays. Future research should therefore investigate the role of *corA* under a broader range of stressors and environmental conditions, including long-term persistence models and mixed-species biofilms, to determine whether its inactivation provides subtle but ecologically significant fitness benefits.

Deletion of *rsbU* resulted in a pronounced reduction in biofilm biomass and short-term surface attachment. This finding is consistent with the established role of the stress

response in promoting robust colonisation, as SigB (activated by RsbU) regulates a wide regulon involved in stress adaptation and biofilm formation (van der Veen and Abee, 2010). Our microscopy data also revealed that Δ*rsbU* biofilms were thinner and had reduced biovolume, highlighting that disruption of the SigB pathway compromises not only biofilm initiation but also subsequent structural development. These results are consistent with previous findings that *rsbU* influences biofilm formation (Hsu et al., 2020).

Our results, however, contrast with the report of Hsu et al., 2020, who observed increased biofilm formation in Δ*rsbU* mutant. The discrepancy may reflect differences in experimental context. Hsu et al., 2020, assays were performed in MWB medium at 30 °C, whereas we used 1/10-strength BHI at 20 °C. Strain-specific regulatory variation may also play its role, as *L. monocytogenes* biofilm composition is highly complex and influenced by multiple overlapping pathways (Wang et al., 2022), making it plausible that the outcome of SigB disruption varies between sequence types. In our ST121 background, SigB activity appears important for sustained biofilm development, whereas in other genetic contexts loss of SigB regulation may derepress alternative adhesion pathways.

Notably, both our study and that of Hsu et al., identified unusual structural features in Δ*rsbU* biofilms. SEM imaging revealed that web-like filaments were not present in the parental strain, suggesting that *rsbU* deletion may alter matrix composition. We hypothesised that these filaments could represent extracellular DNA (eDNA), which is frequently associated with filamentous structures in biofilms (Holliday et al., 2015). Given that SigB regulates genes involved in autolysis and lysis-dependent eDNA release (Rice et al., 2004; Xie et al., 2020), *rsbU* disruption may indirectly increase eDNA release despite the overall reduction in biomass. Such structural adaptation could facilitate cellular aggregation and promote cell carry-over during the subsequent passages of the BPM.

Future research should aim to clarify whether SigB disruption directly enhances eDNA release, and how this structural adaptation contributes to persistence in food-related environments. Combining genetic, biochemical, and high-resolution imaging approaches across multiple sequence types and environmental conditions will be key to understanding whether these filaments represent an adaptive mechanism of biofilm resilience or a strain-specific artefact. Additionally, understanding how *rsbU*-linked

changes in matrix composition influence biofilm persistence could inform the development of targeted control strategies, such as enzymatic disruption of eDNA or interventions that impair SigB-mediated stress responses.

Our findings highlight the central role of pyrimidine biosynthesis in *L. monocytogenes* biofilm formation. The Δ*pyrD* mutant displayed reduced biofilm biomass and short-term cell attachment capacity. Both also exhibited structural defects, with increased base area for Δ*carB* mutant and reduced biofilm thickness in Δ*pyrD*. These findings align with observations in *E. coli* (Rossi et al., 2022), *Xanthomonas citri* subsp. *citri* (Zhuo et al., 2015), and *P. aeruginosa* (Ueda et al., 2009; Kim-Holzapfel et al., 2023), highlighting that pyrimidine metabolism is not merely a housekeeping function but also a regulatory node for biofilm development. One plausible explanation for these observations is that pyrimidine biosynthesis disruption may act as a signal of nutrient limitation and metabolic stress, triggering biofilm dispersal or promoting a shift toward planktonic growth. This hypothesis aligns with previously observed stress-induced dispersal mechanisms in *P. aeruginosa* (Nair et al., 2021). Future research should explore whether targeting pyrimidine biosynthesis could serve as a strategy to destabilise biofilms in FPEs. Identifying small molecules or metabolic inhibitors that selectively impair pyrimidine metabolism may provide novel avenues for biofilm control without relying solely on traditional biocides.

Mg^{2+} availability had a strong impact on biofilm formation. Supplementation with Mg^{2+} increased the biofilm base area in both the Δ*mgtA* and Δ*ykoK* mutants, as well as in the parental strain, and also produced mutant-specific changes in cell attachment profiles under different supplementation levels. These results are consistent with previous work showing that Mg^{2+} plays an important role in biofilm development. For example, Chalke et al., 2022, reported that Mg^{2+} concentrations up to 50 mM promoted *L. monocytogenes* biofilm formation and influenced later stages of development. This agrees with the increase in base area we observed in our mutants with higher Mg^{2+} supplementation. However, we also found that high Mg^{2+} levels (50 mM) impaired cell attachment in both the Δ*ykoK* mutant and the parental strain, while even a lower concentration (1 mM) had a similar effect in Δ*mgtA*. In this respect, our findings are in line with Oknin et al., 2015, who described in *B. subtilis* that Mg^{2+} supplementation above 25 mM reversed its positive effects on biofilm formation and instead led to biofilm dispersal.

In Δ*mgtA*, SEM revealed porous matrix structures absent in the parental strain. A similar porous matrix has previously been described in *L. monocytogenes* (Ceruso et al., 2020), where it was attributed to the 'leakage of intracellular components'. This intracellular leakage may provide a potential hypothesis for the porous matrix observed in the Δ*mgtA* mutants. In the absence of proper Mg^{2+} homeostasis, membrane stability and permeability properties are likely altered (Groisman et al., 2013; Li et al., 2025), resulting in compromised membrane integrity. As a result, cells may be more prone to releasing intracellular constituents. Since SYTO 9 staining did not indicate increased eDNA in Δ*mgtA* strain, these structures may be of proteinaceous nature, consistent with the protein-dominant nature of *L. monocytogenes* biofilms (Combrouse et al., 2013). Alternatively, this observation raises the possibility that MgtA, beyond its role as a metal ion transporter, may influence matrix secretion pathways. Further investigation is needed to determine whether MgtA affects the export of specific matrix-associated proteins or modulates cellular physiology in a way that alters biofilm architecture. Additional research should examine how Mg^{2+} availability and MgtA function shape the biochemical composition and mechanical persistence of *L. monocytogenes* biofilms under the FPE conditions. Such studies could clarify whether manipulation of Mg^{2+} levels or interference with transporter-linked pathways offers a viable strategy to destabilise biofilms in industrial environments.

6.7. Conclusion

In **Chapter 6**, we focused on phenotypic characterisation of genes associated with biofilm persistence and reduced disinfectant susceptibility. These genes were initially detected in **Chapter 4** using an in vitro BPM and were subsequently disrupted through targeted knockouts in **Chapter 5**.

Initial observations made with conventional assays to evaluate biofilm formation was supported by microscopic analysis and quantification of key biofilm structural parameters, including biofilm coverage, thickness, and biovolume. Biofilm thickness was significantly reduced in Δ*rsbU* and Δ*pyrD* mutant, with base area significantly increased in Δ*bglG* mutant. Likewise, biovolume was notably decreased in Δ*rsbU* mutant, consistent with the crystal violet data. We also detected presence of unique structural components in the Δ*rsbU* and Δ*mgtA* mutants, which resembled web-like filaments and porous matrix respectively. Notably, in several tested mutants, short-term cell attachment capacity was significantly reduced. Overall, we revealed that deletion of *rsbU* gene,

involved in transcription and stress response initiation, exhibited the most notable impact on biofilm-forming properties and physiology of the strain. In addition, we also detected that Mg^{2+} supplementation affects the cell attachment capacity and increases the biofilm base area but does not have an effect on other structural parameters.

Our findings reveal that persistence-associated loci in *L. monocytogenes* influence biofilm formation through multiple, distinct mechanisms. Transport systems such as *corA*, *mgtA*/*ykoK* appear to modulate matrix composition and potentially susceptibility to BC, while stress response regulation via *rsbU* shapes the balance between maintaining robust architecture and enabling stress-related adjustments. In parallel, metabolic pathways including *pyr* operon, connect nutrient availability to structural integrity and dispersal. This multifactorial control highlights that persistence in disinfectant-exposed environments is not driven by a single dominant pathway, but rather by the interplay of transport, stress adaptation, and metabolism.

Future work should aim to dissect the molecular mechanisms underlying the biofilm phenotypes described in this chapter, with an emphasis on characterising the FPE-associated matrix components of *L. monocytogenes* biofilms and determining how the disruption of metal homeostasis, stress response and pyrimidine synthesis pathways impact matrix composition.

Chapter 7: General Discussion

The overall aim of this work was to advance our understanding of the mechanisms that enable *L. monocytogenes* to persist in FPEs. We hypothesised that *L. monocytogenes* adaptation to FPE-associated stressors is facilitated by the acquisition of mutations that enhance biofilm formation and confer reduced biocide susceptibility. However, the specific genetic determinants of persistence, particularly in biofilm-associated cells, remain poorly understood. In this study, we aimed to address this gap by replicating realistic FPE conditions to model the transition of *L. monocytogenes* from a naïve, biocide-susceptible strain to one exhibiting traits associated with persistence. Using an adaptive evolution approach, we investigated the genetic and phenotypic changes that arise under repeated biocide exposure. After 30 consecutive passages, followed by WGS of the evolved populations, we identified mutations that became fixed over time and linked them to adaptative mechanisms supporting reduced disinfectant susceptibility and biofilm formation.

Emergence of Reduced Disinfectant Susceptibility in FPE Settings

We detected a diverse landscape of genetic changes associated with reduced susceptibility to BC, with the central genetic target being the *fepRA* operon. This finding supports previous studies (Douarre et al., 2022) and confirms the rapid acquisition of a phenotype showing a two-fold increase in MIC of BC. Importantly, we observed that adaptation to subinhibitory BC concentrations consistently targeted *fepR* not only in planktonic populations but also in biofilms, which was not detected by previous work. This suggests that the biofilm matrix alone is insufficient to protect against BC exposure, as the disinfectant likely penetrates the matrix and imposes stress on embedded cells. In such cases, mutations leading to FepR overexpression would therefore remain adaptively beneficial.

In our model, we observed non-synonymous mutations both within and outside of the DBD of *fepR*, with mutations outside the DBD showing higher prevalence. This contrasts with previous reports suggesting that approximately 75% of *fepR* mutations occur within the DBD (Bolten et al., 2022; Douarre et al., 2022). Additionally, we detected mutations not only in *fepR* and its intergenic region but also background mutations that consistently co-occurred with changes in the *fepRA* operon. Unlike earlier studies that primarily focused on isolated point mutations, our data provide a view of the mutational landscape accompanying *fepR* alterations. The persistence of clones harbouring specific

combinations of mutations into the later stages of the evolution experiment suggests that these combinations confer selective advantage. Although we did not observe a standalone effect of mutations in genes such as *corA* or *bglG* on reduced BC susceptibility, their consistent co-occurrence with *fepRA* mutations implies a potential complementary function. We hypothesise, *bglG* mutations may facilitate a metabolic shift to slow down metabolic processes, as a result reducing potential cellular targets for BC. This would parallel mechanisms described in antibiotic tolerance, where reduced metabolic activity or dormancy confers transient protection against antimicrobials (Balaban et al., 2019). In another hand, alterations in *corA* could contribute to improved export of the disinfectant. Both mechanisms may impact tolerance or reduced susceptibility indirectly, though further work will be required to validate their contributions.

Adaptation to Biofilm Lifestyle Under FPE Pressures

We identified a diverse repertoire of pathways that have not previously been associated with biofilm formation in *L. monocytogenes* (**Figure 52**). Although biofilm hyperproduction has been seen as an advantageous trait in long-term bead model evolution experiments (Trampari et al., 2021), we demonstrated that this is not the preferred trajectory for *L. monocytogenes.* Instead, we observed an early evolutionary shift towards reduced cell attachment. Our work challanges the traditional view that biofilm evolution consistently selects for stronger biofilm-forming phenotypes and aligns with recent findings by Amador et al., 2025, who suggested that adaptation may instead favor traits that optimise resource competition or metabolic efficiency over biofilm reinforcement.

rsb Operon

One of the most prominent findings of this study was the recurrent selection of mutations in the *rsb* operon during the BPM (**Figure 52**), and the impact of *rsbU* deletion on biofilm phenotypes. Deletion of *rsbU* led to a substantial reduction in biomass, a marked decrease in initial attachment to stainless steel, and significantly reduced biofilm thickness. SEM analysis also revealed the presence of web-like filaments in the Δ*rsbU* mutant, which we hypothesise may contribute to cell entrapment, aggregation, and carry-over. Our findings are consistent with the established role of stress response in supporting biofilm development. Van der Veen and Abee in 2010, reported that deletion of *sigB* impaired biofilm formation. Given that *rsbU* is critical for activation of *sigB* (Dessaux et al., 2021),

deletion of either gene is expected to result in comparable phenotypes. However, our findings also contrast with those of Hsu et al., 2020, who reported that Δ*rsbU* produced significantly more biomass and exhibited increased attachment. According to the current model, *rsbU* deletion prevents *sigB* activation, leaving SigB bound to the anti-sigma factor RsbW, preventing its interaction with the RNA polymerase and subsequent induction of the general stress regulon. In our parental strain, the initiation of biofilm formation could also be dependent on SigB activation of specific biofilm-related pathways, as loss of *rsbU* led to a significant reduction of biofilm. By contrast, in the EGD-e strain used by Hsu et al., SigB may repress pathways that enhance biofilm formation. In that context, *rsbU* deletion would derepress those pathways, leading to increase in biomass production. This hypothesis supports a strain- or sequence-type-specific variation in SigB-mediated regulation, with wild-type isolates like BL87-028 behaving differently from long-term laboratory strains.

Magnesium Homeostasis

Non-synonymous mutations in magnesium homeostasis systems emerged as a predominant feature of evolved biofilm lineages (**Figure 52**). The *ykoK* leader (M-box riboswitch) carried mutations near predicted magnesium-interactive sites and long-range base-pairing sites, suggesting potential disruption of riboswitch folding. Such disruption may affect M-box sensitivity to intracellular magnesium concentrations and, consequently, dysregulate *mgtA* expression. Alongside *ykoK* mutations, we observed co-occurring mutations in *mgtA* and *pitA*, particularly in predicted transmembrane domains, suggesting functional fine-tuning of ion transport activity. Coordinated changes in multiple transporters likely reflect an adaptive strategy to balance magnesium acquisition with energy cost. Such balance seems to be more critical to be maintained in biofilms, where ionic gradients, nutrient limitations, and metabolic stress differ significantly from planktonic conditions (Booth et al., 2011).

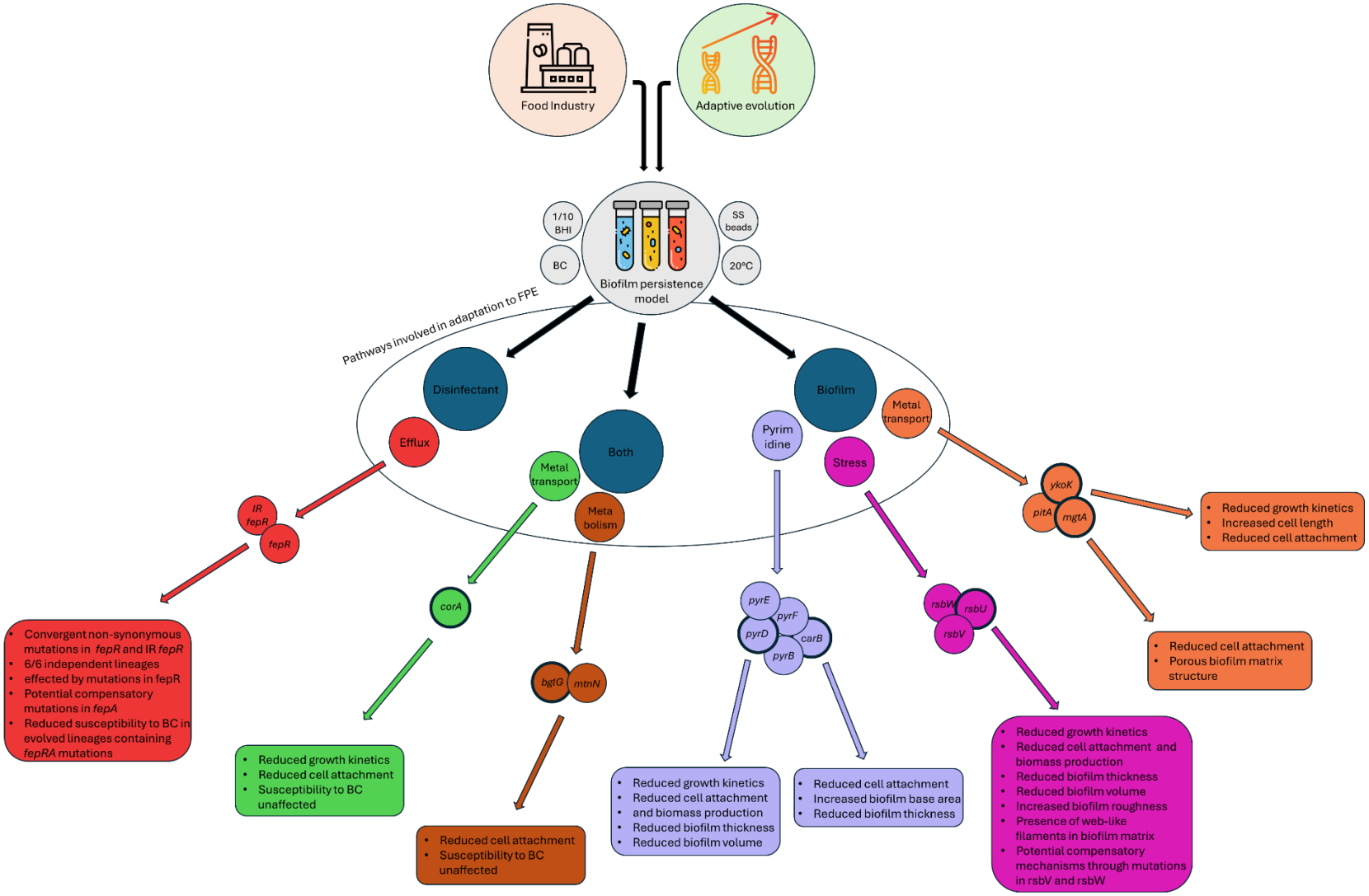

Food Industry
Adaptive evolution
1/10 BHI
BC
Biofilm persistence model
SS beads
20°C
Pathways involved in adaptation to FPE
Disinfectant
Efflux
Both
Metal transport
Meta bolism
Biofilm
Pyrim idine
Stress
Metal transport
IR fepR
fepR
corA
bglG
mtnN
pyrE
pyrF
pyrD
carB
pyrB
rsbW
rsbU
rsbV
ykoK
pitA
mgtA
• Convergent non-synonymous mutations in fepR and IR fepR
• 6/6 independent lineages
• effected by mutations in fepR
• Potential compensatory mutations in fepA
• Reduced susceptibility to BC in evolved lineages containing fepRA mutations
• Reduced growth kinetics
• Reduced cell attachment
• Susceptibility to BC unaffected
• Reduced cell attachment
• Susceptibility to BC unaffected
• Reduced growth kinetics
• Reduced cell attachment
• and biomass production
• Reduced biofilm thickness
• Reduced biofilm volume
• Reduced cell attachment
• Increased biofilm base area
• Reduced biofilm thickness
• Reduced growth kinetics
• Reduced cell attachment and biomass production
• Reduced biofilm thickness
• Reduced biofilm volume
• Increased biofilm roughness
• Presence of web-like filaments in biofilm matrix
• Potential compensatory mechanisms through mutations in rsbV and rsbW
• Reduced cell attachment
• Porous biofilm matrix structure
• Reduced growth kinetics
• Increased cell length
• Reduced cell attachment

Figure 52. Schematic representation of the experimental design and key scientific findings related to adaptive evolution under biofilm persistence and disinfectant exposure. The figure outlines the project workflow, highlighting the evolution experiments conducted under biofilm-forming and disinfectant-stressed conditions. Distinct groups of evolved populations are indicated: those evolved solely under disinfectant exposure, solely under biofilm conditions, and those exhibiting shared adaptive signatures under both conditions. Major genetic pathways impacted by adaptive evolution are labelled, including metabolism, stress response, metabolic pathways, efflux activity and metal homeostasis. Mutations that accumulated during adaptation are mapped to specific genes, with gene names indicated. Genes enclosed in blue rings were selected for targeted gene knockout to dissect their functional roles. Functional analysis of these gene deletions revealed phenotypic consequences in terms of biofilm formation capacity and biofilm architecture, reduced disinfectant susceptibility, growth kinetics, as indicated in the figure by directional arrows.

Metabolic Shift Under Sessile Lifestyle and Reduced Disinfectant Susceptibility

Metabolic processes differ substantially between biofilm and planktonic lifestyles, with shifts in glycolipid, amino acid, and carbohydrate metabolism (Lu et al., 2019). Biofilm formation is thought to begin with an initial burst of metabolic activity, which supports the production of extracellular matrix, followed by a reduction in metabolic activity in mature biofilms (Pisithkul et al., 2019). Reflecting this dynamic, many mutations selected under the BPM evolution affected metabolic pathways. Genes such as *bglG* and *mtnN* arose under both biofilm and BC selection, suggesting shared adaptations under different selective pressures. Other mutations (*rpiB*, *ndk*) appeared uniquely in disinfectant-treated populations, supporting the hypothesis that reduced metabolic activity decrease the number of active antimicrobial targets. These findings are consistent with previous work by Crabbé et al., in 2019, which demonstrated that regions of low metabolic activity within biofilms contribute to antibiotic tolerance.

The Strength of the Adaptive Evolution Bead Model

Captures a Complex Selective Landscape of Adaptation

Lineages evolved under both biofilm and disinfectant conditions accumulated mutations in a wide range of functional gene groups, highlighting that adaptation involves many overlapping mechanisms rather than a single dominant pathway. Although this complexity may make it difficult to link specific mutations to phenotypic outcomes, since numerous genes are affected within the same isolate, this diversity of responses is also informative, because it reflects bacterial adaptation in real-world environments.

Captures Convergent Evolution and Reproducibility

The bead model also revealed a high degree of reproducibility across independent lineages. We consistently observed convergent mutations in the same pathways, even though the specific genetic changes varied between lineages. This pattern indicates that adaptation follows predictable trajectories shaped by selective pressures. Such consistency across replicates strengthens confidence in the model as a robust tool for identifying key adaptive pathways and mechanisms.

Captures Emergence of Compensatory Mechanisms

The strength of the BPM lies not only in detecting acquisition of adaptation mechanisms against disinfectants, but also in uncovering long-term compensatory mechanisms. For example, we identified previously unreported mutations in *fepA* that co-occurred with a premature stop codon in *fepR*. These mutations are likely to reduce FepA function, potentially counteracting the constitutive overexpression driven by *fepR* inactivation and alleviating the fitness cost associated with efflux hyperactivity.

Unlike the straightforward *fepR–fepA* compensatory pair, compensation within the *rsb* operon occurs at the regulatory-network level. Loss of *rsbU* prevents activation of SigB, locking it in an inactive state. A premature stop codon in *rsbW,* found within the same lineage as the premature stop codon in *rsbU,* may provide a compensatory solution. We hypothesise that by removing the anti-sigma factor (*RsbW*) that normally sequesters SigB, the cell bypasses the need for *rsbU*-mediated activation and restores SigB activity.

Overall, identification of compensatory mechanisms is a strong advantage of using the bead model, as it not only detects adaptations to stress that often involve fitness trade-offs, but also reveals how bacteria balance out these trade-offs to stabilise the phenotype.

Limitations of the Study

Although we believe this work offers important mechanistic insights into the adaptation of *L. monocytogenes* to the FPE niche, several limitations must be considered. Firstly, we used a modelling approach, which is a simplified representation of a more complex biological system. Although we mimicked real-world FPE conditions, including low nutrient availability, stainless steel as the contact surface, and sub-inhibitory concentrations of disinfectants, other factors could not be fully replicated. One such factor is organic load. In real FPEs, residues such as grease, proteins, and carbohydrates can neutralize disinfectants and reduce their activity (Gélinas and Goulet, 1983; Iñiguez-Moreno, Avila-Novoa and Gutiérrez-Lomelí, 2018; Asli Şahiner et al., 2022), whereas our bead system used clean stainless steel without organic matter. Similarly, flow dynamics and spatial heterogeneity of factory environments are not captured by the bead setup. Temperature is another important limitation. We maintained 20 °C throughout the adaptive experiment to compensate for the extension of replication time associated with lower temperatures, whereas in real-world FPEs cold storage temperatures are typically 8 °C or below to suppress pathogen growth and toxin production (FSA, 2016). We

acknowledge that *L. monocytogenes* may respond differently to the same stressors under lower temperatures.

Another limitation is the use of a single-species model rather than a multi-species community, as it overlooks the impact of the wider FPE microbiome, which often includes strong biofilm matrix producers that can offer protection by creating diffusion barriers. Studies that aim to model FPE adaptation should seek to incorporate microbial community complexity. Using single species also prevents capture of horizontal gene transfer (HGT), a process that can fundamentally alter evolutionary trajectories by introducing advantageous traits from neighbouring species (Cooper, 2018). In addition, our study was performed using a single isolate belonging to ST121. While this choice was deliberate, allowing us to track *de novo* adaptation in a biocide-susceptible background, it limits generalisation of the results. Many ST121 isolates already display elevated tolerance levels to BC. In particular, *qacH,* a transposon harboured efflux pump gene, is now widely carried by *L. monocytogenes* and raises the MIC for BC (Gutiérrez et al., 2025). Our baseline strain therefore may not reflect the tolerance levels typically found in today's industrial isolates.

Finally, we used analytical-grade BC rather than a formulated disinfectant product. Commercial disinfectants contain surfactants that can influence antimicrobial activity and microbial adaptation which is not captured by pure compounds. In addition, C&D is not limited to disinfectants but also involves detergents that remove soil and organic residues, adding further selective pressures. Together, these considerations highlight that while our model provides valuable insights into evolutionary mechanisms, its translation to FPE realities must be made with caution.

Future Work

One important unresolved question from our work concerns the survival advantage conferred by background mutations that were not the central target of adaptation but nonetheless became fixed in evolved populations. These mutations outside of primary adaptive targets remain underexplored in studies of microbial evolution. Future work could focus on constructing mutant panels that include different combinations of background mutations and assessing their competitive fitness under FPE relevant stresses. Such experiments could also examine how combinations of mutations influence cross-tolerance to commonly used antimicrobial classes against *L. monocytogenes*. Finally, we

could also evaluate the fitness costs associated with the most prevalent mutations in larger microbial communities to see whether they confer survival advantages against competing species.

In parallel, surveillance of isolates from our own collections and from publicly available genomes could help determine the prevalence of detected mutations across clinical, food, and environmental sources, to evaluate if detected patterns of mutation acquisition are seen in a wider range of isolates.

The Future of the Bead Model

Having demonstrated the viability and strength of the bead model for tracking evolutionary trajectories in a Gram-positive single-species system, future work should focus on expanding the model to represent the community dynamics observed in real-world FPEs. This could be achieved by incorporating other bacterial genera that frequently co-occur with *Listeria* in these environments, such as *Pseudomonas* (with *P. fluorescens* being most abundant, alongside *P. caeni*, *P. viridiflava*, and *P. rhizosphaerae*), as well as *Psychrobacter*, *Sphingomonas*, *Chryseobacterium*, *Streptococcus thermophilus*, and *Galactobacter caseinivorans*, all of which have been reported in the shared niches (Diaz et al., 2025; Tan et al., 2019; Zwirzitz et al., 2021).

Conclusion

Collectively, this study demonstrates that the in vitro bead-based model provides a powerful framework for investigating the evolutionary trajectories of Gram-positive bacteria and can be adapted to a variety of selective pressures and environmental conditions. We demonstrated that mutants with a reduced susceptibility to QAC biocides such as BC can be rapidly selected under both biofilm and planktonic lifestyles. While biofilms were not inherently predisposed to developing tolerance, biofilm lineages survived higher disinfectant concentrations in our model than planktonic lineages. Our findings also evidence new insights into the genetic traits of biofilm persistence in FPEs and highlight potential targets exploited by *L. monocytogenes* to establish and maintain niches under otherwise unfavourable conditions. In particular, magnesium homeostasis, stress response, and pyrimidine synthesis pathways emerged as key contributors of biofilm resilience. Finally, using a longitudinal experimental evolution approach, enabled us to detect compensatory mechanisms that would likely remain undetected in single time-point studies.

References

Abachin, E., Poyart, C., Pellegrini, E., Milohanic, E., Fiedler, F., Berche, P. and Trieu-Cuot, P. (2002). Formation of D-alanyl-lipoteichoic acid is required for adhesion and virulence of *Listeria monocytogenes*. *Molecular Microbiology*, 43(1), pp.1–14. doi:https://doi.org/10.1046/j.1365-2958.2002.02723.x.

Abdelhamed, H., Lawrence, M., Ramachandran, R. and Karsi, A. (2019). Validation of Predicted Virulence Factors in *Listeria monocytogenes* Identified Using Comparative Genomics. *Toxins*, 11(9), p.508. doi:https://doi.org/10.3390/toxins11090508.

Abdelhamed, H., Lawrence, M.L. and Karsi, A. (2015). A novel suicide plasmid for efficient gene mutation in *Listeria monocytogenes*. *Plasmid*, 81, pp.1–8. doi:https://doi.org/10.1016/j.plasmid.2015.05.003.

Adams, J. and Rosenzweig, F. (2014). Experimental microbial evolution: history and conceptual underpinnings. *Genomics*, 104(6), pp.393–398. doi:https://doi.org/10.1016/j.ygeno.2014.10.004.

Adams, J.L. and McLean, R.J.C. (1999). Impact of *rpoS* Deletion on *Escherichia coli* Biofilms. *Applied and Environmental Microbiology*, 65(9), pp.4285–4287. doi:https://doi.org/10.1128/aem.65.9.4285-4287.1999.

Afgan, E., Baker, D., Batut, B., van den Beek, M., Bouvier, D., Čech, M., Chilton, J., Clements, D., Coraor, N., Grüning, B.A., Guerler, A., Hillman-Jackson, J., Hiltemann, S., Jalili, V., Rasche, H., Soranzo, N., Goecks, J., Taylor, J., Nekrutenko, A. and Blankenberg, D. (2018). The Galaxy platform for accessible, reproducible reproducible, and collaborative biomedical analyses: 2018 update. *Nucleic Acids Research*, 46(W1), pp.W537–W544.

Allkja, J., van Charante, F., Aizawa, J., Reigada, I., Guarch-Pérez, C., Vazquez-Rodriguez, J.A., Cos, P., Coenye, T., Fallarero, A., Zaat, S.A.J., Felici, A., Ferrari, L., Azevedo, N.F., Parker, A.E. and Goeres, D.M. (2021). Interlaboratory study for the evaluation of three microtiter plate-based biofilm quantification methods. *Scientific Reports*, [online] 11(1). doi:https://doi.org/10.1038/s41598-021-93115-w.

Allwood, A.C., Walter, M.R., Burch, I.W. and Kamber, B.S. (2007). 3.43 billion-year-old stromatolite reef from the Pilbara Craton of Western Australia: Ecosystem-scale insights to early life on Earth. *Precambrian Research*, 158(3-4), pp.198–227. doi:https://doi.org/10.1016/j.precamres.2007.04.013.

Altschul, S.F., Gish, W., Miller, W., Myers, E.W. and Lipman, D.J. (1990). Basic local alignment search tool. *Journal of Molecular Biology*, 215(3), pp.403–410. doi:https://doi.org/10.1016/S0022-2836(05)80360-2.

Amador, C.I., Moscovitz, S.Z., Maccario, L., Jakob Herschend, Kramer, I.-S., Jeckel, H., Cooper, V.S., Drescher, K., Neu, T.R., Mette Burmølle and Røder, H.L. (2025). Evolution of genotypic and phenotypic diversity in multispecies biofilms. *npj Biofilms and Microbiomes*, 11(1). doi:https://doi.org/10.1038/s41522-025-00755-1.

Amaya-Villar, R., García-Cabrera, E., Sulleiro-Igual, E., Fernández-Viladrich, P., Dionisi Fontanals-Aymerich, Catalán-Alonso, P., Rodrigo, C., Coloma-Conde, A., Fabio Grill-Díaz, Guerrero-Espejo, A., Jerónimo Pachón and Guillén Prats-Pastor (2010). Three-year multicenter

surveillance of community-acquired *L. monocytogenes* meningitis in adults. *BMC Infectious Diseases*, 10(1).

Amster-Choder, O. and Wright, A. (1993). Transcriptional regulation of thebgl operon of *Escherichia coli* involves phosphotransferase system-mediated phosphorylation of a transcriptional antiterminator. *Journal of Cellular Biochemistry*, 51(1), pp.83–90. doi:https://doi.org/10.1002/jcb.240510115.

Andersen, J.T., Petersen, M., Jimenez-Solem, E., Broedbaek, K., Andersen, E.W., Andersen, N.L., Afzal, S., Torp-Pedersen, C., Keiding, N. and Poulsen, H.E. (2012). Trimethoprim use in early pregnancy and the risk of miscarriage: a register-based nationwide cohort study. *Epidemiology and Infection*, 141(8), pp. 1749–1755. doi: https://doi.org/10.1017/s0950268812002178.

Arnaud, M., Chastanet, A. and Debarbouille, M. (2004). New Vector for Efficient Allelic Replacement in Naturally Non-transformable, Low-GC-Content, Gram-Positive Bacteria. *Applied and Environmental Microbiology*, [online] 70(11), pp.6887–6891. doi:https://doi.org/10.1128/aem.70.11.6887-6891.2004.

Arnold, J.W. and Bailey, G.W. (2000). Surface finishes on stainless steel reduce bacterial attachment and early biofilm formation: scanning electron and atomic force microscopy study. *Poultry Science*, 79(12), pp.1839–1845. doi:https://doi.org/10.1093/ps/79.12.1839.

Aryal, M. and Muriana, P.M. (2019). Efficacy of Commercial Sanitizers Used in Food Processing Facilities for Inactivation of *L. monocytogenes, E. Coli* O157:H7, and Salmonella Biofilms. *Foods*, 8(12), p.639.

Şahiner, A., Halat, E., Algın Yapar, E., & Kara, B. A. (2022). Evaluation of organic load related efficacy changes in antiseptic solutions used in hospitals. *Turkish Journal of Medical Sciences*, 52(3), 825–833. https://doi.org/10.55730/1300-0144.5379.

Autret, N., Raynaud, C., Dubail, I., Berche, P. and Charbit, A. (2003). Identification of the agr Locus of *L. monocytogenes*: Role in Bacterial Virulence. *Infection and Immunity*, 71(8), pp.4463–4471. doi:https://doi.org/10.1128/iai.71.8.4463-4471.2003.

Bae, T. and Schneewind, O. (2006). Allelic replacement in *Staphylococcus aureus* with inducible counter-selection. *Plasmid*, 55(1), pp.58–63. doi:https://doi.org/10.1016/j.plasmid.2005.05.005.

Balaban, N.Q. (2004). Bacterial Persistence as a Phenotypic Switch. *Science*, 305(5690), pp.1622–1625.

Balaban, N.Q., Helaine, S., Lewis, K., Ackermann, M., Aldridge, B., Andersson, D.I., Brynildsen, M.P., Bumann, D., Camilli, A., Collins, J.J., Dehio, C., Fortune, S., Ghigo, J.-M., Hardt, W.-D., Harms, A., Heinemann, M., Hung, D.T., Jenal, U., Levin, B.R. and Michiels, J. (2019). Definitions and guidelines for research on antibiotic persistence. *Nature Reviews Microbiology*, [online] 17(7), pp.441–448. doi:https://doi.org/10.1038/s41579-019-0196-3.

Barbosa, J., Borges, S., Camilo, R., Magalhães, R., Ferreira, V., Santos, I., Silva, J., Almeida, G. and Teixeira, P. (2013). Biofilm Formation among Clinical and Food Isolates of *L.*

monocytogenes. *International Journal of Microbiology*, 2013, pp.1–6. doi:https://doi.org/10.1155/2013/524975.

Barnett, M., Meister, L. and Rainey, P.B. (2025). Experimental evolution of evolvability. *Science*, 387(6736). doi:https://doi.org/10.1126/science.adr2756.

Barnhart, M.M. and Chapman, M.R. (2006). Curli Biogenesis and Function. *Annual Review of Microbiology*, 60(1), pp.131–147. doi:https://doi.org/10.1146/annurev.micro.60.080805.142106.

Bechtel, T.D., Hershelman, J., Ghoshal, M., McLandsborough, L. and Gibbons, J.G. (2024). Chemical mutagenesis of *Listeria monocytogenes* for increased tolerance to benzalkonium chloride shows independent genetic underpinnings and off-target antibiotic resistance. PLoS ONE, 19(7), pp.e0305663–e0305663. doi:https://doi.org/10.1371/journal.pone.0305663.

Becker, L.A., Mehmet Sevket Çetin, Hutkins, R.W. and Benson, A.K. (1998). Identification of the Gene Encoding the Alternative Sigma Factor ς ^{B} from *Listeria monocytogenes* and Its Role in Osmotolerance. *Journal of Bacteriology*, 180(17), pp.4547–4554. doi:https://doi.org/10.1128/jb.180.17.4547-4554.1998.

Bejder, B.S., Monda, F., Gless, B.H., Bojer, M.S., Ingmer, H. and Olsen, C.A. (2024). A short-lived peptide signal regulates cell-to-cell communication in *L. monocytogenes*. *Communications Biology*, 7(1). doi:https://doi.org/10.1038/s42003-024-06623-6.

Beloin, C., Roux, A. and Ghigo, J.M. (2008). *Escherichia coli* biofilms. *Current topics in microbiology and immunology*, [online] 322, pp.249–89. doi:https://doi.org/10.1007/978-3-540-75418-3_12.

Benoit, M., Conant, C.G., Ionescu-Zanetti, C., Schwartz, M.A. and Matin, A. (2010). New Device for High-Throughput Viability Screening of Flow Biofilms. *Applied and Environmental Microbiology*, 76(13), pp.4136–4142. doi:https://doi.org/10.1128/aem.03065-09.

Berman, H.M. (2000). The Protein Data Bank. *Nucleic Acids Research*, [online] 28(1), pp.235–242. doi:https://doi.org/10.1093/nar/28.1.235.

Berrang, M.E. and Frank, J.F. (2012). Generation of airborne *Listeria innocua* from model floor drains. *Journal of Food Protection*, 75(7), pp. 1328–1331. doi: https://doi.org/10.4315/0362-028x.jfp-12-021.

Bhomkar, P., Materi, W., Semenchenko, V. and Wishart, D.S. (2010). Transcriptional Response of E. coli Upon FimH-mediated Fimbrial Adhesion. *Gene Regulation and Systems Biology*, 4, p.GRSB.S4525. doi:https://doi.org/10.4137/grsb.s4525.

Bigot, A., Pagniez, H., Botton, E., Fréhel, C., Dubail, I., Jacquet, C., Charbit, A. and Raynaud, C. (2005). Role of FliF and FliI of *Listeria monocytogenes* in Flagellar Assembly and Pathogenicity. *Infection and Immunity*, 73(9), pp.5530–5539. doi:https://doi.org/10.1128/iai.73.9.5530-5539.2005.

Blackman, I.C. and Frank, J.F. (1996). Growth of *Listeria monocytogenes* as a biofilm on various food-processing surfaces. *Journal of Food Protection*, 59(8), pp. 827–831. doi: https://doi.org/10.4315/0362-028x-59.8.827

Blanco-Cabra, N., López-Martínez, M.J., Arévalo-Jaimes, B.V., Martin-Gómez, M.T., Samitier, J. and Torrents, E. (2021). A new BiofilmChip device for testing biofilm formation and antibiotic susceptibility. *npj Biofilms and Microbiomes*, [online] 7(1), pp.1–9. doi:https://doi.org/10.1038/s41522-021-00236-1.

Blum, M., Andreeva, A., Florentino, L., Chuguransky, S., Grego, T., Hobbs, E., Pinto, B., Orr, A., Paysan-Lafosse, T., Ponamareva, I., Salazar, G., Bordin, N., Bork, P., Bridge, A., Colwell, L., Gough, J., Haft, D., Letunic, I., Llinares-López, F. and Marchler-Bauer, A. (2024). InterPro: the protein sequence classification resource in 2025. Nucleic Acids Research, [online] 53(D1). doi:https://doi.org/10.1093/nar/gkae1082.

Blum, M., Chang, H.-Y., Chuguransky, S., Grego, T., Kandasaamy, S., Mitchell, A., Nuka, G., Paysan-Lafosse, T., Qureshi, M., Raj, S., Richardson, L., Salazar, G.A., Williams, L., Bork, P., Bridge, A., Gough, J., Haft, D.H., Letunic, I., Marchler-Bauer, A. and Mi, H. (2020). The InterPro protein families and domains database: 20 years on. *Nucleic Acids Research*, 49(D1), pp.D344–D354. doi:https://doi.org/10.1093/nar/gkaa977.

Boles, B.R., Thoendel, M. and Singh, P.K. (2005). Rhamnolipids mediate detachment ofPseudomonas aeruginosafrom biofilms. *Molecular Microbiology*, 57(5), pp.1210–1223. doi:https://doi.org/10.1111/j.1365-2958.2005.04743.x.

Bolten, S., Harrand, A. S., Skeens, J., & Wiedmann, M. (2022). Nonsynonymous Mutations in *fepR* Are Associated with Adaptation of *Listeria monocytogenes* and Other *Listeria* spp. to Low Concentrations of Benzalkonium Chloride but Do Not Increase Survival of *L. monocytogenes* and Other *Listeria* spp. after Exposure to Benzalkonium Chloride Concentrations Recommended for Use in Food Processing Environments. *Applied and Environmental Microbiology*, *88*(11). https://doi.org/10.1128/aem.00486-22

Booth, S.C., Workentine, M.L., Wen, J., Shaykhutdinov, R., Vogel, H.J., Ceri, H., Turner, R.J. and Weljie, A.M. (2011). Differences in Metabolism between the Biofilm and Planktonic Response to Metal Stress. Journal of Proteome Research, 10(7), pp.3190–3199. doi:https://doi.org/10.1021/pr2002353.

Borucki, M.K. and Call, D.R. (2003). *Listeria monocytogenes* Serotype Identification by PCR. *Journal of Clinical Microbiology*, 41(12), pp.5537–5540. doi:https://doi.org/10.1128/jcm.41.12.5537-5540.2003.

Bos, R., van der Mei, H.C. and Busscher, H.J. (1999). Physico-chemistry of initial microbial adhesive interactions - its mechanisms and methods for study. *FEMS Microbiology Reviews*, 23(2), pp.179–230. doi:https://doi.org/10.1111/j.1574-6976.1999.tb00396.x.

Bridier, A., Dubois-Brissonnet, F., Boubetra, A., Thomas, V. and Briandet, R. (2010). The biofilm architecture of sixty opportunistic pathogens deciphered using a high throughput CLSM method. *Journal of Microbiological Methods*, 82(1), pp.64–70.

British Stainless Steel Association Stainless Steel Advisory Service Corrosion of Stainless Steels in Supply (Drinking) and Waste (Sewage) Water Systems. (2001). Available at: https://bssa.org.uk/wp-content/uploads/2021/04/SSAS4.92-Stainless-Steels-in-Supply-Waste-Waters.pdf [Accessed 26 Sep. 2025].

Brito, I.L. (2021). Examining horizontal gene transfer in microbial communities. *Nature Reviews Microbiology*, 19(7), pp.442–453. doi:https://doi.org/10.1038/s41579-021-00534-7.

Bronesky, D., Wu, Z., Marzi, S., Walter, P., Geissmann, T., Moreau, K., Vandenesch, F., Caldelari, I. and Romby, P. (2016). *Staphylococcus aureus* RNAIII and Its Regulon Link Quorum Sensing, Stress Responses, Metabolic Adaptation, and Regulation of Virulence Gene Expression. *Annual Review of Microbiology*, 70(1), pp.299–316. doi:https://doi.org/10.1146/annurev-micro-102215-095708.

Brooun, A., Liu, S. and Lewis, K. (2000). A Dose-Response Study of Antibiotic Tolerance in Pseudomonas aeruginosa Biofilms. *Antimicrobial Agents and Chemotherapy*, 44(3), pp.640–646. doi:https://doi.org/10.1128/aac.44.3.640-646.2000.

Brouwer, M. C., & van de Beek, D. (2023). Adjunctive dexamethasone treatment in adults with *Listeria monocytogenes* meningitis: A prospective nationwide cohort study. *EClinicalMedicine, 58*, 101922. https://doi.org/10.1016/j.eclinm.2023.101922.

Brown, P., Chen, Y., Siletzky, R.M., Parsons, C., Lee-Ann Jaykus, Eifert, J.D., Ryser, E.T., Logue, C.M., Stam, C.M., Brown, E.W. and Kathariou, S. (2021). Harnessing Whole Genome Sequence Data for Facility-Specific Signatures for *Listeria monocytogenes*: A Case Study With Turkey Processing Plants in the United States. *Frontiers in sustainable food systems*, 5. doi:https://doi.org/10.3389/fsufs.2021.742353.

Buffet-Bataillon, S., Tattevin, P., Maillard, J.-Y., Bonnaure-Mallet, M. and Jolivet-Gougeon, A. (2016). Efflux pump induction by quaternary ammonium compounds and fluoroquinolone tolerance in bacteria. *Future Microbiology*, 11(1), pp.81–92.

Burn, C. G. (1935). Characteristics of a new species of the genus *Listerella* obtained from human sources. *Journal of Bacteriology, 30*(6), 573–591.

Butler, J.P., Tolić-Nørrelykke, I.M., Fabry, B. and Fredberg, J.J. (2002). Traction fields, moments, and strain energy that cells exert on their surroundings. *American Journal of Physiology-Cell Physiology*, 282(3), pp.C595–C605.

Buzzo, J.R., Devaraj, A., Gloag, E.S., Jurcisek, J.A., Robledo-Avila, F., Kesler, T., Wilbanks, K., Mashburn-Warren, L., Balu, S., Wickham, J., Novotny, L.A., Stoodley, P., Bakaletz, L.O. and Goodman, S.D. (2021). Z-form extracellular DNA is a structural component of the bacterial biofilm matrix. *Cell*, 184(23), pp.5740-5758.e17. doi:https://doi.org/10.1016/j.cell.2021.10.010.

C., Van Domselaar, G., Pagotto, F. and Graham, M. (2019). Shared genome analyses of notable listeriosis outbreaks, highlighting the critical importance of epidemiological evidence, input datasets and interpretation criteria. *Microbial Genomics*, 5(1).

Cai, Y., Tao, H., Gaballa, A., Pi, H. and Helmann, J.D. (2025). The extracytoplasmic sigma factor σX supports biofilm formation and increases biocontrol efficacy in *Bacillus velezensis* 118. *Scientific Reports*, 15(1). doi:https://doi.org/10.1038/s41598-025-89284-7.

Carstens, C.K., Salazar, J.K., Bathija, V.M., Narula, S.S., Wang, P. and Tortorello, M.L. (2018). Control of *Listeria monocytogenes* in caramel apples by use of sticks pretreated with potassium sorbate. *Journal of Food Protection*, 81(12), pp. 1921–1928. doi: https://doi.org/10.4315/0362-028x.jfp-18-175.

CDC (2024). *Disinfection and Sterilization Guideline*. [online] Infection Control. Available at: https://www.cdc.gov/infection-control/hcp/disinfection-and-sterilization/index.html.

CDC (2024). *Factors Affecting the Efficacy of Disinfection and Sterilization*. [online] Infection Control. Available at: https://www.cdc.gov/infection-control/hcp/disinfection-sterilization/efficacy-factors.html?utm_source=chatgpt.com.

CDC (2024). *Multistate Outbreak of Listeriosis Linked to Frozen Vegetables | Listeria | CDC*. [online] Available at: https://archive.cdc.gov/www_cdc_gov/listeria/outbreaks/frozen-vegetables-05-16/index.html?utm_source=chatgpt.com [Accessed 26 Sep. 2025].

Center for Veterinary Medicine (2019). *Get the Facts about Listeria!* [online] U.S. Food and Drug Administration. Available at: https://www.fda.gov/animal-veterinary/animal-health- literacy/get-facts-about-listeria.

Ceri, H., Olson, M.E., Stremick, C., Read, R.R., Morck, D. and Buret, A. (1999). The Calgary Biofilm Device: New Technology for Rapid Determination of Antibiotic Susceptibilities of Bacterial Biofilms. *Journal of Clinical Microbiology*, 37(6), pp.1771–1776. doi:https://doi.org/10.1128/jcm.37.6.1771-1776.1999.

Ceruso, M., Clement, J.A., Todd, M.J., Zhang, F., Huang, Z., Anastasio, A., Pepe, T. and Liu, Y. (2020). The Inhibitory Effect of Plant Extracts on Growth of the Foodborne Pathogen, *Listeria monocytogenes. Antibiotics (Basel, Switzerland)*, [online] 9(6). doi:https://doi.org/10.3390/antibiotics9060319.

Chaitiemwong, N., Hazeleger, W.C. and Beumer, R.R. (2010). Survival of *L. monocytogenes* on a conveyor belt material with or without antimicrobial additives. *International Journal of Food Microbiology*, [online] 142(1), pp.260–263. doi:https://doi.org/10.1016/j.ijfoodmicro.2010.06.021.

Chalke, S., Vidović, S., Fletcher, G.C., Palmer, J.W. and Flint, S. (2022). Differential effects of magnesium, calcium, and sodium on *Listeria monocytogenes* biofilm formation. *Biofouling*, 38(8), pp.786–795. doi:https://doi.org/10.1080/08927014.2022.2131398.

Challan Belval, S., Gal, L., Margiewes, S., Garmyn, D., Piveteau, P. and Guzzo, J. (2006). Assessment of the Roles of LuxS, *S*-Ribosyl Homocysteine, and Autoinducer 2 in Cell Attachment during Biofilm Formation by *Listeria monocytogenes* EGD-e. *Applied and Environmental Microbiology*, 72(4), pp.2644–2650. doi:https://doi.org/10.1128/aem.72.4.2644-2650.2006.

Charlier, C., Perrodeau, É., Leclercq, A., Cazenave, B., Pilmis, B., Henry, B., Lopes, A., Maury, M.M., Moura, A., Goffinet, F., Dieye, H.B., Thouvenot, P., Ungeheuer, M.-N., Tourdjman, M., Goulet, V., de Valk, H., Lortholary, O., Ravaud, P., Lecuit, M. and Hausfater, P. (2017). Clinical features and prognostic factors of listeriosis: the MONALISA national prospective cohort study. *The Lancet Infectious Diseases*, 17(5), pp.510–519. doi:https://doi.org/10.1016/s1473-3099(16)30521-7.

Chatterjee, D., Daya Manasi, A.R., Rastogi, S.K., Panda, A.P., Biju, B., Bhattacharyya, D. and Ghosh, A.S. (2024). Involvement of CorA of *Mycobacterium smegmatis* in exerting intrinsic resistance towards structurally unrelated antibiotics. Journal of Applied Microbiology, 135(12). doi:https://doi.org/10.1093/jambio/lxae298.

Chaturongakul, S. and Boor, K.J. (2004). RsbT and RsbV Contribute to B-Dependent Survival under Environmental, Energy, and Intracellular Stress Conditions in L. monocytogenes. *Applied and Environmental Microbiology*, 70(9), pp.5349–5356. doi:https://doi.org/10.1128/aem.70.9.5349-5356.2004.

Chaturongakul, S., Raengpradub, S., Palmer, M. E., Bergholz, T. M., Orsi, R. H., Hu, Y., Ollinger, J., Wiedmann, M., & Boor, K. J. (2011). Transcriptomic and Phenotypic Analyses Identify Coregulated, Overlapping Regulons among PrfA, CtsR, HrcA, and the Alternative Sigma Factors σ^B, σ^C, σ^H, and σ^L in *Listeria monocytogenes*. *Applied and Environmental Microbiology*, *77*(1), 187–200. https://doi.org/10.1128/aem.00952-10

Chaturongkasumrit, Y., Takahashi, H., Keeratipibul, S., Kuda, T. and Kimura, B. (2011). The effect of polyesterurethane belt surface roughness on *Listeria monocytogenes* biofilm formation and its cleaning efficiency. *Food Control*, 22(12), pp.1893–1899. doi:https://doi.org/10.1016/j.foodcont.2011.04.032.

Chen, S., Zhou, Y., Chen, Y. and Gu, J. (2018). fastp: an ultra-fast all-in-one FASTQ preprocessor. *Bioinformatics*, [online] 34(17), pp.i884–i890. Available at: https://academic.oup.com/bioinformatics/article/34/17/i884/5093234.

Chen, Y., Gonzalez-Escalona, N., Hammack, T.S., Allard, M.W., Strain, E.A. and Brown, E.W. (2016). Core Genome Multilocus Sequence Typing for Identification of Globally Distributed Clonal Groups and Differentiation of Outbreak Strains of *Listeria monocytogenes*. *Applied and Environmental Microbiology*, 82(20), pp.6258–6272. doi:https://doi.org/10.1128/aem.01532-16.

Chiang, W.-C., Pamp, S.J., Nilsson, M., Givskov, M. and Tolker-Nielsen, T. (2012). The metabolically active subpopulation in *Pseudomonas aeruginosa* biofilms survives exposure to membrane-targeting antimicrobials via distinct molecular mechanisms. *FEMS Immunology & Medical Microbiology*, 65(2), pp.245–256. doi:https://doi.org/10.1111/j.1574-695x.2012.00929.x.

Chiaverini, A., Guidi, F., Torresi, M., Vicdalia Aniela Acciari, Centorotola, G., Cornacchia, A., Patrizia Centorame, Marfoglia, C., Blasi, G., Marco Di Domenico, Giacomo Migliorati, Roussel, S., Pomilio, F. and Yann Sevellec (2021). Phylogenetic Analysis and Genome-Wide Association Study Applied to an Italian *L. monocytogenes* Outbreak. *Frontiers in Microbiology*, 12. doi:https://doi.org/10.3389/fmicb.2021.750065.

Christensen, G.D., Simpson, W.A., Younger, J.J., Baddour, L.M., Barrett, F.F., Melton, D.M. and Beachey, E.H. (1985). Adherence of coagulase-negative *staphylococci* to plastic tissue culture plates: a quantitative model for the adherence of *staphylococci* to medical devices. *Journal of Clinical Microbiology*, 22(6), pp.996–1006. doi:https://doi.org/10.1128/jcm.22.6.996-1006.1985.

Clark, D.R., Chaturvedi, V., Kinder, J.M., Jiang, T.T., Xin, L., Ertelt, J.M. and Way, S.S. (2014). Perinatal *L. monocytogenes* susceptibility despite preconceptual priming and maintenance of pathogen-specific CD8+ T cells during pregnancy. *Cellular & Molecular Immunology*, 11(6), pp.595–605.

Clinical and laboratory standards institute (2018). *Methods for antimicrobial dilution susceptibility tests for bacteria that grow aerobically*. Wayne, PA, USA: Clinical and laboratory standards institute.

Cobo-Díaz, J.F., Alvarez-Molina, A., Alexa, E.A., Walsh, C.J., Mencía-Ares, O., Puente-Gómez, P., Likotrafiti, E., Fernández-Gómez, P., Prieto, B., Crispie, F., Ruiz, L., González-Raurich, M., López, M., Prieto, M., Cotter, P. and Alvarez-Ordóñez, A. (2021). Microbial colonization and resistome dynamics in food processing environments of a newly opened pork cutting industry during 1.5 years of activity. Microbiome, 9(1). doi:https://doi.org/10.1186/s40168-021-01131-9.
Colagiorgi, A., Bruini, I., Di Ciccio, P. A., Zanardi, E., Ghidini, S., & Ianieri, A. (2017). Listeria monocytogenes Biofilms in the Wonderland of Food Industry. *Pathogens*, *6*(3), 41. https://doi.org/10.3390/pathogens6030041

Colagiorgi, A., Bruini, I., Di Ciccio, P.A., Zanardi, E., Ghidini, S. and Ianieri, A. (2017). *L. monocytogenes* Biofilms in the Wonderland of Food Industry. P*athogens*, 6(3), p.41.

Colagiorgi, A., Di Ciccio, P., Zanardi, E., Ghidini, S. and Ianieri, A. (2016). A Look inside the *Listeria monocytogenes* Biofilms Extracellular Matrix. *Microorganisms*, 4(3), p.22. doi:https://doi.org/10.3390/microorganisms4030022.

Combrouse, T., Sadovskaya, I., Faille, C., Kol, O., Guérardel, Y. and Midelet-Bourdin, G. (2013). Quantification of the extracellular matrix of the *Listeria monocytogenes* biofilms of different phylogenic lineages with optimization of culture conditions. *Journal of Applied Microbiology*, 114(4), pp.1120–1131. doi:https://doi.org/10.1111/jam.12127.

Cooper, R., Lev Tsimring and Hasty, J. (2018). Microfluidics-Based Analysis of Contact-dependent Bacterial Interactions. *BIO-PROTOCOL*, 8(16). doi:https://doi.org/10.21769/bioprotoc.2970.

Corte, L., Casagrande Pierantoni, D., Tascini, C., Roscini, L. and Cardinali, G. (2019). Biofilm Specific Activity: A Measure to Quantify Microbial Biofilm. *Microorganisms*, 7(3), p.73. doi:https://doi.org/10.3390/microorganisms7030073.

Costerton, J.W., Cheng, K.J., Geesey, G.G., Ladd, T.I., Nickel, J.C., Dasgupta, M. and Marrie, T.J. (1987). Bacterial Biofilms in Nature and Disease. *Annual Review of Microbiology*, 41(1), pp.435–464. doi:https://doi.org/10.1146/annurev.mi.41.100187.002251.

Coughlan, L.M., Cotter, P.D., Hill, C. and Alvarez-Ordóñez, A. (2016). New Weapons to Fight Old Enemies: Novel Strategies for the (Bio)control of Bacterial Biofilms in the Food Industry. Frontiers in Microbiology, 7. doi:https://doi.org/10.3389/fmicb.2016.01641.

Cromie, M.J., Shi, Y., Latifi, T. and Groisman, E.A. (2006). An RNA Sensor for Intracellular Mg^{2+}. *Cell*, 125(1), pp.71–84. doi:https://doi.org/10.1016/j.cell.2006.01.043.

Crooks, G.E. (2004). WebLogo: A Sequence Logo Generator. *Genome Research*, 14(6), pp.1188–1190. doi:https://doi.org/10.1101/gr.849004.

Croucher, N.J., Page, A.J., Connor, T.R., Delaney, A.J., Keane, J.A., Bentley, S.D., Parkhill, J. and Harris, S.R. (2014). Rapid phylogenetic analysis of large samples of recombinant bacterial whole genome sequences using Gubbins. *Nucleic Acids Research*, 43(3), pp.e15–e15. doi:https://doi.org/10.1093/nar/gku1196.

Crouzet, M., Le Senechal, C., Brözel, V.S., Costaglioli, P., Barthe, C., Bonneu, M., Garbay, B. and Vilain, S. (2014). Exploring early steps in biofilm formation: set-up of an experimental system for molecular studies. *BMC Microbiology*, 14(1). doi:https://doi.org/10.1186/s12866-014-0253-z.

Crusz, S.A., Popat, R., Rybtke, M.T., Cámara, M., Givskov, M., Tolker-Nielsen, T., Diggle, S.P. and Williams, P. (2012). Bursting the bubble on bacterial biofilms: a flow cell methodology. *Biofouling*, [online] 28(8), pp.835–842. doi:https://doi.org/10.1080/08927014.2012.716044.

da Silva Fernandes, M., Kabuki, D.Y. and Kuaye, A.Y. (2015). Behaviour of *Listeria monocytogenes* in a multi-species biofilm with *Enterococcus faecalis* and *Enterococcus faecium* and control through sanitation procedures. *International Journal of Food Microbiology*, [online] 200, pp.5–12. doi:https://doi.org/10.1016/j.ijfoodmicro.2015.01.003.

Dávid Szatmári, Péter Sárkány, Kocsis, B., Nagy, T., Attila Miseta, Szilvia Barkó, Beáta Longauer, Robinson, R. and Nyitrai, M. (2020). Intracellular ion concentrations and cation-dependent remodelling of bacterial MreB assemblies. *Scientific Reports*, 10(1). doi:https://doi.org/10.1038/s41598-020-68960-w.

Dawan, J., Zhang, S. and Ahn, J. (2025). Recent Advances in Biofilm Control Technologies for the Food Industry. *Antibiotics*, [online] 14(3), pp.254–254. doi:https://doi.org/10.3390/antibiotics14030254.

Dehkordi, P.H., Moshtaghi, H. and Abbasvali, M. (2022). Effects of magnesium oxide and copper oxide nanoparticles on biofilm formation of *Escherichia coli* and *Listeria monocytogenes*. *Nanotechnology*, 34(15), pp.155102–155102. doi:https://doi.org/10.1088/1361-6528/acab6f.

Dessaux, C., Pucciarelli, M.G., Guerreiro, D.N., O'Byrne, C.P. and Portillo, F.G. (2021). Activation of the *Listeria monocytogenes* Stressosome in the Intracellular Eukaryotic Environment. *Applied and Environmental Microbiology*, 87(12). doi:https://doi.org/10.1128/aem.00397-21.

Deutscher, J., Francke, C. and Postma, P.W. (2006). How Phosphotransferase System-Related Protein Phosphorylation Regulates Carbohydrate Metabolism in Bacteria. *Microbiology and Molecular Biology Reviews*, 70(4), pp.939–1031. doi:https://doi.org/10.1128/mmbr.00024-06.

Di Bonaventura, G., Piccolomini, R., Paludi, D., D'Orio, V., Vergara, A., Conter, M. and Ianieri, A. (2008). Influence of temperature on biofilm formation by *Listeria monocytogenes* on various food-contact surfaces: relationship with motility and cell surface hydrophobicity. Journal of Applied Microbiology, 104(6), pp.1552–1561. doi:https://doi.org/10.1111/j.1365-2672.2007.03688.x.

Di Ciccio, P., Rubiola, S., Panebianco, F., Lomonaco, S., Allard, M., Bianchi, D.M., Civera, T. and Chiesa, F. (2022). Biofilm formation and genomic features of *L. monocytogenes* strains isolated from meat and dairy industries located in Piedmont (Italy). *International Journal of Food Microbiology*, 378, p.109784. doi:https://doi.org/10.1016/j.ijfoodmicro.2022.109784.

Diaz, M., Aird, H., Viet, T. L., Gutiérrez, A. V., Nasmille Larke-Mejia, Oleksii Omelchenko, Lluis Moragues-Solanas, Fritscher, J., Som, N., McLauchlin, J., Hildebrand, F., Jørgensen, F., & Gilmour, M. (2024). Microbial composition and dynamics in environmental samples from a ready-to-eat food production facility with a long-term colonisation of *Listeria monocytogenes*. *Food Microbiology*, *125*, 104649–104649. https://doi.org/10.1016/j.fm.2024.104649

Dickstein, Y., Oster, Y., Shimon, O., Nesher, L., Yahav, D., Yonit Wiener-Well, Cohen, R., Ben-Ami, R., Weinberger, M., Rahav, G., Maor, Y., Chowers, M., Nir-Paz, R. and Paul, M. (2019). Antibiotic treatment for invasive nonpregnancy-associated listeriosis and mortality: a retrospective cohort study. *European Journal of Clinical Microbiology & Infectious Diseases*, 38(12), pp.2243–2251. doi:https://doi.org/10.1007/s10096-019-03666-0.

Donlan, R.M. (2002). Biofilms: Microbial Life on Surfaces. *Emerging Infectious Diseases*, 8(9), pp.881–890. doi:https://doi.org/10.3201/eid0809.020063.

Dorey, A.L., Lee, B.-H., Rotter, B. and O'Byrne, C.P. (2019). Blue Light Sensing in *Listeria monocytogenes* Is Temperature-Dependent and the Transcriptional Response to It Is Predominantly SigB-Dependent. *Frontiers in Microbiology*, 10. doi:https://doi.org/10.3389/fmicb.2019.02497.

Dörr, T., Vulić, M. and Lewis, K. (2010). Ciprofloxacin Causes Persister Formation by Inducing the TisB toxin in *Escherichia coli*. *PLoS Biology*, 8(2), p.e1000317. doi:https://doi.org/10.1371/journal.pbio.1000317.

Doumith, M., Buchrieser, C., Glaser, P., Jacquet, C. and Martin, P. (2004). Differentiation of the Major *Listeria monocytogenes* Serovars by Multiplex PCR. *Journal of Clinical Microbiology*, [online] 42(8), pp.3819–3822. doi:https://doi.org/10.1128/JCM.42.8.3819-3822.2004.

Dramsi, S., Dehoux, P., Lebrun, M., Goossens, P.L. and Cossart, P. (1997). Identification of four new members of the internalin multigene family of *Listeria monocytogenes* EGD. *Infection and immunity*, 65(5), pp.1615–1625. doi:https://doi.org/10.1128/iai.65.5.1615-1625.1997.

Du, X., Zhang, X., Wang, X., Su, Y., Li, P. and Wang, S. (2017). Isolation and characterization of *L. monocytogenes* in Chinese food obtained from the central area of China. *Food Control*, 74, pp.9–16.

Dunsmore, D.G. (1981). Bacteriological Control of Food Equipment Surfaces by Cleaning Systems. I. Detergent Effects. *Journal of Food Protection*, 44(1), pp.15–20. doi:https://doi.org/10.4315/0362-028x-44.1.15.

Durão, P., Balbontín, R. and Gordo, I. (2018). Evolutionary Mechanisms Shaping the Maintenance of Antibiotic Tolerance. *Trends in Microbiology*, [online] 26(8), pp.677–691. doi:https://doi.org/10.1016/j.tim.2018.01.005.

Dussurget, O., Cabanes, D., Dehoux, P., Lecuit, M., Buchrieser, C., Glaser, P. and Cossart, P. (2002). *L. monocytogenes* bile salt hydrolase is a virulence factor involved in the intestinal and hepatic phases of listeriosis. *Molecular Microbiology*, 46(3), pp.903–903. doi:https://doi.org/10.1046/j.1365-2958.2002.03230.x.

Dutta, V., Elhanafi, D. and Kathariou, S. (2013). Conservation and Distribution of the Benzalkonium Chloride Tolerance Cassette *bcrABC* in *L. monocytogenes*. *Applied and Environmental Microbiology*, 79(19), pp.6067–6074.

Elfmann, C., Zhu, B., Stülke, J. and Halbedel, S. (2023). *ListiWiki*: A database for the foodborne pathogen *Listeria monocytogenes*. *International Journal of Medical Microbiology*, [online] 313(6), p.151591. doi:https://doi.org/10.1016/j.ijmm.2023.151591.

Elhanafi, D., Dutta, V. and Kathariou, S. (2010). Genetic Characterization of Plasmid-Associated Benzalkonium Chloride Tolerance Determinants in a *L. monocytogenes* Strain from the 1998-1999 Outbreak. *Applied and Environmental Microbiology*, 76(24), pp.8231–8238. doi:https://doi.org/10.1128/aem.02056-10.

Elinav, H., Hershko-Klement, A., Valinsky, L., Jaffe, J., Wiseman, A., Shimon, H., Braun, E., Paitan, Y., Block, C., Sorek, R., Nir-Paz, R., Miron, D., Glikman, D., Soboh, S., Nseir, W., Paz, A., Cohen, E., Mendelson, B., Paz, E. and Shimoni, Z. (2014). Pregnancy-Associated Listeriosis: Clinical Characteristics and Geospatial Analysis of a 10-Year Period in Israel. *Clinical Infectious Diseases*, 59(7), pp.953–961. doi:https://doi.org/10.1093/cid/ciu504.

Europa.eu. (2020). *EUR-Lex - 32005R2073 - EN - EUR-Lex*. [online] Available at: https://eur-lex.europa.eu/legal-content/EN/TXT/?uri=CELEX%3A32005R2073 [Accessed 13 Nov. 2021].

European Centre for Disease Prevention and Control. Expert opinion on whole genome sequencing for public health surveillance. Stockholm: ECDC; 2016

European Food Safety Authority (EFSA) and European Centre for Disease Prevention and Control (ECDC) (2023). The European Union One Health Zoonoses Report. *EFSA Journal*, 21(12), e8442. doi: https://doi.org/10.2903/j.efsa.2023.8442.

Evans, C.R., Smiley, M.K., Sean Asahara Thio, Wei, M., Florek, L.C., Dayton, H., Price-Whelan, A., Min, W. and Lars (2023). Spatial heterogeneity in biofilm metabolism elicited by local control

of phenazine methylation. *Proceedings of the National Academy of Sciences of the United States of America*, 120(43). doi:https://doi.org/10.1073/pnas.2313208120.

Even, S. (2005). Ribonucleases J1 and J2: two novel endoribonucleases in *B. subtilis* with functional homology to *E.coli* RNase E. *Nucleic Acids Research*, 33(7), pp.2141–2152. doi:https://doi.org/10.1093/nar/gki505.

Ewels, P., Magnusson, M., Lundin, S. and Käller, M. (2016). MultiQC: summarize analysis results for multiple tools and samples in a single report. *Bioinformatics*, 32(19), pp.3047– 3048.

Fagerlund, A., Heir, E., Møretrø, T. and Langsrud, S. (2020). *L. monocytogenes* Biofilm Removal Using Different Commercial Cleaning Agents. *Molecules*, 25(4), p.792. doi:https://doi.org/10.3390/molecules25040792.

Fagerlund, A., Langsrud, S., Heir, E., Mikkelsen, M.I. and Møretrø, T. (2016). Biofilm Matrix Composition Affects the Susceptibility of Food Associated *Staphylococci* to C&D Agents. *Frontiers in Microbiology*, 7.

Fagerlund, A., Langsrud, S., Schirmer, B.C.T., Møretrø, T. and Heir, E. (2016). Genome Analysis of *Listeria monocytogenes* Sequence Type 8 Strains Persisting in Salmon and Poultry Processing Environments and Comparison with Related Strains. *PLOS ONE*, 11(3), p.e0151117. doi:https://doi.org/10.1371/journal.pone.0151117.

Fagerlund, A., Møretrø, T., Heir, E., Briandet, R. and Langsrud, S. (2017). C&D of Biofilms Composed of *L. monocytogenes* and Background Microbiota from Meat Processing Surfaces. *Applied and Environmental Microbiology*, [online] 83(17). doi:https://doi.org/10.1128/AEM.01046-17.

Fagerlund, A., Wagner, E., Møretrø, T., Heir, E., Moen, B., Rychli, K., & Langsrud, S. (2022). Pervasive Listeria monocytogenes Is Common in the Norwegian Food System and Is Associated with Increased Prevalence of Stress Survival and Resistance Determinants. *Applied and Environmental Microbiology*, *88*(18), e0086122. https://doi.org/10.1128/aem.00861-22

FAO/WHO (2008). *Benefits and Risks of the Use of Chlorine-containing Disinfectants in Food Production and Food Processing*. Switzerland: WHO Document Production Services.

Fay, M.L., Salazar, J.K., Stewart, D.S., Khouja, B.A., Zhou, X. and Datta, A.R. (2024). Survival of *Listeria monocytogenes* on Frozen Vegetables during Long-term Storage at −18 and −10°C. *Journal of Food Protection*, 87(3), p.100224. doi:https://doi.org/10.1016/j.jfp.2024.100224.

Felix Krueger, Frankie James, Phil Ewels, Ebrahim Afyounian, Michael Weinstein, Benjamin Schuster-Boeckler, Gert Hulselmans, & sclamons. (2023). FelixKrueger/TrimGalore: v0.6.10 - add default decompression path (0.6.10). https://doi.org/10.5281/zenodo.7598955

Félix, B., Feurer, C., Maillet, A., Guillier, L., Boscher, E., Kerouanton, A., Denis, M. and Roussel, S. (2018). Population Genetic Structure of *Listeria monocytogenes* Strains Isolated From the Pig and Pork Production Chain in France. *Frontiers in Microbiology*, 9. doi:https://doi.org/10.3389/fmicb.2018.00684

Feng, Y., Wu, S., Varma, J.K., Klena, J.D., Angulo, F.J. and Ran, L. (2013). Systematic review of human listeriosis in China, 1964-2010. *Tropical Medicine & International Health*, 18(10), pp.1248–1256. doi:https://doi.org/10.1111/tmi.12173.

Fernández Guerrero, M. L., Torres, R., Mancebo, B., González-López, J. J., Górgolas, M., Jusdado, J. J., & Roblas, R. F. (2012). Antimicrobial treatment of invasive non-perinatal human listeriosis and the impact of the underlying disease on prognosis. *Clinical Microbiology and Infection, 18*(7), 690–695. https://doi.org/10.1111/j.1469-0691.2011.03616.x.

Ferreira, V., Wiedmann, M., Teixeira, P. and Stasiewicz, M.J. (2014). *L. monocytogenes* Persistence in Food-Associated Environments: Epidemiology, Strain Characteristics, and Implications for Public Health. *Journal of Food Protection*, 77(1), pp.150–170.

Finn, L., Onyeaka, H. and O'Neill, S.L. (2023). Listeria monocytogenes Biofilms in Food-Associated Environments: A Persistent Enigma. *Foods*, 12(18), pp.3339–3339. doi:https://doi.org/10.3390/foods12183339.

Fleming, D.W., Cochi, S.L., MacDonald, K.L., Brondum, J., Hayes, P.S., Plikaytis, B.D., Holmes, M.B., Audurier, A., Broome, C.V. and Reingold, A.L. (1985). Pasteurized Milk as a Vehicle of Infection in an Outbreak of Listeriosis. *New England Journal of Medicine*, 312(7), pp.404–407. doi:https://doi.org/10.1056/nejm198502143120704.

Flemming, H.-C. and Wingender, J. (2010). The biofilm matrix. *Nature reviews. Microbiology*, [online] 8(9), pp.623–33.

Flemming, H.-C., Wingender, J., Szewzyk, U., Steinberg, P., Rice, S.A. and Kjelleberg, S. (2016). Biofilms: an emergent form of bacterial life. *Nature reviews. Microbiology*, [online] 14(9), pp.563–75. Available at: https://www.ncbi.nlm.nih.gov/pubmed/27510863.

Food Standards Agency. (2023). *Chapter 4.2 HACCP Based Procedures*. [online] Available at: https://www.food.gov.uk/business-guidance/chapter-42-haccp-based-procedures?utm_source=chatgpt.com [Accessed 4 Sep. 2025].

Food Standards Agency. (2025). *Cleaning effectively in your business*. [online] Available at: https://www.food.gov.uk/business-guidance/cleaning-effectively-in-your-business?utm_source=chatgpt.com [Accessed 5 Apr. 2025].

Food Standards Scotland. (2020). *Cleaning Food Standards Scotland*. [online] Available at: https://www.foodstandards.gov.scot/self-assessment-resources/cleaning?utm_source=chatgpt.com [Accessed 14 Sep. 2025].

Fox, E.M., Allnutt, T., Bradbury, M.I., Fanning, S. and Chandry, P.S. (2016). Comparative Genomics of the *L. monocytogenes* ST204 Subgroup. *Frontiers in Microbiology*, 7. doi:https://doi.org/10.3389/fmicb.2016.02057.

François Guérin, Galimand, M., Fabrice Tuambilangana, Courvalin, P. and Cattoir, V. (2014). Overexpression of the Novel MATE Fluoroquinolone Efflux Pump FepA in *L. monocytogenes* Is Driven by Inactivation of Its Local Repressor FepR. *PLOS ONE*, 9(9), pp.e106340–e106340. doi:https://doi.org/10.1371/journal.pone.0106340.

Frankel, G.S. (1998). Pitting Corrosion of Metals. *Journal of The Electrochemical Society*, [online] 145(6), p.2186. doi:https://doi.org/10.1149/1.1838615.

Freitag, N.E., Rong, L. and Portnoy, D.A. (1993). Regulation of the *prfA* transcriptional activator of *L. monocytogenes*: multiple promoter elements contribute to intracellular growth and cell-to-cell spread. *Infection and Immunity*, 61(6), pp.2537–2544. doi:https://doi.org/10.1128/iai.61.6.2537-2544.1993.

Gabriel Antonio Salvador Minero, Møllebjerg, A., Thiesen, C., Johansen, M., Nis Pedersen Jørgensen, Birkedal, V., Daniel Erik Otzen and Meyer, R. (2024). Extracellular G-quadruplexes and Z-DNA protect biofilms from DNase I, and G-quadruplexes form a DNAzyme with peroxidase activity. *Nucleic Acids Research*, [online] 52(4), pp.1575–1590. doi:https://doi.org/10.1093/nar/gkae034.

Gacy, A.M. and McMurray, C.T. (1998). Influence of Hairpins on Template Reannealing at Trinucleotide Repeat Duplexes: A Model for Slipped DNA†. *Biochemistry*, 37(26), pp.9426–9434. doi:https://doi.org/10.1021/bi980157s.

Gallandat, K., Kolus, R.C., Julian, T.R. and Lantagne, D.S. (2021). A systematic review of chlorine-based surface disinfection efficacy to inform recommendations for low-resource outbreak settings. *American Journal of Infection Control*, [online] 49(1), pp.90–103. doi:https://doi.org/10.1016/j.ajic.2020.05.014.

Garmyn, D., Gal, L., Briandet, R., Guilbaud, M., Lemaître, J.-P., Hartmann, A. and Piveteau, P. (2011). Evidence of Autoinduction Heterogeneity via Expression of the Agr System of *Listeria monocytogenes* at the Single-Cell Level. *Applied and Environmental Microbiology*, 77(17), pp.6286–6289. doi:https://doi.org/10.1128/aem.02891-10.

Gélinas, P. and Goulet, J. (1983). Neutralization of the activity of eight disinfectants by organic matter. *Journal of Applied Bacteriology*, 54(2), pp.243–247. doi:https://doi.org/10.1111/j.1365-2672.1983.tb02613.x.

Gerba, C.P. (2015). Quaternary Ammonium Biocides: Efficacy in Application. *Applied and Environmental Microbiology*, [online] 81(2), pp.464–469. doi:https://doi.org/10.1128/AEM.02633-14.

Giaouris, E., Chapot-Chartier, M.-P. and Briandet, R. (2009). Surface physicochemical analysis of natural *Lactococcus lactis* strains reveals the existence of hydrophobic and low charged strains with altered adhesive properties. *International Journal of Food Microbiology*, 131(1), pp.2–9. doi:https://doi.org/10.1016/j.ijfoodmicro.2008.09.006.

Giaouris, E., Heir, E., Desvaux, M., Hébraud, M., Møretrø, T., Langsrud, S., Doulgeraki, A., Nychas, G.-J., Kačániová, M., Czaczyk, K., Ölmez, H. and Simões, M. (2015). Intra- and inter-species interactions within biofilms of important foodborne bacterial pathogens. *Frontiers in Microbiology*, 6.

Gibson, H., Taylor, J.H., Hall, K.E. and Holah, J.T. (1999). Effectiveness of cleaning techniques used in the food industry in terms of the removal of bacterial biofilms. *Journal of Applied Microbiology*, 87(1), pp.41–48. doi:https://doi.org/10.1046/j.1365-2672.1999.00790.x.

Gilbreth, S.E., Call, J.E., Wallace, F.M., Scott, V.N., Chen, Y. and Luchansky, J.B. (2005). Relatedness of *Listeria monocytogenes* Isolates Recovered from Selected Ready-To-Eat Foods and Listeriosis Patients in the United States. *Applied and Environmental Microbiology*, 71(12), pp.8115–8122. doi:https://doi.org/10.1128/aem.71.12.8115-8122.2005.

Gilmour, M.W., Graham, M., Van Domselaar, G., Tyler, S., Kent, H., Trout-Yakel, K.M., Larios, O., Allen, V., Lee, B. and Nadon, C. (2010). High-throughput genome sequencing of two *Listeria monocytogenes* clinical isolates during a large foodborne outbreak. *BMC Genomics*, 11(1), p.120. doi:https://doi.org/10.1186/1471-2164-11-120.

Girard, D., Leclercq, A., Laurent, E., Lecuit, M., de Valk, H. and Goulet, V. (2014). Pregnancy-related listeriosis in France, 1984 to 2011, with a focus on 606 cases from 1999 to 2011. *Eurosurveillance*, 19(38). doi:https://doi.org/10.2807/1560-7917.es2014.19.38.20909.

Gjermansen, M., Ragas, P., Sternberg, C., Molin, S. and Tolker-Nielsen, T. (2005). Characterization of starvation-induced dispersion in *Pseudomonas putida* biofilms. *Environmental Microbiology*, 7(6), pp.894–904. doi:https://doi.org/10.1111/j.1462-2920.2005.00775.x.

Goeres, D.M., Loetterle, L.R., Hamilton, M.A., Murga, R., Kirby, D.W. and Donlan, R.M. (2005). Statistical assessment of a laboratory method for growing biofilms. *Microbiology*, 151(3), pp.757–762. doi:https://doi.org/10.1099/mic.0.27709-0.

Goetz, C., Larouche, J., Velez Aristizabal, M., Niboucha, N. and Jean, J. (2021). Efficacy of organic peroxyacids for eliminating biofilm preformed by microorganisms isolated from dairy processing plants. *Applied and Environmental Microbiology*. doi:https://doi.org/10.1128/aem.01889-21.

Gottschalk, N., Augustin, W., Scholl, S., Ian Wilson, D. and Mercadé-Prieto, R. (2022). Model food soils for investigating cleaning: a review. *Food and Bioproducts Processing*. doi:https://doi.org/10.1016/j.fbp.2022.09.013.

GOV.UK [Internet]. [cited 2024 May 22]. Listeriosis in England and Wales: summary for 2022. Available from: https://www.gov.uk/government/publications/listeria-monocytogenes-surveillance-reports/listeriosis-in-england-and-wales-summary-for-2022

GOV.UK. (2021). *Listeriosis in England and Wales: summary for 2018*. [online] Available at: https://www.gov.uk/government/publications/listeria-monocytogenes-surveillance-reports/listeriosis-in-england-and-wales-summary-for-2018.

Grigore-Gurgu, L., Bucur, F.I., Mihalache, O.A. and Nicolau, A.I. (2024). Comprehensive Review on the Biocontrol of *Listeria monocytogenes* in Food Products. *Foods*, 13(5), pp.734–734. doi:https://doi.org/10.3390/foods13050734.

Groisman, E.A., Hollands, K., Kriner, M.A., Lee, E.-J., Park, S.-Y. and Pontes, M.H. (2013). Bacterial Mg^{2+} Homeostasis, Transport, and Virulence. *Annual review of genetics*, [online] 47, pp.625–646. doi:https://doi.org/10.1146/annurev-genet-051313-051025.

Grotzinger, J.P. and Knoll, A.H. (1999). STROMATOLITES IN PRECAMBRIAN CARBONATES: Evolutionary Mileposts or Environmental Dipsticks? *Annual Review of Earth and Planetary Sciences*, 27(1), pp.313–358. doi:https://doi.org/10.1146/annurev.earth.27.1.313.

Guérin, A., Bridier, A., Le Grandois, P., Sévellec, Y., Palma, F., Félix, B., Roussel, S. and Soumet, C. (2021). Exposure to Quaternary Ammonium Compounds Selects Resistance to Ciprofloxacin in *Listeria monocytogenes*. Pathogens, 10(2), p.220. doi:https://doi.org/10.3390/pathogens10020220.

Guerreiro, D.N., Arcari, T. and O'Byrne, C.P. (2020). The σB-Mediated General Stress Response of *Listeria monocytogenes*: Life and Death Decision Making in a Pathogen. *Frontiers in Microbiology*, 11. doi:https://doi.org/10.3389/fmicb.2020.01505.

Guilbaud, M., Piveteau, P., Desvaux, M., Brisse, S. and Briandet, R. (2014). Exploring the Diversity of *L. monocytogenes* Biofilm Architecture by High-Throughput Confocal Laser Scanning Microscopy and the Predominance of the Honeycomb-Like Morphotype. *Applied and Environmental Microbiology*, 81(5), pp.1813–1819.

Guo, R. and Lu, H. (2020). Targeted Metabolomics Revealed the Regulatory Role of Manganese on Small-Molecule Metabolism of Biofilm Formation in *Escherichia coli*. *Journal of Analysis and Testing*, 4(3), pp.226–237. doi:https://doi.org/10.1007/s41664-020-00139-8.

Gutiérrez, A.V., Matthews, M., Diaz, M., Viet, T.L., Leonardo, Jørgensen, F., Aird, H., Anaïs Painset, Som, N., Omelchenko,, O., Adriaenssens, E.M., Kingsley, R.A. and Gilmour, M.W. (2025). Population structure and gene flux of *L. monocytogenes* ST121 reveal prophages as a candidate driver of adaptation and persistence in food production environments. *Microbial Genomics*, 11(4). doi:https://doi.org/10.1099/mgen.0.001397.

Haase, J.K., Didelot, X., Lecuit, M., Korkeala, H. and Achtman, M. (2013). The ubiquitous nature of *Listeria monocytogenes* clones: a large-scale Multilocus Sequence Typing study. *Environmental Microbiology*, 16(2), pp.405–416. doi:https://doi.org/10.1111/1462-2920.12342.

Hall, M.B. (2022). Rasusa: Randomly subsample sequencing reads to a specified coverage. *Journal of open source software*, 7(69), pp.3941–3941. doi:https://doi.org/10.21105/joss.03941.

Harmsen, M., Lappann, M., Knøchel, S. and Molin, S. (2010). Role of Extracellular DNA during Biofilm Formation by *Listeria monocytogenes*. *Applied and Environmental Microbiology*, 76(7), pp.2271–2279. doi:https://doi.org/10.1128/aem.02361-09.

Harris, R.M., Webb, D.C., Howitt, S.M. and Cox, G.B. (2001). Characterization of PitA and PitB from Escherichia coli. *Journal of Bacteriology*, [online] 183(17), pp.5008–5014. doi:https://doi.org/10.1128/jb.183.17.5008-5014.2001.

Harris, R.M., Webb, D.C., Howitt, S.M. and Cox, G.B. (2001). Characterization of PitA and PitB from *Escherichia coli*. Journal of Bacteriology, [online] 183(17), pp.5008–5014. doi:https://doi.org/10.1128/jb.183.17.5008-5014.2001.

Harter, E., Wagner, E.M., Zaiser, A., Halecker, S., Wagner, M. and Rychli, K. (2017). Stress Survival Islet 2, Predominantly Present in *L. monocytogenes* Strains of Sequence Type 121, Is

Involved in the Alkaline and Oxidative Stress Responses. *Applied and Environmental Microbiology*, 83(16). doi:https://doi.org/10.1128/aem.00827-17.

Hartmann, I., Carranza, P., Lehner, A., Stephan, R., Eberl, L., & Riedel, K. (2010). Genes Involved in *Cronobacter sakazakii* Biofilm Formation. *Applied and Environmental Microbiology*, *76*(7), 2251–2261. https://doi.org/10.1128/AEM.00930-09

Hartmann, R., Jeckel, H., Jelli, E., Singh, P., Vaidya, S., Bayer, M., Hartmann, R., Vidakovic, L., Chávez, F.P., Fong, N., Dragoš, A., Lamprecht, O., Thöming, J.G., Netter, N., Häussler, S., Nadell, C.D., Sourjik, V., Kovács, Á.T., Yildiz, F.H. and Drescher, K. (2021). Quantitative image analysis of microbial communities with BiofilmQ. 6(2), pp.151–156. doi:https://doi.org/10.1038/s41564-020-00817-4.

He, X., Zhang, W., Liu, J., Liu, J., Chen, Y., Luan, C., Zhang, J., Bao, G., Lin, X., Muh, F., Lin, T. and Lu, F. (2025). The global regulatory role of RsbUVW in virulence and biofilm formation in MRSA. *Microbial Pathogenesis*, [online] 203, p.107508. doi:https://doi.org/10.1016/j.micpath.2025.107508.

Heacock-Kang, Y., Sun, Z., Zarzycki-Siek, J., McMillan, I.A., Norris, M.H., Bluhm, A.P., Cabanas, D., Fogen, D., Vo, H., Donachie, S.P., Borlee, B.R., Sibley, C.D., Lewenza, S., Schurr, M.J., Schweizer, H.P. and Hoang, T.T. (2017). Spatial transcriptomes within the *Pseudomonas aeruginosa* biofilm architecture. *Molecular Microbiology*, [online] 106(6), pp.976–985. doi:https://doi.org/10.1111/mmi.13863.

Heberle, H., Meirelles, G.V., da Silva, F.R., Telles, G.P. and Minghim, R. (2015). InteractiVenn: a web-based tool for the analysis of sets through Venn diagrams. BMC Bioinformatics, [online] 16(1). doi:https://doi.org/10.1186/s12859-015-0611-3.

Heir, E., Sundheim, G. and Holck, A.L. (1999). Identification and characterization of quaternary ammonium compound resistant *staphylococci* from the food industry. *International Journal of Food Microbiology*, 48(3), pp.211–219.

Henri, C., Félix, B., Laurent Guillier, Pimlapas Leekitcharoenphon, Michelon, D., Jean-François Mariet, Frank Møller Aarestrup, Michel-Yves Mistou, Hendriksen, R.S. and Roussel, S. (2016). Population Genetic Structure of *Listeria monocytogenes* Strains as Determined by Pulsed-Field Gel Electrophoresis and Multilocus Sequence Typing. 82(18), pp.5720–5728. doi:https://doi.org/10.1128/aem.00583-16.

Hilbert, L.R., Bagge-Ravn, D., Kold, J. and Gram, L. (2003). Influence of surface roughness of stainless steel on microbial adhesion and corrosion resistance. *International Biodeterioration & Biodegradation*, [online] 52(3), pp.175–185. doi:https://doi.org/10.1016/S0964-8305(03)00104-5.

Hingston, P., Chen, J.A., Dhillon, B.K., Laing, C.R., Bertelli, C., Victor, Taurai Tasara, Kevin Fiona, Lisbeth Truelstrup Hansen and Wang, S. (2017). Genotypes Associated with *Listeria monocytogenes* Isolates Displaying Impaired or Enhanced Tolerances to Cold, Salt, Acid, or Desiccation Stress. *Frontiers in Microbiology*, 8. doi:https://doi.org/10.3389/fmicb.2017.00369.

Hmiel, S.P., Snavely, M.D., Florer, J.B., Maguire, M.G. and Miller, C.A. (1989). Magnesium transport in *Salmonella typhimurium*: genetic characterization and cloning of three magnesium transport loci. *Journal of Bacteriology*, 171(9), pp.4742–4751. doi:https://doi.org/10.1128/jb.171.9.4742-4751.1989.

Hof, H., Nichterlein, T. and Kretschmar, M. (1997). Management of listeriosis. *Clinical Microbiology Reviews*, 10(2), pp.345–357. doi:https://doi.org/10.1128/cmr.10.2.345.

Holch, A., Webb, K., Lukjancenko, O., Ussery, D., Rosenthal, B.M. and Gram, L. (2013). Genome Sequencing Identifies Two Nearly Unchanged Strains of Persistent *L. monocytogenes* Isolated at Two Different Fish Processing Plants Sampled 6 Years Apart.*Applied and Environmental Microbiology*, 79(9), pp.2944–2951.

Holliday, R., Preshaw, P.M., Bowen, L. and Jakubovics, N.S. (2015). The ultrastructure of subgingival dental plaque, revealed by high-resolution field emission scanning electron microscopy. *BDJ Open*, 1(1). doi:https://doi.org/10.1038/bdjopen.2015.3.

Horton, R.M., Hunt, H.D., Ho, S.N., Pullen, J.K. and Pease, L.R. (1990). Engineering hybrid genes without the use of restriction enzymes: gene splicing by overlap extension. *Gene*, [online] 77(1), pp.61–68. doi:https://doi.org/10.1016/0378-1119(89)90359-4.

Hsu, C.-Y. (2019). *Investigation of molecular mechanisms of biofilm formation by Listeria monocytogenes*. Doctoral Thesis.

Hsu, C.-Y., Cairns, L., Hobley, L., Abbott, J., O'Byrne, C. and Stanley-Wall, N.R. (2020). Genomic Differences between *L. monocytogenes* EGD-e Isolates Reveal Crucial Roles for SigB and Wall Rhamnosylation in Biofilm Formation. *Journal of Bacteriology*, 202(7). doi:https://doi.org/10.1128/jb.00692-19.

Hua, Z. and Zhu, M. (2024). Comprehensive strategies for controlling *Listeria monocytogenes* biofilms on food-contact surfaces. *Comprehensive reviews in food science and food safety*, 23(3). doi:https://doi.org/10.1111/1541-4337.13348.

Huang, H., Juhasz, A., Brunetti, G., Roccisano, A. and Stanford, N. (2023). Enhanced pitting tolerance and antibacterial durability of Cu-bearing stainless steels via tailoring Cu distributions. *Materialia*, 31, p.101880. doi:https://doi.org/10.1016/j.mtla.2023.101880.

Hue, C., Sahin, N. and Andrews, B. (2022). Phenomics approaches to understand genetic networks and gene function in yeast. *Biochemical Society Transactions*, 50(2), pp.713–721. doi:https://doi.org/10.1042/bst20210285.

Hunter, P. (2022). Understanding redundancy and resilience. *EMBO reports*, 23(3). doi:https://doi.org/10.15252/embr.202254742.

Hurley, D., Luque-Sastre, L., Parker, C.T., Huynh, S., Eshwar, A.K., Nguyen, S.V., Andrews, N., Moura, A., Fox, E.M., Jordan, K., Lehner, A., Stephan, R. and Fanning, S. (2019). Whole-Genome Sequencing-Based Characterization of 100 *L. monocytogenes* Isolates Collected from FPEs over a Four-Year Period. *mSphere*, 4(4).

Hutchison, C.A., Merryman, C., Sun, L., Assad-Garcia, N., Richter, R.A., Smith, H.O. and Glass, J.I. (2019). Polar Effects of Transposon Insertion into a Minimal Bacterial Genome. *Journal of Bacteriology*, 201(19). doi:https://doi.org/10.1128/jb.00185-19.

Hyden, P., Pietzka, A., Lennkh, A., Murer, A., Springer, B., Blaschitz, M., Indra, A., Huhulescu, S., Allerberger, F., Ruppitsch, W. and Sensen, C.W. (2016). Whole genome sequence-based serogrouping of *L. monocytogenes* isolates. *Journal of Biotechnology*, 235(4), pp.181– 186.

Inagaki, S., Kuramitsu, H.K. and Sharma, A. (2005). Contact-dependent regulation of a *Tannerella forsythia*virulence factor, BspA, in biofilms. *Fems Microbiology Letters*, 249(2), pp.291–296. doi:https://doi.org/10.1016/j.femsle.2005.06.032.

Iñiguez-Moreno, M., Avila-Novoa, M.G. and Gutiérrez-Lomelí, M. (2018). Tolerance of pathogenic and spoilage microorganisms to disinfectants in the presence of organic matter and their residual effect on stainless steel and polypropylene. *Journal of Global Antimicrobial Tolerance*, 14, pp.197–201. doi:https://doi.org/10.1016/j.jgar.2018.04.010.

Iqbal, Q., Lubeck-Schricker, M., Wells, E., Wolfe, M.K. and Lantagne, D. (2016). Shelf-Life of Chlorine Solutions Recommended in Ebola Virus Disease Response. *PLOS ONE*, 11(5), p.e0156136. doi:https://doi.org/10.1371/journal.pone.0156136.

Ishihara, Y. and Akazawa, K. (2023). Treatment of *L. monocytogenes* bacteremia with oral levofloxacin in an immunocompromised patient. *IDCases*, 31, p.e01680. doi:https://doi.org/10.1016/j.idcr.2023.e01680.

Ishikawa, M. and Hori, K. (2013). A new simple method for introducing an unmarked mutation into a large gene of non-competent Gram-negative bacteria by FLP/FRT recombination. *BMC Microbiology*, 13(1), p.86. doi:https://doi.org/10.1186/1471-2180-13-86.

Jackson, R.J., Binet, M.R.B., Lee, L.J., Ma, R., Graham, A.I., McLeod, C.W. and Poole, R.K. (2008). Expression of the PitA phosphate/metal transporter of *Escherichia coli* is responsive to zinc and inorganic phosphate levels. *FEMS Microbiology Letters*, 289(2), pp.219–224. doi:https://doi.org/10.1111/j.1574-6968.2008.01386.x.

Jacquet, C., Gouin, E., Jeannel, D., Cossart, P. and Rocourt, J. (2002). Expression of ActA, Ami, InlB, and Listeriolysin O in *L. monocytogenes* of Human and Food Origin. *Applied and Environmental Microbiology*, 68(2), pp.616–622.

Jagadeesan, B., Koo, O.K., Kim, K.-P., Burkholder, K.M., Mishra, K.K., Aroonnual, A. and Bhunia, A.K. (2010). LAP, an alcohol acetaldehyde dehydrogenase enzyme in *Listeria*, promotes bacterial adhesion to enterocyte-like Caco-2 cells only in pathogenic species. *Microbiology*, 156(9), pp.2782–2795. doi:https://doi.org/10.1099/mic.0.036509-0.

James, G.A., Korber, D.R., Caldwell, D.E. and Costerton, J.W. (1995). Digital image analysis of growth and starvation responses of a surface-colonizing Acinetobacter sp. *Journal of bacteriology*, 177(4), pp.907–915. doi:https://doi.org/10.1128/jb.177.4.907-915.1995.

Janež, N., Škrlj, B., Sterniša, M., Klančnik, A. and Sabotič, J. (2021). The role of the *L. monocytogenes* surfactome in biofilm formation. *Microbial Biotechnology*, 14(4), pp.1269–1281. doi:https://doi.org/10.1111/1751-7915.13847.

Jiang, M., Chen, X., Guo, Z.-F., Cao, Y., Chen, M. and Guo, Z. (2008). Identification and Characterization of (1R,6R)-2-Succinyl-6-hydroxy-2,4-cyclohexadiene-1-carboxylate Synthase in the Menaquinone Biosynthesis of *Escherichia coli*. Biochemistry, 47(11), pp.3426–3434. doi:https://doi.org/10.1021/bi7023755.

Jiang, X., Yu, T., Xu, Y., Wang, H., Korkeala, H. and Shi, L. (2018). MdrL, a major facilitator superfamily efflux pump of *Listeria monocytogenes* involved in tolerance to benzalkonium chloride. *Applied Microbiology and Biotechnology*, 103(3), pp.1339–1350. doi:https://doi.org/10.1007/s00253-018-9551-y.

Jo, J., Cortez, K.L., Cornell, W.C., Price-Whelan, A. and Dietrich, L.E. (2017). An orphan cbb3-type cytochrome oxidase subunit supports *Pseudomonas aeruginosa* biofilm growth and virulence. *eLife*, [online] 6, p.e30205. doi:https://doi.org/10.7554/eLife.30205.

Jo, J., Price-Whelan, A. and Dietrich, L.E.P. (2022). Gradients and consequences of heterogeneity in biofilms. *Nature Reviews Microbiology*, 20(10), pp.593–607. doi:https://doi.org/10.1038/s41579-022-00692-2.

Jobling, M.G., Raleigh, E.A. and Frank, D.N. (2016). Complete Genome Sequence of *Escherichia coli* ER1821R, a Laboratory K-12 Derivative Engineered To Be Deficient in All Methylcytosine and Methyladenine Restriction Systems. *Genome Announcements*, 4(4). doi:https://doi.org/10.1128/genomea.00763-16.

Jolley, K.A. and Maiden, M.C. (2010). BIGSdb: Scalable analysis of bacterial genome variation at the population level. *BMC Bioinformatics*, 11(1). doi:https://doi.org/10.1186/1471-2105-11-595.

Jolley, K.A., Bray, J.E. and Maiden, M.C.J. (2018). Open-access bacterial population genomics: BIGSdb software, the PubMLST.org website and their applications. *Wellcome Open Research*, 3, p.124.

Jumper, J., Evans, R., Pritzel, A., Green, T., Figurnov, M., Ronneberger, O., Tunyasuvunakool, K., Bates, R., Žídek, A., Potapenko, A., Bridgland, A., Meyer, C., Kohl, S.A.A., Ballard, A.J., Cowie, A., Romera-Paredes, B., Nikolov, S., Jain, R., Adler, J. and Back, T. (2021). Highly Accurate Protein Structure Prediction with Alphafold. *Nature*, 596(7873), pp.583–589. doi:https://doi.org/10.1038/s41586-021-03819-2.

Justin Abi Assaf, Holden, E.R., Eleftheria Trampari and Webber, M.A. (2024). Common food preservatives impose distinct selective pressures on *Salmonella* Typhimurium planktonic and biofilm populations. *Food microbiology*, pp.104517–104517. doi:https://doi.org/10.1016/j.fm.2024.104517.

Kaiser, D. (2001). Building a Multicellular Organism. *Annual Review of Genetics*, 35(1), pp.103–123. doi:https://doi.org/10.1146/annurev.genet.35.102401.090145.

Kakurinov, V. (2014). Food Safety Assurance Systems: C&D. *Encyclopedia of Food Safety*, pp.211–225. doi:https://doi.org/10.1016/b978-0-12-378612-8.00356-5.

Karatan, E. and Watnick, P. (2009). Signals, regulatory networks, and materials that build and break bacterial biofilms. *Microbiology and molecular biology reviews: MMBR*, [online] 73(2), pp.310–347. doi:https://doi.org/10.1128/MMBR.00041-08.

Karygianni, L., Ren, Z., Koo, H. and Thurnheer, T. (2020). Biofilm Matrixome: Extracellular Components in Structured Microbial Communities. *Trends in Microbiology*, [online] 28(8). doi:https://doi.org/10.1016/j.tim.2020.03.016.

Katharios-Lanwermeyer, S., Rakic-Martinez, M., Elhanafi, D., Ratani, S., Tiedje, J.M. and Kathariou, S. (2012). Coselection of Cadmium and Benzalkonium Chloride Tolerance in Conjugative Transfers from Nonpathogenic *Listeria* spp. to Other Listeriae. *Applied and Environmental Microbiology*, 78(21), pp.7549–7556.

Kehres, D.G., Lawyer, C.H. and Maguire, M.E. (1998). The CorA Magnesium Transporter Gene Family. Microbial & Comparative Genomics, 3(3), pp.151–169. doi:https://doi.org/10.1089/omi.1.1998.3.151.

Kersey, C.M., Aguemang, P.A. and C. Korsi Dumenyo (2011). CorA, the Mg^{2+}/nickel/cobalt transporter, affects virulence and extracellular enzyme production in the soft rot pathogen *Pectobacterium carotovorum*. *Molecular Plant Pathology*, 13(1), pp.58–71. doi:https://doi.org/10.1111/j.1364-3703.2011.00726.x.

Khalil, A., Samara, A., O'Brien, P., Ladhani, S. (2023). *Listeria* outbreaks cause maternal and perinatal mortality and morbidity: we must do better. The Lancet Microbe. https://doi.org/10.1016/s2666-5247(22)00388-3

Kim-Holzapfel, D.M., Dey, R., Richardson, B.C., Arachchige, D., Reddy, K., De Vitto, H., Bhandari, J. and French, J.B. (2023). Human uridine 5'-monophosphate synthase stores metabolic potential in inactive biomolecular condensates. *The Journal of Biological Chemistry*, [online] 299(3), p.102949. doi:https://doi.org/10.1016/j.jbc.2023.102949.

Kim, M., Weigand, M.R., Oh, S., Hatt, J.K., Krishnan, R., Tezel, U., Pavlostathis, S.G. and Konstantinidis, K.T. (2018). Widely Used Benzalkonium Chloride Disinfectants Can Promote Antibiotic Resistance. *Applied and Environmental Microbiology*, 84(17). doi:https://doi.org/10.1128/aem.01201-18.

Knudsen, G.M., Nielsen, J.B., Marvig, R.L., Ng, Y., Worning, P., Westh, H. and Gram, L. (2017). Genome-wide-analyses of *Listeria monocytogenes* from food-processing plants reveal clonal diversity and date the emergence of persisting sequence types. *Environmental Microbiology Reports*, 9(4), pp.428–440. doi:https://doi.org/10.1111/1758-2229.12552.

Kochkodan, V., Tsarenko, S., Potapchenko, N., Kosinova, V. and Goncharuk, V. (2008). Adhesion of microorganisms to polymer membranes: a photobactericidal effect of surface treatment with TiO2. *Desalination*, [online] 220(1), pp.380–385. doi:https://doi.org/10.1016/j.desal.2007.01.042.

Kolmogorov, M., Yuan, J., Lin, Y. and Pevzner, P.A. (2019). Assembly of long, error-prone reads using repeat graphs. *Nature Biotechnology*, 37(5), pp.540–546.

Koren, S., Walenz, B.P., Berlin, K., Miller, J.R., Bergman, N.H. and Phillippy, A.M. (2017). Canu: scalable and accurate long-read assembly via adaptive k-mer weighting and repeat separation. *Genome Research*, 27(5), pp.722–736. doi:https://doi.org/10.1101/gr.215087.116.

Koutsoumanis, K., Pavlis, A., Nychas, G.-J.E. and Xanthiakos, K. (2010). Probabilistic model for *Listeria monocytogenes* growth during distribution, retail storage, and domestic storage of pasteurized milk. *Applied and environmental microbiology*, [online] 76(7), pp.2181–91. doi:https://doi.org/10.1128/AEM.02430-09.

Kovacevic, J., Ziegler, J., Wałecka-Zacharska, E., Reimer, A., Kitts, D.D. and Gilmour, M.W. (2016). Tolerance of *Listeria monocytogenes* to Quaternary Ammonium Sanitizers Is Mediated by a Novel Efflux Pump Encoded by *emrE*. *Applied and Environmental Microbiology*, 82(3), pp.939–953. doi:https://doi.org/10.1128/aem.03741-15.

Kow, R. L., Whicher, J. R., McDonald, C. A., Palfey, B. A., & Fagan, R. L. (2009). Disruption of the Proton Relay Network in the Class 2 Dihydroorotate Dehydrogenase from *Escherichia coli*. *Biochemistry*, *48*(41), 9801–9809. https://doi.org/10.1021/bi901024m

Kozlov, A.M., Darriba, D., Flouri, T., Morel, B. and Stamatakis, A. (2019). RAxML-NG: a fast, scalable and user-friendly tool for maximum likelihood phylogenetic inference. *Bioinformatics*, 35(21). doi:https://doi.org/10.1093/bioinformatics/btz305.

Kragh, M.L. and Truelstrup Hansen, L. (2020). Initial Transcriptomic Response and Adaption of *L. monocytogenes* to Desiccation on Food Grade Stainless-steel.*Frontiers in Microbiology*, 10.

Krasowska, A. and Sigler, K. (2014). How microorganisms use hydrophobicity and what does this mean for human needs? *Frontiers in Cellular and Infection Microbiology*, 4. doi:https://doi.org/10.3389/fcimb.2014.00112.

Krawczyk-Balska, A. and Markiewicz, Z. (2015). The intrinsic cephalosporin resistome of *L. monocytogenes* in the context of stress response, gene regulation, pathogenesis and therapeutics. *Journal of Applied Microbiology*, 120(2), pp.251–265. doi:https://doi.org/10.1111/jam.12989.

Kuenne, C., Billion, A., Mraheil, M.A., Strittmatter, A., Daniel, R., Goesmann, A., Barbuddhe, S., Hain, T. and Chakraborty, T. (2013). Reassessment of the *Listeria monocytogenes* pan-genome reveals dynamic integration hotspots and mobile genetic elements as major components of the accessory genome. *BMC Genomics*, 14(1). doi:https://doi.org/10.1186/1471-2164-14-47.

Kumar, S., Datta, S., Dey, V. and Dijendra Nath Roy (2024). Alteration of stainless-steel surface potential by modifying topography inhibits the development of bacterial biofilm. *Journal of materials research/Pratt's guide to venture capital sources*. doi:https://doi.org/10.1557/s43578-024-01308-6.

Kung, S.H., Retchless, A.C., Kwan, J.Y. and Almeida, R.P.P. (2013). Effects of DNA Size on Transformation and Recombination Efficiencies in *Xylella fastidiosa*. *Applied and Environmental Microbiology*, [online] 79(5), pp.1712–1717. doi:https://doi.org/10.1128/AEM.03525-12.

Lake, F.B., Chen, J., van Overbeek, L.S., Baars, J., Abee, T. and M.W, H. (2024). Biofilm formation and desiccation survival of *Listeria monocytogenes* with microbiota on mushroom processing surfaces and the effect of cleaning and disinfection. *International Journal of Food Microbiology*, 411, pp.110509–110509. doi:https://doi.org/10.1016/j.ijfoodmicro.2023.110509.

Lambert, P.A. and Hammond, S.M. (1973). Potassium fluxes, first indications of membrane damage in micro-organisms. Biochemical and Biophysical Research Communications, 54(2), pp.796–799. doi:https://doi.org/10.1016/0006-291x(73)91494-0.

Lappin-Scott, H.M. and Bass, C. (2001). Biofilm formation: Attachment, growth, and detachment of microbes from surfaces. *American Journal of Infection Control*, 29(4), pp.250–251. doi:https://doi.org/10.1067/mic.2001.115674.

Larsen, M.V., Cosentino, S., Rasmussen, S., Friis, C., Hasman, H., Marvig, R.L., Jelsbak, L., Sicheritz-Ponten, T., Ussery, D.W., Aarestrup, F.M. and Lund, O. (2012). Multilocus Sequence Typing of Total-Genome-Sequenced Bacteria. Journal of Clinical Microbiology, 50(4), pp.1355–1361.

Lauderdale, K.J., Boles, B.R., Cheung, A.L. and Horswill, A.R. (2009). Interconnections between Sigma B, agr, and Proteolytic Activity in *Staphylococcus aureus* Biofilm Maturation. *Infection and Immunity*, 77(4), pp.1623–1635. doi:https://doi.org/10.1128/iai.01036-08.

Lecuit, M. (2007). Human listeriosis and animal models. *Microbes and Infection*, 9(10), pp.1216–1225. doi:https://doi.org/10.1016/j.micinf.2007.05.009.

Lee, B.-H., Cole, S., Badel-Berchoux, S., Guillier, L., Felix, B., Krezdorn, N., Hébraud, M., Bernardi, T., Sultan, I. and Piveteau, P. (2019). Biofilm Formation of *Listeria monocytogenes* Strains Under Food Processing Environments and Pan-Genome-Wide Association Study. *Frontiers in Microbiology*, [online] 10. doi:https://doi.org/10.3389/fmicb.2019.02698.

Lee, I.P.A., Eldakar, O.T., Gogarten, J.P. and Andam, C.P. (2021). Bacterial cooperation through horizontal gene transfer. *Trends in Ecology & Evolution*, 37(3). doi:https://doi.org/10.1016/j.tree.2021.11.006.

Lemon, K.P., Freitag, N.E. and Kolter, R. (2010). The Virulence Regulator PrfA Promotes Biofilm Formation by *Listeria monocytogenes*. *Journal of Bacteriology*, 192(15), pp.3969–3976. doi:https://doi.org/10.1128/jb.00179-10.

Lemon, K.P., Higgins, D.E. and Kolter, R. (2007). Flagellar Motility Is Critical for *L. monocytogenes* Biofilm Formation. *Journal of Bacteriology*, 189(12), pp.4418–4424.

Leontina Grigore-Gurgu, Florentina Ionela Bucur, Octavian Augustin Mihalache and Anca Ioana Nicolau (2024). Comprehensive Review on the Biocontrol of *L. monocytogenes* in Food Products. *Foods*, 13(5), pp.734–734. doi:https://doi.org/10.3390/foods13050734.

Lewis, K. (2010). Persister Cells. *Annual Review of Microbiology*, 64(1), pp.357–372. doi:https://doi.org/10.1146/annurev.micro.112408.134306.

Li, G. and Kathariou, S. (2003). An Improved Cloning Vector for Construction of Gene Replacements in *Listeria monocytogenes*. *Applied and Environmental Microbiology*, 69(5), pp.3020–3023. doi:https://doi.org/10.1128/aem.69.5.3020-3023.2003.

Li, H., Yang, J., Kuang, S., Fu, H., Lin, H. and Peng, B. (2025). Magnesium modulates phospholipid metabolism to promote bacterial phenotypic resistance to antibiotics. *eLife*, 13. doi:https://doi.org/10.7554/elife.100427.3.

Li, X., Hospital, X.F., Hierro, E., Fernández, M., Sheng, L. and Wang, L. (2023). Formation of *L. monocytogenes* persister cells in the produce-processing environment. *International journal of food microbiology*, 390, pp.110106–110106. doi:https://doi.org/10.1016/j.ijfoodmicro.2023.110106.

Li, X., Zhang, X., Zhang, M., Luo, X., Zhang, T., Liu, X., Lu, R. and Zhang, Y. (2024). Environmental magnesium ion affects global gene expression, motility, biofilm formation and virulence of *Vibrio parahaemolyticus*. *Biofilm*, 7, pp.100194–100194. doi:https://doi.org/10.1016/j.bioflm.2024.100194.

Lichtenberg, M., Kragh, K.N., Fritz, B., Kirkegaard, J.B., Tolker-Nielsen, T. and Bjarnsholt, T. (2022). Cyclic-di-GMP signaling controls metabolic activity in *Pseudomonas aeruginosa*. *Cell Reports*, 41(3), p.111515. doi:https://doi.org/10.1016/j.celrep.2022.111515.

Linnan, M. J., Mascola, L., Lou, X. D., Goulet, V., May, S., Salminen, C., Hird, D. W., Yonekura, M. L., Hayes, P., Weaver, R., Audurier, A., Plikaytis, B. D., Fannin, S. L., Kleks, A., & Broome, C. V. (1988). Epidemic listeriosis associated with Mexican-style cheese. *The New England Journal of Medicine, 319*(13), 823-828. https://doi.org/10.1056/NEJM198809293191303

Lio, P.A. and Kaye, E.T. (2011). Topical Antibacterial Agents. *Medical Clinics of North America*, 95(4), pp.703–721. doi:https://doi.org/10.1016/j.mcna.2011.03.008.

Liochev, S.I., Hausladen, A. and Fridovich, I. (1999). Nitroreductase A is regulated as a member of the *soxRS* regulon of *Escherichia coli*. *Proceedings of the National Academy of Sciences*, 96(7), pp.3537–3539. doi:https://doi.org/10.1073/pnas.96.7.3537.

Lipscomb, W.N. and Kantrowitz, E.R. (2012). Structure and Mechanisms of *Escherichia coli* Aspartate Transcarbamoylase. *Accounts of Chemical Research*, [online] 45(3), pp.444–453. doi:https://doi.org/10.1021/ar200166p.

Liu, D. (2006). Identification, subtyping and virulence determination of *Listeria monocytogenes*, an important foodborne pathogen. *Journal of Medical Microbiology*, 55(6), pp.645–659. doi:https://doi.org/10.1099/jmm.0.46495-0.

Liu, H. (2012). Optical and digital microscopic imaging techniques and applications in pathology. *Analytical Cellular Pathology (Amsterdam)*, [online] 34(1-2), p.5. doi:https://doi.org/10.3233/ACP-2011-0006.

Liu, J., Zhang, D., Lian, S., Gu, X., Hou, Q., Xia, P. and Zhu, G. (2021). Mechanism of nitrite transporter NirC in motility, biofilm formation, and adhesion of avian pathogenic *Escherichia*

coli. *Archives of Microbiology*, 203(7), pp.4221–4231. doi:https://doi.org/10.1007/s00203-021-02412-5.

Liu, Y., Van, A.M., Minh, Ngoc, B., Chen, R., Raphael, Paulino, A., Thaker, K., Aaryan Somadder, Frost, D.J., Menke, C.C., Slimak, Z.C. and Slonczewski, J.L. (2024). Fitness trade-offs of multidrug efflux pumps in *Escherichia coli* K-12 in acid or base, and with aromatic phytochemicals. *Applied and Environmental Microbiology*, 90(2). doi:https://doi.org/10.1128/aem.02096-23.

Loughlin, M.F., Jones, M.V. and Lambert, P.A. (2002). *Pseudomonas aeruginosa* cells adapted to benzalkonium chloride show tolerance to other membrane-active agents but not to clinically relevant antibiotics. *Journal of Antimicrobial Chemotherapy*, [online] 49(4), pp.631–639. doi:https://doi.org/10.1093/jac/49.4.631.

Løvdal, T., Brandal, L.T., Sundaram, A.Y.M., Naseer, U., Roth, B. and Lunestad, B.T. (2021). Small-Scale Comparative Genomic Analysis of *Listeria monocytogenes* Isolated from Environments of Salmon Processing Plants and Human Cases in Norway. *Hygiene*, 1(1), pp.43–55. doi:https://doi.org/10.3390/hygiene1010005.

Lu, H., Que, Y., Wu, X., Guan, T. and Guo, H. (2019). Metabolomics Deciphered Metabolic Reprogramming Required for Biofilm Formation. *Scientific Reports*, [online] 9(1). doi:https://doi.org/10.1038/s41598-019-49603-1.

Luque-Sastre, L., Arroyo, C., Fox, E.M., McMahon, B.J., Bai, L., Li, F. and Fanning, S. (2018). Antimicrobial Tolerance in *Listeria* Species. *Microbiology Spectrum*, 6(4). doi:https://doi.org/10.1128/microbiolspec.arba-0031-2017.

Lyska, D., Engelmann, K., Meierhoff, K. and Westhoff, P. (2013). pAUL: A Gateway-Based Vector System for Adaptive Expression and Flexible Tagging of Proteins in *Arabidopsis*. *PLOS ONE*, 8(1), pp.e53787–e53787. doi:https://doi.org/10.1371/journal.pone.0053787.

Ma, Q., Zhang, G. and Wood, T.K. (2011). Escherichia coli BdcA controls biofilm dispersal in *Pseudomonas aeruginosa* and Rhizobium meliloti. *BMC Research Notes*, 4(1). doi:https://doi.org/10.1186/1756-0500-4-447.

Ma, X., Tempelaars, M.H., Zwietering, M.H., Boeren, S., O'Byrne, C.P., den Besten, H. and Abee, T. (2024). A single point mutation in the *Listeria monocytogenes* ribosomal gene *rpsU* enables SigB activation independently of the stressosome and the anti-sigma factor antagonist RsbV. *Frontiers in Microbiology*, 15. doi:https://doi.org/10.3389/fmicb.2024.1304325.

Madad, A., Marshall, K.E., Blessington, T., Hardy, C., Salter, M., Basler, C., Conrad, A., Stroika, S., Luo, Y., Dwarka, A., Gerhardt, T., Rosa, Y., Cibulskas, K., Rosen, H.E., Adcock, B., Kiang, D., Hutton, S., Parish, M., Podoski, B. and Patel, B. (2023). Investigation of a Multistate Outbreak of *Listeria monocytogenes* Infections Linked to Frozen Vegetables Produced at Individually Quick-Frozen Vegetable Manufacturing Facilities. *Journal of Food Protection*, [online] 86(8), p.100117. doi:https://doi.org/10.1016/j.jfp.2023.100117.

Mafu, A.A., Plumety, C., Deschênes, L. and Goulet, J. (2011). Adhesion of Pathogenic Bacteria to Food Contact Surfaces: Influence of pH of Culture. *International Journal of Microbiology*, [online] 2011.

Maguire, M., E. (2006). Magnesium Transporters: Properties, Regulation and Structure. *Frontiers in Bioscience*, 11(1), p.3149. doi:https://doi.org/10.2741/2039.

Maguire, M.E. (1992). MgtA and MgtB: Prokaryotic P-type ATPases that mediate Mg^{2+} influx. *Journal of Bioenergetics and Biomembranes*, 24(3), pp.319–328. doi:https://doi.org/10.1007/bf00768852.

Maiden, M.C.J., Bygraves, J.A., Feil, E., Morelli, G., Russell, J.E., Urwin, R., Zhang, Q., Zhou, J., Zurth, K., Caugant, D.A., Feavers, I.M., Achtman, M. and Spratt, B.G. (1998). Multilocus sequence typing: A portable approach to the identification of clones within populations of pathogenic microorganisms. *Proceedings of the National Academy of Sciences*, 95(6), pp.3140–3145. doi:https://doi.org/10.1073/pnas.95.6.3140.

Maillard, J.-Y. (2022). Impact of benzalkonium chloride, benzethonium chloride and chloroxylenol on bacterial antimicrobial resistance. *Journal of Applied Microbiology*, 133(6), pp.3322–3346. doi:https://doi.org/10.1111/jam.15739.

Mangwani, N., Shukla, S.K., Rao, T.S. and Das, S. (2014). Calcium-mediated modulation of *Pseudomonas mendocina* NR802 biofilm influences the phenanthrene degradation. *Colloids and Surfaces B: Biointerfaces*, 114, pp.301–309. doi:https://doi.org/10.1016/j.colsurfb.2013.10.003.

Marinho, C.M., Santos, Kallipolitis, B.H., Johansson, J., Ignatov, D., Guerreiro, D.N., Pascal Piveteau and O'Byrne, C.P. (2019). The σ^B-dependent regulatory sRNA Rli47 represses isoleucine biosynthesis in *Listeria monocytogenes* through a direct interaction with the *ilvA* transcript. *RNA Biology*, 16(10), pp.1424–1437. doi:https://doi.org/10.1080/15476286.2019.1632776.

Martínez-García, S., Peralta, H., Betanzos-Cabrera, G., Chavez-Galan, L., Rodríguez-Martínez, S., Cancino-Diaz, M. E., & Cancino-Diaz, J. C. (2021). Proteomic comparison of biofilm vs. planktonic *Staphylococcus epidermidis* cells suggests key metabolic differences between these conditions. *Research in Microbiology*, *172*(2), 103796. https://doi.org/10.1016/j.resmic.2020.103796

Martínez-Suárez, J. V., Ortiz, S., & López-Alonso, V. (2016). Potential impact of the resistance to quaternary ammonium disinfectants on the persistence of *Listeria monocytogenes* in food processing environments. *Frontiers in Microbiology, 7*, 638. https://doi.org/10.3389/fmicb.2016.00638.

Martínez-Suárez, J.V., Ortiz, S. and López-Alonso, V. (2016). Potential Impact of the Tolerance to Quaternary Ammonium Disinfectants on the Persistence of *L. monocytogenes* in FPEs. *Frontiers in Microbiology*, 638(7).

Mata, M., Baquero, F. and Pérez-Díaz, J.C. (2000). A multidrug efflux transporter in *L. monocytogenes*. *Fems Microbiology Letters*, 187(2), pp.185–188. doi:https://doi.org/10.1111/j.1574-6968.2000.tb09158.x.

Mateus, A., Shah, M.B., Hevler, J.F., Kurzawa, N., Bobonis, J., Athanasios Typas and Savitski, M.M. (2021). Transcriptional and Post-Transcriptional Polar Effects in Bacterial Gene Deletion Libraries. *MSystems*, 6(5). doi:https://doi.org/10.1128/msystems.00813-21.

Matthews, T.C., Bristow, F.R., Griffiths, E.J., Petkau, A., Adam, J., Dooley, D., Kruczkiewicz, P., Curatcha, J., Cabral, J., Fornika, D., Winsor, G.L., Courtot, M., Bertelli, C., Roudgar, A., Feijao, P., Mabon, P., Enns, E., Thiessen, J., Keddy, A. and Isaac-Renton, J. (2018). The Integrated Rapid Infectious Disease Analysis (IRIDA) Platform. *bioRxiv*.

Blum, M., Andreeva, A., Florentino, L. C., Chuguransky, S. R., Grego, T., Hobbs, E., Pinto, B. L., Orr, A., Paysan-Lafosse, T., Ponamareva, I., Salazar, G. A., Bordin, N., Bork, P., Bridge, A., Colwell, L., Gough, J., Haft, D. H., Letunic, I., Llinares-López, F., Bateman, A. (2025). InterPro: The protein sequence classification resource in 2025. *Nucleic Acids Research, 53*(D1), D444–D456.

Mauri, M., Elli, T., Caviglia, G., Uboldi, G., & Azzi, M. (2017). RAWGraphs: A Visualisation Platform to Create Open Outputs. In Proceedings of the 12th Biannual Conference on Italian SIGCHI Chapter (p. 28:1–28:5). New York, NY, USA: ACM. https://doi.org/10.1145/3125571.3125585

Maury, M.M., Bracq-Dieye, H., Huang, L., Vales, G., Lavina, M., Thouvenot, P., Disson, O., Leclercq, A., Brisse, S. and Lecuit, M. (2019). Hypervirulent *Listeria monocytogenes* clones' adaption to mammalian gut accounts for their association with dairy products. *Nature Communications*, [online] 10(1). doi:https://doi.org/10.1038/s41467-019-10380-0.

Mazaheri, T., Cervantes-Huamán, B.R.H., Bermúdez-Capdevila, M., Ripolles-Avila, C. and Rodríguez-Jerez, J.J. (2021). *Listeria monocytogenes* Biofilms in the Food Industry: Is the Current Hygiene Program Sufficient to Combat the Persistence of the Pathogen? *Microorganisms*, [online] 9(1), p.181. doi:https://doi.org/10.3390/microorganisms9010181.

Mazaheri, T., Ripolles-Avila, C., Hascoët, A.S. and Rodríguez-Jerez, J.J. (2020). Effect of an enzymatic treatment on the removal of mature *L. monocytogenes* biofilms: A quantitative and qualitative study. *Food Control*, 114, p.107266.

McDonnell, G. and Russell, A.D. (1999). Antiseptics and Disinfectants: Activity, Action, and Tolerance. *Clinical Microbiology Reviews*, [online] 12(1), pp.147–179.

McGuffie MJ, Barrick JE. (2021). pLannotate: engineered plasmid annotation. *Nucleic Acids Research.* 49(2), W516-W522. doi: 10.1093/nar/gkab374. PMID: 34019636; PMCID:

McLauchlin, J. (1990). Human listeriosis in Britain, 1967–85, a summary of 722 cases: 1. Listeriosis during pregnancy and in the newborn. *Epidemiology and Infection, 104*(2), 181–189. https://doi.org/10.1017/S0950268800059343.

McLauchlin, J., Aird, H., Amar, C., Barker, C., Dallman, T., Lai, S., Painset, A. and Willis, C. (2021). An outbreak of human listeriosis associated with frozen sweet corn consumption: Investigations in the UK. *International Journal of Food Microbiology*, 338, p.108994.

McLauchlin, J., Aird, H., Amar, C., Boyd, G., Brindle, A., Dallman, T., Jalava, K., Painset, A., Simbo, A. and Swindlehurst, M. (2021). Listeriosis associated with pre-prepared sandwich consumption in hospital in England, 2017. *Epidemiology and Infection*, 149. doi:https://doi.org/10.1017/s0950268821001916.

McLauchlin, J., Grant, K. A., & Amar, C. F. L. (2020). Human foodborne listeriosis in England and Wales, 1981 to 2015. *Epidemiology and Infection*, *148*. https://doi.org/10.1017/s0950268820000473

McLauchlin, J., Hall, S.M., Velani, S.K. and Gilbert, R.J. (1991). Human listeriosis and pate: a possible association. *BMJ*, 303(6805), pp.773–775. doi:https://doi.org/10.1136/bmj.303.6805.773.

Méndez Acevedo, M., Rolon, M.L., Johnson, B.B., Burns, L.H., Stacy, J., Aurand-Cravens, A., LaBorde, L. and Kovac, J. (2024). Sanitizer Tolerance and Persistence of *Listeria monocytogenes* Isolates in Tree Fruit Packing Facilities. *Journal of food protection*, [online] 87(10), p.100354. doi:https://doi.org/10.1016/j.jfp.2024.100354.

Mendez, E., Walker, D.K., Vipham, J. and Trinetta, V. (2020). The use of a CDC biofilm reactor to grow multi-strain *L. monocytogenes* biofilm. *Food Microbiology*, 92, p.103592. doi:https://doi.org/10.1016/j.fm.2020.103592.

Merchel Piovesan Pereira, B. and Tagkopoulos, I. (2019). Benzalkonium Chlorides: Uses, Regulatory Status, and Microbial Tolerance. *Applied and Environmental Microbiology*, 85(13). doi:https://doi.org/10.1128/aem.00377-19.

Merle-Melet, M., Dossou-Gbete, L., Maurer, P., Meyer, Ph., Lozniewski, A., Kuntzburger, O., Wéber, M. and Gérard, A. (1996). Is amoxicillin-cotrimoxazole the most appropriate antibiotic regimen for *Listeria meningoencephalitis*? Review of 22 cases and the literature. *Journal of Infection*, 33(2), pp.79–85.

Merritt, J.H., Kadouri, D.E. and O'Toole, G.A. (2005). Growing and Analyzing Static Biofilms. *Current Protocols in Microbiology*, 00(1). doi:https://doi.org/10.1002/9780471729259.mc01b01s00.

Miller, I.A., Chatfield, S., Dougan, G., Desilva, L., Joysey, H.S. and Hormaeche, C. (1989). Bacteriophage P22 as a vehicle for transducing cosmid gene banks between smooth strains of *Salmonella typhimurium*: Use in identifying a role for *aroD* in attenuating virulent Salmonella strains. *MGG Molecular & General Genetics*, 215(2), pp.312–316. doi:https://doi.org/10.1007/bf00339734.

Miller, M.B. and Bassler, B.L. (2001). Quorum sensing in bacteria. *Annual review of microbiology*, 55(1), pp.165–99. doi:https://doi.org/10.1146/annurev.micro.55.1.165.

Minarovičová, J., Véghová, A., Mikulášová, M., Chovanová, R., Šoltýs, K., Drahovská, H. and Kaclíková, E. (2018). Benzalkonium chloride tolerance of *Listeria monocytogenes* strains isolated from a meat processing facility is related to presence of plasmid-borne *bcrABC* cassette. *Antonie Van Leeuwenhoek*, [online] 111(10), pp.1913–1923. doi:https://doi.org/10.1007/s10482-018-1082-0.

Minero, G., Møllebjerg, A., Thiesen, C., Johansen, M., Nis Pedersen Jørgensen, Birkedal, V., Daniel Erik Otzen and Meyer, R. (2024). Extracellular G-quadruplexes and Z-DNA protect biofilms from DNase I, and G-quadruplexes form a DNAzyme with peroxidase activity. *Nucleic Acids Research*, [online] 52(4), pp.1575–1590. doi:https://doi.org/10.1093/nar/gkae034.

Mishra, S., Gupta, A., Upadhye, V., Singh, S.C., Sinha, R.P. and Häder, Donat-P. (2023). Therapeutic Strategies against Biofilm Infections. *Life*, 13(1), p.172. doi:https://doi.org/10.3390/life13010172.

Mitchell, G., Cheng, M.I., Chen, C., Nguyen, B.N., Whiteley, A.T., Kianian, S., Cox, J.S., Green, D.R., McDonald, K.L. and Portnoy, D.A. (2017). *Listeria monocytogenes* triggers noncanonical autophagy upon phagocytosis, but avoids subsequent growth-restricting xenophagy. *Proceedings of the National Academy of Sciences*, 115(2). doi:https://doi.org/10.1073/pnas.1716055115.

Mitja, O., Pigrau, C., Ruiz, I., Vidal, X., Almirante, B., Planes, A.-M. ., Molina, I., Rodriguez, D. and Pahissa, A. (2009). Predictors of mortality and impact of aminoglycosides on outcome in listeriosis in a retrospective cohort study. *Journal of Antimicrobial Chemotherapy*, 64(2), pp.416–423.

Mojzsis, S.J., Arrhenius, G., McKeegan, K.D., Harrison, T.M., Nutman, A.P. and Friend, C.R.L. (1996). Evidence for life on Earth before 3,800 million years ago. *Nature*, 384(6604), pp.55–59. doi:https://doi.org/10.1038/384055a0.

Monk, I.R., Gahan, C.G.M. and Hill, C. (2008). Tools for Functional Postgenomic Analysis of *Listeria monocytogenes*. *Applied and Environmental Microbiology*, 74(13), pp.3921–3934. doi:https://doi.org/10.1128/aem.00314-08.

Monk, I.R., Shah, I.M., Xu, M., Tan, M.-W. and Foster, T.J. (2012). Transforming the Untransformable: Application of Direct Transformation To Manipulate Genetically *Staphylococcus aureus* and *Staphylococcus epidermidis*. *mBio*, 3(2). doi:https://doi.org/10.1128/mbio.00277-11.

Montañez-Izquierdo, V.Y., Salas-Vázquez, D.I. and Rodríguez-Jerez, J.J. (2012). Use of epifluorescence microscopy to assess the effectiveness of phage P100 in controlling *Listeria monocytogenes* biofilms on stainless steel surfaces. *Food Control*, 23(2), pp.470–477. doi:https://doi.org/10.1016/j.foodcont.2011.08.016.

Møretrø, T. and Langsrud, S. (2004). *Listeria monocytogenes*: biofilm formation and persistence in food-processing environments. *Biofilms*, 1(2), pp.107–121. doi:https://doi.org/10.1017/s1479050504001322.

Møretrø, T., & Langsrud, S. (2017). Residential Bacteria on Surfaces in the Food Industry and Their Implications for Food Safety and Quality. Comprehensive Reviews in Food Science and Food Safety, 16(5), 1022–1041. https://doi.org/10.1111/1541-4337.12283

Møretrø, T., Schirmer, B.C.T., Heir, E., Fagerlund, A., HjemLi, P. and Langsrud, S. (2017). Tolerance to quaternary ammonium compound disinfectants may enhance growth of *L. monocytogenes* in the food industry. *International Journal of Food Microbiology*, 241, pp.215–224.

Morganti, M., Scaltriti, E., Cozzolino, P., Luca Bolzoni, Casadei, G., Pierantoni, M., Emanuela Foni and Stefano Pongolini (2016). Processing-Dependent and Clonal Contamination Patterns of Listeria monocytogenes in the Cured Ham Food Chain Revealed by Genetic Analysis. *Applied and Environmental Microbiology*, [online] 82(3), pp.822–831. doi:https://doi.org/10.1128/aem.03103-15.

Morici, L.A., Carterson, A.J., Wagner, V.E., Frisk, A., Schurr, J.R., zu Bentrup, K.H., Hassett, D.J., Iglewski, B.H., Sauer, K. and Schurr, M.J. (2007). *Pseudomonas aeruginosa* AlgR Represses the Rhl Quorum-Sensing System in a Biofilm-Specific Manner. *Journal of Bacteriology*, 189(21), pp.7752–7764. doi:https://doi.org/10.1128/jb.01797-06.

Moura, A., Criscuolo, A., Hannes Pouseele, Maury, M.M., Leclercq, A., Tarr, C.L., Larsson, J., Dallman, T.J., Reimer, A., Enouf, V., Larsonneur, E., Carleton, H.A., Hélène Bracq-Dieye, Katz, L.S., Jones, L., Touchon, M., Mathieu Tourdjman, Walker, M.C., Stroika, S. and Cantinelli, T. (2017). Whole genome-based population biology and epidemiological surveillance of *Listeria monocytogenes*. *Nature microbiology*, 2(2). doi:https://doi.org/10.1038/nmicrobiol.2016.185.

Moura, A., Tourdjman, M., Leclercq, A., Hamelin, E., Laurent, E., Fredriksen, N., Van Cauteren, D., Bracq-Dieye, H., Thouvenot, P., Vales, G., Tessaud-Rita, N., Maury, M.M., Alexandru, A., Criscuolo, A., Quevillon, E., Donguy, M.-P., Enouf, V., de Valk, H., Brisse, S. and Lecuit, M. (2017). Real-Time Whole-Genome Sequencing for Surveillance of *Listeria monocytogenes*, France. *Emerging Infectious Diseases*, 23(9), pp.1462–1470. doi:https://doi.org/10.3201/eid2309.170336.

Mugunthan, S., Wong, L.L., Winnerdy, F.R., Summers, S., Bin Ismail, M.H., Foo, Y.H., Jaggi, T.K., Meldrum, O.W., Tiew, P.Y., Chotirmall, S.H., Rice, S.A., Phan, A.T., Kjelleberg, S. and Seviour, T. (2023). RNA is a key component of extracellular DNA networks in *Pseudomonas aeruginosa* biofilms. *Nature Communications*, [online] 14(1), p.7772. doi:https://doi.org/10.1038/s41467-023-43533-3.

Mulcahy, H. and Lewenza, S. (2011). Magnesium Limitation Is an Environmental Trigger of the *Pseudomonas aeruginosa* Biofilm Lifestyle. *PLoS ONE*, 6(8), p.e23307. doi:https://doi.org/10.1371/journal.pone.0023307.

Müller, A., Rychli, K., Muhterem-Uyar, M., Zaiser, A., Stessl, B., Guinane, C.M., Cotter, P.D., Wagner, M. and Schmitz-Esser, S. (2013). Tn6188 - A Novel Transposon in *Listeria monocytogenes* Responsible for Tolerance to Benzalkonium Chloride. *PLoS ONE*, 8(10), p.e76835. doi:https://doi.org/10.1371/journal.pone.0076835.

Murray, E. G. D., Webb, R. A., & Swann, M. B. R. (1926). A disease of rabbits characterized by a large mononuclear leucocytosis caused by a hitherto undescribed bacillus *Bacterium monocytogenes* n. sp. *Journal of Pathology and Bacteriology, 29*(4), 407-439.

Myintzaw, P., Pennone, V., McAuliffe, O., Begley, M. and Callanan, M. (2023). Association of Virulence, Biofilm, and Antimicrobial Tolerance Genes with Specific Clonal Complex Types of *L. monocytogenes*. *Microorganisms*, [online] 11(6), p.1603. doi:https://doi.org/10.3390/microorganisms11061603.

Mylonakis, E., Hohmann, E.L. and Calderwood, S.B. (1998). Central Nervous System Infection with *Listeria monocytogenes*: 33 Years' Experience at a General Hospital and Review of 776 Episodes from the Literature. *Medicine*, 77(5), pp.313–336. doi:https://doi.org/10.1097/00005792-199809000-00002.

Mylonakis, E., Paliou, M., Hohmann, E. L., Calderwood, S. B., & Wing, E. J. (2002). Listeriosis during pregnancy: A case series and review of 222 cases. *Medicine (Baltimore)*, 81(4), 260–269. https://doi.org/10.1097/00005792-200207000-00002.

Nadon, C.A., Bowen, B.M., Wiedmann, M. and Boor, K.J. (2002). Sigma B Contributes to PrfA-Mediated Virulence in *Listeria monocytogenes*. Infection and Immunity, 70(7), pp.3948–3952. doi:https://doi.org/10.1128/iai.70.7.3948-3952.2002.

Nair, H.A.S., Subramoni, S., Poh, W.H., Hasnuddin, N.T.B., Tay, M., Givskov, M., Tolker-Nielsen, T., Kjelleberg, S., McDougald, D. and Rice, S.A. (2021). Carbon starvation of *Pseudomonas aeruginosa* biofilms selects for dispersal insensitive mutants. *BMC Microbiology*, 21(1). doi:https://doi.org/10.1186/s12866-021-02318-8.

NicAogáin, K. and O'Byrne, C.P. (2016). The Role of Stress and Stress Adaptations in Determining the Fate of the Bacterial Pathogen *Listeria monocytogenes* in the Food Chain. *Frontiers in Microbiology*, [online] 7, p.1865. doi:https://doi.org/10.3389/fmicb.2016.01865.

Nickel, J.C., Ruseska, I., Wright, J.B. and Costerton, J.W. (1985). Tobramycin resistance of *Pseudomonas aeruginosa* cells growing as a biofilm on urinary catheter material. *Antimicrobial Agents and Chemotherapy*, 27(4), pp.619–624. doi:https://doi.org/10.1128/aac.27.4.619.

Niederdorfer, R., Besemer, K., Battin, T.J. and Peter, H. (2017). Ecological strategies and metabolic trade-offs of complex environmental biofilms. *npj Biofilms and Microbiomes*, 3(1). doi:https://doi.org/10.1038/s41522-017-0029-y.

Nittay, Tal Livny, Toledano, G., Sorokin, Y., Nesli Tovi and Friedman, J. (2024). Evolution in microbial microcosms is highly parallel, regardless of the presence of interacting species. Cell Systems, 15(10), pp.930-940.e5. doi:https://doi.org/10.1016/j.cels.2024.09.007.

Nordholt, N., Kanaris, O., Schmidt, S.B.I. and Schreiber, F. (2021). Persistence against benzalkonium chloride promotes rapid evolution of tolerance during periodic disinfection. *Nature Communications*, 12(1). doi:https://doi.org/10.1038/s41467-021-27019-8.

Nowak, J., Visnovsky, S.B., Pitman, A.R., Cruz, C.D., Palmer, J., Fletcher, G.C. and Flint, S. (2021). Biofilm Formation by *Listeria monocytogenes* 15G01, a Persistent Isolate from a

Seafood-Processing Plant, Is Influenced by Inactivation of Multiple Genes Belonging to Different Functional Groups. *Applied and Environmental Microbiology*, 87(10). doi:https://doi.org/10.1128/aem.02349-20.

O'Mahony, A. (2020). *The break-up: ready meals category report 2020*. [online] The Grocer. Available at: https://www.thegrocer.co.uk/category-reports/the-break-up-ready-meals- category-report-2020/601160.article.

O'Toole, G., Kaplan, H.B. and Kolter, R. (2000). Biofilm Formation as Microbial Development. *Annual Review of Microbiology*, 54(1), pp.49–79. doi:https://doi.org/10.1146/annurev.micro.54.1.49.

Oakley, J.D., Taylor, K.G. and Doyle, R.J. (1985). Trypsin-susceptible cell surface characteristics of *Streptococcus sanguis*. *Canadian Journal of Microbiology*, 31(12), pp.1103–1107. doi:https://doi.org/10.1139/m85-208.

Oknin, H., Steinberg, D. and Shemesh, M. (2015). Mg^{2+} ions mitigate biofilm formation of *Bacillus* species via downregulation of matrix genes expression. *Frontiers in Microbiology*, 6. doi:https://doi.org/10.3389/fmicb.2015.00907.

Oliveira, A.H., Tiensuu, T., Guerreiro, D.N., Tükenmez, H., Dessaux, C., García-del Portillo, F., O'Byrne, C. and Johansson, J. (2022). *Listeria monocytogenes* Requires the RsbX Protein To Prevent SigB Activation under Nonstressed Conditions. Journal of Bacteriology, 204(1). doi:https://doi.org/10.1128/jb.00486-21.

Oliveira, F., Lima, T., Correia, A., Ana Margarida Silva, Soares, C., Morais, S., Weißelberg, S., Vilanova, M., Rohde, H. and Nuno Cerca (2022b). Involvement of the Iron-Regulated Loci *hts* and *fhuC* in Biofilm Formation and Survival of *Staphylococcus epidermidis* within the Host. *Microbiology spectrum*, 10(1). doi:https://doi.org/10.1128/spectrum.02168-21.

Orsi, R.H., Bakker, H.C. den and Wiedmann, M. (2011). *L. monocytogenes* lineages: Genomics, evolution, ecology, and phenotypic characteristics. *International Journal of Medical Microbiology*, 301(2), pp.79–96.

Ortiz, S., López-Alonso, V., Gutiérrez Rodríguez, P. and Martínez-Suárez, J.V. (2016). The Connection between Persistent, Disinfectant-Resistant *Listeria monocytogenes* Strains from Two Geographically Separate Iberian Pork Processing Plants: Evidence from Comparative Genome Analysis. *Applied and Environmental Microbiology*, 82(1), pp.308–317. doi:https://doi.org/10.1128/aem.02824-15.

Otto, K. and Silhavy, T.J. (2002). Surface sensing and adhesion of *Escherichia coli* controlled by the Cpx-signaling pathway. *Proceedings of the National Academy of Sciences*, 99(4), pp.2287–2292. doi:https://doi.org/10.1073/pnas.042521699.

Otto, M., Dickey, S.W. and Wolz, C. (2023). Editorial: Quorum-sensing in Gram-positive pathogens – mechanisms, role in infection, and potential as a therapeutic target. *Frontiers in Cellular and Infection Microbiology*, 13. doi:https://doi.org/10.3389/fcimb.2023.1236705.

Page, A.J., Ainsworth, E.V. and Langridge, G.C. (2020). socru: typing of genome-level order and orientation around ribosomal operons in bacteria. *Microbial Genomics*, 6(7). doi:https://doi.org/10.1099/mgen.0.000396.

Page, A.J., Keane, J.A., Delaney, A.J., Taylor, B., Seemann, T., Harris, S.R. and Soares, J. (2016). SNP-sites: rapid efficient extraction of SNPs from multi-FASTA alignments. *Microbial Genomics*, 2(4). doi:https://doi.org/10.1099/mgen.0.000056.

Palma, F., Brauge, T., Radomski, N., Mallet, L., Felten, A., Mistou, M.-Y., Brisabois, A., Guillier, L. and Midelet-Bourdin, G. (2020). Dynamics of mobile genetic elements of *Listeria monocytogenes* persisting in ready-to-eat seafood processing plants in France. *BMC Genomics*, 21(1). doi:https://doi.org/10.1186/s12864-020-6544-x.

Palmer, J., Flint, S., and Brooks, J. (2007). Bacterial cell attachment, the beginning of a biofilm. *J. Ind. Microbiol. Biotechnol.* 34, 577–588.

Parisi, A., Latorre, L., Normanno, G., Miccolupo, A., Fraccalvieri, R., Lorusso, V. and Santagada, G. (2010). Amplified Fragment Length Polymorphism and Multi-Locus Sequence Typing for high-resolution genotyping of *L. monocytogenes* from foods and the environment. *Food Microbiology*, 27(1), pp.101–108.

Park, J., Choi, H. and Won Gon Kim (2020). The Nitrite Transporter Facilitates Biofilm Formation via Suppression of Nitrite Reductase and Is a New Antibiofilm Target in *P. aeruginosa*. *MBio*, 11(4). doi:https://doi.org/10.1128/mbio.00878-20.

Park, S.F. and Stewart, G.S. (1990). High-efficiency transformation of *Listeria monocytogenes* by electroporation of penicillin-treated cells. *Gene*, 94(1), pp.129–132. doi:https://doi.org/10.1016/0378-1119(90)90479-b.

Pasqua, M., Grossi, M., Zennaro, A., Fanelli, G., Micheli, G., Barras, F., Colonna, B. and Prosseda, G. (2019). The Varied Role of Efflux Pumps of the MFS Family in the Interplay of Bacteria with Animal and Plant Cells. *Microorganisms*, [online] 7(9). Available at: https://www.ncbi.nlm.nih.gov/pmc/articles/PMC6780985/ [Accessed 5 Nov. 2020].

Pasquali, F., Palma, F., Guillier, L., Lucchi, A., De Cesare, A. and Manfreda, G. (2018). *Listeria monocytogenes* Sequence Types 121 and 14 Repeatedly Isolated Within One Year of Sampling in a Rabbit Meat Processing Plant: Persistence and Ecophysiology. *Frontiers in Microbiology*, [online] 9, p.596. doi:https://doi.org/10.3389/fmicb.2018.00596.

Pathak, D., Jin, K.S., Tandukar, S., Kim, J.H., Kwon, E. and Kim, D.Y. (2020). Structural insights into the regulation of SigB activity by RsbV and RsbW. *IUCrJ*, 7(4), pp.737–747. doi:https://doi.org/10.1107/s2052252520007617.

Paul, J.H. and Jeffrey, W.H. (1985). Evidence for Separate Adhesion Mechanisms for Hydrophilic and Hydrophobic Surfaces in *Vibrio proteolytica*. *Applied and Environmental Microbiology*, 50(2), pp.431–437.

Paulsen, I.T., Skurray, R.A., Tam, R., Saier, M.H., Turner, R.J., Weiner, J.H., Goldberg, E.B. and Grinius, L.L. (1996). The SMR family: a novel family of multidrug efflux proteins involved with the efflux of lipophilic drugs. *Molecular Microbiology*, 19(6), pp.1167–1175.

Pereira, A.P., Antunes, P., Bierge, P., Willems, R.J.L., Jukka Corander, Coque, T.M., Pich, O.Q., Peixe, L., Freitas, A.R. and Novais, C. (2023). Unravelling *Enterococcus* susceptibility to quaternary ammonium compounds: genes, phenotypes, and the impact of environmental conditions. *Microbiology spectrum*, 11(5).

Pérez-Rodríguez, F., Valero, A., Carrasco, E., García, R.M. and Zurera, G. (2008). Understanding and modelling bacterial transfer to foods: a review. *Trends in Food Science & Technology*, 19(3), pp.131–144. doi:https://doi.org/10.1016/j.tifs.2007.08.003.

Perfeito, L., Fernandes, L., Mota, C. and Gordo, I. (2007). Adaptive mutations in bacteria: high rate and small effects. *Science (New York, N.Y.)*, [online] 317(5839), pp.813–815. doi:https://doi.org/10.1126/science.1142284.

Pessione, E. (2020). The Russian Doll Model: How Bacteria Shape Successful and Sustainable Inter-Kingdom Relationships. *Frontiers in Microbiology*, 11. doi:https://doi.org/10.3389/fmicb.2020.573759.

Piercey, M.J., Hingston, P.A. and Truelstrup Hansen, L. (2016). Genes involved in *Listeria monocytogenes* biofilm formation at a simulated food processing plant temperature of 15°C. *International Journal of Food Microbiology*, 223, pp.63–74. doi:https://doi.org/10.1016/j.ijfoodmicro.2016.02.009.

Pierre-Emmanuel Douarre, Yann Sévellec, Patricia Le Grandois, Christophe Soumet, Arnaud Bridier and Roussel, S. (2022). FepR as a Central Genetic Target in the Adaptation to Quaternary Ammonium Compounds and Cross-Tolerance to Ciprofloxacin in *L. monocytogenes*. *Frontiers in microbiology*, 13. doi:https://doi.org/10.3389/fmicb.2022.864576.

Pightling, A.W., Petronella, N. and Pagotto, F. (2015). The *L. monocytogenes* Core-Genome Sequence Typer (LmCGST): a bioinformatic pipeline for molecular characterization with next-generation sequence data. *BMC Microbiology*, 15(1). doi:https://doi.org/10.1186/s12866-015-0526-1.

Pilkington, A. (2022). *Ready-to-eat foods and Ready Meals Market Report UK 2022*. [online] store.mintel.com. Available at: https://store.mintel.com/report/uk-ready-meals-and-ready-to-cook-foods-market-report-2022 [Accessed 14 Sep. 2025].

Pineda, B., Giménez-Caminero, E., Begoña García-Sogo, María Teresa Antón, Atarés, A., Capel, J., Lozano, R., Angosto, T. and Moreno, V. (2010). Genetic and Physiological Characterization of the Arlequin Insertional Mutant Reveals a Key Regulator of Reproductive Development in Tomato. *Plant and Cell Physiology*, 51(3), pp.435–447. doi:https://doi.org/10.1093/pcp/pcq009.

Pirie, J. H. (1940). *Listeria*: Change of name for a genus of bacteria. *Nature, 145*(3683), 264. https://doi.org/10.1038/145264a0.

Pirone-Davies, C., Chen, Y., Pightling, A., Ryan, G., Wang, Y., Yao, K., Hoffmann, M. and Allard, M.W. (2018). Genes significantly associated with lineage II food isolates of *Listeria monocytogenes.* BMC Genomics, 19(1). doi:https://doi.org/10.1186/s12864-018-5074-2.

Pisithkul, T., Schroeder, J.W., Trujillo, E.A., Yeesin, P., Stevenson, D.M., Chaiamarit, T., Coon, J.J., Wang, J.D. and Amador-Noguez, D. (2019). Metabolic Remodelling during Biofilm Development of *Bacillus subtilis*. *mBio*, [online] 10(3). doi:https://doi.org/10.1128/mBio.00623-19.

Poimenidou, S.V., Dalmasso, M., Papadimitriou, K., Fox, E.M., Skandamis, P.N. and Jordan, K. (2018). Virulence Gene Sequencing Highlights Similarities and Differences in Sequences in *L. monocytogenes* Serotype 1/2a and 4b Strains of Clinical and Food Origin From 3 Different Geographic Locations. *Frontiers in Microbiology*, 9(5).

Poltak, S. R., & Cooper, V. S. (2010). Ecological succession in long-term experimentally evolved biofilms produces synergistic communities. *The ISME Journal*, *5*(3), 369–378. https://doi.org/10.1038/ismej.2010.136

Pomposiello, P.J., Bennik, M.H.J. and Demple, B. (2001). Genome-Wide Transcriptional Profiling of the Escherichia coli Responses to Superoxide Stress and Sodium Salicylate. *Journal of Bacteriology*, 183(13), pp.3890–3902. doi:https://doi.org/10.1128/jb.183.13.3890-3902.2001.

Popovic, I., Heron, B. and Covacin, C. (2014). *Listeria*: An Australian Perspective (2001–2010). *Foodborne Pathogens and Disease*, 11(6), pp.425–432. doi:https://doi.org/10.1089/fpd.2013.1697.

Popowska, M., Krawczyk-Balska, A., Ostrowski, R. and Desvaux, M. (2017). InlL from *L. monocytogenes* Is Involved in Biofilm Formation and Adhesion to Mucin. *Frontiers in Microbiology*, 8.

Post, D. W., Held, J. M., Ketterer, M. R., Phillips, N., Sahu, A. K., Apicella, M. A., & Gibson, B. W. (2014). Comparative analyses of proteins from *Haemophilus influenzae* biofilm and planktonic populations using metabolic labeling and mass spectrometry. *14*(1). https://doi.org/10.1186/s12866-014-0329-9.

Poulsen, L.K., Ballard, G. and Stahl, D.A. (1993). Use of rRNA fluorescence in situ hybridization for measuring the activity of single cells in young and established biofilms. *Applied and environmental microbiology*, 59(5), pp.1354–1360. doi:https://doi.org/10.1128/aem.59.5.1354-1360.1993.

Hashemifard Dehkordi, P., Moshtaghi, H., & Abbasvali, M. (2022). Effects of magnesium oxide and copper oxide nanoparticles on biofilm formation of *Escherichia coli* and *Listeria monocytogenes*. *Nanotechnology, 34*(15), 155102. https://doi.org/10.1088/1361-6528/acab6f.

Prigent-Combaret, C. and Lejeune, P. (1999). [4] Monitoring gene expression in biofilms. *Methods in enzymology on CD-ROM/Methods in enzymology*, pp.56–79. doi:https://doi.org/10.1016/s0076-6879(99)10006-5.

Prjibelski, A., Antipov, D., Meleshko, D., Lapidus, A. and Korobeynikov, A. (2020). Using SPAdes *De Novo* Assembler. *Current Protocols in Bioinformatics*, 70(1).

Promadej, N., Fiedler, F., Cossart, P., Dramsi, S. and Kathariou, S. (1999). Cell Wall Teichoic Acid Glycosylation in *Listeria monocytogenes* Serotype 4b Requires *gtcA*, a Novel, Serogroup-Specific Gene. *Journal of Bacteriology*, 181(2), pp.418–425. doi:https://doi.org/10.1128/jb.181.2.418-425.1999.

Public health England, management team (2020). *Investigation into an outbreak of L. monocytogenes infections associated with hospital-provided pre- prepared sandwiches, UK May to July 2019*. Wellington House 133-155 Waterloo Road London SE1 8UG: PHE publications.

Puga, C.H., Dahdouh, E., SanJose, C. and Orgaz, B. (2018). *Listeria monocytogenes* Colonizes *Pseudomonas fluorescens* Biofilms and Induces Matrix Over-Production. *Frontiers in Microbiology*, 9. doi:https://doi.org/10.3389/fmicb.2018.01706.

Purevdorj-Gage, B. (2005). Phenotypic differentiation and seeding dispersal in non-mucoid and mucoid *Pseudomonas aeruginosa* biofilms. *Microbiology*, 151(5), pp.1569–1576. doi:https://doi.org/10.1099/mic.0.27536-0.

Qu, L., Meng, G.-L., Wang, Q., Yang, L., Wang, L.-B. and Xie, Y. (2022). A comprehensive analysis of listeriosis in 13 pregnant women and 27 newborns in Xi'an from 2011 to 2020. *Translational pediatrics*, [online] 11(9), pp.1482–1490. doi:https://doi.org/10.21037/tp-22-332.

Queiroz, O.C.M., Ogunade, I.M., Weinberg, Z. and Adesogan, A.T. (2018). Silage review: Foodborne pathogens in silage and their mitigation by silage additives. *Journal of Dairy Science*, 101(5), pp.4132–4142.

Quendera, A.P., Pinto, S.N., Pobre, V., Antunes, W., Bonifácio, V.D.B., Arraiano, C.M. and Andrade, J.M. (2023). The ribonuclease PNPase is a key regulator of biofilm formation in *L. monocytogenes* and affects invasion of host cells. *NPJ biofilms and microbiomes*, [online] 9(1), p.34. doi:https://doi.org/10.1038/s41522-023-00397-1.

Quinlan, A.R. and Hall, I.M. (2010). BEDTools: a flexible suite of utilities for comparing genomic features. *Bioinformatics*, 26(6), pp.841–842.

Rahman, M.A., Sahoo, N. and Yemmireddy, V. (2022). Analysis of Sanitizer Rotation on the Susceptibility, Biofilm Forming Ability and Caco-2 Cell Adhesion and Invasion of *Listeria*. *Pathogens (Basel, Switzerland)*, [online] 11(9), p.961. doi:https://doi.org/10.3390/pathogens11090961.

Ramesh, A. and Winkler, W.C. (2010). Magnesium-sensing riboswitches in bacteria. *RNA Biology*, 7(1), pp.77–83. doi:https://doi.org/10.4161/rna.7.1.10490.

Ramesh, A. and Winkler, W.C. (2010). Magnesium-sensing riboswitches in bacteria. *RNA Biology*, 7(1), pp.77–83. doi:https://doi.org/10.4161/rna.7.1.10490.

Ramesh, A., Wakeman, C. A., & Winkler, W. C. (2011). Insights into Metalloregulation by M-box Riboswitch RNAs via Structural Analysis of Manganese-Bound Complexes. *Journal of*

Molecular Biology/Journal of Molecular Biology, *407*(4), 556–570. https://doi.org/10.1016/j.jmb.2011.01.049

Ranjbar, R. and Halaji, M. (2018). Epidemiology of *L. monocytogenes* prevalence in foods, animals and human origin from Iran: a systematic review and meta-analysis. *BMC Public Health*, 18(1).

Ranson, T.M., Barton, M.E. and McLean, R.J.C. (2023). Influence of central metabolism disruption on *Escherichia coli* biofilm formation. *Canadian Journal of Microbiology*, 69(11), pp.432–438. doi:https://doi.org/10.1139/cjm-2023-0096.

Ravishankar, S., Baldelli, V., Angeletti, C., Raffaelli, N., Landini, P. and Rossi, E. (2024). Fluoropyrimidines affect *de novo* pyrimidine synthesis impairing biofilm formation in *E. coli*. *Biofilm*, 7, p.100180. doi:https://doi.org/10.1016/j.bioflm.2024.100180.

Recsei, P., Kreiswirth, B., O'Reilly, M., Schlievert, P., Gruss, A. and Novick, R.P. (1986). Regulation of exoprotein gene expression in *Staphylococcus aureus* by *agr*. *MGG Molecular & General Genetics*, 202(1), pp.58–61. doi:https://doi.org/10.1007/bf00330517.

Reimer, A., Weedmark, K., Petkau, A., Peterson, C.-L., Walker, M., Knox, N., Kent, H., Mabon, P., Berry, C., Tyler, S., Tschetter, L., Jerome, M., Allen, V., Hoang, L., Bekal, S., Clark, C., Nadon, C., Van Domselaar, G., Pagotto, F. and Graham, M. (2019). Shared genome analyses of notable listeriosis outbreaks, highlighting the critical importance of epidemiological evidence, input datasets and interpretation criteria. *Microbial Genomics*, 5(1). doi:https://doi.org/10.1099/mgen.0.000237.

Renier, S., Hébraud, M. and Desvaux, M. (2010). Molecular biology of surface colonization by *Listeria monocytogenes*: an additional facet of an opportunistic Gram-positive foodborne pathogen. *Environmental Microbiology*, 13(4), pp.835–850. doi:https://doi.org/10.1111/j.1462-2920.2010.02378.x.

Ribeiro, M. H., Manha, S., & Brito, L. (2006). The effects of salt and pH stress on the growth rates of persistent strains of Listeria monocytogenes collected from specific ecological niches. *Food Research International*, *39*(7), 816–822. https://doi.org/10.1016/j.foodres.2006.03.005

Ricci, A., Allende, A., Bolton, D., Chemaly, M., Davies, R., Fernández Escámez, P.S., Girones, R., Herman, L., Koutsoumanis, K., Nørrung, B., Robertson, L., Ru, G., Sanaa, M., Simmons, M., Skandamis, P., Snary, E., Speybroeck, N., Ter Kuile, B., Threlfall, J. and Wahlström, H. (2018). *L. monocytogenes* contamination of ready-to-eat foods and the risk for human health in the EU. *EFSA Journal*, 16(1), p.5154.

Rice, K.C., Patton, T., Yang, S.-J., Dumoulin, A., Bischoff, M. and Bayles, K.W. (2004). Transcription of the *Staphylococcus aureus cid* and *lrg* Murein Hydrolase Regulators Is Affected by Sigma Factor B. *Journal of Bacteriology*, 186(10), pp.3029–3037. doi:https://doi.org/10.1128/jb.186.10.3029-3037.2004.

Rieu, A., Briandet, R., Habimana, O., Garmyn, D., Guzzo, J. and Piveteau, P. (2008). *L. monocytogenes* EGD-e Biofilms: No Mushrooms but a Network of Knitted Chains. *Applied and Environmental Microbiology*, 74(14), pp.4491–4497.

Rieu, A., Weidmann, S., Garmyn, D., Piveteau, P. and Guzzo, J. (2007). agr System of Listeria monocytogenes EGD-e: Role in Adherence and Differential Expression Pattern. *Applied and Environmental Microbiology*, 73(19), pp.6125–6133. doi:https://doi.org/10.1128/aem.00608-07.

Ripolles-Avila, C., Hascoët, A.S., Guerrero-Navarro, A.E. and Rodríguez-Jerez, J.J. (2018). Establishment of incubation conditions to optimize the in vitro formation of mature *Listeria monocytogenes* biofilms on food-contact surfaces. Food Control, 92, pp.240–248. doi:https://doi.org/10.1016/j.foodcont.2018.04.054.

Ripolles-Avila, C., Ríos-Castillo, A.G. and Rodríguez-Jerez, J.J. (2018). Development of a peroxide biodetector for a direct detection of biofilms produced by catalase-positive bacteria on food-contact surfaces. *CyTA - Journal of Food*, 16(1), pp.506–515. doi:https://doi.org/10.1080/19476337.2017.1418434.

Robertson, J. and Nash, J.H.E. (2018). MOB-suite: software tools for clustering, reconstruction and typing of plasmids from draft assemblies. *Microbial Genomics*, 4(8). doi:https://doi.org/10.1099/mgen.0.000206.

Rogers, J.R., Gustavo Espinoza Garcia and Geissler, P.L. (2021). Membrane hydrophobicity determines the activation free energy of passive lipid transport. *Biophysical Journal*, 120(17), pp.3718–3731.

Romanova, N. A., Wolffs, P. F. G., Brovko, L. Y., & Griffiths, M. W. (2006). Role of Efflux Pumps in Adaptation and Resistance of *Listeria monocytogenes* to Benzalkonium Chloride. *Applied and Environmental Microbiology*, *72*(5), 3498–3503. https://doi.org/10.1128/aem.72.5.3498-3503.2006

Ronholm, J., Nasheri, N., Petronella, N. and Pagotto, F. (2016). Navigating Microbiological Food Safety in the Era of Whole-Genome Sequencing. *Clinical Microbiology Reviews*, 29(4), pp.837–857. doi:https://doi.org/10.1128/cmr.00056-16.

Rosing, M.T. (1999). 13C-Depleted Carbon Microparticles in >3700-Ma Sea-Floor Sedimentary Rocks from West Greenland. *Science*, 283(5402), pp.674–676. doi:https://doi.org/10.1126/science.283.5402.674.

Rossi, E., Leccese, G., Baldelli, V., Bibi, A., Scalone, E., Camilloni, C., Paroni, M. and Landini, P. (2022). Inactivation of the Pyrimidine Biosynthesis *pyrD* Gene Negatively Affects Biofilm Formation and Virulence Determinants in the Crohn's Disease-Associated Adherent Invasive *Escherichia coli* LF82 Strain. *Microorganisms*, [online] 10(3), p.537. doi:https://doi.org/10.3390/microorganisms10030537.

Rosso, L., Bajard, S., Flandrois, J.P., Lahellec, C., Fournaud, J. and Veit, P. (1996). Differential growth of *Listeria monocytogenes* at 4 and 8°C: Consequences for the Shelf Life of Chilled Products. *Journal of Food Protection*, 59(9), pp.944–949. doi:https://doi.org/10.4315/0362-028x-59.9.944.

Ruppitsch, W., Pietzka, A., Prior, K., Bletz, S., Fernandez, H.L., Allerberger, F., Harmsen, D. and Mellmann, A. (2015). Defining and Evaluating a Core Genome Multilocus Sequence Typing

Scheme for Whole-Genome Sequence-Based Typing of *L. monocytogenes*. *Journal of Clinical Microbiology*, 53(9), pp.2869–2876.

Rutala, W.A. and Weber, D.J. (2015). Disinfection, Sterilization, and Control of Hospital Waste. *Mandell, Douglas, and Bennett's Principles and Practice of Infectious Diseases*, [online] 2(3), pp.3294-3309.e4. doi:https://doi.org/10.1016/B978-1-4557-4801-3.00301-5.

Rychli, K., Guinane, C.M., Daly, K., Hill, C. and Cotter, P.D. (2014). Generation of Nonpolar Deletion Mutants in *Listeria monocytogenes* Using the 'SOEing' Method. *Methods in Molecular Biology*, pp.187–200. doi:https://doi.org/10.1007/978-1-4939-0703-8_16.

Rychli, K., Wagner, E., Guinane, C.M., Daly, K., Hill, C. and Cotter, P.D. (2020). Generation of Nonpolar Deletion Mutants in *Listeria monocytogenes* Using the 'SOEing' Method. *Methods in molecular biology*, pp.165–175. doi:https://doi.org/10.1007/978-1-0716-0982-8_13.

Rychli, K., Wagner, E.M., Ciolacu, L., Zaiser, A., Tasara, T., Wagner, M. and Schmitz-Esser, S. (2017). Comparative genomics of human and non-human *Listeria monocytogenes* sequence type 121 strains. PLOS ONE, 12(5), p.e0176857. doi:https://doi.org/10.1371/journal.pone.0176857.

Sabet, C., Lecuit, M., Cabanes, D., Cossart, P. and Bierne, H. (2005). LPXTG Protein InlJ, a Newly Identified Internalin Involved in *Listeria monocytogenes* Virulence. *Infection and Immunity*, [online] 73(10), pp.6912–6922. doi:https://doi.org/10.1128/IAI.73.10.6912-6922.2005.

Sadekuzzaman, M., Yang, S., Mizan, M.F.R., Kim, H.-S. and Ha, S.-D. (2017). Effectiveness of a phage cocktail as a biocontrol agent against *L. monocytogenes* biofilms. *Food Control*, [online] C(78), pp.256–263. doi:https://doi.org/10.1016/j.foodcont.2016.10.056.

Saeed-Kothe, A. and Powers-Lee, S.G. (2002). Specificity Determining Residues in Ammonia- and Glutamine-dependent Carbamoyl Phosphate Synthetases. *Journal of Biological Chemistry*, 277(9), pp.7231–7238. doi:https://doi.org/10.1074/jbc.m110926200.

Şahiner, A., Halat, E., Evren Algın Yapar, and Bilge Ahsen Kara (2022). Evaluation of organic load related efficacy changes in antiseptic solutions used in hospitals. *Turkish Journal of Medical Sciences*, 52(3), pp. 825–833. doi: https://doi.org/10.55730/1300-0144.5379.

Salama, M., Amitai, Z., Ezernitchi, A.V., Sheffer, R., Jaffe, J., Rahmani, S., Leshem, E. and Valinsky, L. (2018). Surveillance of listeriosis in the Tel Aviv District, Israel, 2010-2015. *Epidemiology and infection*, [online] 146(3), pp.283–290. doi:https://doi.org/10.1017/S0950268817003004.

Samad, A., Li, Y., Zhang, C., Chen, F., Zeng, W., Fan, X., & Jin, T. (2019). X-ray crystal structure of putative transcription regulator *lmo2088* from *Listeria monocytogenes*. *Biochemical and Biophysical Research Communications*, *520*(2), 434–440. https://doi.org/10.1016/j.bbrc.2019.10.033

Sauer, K., Camper, A.K., Ehrlich, G.D., Costerton, J.W. and Davies, D.G. (2002). *Pseudomonas aeruginosa* Displays Multiple Phenotypes during Development as a Biofilm. *Journal of Bacteriology*, 184(4), pp.1140–1154. doi:https://doi.org/10.1128/jb.184.4.1140-1154.2002.

Sauer, K., Stoodley, P., Goeres, D.M., Hall-Stoodley, L., Burmølle, M., Stewart, P.S. and Bjarnsholt, T. (2022). The biofilm life cycle: expanding the conceptual model of biofilm formation. *Nature Reviews Microbiology*, [online] 20(10), pp.608–620.

Sawyer, L.K. and Hermanowicz, S.W. (1998). Detachment of biofilm bacteria due to variations in nutrient supply. *Water Science and Technology*, 37(4-5). doi:https://doi.org/10.1016/s0273-1223(98)00108-5.

Schlech, W. F., Lavigne, P. M., Bortolussi, R. A., Allen, A. C., Haldane, E. V., Wort, A. J., Hightower, A. W., Johnson, S. E., King, S. H., Nicholls, E. S., & Broome, C. V. (1983). Epidemic listeriosis — evidence for transmission by food. *The New England Journal of Medicine, 308*(4), 203-206.

Schmid, B., Klumpp, J., Raimann, E., Loessner, M.J., Stephan, R. and Tasara, T. (2009). Role of Cold Shock Proteins in Growth of *Listeria monocytogenes* under Cold and Osmotic Stress Conditions. *Applied and Environmental Microbiology*, 75(6), pp.1621–1627. doi:https://doi.org/10.1128/aem.02154-08.

Schmitz-Esser, S., Müller, A., Stessl, B. and Wagner, M. (2015). Genomes of sequence type 121 *Listeria monocytogenes* strains harbor highly conserved plasmids and prophages. *Frontiers in Microbiology*, 6. doi:https://doi.org/10.3389/fmicb.2015.00380.

Schneewind, O. and Missiakas, D. (2014). Genetic Manipulation of *Staphylococcus aureus*. *Current Protocols in Microbiology*, [online] 32(1). doi:https://doi.org/10.1002/9780471729259.mc09c03s32.

Schneider, T.D. and Stephens, R.Michael. (1990). Sequence logos: a new way to display consensus sequences. *Nucleic Acids Research*, 18(20), pp.6097–6100. doi:https://doi.org/10.1093/nar/18.20.6097.

Schulz, L.M., Dreier, F., Marie, L. and Rismondo, J. (2023). Adaptation mechanisms of *Listeria monocytogenes* to quaternary ammonium compounds. *Microbiology spectrum*, 11(5). doi:https://doi.org/10.1128/spectrum.01441-23.

Schuster, C.F., Howard, S.A. and Gründling, A. (2019). Use of the counter selectable marker PheS* for genome engineering in *Staphylococcus aureus*. *Microbiology*, 165(5), pp.572–584. doi:https://doi.org/10.1099/mic.0.000791.

Schwengers, O., Jelonek, L., Dieckmann, M.A., Beyvers, S., Blom, J. and Goesmann, A. (2021). Bakta: rapid and standardized annotation of bacterial genomes via alignment-free sequence identification. *Microbial Genomics*, 7(11). doi:https://doi.org/10.1099/mgen.0.000685.

Scobie, A., Kanagarajah, S., Harris, R.J., Byrne, L., Amar, C., Grant, K. and Godbole, G. (2019). Mortality risk factors for listeriosis – A 10 year10-year review of non-pregnancy associated cases in England 2006–2015. *Journal of Infection*, 78(3), pp.208–214.

Seemann, T. (2014). Prokka: rapid prokaryotic genome annotation. *Bioinformatics*, [online] 30(14), pp.2068–2069.

Seemann, T. (2015). Snippy: rapid haploid variant calling and core SNP phylogeny. *GitHub. Available at: github. com/tseemann/snippy*.

Seemann, T. (2020). ABRicate: Mass screening of contigs for antimicrobial tolerance or virulence genes. *GitHub. Available at: github. com/tseemann/abricate*.

Seemann, T. (2020). Shovil: Assemble bacterial isolate genomes from Illumina paired-end reads. *GitHub. Available at: github. com/tseemann/shovil*.

Sela, S., Frank, S., Belausov, E. and Pinto, R. (2006). A Mutation in the *luxS* Gene Influences *Listeria monocytogenes* Biofilm Formation. *Applied and Environmental Microbiology*, 72(8), pp.5653–5658. doi:https://doi.org/10.1128/aem.00048-06.

Serra, D.O. and Hengge, R. (2014). Stress responses go three dimensional - the spatial order of physiological differentiation in bacterial macrocolony biofilms. *Environmental Microbiology*, 16(6), pp.1455–1471. doi:https://doi.org/10.1111/1462-2920.12483.

Seveau, S., Pizarro-Cerda, J. and Cossart, P. (2007). Molecular mechanisms exploited by *L. monocytogenes* during host cell invasion. *Microbes and Infection*, 9(10), pp.1167–1175. doi:https://doi.org/10.1016/j.micinf.2007.05.004.

Seviour, T., Winnerdy, F.R., Wong, L.L., Shi, X., Mugunthan, S., Foo, Y.H., Castaing, R., Adav, S.S., Subramoni, S., Kohli, G.S., Shewan, H.M., Stokes, J.R., Rice, S.A., Phan, A.T. and Kjelleberg, S. (2021). The biofilm matrix scaffold of *Pseudomonas aeruginosa* contains G-quadruplex extracellular DNA structures. *npj Biofilms and Microbiomes*, 7(1). doi:https://doi.org/10.1038/s41522-021-00197-5.

Shen, W., Le, S., Li, Y. and Hu, F. (2016). SeqKit: A Cross-Platform and Ultrafast Toolkit for FASTA/Q File Manipulation. *PLOS ONE*, 11(10), p.e0163962. doi:https://doi.org/10.1371/journal.pone.0163962.

Shi, W., Zhang, Q., Li, H., Du, D., Ma, X., Wang, J., Jiang, J., Liu, C., Kou, L. and Ren, J. (2024). Biofilm Formation, Motility, and Virulence of *Listeria monocytogenes* Are Reduced by Deletion of the Gene *lmo0159*, a Novel *Listerial* LPXTG Surface Protein. Microorganisms, 12(7), pp.1354 –1354. doi:https://doi.org/10.3390/microorganisms12071354.

Shin, J.-H., Brody, M.S. and Price, C.W. (2010). Physical and antibiotic stresses require activation of the RsbU phosphatase to induce the general stress response in Listeria monocytogenes. *Microbiology*,156(9),pp.2660–2669. doi:https://doi.org/10.1099/mic.0.041202-0.

Sibanda, T. and Buys, E.M. (2022). *Listeria monocytogenes* Pathogenesis: The Role of Stress Adaptation. *Microorganisms*, [online] 10(8), p.1522. doi:https://doi.org/10.3390/microorganisms10081522.

Sievers, F., Wilm, A., Dineen, D., Gibson, T.J., Karplus, K., Li, W., Lopez, R., McWilliam, H., Remmert, M., Soding, J., Thompson, J.D. and Higgins, D.G. (2014). Fast, scalable generation of high-quality protein multiple sequence alignments using Clustal Omega. *Molecular Systems Biology*, 7(1), pp.539–539. doi:https://doi.org/10.1038/msb.2011.75.

Singh, A.V., Vyas, V., Patil, R., Sharma, V., Scopelliti, P.E., Bongiorno, G., Podestà, A., Lenardi, C., Gade, W.N. and Milani, P. (2011). Quantitative Characterization of the Influence of the Nanoscale Morphology of Nanostructured Surfaces on Bacterial Adhesion and Biofilm Formation. *PLoS ONE*, 6(9), p.e25029. doi:https://doi.org/10.1371/journal.pone.0025029.

Singh, R., Ray, P., Das, A. and Sharma, M. (2009). Role of persisters and small-colony variants in antibiotic tolerance of planktonic and biofilm-associated *Staphylococcus aureus*: an in vitro study. *Journal of Medical Microbiology*, 58(8), pp.1067–1073. doi:https://doi.org/10.1099/jmm.0.009720-0.

Song, B. and Leff, L.G. (2006). Influence of magnesium ions on biofilm formation by *Pseudomonas fluorescens*. *Microbiological Research*, 161(4), pp.355–361. doi:https://doi.org/10.1016/j.micres.2006.01.004.

Soni, K.A., Nannapaneni, R. and Hagens, S. (2010). Reduction of *Listeria monocytogenes* on the Surface of Fresh Channel Catfish Fillets by Bacteriophage Listex P100. *Foodborne Pathogens and Disease*, [online] 7(4), pp.427–434. doi:https://doi.org/10.1089/fpd.2009.0432.

Sosnowski, M., Lachtara, B., Wieczorek, K. and Osek, J. (2019). Antimicrobial resistance and genotypic characteristics of *Listeria monocytogenes* isolated from food in Poland. *International Journal of Food Microbiology*, 289, pp.1–6. doi:https://doi.org/10.1016/j.ijfoodmicro.2018.08.029.

Soumet, C., Ragimbeau, C. and Maris, P. (2005). Screening of benzalkonium chloride tolerance in *L. monocytogenes* strains isolated during cold smoked fish production. *Letters in Applied Microbiology*, 41(3), pp.291–296.

Southwick, F. S., & Purich, D. L. (1996). Intracellular pathogenesis of listeriosis. *The New England Journal of Medicine, 334*(12), 770–776. https://doi.org/10.1056/NEJM199603213341206.

Spinelli, S.V., Pontel, L.B., GarcÃa VÃ©scovi, E. and Soncini, F.C. (2008). Regulation of magnesium homeostasis in Salmonella: Mg^{2+} targets the *mgtA* transcript for degradation by RNase E. *FEMS Microbiology Letters*, 280(2), pp.226–234. doi:https://doi.org/10.1111/j.1574-6968.2008.01065.x.

Srinivasan, S., Vladescu, I.D., Koehler, S.A., Wang, X., Mani, M. and Rubinstein, S.M. (2018). Matrix Production and Sporulation in *Bacillus subtilis* Biofilms Localize to Propagating Wave Fronts. 114(6), pp.1490–1498. doi:https://doi.org/10.1016/j.bpj.2018.02.002.

Sternberg, C., Christensen, B.B., Johansen, T., Toftgaard Nielsen, A., Andersen, J.B., Givskov, M. and Molin, S. (1999). Distribution of bacterial growth activity in flow-chamber biofilms. *Applied and Environmental Microbiology*, [online] 65(9), pp.4108–4117. doi:https://doi.org/10.1128/AEM.65.9.4108-4117.1999.

Stewart, P.S. and Franklin, M.J. (2008). Physiological heterogeneity in biofilms. *Nature Reviews Microbiology*, 6(3), pp.199–210. doi:https://doi.org/10.1038/nrmicro1838.

Stoodley, P., Hall-Stoodley, L. and Lappin-Scott, H.M. (2001). [21] Detachment, surface migration, and other dynamic behavior in bacterial biofilms revealed by digital time-lapse imaging. pp.306–319. doi:https://doi.org/10.1016/s0076-6879(01)37023-4.

Stoodley, P., Sauer, K., Davies, D.G. and Costerton, J.W. (2002). Biofilms as Complex Differentiated Communities. *Annual Review of Microbiology*, [online] 56(1), pp.187–209. doi:https://doi.org/10.1146/annurev.micro.56.012302.160705.

Suárez, M. M., Bautista, R. M., Almela, M., Soriano, A., Marco, F., Bosch, J., Martínez, J. A., Bové, A., Trilla, A., & Mensa, J. (2007). *Listeria monocytogenes* bacteremia: Analysis of 110 episodes. *Medicina Clínica (Barcelona), 129*(6), 218–221. https://doi.org/10.1157/13107920.

Sugimoto, S., Sato, F., Miyakawa, R., Chiba, A., Onodera, S., Hori, S. and Mizunoe, Y. (2018). Broad impact of extracellular DNA on biofilm formation by clinically isolated Methicillin-resistant and -sensitive strains of *Staphylococcus aureus*. *Scientific Reports*, 8(1).

Sullivan, C.B., Diggle, M.A. and Clarke, S.C. (2005). Multilocus Sequence Typing: Data Analysis in Clinical Microbiology and Public Health. *Molecular Biotechnology*, 29(3), pp.245–254.

Sykes, D.B. (2018). The emergence of dihydroorotate dehydrogenase (DHODH) as a therapeutic target in acute myeloid leukemia. Expert Opinion on Therapeutic Targets, 22(11), pp.893–898. doi:https://doi.org/10.1080/14728222.2018.1536748.

Tan, X., Chung, T., Chen, Y., Macarisin, D., LaBorde, L. and Kovac, J. (2019). The occurrence of *Listeria monocytogenes* is associated with built environment microbiota in three tree fruit processing facilities. *Microbiome*, [online] 7(1). doi:https://doi.org/10.1186/s40168-019-0726-2.

Tang, D., Gao, Q., Zhao, Y., Li, Y., Chen, P., Zhou, J., Xu, R., Wu, Z., Xu, Y. and Li, H. (2018). Mg^{2+} reduces biofilm quantity in *Acidithiobacillus ferrooxidans* through inhibiting Type IV pili formation. *FEMS microbiology letters*, [online] 365(4). doi:https://doi.org/10.1093/femsle/fnx266.

Tao, T., Grulich, P.F., Kucharski, L.M., Smith, R.L. and Maguire, M.E. (1998). Magnesium transport in *Salmonella typhimurium*: biphasic magnesium and time dependence of the transcription of the *mgtA* and *mgtCB* loci. *Microbiology*, 144(3), pp.655–664. doi:https://doi.org/10.1099/00221287-144-3-655.

Temple, M.E. and Nahata, M.C. (2000). Treatment of Listeriosis. *Annals of Pharmacotherapy*, [online] 34(5), pp.656–661. doi:https://doi.org/10.1345/aph.19315.

The Food Hygiene Regulations 1970. Available at: https://www.legislation.gov.uk/uksi/1970/1172/pdfs/uksi_19701172_en.pdf [Accessed 27 Sep. 2025].

Thomassen, G.M.B., Reiche, T., Hjørungnes, M. and Mehli, L. (2023). High Disinfectant Tolerance in *Pseudomonas* spp. Biofilm Aids the Survival of *Listeria monocytogenes*. *Microorganisms*, [online] 11(6), p.1414. doi:https://doi.org/10.3390/microorganisms11061414.

To, M.S. et al. (2002) 'Postadaptational Resistance to Benzalkonium Chloride and Subsequent Physicochemical Modifications of *Listeria monocytogenes'*, Applied and Environmental Microbiology, 68(11), pp. 5258–5264. Available at: https://doi.org/10.1128/aem.68.11.5258-5264.2002.

Tokuoka, K., Kusakari, Y., Krungkrai, S.R., Matsumura, H., Kai, Y., Krungkrai, J., Horii, T. and Inoue, T. (2007). Structural Basis for the Decarboxylation of Orotidine 5'-Monophosphate (OMP) by Plasmodium Falciparum OMP Decarboxylase. *Journal of Biochemistry*, 143(1), pp.69–78. doi:https://doi.org/10.1093/jb/mvm193.

Trampari, E., Holden, E. R., Wickham, G. J., Ravi, A., Martins, L. de O., Savva, G. M., & Webber, M. A. (2021). Exposure of *Salmonella* biofilms to antibiotic concentrations rapidly selects resistance with collateral tradeoffs. *Npj Biofilms and Microbiomes*, 7(1). https://doi.org/10.1038/s41522-020-00178-0.

Tripathi, A., Park, J., Pho, T. and Champion, J.A. (2024). Dual Antibacterial Properties of Copper -Coated Nanotextured Stainless Steel. *Small*. [online] doi:https://doi.org/10.1002/smll.202311546.

Turnbough, C.L. and Switzer, R.L. (2008). Regulation of Pyrimidine Biosynthetic Gene Expression in Bacteria: Repression without Repressors. *Microbiology and Molecular Biology Reviews*, 72(2), pp.266–300. doi:https://doi.org/10.1128/mmbr.00001-08.

Ueda, A., Attila, C., Whiteley, M. and Wood, T.K. (2009). Uracil influences quorum sensing and biofilm formation in *Pseudomonas aeruginosa* and fluorouracil is an antagonist. *Microbial Biotechnology*, [online] 2(1), pp.62–74. doi:https://doi.org/10.1111/j.1751-7915.2008.00060.x.

UK Health Security Agency. (2023). *L. monocytogenes laboratory reports and listeriosis cases in England and Wales: 2023*. UKHSA.

UK Health Security Agency. (2025). *Listeriosis in England and Wales: summary for 2024*. GOV.UK. Retrieved from https://www.gov.uk/government/publications/listeria-monocytogenes-surveillance-reports/listeriosis-in-england-and-wales-summary-for-2024.

Valentini, M. and Filloux, A. (2016). Biofilms and Cyclic di-GMP (c-di-GMP) Signalling: Lessons from *Pseudomonas aeruginosa* and Other Bacteria. *Journal of Biological Chemistry*, 291(24), pp.12547–12555. doi:https://doi.org/10.1074/jbc.r115.711507.

Van de Lagemaat, M., Stockbroekx, V., Geertsema-Doornbusch, G.I., Dijk, M., Carniello, V., Woudstra, W., van der Mei, H.C., Busscher, H.J. and Ren, Y. (2022). A Comparison of the Adaptive Response of *Staphylococcus aureus* vs. *Streptococcus mutans* and the Development of Chlorhexidine Tolerance. Frontiers in Microbiology, [online] 13, p.861890. doi:https://doi.org/10.3389/fmicb.2022.861890.

Van der Veen, S. and Abee, T. (2010). Importance of SigB for *L. monocytogenes* Static and Continuous-Flow Biofilm Formation and Disinfectant Tolerance. *Applied and Environmental Microbiology*, 76(23), pp.7854–7860.

Van Dijk, H.F.G., Verbrugh, H.A., Abee, T., Andriessen, J.W., van Dijk, H.F.G., ter Kuile, B.H., Mevius, D.J., Montforts, M.H.M.M., van Schaik, W., Schmitt, H., Smidt, H., Veening, J.-W. and Voss, A. (2022). Resisting disinfectants. *Communications Medicine*, 2(1). doi:https://doi.org/10.1038/s43856-021-00070-8.

Van Oss, C.J., Good, R.J. and Chaudhury, M.K. (1986). The role of van der Waals forces and hydrogen bonds in 'hydrophobic interactions' between biopolymers and low energy surfaces. *Journal of Colloid and Interface Science*, 111(2), pp.378–390. doi:https://doi.org/10.1016/0021-9797(86)90041-x.

Varadi, M., Anyango, S., Deshpande, M., Nair, S., Natassia, C., Yordanova, G., Yuan, D., Stroe, O., Wood, G., Laydon, A., Žídek, A., Green, T., Tunyasuvunakool, K., Petersen, S., Jumper, J., Clancy, E., Green, R., Vora, A., Lutfi, M. and Figurnov, M. (2021). AlphaFold Protein Structure Database: massively expanding the structural coverage of protein-sequence space with high-accuracy models. *Nucleic Acids Research*, 50(D1).

Váradi, M., Bertoni, D., Magaña, P., Paramval, U., Pidruchna, I., Radhakrishnan, M., Tsenkov, M., Nair, S., Mirdita, M., Yeo, J., Kovalevskiy, O., Tunyasuvunakool, K., Laydon, A., Žídek, A., Tomlinson, H., Hariharan, D., Abrahamson, J., Green, T., Jumper, J. and Birney, E. (2023). AlphaFold Protein Structure Database in 2024: providing structure coverage for over 214 million protein sequences. *Nucleic Acids Research*, 52(D1). doi:https://doi.org/10.1093/nar/gkad1011.

Vázquez-Boland, J.A., Domínguez-Bernal, G., González-Zorn, B., Kreft, J. and Goebel, W. (2001). Pathogenicity islands and virulence evolution in *Listeria*. *Microbes and Infection*, 3(7), pp.571–584.

Verghese, B., Lok, M., Wen, J., Alessandria, V., Chen, Y., Kathariou, S. and Knabel, S. (2011). *comK* Prophage Junction Fragments as Markers for *L. monocytogenes* Genotypes Unique to Individual Meat and Poultry Processing Plants and a Model for Rapid Niche-Specific Adaptation, Biofilm Formation, and Persistence. *Applied and Environmental Microbiology*, 77(10), pp.3279–3292. doi:https://doi.org/10.1128/aem.00546-11.

Verran, J. and Whitehead, K. (2005). Factors Affecting Microbial Adhesion to Stainless Steel and Other Materials Used in Medical Devices. *The International Journal of Artificial Organs*, 28(11), pp.1138–1145. doi:https://doi.org/10.1177/039139880502801111.

Voglauer, E.M., Alteio, L.V., Pracser, N., Thalguter, S., Quijada, N.M., Wagner, M. and Rychli, K. (2024). *Listeria monocytogenes* colonises established multispecies biofilms and resides within them without altering biofilm composition or gene expression. *Microbiological Research*, [online] 292, p.127997. doi:https://doi.org/10.1016/j.micres.2024.127997.

Voloshchuk, O., Rolon, M.L., Bartlett, K.V., Acevedo, M.M., LaBorde, L.F. and Kovac, J. (2024). *Pseudomonadaceae* increased the tolerance of *Listeria monocytogenes* to sanitizers in multi-species biofilms. *Food Microbiology*, pp.104687–104687. doi:https://doi.org/10.1016/j.fm.2024.104687.

Walker, B.J., Abeel, T., Shea, T., Priest, M., Abouelliel, A., Sakthikumar, S., Cuomo, C.A., Zeng, Q., Wortman, J., Young, S.K. and Earl, A.M. (2014). Pilon: An Integrated Tool for

Comprehensive Microbial Variant Detection and Genome Assembly Improvement. *PLoS ONE*, 9(11), p.e112963.

Walker, S.J., Archer, P. and Banks, J.G. (1990). Growth of *L. monocytogenes* at refrigeration temperatures. *Journal of Applied Bacteriology*, 68(2), pp.157–162.

Walter, M.R., Buick, R. and Dunlop, J.S.R. (1980). Stromatolites 3,400–3,500 Myr old from the North Pole area, Western Australia. *Nature*, 284(5755), pp.443–445. doi:https://doi.org/10.1038/284443a0.

Wang, H., Hou, X., Shen, J., Wang, W., Ye, Y., Yu, J. and Xue, T. (2022). Alternative sigma factor B reduces biofilm formation and stress response in milk-derived *Staphylococcus aureus*. *LWT*, 162, p.113515. doi:https://doi.org/10.1016/j.lwt.2022.113515.

Wang, Z., Tao, X., Liu, S., Zhao, Y. and Yang, X. (2021). An Update Review on *Listeria* Infection in Pregnancy. *Infection and Drug Tolerance*, [online] 14, pp.1967–1978. doi:https://doi.org/10.2147/IDR.S313675.

Webb, A.J., Karatsa-Dodgson, M. and Gründling, A. (2009). Two-enzyme systems for glycolipid and polyglycerolphosphate lipoteichoic acid synthesis in *Listeria monocytogenes*. *Molecular Microbiology*, 74(2), pp.299–314. doi:https://doi.org/10.1111/j.1365-2958.2009.06829.x.

Webb, J.S., Lau, M. and Kjelleberg, S. (2004). Bacteriophage and Phenotypic Variation in *P. aeruginosa* Biofilm Development. *Journal of Bacteriology*, 186(23), pp.8066–8073. doi:https://doi.org/10.1128/jb.186.23.8066-8073.2004.

Wessels, S. and Ingmer, H. (2013). Modes of action of three disinfectant active substances: A review. *Regulatory Toxicology and Pharmacology*, 67(3), pp.456–467.

Whitchurch, C.B. (2002). Extracellular DNA Required for Bacterial Biofilm Formation. *Science*, 295(5559), pp.1487–1487. doi:https://doi.org/10.1126/science.295.5559.1487.

Wick, R.R., Kupfer, S.S., Cerdeira, L., Hawkey, J., Guillaume Méric, Vezina, B., Holt, K.E. and Holt, K.E. (2021). Trycycler: consensus long-read assemblies for bacterial genomes. *Genome Biology*, 22(1). doi:https://doi.org/10.1186/s13059-021-02483-z.

Wickham, G.J. (2021). *Collateral selective landscape of drug resistance in experimentally evolved biofilms of Pseudomonas aeruginosa*. Doctoral Thesis.

Wiedmann, M., Arvik, T.J., Hurley, R.J. and Boor, K.J. (1998). General Stress Transcription Factor ς ^{B} and Its Role in Acid Tolerance and Virulence of *Listeria monocytogenes*. *Journal of Bacteriology*, 180(14), pp.3650–3656. doi:https://doi.org/10.1128/jb.180.14.3650-3656.1998.

Williamson, K.S., Richards, L.A., Perez-Osorio, A.C., Pitts, B., McInnerney, K., Stewart, P.S. and Franklin, M.J. (2012). Heterogeneity in *Pseudomonas aeruginosa* Biofilms Includes Expression of Ribosome Hibernation Factors in the Antibiotic-Tolerant Subpopulation and Hypoxia-Induced Stress Response in the Metabolically Active Population. *Journal of Bacteriology*, 194(8), pp.2062–2073. doi:https://doi.org/10.1128/jb.00022-12.

Wise, A.A. and Price, C.W. (1995). Four additional genes in the *sigB* operon of *Bacillus subtilis* that control activity of the general stress factor sigma B in response to environmental signals. *Journal of bacteriology*, 177(1), pp.123–133. doi:https://doi.org/10.1128/jb.177.1.123-133.1995.

Wishart, D. S., Ren, L., Leong-Sit, J., Saha, S., Grant, J. R., Stothard, P., Singh, U., Kropielnicki, A., Oler, E., Peters, H., Gautam, V. (2023). PlasMapper 3.0 - A Web Server for Generating, Editing, Annotating and Visualizing Publication Quality Plasmid Maps. *Nucleic Acids Research, https://doi.org/10.1093/NAR/GKAD276*

Wolfaardt, G.M., Lawrence, J.R., Robarts, R.D., Caldwell, S.J. and Caldwell, D.E. (1994). Multicellular Organization in a Degradative Biofilm Community. *Applied and Environmental Microbiology*, 60(2), pp.434–446. doi:https://doi.org/10.1128/aem.60.2.434-446.1994.

Wood, D.E. and Salzberg, S.L. (2014). Kraken: ultrafast metagenomic sequence classification using exact alignments. *Genome Biology*, 15(3), p.R46.

Wood, D.E., Lu, J. and Langmead, B. (2019). Improved metagenomic analysis with Kraken 2. *Genome Biology*, 20(1). doi:https://doi.org/10.1186/s13059-019-1891-0.

Wu-Chen, R.A., Feng, J., Elhadidy, M., Nambiar, R.B., Liao, X., Yue, M. and Ding, T. (2023). Benzalkonium chloride forces selective evolution of tolerance towards antibiotics in *Salmonella enterica* serovar Typhimurium. Journal of Infection and Public Health, [online] 16, pp.225–235. doi:https://doi.org/10.1016/j.jiph.2023.10.022.

Wu, S., Wu, Q., Zhang, J., Chen, M. and Guo, W. (2016). Analysis of Multilocus Sequence Typing and Virulence Characterization of *L. monocytogenes* Isolates from Chinese Retail Ready-to-Eat Food. Frontiers in Microbiology, 7(3).

Wuenscher, M.D., Köhler, S., Goebel, W. and Chakraborty, T. (1991). Gene disruption by plasmid integration in *Listeria monocytogenes*: Insertional inactivation of the listeriolysin determinant *IisA*. *Molecular and General Genetics MGG*, 228(1-2), pp.177–182. doi:https://doi.org/10.1007/bf00282463.

Wunsch, N.-G. (2025). *Topic: Food Industry in the UK*. [online] Statista. Available at: https://www.statista.com/topics/7229/food-industry-in-the-uk/#topicOverview.

Xayarath, B. and Freitag, N.E. (2012). Optimizing the balance between host and environmental survival skills: lessons learned from *Listeria monocytogenes*. *Future Microbiology*, 7(7), pp.839 –852. doi:https://doi.org/10.2217/fmb.12.57.

Xie, X., Liu, X., Li, Y., Luo, L., Yuan, W., Chen, B., Liang, G., Shen, R., Li, H., Huang, S. and Duan, C. (2020). Advanced Glycation End Products Enhance Biofilm Formation by Promoting Extracellular DNA Release Through *sigB* Upregulation in *Staphylococcus aureus*. *Frontiers in microbiology*, 11. doi:https://doi.org/10.3389/fmicb.2020.01479.

Yang, Z., Khan, S.A., Walsh, L.J., Ziora, Z.M. and Seneviratne, C.J. (2024). Classical and Modern Models for Biofilm Studies: A Comprehensive Review. *Antibiotics*, 13(12), pp.1228–1228. doi:https://doi.org/10.3390/antibiotics13121228.

Yannarell, S.M., Beaudoin, E.S., Talley, H.S., Schoenborn, A.A., Orr, G., Anderton, C.R., Chrisler, W.B. and Shank, E.A. (2022). Extensive cellular multitasking within *Bacillus subtilis* biofilms. *bioRxiv (Cold Spring Harbor Laboratory)*. doi:https://doi.org/10.1101/2022.09.02.506450.

Yu, T., Jiang, X., Zhang, Y., Ji, S., Gao, W. and Shi, L. (2018). Effect of Benzalkonium Chloride Adaptation on Sensitivity to Antimicrobial Agents and Tolerance to Environmental Stresses in *L. monocytogenes*. *Frontiers in Microbiology*, 9. doi:https://doi.org/10.3389/fmicb.2018.02906.

Zeinert, R., Zhou, F., Franco, P., Zöller, J., Madni, Z.K., Lessen, H., L Aravind, Langer, J.D., Sodt, A.J., Storz, G. and Matthies, D. (2025). P-type ATPase magnesium transporter MgtA acts as a dimer. *Nature Structural & Molecular Biology*. doi:https://doi.org/10.1038/s41594-025-01593-7.

Zetzmann, M., Bucur, F.I., Crauwels, P., Borda, D., Nicolau, A.I., Grigore-Gurgu, L., Seibold, G.M. and Riedel, C.U. (2019). Characterization of the biofilm phenotype of a *Listeria monocytogenes* mutant deficient in *agr* peptide sensing. *MicrobiologyOpen*, 8(9). doi:https://doi.org/10.1002/mbo3.826.

Zgurskaya, H.I. (2009). Multicomponent drug efflux complexes: architecture and mechanism of assembly. *Future Microbiology*, 4(7), pp.919–932. doi:https://doi.org/10.2217/fmb.09.62.

Zhang, X. and Bishop, P.L. (2003). Biodegradability of biofilm extracellular polymeric substances. *Chemosphere*, 50(1), pp.63–69. doi:https://doi.org/10.1016/s0045-6535(02)00319-3.

Zhang, Z., Zhang, X.-R., Jin, T., Yang, C.-G., Sun, Y.-P., Li, Q. and Yang, K. (2021). Antibacterial mechanism of Cu-bearing 430 ferritic stainless steel. *Rare metals/Rare Metals*, 41(2), pp.559–569. doi:https://doi.org/10.1007/s12598-021-01751-y.

Zhao, X., Xu, C., Qu, J., Jin, Y., Bai, F., Cheng, Z., Wu, W., & Pan, X. (2023). PitA Controls the H2- and H3-T6SSs through PhoB in *Pseudomonas aeruginosa*. *Applied and Environmental Microbiology*, *89*(6). https://doi.org/10.1128/aem.02094-22.

Zhuo, T., Rou, W., Song, X., Guo, J., Fan, X., Kamau, G. G., & Zou, H. (2015). Molecular study on the *carAB* operon reveals that *carB* gene is required for swimming and biofilm formation in *Xanthomonas citri* subsp. *citri*. *BMC Microbiology*, *15*(1). https://doi.org/10.1186/s12866-015-0555-9

Zobell, C.E. and Allen, E.C. (1935). The Significance of Marine Bacteria in the Fouling of Submerged Surfaces. *Journal of Bacteriology*, [online] 29(3), pp.239–251. doi:https://doi.org/10.1128/jb.29.3.239-251.1935.

Zogaj, X., Nimtz, M., Rohde, M., Bokranz, W. and Romling, U. (2001). The multicellular morphotypes of *Salmonella* typhimurium and *Escherichia coli* produce cellulose as the second component of the extracellular matrix. *Molecular Microbiology*, 39(6), pp.1452–1463. doi:https://doi.org/10.1046/j.1365-2958.2001.02337.x.

Zolotarev, A.S., Meera Unnikrishnan, Shmukler, B.E., Clark, J.S., Vandorpe, D.H., Nikolaus Grigorieff, Rubin, E.J. and Alper, S.L. (2007). Increased sulfate uptake by *E. coli* overexpressing the SLC26-related SulP protein Rv1739c from *Mycobacterium tuberculosis*. *Comparative Biochemistry and Physiology Part A Molecular & Integrative Physiology*, 149(3), pp.255–266. doi:https://doi.org/10.1016/j.cbpa.2007.12.005.

Zwirzitz, B., Wetzels, S.U., Dixon, E.D., Fleischmann, S., Selberherr, E., Thalguter, S., Quijada, N.M., Dzieciol, M., Wagner, M. and Stessl, B. (2021). Co-Occurrence of *Listeria* spp. and Spoilage Associated Microbiota During Meat Processing Due to Cross-Contamination Events. *Frontiers in Microbiology*, 12. doi:https://doi.org/10.3389/fmicb.2021.632935.

Appendices

Appendix 1. Isolate collection from Food Standards Agency (FSA)-sponsored food surveys conducted in Northern Ireland between September 2007 and February 2013. The collection includes a total of 198 *Listeria* spp. isolates, comprising 115 *Listeria monocytogenes*, 36 *Listeria welshimeri*, 32 *Listeria innocua*, 14 *Listeria seelegeri* and 1 *Listeria ivanovii*. Isolates were obtained from a variety of sources, including milk, meat, fish, environmental samples, quality assurance swabs, and samples of unknown origin.

Type of source	Source	Species	Year of isolation	Sequenced and phenotyped
Milk	Raw milk	*L. innocua*	2007	No
Milk	Raw milk	*L. innocua*	2008	No
Milk	Raw milk	*L. innocua*	2008	No
Milk	Raw milk	*L. innocua*	2009	No
Milk	Raw milk	*L. innocua*	2009	No
Milk	Raw milk	*L. innocua*	2009	No
Milk	Raw milk	*L. innocua*	2009	No
Milk	Raw milk	*L. innocua*	2009	No
Other	Croquette	*L. innocua*	2009	No
Other	Croquette	*L. innocua*	2009	No
Other	Croquette	*L. innocua*	2009	No
Other	Not given	*L. innocua*	2009	No
Milk	Raw milk	*L. innocua*	2009	No
Quality assurance sample	Quality assurance sample	*L. innocua*	2009	No
Milk	Raw milk	*L. innocua*	2009	No
Milk	Raw milk	*L. innocua*	2009	No
Milk	Raw milk	*L. innocua*	2009	No
Meat	Raw meat	*L. innocua*	2010	No
Milk	Raw milk	*L. innocua*	2010	No
Milk	Raw milk	*L. innocua*	2010	No
Milk	Raw milk	*L. innocua*	2010	No
Meat	Cooked meat	*L. innocua*	2010	No
Milk	Raw milk	*L. innocua*	2010	No
Quality assurance sample	Quality assurance sample	*L. innocua*	2010	No
Quality assurance sample	Quality assurance sample	*L. innocua*	2010	No
Quality assurance sample	Quality assurance sample	*L. innocua*	2011	No
Meat	RTE sliced meat survey	*L. innocua*	2012	No
Meat	RTE sliced meat survey	*L. innocua*	2012	No
Meat	RTE sliced meat survey	*L. innocua*	2012	No
Meat	RTE sliced meat survey	*L. innocua*	2012	No
Meat	RTE sliced meat survey	*L. innocua*	2013	No
Milk	Raw milk	*L. ivanovii*	2009	No
Meat	Cooked meat	*L. monocytogenes*	2009	No
Meat	Cooked meat	*L. monocytogenes*	2009	No
Milk	Raw milk	*L. monocytogenes*	2009	No
Other	Croquette	*L. monocytogenes*	2009	No

Meat	Raw meat	*L. monocytogenes*	2009	No
Meat	Cooked meat	*L. monocytogenes*	2009	No
Meat	Cooked meat	*L. monocytogenes*	2009	No
Meat	Cooked meat	*L. monocytogenes*	2009	No
Meat	Cooked meat	*L. monocytogenes*	2010	No
Other	Not given	*L. monocytogenes*	2010	No
Meat	Raw meat	*L. monocytogenes*	2010	No
Meat	Raw meat	*L. monocytogenes*	2010	No
Meat	Raw meat	*L. monocytogenes*	2010	No
Meat	Raw meat	*L. monocytogenes*	2011	No
Environmental	Environmental swab	*L. monocytogenes*	2011	No
Environmental	Environmental swab	*L. monocytogenes*	2011	No
Environmental	Environmental swab	*L. monocytogenes*	2011	No
Environmental	Environmental swab	*L. monocytogenes*	2011	No
Environmental	Environmental swab	*L. monocytogenes*	2011	No
Environmental	Environmental swab	*L. monocytogenes*	2011	No
Environmental	Environmental swab	*L. monocytogenes*	2011	No
Meat	RTE sliced meat survey	*L. monocytogenes*	2012	Yes
Meat	RTE sliced meat survey	*L. monocytogenes*	2012	Yes
Meat	RTE sliced meat survey	*L. monocytogenes*	2012	Yes
Meat	RTE sliced meat survey	*L. monocytogenes*	2012	Yes
Meat	Cooked meat	*L. monocytogenes*	2012	No
Meat	RTE sliced meat survey	*L. monocytogenes*	2012	No
Environmental	Environmental swab	*L. monocytogenes*	2012	No
Meat	RTE sliced meat survey	*L. monocytogenes*	2012	Yes
Meat	RTE sliced meat survey	*L. monocytogenes*	2012	Yes
Quality assurance sample	Quality assurance sample	*L. monocytogenes*	2008	No
Milk	Raw milk	*L. monocytogenes*	2008	No
Quality assurance sample	Quality assurance sample	*L. monocytogenes*	2008	No
Quality assurance sample	Quality assurance sample	*L. monocytogenes*	2009	No
Meat	Cooked meat	*L. monocytogenes*	2009	No
Quality assurance sample	Quality assurance sample	*L. monocytogenes*	2009	No
Milk	Raw milk	*L. monocytogenes*	2009	No
Other	Croquette	*L. monocytogenes*	2009	No
Other	Croquette	*L. monocytogenes*	2009	No
Other	Not given	*L. monocytogenes*	2009	No
Quality assurance sample	Quality assurance sample	*L. monocytogenes*	2009	No
Quality assurance sample	Quality assurance sample	*L. monocytogenes*	2009	No
Other	Croquette	*L. monocytogenes*	2009	No
Milk	Raw milk	*L. monocytogenes*	2009	No
Other	Croquette	*L. monocytogenes*	2009	No
Milk	Raw milk	*L. monocytogenes*	2009	No

Fish	Smoked salmon	*L. monocytogenes*	2009	No
Fish	Smoked salmon	*L. monocytogenes*	2009	No
Fish	Smoked salmon	*L. monocytogenes*	2009	No
Fish	Smoked salmon	*L. monocytogenes*	2009	No
Meat	Cooked meat	*L. monocytogenes*	2009	No
Meat	Cooked meat	*L. monocytogenes*	2009	No
Quality assurance sample	Quality assurance sample	*L. monocytogenes*	2009	No
Meat	Cooked meat	*L. monocytogenes*	2010	No
Milk	Raw milk	*L. monocytogenes*	2010	No
Milk	Raw milk	*L. monocytogenes*	2010	No
Quality assurance sample	Quality assurance sample	*L. monocytogenes*	2010	No
Meat	Raw meat	*L. monocytogenes*	2010	No
Milk	Raw milk	*L. monocytogenes*	2010	No
Quality assurance sample	Quality assurance sample	*L. monocytogenes*	2010	No
Milk	Raw milk	*L. monocytogenes*	2010	No
Milk	Raw milk	*L. monocytogenes*	2010	No
Milk	Raw milk	*L. monocytogenes*	2010	No
Quality assurance sample	Quality assurance sample	*L. monocytogenes*	2010	No
Quality assurance sample	Quality assurance sample	*L. monocytogenes*	2010	No
Meat	Raw meat	*L. monocytogenes*	2010	No
Quality assurance sample	Quality assurance sample	*L. monocytogenes*	2011	No
Meat	Raw meat	*L. monocytogenes*	2011	No
Quality assurance sample	Quality assurance sample	*L. monocytogenes*	2011	No
Meat	Cooked meat	*L. monocytogenes*	2012	No
Quality assurance sample	Quality assurance sample	*L. monocytogenes*	2012	No
Meat	RTE sliced meat survey	*L. monocytogenes*	2012	Yes
Meat	RTE sliced meat survey	*L. monocytogenes*	2012	No
Meat	RTE sliced meat survey	*L. monocytogenes*	2012	Yes
Meat	RTE sliced meat survey	*L. monocytogenes*	2012	No
Quality assurance sample	Quality assurance sample	*L. monocytogenes*	2012	No
Meat	RTE sliced meat survey	*L. monocytogenes*	2012	No
Meat	RTE sliced meat survey	*L. monocytogenes*	2012	No
Meat	RTE sliced meat survey	*L. monocytogenes*	2012	Yes
Meat	RTE sliced meat survey	*L. monocytogenes*	2012	Yes
Meat	RTE sliced meat survey	*L. monocytogenes*	2012	No
Environmental	Environmental swab	*L. monocytogenes*	2012	No
Meat	RTE sliced meat survey	*L. monocytogenes*	2012	No
Meat	RTE sliced meat survey	*L. monocytogenes*	2012	No
Meat	RTE sliced meat survey	*L. monocytogenes*	2012	Yes
Meat	RTE sliced meat survey	*L. monocytogenes*	2012	No

Meat	RTE sliced meat survey	*L. monocytogenes*	2012	Yes
Meat	RTE sliced meat survey	*L. monocytogenes*	2012	Yes
Meat	RTE sliced meat survey	*L. monocytogenes*	2012	No
Meat	RTE sliced meat survey	*L. monocytogenes*	2012	No
Meat	RTE sliced meat survey	*L. monocytogenes*	2012	No
Meat	RTE sliced meat survey	*L. monocytogenes*	2012	Yes
Meat	RTE sliced meat survey	*L. monocytogenes*	2012	Yes
Meat	RTE sliced meat survey	*L. monocytogenes*	2012	No
Meat	RTE sliced meat survey	*L. monocytogenes*	2012	No
Meat	RTE sliced meat survey	*L. monocytogenes*	2012	Yes
Meat	RTE sliced meat survey	*L. monocytogenes*	2012	No
Meat	RTE sliced meat survey	*L. monocytogenes*	2012	Yes
Meat	RTE sliced meat survey	*L. monocytogenes*	2012	No
Meat	RTE sliced meat survey	*L. monocytogenes*	2012	No
Meat	RTE sliced meat survey	*L. monocytogenes*	2012	Yes
Meat	RTE sliced meat survey	*L. monocytogenes*	2012	No
Meat	RTE sliced meat survey	*L. monocytogenes*	2012	No
Meat	RTE sliced meat survey	*L. monocytogenes*	2012	Yes
Meat	RTE sliced meat survey	*L. monocytogenes*	2012	Yes
Meat	RTE sliced meat survey	*L. monocytogenes*	2012	Yes
Meat	RTE sliced meat survey	*L. monocytogenes*	2012	Yes
Meat	RTE sliced meat survey	*L. monocytogenes*	2012	Yes
Meat	RTE sliced meat survey	*L. monocytogenes*	2012	No
Quality assurance sample	Quality assurance sample	*L. monocytogenes*	2013	No
Environmental	Environmental swab	*L. monocytogenes*	2013	No
Environmental	Environmental swab	*L. monocytogenes*	2013	No
Meat	RTE sliced meat survey	*L. monocytogenes*	2012	No
Meat	Cooked meat	*L. seeligeri*	2012	No
Meat	RTE sliced meat survey	*L. seeligeri*	2012	No
Meat	RTE sliced meat survey	*L. seeligeri*	2012	No
Meat	Cooked meat	*L. seeligeri*	2012	No
Meat	RTE sliced meat survey	*L. seeligeri*	2012	No
Meat	RTE sliced meat survey	*L. seeligeri*	2012	No
Meat	RTE sliced meat survey	*L. welshimeri*	2012	No
Meat	RTE sliced meat survey	*L. seeligeri*	2012	No
Meat	RTE sliced meat survey	*L. welshimeri*	2013	No
Quality assurance sample	Quality assurance sample	*L. welshimeri*	2011	No
Quality assurance sample	Quality assurance sample	*L. welshimeri*	2011	No
Quality assurance sample	Quality assurance sample	*L. welshimeri*	2012	No
Meat	RTE sliced meat survey	*L. welshimeri*	2012	No
Meat	RTE sliced meat survey	*L. welshimeri*	2012	No
Meat	RTE sliced meat survey	*L. welshimeri*	2012	No
Meat	RTE sliced meat survey	*L. welshimeri*	2012	No

Meat	RTE sliced meat survey	*L. welshimeri*	2012	No
Meat	RTE sliced meat survey	*L. welshimeri*	2012	No
Meat	RTE sliced meat survey	*L. welshimeri*	2012	No
Meat	RTE sliced meat survey	*L. welshimeri*	2012	No
Meat	RTE sliced meat survey	*L. welshimeri*	2012	No
Meat	RTE sliced meat survey	*L. welshimeri*	2012	No
Meat	RTE sliced meat survey	*L. welshimeri*	2012	No
Meat	RTE sliced meat survey	*L. welshimeri*	2012	No
Meat	RTE sliced meat survey	*L. welshimeri*	2012	No
Meat	RTE sliced meat survey	*L. welshimeri*	2012	No
Meat	RTE sliced meat survey	*L. welshimeri*	2012	No
Meat	RTE sliced meat survey	*L. welshimeri*	2012	No
Meat	RTE sliced meat survey	*L. welshimeri*	2012	No
Meat	RTE sliced meat survey	*L. welshimeri*	2012	No
Meat	RTE sliced meat survey	*L. welshimeri*	2012	No
Meat	RTE sliced meat survey	*L. welshimeri*	2012	No
Meat	RTE sliced meat survey	*L. welshimeri*	2012	No
Meat	Cooked meat	*L. welshimeri*	2010	No
Quality assurance sample	Quality assurance sample	*L. welshimeri*	2009	No
Other	Not given	*L. welshimeri*	2009	No
Quality assurance sample	Quality assurance sample	*L. welshimeri*	2009	No
Fish	Smoked salmon	*L. welshimeri*	2009	No
Fish	Smoked salmon	*L. welshimeri*	2009	No
Meat	Cooked meat	*L. welshimeri*	2009	No
Meat	Cooked meat	*L. welshimeri*	2010	No
Meat	Cooked meat	*L. welshimeri*	2010	No
Quality assurance sample	Quality assurance sample	*L. innocua*	2012	No
Meat	Raw meat	*L. monocytogenes*	2010	No
Milk	Raw milk	*L. monocytogenes*	2010	No
Other	Cream	*L. seeligeri*	2008	No
Quality assurance sample	Quality assurance sample	*L. seeligeri*	2008	No
Other	Cream	*L. seeligeri*	2009	No
Milk	Raw milk	*L. seeligeri*	2009	No
Milk	Raw milk	*L. seeligeri*	2009	No
Meat	Cooked meat	*L. seeligeri*	2009	No
Meat	Cooked meat	*L. seeligeri*	2009	No

Appendix 2. **Quality metrics of the short-read Illumina sequencing data generated for the FSA panel isolates.** The table reports the total reads, reads passing quality filtering, total bases post-filtering, and Q20 bases post-filtering. This table is complementary to **Table 10**.

Order	Strain	Total reads	Reads passed filtering	Total bases post filtering	Q20 bases post filtering
1	LS12/71	3.29M	3.24M	473.1M	454.0M
2	LS12/142	2.76M	2.72M	401.1M	383.8M
3	LS12/177	3.4M	3.3M	491.9M	472.0M
4	LS12/211	3.79M	3.75M	546.4M	523.9M
5	LS12/257	3.89M	3.83M	558.5M	535.5M
6	LS12/426	2.96M	2.91M	425.9M	408.1M
7	LS12/453	2.52M	2.48M	365.5M	350.5M
8	LS12/495	4.30M	4.23M	616.0M	590.5M
9	LS12/505	2.79M	2.75M	405.9M	389.5M
10	LS12/519	2.37M	2.33M	344.1M	329.3M
11	LS12/521	2.87M	2.83M	417.3M	400.4M
12	LS12/522	2.43M	2.39M	353.1M	338.1M
13	LS12/570	1.46M	1.43M	209.9M	198.4M
14	LS12/579	1.66M	1.63M	241.3M	231.3M
15	LS12/580	1.57M	1.53M	225.8M	213.4M
16	LS12/646	1.27M	1.24M	183.2M	172.9M
17	LS12/685	1.79M	1.74M	255.4M	240.9M
18	LS12/741	2.89M	2.83M	420.2M	402.4M
19	LS12/808	2.76M	2.72M	401.3M	384.2M
20	LS12/847	2.94M	2.89M	427.1M	409.1M
21	LS12/859	3.35M	3.29M	485.9M	465.1M
22	LS12/964	1.13M	1.11M	163.8M	156.4M
23	LS12/970	1.61M	1.59M	233.9M	223.9M

Appendix 3. Gene database used for ABRicate analysis of gene presence/absence. The list includes genes associated with various stress adaptations and virulence factors: low pH adaptation, adherence, alkaline and oxidative stress, antibiotic tolerance, arsenic tolerance, bile tolerance, biofilm formation, virulence, cold adaptation, desiccation tolerance, cadmium tolerance, detergent tolerance, salt tolerance, intracellular survival, and invasion. Gene selection based on several publications (Dumith et al., 2004; Hingston et al., 2017; Maury et al., 2019; Moura et al., 2016; Pasquali et al., 2018).

Gene of Interest	Function
lmo0036 (arcB)	Adaptation to low pH
lmo0037 (arcD)	Adaptation to low pH
lmo0039 (arcC)	Adaptation to low pH
lmo0043 (arcA_1)	Adaptation to low pH
lmo0043 (arcA_2)	Adaptation to low pH
lmo0796	Adaptation to low pH
lmo0913	Adaptation to low pH
lmo1367 (argR)	Adaptation to low pH
lmo2362 (gadT2)	Adaptation to low pH
lmo2363 (gadD2_1)	Adaptation to low pH
lmo2363 (gadD2_2)	Adaptation to low pH
lmo2391	Adaptation to low pH
lmo2434 (gadD3)	Adaptation to low pH
SSI1_lmo0447 (gadD1)	Adaptation to low pH
SSI1_lmo0448 (gadT1)	Adaptation to low pH
SSI1_lmo0444	Adaptation to low pH and high salt conc
SSI1_lmo0445	Adaptation to low pH and high salt conc
SSI1_lmo0446 (pva)	Adaptation to low pH and high salt conc
ami	Adherence
dltA	Adherence
fbpA	Adherence
lap	Adherence
lapB	Adherence
LM6179 and SSI2_lin0464	Alkaline and oxidative stress
SSI2_lin0465 and yoaZ	Alkaline and oxidative stress
aacA4	Antibiotic Tolerance
fosX	Antibiotic Tolerance
lmo0441	Antibiotic Tolerance
lmo0540 (ampC)	Antibiotic Tolerance
lmo0919	Antibiotic Tolerance
lmo2741 and tetA_3	Antibiotic Tolerance
norB_1	Antibiotic Tolerance
norB_2	Antibiotic Tolerance
sul_1	Antibiotic Tolerance
sul_2	Antibiotic Tolerance

tetA_1	Antibiotic Tolerance
tetA_2_1	Antibiotic Tolerance
tetA_2_2	Antibiotic Tolerance
arsA1	Arsenic Tolerance
arsA2	Arsenic Tolerance
arsB1	Arsenic Tolerance
arsB2	Arsenic Tolerance
arsD1	Arsenic Tolerance
arsD2	Arsenic Tolerance
arsR1	Arsenic Tolerance
arsR2	Arsenic Tolerance
bsh	Bile-tolerance
lmo2588 (mdrT)	Bile-tolerance
lmo2589 (brtA_1)	Bile-tolerance
mdrM	Bile-tolerance
lmo2589 (brtA_2)	Bile-tolerance
inlL	Biofilm formation and virulence
lmo0435 (bapL)	Biofilm formation and virulence
lmo0673	Biofilm formation and virulence
lmo1288 (luxS)	Biofilm formation and virulence
lmo1460_1	Biofilm formation and virulence
lmo1460_2	Biofilm formation and virulence
lmo2504	Biofilm formation and virulence
comK	Biofilm formation and virulence
cadA1	Cadmium tolerance
cadA2	Cadmium tolerance
cadC1	Cadmium tolerance
cadC2	Cadmium tolerance
cadA4	Cadmium Tolerance and biofilm
cadC4	Cadmium Tolerance and biofilm
lmo1022 (liaR)	cell-envelope stress response (nisin tolerance)
lmo2115 (anrB)	cell-envelope stress response (nisin tolerance)
mprF	cell-envelope stress response (nisin tolerance)
lmo0288 (yycG)	Cold adaption
lmo0866	Cold adaption
lmo1078	Cold adaption
lmo1722	Cold adaption
lmo1879 (cspD_1)	Cold adaption
lmo1879 (cspD_2)	Cold adaption
lmo2016 (cspB)	Cold adaption
lmo0676 (fliP)	Dessication

lmo0679 (flhB)	Dessication
lmo0686 (motB)	Dessication
lmo0693 (fliY)	Dessication
lmo0696 (flgD)	Dessication
lmo0699 (fliM)	Dessication
lmo0706 (flgL)	Dessication
bcrA	Benzalkonium chloride tolerance
bcrB	Benzalkonium chloride tolerance
bcrC	Benzalkonium chloride tolerance
ermC_1	Benzalkonium chloride tolerance
ermC_2	Benzalkonium chloride tolerance
lmo1408 (ladR)	Benzalkonium chloride tolerance
lmo1409 (mdrL)	Benzalkonium chloride tolerance
inlD_1	General Virulence
inlD_2	General Virulence
lmo0333 (inll)	General Virulence
lmo1280 (codY)	General Virulence
lmo2470 (inlP)	General Virulence
lmo2491 (pdeE)	General Virulence
lmo2092 (betL)	High salt
lmo2748_1	High salt
lmo2748_2	High salt
lmo1014 (gbuA)	High salt and cold
lmo1015 (gbuB)	High salt and cold
lmo1016 (gbuC)	High salt and cold
lmo1425 (opuCD)	High salt and cold
lmo1426 (opuCC)	High salt and cold
lmo1427 (opuCB)	High salt and cold
lmo1428 (opuCA)	High salt and cold
lntA_1	Immune modulation
lntA_2	Immune modulation
inlA_1	Internalins
inlA_2	Internalins
inlA_3	Internalins
inlB_1	Internalins
inlC	Internalins
inlC2 and inlH	Internalins
inlE_2	Internalins
inlE_3	Internalins
inlF_1	Internalins
inlF_2	Internalins

inlG_1	Internalins
inlG_2	Internalins
inlJ_1	Internalins
inlJ_2	Internalins
inlK_1	Internalins
inlK_2	Internalins
inlE_1	Internalins
inlB_2	Internalins
hpt	Intracellular survival
lplA1	Intracellular survival
oppA	Intracellular survival
prsA2_1	Intracellular survival
prsA2_2	Intracellular survival
purQ	Intracellular survival
svpA_1	Intracellular survival
svpA_2	Intracellular survival
aut	Invasion
aut_2	Invasion
cwhA_1	Invasion
cwhA_2	Invasion
cwhA_3	Invasion
cwhA_5	Invasion
lpeA	Invasion
vip_1	Invasion
vip_3	Invasion
vip_2	Invasion
cwhA_4	Invasion
LIPI3_llsA	Lineage I associated
LIPI3_llsB	Lineage I associated
LIPI3_llsD	Lineage I associated
LIPI3_llsG	Lineage I associated
LIPI3_llsH	Lineage I associated
LIPI3_llsP	Lineage I associated
LIPI3_llsX	Lineage I associated
LIPI3_llsY	Lineage I associated
actA_1	LIPI-1
actA_2	LIPI-1
actA_3	LIPI-1
hly	LIPI-1
mpl	LIPI-1
plcA	LIPI-1

plcB	LIPI-1
prfA and *prfA**	LIPI-1 / Biofilm formation and virulence
LM9005581_70009	LIPI-4 – CC4 associated, also found in Lineage III and IV
LM9005581_70010	LIPI-4 – CC4 associated, also found in Lineage III and IV
LM9005581_70011	LIPI-4 – CC4 associated, also found in Lineage III and IV
LM9005581_70012	LIPI-4 – CC4 associated, also found in Lineage III and IV
LM9005581_70013	LIPI-4 – CC4 associated, also found in Lineage III and IV
LM9005581_70014	LIPI-4 – CC4 associated, also found in Lineage III and IV
lmo0196 (SpoVGI)	lysozyme tolerance, global posttranscriptional gene regulator
lmo0197 (SpoVGII_1)	lysozyme tolerance, global posttranscriptional gene regulator
lmo0197 (SpoVGII_2)	lysozyme tolerance, global posttranscriptional gene regulator
lmo0737	PCR-serogroup
lmo1118	PCR-serogroup
ORF2110	PCR-serogroup
ORF2819	PCR-serogroup
prs	PCR-serogroup
oatA	Peptidoglycan modification
pdgA	Peptidoglycan modification
agrA	Regulation of transcription and translation
agrC	Regulation of transcription and translation
cheA	Regulation of transcription and translation
cheY	Regulation of transcription and translation
fur	Regulation of transcription and translation
lisR	Regulation of transcription and translation
stp	Regulation of transcription and translation
*virR*_1 and *virR*_1	Regulation of transcription and translation / cell-envelope stress response (nisin tolerance)
virS and *virS*	Regulation of transcription and translation / cell-envelope stress response (nisin tolerance)
*virR*_2 and *virR*_2	Regulation of transcription and translation / cell-envelope stress response (nisin tolerance)
lisK and *lmo1378*	Regulation of transcription and translation / Cold adaption
lmo1080 (rmlT)	Rhamnose operon
lmo1081 (rmlA)	Rhamnose operon
lmo1082 (rmlC)	Rhamnose operon
lmo1083 (rmlB)	Rhamnose operon
lmo1084 (rmlD)	Rhamnose operon
lmo1118	Serogroup
lmo0737	Serogroup
ORF2110	Serogroup

ORF2819	Serogroup
lmo0889 (rsbR)	*sigB* operon
lmo0890 (rsbS)	*sigB* operon
lmo0891 (rsbT)	*sigB* operon
lmo0892 (rsbY)	*sigB* operon
lmo0894 (rsbW)	*sigB* operon
lmo0896 (rsbX)	*sigB* operon
lmo0893 (*rsbV* and *rsbV**)	SigB operon and Regulation of transcription and translation
lmo0895 (*sigB, sigB** and *sigB***)	SigB operon, Regulation of transcription and translation / Stress tolerance
Staph pT48 ermC_3	Staph specific plasmid *ermC*
repA	Stress tolerance
lgt	Surface protein anchoring
lspA	Surface protein anchoring
srtA	Surface protein anchoring
srtB	Surface protein anchoring
gltA	Teichoic acid biosynthesis
gltB	Teichoic acid biosynthesis
gtcA_1	Teichoic acid biosynthesis
gtcA_2	Teichoic acid biosynthesis
tagB	Teichoic acid biosynthesis
tagB	Teichoic acid biosynthesis
emrE	Benzalkonium chloride tolerance

Appendix 4(I). Provides details of 50 sequences homologous to *ykoK* to assess the conservation of *ykoK* within the *Listeria* genus, but excluding *L. monocytogenes* sequences, retrieved from the NCBI database using a BLAST search. The table includes the following information for each sequence: accession number, nucleotide range within the genome, strain, genome location, and the completeness of the genome.

Number	Accession Number	Nucleotide Range	Strain	Position	Genome completeness
1	CP093384.1	188384-188521	*Vagococcus sp.* CY52-2	Chromosome	Complete
2	CP102451.1	288953-289087	*Vagococcus luciliae* G314F	Chromosome	Complete
3	HE999757.2	3266477-3266633	*Carnobacterium maltaromaticum* LMA28	Chromosome	Complete
4	CP045040.1	3144358-3144514	*Carnobacterium maltaromaticum* 18ISCm	Chromosome	Complete
5	OQ263311.1	38747-38903	*Carnobacterium maltaromaticum* NFICC546	PrtP Gene (prtP)	Complete
6	OX460976.10	343844-344000	*Carnobacterium maltaromaticum* SF2022	Chromosome	Complete
7	CP016844.1	2598270-2598426	*Carnobacterium maltaromaticum* TMW 2.1581	Chromosome	Complete
8	CP045585.1	3386044-3386205	*Bacillus thuringiensis* x023	Chromosome	Complete
9	CP083101.1	1686260-1686421	*Bacillus thuringiensis* ABTS-351	Chromosome	Complete
10	CP130743.1	2556206-2556367	*Bacillus thuringiensis* PS3	Chromosome	Complete
11	CP009336.1	166979-167140	*Bacillus thuringiensis* HD1011	Plasmid	Complete
12	CP020755.1	80179-80343	*Bacillus thuringiensis* ATCC 10792	Plasmid pLDW-16	Complete
13	CP046512.1	156644-156805	*Bacillus cereus* JHU	Plasmid	Complete
14	CP004137.1	139298-139462	*Bacillus thuringiensis* IS5056	Plasmid pIS56-328	Complete
15	CP016194.1	2566286-2566447	*Bacillus thuringiensis* ST7	Chromosome	Complete
16	CP126474.1	2431736-	*Bacillus thuringiensis*	Chromosome	Complete

		2431897	DHC4		
17	CP152438.1	236200-236361	*Bacillus sp.* BR3(2024)	Plasmid	Complete
18	CP042875.1	44865-45026	*Bacillus cereus* 09	Plasmid	Complete
19	CP010106.1	2449119-2449280	*Bacillus thuringiensis* HD521	Chromosome	Complete
20	CP015150.1	3340053-3340214	*Bacillus thuringiensis* Bc601	Chromosome	Complete
21	CP043234.1	2461572-2461733	*Bacillus thuringiensis* Bt-GS57	Chromosome	Complete
22	CP083156.1	2223304-2223465	*Bacillus thuringiensis* ABTS-1857	Chromosome	Complete
23	CP130335.1	2506604-2506765	*Bacillus cereus* DW444	Chromosome	Complete
24	CP010005.1	2469104-2469265	*Bacillus thuringiensis* HD 1	Chromosome	Complete
25	CP068720.1	234449-234610	*Bacillus cereus* 21155	Plasmid	Complete
26	CP095377.1	2365290-2365451	*Bacillus cereus* SEM-15	Chromosome	Complete
27	CP032614.1	236285-236446	*Bacillus thuringiensis* QZL38	Plasmid	Complete
28	CP106948.1	592135-592296	*Bacillus thuringiensis* 4F5	Plasmid p_4F5-1	Complete
29	CP083144.1	2269754-2269915	*Bacillus thuringiensis* GC-91	Chromosome	Complete
30	CP162507.1	3035-3196	*Bacillus cereus* DJ29	Plasmid	Complete
31	CP022446.1	59951-60115	*Bacillus cereus* C1L	Plasmid pC1L1	Complete
32	CP068718.1	179858-180019	*Bacillus cereus* CH	Plasmid	Complete
33	CP011349.1	5075377-5075538	*Bacillus thuringiensis* YC-10	Chromosome	Complete
34	CP152429.1	339872-340033	*Bacillus paramycoides* JYZ-SD5	Plasmid	Complete
35	CP072774.1	2434656-2434817	*Bacillus cereus* BC33	Chromosome	Complete
36	CP004069.1	3360193-3360354	*Bacillus thuringiensis* HD73	Complete Genome	Complete
37	CP135061.1	261961-262122	*Bacillus cereus* B126_1	Plasmid	Complete
38	CP011154.1	575515-575676	*Bacillus cereus*	Plasmid pRML05	Complete

			CMCC P0011		
39	CP116313.1	2696989-2697150	*Bacillus thuringiensis* Lip	Chromosome	Complete
40	CP016595.1	2340630-2340791	*Bacillus cereus* K8	Chromosome	Complete
41	CP106675.1	2376033-2376194	*Bacillus cereus* SRCM116293	Chromosome	Complete
42	CP017267.1	2030365-2030499	*Vagococcus teuberi* DSM 21459	Chromosome	Complete
43	CP116325.1	2564636-2564797	*Bacillus thuringiensis* BLB1	Chromosome	Complete
44	CP004870.1	3348886-3349047	*Bacillus thuringiensis* HD-1	Chromosome	Complete
45	CP139215.1	289770-289931	*Bacillus cereus* A01	Plasmid	Complete
46	CP020005.1	283014-283175	*Bacillus thuringiensis* L-7601	Plasmid	Complete
47	CP014283.1	547101-547262	*Bacillus thuringiensis* Bt185	Plasmid pBT1850636	Complete
48	CP129006.1	79009-79170	*Bacillus cereus* strain lycx	Plasmid unnamed	Complete
49	CP106947.1	3321726-3321887	*Bacillus thuringiensis* strain 4F5	Chromosome	Complete
50	CP011152.1	562351-562512	*Bacillus cereus* strain CMCC P0021	Plasmid pRML04	Complete

Appendix 4 (II). Provides details of 50 sequences homologous to *ykoK* to assess the conservation of *ykoK* outside the *Listeria* genus, retrieved from the NCBI database using a BLAST search. The table includes the following information for each sequence: accession number, nucleotide range within the genome, strain, genome location, and the completeness of the genome.

Number	Accession Number	Nucleotide Range	Strain	Position	Genome completeness
1	CP009576.1	2944163-2944329	*Listeria ivanovii subsp. londoniensis* strain WSLC 30151	Chromosome	Complete
2	CP063071.1	2717401-2717567	*Listeria seeligeri* strain Sr73	Chromosome	Complete
3	CP034772.1	2772613-2772779	*Listeria seeligeri* strain RR4	Chromosome	Complete
4	CP149496.1	2669560-2669726	*Listeria welshimeri* strain DSM 20650 V8	Chromosome	Complete
5	CP124262.1	165906-166072	*Listeria seeligeri* strain L182	Chromosome	Complete
6	CP151430.1	2658561-2658727	*Listeria welshimeri* strain 4-43	Chromosome	Complete
7	LT906444.1	2669560-2669726	*Listeria welshimeri* strain NCTC11857	Chromosome	Complete
8	CP124268.1	2718342-2718508	*Listeria seeligeri* strain L140	Chromosome	Complete
9	FN557490.1	2660400-2660566	*Listeria seeligeri* serovar 1/2b str. SLCC3954	Chromosome	Complete
10	CP122330.1	2680951-2681117	*Listeria welshimeri* strain GIMC2051:LmcC15	Chromosome	Complete
11	CP156021.1	2654995-2655161	*Listeria swaminathanii* strain UTK S2-0008	Chromosome	Complete
12	LR134394.1	2858398-2858564	*Listeria ivanovii subsp. londoniensis* strain NCTC12701	Chromosome	Complete
13	CP148898.1	359139-359305	*Listeria seeligeri* strain 43-1	Chromosome	Complete
14	CP009575.1	2887502-2887668	*Listeria ivanovii subsp. londoniensis* strain WSLC 30167	Chromosome	Complete
15	CP046449.1	2738696-2738862	*Listeria sp.* LM90SB2	Chromosome	Complete
16	AM263198.1	2669870-2670036	*Listeria welshimeri* serovar 6b str. SLCC5334	Chromosome	Complete
17	CP009577.1	2795135-2795301	*Listeria ivanovii subsp. ivanovii* strain WSLC 3010	Chromosome	Complete
18	CP165993.1	2246389-2246555	*Listeria ivanovii subsp. ivanovii* strain PNUSAL001964	Chromosome	Complete
19	LT906478.1	2739502-2739668	*Listeria ivanovii subsp. ivanovii* strain NCTC11846	Chromosome	Complete
20	CP165991.1	2709970-2710136	*Listeria ivanovii* strain F5999	Chromosome	Complete
21	CP034771.1	251459-251625	*Listeria ivanovii* strain RR3	Chromosome	Complete
22	FR687253.1	2748962-2749128	*Listeria ivanovii subsp. ivanovii* PAM 55		Complete

23	CP007172.1	2795136-2795302	*Listeria ivanovii* WSLC3009		Complete
24	CP165992.1	2794695-2794861	*Listeria ivanovii* strain ATCC 19119	Chromosome	Complete
25	LT906466.1	2739505-2739671	*Listeria ivanovii subsp. ivanovii* strain NCTC11007	Chromosome	Complete
26	CP151428.1	2739500-2739666	*Listeria ivanovii* strain 1-1	Chromosome	
27	CP149497.1	2739501-2739667	*Listeria ivanovii* strain Li 1979	Chromosome	Complete
28	CP165994.1	1516230-1516396	*Listeria ivanovii* strain PNUSAL004272	Chromosome	Complete
29	CP124258.1	181001-181167	*Listeria ivanovii* strain L195	Chromosome	Complete
30	CP102626.1	2419110-2419277	*Listeria innocua* strain 2012L-5520	Chromosome	Complete
31	CP071157.1	2764158-2764325	*Listeria innocua* strain LI203	Chromosome	Complete
32	CP096148.1	1027271-1027438	*Listeria innocua* strain FSL L7-0007	Chromosome	Complete
33	CP095726.1	1976832-1976999	*Listeria innocua* strain 2010L-2059	Chromosome	Complete
34	CP025202.1	2631966-2632133	*Listeria innocua* strain WSLC_2021_parental	Chromosome	Complete
35	CP151431.1	2754227-2754394	*Listeria innocua* strain 4-99	Chromosome	Complete
36	CP102627.1	2626195-2626362	*Listeria innocua* strain F4078	Chromosome	Complete
37	CP095724.1	1468936-1469103	*Listeria innocua* strain F6217	Chromosome	Complete
38	CP095730.1	1892007-1892174	*Listeria innocua* strain H0996	Chromosome	Complete
39	CP103399.1	368698-368865	*Listeria innocua* strain F6215	Chromosome	Complete
40	AL596173.1	245167-245334	*Listeria innocua* Clip11262		Complete
41	CP095727.1	2792513-2792680	*Listeria innocua* strain 2010L-1951	Chromosome	Complete
42	CP168261.1	1542377-1542544	*Listeria innocua* strain Lin_NWU_CNKT	Chromosome	Complete
43	CP045743.1	1833151-1833318	*Listeria innocua* strain CFSAN044836	Chromosome	Complete
44	CP095728.1	732667-732834	*Listeria innocua* strain 2015L-6726	Chromosome	Complete
45	CP071179.1	2771341-2771508	*Listeria innocua* strain LI47	Chromosome	Complete
46	CP084086.1	91625-91792	*Listeria innocua* strain ZM39	Chromosome	Complete
47	CP095723.1	2338908-2339075	*Listeria innocua* strain 2015L-6714	Chromosome	Complete
48	CP117229.1	2626228-2626395	*Listeria innocua* strain ATCC 33090	Chromosome	Complete
49	CP176674.1	157311-157478	*Listeria innocua* strain GTVSS-019	Chromosome	Complete
50	CP071155.1	2754362-2754529	*Listeria innocua* strain LI42	Chromosome	Complete

Appendix 5. Overview table of all 272 evolved isolates recovered from the Biofilm Persistence Model (BPM). For each isolate, the following information is provided: sample name, sample ID, growth type (biofilm or planktonic), lineage, storage stage (early, mid, late), BC treatment exposure, sample type (population/whole culture or individual colony), MIC of BC, phenotyping status (+ or nothing, indicating whether the isolate was phenotyped), and whole-genome sequencing status (+ or nothing, indicating whether the isolate was sequenced).

Sample name	Sample ID	Type of growth	Lineage	Passage	Treatment	Sample type	MIC (µg/mL)	Phenotyping	Whole-genome sequencing
BL87-028-T10-0-625-Biofilm1-P	Steady_001	Biofilm	L1	P11 - Early	0.625 µg/mL	Population	7.50	+	+
BL87-028-T10-0-625-Biofilm2-P	Steady_002	Biofilm	L2	P11 - Early	0.625 µg/mL	Population	7.50	+	+
BL87-028-T10-0-625-Biofilm3-P	Steady_003	Biofilm	L3	P11 - Early	0.625 µg/mL	Population	7.22	+	+
BL87-028-T10-0-625-Biofilm4-P	Steady_004	Biofilm	L4	P11 - Early	0.625 µg/mL	Population	5.00	+	
BL87-028-T10-No-BC-Biofilm1-P	Steady_005	Biofilm	L1	P11 - Early	No BC	Population	4.17	+	+
BL87-028-T10-No-BC-Biofilm2-P	Steady_006	Biofilm	L2	P11 - Early	No BC	Population	5.00	+	+
BL87-028-T10-No-BC-Biofilm3-P	Steady_007	Biofilm	L3	P11 - Early	No BC	Population	5.56	+	+
BL87-028-T10-No-BC-Biofilm4-P	Steady_008	Biofilm	L4	P11 - Early	No BC	Population	5.00	+	
BL87-028-T10-0-625-Planktonic1-P	Steady_009	Planktonic	L1	P11 - Early	0.625 µg/mL	Population	7.50	+	+
BL87-028-T10-0-625-Planktonic2-P	Steady_010	Planktonic	L2	P11 - Early	0.625 µg/mL	Population	7.20	+	+
BL87-028-T10-0-625-Planktonic3-P	Steady_011	Planktonic	L3	P11 - Early	0.625 µg/mL	Population	7.50	+	+
BL87-028-T10-0-625-Planktonic4-P	Steady_012	Planktonic	L4	P11 - Early	0.625 µg/mL	Population	7.50	+	
BL87-028-T10-No-BC-Planktonic1-P	Steady_013	Planktonic	L1	P11 - Early	No BC	Population	2.50	+	+
BL87-028-T10-No-BC-Planktonic2-P	Steady_014	Planktonic	L2	P11 - Early	No BC	Population	2.50	+	+
BL87-028-T10-No-BC-Planktonic3-	Steady_015	Planktonic	L3	P11 - Early	No BC	Population	2.50	+	+

P									
BL87-028-T10-No-BC-Planktonic4-P	Steady_016	Planktonic	L4	P11 - Early	No BC	Population	2.50	+	
BL87-028-T23-0-625-Biofilm1-P	Steady_and_Ladder_017	Biofilm	L1	P22 - Middle	0.625 µg/mL	Population	5.00	+	+
BL87-028-T23-0-625-Biofilm2-P	Steady_and_Ladder_018	Biofilm	L2	P22 - Middle	0.625 µg/mL	Population	6.94	+	+
BL87-028-T23-0-625-Biofilm3-P	Steady_and_Ladder_019	Biofilm	L3	P22 - Middle	0.625 µg/mL	Population	5.00	+	+
BL87-028-T23-0-625-Biofilm4-P	Steady_and_Ladder_020	Biofilm	L4	P22 - Middle	0.625 µg/mL	Population	5.00	+	
BL87-028-T23-No-BC-Biofilm1-P	Steady_and_Ladder_021	Biofilm	L1	P22 - Middle	No BC	Population	2.50	+	+
BL87-028-T23-No-BC-Biofilm2-P	Steady_and_Ladder_022	Biofilm	L2	P22 - Middle	No BC	Population	2.50	+	+
BL87-028-T23-No-BC-Biofilm3-P	Steady_and_Ladder_023	Biofilm	L3	P22 - Middle	No BC	Population	2.50	+	+
BL87-028-T23-No-BC-Biofilm4-P	Steady_and_Ladder_024	Biofilm	L4	P22 - Middle	No BC	Population	5.00	+	
BL87-028-T23-0-625-Planktonic1-P	Steady_and_Ladder_025	Planktonic	L1	P22 - Middle	0.625 µg/mL	Population	5.00	+	+
BL87-028-T23-0-625-Planktonic2-P	Steady_and_Ladder_026	Planktonic	L2	P22 - Middle	0.625 µg/mL	Population	5.83	+	+
BL87-028-T23-0-625-Planktonic3-P	Steady_and_Ladder_027	Planktonic	L3	P22 - Middle	0.625 µg/mL	Population	5.83	+	+
BL87-028-T23-0-625-Planktonic4-P	Steady_and_Ladder_028	Planktonic	L4	P22 - Middle	0.625 µg/mL	Population	5.56	+	
BL87-028-T23-No-BC-Planktonic1-P	Steady_and_Ladder_029	Planktonic	L1	P22 - Middle	No BC	Population	2.50	+	+
BL87-028-T23-No-BC-Planktonic2-P	Steady_and_Ladder_030	Planktonic	L2	P22 - Middle	No BC	Population	2.78	+	+
BL87-028-T23-No-BC-Planktonic3-P	Steady_and_Ladder_031	Planktonic	L3	P22 - Middle	No BC	Population	3.33	+	+
BL87-028-T23-No-BC-Planktonic4-P	Steady_and_Ladder_032	Planktonic	L4	P22 - Middle	No BC	Population	2.50	+	
BL87-028-T30-0-625-Biofilm1-P	Steady_and_Ladder_033	Biofilm	L1	P30 - Late	0.625 µg/mL	Population	6.67	+	+

BL87-028-T30-0-625-Biofilm2-P	Steady_and_Ladder_034	Biofilm	L2	P30 - Late	0.625 µg/mL	Population	7.50	+	+
BL87-028-T30-0-625-Biofilm3-P	Steady_and_Ladder_035	Biofilm	L3	P30 - Late	0.625 µg/mL	Population	7.22	+	+
BL87-028-T30-0-625-Biofilm4-P	Steady_and_Ladder_036	Biofilm	L4	P30 - Late	0.625 µg/mL	Population	6.39	+	
BL87-028-T30-No-BC-Biofilm1-P	Steady_and_Ladder_037	Biofilm	L1	P30 - Late	No BC	Population	2.50	+	+
BL87-028-T30-No-BC-Biofilm2-P	Steady_and_Ladder_038	Biofilm	L2	P30 - Late	No BC	Population	2.50	+	+
BL87-028-T30-No-BC-Biofilm3-P	Steady_and_Ladder_039	Biofilm	L3	P30 - Late	No BC	Population	2.50	+	+
BL87-028-T30-No-BC-Biofilm4-P	Steady_and_Ladder_040	Biofilm	L4	P30 - Late	No BC	Population	2.50	+	
BL87-028-T30-0-625-Planktonic1-P	Steady_and_Ladder_041	Planktonic	L1	P30 - Late	0.625 µg/mL	Population	7.50	+	+
BL87-028-T30-0-625-Planktonic2-P	Steady_and_Ladder_042	Planktonic	L2	P30 - Late	0.625 µg/mL	Population	7.50	+	+
BL87-028-T30-0-625-Planktonic3-P	Steady_and_Ladder_043	Planktonic	L3	P30 - Late	0.625 µg/mL	Population	7.50	+	+
BL87-028-T30-0-625-Planktonic4-P	Steady_and_Ladder_044	Planktonic	L4	P30 - Late	0.625 µg/mL	Population	7.50	+	
BL87-028-T30-No-BC-Planktonic1-P	Steady_and_Ladder_045	Planktonic	L1	P30 - Late	No BC	Population	2.50	+	+
BL87-028-T30-No-BC-Planktonic2-P	Steady_and_Ladder_046	Planktonic	L2	P30 - Late	No BC	Population	2.50	+	+
BL87-028-T30-No-BC-Planktonic3-P	Steady_and_Ladder_047	Planktonic	L3	P30 - Late	No BC	Population	2.50	+	+
BL87-028-T30-No-BC-Planktonic4-P	Steady_and_Ladder_048	Planktonic	L4	P30 - Late	No BC	Population	2.50		
BL87-028-T10-0-625-Biofilm1-1	Steady_049	Biofilm	L1	P11 - Early	0.625 µg/mL	Colony 1	7.22	+	+
BL87-028-T10-0-625-Biofilm1-2	Steady_050	Biofilm	L1	P11 - Early	0.625 µg/mL	Colony 2	7.50	+	+
BL87-028-T10-0-625-Biofilm1-3	Steady_051	Biofilm	L1	P11 - Early	0.625 µg/mL	Colony 3	7.50	+	+
BL87-028-T10-0-625-Biofilm2-1	Steady_052	Biofilm	L2	P11 - Early	0.625	Colony 1	7.50	+	+

					µg/mL				
BL87-028-T10-0-625-Biofilm2-2	Steady_053	Biofilm	L2	P11 - Early	0.625 µg/mL	Colony 2	7.50	+	+
BL87-028-T10-0-625-Biofilm2-3	Steady_054	Biofilm	L2	P11 - Early	0.625 µg/mL	Colony 3	7.50	+	+
BL87-028-T10-0-625-Biofilm3-1	Steady_055	Biofilm	L3	P11 - Early	0.625 µg/mL	Colony 1	6.67	+	+
BL87-028-T10-0-625-Biofilm3-2	Steady_056	Biofilm	L3	P11 - Early	0.625 µg/mL	Colony 2	6.94	+	+
BL87-028-T10-0-625-Biofilm3-3	Steady_057	Biofilm	L3	P11 - Early	0.625 µg/mL	Colony 3	5.83	+	+
BL87-028-T10-0-625-Biofilm4-1	Steady_058	Biofilm	L4	P11 - Early	0.625 µg/mL	Colony 1	5.00	+	
BL87-028-T10-0-625-Biofilm4-2	Steady_059	Biofilm	L4	P11 - Early	0.625 µg/mL	Colony 2	5.56	+	
BL87-028-T10-0-625-Biofilm4-3	Steady_060	Biofilm	L4	P11 - Early	0.625 µg/mL	Colony 3	5.83	+	
BL87-028-T10-No-BC-Biofilm1-1	Steady_061	Biofilm	L1	P11 - Early	No BC	Colony 1	2.50	+	+
BL87-028-T10-No-BC-Biofilm1-2	Steady_062	Biofilm	L1	P11 - Early	No BC	Colony 2	2.50	+	+
BL87-028-T10-No-BC-Biofilm1-3	Steady_063	Biofilm	L1	P11 - Early	No BC	Colony 3	2.50	+	+
BL87-028-T10-No-BC-Biofilm2-1	Steady_064	Biofilm	L2	P11 - Early	No BC	Colony 1	2.50	+	+
BL87-028-T10-No-BC-Biofilm2-2	Steady_065	Biofilm	L2	P11 - Early	No BC	Colony 2	2.50	+	+
BL87-028-T10-No-BC-Biofilm2-3	Steady_066	Biofilm	L2	P11 - Early	No BC	Colony 3	2.50	+	+
BL87-028-T10-No-BC-Biofilm3-1	Steady_067	Biofilm	L3	P11 - Early	No BC	Colony 1	2.50	+	+
BL87-028-T10-No-BC-Biofilm3-2	Steady_068	Biofilm	L3	P11 - Early	No BC	Colony 2	2.50	+	+
BL87-028-T10-No-BC-Biofilm3-3	Steady_069	Biofilm	L3	P11 - Early	No BC	Colony 3	2.50	+	+
BL87-028-T10-No-BC-Biofilm4-1	Steady_070	Biofilm	L4	P11 - Early	No BC	Colony 1	2.50	+	
BL87-028-T10-No-BC-Biofilm4-2	Steady_071	Biofilm	L4	P11 - Early	No BC	Colony 2	2.50	+	
BL87-028-T10-No-BC-Biofilm4-3	Steady_072	Biofilm	L4	P11 - Early	No BC	Colony 3	2.50	+	
BL87-028-T10-0-625-Planktonic1-1	Steady_073	Planktonic	L1	P11 - Early	0.625 µg/mL	Colony 1	7.50	+	+

BL87-028-T10-0-625-Planktonic1-2	Steady_074	Planktonic	L1	P11 - Early	0.625 µg/mL	Colony 2	5.00	+	+
BL87-028-T10-0-625-Planktonic1-3	Steady_075	Planktonic	L1	P11 - Early	0.625 µg/mL	Colony 3	5.00	+	+
BL87-028-T10-0-625-Planktonic2-1	Steady_076	Planktonic	L2	P11 - Early	0.625 µg/mL	Colony 1	5.00	+	+
BL87-028-T10-0-625-Planktonic2-2	Steady_077	Planktonic	L2	P11 - Early	0.625 µg/mL	Colony 2	5.00	+	+
BL87-028-T10-0-625-Planktonic2-3	Steady_078	Planktonic	L2	P11 - Early	0.625 µg/mL	Colony 3	7.50	+	+
BL87-028-T10-0-625-Planktonic3-1	Steady_079	Planktonic	L3	P11 - Early	0.625 µg/mL	Colony 1	7.50	+	+
BL87-028-T10-0-625-Planktonic3-2	Steady_080	Planktonic	L3	P11 - Early	0.625 µg/mL	Colony 2	7.50	+	+
BL87-028-T10-0-625-Planktonic3-3	Steady_081	Planktonic	L3	P11 - Early	0.625 µg/mL	Colony 3	7.50	+	+
BL87-028-T10-0-625-Planktonic4-1	Steady_082	Planktonic	L4	P11 - Early	0.625 µg/mL	Colony 1	5.00	+	
BL87-028-T10-0-625-Planktonic4-2	Steady_083	Planktonic	L4	P11 - Early	0.625 µg/mL	Colony 2	7.22	+	
BL87-028-T10-0-625-Planktonic4-3	Steady_084	Planktonic	L4	P11 - Early	0.625 µg/mL	Colony 3	6.94	+	
BL87-028-T10-No-BC-Planktonic1-1	Steady_085	Planktonic	L1	P11 - Early	No BC	Colony 1	2.50	+	+
BL87-028-T10-No-BC-Planktonic1-2	Steady_086	Planktonic	L1	P11 - Early	No BC	Colony 2	2.50	+	+
BL87-028-T10-No-BC-Planktonic1-3	Steady_087	Planktonic	L1	P11 - Early	No BC	Colony 3	2.50	+	+
BL87-028-T10-No-BC-Planktonic2-1	Steady_088	Planktonic	L2	P11 - Early	No BC	Colony 1	2.50	+	+
BL87-028-T10-No-BC-Planktonic2-2	Steady_089	Planktonic	L2	P11 - Early	No BC	Colony 2	2.50	+	+
BL87-028-T10-No-BC-Planktonic2-3	Steady_090	Planktonic	L2	P11 - Early	No BC	Colony 3	2.50	+	+

BL87-028-T10-No-BC-Planktonic3-1	Steady_091	Planktonic	L3	P11 - Early	No BC	Colony 1	2.50	+	+
BL87-028-T10-No-BC-Planktonic3-2	Steady_092	Planktonic	L3	P11 - Early	No BC	Colony 2	2.50	+	+
BL87-028-T10-No-BC-Planktonic3-3	Steady_093	Planktonic	L3	P11 - Early	No BC	Colony 3	2.50	+	+
BL87-028-T10-No-BC-Planktonic4-1	Steady_094	Planktonic	L4	P11 - Early	No BC	Colony 1	2.50	+	
BL87-028-T10-No-BC-Planktonic4-2	Steady_095	Planktonic	L4	P11 - Early	No BC	Colony 2	2.50	+	
BL87-028-T10-No-BC-Planktonic4-3	Steady_096	Planktonic	L4	P11 - Early	No BC	Colony 3	2.50	+	
BL87-028-T23-0-625-Biofilm1-1	Steady_and_Ladder_097	Biofilm	L1	P22 - Middle	0.625 µg/mL	Colony 1	5.00	+	+
BL87-028-T23-0-625-Biofilm1-2	Steady_and_Ladder_098	Biofilm	L1	P22 - Middle	0.625 µg/mL	Colony 2	5.28	+	+
BL87-028-T23-0-625-Biofilm1-3	Steady_and_Ladder_099	Biofilm	L1	P22 - Middle	0.625 µg/mL	Colony 3	6.11	+	+
BL87-028-T23-0-625-Biofilm2-1	Steady_and_Ladder_100	Biofilm	L2	P22 - Middle	0.625 µg/mL	Colony 1	6.94	+	+
BL87-028-T23-0-625-Biofilm2-2	Steady_and_Ladder_101	Biofilm	L2	P22 - Middle	0.625 µg/mL	Colony 2	7.22	+	+
BL87-028-T23-0-625-Biofilm2-3	Steady_and_Ladder_102	Biofilm	L2	P22 - Middle	0.625 µg/mL	Colony 3	6.94	+	+
BL87-028-T23-0-625-Biofilm3-1	Steady_and_Ladder_103	Biofilm	L3	P22 - Middle	0.625 µg/mL	Colony 1	5.00	+	+
BL87-028-T23-0-625-Biofilm3-2	Steady_and_Ladder_104	Biofilm	L3	P22 - Middle	0.625 µg/mL	Colony 2	5.00	+	+
BL87-028-T23-0-625-Biofilm3-3	Steady_and_Ladder_105	Biofilm	L3	P22 - Middle	0.625 µg/mL	Colony 3	5.00	+	+
BL87-028-T23-0-625-Biofilm4-1	Steady_and_Ladder_106	Biofilm	L4	P22 - Middle	0.625 µg/mL	Colony 1	5.00	+	
BL87-028-T23-0-625-Biofilm4-2	Steady_and_Ladder_107	Biofilm	L4	P22 - Middle	0.625 µg/mL	Colony 2	5.00	+	

BL87-028-T23-0-625-Biofilm4-3	Steady_and_Ladder_108	Biofilm	L4	P22 - Middle	0.625 µg/mL	Colony 3	4.17	+	
BL87-028-T23-No-BC-Biofilm1-1	Steady_and_Ladder_109	Biofilm	L1	P22 - Middle	No BC	Colony 1	2.50	+	+
BL87-028-T23-No-BC-Biofilm1-2	Steady_and_Ladder_110	Biofilm	L1	P22 - Middle	No BC	Colony 2	3.89	+	+
BL87-028-T23-No-BC-Biofilm1-3	Steady_and_Ladder_111	Biofilm	L1	P22 - Middle	No BC	Colony 3	2.50	+	+
BL87-028-T23-No-BC-Biofilm2-1	Steady_and_Ladder_112	Biofilm	L2	P22 - Middle	No BC	Colony 1	2.50	+	+
BL87-028-T23-No-BC-Biofilm2-2	Steady_and_Ladder_113	Biofilm	L2	P22 - Middle	No BC	Colony 2	2.50	+	+
BL87-028-T23-No-BC-Biofilm2-3	Steady_and_Ladder_114	Biofilm	L2	P22 - Middle	No BC	Colony 3	3.06	+	+
BL87-028-T23-No-BC-Biofilm3-1	Steady_and_Ladder_115	Biofilm	L3	P22 - Middle	No BC	Colony 1	3.06	+	+
BL87-028-T23-No-BC-Biofilm3-2	Steady_and_Ladder_116	Biofilm	L3	P22 - Middle	No BC	Colony 2	2.50	+	+
BL87-028-T23-No-BC-Biofilm3-3	Steady_and_Ladder_117	Biofilm	L3	P22 - Middle	No BC	Colony 3	4.44	+	+
BL87-028-T23-No-BC-Biofilm4-1	Steady_and_Ladder_118	Biofilm	L4	P22 - Middle	No BC	Colony 1	3.06	+	
BL87-028-T23-No-BC-Biofilm4-2	Steady_and_Ladder_119	Biofilm	L4	P22 - Middle	No BC	Colony 2	3.89	+	
BL87-028-T23-No-BC-Biofilm4-3	Steady_and_Ladder_120	Biofilm	L4	P22 - Middle	No BC	Colony 3	3.61	+	
BL87-028-T23-0-625-Planktonic1-1	Steady_and_Ladder_121	Planktonic	L1	P22 - Middle	0.625 µg/mL	Colony 1	5.83	+	+
BL87-028-T23-0-625-Planktonic1-2	Steady_and_Ladder_122	Planktonic	L1	P22 - Middle	0.625 µg/mL	Colony 2	6.39	+	+
BL87-028-T23-0-625-Planktonic1-3	Steady_and_Ladder_123	Planktonic	L1	P22 - Middle	0.625 µg/mL	Colony 3	3.33	+	+
BL87-028-T23-0-625-Planktonic2-1	Steady_and_Ladder_124	Planktonic	L2	P22 - Middle	0.625 µg/mL	Colony 1	5.00	+	+
BL87-028-T23-0-625-Planktonic2-2	Steady_and_Ladder_125	Planktonic	L2	P22 - Middle	0.625 µg/mL	Colony 2	5.00	+	+
BL87-028-T23-0-625-Planktonic2-3	Steady_and_Ladder_126	Planktonic	L2	P22 - Middle	0.625 µg/mL	Colony 3	5.83	+	+
BL87-028-T23-0-625-Planktonic3-1	Steady_and_Ladder_127	Planktonic	L3	P22 - Middle	0.625 µg/mL	Colony 1	5.00	+	+
BL87-028-T23-0-625-Planktonic3-2	Steady_and_Ladder_128	Planktonic	L3	P22 - Middle	0.625 µg/mL	Colony 2	5.83	+	+
BL87-028-T23-0-625-Planktonic3-3	Steady_and_Ladder_129	Planktonic	L3	P22 - Middle	0.625	Colony 3	5.00	+	+

					µg/mL				
BL87-028-T23-0-625-Planktonic4-1	Steady_and_Ladder_130	Planktonic	L4	P22 - Middle	0.625 µg/mL	Colony 1	5.00	+	
BL87-028-T23-0-625-Planktonic4-2	Steady_and_Ladder_131	Planktonic	L4	P22 - Middle	0.625 µg/mL	Colony 2	5.83	+	
BL87-028-T23-0-625-Planktonic4-3	Steady_and_Ladder_132	Planktonic	L4	P22 - Middle	0.625 µg/mL	Colony 3	5.83	+	
BL87-028-T23-No-BC-Planktonic1-1	Steady_and_Ladder_133	Planktonic	L1	P22 - Middle	No BC	Colony 1	2.50	+	+
BL87-028-T23-No-BC-Planktonic1-2	Steady_and_Ladder_134	Planktonic	L1	P22 - Middle	No BC	Colony 2	2.50	+	+
BL87-028-T23-No-BC-Planktonic1-3	Steady_and_Ladder_135	Planktonic	L1	P22 - Middle	No BC	Colony 3	3.33	+	+
BL87-028-T23-No-BC-Planktonic2-1	Steady_and_Ladder_136	Planktonic	L2	P22 - Middle	No BC	Colony 1	3.06	+	+
BL87-028-T23-No-BC-Planktonic2-2	Steady_and_Ladder_137	Planktonic	L2	P22 - Middle	No BC	Colony 2	3.89	+	+
BL87-028-T23-No-BC-Planktonic2-3	Steady_and_Ladder_138	Planktonic	L2	P22 - Middle	No BC	Colony 3	3.33	+	+
BL87-028-T23-No-BC-Planktonic3-1	Steady_and_Ladder_139	Planktonic	L3	P22 - Middle	No BC	Colony 1	3.33	+	+
BL87-028-T23-No-BC-Planktonic3-2	Steady_and_Ladder_140	Planktonic	L3	P22 - Middle	No BC	Colony 2	2.50	+	+
BL87-028-T23-No-BC-Planktonic3-3	Steady_and_Ladder_141	Planktonic	L3	P22 - Middle	No BC	Colony 3	2.50	+	+
BL87-028-T23-No-BC-Planktonic4-1	Steady_and_Ladder_142	Planktonic	L4	P22 - Middle	No BC	Colony 1	2.50	+	
BL87-028-T23-No-BC-Planktonic4-2	Steady_and_Ladder_143	Planktonic	L4	P22 - Middle	No BC	Colony 2	2.50	+	
BL87-028-T23-No-BC-Planktonic4-3	Steady_and_Ladder_144	Planktonic	L4	P22 - Middle	No BC	Colony 3	4.17	+	
BL87-028-T30-0-625-Biofilm1-1	Steady_and_Ladder_145	Biofilm	L1	P30 - Late	0.625 µg/mL	Colony 1	7.50	+	+
BL87-028-T30-0-625-Biofilm1-2	Steady_and_Ladder_146	Biofilm	L1	P30 - Late	0.625	Colony 2	7.50	+	+

					µg/mL				
BL87-028-T30-0-625-Biofilm1-3	Steady_and_Ladder_147	Biofilm	L1	P30 - Late	0.625 µg/mL	Colony 3	7.50	+	+
BL87-028-T30-0-625-Biofilm2-1	Steady_and_Ladder_148	Biofilm	L2	P30 - Late	0.625 µg/mL	Colony 1	7.50	+	+
BL87-028-T30-0-625-Biofilm2-2	Steady_and_Ladder_149	Biofilm	L2	P30 - Late	0.625 µg/mL	Colony 2	7.50	+	+
BL87-028-T30-0-625-Biofilm2-3	Steady_and_Ladder_150	Biofilm	L2	P30 - Late	0.625 µg/mL	Colony 3	7.50	+	+
BL87-028-T30-0-625-Biofilm3-1	Steady_and_Ladder_151	Biofilm	L3	P30 - Late	0.625 µg/mL	Colony 1	5.28	+	+
BL87-028-T30-0-625-Biofilm3-2	Steady_and_Ladder_152	Biofilm	L3	P30 - Late	0.625 µg/mL	Colony 2	7.22	+	+
BL87-028-T30-0-625-Biofilm3-3	Steady_and_Ladder_153	Biofilm	L3	P30 - Late	0.625 µg/mL	Colony 3	5.00	+	+
BL87-028-T30-0-625-Biofilm4-1	Steady_and_Ladder_154	Biofilm	L4	P30 - Late	0.625 µg/mL	Colony 1	5.83	+	
BL87-028-T30-0-625-Biofilm4-2	Steady_and_Ladder_155	Biofilm	L4	P30 - Late	0.625 µg/mL	Colony 2	6.39	+	
BL87-028-T30-0-625-Biofilm4-3	Steady_and_Ladder_156	Biofilm	L4	P30 - Late	0.625 µg/mL	Colony 3	6.67	+	
BL87-028-T30-No-BC-Biofilm1-1	Steady_and_Ladder_157	Biofilm	L1	P30 - Late	No BC	Colony 1	2.50	+	+
BL87-028-T30-No-BC-Biofilm1-2	Steady_and_Ladder_158	Biofilm	L1	P30 - Late	No BC	Colony 2	2.50	+	+
BL87-028-T30-No-BC-Biofilm1-3	Steady_and_Ladder_159	Biofilm	L1	P30 - Late	No BC	Colony 3	2.50	+	+
BL87-028-T30-No-BC-Biofilm2-1	Steady_and_Ladder_160	Biofilm	L2	P30 - Late	No BC	Colony 1	2.50	+	+
BL87-028-T30-No-BC-Biofilm2-2	Steady_and_Ladder_161	Biofilm	L2	P30 - Late	No BC	Colony 2	3.06	+	+
BL87-028-T30-No-BC-Biofilm2-3	Steady_and_Ladder_162	Biofilm	L2	P30 - Late	No BC	Colony 3	2.50	+	+
BL87-028-T30-No-BC-Biofilm3-1	Steady_and_Ladder_163	Biofilm	L3	P30 - Late	No BC	Colony 1	2.50	+	+
BL87-028-T30-No-BC-Biofilm3-2	Steady_and_Ladder_164	Biofilm	L3	P30 - Late	No BC	Colony 2	2.50	+	+
BL87-028-T30-No-BC-Biofilm3-3	Steady_and_Ladder_165	Biofilm	L3	P30 - Late	No BC	Colony 3	2.50	+	+
BL87-028-T30-No-BC-Biofilm4-1	Steady_and_Ladder_166	Biofilm	L4	P30 - Late	No BC	Colony 1	2.50	+	

BL87-028-T30-No-BC-Biofilm4-2	Steady_and_Ladder_167	Biofilm	L4	P30 - Late	No BC	Colony 2	2.50	+	
BL87-028-T30-No-BC-Biofilm4-3	Steady_and_Ladder_168	Biofilm	L4	P30 - Late	No BC	Colony 3	2.50	+	
BL87-028-T30-BC-0-625-P1-1	Steady_and_Ladder_169	Planktonic	L1	P30 - Late	0.625 µg/mL	Colony 1	7.50	+	+
BL87-028-T30-BC-0-625-P1-2	Steady_and_Ladder_170	Planktonic	L1	P30 - Late	0.625 µg/mL	Colony 2	7.50	+	+
BL87-028-T30-BC-0-625-P1-3	Steady_and_Ladder_171	Planktonic	L1	P30 - Late	0.625 µg/mL	Colony 3	7.50	+	+
BL87-028-T30-BC-0-625-P2-1	Steady_and_Ladder_172	Planktonic	L2	P30 - Late	0.625 µg/mL	Colony 1	6.94	+	+
BL87-028-T30-BC-0-625-P2-2	Steady_and_Ladder_173	Planktonic	L2	P30 - Late	0.625 µg/mL	Colony 2	6.94	+	+
BL87-028-T30-BC-0-625-P2-3	Steady_and_Ladder_174	Planktonic	L2	P30 - Late	0.625 µg/mL	Colony 3	7.50	+	+
BL87-028-T30-BC-0-625-P3-1	Steady_and_Ladder_175	Planktonic	L3	P30 - Late	0.625 µg/mL	Colony 1	7.50	+	+
BL87-028-T30-BC-0-625-P3-2	Steady_and_Ladder_176	Planktonic	L3	P30 - Late	0.625 µg/mL	Colony 2	7.22	+	+
BL87-028-T30-BC-0-625-P3-3	Steady_and_Ladder_177	Planktonic	L3	P30 - Late	0.625 µg/mL	Colony 3	7.50	+	+
BL87-028-T30-BC-0-625-P4-1	Steady_and_Ladder_178	Planktonic	L4	P30 - Late	0.625 µg/mL	Colony 1	7.50	+	
BL87-028-T30-BC-0-625-P4-2	Steady_and_Ladder_179	Planktonic	L4	P30 - Late	0.625 µg/mL	Colony 2	5.83	+	
BL87-028-T30-BC-0-625-P4-3	Steady_and_Ladder_180	Planktonic	L4	P30 - Late	0.625 µg/mL	Colony 3	7.50	+	
BL87-028-T30-No-BC-Planktonic1-1	Steady_and_Ladder_181	Planktonic	L1	P30 - Late	No BC	Colony 1	2.50	+	+
BL87-028-T30-No-BC-Planktonic1-2	Steady_and_Ladder_182	Planktonic	L1	P30 - Late	No BC	Colony 2	2.50	+	+
BL87-028-T30-No-BC-Planktonic1-3	Steady_and_Ladder_183	Planktonic	L1	P30 - Late	No BC	Colony 3	2.50	+	+
BL87-028-T30-No-BC-Planktonic2-	Steady_and_Ladder_184	Planktonic	L2	P30 - Late	No BC	Colony 1	2.50	+	+

1									
BL87-028-T30-No-BC-Planktonic2-2	Steady_and_Ladder_185	Planktonic	L2	P30 - Late	No BC	Colony 2	2.50	+	+
BL87-028-T30-No-BC-Planktonic2-3	Steady_and_Ladder_186	Planktonic	L2	P30 - Late	No BC	Colony 3	2.50	+	+
BL87-028-T30-No-BC-Planktonic3-1	Steady_and_Ladder_187	Planktonic	L3	P30 - Late	No BC	Colony 1	2.50	+	+
BL87-028-T30-No-BC-Planktonic3-2	Steady_and_Ladder_188	Planktonic	L3	P30 - Late	No BC	Colony 2	2.50	+	+
BL87-028-T30-No-BC-Planktonic3-3	Steady_and_Ladder_189	Planktonic	L3	P30 - Late	No BC	Colony 3	2.50	+	+
BL87-028-T30-No-BC-Planktonic4-1	Steady_and_Ladder_190	Planktonic	L4	P30 - Late	No BC	Colony 1	4.17	+	
BL87-028-T30-No-BC-Planktonic4-2	Steady_and_Ladder_191	Planktonic	L4	P30 - Late	No BC	Colony 2	2.50	+	
BL87-028-T30-No-BC-Planktonic4-3	Steady_and_Ladder_192	Planktonic	L4	P30 - Late	No BC	Colony 3	2.50	+	
BL87-028-T23-1-3-Biofilm1-P	Ladder_193	Biofilm	L1	P22 - Middle	1.3 µg/mL	Population	5.83	+	+
BL87-028-T23-1-3-Biofilm2-P	Ladder_194	Biofilm	L2	P22 - Middle	1.3 µg/mL	Population	6.11	+	+
BL87-028-T23-1-3-Biofilm3-P	Ladder_195	Biofilm	L3	P22 - Middle	1.3 µg/mL	Population	6.67	+	+
BL87-028-T23-1-3-Biofilm4-P	Ladder_196	Biofilm	L4	P22 - Middle	1.3 µg/mL	Population	6.94	+	
BL87-028-T23-1-3-Planktonic1-P	Ladder_197	Planktonic	L1	P22 - Middle	1.3 µg/mL	Population	6.11	+	
BL87-028-T23-1-3-Planktonic2-P	Ladder_198	Planktonic	L2	P22 - Middle	1.3 µg/mL	Population	6.39	+	
BL87-028-T23-1-3-Planktonic3-P	Ladder_199	Planktonic	L3	P22 - Middle	1.3 µg/mL	Population	6.67	+	
BL87-028-T23-1-3-Planktonic4-P	Ladder_200	Planktonic	L4	P22 - Middle	1.3 µg/mL	Population	5.83	+	
BL87-028-T30-BC-1-3-B1-P	Ladder_201	Biofilm	L1	P30 - Late	1.3 µg/mL	Population	7.50	+	+
BL87-028-T30-BC-1-3-B2-P	Ladder_202	Biofilm	L2	P30 - Late	1.3 µg/mL	Population	7.50	+	+
BL87-028-T30-BC-1-3-B3-P	Ladder_203	Biofilm	L3	P30 - Late	1.3 µg/mL	Population	7.50	+	+
BL87-028-T30-BC-1-3-B4-P	Ladder_204	Biofilm	L4	P30 - Late	1.3 µg/mL	Population	7.50	+	
BL87-028-T30-1-75-Biofilm1-P	Ladder_205	Biofilm	L1	P30 - Late	1.75 µg/mL	Population	7.50	+	+

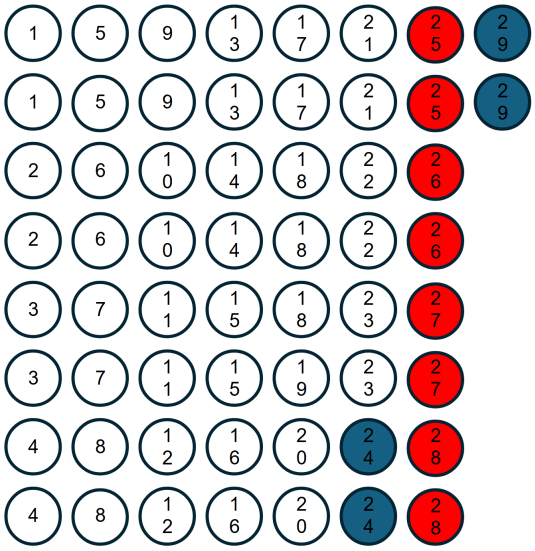
BL87-028-T30-1-75-Biofilm2-P	Ladder_206	Biofilm	L2	P30 - Late	1.75 µg/mL	Population	7.50	+	+
BL87-028-T30-1-75-Biofilm3-P	Ladder_207	Biofilm	L3	P30 - Late	1.75 µg/mL	Population	7.50	+	+
BL87-028-T30-1-75-Biofilm4-P	Ladder_208	Biofilm	L4	P30 - Late	1.75 µg/mL	Population	7.50	+	
BL87-028-T30-BC-1-3-P1-P	Ladder_209	Planktonic	L1	P30 - Late	1.3 µg/mL	Population	7.50	+	+
BL87-028-T30-BC-1-3-P2-P	Ladder_210	Planktonic	L2	P30 - Late	1.3 µg/mL	Population	7.50	+	+
BL87-028-T30-BC-1-3-P3-P	Ladder_211	Planktonic	L3	P30 - Late	1.3 µg/mL	Population	7.50	+	+
BL87-028-T30-BC-1-3-P4-P	Ladder_212	Planktonic	L4	P30 - Late	1.3 µg/mL	Population	7.50	+	
BL87-028-T23-1-3-Biofilm1-1	Ladder_213	Biofilm	L1	P22 - Middle	1.3 µg/mL	Colony 1	5.56	+	+
BL87-028-T23-1-3-Biofilm1-2	Ladder_214	Biofilm	L1	P22 - Middle	1.3 µg/mL	Colony 2	6.11	+	+
BL87-028-T23-1-3-Biofilm1-3	Ladder_215	Biofilm	L1	P22 - Middle	1.3 µg/mL	Colony 3	5.83	+	+
BL87-028-T23-1-3-Biofilm2-1	Ladder_216	Biofilm	L2	P22 - Middle	1.3 µg/mL	Colony 1	5.83	+	+
BL87-028-T23-1-3-Biofilm2-2	Ladder_217	Biofilm	L2	P22 - Middle	1.3 µg/mL	Colony 2	5.83	+	+
BL87-028-T23-1-3-Biofilm2-3	Ladder_218	Biofilm	L2	P22 - Middle	1.3 µg/mL	Colony 3	6.67	+	+
BL87-028-T23-1-3-Biofilm3-1	Ladder_219	Biofilm	L3	P22 - Middle	1.3 µg/mL	Colony 1	6.11	+	+
BL87-028-T23-1-3-Biofilm3-2	Ladder_220	Biofilm	L3	P22 - Middle	1.3 µg/mL	Colony 2	6.39	+	+
BL87-028-T23-1-3-Biofilm3-3	Ladder_221	Biofilm	L3	P22 - Middle	1.3 µg/mL	Colony 3	7.22	+	+
BL87-028-T23-1-3-Biofilm4-1	Ladder_222	Biofilm	L4	P22 - Middle	1.3 µg/mL	Colony 1	7.22	+	
BL87-028-T23-1-3-Biofilm4-2	Ladder_223	Biofilm	L4	P22 - Middle	1.3 µg/mL	Colony 2	6.94	+	
BL87-028-T23-1-3-Biofilm4-3	Ladder_224	Biofilm	L4	P22 - Middle	1.3 µg/mL	Colony 3	7.22	+	
BL87-028-T23-1-3-Planktonic1-1	Ladder_225	Planktonic	L1	P22 - Middle	1.3 µg/mL	Colony 1	5.83	+	
BL87-028-T23-1-3-Planktonic1-2	Ladder_226	Planktonic	L1	P22 - Middle	1.3 µg/mL	Colony 2	5.56	+	
BL87-028-T23-1-3-Planktonic1-3	Ladder_227	Planktonic	L1	P22 - Middle	1.3 µg/mL	Colony 3	5.56	+	
BL87-028-T23-1-3-Planktonic2-1	Ladder_228	Planktonic	L2	P22 - Middle	1.3 µg/mL	Colony 1	5.83	+	
BL87-028-T23-1-3-Planktonic2-2	Ladder_229	Planktonic	L2	P22 - Middle	1.3 µg/mL	Colony 2	6.11	+	
BL87-028-T23-1-3-Planktonic2-3	Ladder_230	Planktonic	L2	P22 - Middle	1.3 µg/mL	Colony 3	6.94	+	

BL87-028-T23-1-3-Planktonic3-1	Ladder_231	Planktonic	L3	P22 - Middle	1.3 µg/mL	Colony 1	6.11	+	
BL87-028-T23-1-3-Planktonic3-2	Ladder_232	Planktonic	L3	P22 - Middle	1.3 µg/mL	Colony 2	6.11	+	
BL87-028-T23-1-3-Planktonic3-3	Ladder_233	Planktonic	L3	P22 - Middle	1.3 µg/mL	Colony 3	6.11	+	
BL87-028-T23-1-3-Planktonic4-1	Ladder_234	Planktonic	L4	P22 - Middle	1.3 µg/mL	Colony 1	5.00	+	
BL87-028-T23-1-3-Planktonic4-2	Ladder_235	Planktonic	L4	P22 - Middle	1.3 µg/mL	Colony 2	6.67	+	
BL87-028-T23-1-3-Planktonic4-3	Ladder_236	Planktonic	L4	P22 - Middle	1.3 µg/mL	Colony 3	5.83	+	
BL87-028-T30-BC-1-3-B1-1	Ladder_237	Biofilm	L1	P30 - Late	1.3 µg/mL	Colony 1	7.50	+	+
BL87-028-T30-BC-1-3-B1-2	Ladder_238	Biofilm	L1	P30 - Late	1.3 µg/mL	Colony 2	7.50	+	+
BL87-028-T30-BC-1-3-B1-3	Ladder_239	Biofilm	L1	P30 - Late	1.3 µg/mL	Colony 3	7.50	+	+
BL87-028-T30-BC-1-3-B2-1	Ladder_240	Biofilm	L2	P30 - Late	1.3 µg/mL	Colony 1	7.50	+	+
BL87-028-T30-BC-1-3-B2-2	Ladder_241	Biofilm	L2	P30 - Late	1.3 µg/mL	Colony 2	7.50	+	+
BL87-028-T30-BC-1-3-B2-3	Ladder_242	Biofilm	L2	P30 - Late	1.3 µg/mL	Colony 3	7.50	+	+
BL87-028-T30-BC-1-3-B3-1	Ladder_243	Biofilm	L3	P30 - Late	1.3 µg/mL	Colony 1	7.50	+	+
BL87-028-T30-BC-1-3-B3-2	Ladder_244	Biofilm	L3	P30 - Late	1.3 µg/mL	Colony 2	7.50	+	+
BL87-028-T30-BC-1-3-B3-3	Ladder_245	Biofilm	L3	P30 - Late	1.3 µg/mL	Colony 3	7.50	+	+
BL87-028-T30-BC-1-3-B4-1	Ladder_246	Biofilm	L4	P30 - Late	1.3 µg/mL	Colony 1	7.50	+	
BL87-028-T30-BC-1-3-B4-2	Ladder_247	Biofilm	L4	P30 - Late	1.3 µg/mL	Colony 2	7.50	+	
BL87-028-T30-BC-1-3-B4-3	Ladder_248	Biofilm	L4	P30 - Late	1.3 µg/mL	Colony 3	7.50	+	
BL87-028-T30-1-75-Biofilm1-1	Ladder_249	Biofilm	L1	P30 - Late	1.75 µg/mL	Colony 1	7.50	+	+
BL87-028-T30-1-75-Biofilm1-2	Ladder_250	Biofilm	L1	P30 - Late	1.75 µg/mL	Colony 2	7.50	+	+
BL87-028-T30-1-75-Biofilm1-3	Ladder_251	Biofilm	L1	P30 - Late	1.75 µg/mL	Colony 3	7.50	+	+
BL87-028-T30-1-75-Biofilm2-1	Ladder_252	Biofilm	L2	P30 - Late	1.75 µg/mL	Colony 1	7.50	+	+
BL87-028-T30-1-75-Biofilm2-2	Ladder_253	Biofilm	L2	P30 - Late	1.75 µg/mL	Colony 2	7.50	+	+
BL87-028-T30-1-75-Biofilm2-3	Ladder_254	Biofilm	L2	P30 - Late	1.75	Colony 3	7.50	+	+

					µg/mL				
BL87-028-T30-1-75-Biofilm3-1	Ladder_255	Biofilm	L3	P30 - Late	1.75 µg/mL	Colony 1	7.50	+	+
BL87-028-T30-1-75-Biofilm3-2	Ladder_256	Biofilm	L3	P30 - Late	1.75 µg/mL	Colony 2	7.08	+	+
BL87-028-T30-1-75-Biofilm3-3	Ladder_257	Biofilm	L3	P30 - Late	1.75 µg/mL	Colony 3	7.50	+	+
BL87-028-T30-1-75-Biofilm4-1	Ladder_258	Biofilm	L4	P30 - Late	1.75 µg/mL	Colony 1	7.50	+	
BL87-028-T30-1-75-Biofilm4-2	Ladder_259	Biofilm	L4	P30 - Late	1.75 µg/mL	Colony 2	7.50	+	
BL87-028-T30-1-75-Biofilm4-3	Ladder_260	Biofilm	L4	P30 - Late	1.75 µg/mL	Colony 3	7.50	+	
BL87-028-T30-BC-1-3-P1-1	Ladder_261	Planktonic	L1	P30 - Late	1.3 µg/mL	Colony 1	7.50	+	+
BL87-028-T30-BC-1-3-P1-2	Ladder_262	Planktonic	L1	P30 - Late	1.3 µg/mL	Colony 2	7.50	+	+
BL87-028-T30-BC-1-3-P1-3	Ladder_263	Planktonic	L1	P30 - Late	1.3 µg/mL	Colony 3	7.50	+	+
BL87-028-T30-BC-1-3-P2-1	Ladder_264	Planktonic	L2	P30 - Late	1.3 µg/mL	Colony 1	7.50	+	+
BL87-028-T30-BC-1-3-P2-2	Ladder_265	Planktonic	L2	P30 - Late	1.3 µg/mL	Colony 2	7.50	+	+
BL87-028-T30-BC-1-3-P2-3	Ladder_266	Planktonic	L2	P30 - Late	1.3 µg/mL	Colony 3	7.50	+	+
BL87-028-T30-BC-1-3-P3-1	Ladder_267	Planktonic	L3	P30 - Late	1.3 µg/mL	Colony 1	7.50	+	
BL87-028-T30-BC-1-3-P3-2	Ladder_268	Planktonic	L3	P30 - Late	1.3 µg/mL	Colony 2	7.50	+	+
BL87-028-T30-BC-1-3-P3-3	Ladder_269	Planktonic	L3	P30 - Late	1.3 µg/mL	Colony 3	7.50	+	+
BL87-028-T30-BC-1-3-P4-1	Ladder_270	Planktonic	L4	P30 - Late	1.3 µg/mL	Colony 1	7.50	+	
BL87-028-T30-BC-1-3-P4-2	Ladder_271	Planktonic	L4	P30 - Late	1.3 µg/mL	Colony 2	7.50	+	
BL87-028-T30-BC-1-3-P4-3	Ladder_272	Planktonic	L4	P30 - Late	1.3 µg/mL	Colony 3	7.50	+	

Appendix 6. Layout of the MIC of BC test for the FSA panel isolates performed by agar dilution method, corresponding to the results demonstrated in **Figure 6**. For the control, strain 08-5578 that exhibits reduced susceptibility to BC was used, while strain 81-0861 served as the susceptible control (Kovacevic et al., 2016).

A



B

1	LS12/71
2	LS12/142
3	LS12/177
4	LS12/211
5	LS12/257
6	LS12/426
7	LS12/453
8	LS12/495
9	LS12/505
10	LS12/519
11	LS12/521
12	LS12/522
13	LS12/570
14	LS12/579
15	LS12/580

16	LS12/646
17	LS12/685
18	LS12/741
19	LS12/808
20	LS12/847
21	LS12/859
22	LS12/964
23	LS12/970
24	Sensitive
25	Tolerant
26	Tolerant
27	Tolerant
28	Tolerant
29	Sensitive

Appendix 7. Statistical analysis using one-way ANOVA, corresponding to **Figure 7**, assessing the biofilm-forming capacity of FSA panel isolates as measured by the crystal violet assay. The table includes mean differences, q values (adjusted for multiple comparisons), statistical significance, a significance of group comparisons ($p < 0.05$ (*), $p < 0.01$ (**), $p < 0.001$ (***), and $p < 0.0001$ (****)), and the 95% confidence intervals (CIs) for the differences. Analysis was performed using GraphPad Prism.

Tukey's Multiple Comparison Test	Mean Diff.	q	Significant ? P < 0.05?	Summary	95% CI of diff
LS12/71 vs LS12/142	-0.2906	5.95	Yes	**	-0.5454 to -0.03583
LS12/71 vs LS12/177	-0.2078	4.208	No	ns	-0.4655 to 0.04983
LS12/71 vs LS12/211	-0.5127	10.38	Yes	***	-0.7704 to -0.2551
LS12/71 vs LS12/257	0.2602	5.383	Yes	*	0.008059 to 0.5123
LS12/71 vs LS12/426	-0.5087	10.18	Yes	***	-0.7694 to -0.2479
LS12/71 vs LS12/453	-0.07688	1.591	No	ns	-0.3290 to 0.1752
LS12/71 vs LS12/495	-0.2287	4.732	No	ns	-0.4808 to 0.02343
LS12/71 vs LS12/505	-0.3481	6.964	Yes	***	-0.6089 to -0.08736
LS12/71 vs LS12/519	0.4954	10.25	Yes	***	0.2433 to 0.7475
LS12/71 vs LS12/521	0.08163	1.689	No	ns	-0.1705 to 0.3337
LS12/71 vs LS12/522	-0.1905	3.857	No	ns	-0.4482 to 0.06715
LS12/71 vs LS12/570	-0.1741	3.602	No	ns	-0.4262 to 0.07805
LS12/71 vs LS12/579	-0.04486	0.9283	No	ns	-0.2970 to 0.2072
LS12/71 vs LS12/580	-0.05416	1.121	No	ns	-0.3063 to 0.1979
LS12/71 vs LS12/646	-0.4647	9.296	Yes	***	-0.7254 to -0.2039
LS12/71 vs LS12/685	-0.4255	8.805	Yes	***	-0.6776 to -0.1734
LS12/71 vs LS12/741	-1.774	36.33	Yes	***	-2.029 to -1.520
LS12/71 vs LS12/808	-0.3049	6.309	Yes	**	-0.5570 to -0.05280
LS12/71 vs LS12/847	-0.3961	8.195	Yes	***	-0.6482 to -0.1440
LS12/71 vs LS12/859	0.1032	2.135	No	ns	-0.1489 to 0.3553
LS12/71 vs LS12/970	-0.6784	14.04	Yes	***	-0.9305 to -0.4263
LS12/71 vs LS12/964	-0.417	8.629	Yes	***	-0.6691 to -0.1649
LS12/142 vs LS12/177	0.08278	1.676	No	ns	-0.1749 to 0.3404
LS12/142 vs LS12/211	-0.2222	4.498	No	ns	-0.4798 to 0.03550
LS12/142 vs LS12/257	0.5508	11.4	Yes	***	0.2987 to 0.8029
LS12/142 vs LS12/426	-0.2181	4.362	No	ns	-0.4788 to 0.04270
LS12/142 vs LS12/453	0.2137	4.422	No	ns	-0.03838 to 0.4658
LS12/142 vs LS12/495	0.06193	1.281	No	ns	-0.1902 to 0.3140
LS12/142 vs LS12/505	-0.05753	1.151	No	ns	-0.3183 to 0.2032
LS12/142 vs LS12/519	0.786	16.27	Yes	***	0.5339 to 1.038
LS12/142 vs LS12/521	0.3722	7.702	Yes	***	0.1201 to 0.6243
LS12/142 vs LS12/522	0.1001	2.027	No	ns	-0.1576 to 0.3577
LS12/142 vs LS12/570	0.1165	2.412	No	ns	-0.1356 to 0.3686
LS12/142 vs LS12/579	0.2457	5.085	No	ns	-0.006367 to 0.4978
LS12/142 vs LS12/580	0.2364	4.893	No	ns	-0.01566 to 0.4885
LS12/142 vs LS12/646	-0.1741	3.482	No	ns	-0.4348 to 0.08669

LS12/142 vs LS12/685	-0.1349	2.791	No	ns	-0.3870 to 0.1172
LS12/142 vs LS12/741	-1.484	30.38	Yes	***	-1.738 to -1.229
LS12/142 vs LS12/808	-0.01431	0.2961	No	ns	-0.2664 to 0.2378
LS12/142 vs LS12/847	-0.1055	2.182	No	ns	-0.3576 to 0.1466
LS12/142 vs LS12/859	0.3938	8.148	Yes	***	0.1417 to 0.6459
LS12/142 vs LS12/970	-0.3878	8.025	Yes	***	-0.6399 to -0.1357
LS12/142 vs LS12/964	-0.1264	2.616	No	ns	-0.3785 to 0.1257
LS12/177 vs LS12/211	-0.3049	6.106	Yes	**	-0.5654 to -0.04443
LS12/177 vs LS12/257	0.468	9.573	Yes	***	0.2130 to 0.7230
LS12/177 vs LS12/426	-0.3008	5.954	Yes	**	-0.5644 to -0.03726
LS12/177 vs LS12/453	0.1309	2.679	No	ns	-0.1241 to 0.3860
LS12/177 vs LS12/495	-0.02085	0.4266	No	ns	-0.2759 to 0.2342
LS12/177 vs LS12/505	-0.1403	2.777	No	ns	-0.4039 to 0.1233
LS12/177 vs LS12/519	0.7033	14.39	Yes	***	0.4482 to 0.9583
LS12/177 vs LS12/521	0.2894	5.921	Yes	**	0.03443 to 0.5445
LS12/177 vs LS12/522	0.01731	0.3467	No	ns	-0.2432 to 0.2778
LS12/177 vs LS12/570	0.03377	0.6907	No	ns	-0.2212 to 0.2888
LS12/177 vs LS12/579	0.163	3.334	No	ns	-0.09205 to 0.4180
LS12/177 vs LS12/580	0.1537	3.143	No	ns	-0.1013 to 0.4087
LS12/177 vs LS12/646	-0.2569	5.084	No	ns	-0.5204 to 0.006723
LS12/177 vs LS12/685	-0.2177	4.453	No	ns	-0.4727 to 0.03734
LS12/177 vs LS12/741	-1.566	31.72	Yes	***	-1.824 to -1.309
LS12/177 vs LS12/808	-0.09709	1.986	No	ns	-0.3521 to 0.1579
LS12/177 vs LS12/847	-0.1882	3.851	No	ns	-0.4432 to 0.06678
LS12/177 vs LS12/859	0.311	6.362	Yes	**	0.05597 to 0.5660
LS12/177 vs LS12/970	-0.4706	9.626	Yes	***	-0.7256 to -0.2156
LS12/177 vs LS12/964	-0.2092	4.279	No	ns	-0.4642 to 0.04582
LS12/211 vs LS12/257	0.7729	15.81	Yes	***	0.5179 to 1.028
LS12/211 vs LS12/426	0.004086	0.08088	No	ns	-0.2595 to 0.2677
LS12/211 vs LS12/453	0.4359	8.916	Yes	***	0.1809 to 0.6909
LS12/211 vs LS12/495	0.2841	5.811	Yes	*	0.02907 to 0.5391
LS12/211 vs LS12/505	0.1646	3.258	No	ns	-0.09896 to 0.4282
LS12/211 vs LS12/519	1.008	20.62	Yes	***	0.7532 to 1.263
LS12/211 vs LS12/521	0.5944	12.16	Yes	***	0.3394 to 0.8494
LS12/211 vs LS12/522	0.3222	6.453	Yes	**	0.06175 to 0.5827
LS12/211 vs LS12/570	0.3387	6.929	Yes	***	0.08368 to 0.5937
LS12/211 vs LS12/579	0.4679	9.571	Yes	***	0.2129 to 0.7229
LS12/211 vs LS12/580	0.4586	9.381	Yes	***	0.2036 to 0.7136
LS12/211 vs LS12/646	0.04807	0.9514	No	ns	-0.2155 to 0.3117
LS12/211 vs LS12/685	0.08725	1.785	No	ns	-0.1678 to 0.3423
LS12/211 vs LS12/741	-1.262	25.54	Yes	***	-1.519 to -1.004
LS12/211 vs LS12/808	0.2078	4.252	No	ns	-0.04717 to 0.4629
LS12/211 vs LS12/847	0.1167	2.387	No	ns	-0.1383 to 0.3717
LS12/211 vs LS12/859	0.6159	12.6	Yes	***	0.3609 to 0.8709
LS12/211 vs LS12/970	-0.1657	3.389	No	ns	-0.4207 to 0.08936

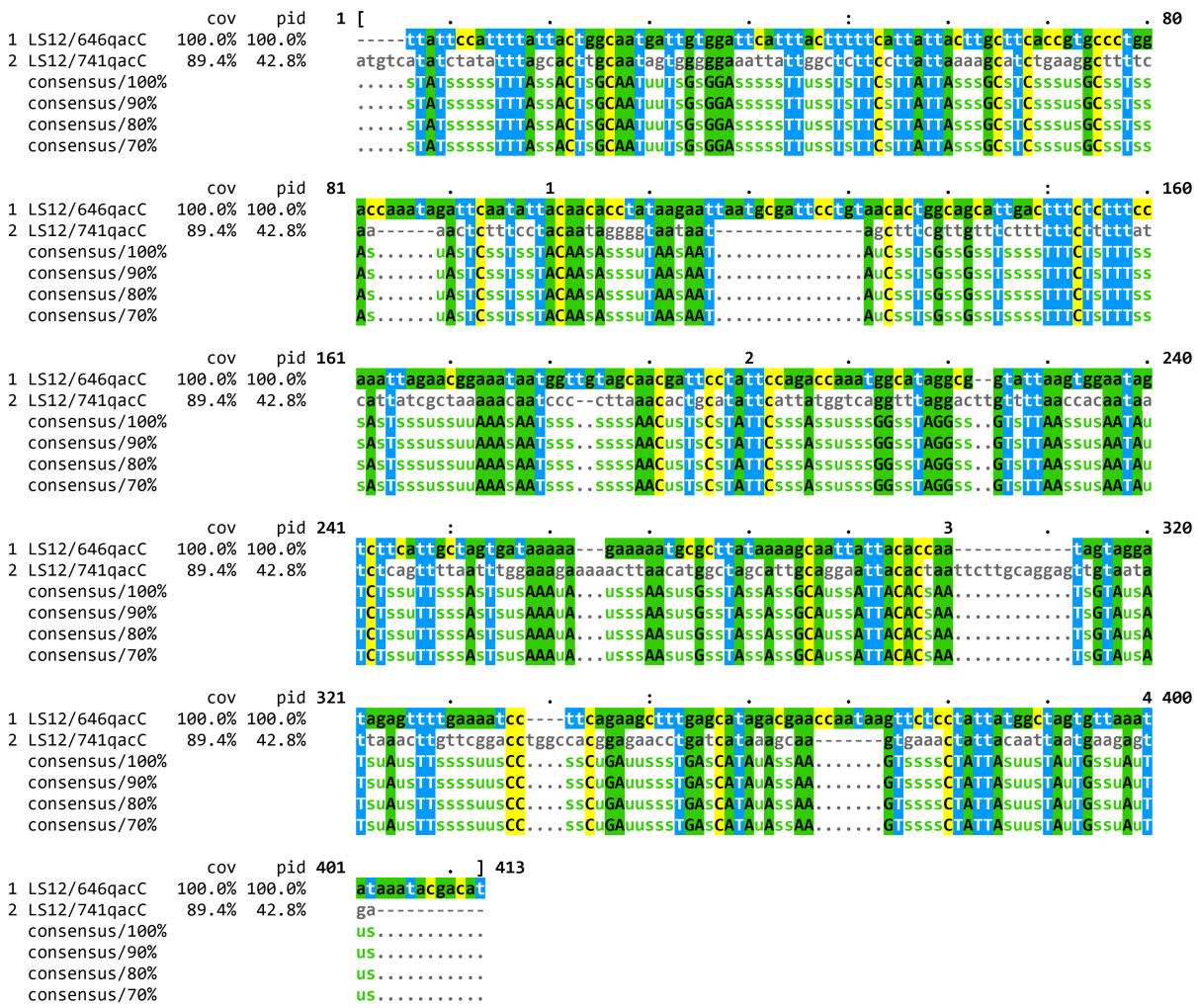
LS12/211 vs LS12/964	0.09574	1.959	No	ns	-0.1593 to 0.3508
LS12/257 vs LS12/426	-0.7688	15.54	Yes	***	-1.027 to -0.5107
LS12/257 vs LS12/453	-0.337	7.05	Yes	***	-0.5864 to -0.08763
LS12/257 vs LS12/495	-0.4888	10.22	Yes	***	-0.7382 to -0.2394
LS12/257 vs LS12/505	-0.6083	12.29	Yes	***	-0.8665 to -0.3501
LS12/257 vs LS12/519	0.2353	4.921	No	ns	-0.01413 to 0.4847
LS12/257 vs LS12/521	-0.1785	3.734	No	ns	-0.4279 to 0.07087
LS12/257 vs LS12/522	-0.4507	9.219	Yes	***	-0.7057 to -0.1957
LS12/257 vs LS12/570	-0.4342	9.082	Yes	***	-0.6836 to -0.1848
LS12/257 vs LS12/579	-0.305	6.38	Yes	**	-0.5544 to -0.05562
LS12/257 vs LS12/580	-0.3143	6.574	Yes	**	-0.5637 to -0.06491
LS12/257 vs LS12/646	-0.7248	14.65	Yes	***	-0.9830 to -0.4667
LS12/257 vs LS12/685	-0.6857	14.34	Yes	***	-0.9351 to -0.4362
LS12/257 vs LS12/741	-2.034	42.1	Yes	***	-2.287 to -1.782
LS12/257 vs LS12/808	-0.5651	11.82	Yes	***	-0.8145 to -0.3157
LS12/257 vs LS12/847	-0.6562	13.73	Yes	***	-0.9056 to -0.4068
LS12/257 vs LS12/859	-0.157	3.284	No	ns	-0.4064 to 0.09241
LS12/257 vs LS12/970	-0.9386	19.63	Yes	***	-1.188 to -0.6892
LS12/257 vs LS12/964	-0.6772	14.16	Yes	***	-0.9266 to -0.4278
LS12/426 vs LS12/453	0.4318	8.725	Yes	***	0.1736 to 0.6899
LS12/426 vs LS12/495	0.28	5.658	Yes	*	0.02183 to 0.5382
LS12/426 vs LS12/505	0.1605	3.141	No	ns	-0.1061 to 0.4272
LS12/426 vs LS12/519	1.004	20.29	Yes	***	0.7459 to 1.262
LS12/426 vs LS12/521	0.5903	11.93	Yes	***	0.3321 to 0.8484
LS12/426 vs LS12/522	0.3182	6.297	Yes	**	0.05458 to 0.5817
LS12/426 vs LS12/570	0.3346	6.761	Yes	***	0.07645 to 0.5928
LS12/426 vs LS12/579	0.4638	9.372	Yes	***	0.2056 to 0.7220
LS12/426 vs LS12/580	0.4545	9.184	Yes	***	0.1963 to 0.7127
LS12/426 vs LS12/646	0.04399	0.8606	No	ns	-0.2226 to 0.3106
LS12/426 vs LS12/685	0.08317	1.681	No	ns	-0.1750 to 0.3413
LS12/426 vs LS12/741	-1.266	25.32	Yes	***	-1.526 to -1.005
LS12/426 vs LS12/808	0.2038	4.117	No	ns	-0.05441 to 0.4619
LS12/426 vs LS12/847	0.1126	2.275	No	ns	-0.1456 to 0.3708
LS12/426 vs LS12/859	0.6118	12.36	Yes	***	0.3537 to 0.8700
LS12/426 vs LS12/970	-0.1697	3.43	No	ns	-0.4279 to 0.08842
LS12/426 vs LS12/964	0.09165	1.852	No	ns	-0.1665 to 0.3498
LS12/453 vs LS12/495	-0.1518	3.175	No	ns	-0.4012 to 0.09761
LS12/453 vs LS12/505	-0.2713	5.481	Yes	*	-0.5294 to -0.01309
LS12/453 vs LS12/519	0.5723	11.97	Yes	***	0.3229 to 0.8217
LS12/453 vs LS12/521	0.1585	3.315	No	ns	-0.09091 to 0.4079
LS12/453 vs LS12/522	-0.1136	2.324	No	ns	-0.3686 to 0.1414
LS12/453 vs LS12/570	-0.09718	2.033	No	ns	-0.3466 to 0.1522
LS12/453 vs LS12/579	0.03202	0.6696	No	ns	-0.2174 to 0.2814
LS12/453 vs LS12/580	0.02272	0.4752	No	ns	-0.2267 to 0.2721
LS12/453 vs LS12/646	-0.3878	7.836	Yes	***	-0.6460 to -0.1296

LS12/453 vs LS12/685	-0.3486	7.292	Yes	***	-0.5980 to -0.09921
LS12/453 vs LS12/741	-1.697	35.12	Yes	***	-1.950 to -1.445
LS12/453 vs LS12/808	-0.228	4.77	No	ns	-0.4774 to 0.02138
LS12/453 vs LS12/847	-0.3192	6.676	Yes	**	-0.5686 to -0.06977
LS12/453 vs LS12/859	0.18	3.766	No	ns	-0.06937 to 0.4294
LS12/453 vs LS12/970	-0.6015	12.58	Yes	***	-0.8509 to -0.3521
LS12/453 vs LS12/964	-0.3401	7.114	Yes	***	-0.5895 to -0.09072
LS12/495 vs LS12/505	-0.1195	2.414	No	ns	-0.3776 to 0.1387
LS12/495 vs LS12/519	0.7241	15.15	Yes	***	0.4747 to 0.9735
LS12/495 vs LS12/521	0.3103	6.49	Yes	**	0.06089 to 0.5597
LS12/495 vs LS12/522	0.03817	0.7808	No	ns	-0.2168 to 0.2932
LS12/495 vs LS12/570	0.05462	1.142	No	ns	-0.1948 to 0.3040
LS12/495 vs LS12/579	0.1838	3.845	No	ns	-0.06560 to 0.4332
LS12/495 vs LS12/580	0.1745	3.65	No	ns	-0.07489 to 0.4239
LS12/495 vs LS12/646	-0.236	4.769	No	ns	-0.4942 to 0.02216
LS12/495 vs LS12/685	-0.1968	4.117	No	ns	-0.4462 to 0.05258
LS12/495 vs LS12/741	-1.546	31.98	Yes	***	-1.798 to -1.294
LS12/495 vs LS12/808	-0.07624	1.595	No	ns	-0.3256 to 0.1732
LS12/495 vs LS12/847	-0.1674	3.501	No	ns	-0.4168 to 0.08202
LS12/495 vs LS12/859	0.3318	6.941	Yes	***	0.08242 to 0.5812
LS12/495 vs LS12/970	-0.4497	9.407	Yes	***	-0.6991 to -0.2003
LS12/495 vs LS12/964	-0.1883	3.939	No	ns	-0.4377 to 0.06107
LS12/505 vs LS12/519	0.8436	17.05	Yes	***	0.5854 to 1.102
LS12/505 vs LS12/521	0.4298	8.684	Yes	***	0.1716 to 0.6879
LS12/505 vs LS12/522	0.1576	3.12	No	ns	-0.1060 to 0.4212
LS12/505 vs LS12/570	0.1741	3.518	No	ns	-0.08408 to 0.4322
LS12/505 vs LS12/579	0.3033	6.128	Yes	**	0.04511 to 0.5614
LS12/505 vs LS12/580	0.294	5.94	Yes	**	0.03581 to 0.5521
LS12/505 vs LS12/646	-0.1165	2.28	No	ns	-0.3832 to 0.1501
LS12/505 vs LS12/685	-0.07736	1.563	No	ns	-0.3355 to 0.1808
LS12/505 vs LS12/741	-1.426	28.53	Yes	***	-1.687 to -1.165
LS12/505 vs LS12/808	0.04322	0.8734	No	ns	-0.2149 to 0.3014
LS12/505 vs LS12/847	-0.04792	0.9684	No	ns	-0.3061 to 0.2102
LS12/505 vs LS12/859	0.4513	9.119	Yes	***	0.1931 to 0.7095
LS12/505 vs LS12/970	-0.3303	6.674	Yes	**	-0.5884 to -0.07211
LS12/505 vs LS12/964	-0.06888	1.392	No	ns	-0.3270 to 0.1893
LS12/519 vs LS12/521	-0.4138	8.655	Yes	***	-0.6632 to -0.1644
LS12/519 vs LS12/522	-0.6859	14.03	Yes	***	-0.9410 to -0.4309
LS12/519 vs LS12/570	-0.6695	14	Yes	***	-0.9189 to -0.4201
LS12/519 vs LS12/579	-0.5403	11.3	Yes	***	-0.7897 to -0.2909
LS12/519 vs LS12/580	-0.5496	11.5	Yes	***	-0.7990 to -0.3002
LS12/519 vs LS12/646	-0.9601	19.4	Yes	***	-1.218 to -0.7020
LS12/519 vs LS12/685	-0.9209	19.26	Yes	***	-1.170 to -0.6715
LS12/519 vs LS12/741	-2.27	46.97	Yes	***	-2.522 to -2.018
LS12/519 vs LS12/808	-0.8003	16.74	Yes	***	-1.050 to -0.5509

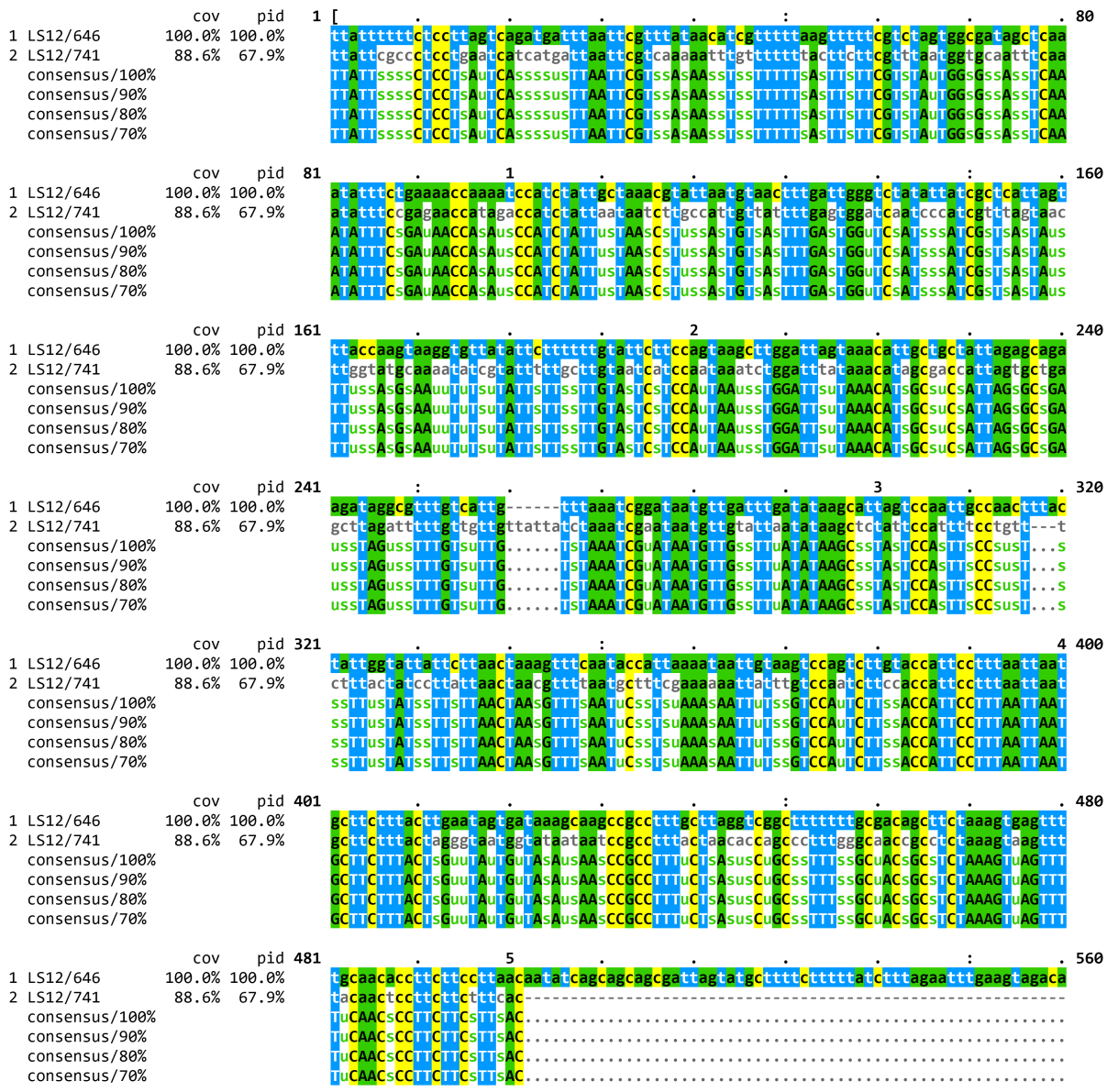
LS12/519 vs LS12/847	-0.8915	18.65	Yes	***	-1.141 to -0.6421
LS12/519 vs LS12/859	-0.3923	8.205	Yes	***	-0.6417 to -0.1429
LS12/519 vs LS12/970	-1.174	24.55	Yes	***	-1.423 to -0.9244
LS12/519 vs LS12/964	-0.9124	19.08	Yes	***	-1.162 to -0.6630
LS12/521 vs LS12/522	-0.2721	5.567	Yes	*	-0.5271 to -0.01712
LS12/521 vs LS12/570	-0.2557	5.348	Yes	*	-0.5051 to -0.006270
LS12/521 vs LS12/579	-0.1265	2.646	No	ns	-0.3759 to 0.1229
LS12/521 vs LS12/580	-0.1358	2.84	No	ns	-0.3852 to 0.1136
LS12/521 vs LS12/646	-0.5463	11.04	Yes	***	-0.8045 to -0.2881
LS12/521 vs LS12/685	-0.5071	10.61	Yes	***	-0.7565 to -0.2577
LS12/521 vs LS12/741	-1.856	38.4	Yes	***	-2.108 to -1.604
LS12/521 vs LS12/808	-0.3865	8.085	Yes	***	-0.6359 to -0.1371
LS12/521 vs LS12/847	-0.4777	9.991	Yes	***	-0.7271 to -0.2283
LS12/521 vs LS12/859	0.02154	0.4504	No	ns	-0.2279 to 0.2709
LS12/521 vs LS12/970	-0.76	15.9	Yes	***	-1.009 to -0.5106
LS12/521 vs LS12/964	-0.4986	10.43	Yes	***	-0.7480 to -0.2492
LS12/522 vs LS12/570	0.01645	0.3365	No	ns	-0.2386 to 0.2715
LS12/522 vs LS12/579	0.1456	2.979	No	ns	-0.1094 to 0.4007
LS12/522 vs LS12/580	0.1363	2.789	No	ns	-0.1187 to 0.3914
LS12/522 vs LS12/646	-0.2742	5.426	Yes	*	-0.5378 to -0.01059
LS12/522 vs LS12/685	-0.235	4.807	No	ns	-0.4900 to 0.02002
LS12/522 vs LS12/741	-1.584	32.07	Yes	***	-1.841 to -1.326
LS12/522 vs LS12/808	-0.1144	2.34	No	ns	-0.3694 to 0.1406
LS12/522 vs LS12/847	-0.2056	4.205	No	ns	-0.4606 to 0.04946
LS12/522 vs LS12/859	0.2937	6.007	Yes	**	0.03865 to 0.5487
LS12/522 vs LS12/970	-0.4879	9.981	Yes	***	-0.7429 to -0.2329
LS12/522 vs LS12/964	-0.2265	4.633	No	ns	-0.4815 to 0.02851
LS12/570 vs LS12/579	0.1292	2.702	No	ns	-0.1202 to 0.3786
LS12/570 vs LS12/580	0.1199	2.508	No	ns	-0.1295 to 0.3693
LS12/570 vs LS12/646	-0.2906	5.873	Yes	*	-0.5488 to -0.03246
LS12/570 vs LS12/685	-0.2514	5.259	Yes	*	-0.5008 to -0.002035
LS12/570 vs LS12/741	-1.6	33.11	Yes	***	-1.852 to -1.348
LS12/570 vs LS12/808	-0.1309	2.737	No	ns	-0.3803 to 0.1186
LS12/570 vs LS12/847	-0.222	4.643	No	ns	-0.4714 to 0.02741
LS12/570 vs LS12/859	0.2772	5.798	Yes	*	0.02781 to 0.5266
LS12/570 vs LS12/970	-0.5043	10.55	Yes	***	-0.7538 to -0.2549
LS12/570 vs LS12/964	-0.243	5.082	No	ns	-0.4924 to 0.006452
LS12/579 vs LS12/580	-0.0093	0.1944	No	ns	-0.2587 to 0.2401
LS12/579 vs LS12/646	-0.4198	8.483	Yes	***	-0.6780 to -0.1617
LS12/579 vs LS12/685	-0.3806	7.961	Yes	***	-0.6300 to -0.1312
LS12/579 vs LS12/741	-1.729	35.79	Yes	***	-1.982 to -1.477
LS12/579 vs LS12/808	-0.26	5.439	Yes	*	-0.5095 to -0.01064
LS12/579 vs LS12/847	-0.3512	7.346	Yes	***	-0.6006 to -0.1018
LS12/579 vs LS12/859	0.148	3.096	No	ns	-0.1014 to 0.3974
LS12/579 vs LS12/970	-0.6335	13.25	Yes	***	-0.8829 to -0.3841

LS12/579 vs LS12/964	-0.3721	7.784	Yes	***	-0.6216 to -0.1227
LS12/580 vs LS12/646	-0.4105	8.295	Yes	***	-0.6687 to -0.1524
LS12/580 vs LS12/685	-0.3713	7.767	Yes	***	-0.6207 to -0.1219
LS12/580 vs LS12/741	-1.72	35.59	Yes	***	-1.972 to -1.468
LS12/580 vs LS12/808	-0.2508	5.245	Yes	*	-0.5002 to -0.001344
LS12/580 vs LS12/847	-0.3419	7.151	Yes	***	-0.5913 to -0.09249
LS12/580 vs LS12/859	0.1573	3.29	No	ns	-0.09209 to 0.4067
LS12/580 vs LS12/970	-0.6242	13.06	Yes	***	-0.8737 to -0.3748
LS12/580 vs LS12/964	-0.3629	7.589	Yes	***	-0.6123 to -0.1134
LS12/646 vs LS12/685	0.03918	0.7917	No	ns	-0.2190 to 0.2973
LS12/646 vs LS12/741	-1.31	26.2	Yes	***	-1.570 to -1.049
LS12/646 vs LS12/808	0.1598	3.228	No	ns	-0.09839 to 0.4179
LS12/646 vs LS12/847	0.06862	1.387	No	ns	-0.1895 to 0.3268
LS12/646 vs LS12/859	0.5678	11.47	Yes	***	0.3097 to 0.8260
LS12/646 vs LS12/970	-0.2137	4.319	No	ns	-0.4719 to 0.04443
LS12/646 vs LS12/964	0.04767	0.9632	No	ns	-0.2105 to 0.3058
LS12/685 vs LS12/741	-1.349	27.91	Yes	***	-1.601 to -1.097
LS12/685 vs LS12/808	0.1206	2.522	No	ns	-0.1288 to 0.3700
LS12/685 vs LS12/847	0.02944	0.6158	No	ns	-0.2200 to 0.2788
LS12/685 vs LS12/859	0.5287	11.06	Yes	***	0.2792 to 0.7781
LS12/685 vs LS12/970	-0.2529	5.29	Yes	*	-0.5023 to -0.003500
LS12/685 vs LS12/964	0.00848 7	0.1775	No	ns	-0.2409 to 0.2579
LS12/741 vs LS12/808	1.469	30.41	Yes	***	1.217 to 1.722
LS12/741 vs LS12/847	1.378	28.52	Yes	***	1.126 to 1.630
LS12/741 vs LS12/859	1.877	38.85	Yes	***	1.625 to 2.130
LS12/741 vs LS12/970	1.096	22.68	Yes	***	0.8438 to 1.348
LS12/741 vs LS12/964	1.357	28.09	Yes	***	1.105 to 1.609
LS12/808 vs LS12/847	-0.09115	1.906	No	ns	-0.3406 to 0.1583
LS12/808 vs LS12/859	0.4081	8.535	Yes	***	0.1587 to 0.6575
LS12/808 vs LS12/970	-0.3735	7.812	Yes	***	-0.6229 to -0.1241
LS12/808 vs LS12/964	-0.1121	2.345	No	ns	-0.3615 to 0.1373
LS12/847 vs LS12/859	0.4992	10.44	Yes	***	0.2498 to 0.7486
LS12/847 vs LS12/970	-0.2823	5.906	Yes	**	-0.5318 to -0.03294
LS12/847 vs LS12/964	-0.02095	0.4383	No	ns	-0.2704 to 0.2285
LS12/859 vs LS12/970	-0.7816	16.35	Yes	***	-1.031 to -0.5322
LS12/859 vs LS12/964	-0.5202	10.88	Yes	***	-0.7696 to -0.2708
LS12/970 vs LS12/964	0.2614	5.467	Yes	*	0.01199 to 0.5108

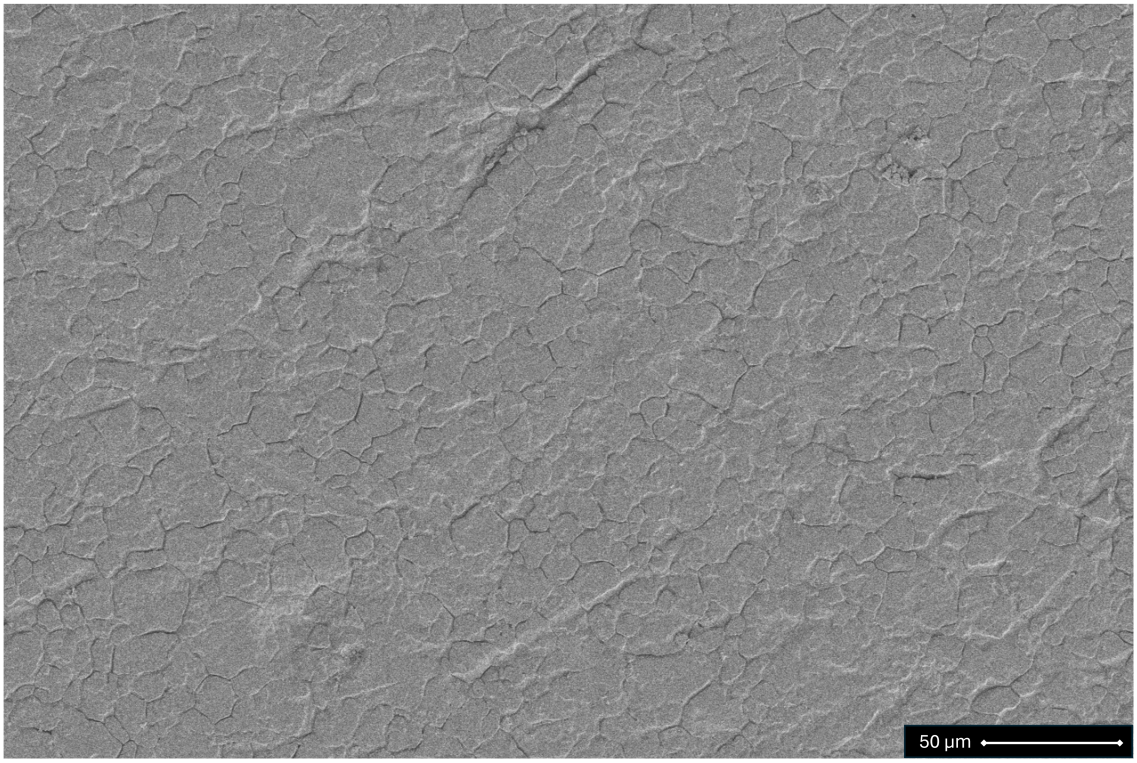
Appendix 8(I). Base pair alignment of the *qac* gene sequences from isolates LS12/646 (top) and LS12/741 (bottom), performed using the Clustal Omega Multiple Sequence Alignment (MSA) tool.



Appendix 8(II). Base pair alignment of the tetR gene sequences from isolates LS12/646 (top) and LS12/741 (bottom), performed using the Clustal Omega Multiple Sequence Alignment (MSA) tool.



Appendix 9. Scanning electron microscopy (SEM) image of the sterile surface topography of a stainless-steel grade 316 coupon at 1000× magnification. Scale bar: 50 µm.



Appendix 10. Full set of statistical analysis that was determined using one-way ANOVA followed by Tukey's multiple comparison test to analyse the results shown in Figures 19 - 20, which demonstrates the emergence of BC-tolerant planktonic and biofilm lineages in evolved *L. monocytogenes* isolates.

Sub-section	Tukey's Multiple Comparison Test	Mean Diff.	q	Significant? P < 0.05?	Summary
Fig. 19A.	Early passage (0.625 BC) vs Early passage non-exposed	0.6127	4.451	No	ns
	Early passage (0.625 BC) vs Mid passage (0.625 BC)	0.4312	3.132	No	ns
	Early passage (0.625 BC) vs Mid passage non-exposed	1.157	8.407	Yes	***
	Early passage (0.625 BC) vs Late passage (0.625 BC)	-0.06808	0.4945	No	ns
	Early passage (0.625 BC) vs Late passage non-exposed	1.407	10.22	Yes	***
	Early passage (0.625 BC) vs Parental strain	1.225	8.241	Yes	***
	Early passage non-exposed vs Mid passage (0.625 BC)	-0.1816	1.319	No	ns
	Early passage non-exposed vs Mid passage non-exposed	0.5447	3.956	No	ns
	Early passage non-exposed vs Late passage (0.625 BC)	-0.6808	4.945	Yes	*
	Early passage non-exposed vs Late passage non-exposed	0.7943	5.77	Yes	**
	Early passage non-exposed vs Parental strain	0.6127	4.121	No	ns
	Mid passage (0.625 BC) vs Mid passage non-exposed	0.7262	5.275	Yes	*
	Mid passage (0.625 BC) vs Late passage (0.625 BC)	-0.4993	3.627	No	ns
	Mid passage (0.625 BC) vs Late passage non-exposed	0.9759	7.088	Yes	**
	Mid passage (0.625 BC) vs Parental strain	0.7943	5.342	Yes	*
	Mid passage non-exposed vs Late passage (0.625 BC)	-1.225	8.902	Yes	***
	Mid passage non-exposed vs Late passage non-exposed	0.2496	1.813	No	ns
	Mid passage non-exposed vs Parental strain	0.06808	0.4578	No	ns
	Late passage (0.625 BC) vs Late passage non-exposed	1.475	10.71	Yes	***
	Late passage (0.625 BC) vs Parental strain	1.294	8.699	Yes	***
	Late passage non-exposed vs Parental strain	-0.1816	1.221	No	ns
B	Early passage (0.625 BC) vs Early passage non-exposed	1.611	30.7	Yes	***
	Early passage (0.625 BC) vs Mid passage (0.625 BC)	0.6127	11.67	Yes	***
	Early passage (0.625 BC) vs Mid passage non-exposed	1.521	28.97	Yes	***
	Early passage (0.625 BC) vs Late passage (0.625 BC)	-0.02269	0.4323	No	ns
	Early passage (0.625 BC) vs Late passage non-exposed	1.611	30.7	Yes	***
	Early passage (0.625 BC) vs Parental strain	1.43	25.22	Yes	***
	Early passage non-exposed vs Mid passage (0.625 BC)	-0.9985	19.02	Yes	***
	Early passage non-exposed vs Mid passage	-0.0907	1.729	No	ns

	non-exposed	8			
	Early passage non-exposed vs Late passage (0.625 BC)	-1.634	31.13	Yes	***
	Early passage non-exposed vs Late passage non-exposed	0	0	No	ns
	Early passage non-exposed vs Parental strain	-0.1816	3.202	No	ns
	Mid passage (0.625 BC) vs Mid passage non-exposed	0.9078	17.29	Yes	***
	Mid passage (0.625 BC) vs Late passage (0.625 BC)	-0.6354	12.11	Yes	***
	Mid passage (0.625 BC) vs Late passage non-exposed	0.9985	19.02	Yes	***
	Mid passage (0.625 BC) vs Parental strain	0.817	14.41	Yes	***
	Mid passage non-exposed vs Late passage (0.625 BC)	-1.543	29.4	Yes	***
	Mid passage non-exposed vs Late passage non-exposed	0.09078	1.729	No	ns
	Mid passage non-exposed vs Parental strain	-0.09078	1.601	No	ns
	Late passage (0.625 BC) vs Late passage non-exposed	1.634	31.13	Yes	***
	Late passage (0.625 BC) vs Parental strain	1.452	25.62	Yes	***
	Late passage non-exposed vs Parental strain	-0.1816	3.202	No	ns
Fig. 19C.	Early passage (0.625 BC) vs Early passage non-exposed	1.339	10.61	Yes	***
	Early passage (0.625 BC) vs Mid passage (0.625 BC)	0.3631	2.878	No	ns
	Early passage (0.625 BC) vs Mid passage non-exposed	1.248	9.894	Yes	***
	Early passage (0.625 BC) vs Late passage (0.625 BC)	0.02269	0.1799	No	ns
	Early passage (0.625 BC) vs Late passage non-exposed	1.339	10.61	Yes	***
	Early passage (0.625 BC) vs Parental strain	1.157	8.494	Yes	***
	Early passage non-exposed vs Mid passage (0.625 BC)	-0.9759	7.736	Yes	***
	Early passage non-exposed vs Mid passage non-exposed	-0.09078	0.7196	No	ns
	Early passage non-exposed vs Late passage (0.625 BC)	-1.316	10.43	Yes	***
	Early passage non-exposed vs Late passage non-exposed	0	0	No	ns
	Early passage non-exposed vs Parental strain	-0.1816	1.332	No	ns
	Mid passage (0.625 BC) vs Mid passage non-exposed	0.8851	7.016	Yes	**
	Mid passage (0.625 BC) vs Late passage (0.625 BC)	-0.3404	2.698	No	ns
	Mid passage (0.625 BC) vs Late passage non-exposed	0.9759	7.736	Yes	***
	Mid passage (0.625 BC) vs Parental strain	0.7943	5.829	Yes	**
	Mid passage non-exposed vs Late passage (0.625 BC)	-1.225	9.714	Yes	***
	Mid passage non-exposed vs Late passage non-exposed	0.09078	0.7196	No	ns
	Mid passage non-exposed vs Parental strain	-0.09078	0.6662	No	ns
	Late passage (0.625 BC) vs Late passage non-	1.316	10.43	Yes	***

	exposed				
	Late passage (0.625 BC) vs Parental strain	1.135	8.328	Yes	***
	Late passage non-exposed vs Parental strain	-0.1816	1.332	No	ns
Fig 19D.	Early passage (0.625 BC) vs Early passage non-exposed	1.225	10.26	Yes	***
	Early passage (0.625 BC) vs Mid passage (0.625 BC)	0.3404	2.85	No	ns
	Early passage (0.625 BC) vs Mid passage non-exposed	1.112	9.31	Yes	***
	Early passage (0.625 BC) vs Late passage (0.625 BC)	-0.3631	3.04	No	ns
	Early passage (0.625 BC) vs Late passage non-exposed	1.089	9.12	Yes	***
	Early passage (0.625 BC) vs Parental strain	1.044	8.092	Yes	***
	Early passage non-exposed vs Mid passage (0.625 BC)	-0.8851	7.41	Yes	***
	Early passage non-exposed vs Mid passage non-exposed	-0.1135	0.95	No	ns
	Early passage non-exposed vs Late passage (0.625 BC)	-1.589	13.3	Yes	***
	Early passage non-exposed vs Late passage non-exposed	-0.1362	1.14	No	ns
	Early passage non-exposed vs Parental strain	-0.1816	1.407	No	ns
	Mid passage (0.625 BC) vs Mid passage non-exposed	0.7716	6.46	Yes	**
	Mid passage (0.625 BC) vs Late passage (0.625 BC)	-0.7035	5.89	Yes	**
	Mid passage (0.625 BC) vs Late passage non-exposed	0.7489	6.27	Yes	**
	Mid passage (0.625 BC) vs Parental strain	0.7035	5.453	Yes	*
	Mid passage non-exposed vs Late passage (0.625 BC)	-1.475	12.35	Yes	***
	Mid passage non-exposed vs Late passage non-exposed	-0.02269	0.19	No	ns
	Mid passage non-exposed vs Parental strain	-0.06808	0.5277	No	ns
	Late passage (0.625 BC) vs Late passage non-exposed	1.452	12.16	Yes	***
	Late passage (0.625 BC) vs Parental strain	1.407	10.91	Yes	***
	Late passage non-exposed vs Parental strain	-0.04539	0.3518	No	ns
Fig 20A.	Early passage (0.625 BC) vs Early passage non-exposed	0.6127	5.22	Yes	*
	Early passage (0.625 BC) vs Mid passage (0.625 BC)	0.4312	3.673	No	ns
	Early passage (0.625 BC) vs Mid passage (1.3 BC)	0.1362	1.16	No	ns
	Early passage (0.625 BC) vs Mid passage non-exposed	1.157	9.859	Yes	***
	Early passage (0.625 BC) vs Late passage (0.625 BC)	-0.06808	0.5799	No	ns
	Early passage (0.625 BC) vs Late passage (1.3 BC)	-0.2269	1.933	No	ns
	Early passage (0.625 BC) vs Late passage (1.75 BC)	-0.2269	1.933	No	ns
	Early passage (0.625 BC) vs Late passage non-exposed	1.407	11.99	Yes	***

	Early passage (0.625 BC) vs Parental strain	1.225	9.665	Yes	***
	Early passage non-exposed vs Mid passage (0.625 BC)	-0.1816	1.547	No	ns
	Early passage non-exposed vs Mid passage (1.3 BC)	-0.4766	4.06	No	ns
	Early passage non-exposed vs Mid passage non-exposed	0.5447	4.64	No	ns
	Early passage non-exposed vs Late passage (0.625 BC)	-0.6808	5.799	Yes	**
	Early passage non-exposed vs Late passage (1.3 BC)	-0.8397	7.153	Yes	***
	Early passage non-exposed vs Late passage (1.75 BC)	-0.8397	7.153	Yes	***
	Early passage non-exposed vs Late passage non-exposed	0.7943	6.766	Yes	**
	Early passage non-exposed vs Parental strain	0.6127	4.832	No	ns
	Mid passage (0.625 BC) vs Mid passage (1.3 BC)	-0.295	2.513	No	ns
	Mid passage (0.625 BC) vs Mid passage non-exposed	0.7262	6.186	Yes	**
	Mid passage (0.625 BC) vs Late passage (0.625 BC)	-0.4993	4.253	No	ns
	Mid passage (0.625 BC) vs Late passage (1.3 BC)	-0.6581	5.606	Yes	*
	Mid passage (0.625 BC) vs Late passage (1.75 BC)	-0.6581	5.606	Yes	*
	Mid passage (0.625 BC) vs Late passage non-exposed	0.9759	8.313	Yes	***
	Mid passage (0.625 BC) vs Parental strain	0.7943	6.264	Yes	**
	Mid passage (1.3 BC) vs Mid passage non-exposed	1.021	8.699	Yes	***
	Mid passage (1.3 BC) vs Late passage (0.625 BC)	-0.2042	1.74	No	ns
	Mid passage (1.3 BC) vs Late passage (1.3 BC)	-0.3631	3.093	No	ns
	Mid passage (1.3 BC) vs Late passage (1.75 BC)	-0.3631	3.093	No	ns
	Mid passage (1.3 BC) vs Late passage non-exposed	1.271	10.83	Yes	***
	Mid passage (1.3 BC) vs Parental strain	1.089	8.591	Yes	***
	Mid passage non-exposed vs Late passage (0.625 BC)	-1.225	10.44	Yes	***
	Mid passage non-exposed vs Late passage (1.3 BC)	-1.384	11.79	Yes	***
	Mid passage non-exposed vs Late passage (1.75 BC)	-1.384	11.79	Yes	***
	Mid passage non-exposed vs Late passage non-exposed	0.2496	2.126	No	ns
	Mid passage non-exposed vs Parental strain	0.06808	0.5369	No	ns
	Late passage (0.625 BC) vs Late passage (1.3 BC)	-0.1589	1.353	No	ns
	Late passage (0.625 BC) vs Late passage (1.75 BC)	-0.1589	1.353	No	ns
	Late passage (0.625 BC) vs Late passage non-exposed	1.475	12.57	Yes	***
	Late passage (0.625 BC) vs Parental strain	1.294	10.2	Yes	***
	Late passage (1.3 BC) vs Late passage (1.75 BC)	0	0	No	ns

	Late passage (1.3 BC) vs Late passage non-exposed	1.634	13.92	Yes	***
	Late passage (1.3 BC) vs Parental strain	1.452	11.45	Yes	***
	Late passage (1.75 BC) vs Late passage non-exposed	1.634	13.92	Yes	***
	Late passage (1.75 BC) vs Parental strain	1.452	11.45	Yes	***
	Late passage non-exposed vs Parental strain	-0.1816	1.432	No	ns
Fig 20B.	Early passage (0.625 BC) vs Early passage non-exposed	1.611	32.12	Yes	***
	Early passage (0.625 BC) vs Mid passage (0.625 BC)	0.6127	12.22	Yes	***
	Early passage (0.625 BC) vs Mid passage (1.3 BC)	0.3858	7.692	Yes	***
	Early passage (0.625 BC) vs Mid passage non-exposed	1.521	30.32	Yes	***
	Early passage (0.625 BC) vs Late passage (0.625 BC)	-0.02269	0.4525	No	ns
	Early passage (0.625 BC) vs Late passage (1.3 BC)	-0.02269	0.4525	No	ns
	Early passage (0.625 BC) vs Late passage non-exposed	1.611	32.12	Yes	***
	Early passage (0.625 BC) vs Parental strain	1.43	26.39	Yes	***
	Early passage non-exposed vs Mid passage (0.625 BC)	-0.9985	19.91	Yes	***
	Early passage non-exposed vs Mid passage (1.3 BC)	-1.225	24.43	Yes	***
	Early passage non-exposed vs Mid passage non-exposed	-0.09078	1.81	No	ns
	Early passage non-exposed vs Late passage (0.625 BC)	-1.634	32.58	Yes	***
	Early passage non-exposed vs Late passage (1.3 BC)	-1.634	32.58	Yes	***
	Early passage non-exposed vs Late passage non-exposed	0	0	No	ns
	Early passage non-exposed vs Parental strain	-0.1816	3.351	No	ns
	Mid passage (0.625 BC) vs Mid passage (1.3 BC)	-0.2269	4.525	No	ns
	Mid passage (0.625 BC) vs Mid passage non-exposed	0.9078	18.1	Yes	***
	Mid passage (0.625 BC) vs Late passage (0.625 BC)	-0.6354	12.67	Yes	***
	Mid passage (0.625 BC) vs Late passage (1.3 BC)	-0.6354	12.67	Yes	***
	Mid passage (0.625 BC) vs Late passage non-exposed	0.9985	19.91	Yes	***
	Mid passage (0.625 BC) vs Parental strain	0.817	15.08	Yes	***
	Mid passage (1.3 BC) vs Mid passage non-exposed	1.135	22.62	Yes	***
	Mid passage (1.3 BC) vs Late passage (0.625 BC)	-0.4085	8.144	Yes	***
	Mid passage (1.3 BC) vs Late passage (1.3 BC)	-0.4085	8.144	Yes	***
	Mid passage (1.3 BC) vs Late passage non-exposed	1.225	24.43	Yes	***
	Mid passage (1.3 BC) vs Parental strain	1.044	19.27	Yes	***
	Mid passage non-exposed vs Late passage (0.625 BC)	-1.543	30.77	Yes	***
	Mid passage non-exposed vs Late passage (1.3	-1.543	30.77	Yes	***

	BC)				
	Mid passage non-exposed vs Late passage non-exposed	0.09078	1.81	No	ns
	Mid passage non-exposed vs Parental strain	-0.09078	1.676	No	ns
	Late passage (0.625 BC) vs Late passage (1.3 BC)	0	0	No	ns
	Late passage (0.625 BC) vs Late passage non-exposed	1.634	32.58	Yes	***
	Late passage (0.625 BC) vs Parental strain	1.452	26.81	Yes	***
	Late passage (1.3 BC) vs Late passage non-exposed	1.634	32.58	Yes	***
	Late passage (1.3 BC) vs Parental strain	1.452	26.81	Yes	***
	Late passage non-exposed vs Parental strain	-0.1816	3.351	No	ns
Fig 20C.	Early passage (0.625 BC) vs Early passage non-exposed	1.339	12	Yes	***
	Early passage (0.625 BC) vs Mid passage (0.625 BC)	0.3631	3.254	No	ns
	Early passage (0.625 BC) vs Mid passage (1.3 BC)	0.1362	1.22	No	ns
	Early passage (0.625 BC) vs Mid passage non-exposed	1.248	11.19	Yes	***
	Early passage (0.625 BC) vs Late passage (0.625 BC)	0.02269	0.2034	No	ns
	Early passage (0.625 BC) vs Late passage (1.3 BC)	-0.295	2.644	No	ns
	Early passage (0.625 BC) vs Late passage (1.75 BC)	-0.295	2.644	No	ns
	Early passage (0.625 BC) vs Late passage non-exposed	1.339	12	Yes	***
	Early passage (0.625 BC) vs Parental strain	1.157	9.604	Yes	***
	Early passage non-exposed vs Mid passage (0.625 BC)	-0.9759	8.746	Yes	***
	Early passage non-exposed vs Mid passage (1.3 BC)	-1.203	10.78	Yes	***
	Early passage non-exposed vs Mid passage non-exposed	-0.09078	0.8136	No	ns
	Early passage non-exposed vs Late passage (0.625 BC)	-1.316	11.8	Yes	***
	Early passage non-exposed vs Late passage (1.3 BC)	-1.634	14.64	Yes	***
	Early passage non-exposed vs Late passage (1.75 BC)	-1.634	14.64	Yes	***
	Early passage non-exposed vs Late passage non-exposed	0	0	No	ns
	Early passage non-exposed vs Parental strain	-0.1816	1.506	No	ns
	Mid passage (0.625 BC) vs Mid passage (1.3 BC)	-0.2269	2.034	No	ns
	Mid passage (0.625 BC) vs Mid passage non-exposed	0.8851	7.932	Yes	***
	Mid passage (0.625 BC) vs Late passage (0.625 BC)	-0.3404	3.051	No	ns
	Mid passage (0.625 BC) vs Late passage (1.3 BC)	-0.6581	5.898	Yes	**
	Mid passage (0.625 BC) vs Late passage (1.75 BC)	-0.6581	5.898	Yes	**
	Mid passage (0.625 BC) vs Late passage non-exposed	0.9759	8.746	Yes	***

	Mid passage (0.625 BC) vs Parental strain	0.7943	6.591	Yes	**
	Mid passage (1.3 BC) vs Mid passage non-exposed	1.112	9.966	Yes	***
	Mid passage (1.3 BC) vs Late passage (0.625 BC)	-0.1135	1.017	No	ns
	Mid passage (1.3 BC) vs Late passage (1.3 BC)	-0.4312	3.865	No	ns
	Mid passage (1.3 BC) vs Late passage (1.75 BC)	-0.4312	3.865	No	ns
	Mid passage (1.3 BC) vs Late passage non-exposed	1.203	10.78	Yes	***
	Mid passage (1.3 BC) vs Parental strain	1.021	8.474	Yes	***
	Mid passage non-exposed vs Late passage (0.625 BC)	-1.225	10.98	Yes	***
	Mid passage non-exposed vs Late passage (1.3 BC)	-1.543	13.83	Yes	***
	Mid passage non-exposed vs Late passage (1.75 BC)	-1.543	13.83	Yes	***
	Mid passage non-exposed vs Late passage non-exposed	0.09078	0.8136	No	ns
	Mid passage non-exposed vs Parental strain	-0.09078	0.7532	No	ns
	Late passage (0.625 BC) vs Late passage (1.3 BC)	-0.3177	2.848	No	ns
	Late passage (0.625 BC) vs Late passage (1.75 BC)	-0.3177	2.848	No	ns
	Late passage (0.625 BC) vs Late passage non-exposed	1.316	11.8	Yes	***
	Late passage (0.625 BC) vs Parental strain	1.135	9.415	Yes	***
	Late passage (1.3 BC) vs Late passage (1.75 BC)	0	0	No	ns
	Late passage (1.3 BC) vs Late passage non-exposed	1.634	14.64	Yes	***
	Late passage (1.3 BC) vs Parental strain	1.452	12.05	Yes	***
	Late passage (1.75 BC) vs Late passage non-exposed	1.634	14.64	Yes	***
	Late passage (1.75 BC) vs Parental strain	1.452	12.05	Yes	***
	Late passage non-exposed vs Parental strain	-0.1816	1.506	No	ns
Fig 20D.	Early passage (0.625 BC) vs Early passage non-exposed	1.225	11.34	Yes	***
	Early passage (0.625 BC) vs Mid passage (0.625 BC)	0.3404	3.149	No	ns
	Early passage (0.625 BC) vs Mid passage (1.3 BC)	0.1816	1.679	No	ns
	Early passage (0.625 BC) vs Mid passage non-exposed	1.112	10.29	Yes	***
	Early passage (0.625 BC) vs Late passage (0.625 BC)	-0.3631	3.359	No	ns
	Early passage (0.625 BC) vs Late passage (1.3 BC)	-0.4085	3.779	No	ns
	Early passage (0.625 BC) vs Late passage non-exposed	1.089	10.08	Yes	***
	Early passage (0.625 BC) vs Parental strain	1.044	8.94	Yes	***
	Early passage non-exposed vs Mid passage (0.625 BC)	-0.8851	8.187	Yes	***
	Early passage non-exposed vs Mid passage (1.3 BC)	-1.044	9.656	Yes	***
	Early passage non-exposed vs Mid passage	-0.1135	1.05	No	ns

	non-exposed				
	Early passage non-exposed vs Late passage (0.625 BC)	-1.589	14.69	Yes	***
	Early passage non-exposed vs Late passage (1.3 BC)	-1.634	15.11	Yes	***
	Early passage non-exposed vs Late passage non-exposed	-0.1362	1.26	No	ns
	Early passage non-exposed vs Parental strain	-0.1816	1.555	No	ns
	Mid passage (0.625 BC) vs Mid passage (1.3 BC)	-0.1589	1.469	No	ns
	Mid passage (0.625 BC) vs Mid passage non-exposed	0.7716	7.137	Yes	***
	Mid passage (0.625 BC) vs Late passage (0.625 BC)	-0.7035	6.508	Yes	**
	Mid passage (0.625 BC) vs Late passage (1.3 BC)	-0.7489	6.927	Yes	**
	Mid passage (0.625 BC) vs Late passage non-exposed	0.7489	6.927	Yes	**
	Mid passage (0.625 BC) vs Parental strain	0.7035	6.025	Yes	**
	Mid passage (1.3 BC) vs Mid passage non-exposed	0.9305	8.607	Yes	***
	Mid passage (1.3 BC) vs Late passage (0.625 BC)	-0.5447	5.038	Yes	*
	Mid passage (1.3 BC) vs Late passage (1.3 BC)	-0.5901	5.458	Yes	*
	Mid passage (1.3 BC) vs Late passage non-exposed	0.9078	8.397	Yes	***
	Mid passage (1.3 BC) vs Parental strain	0.8624	7.385	Yes	***
	Mid passage non-exposed vs Late passage (0.625 BC)	-1.475	13.65	Yes	***
	Mid passage non-exposed vs Late passage (1.3 BC)	-1.521	14.06	Yes	***
	Mid passage non-exposed vs Late passage non-exposed	-0.02269	0.2099	No	ns
	Mid passage non-exposed vs Parental strain	-0.06808	0.5831	No	ns
	Late passage (0.625 BC) vs Late passage (1.3 BC)	-0.04539	0.4198	No	ns
	Late passage (0.625 BC) vs Late passage non-exposed	1.452	13.44	Yes	***
	Late passage (0.625 BC) vs Parental strain	1.407	12.05	Yes	***
	Late passage (1.3 BC) vs Late passage non-exposed	1.498	13.85	Yes	***
	Late passage (1.3 BC) vs Parental strain	1.452	12.44	Yes	***
	Late passage non-exposed vs Parental strain	-0.04539	0.3887	No	ns

Appendix 11(I). Demonstrates the genes that exhibited non-synonymous and intergenic mutations under BC exposure and were included into each of the functional subgroups predicted with *ListiWiki.* Corresponding to the **Figure 23**.

Unknown	Inorganic ion transport and metabolism	Nucleotide transport and metabolism	Posttranslational modification, protein turnover, chaperones	Signal transduction mechanisms	Transcription	Carbohydrate transport and metabolism	Amino acid transport and metabolism	Replication, recombination and repair
locus_13460	*corA*	*mtnN*	*cyoE*	*lipA*	*fepR*	*rpiB*	*locus_06315*	*srmB*
lmo2805	*focA*	*ndk*	*sufD*	*lmo0689*	*bglG*			
lmo1289	*locus_05680*	*pyrF*						
lmo2410								
locus_03235								
arA1								

Appendix 11(II). Demonstrates the genes that exhibited non-synonymous and intergenic mutations under biofilm lifestyle exposure and were included into each of the functional subgroups predicted with *ListiWiki.* Corresponding to the **Figure 27**.

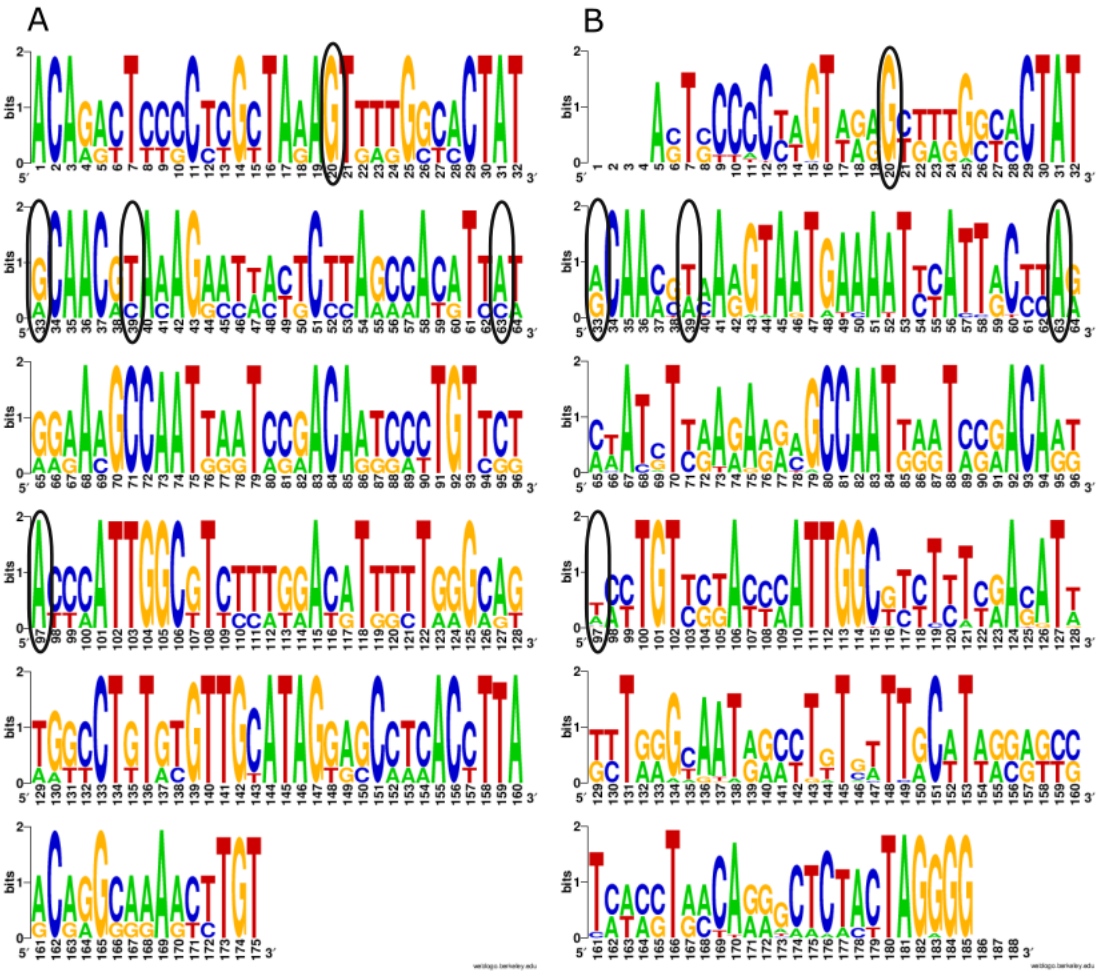
Transcription	**Nucleotide transport and metabolism**	**Energy production and conversion**	**Uknown**	**Inorganic ion transport and metabolism**	**Signal transduction mechanisms**	**Cell wall/membrane biogenesis**	**Carbohydrate transport and metabolism**	**Defense/ virulence mechanisms**	**Posttranslational modification, protein turnover, chaperones**	**Translation**	**Replication, recombination and repair**	**Secondary metabolites biosynthesis, transport and catabolism**
marR	*mtnN*	*glpK*	*tlyC*	*mgtA*	*rsbW*	*inlH*	*araJ*	*lolE*	*sufD*	dtd	*srmB*	*bdS1*
bglG	*pyrD*	*aceF*	*yurZ*	*pitA*	*rsbV*	*iap*	*fbp*					
golR	*pyrB*	*rnfC*	DUF1310	*corA*	*walK*							
degU	*pyrF*	*ndh*	*yvaK*	*feoB*								
yhcF	*pyrE*	*atpA1*	*lmo0331*									
rsbU	*guA1*	*ply*	*ykoK*									

Appendix 12. Demonstrates non-synonymous mutations within *fepR* indicating their position, domain structural element, amino acid substitution, change in polarity, bulkiness, charge, side chain change and hydrogen forming capacity of the side chain.

Position	Domain	Structural element	Amino acid change	Hydrophilicity change	Bulkiness	Charge change	Side chain	Hydrogen bond formation (side chain)
7	DNA binding domain	α-helix 1	Lysine → Glutamic acid	Remained hydrophilic	Increased	Positive → Negative	Amino group → Carboxyl group	Retained ability
10	DNA binding domain	α-helix 1	Alanine → Threonine	Hydrophobic → hydrophilic	Increased	Remained neutral	Methyl group → Hydroxyl group	Gained ability
24	DNA binding domain (HTH)	α-helix 2	Leucine → Proline	Became less hydrophobic	Decreased	Remained neutral	Isobutyl group → Pyrrolidine ring	Lost ability
30	DNA binding domain (HTH)	α-helix 2	Valine → Phenylalanine	Became more hydrophobic	Increased	Remained neutral	Isopropyl group → Benzyl ring	No ability
37	DNA binding domain (HTH)	α-helix 3	Serine → Threonine	Remained hydrophilic	Increased	Remained neutral	Hydroxymethyl group → Hydroxyl group	Retained ability
41	DNA binding domain (HTH)	-	Histidine → Glutamine	Became more hydrophillic	Increased	Neutral/ positive → neutral	Imidazole ring → Amide group	Retained ability
76	Effector binding domain	α-helix 5	Proline → Leucine	Became more hydrophobic	Increased	Remained neutral	Pyrrolidine ring → Isobutyl group	No ability
96	Effector binding domain	α-helix 6	Alanine → Valine	Became more hydrophobic	Increased	Remained neutral	Methyl group → Isopropryl group	No ability
105	Effector binding domain	α-helix 6	Phenylalanine → Valine	Became less hydrophobic	Decreased	Remained neutral	Benzyl ring → Isopropryl group	No ability
105	Effector binding domain	α-helix 6	Phenylalanine → Alanine	Became less hydrophobic	Decreased	Remained neutral	Benzyl ring → Methyl group	No ability
107	Effector binding domain	-	Proline → Leucine	Became more hydrophobic	Increased	Remained neutral	Pyrrolidine ring → Isobutyl group	No ability
157	Effector binding domain	α-helix 8	Glycine → Arginine	Became more hydrophillic	Increased	Neutral → Positive	Hydrogen atom → Guanidinium group	Gained ability
157	Effector	α-helix	Glycine	Became	Increa	Remained	Hydrogen	No

	binding domain	8	→ Valine	more hydrophobic	sed	neutral	atom → Isopropyl group	ability
181	Effector binding domain	α-helix 9	Alanine → Valine	Became more hydrophobic	Increased	Remained neutral	Methyl group → Isopropyl group	No ability

Appendix 13. Conservation of mutations in YkoK leader within (A) and outside (B) of *Listeria* genus. Sequence logos of nucleic acids multiple in sequence alignment, consisting of 50 sequences each. The overall height of the stack indicates the sequence conservation of nucleic acid residue, while the height of symbols within the stack indicates the relative frequency of each nucleic acid. Visualised with WebLogo (v2.8.2).

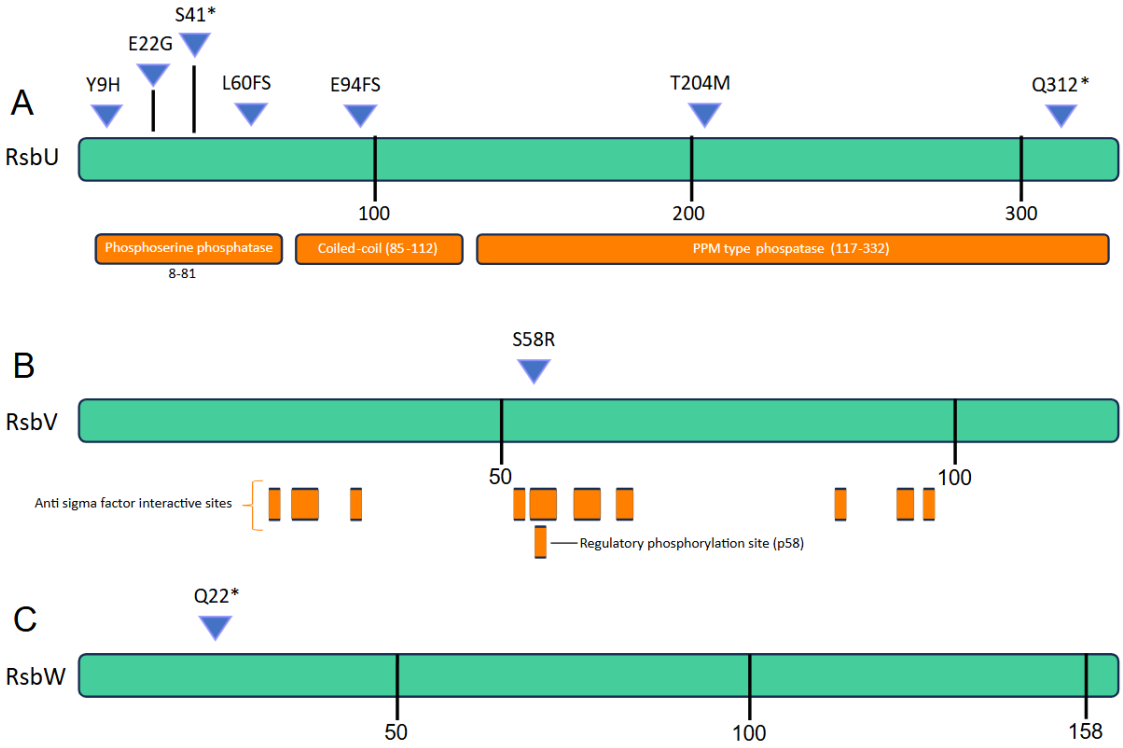


Appendix 14. Demonstrates non-synonymous mutations in regions associated with biofilm persistence indicating their position, domain structural element, amino acid substitution, change in polarity, bulkiness, charge, side chain change and hydrogen forming capacity of the side chain.

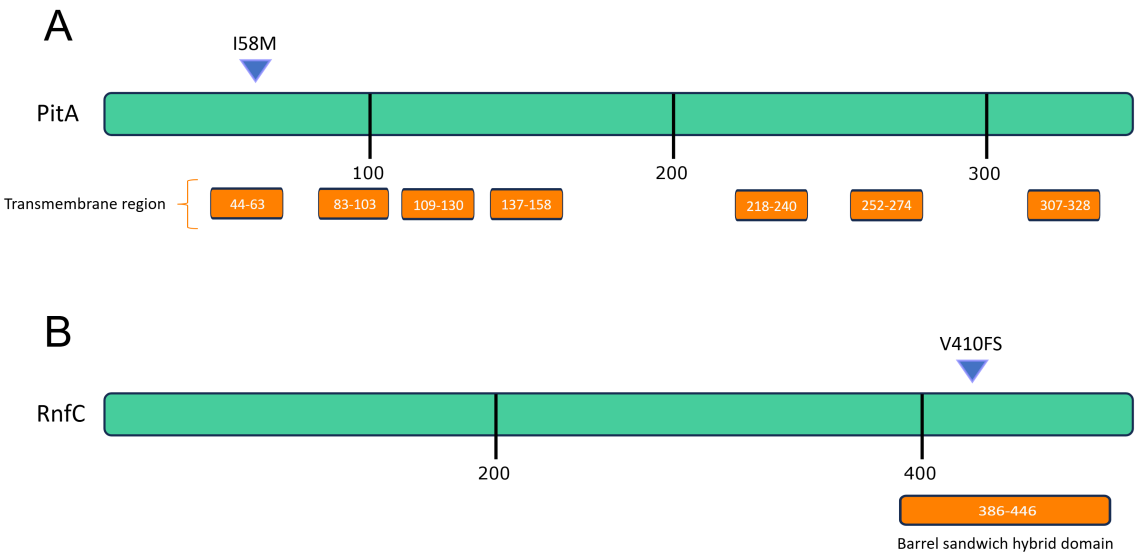
Gene	Position	Predicted Domain	Predicted Structural Element	Amino Acid Change	Hydrophilicity Change	Bulkiness	Charge Change	Side Chain	Hydrogen Bond Formation (side chain)
mgtA	286	Transmembrane domain	α-helix	Alanine → Glycine	Hydrophobic → Neutral	Smaller	Remained neutral	Methyl group → Hydrogen atom	No ability
mgtA	687	Transmembrane domain	-	Lysine → Isoleucine	Hydrophilic → Hydrophobic	Increased	Positive → Neutral	Amino group → Isopropyl group	Lost ability
rsbU	9	-	α-helix	Tyrosine → Histidine	Hydrophobic → Hydrophilic	Decreased	Neutral → Positive	Phenol group → Imidazole group	Gained ability
rsbU	22	-	α-helix	Alanine → Threonine	Hydrophobic → Hydrophilic	Increased	Remained neutral	Methyl group → Hydroxymethyl group	Gained ability
rsbU	41	-	-	Serine → *	N/A	N/A	N/A	N/A	Lost ability
rsbU	60	-	α-helix	Valine → FS	N/A	N/A	N/A	N/A	Lost ability
rsbU	94	-	α-helical coiled coil	Serine → *	N/A	N/A	N/A	N/A	Lost ability
rsbU	204	PPM-type phosphatase	β-pleated sheet	Histidine → Glutamine	Remained hydrophilic	Increased	Positive → Neutral	Imidazole group → Amide group	Retained ability

rsbU	312	PPM-type phosphatase	β-pleated sheet	Glutamine → *	N/A	N/A	N/A	N/A	Lost ability
pyrB	22	-	α-helix	Alanine → Glutamic acid	Hydrophobic → Hydrophilic	Increased	Neutral → Negative	Methyl group → Carboxylic acid	Gained ability
pyrB	153	-	-	Glycine → Arginine	Hydrophobic → Hydrophilic	Increased	Neutral → Positive	Hydrogen atom → Guanidinium group	Gained ability
carB	175	ATP grasp1	-	Glycine → Valine	More hydrophobic	Increased	Remained neutral	Hydrogen atom → Isopropyl group	No ability
carB	262	ATP grasp1	α-helix	Glutamine → *	N/A	N/A	N/A	N/A	Lost ability
carB	599	Carbomoyl phosphate synthetic domain	-	Serine → Methionine	Hydrophilic → Hydrophobic	Increased	Remained neutral	Hydroxymethyl group → Thioether	Lost ability
carB	781	Carbomoyl phosphate synthetic domain	-	Glycine → Glutamic acid	More hydrophillic	Increased	Neutral → Negative	Hydrogen atom → Carboxylic acid	Gained ability
carB	969	MGS-like domain	α-helix	Glycine → FS	N/A	N/A	N/A	N/A	No ability
pyrF	63	-	-	Aspartic acid → Histidine	Remained hydrophilic	Increased	Negative → Positive	Carboxyl group → Imidazole group	Retained ability
pyrd	138	-	α-helix	Isoleucine → FS	N/A	N/A	N/A	N/A	Lost ability
pyrd	192	Substrate binding site	-	Asparagine → Lysine	Remained hydrophilic	Increased	Neutral → Positive	Amide group → Amino group	Retained ability
pyrd	285	-	α-helix	Arginine → *	N/A	N/A	N/A	N/A	Lost ability

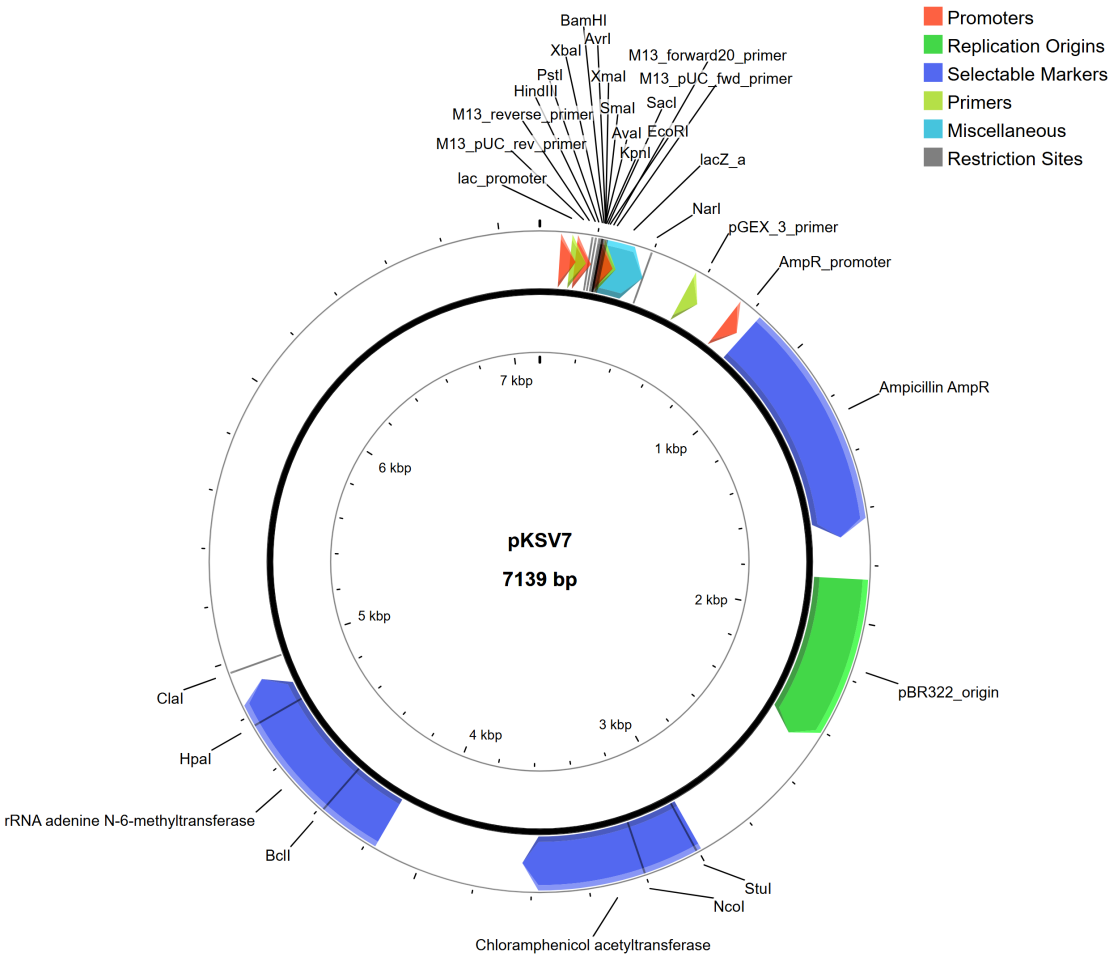
Appendix 15. Graphical overview of substitutions in SigB regulating operon for (**A; B; C**) RsbU, RsbV, RsbW. Substitutions are indicated by triangles. Predicted structural and functional domains are indicated by the orange boxes. * Indicates an early stop codon, FS – frameshift mutation. Domains predicted with InterPro.



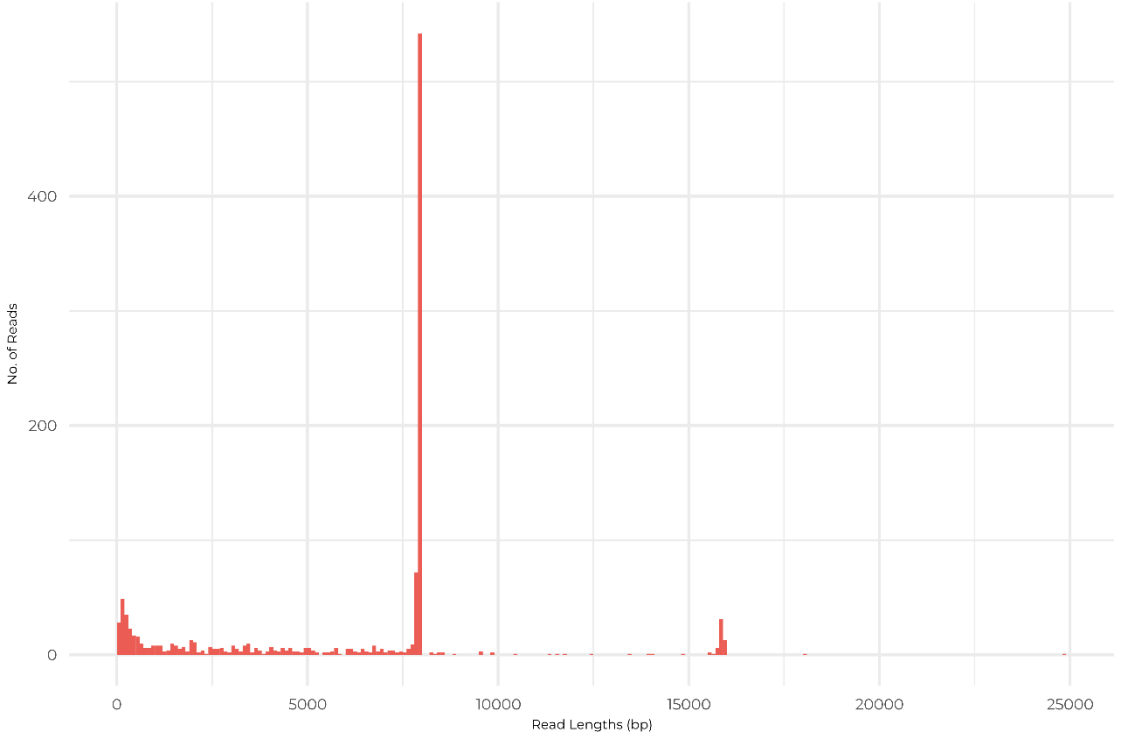
Appendix 16. Graphical overview of substitutions in (A) PitA and (B) RnfC. Non-synonymous mutations are indicated by triangle. Predicted structural and functional domains are indicated by the orange boxes. Domains predicted with InterPro.



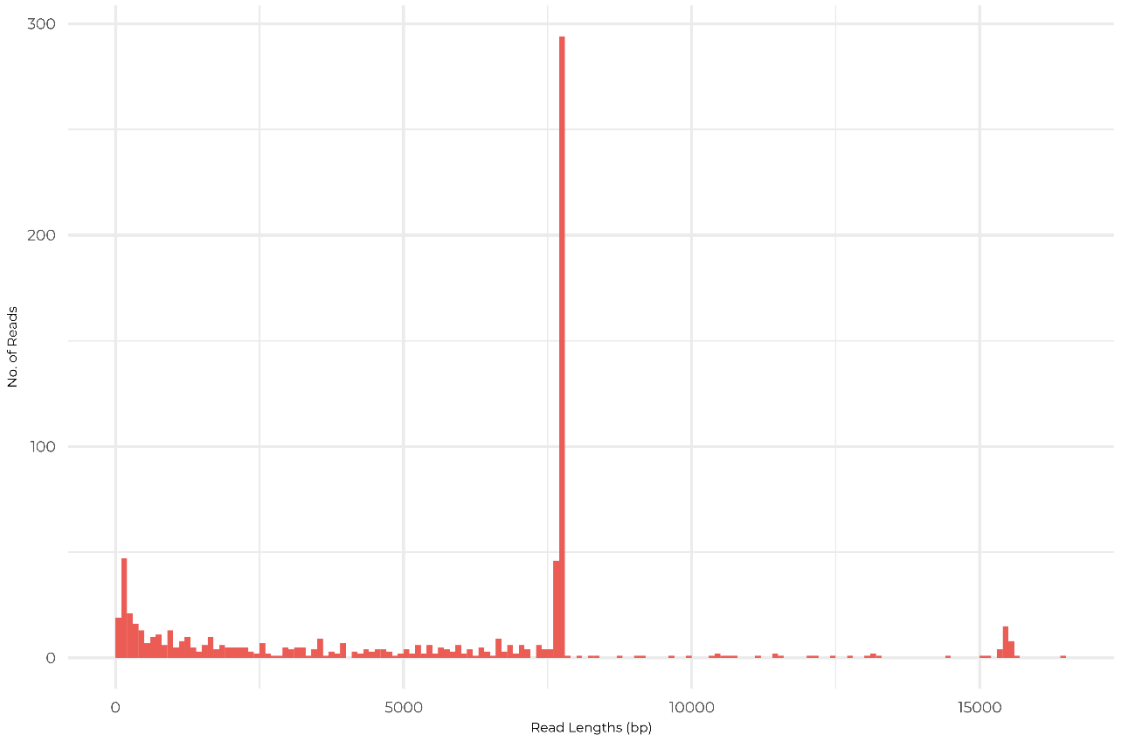
Appendix 17. Annotated map of the pKSV7 vector, generated using PlasMapper 3.0 (Wishart et al., 2023). The map highlights key features including the origin of replication, multiple cloning site (MCS) with annotated restriction enzyme sites, and selectable markers: ampicillin tolerance (AmpR) and chloramphenicol acetyltransferase (cat). Features are colour-coded as indicated in the legend.



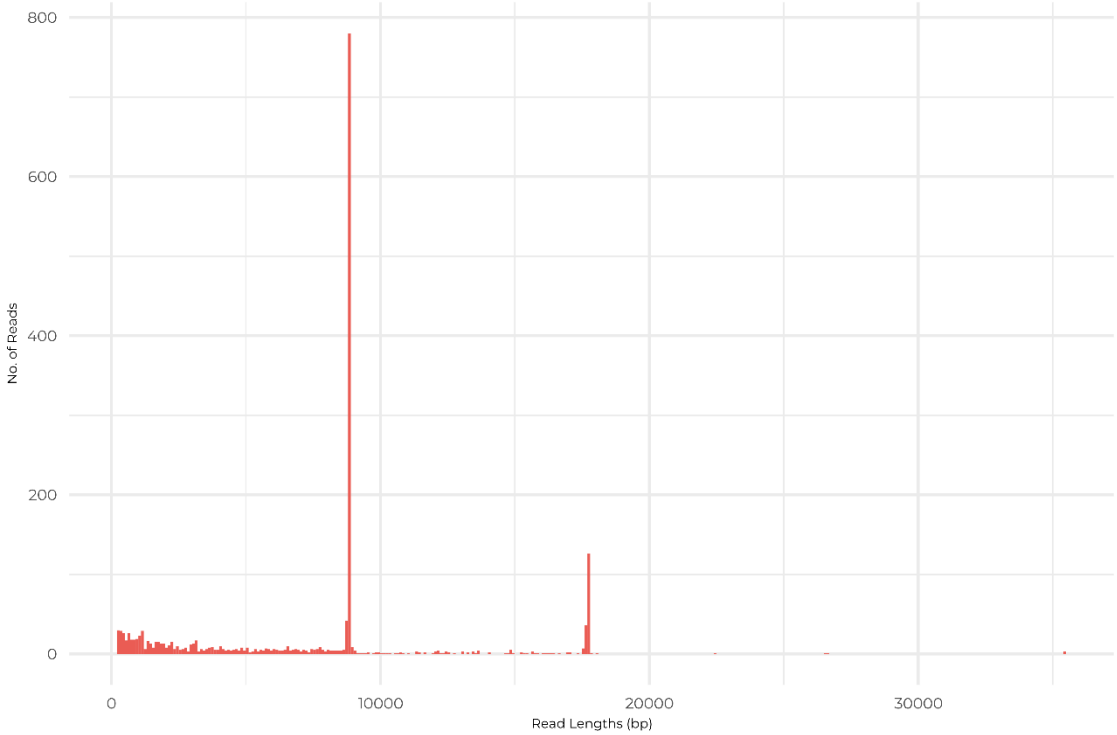
Appendix 18(I). Read length histogram generated from the whole plasmid sequencing data for pKSV7-ΔykoK construct. The histogram displays the number of reads corresponding to each read length.



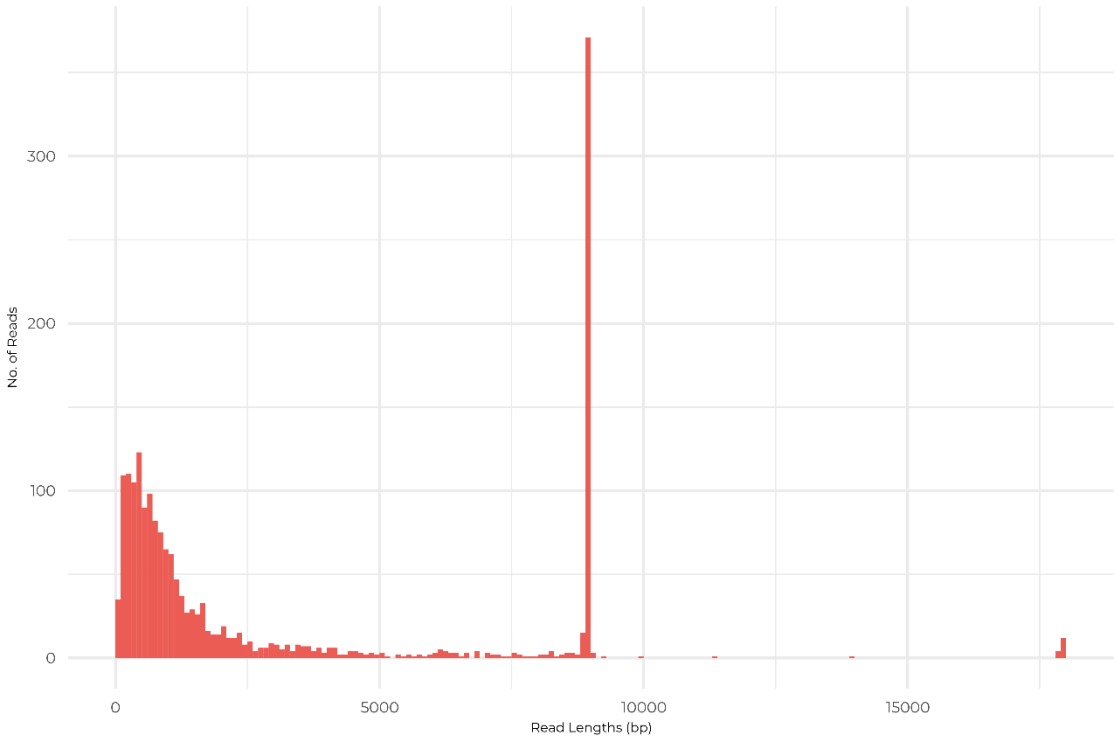
Appendix 18(II). Read length histogram generated from the whole plasmid sequencing data for pKSV7-Δ*mgtA* construct. The histogram displays the number of reads corresponding to each read length.



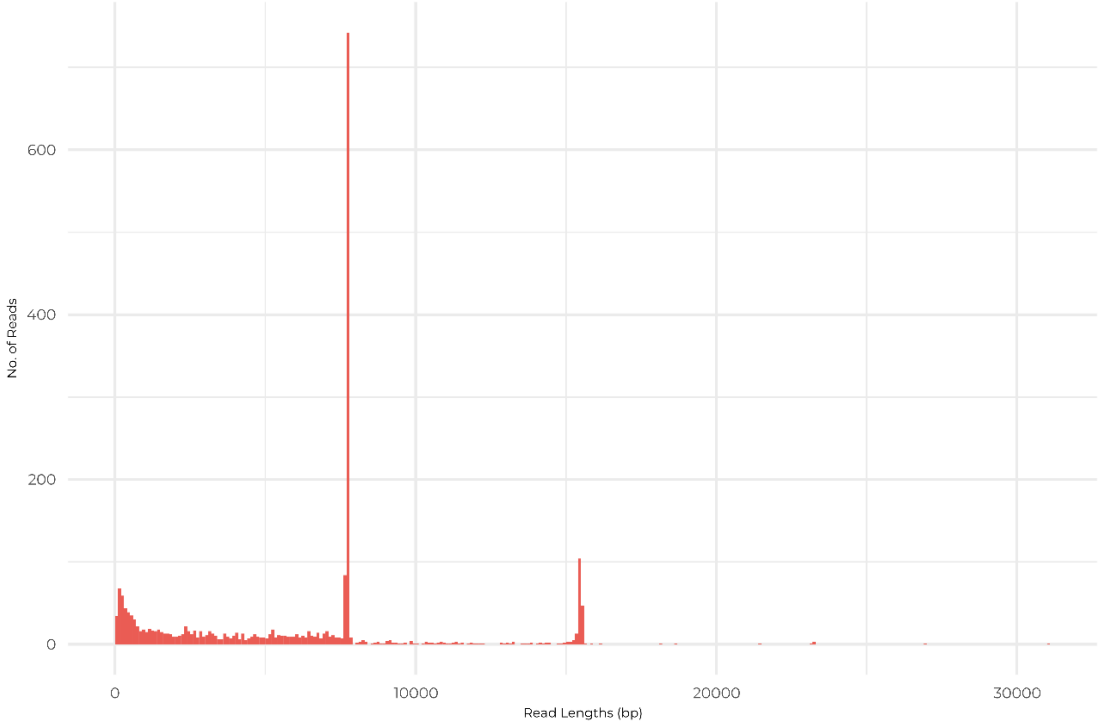
Appendix 18(III). Read length histogram generated from the whole plasmid sequencing data for pKSV7-Δ*rsbU* construct. The histogram displays the number of reads corresponding to each read length.



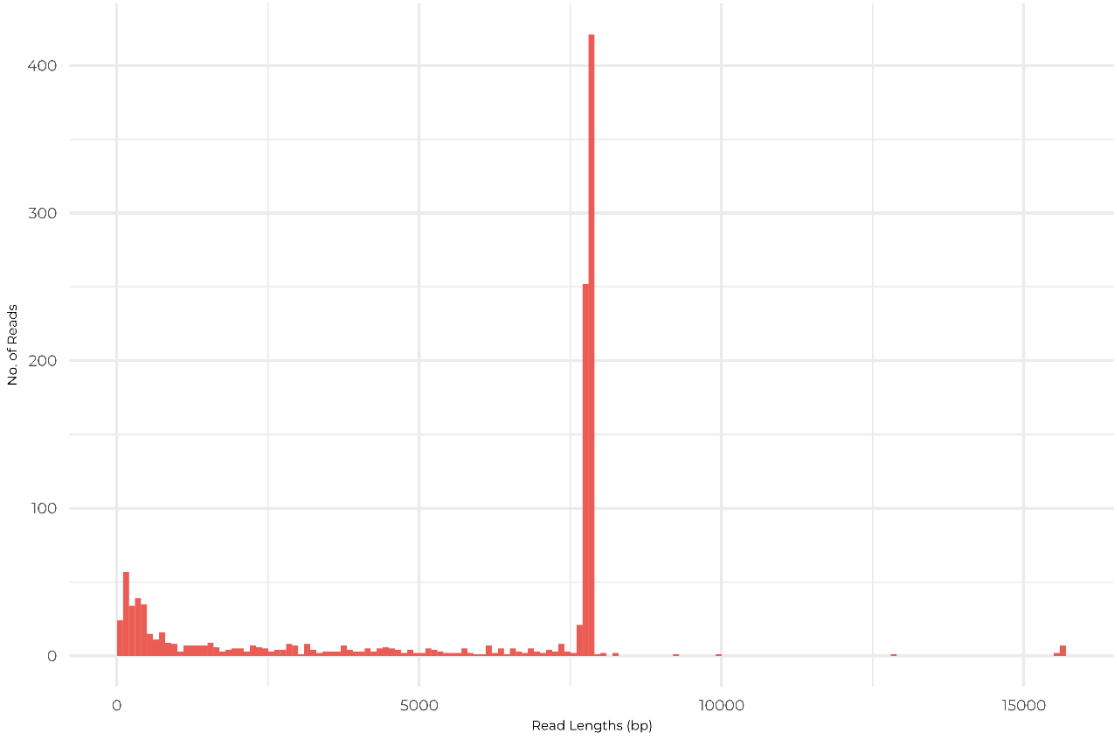
Appendix 18(IV). Read length histogram generated from the whole plasmid sequencing data for pKSV7-Δ*pyrD* construct. The histogram displays the number of reads corresponding to each read length.



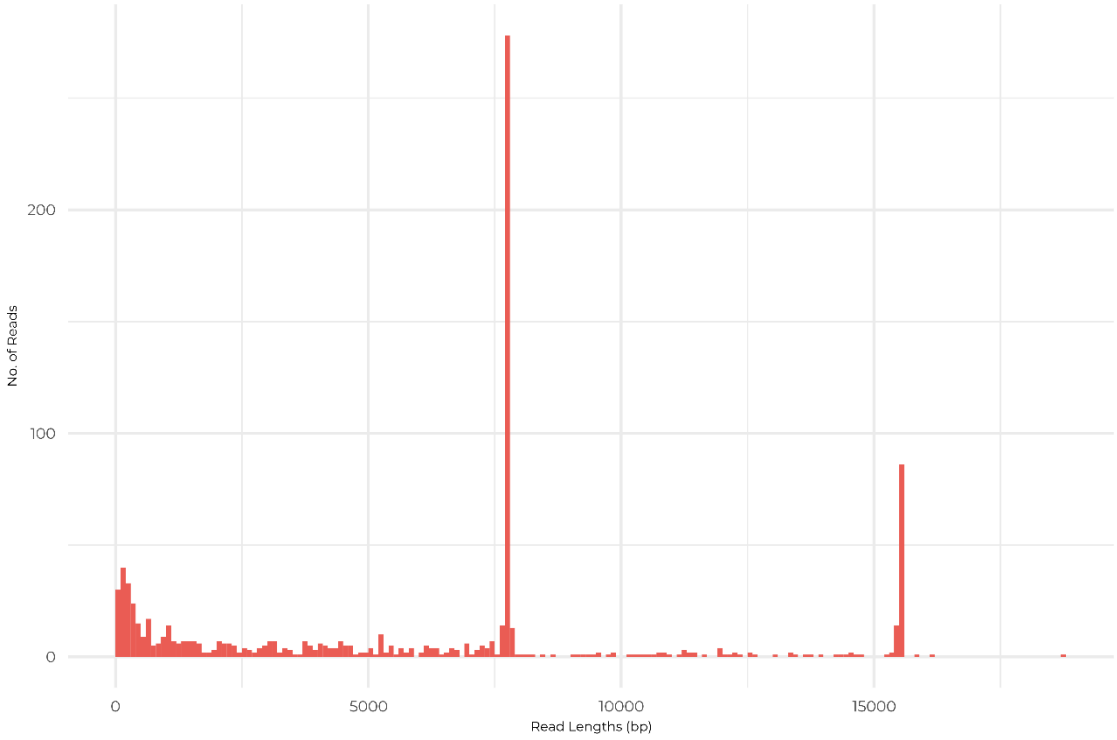
Appendix 18(V). Read length histogram generated from the whole plasmid sequencing data for pKSV7-Δ*carB* construct. The histogram displays the number of reads corresponding to each read length.



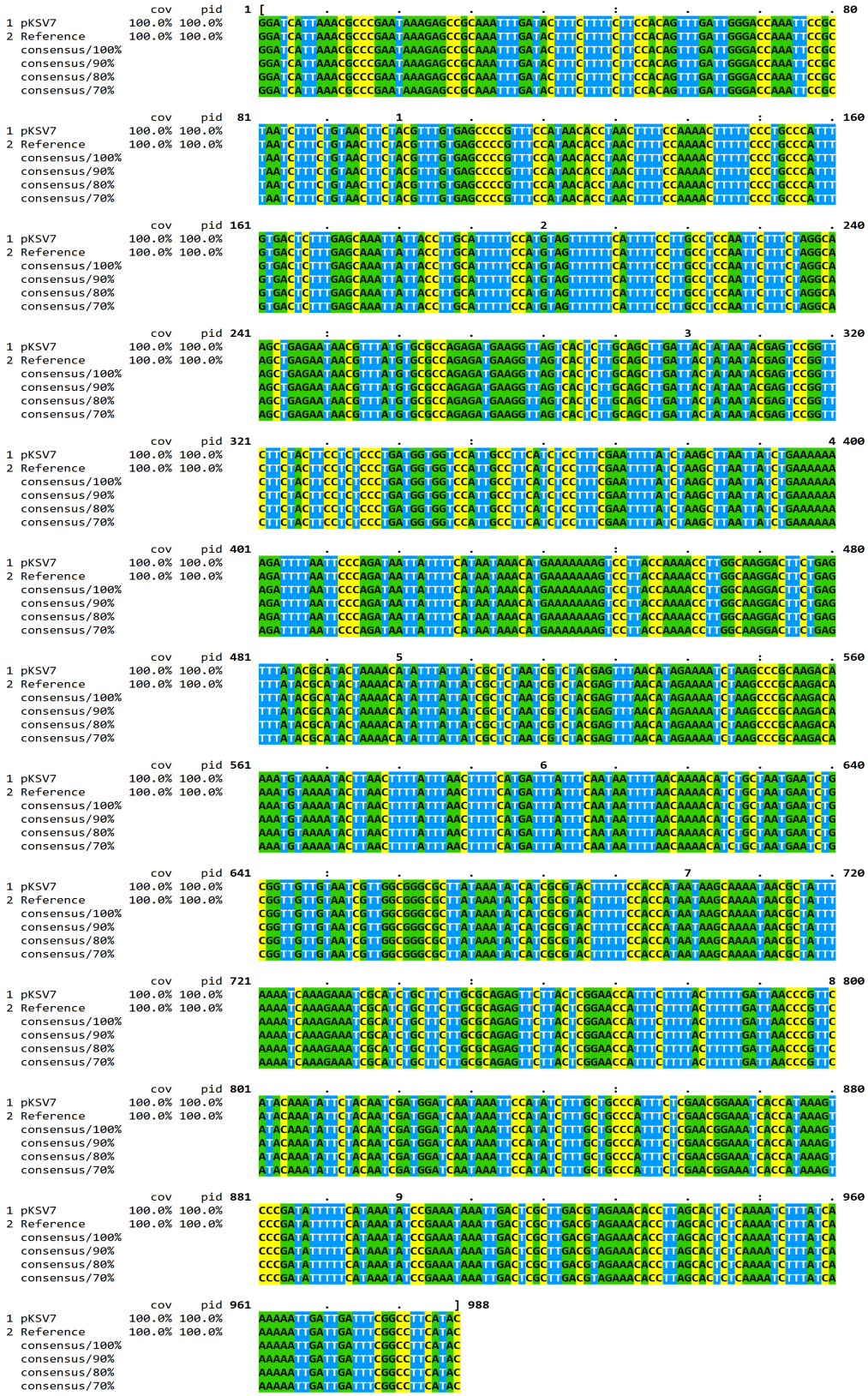
Appendix 18(VI). Read length histogram generated from the whole plasmid sequencing data for pKSV7-Δ*corA* construct. The histogram displays the number of reads corresponding to each read length.



Appendix 18(VII). Read length histogram generated from the whole plasmid sequencing data for pKSV7-Δ*bglG* construct. The histogram displays the number of reads corresponding to each read length.



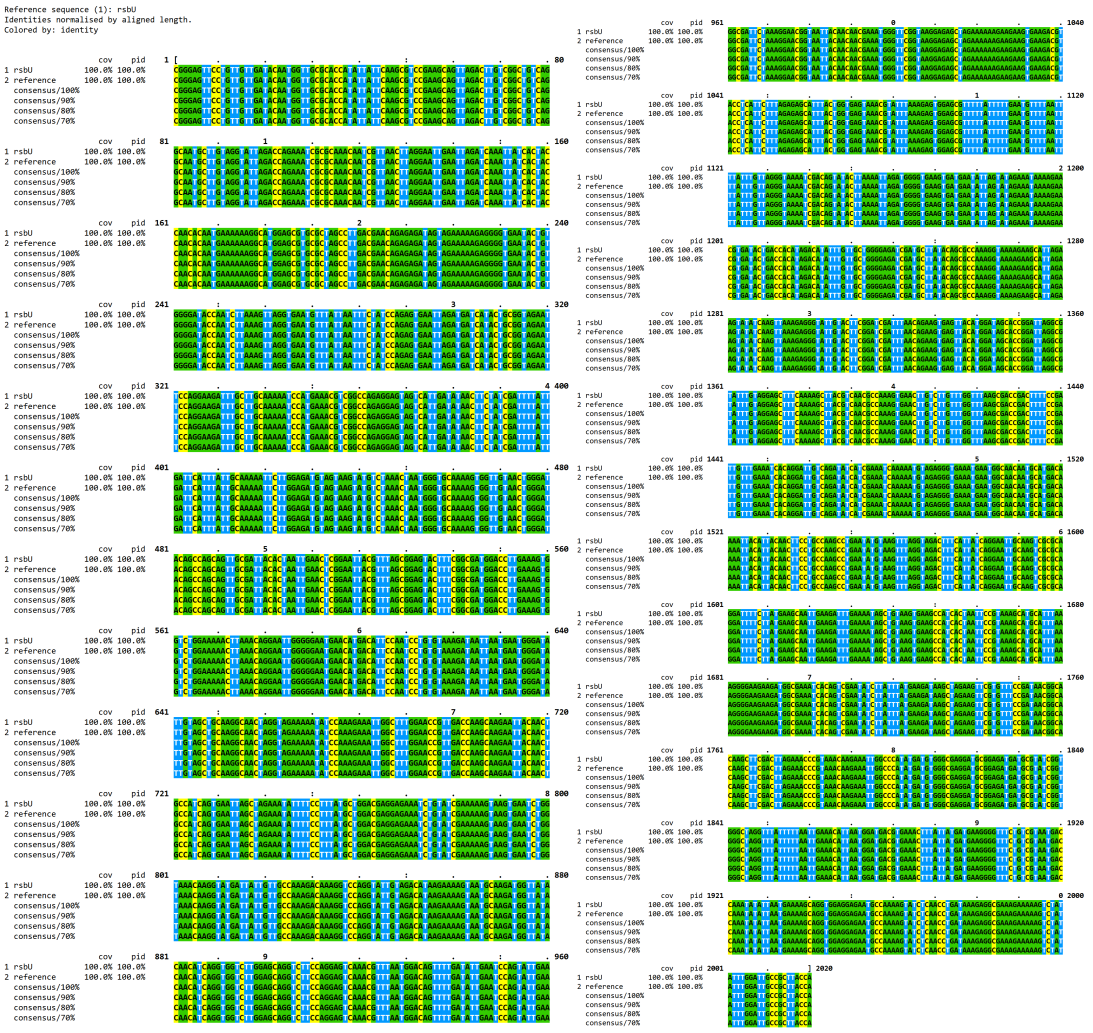
Appendix 19(I). Sequence alignment of the pKSV7-ΔykoK insert against the *ykoK*-deficient reference sequence. Alignment was performed using the Clustal Omega multiple sequence alignment tool. Sequence 1: pKSV7-**ΔykoK** fragment. Sequence 2: *ykoK*-deficient reference sequence.



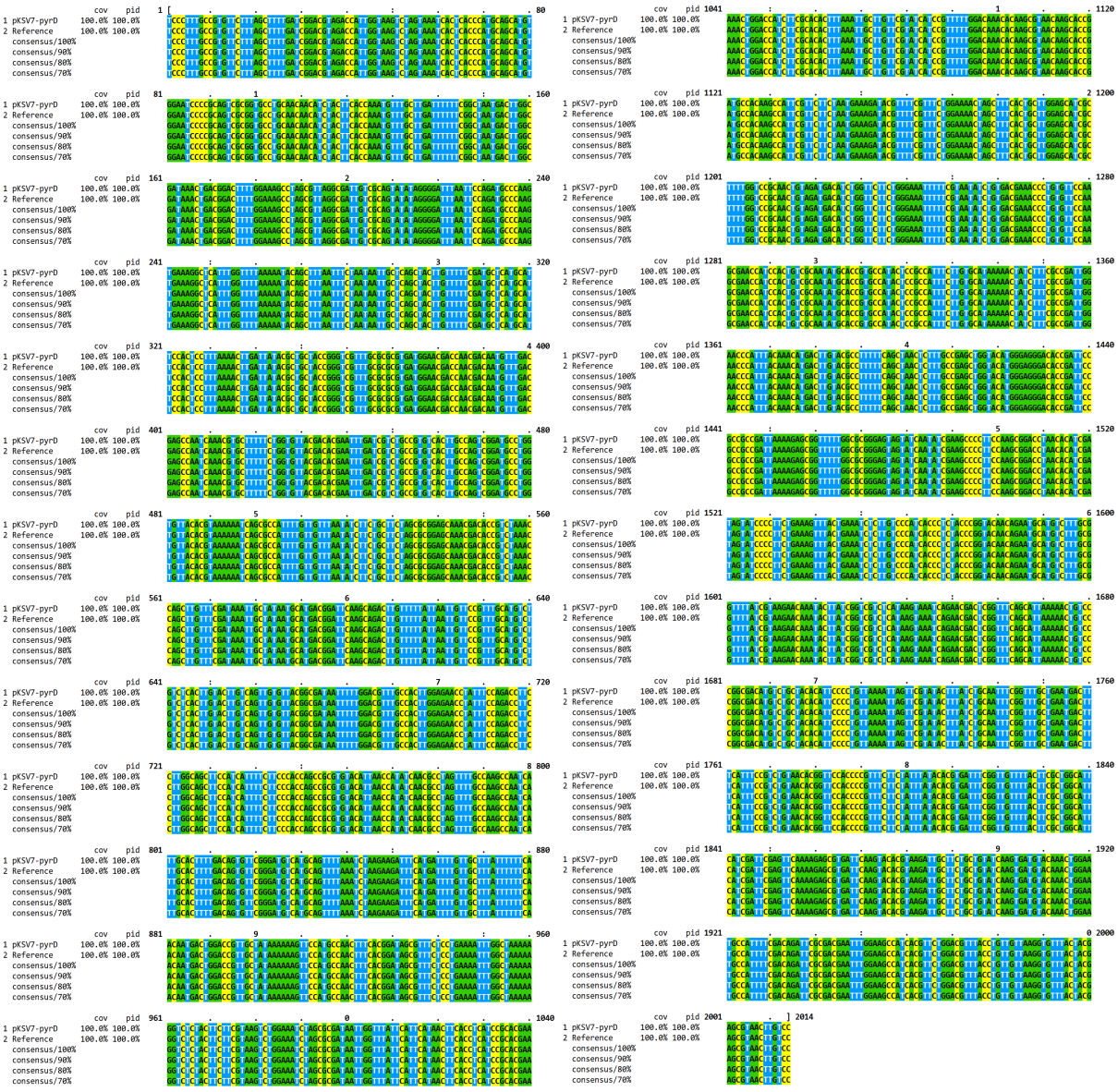
Appendix 19(II). Sequence alignment of the pKSV7-Δ*mgtA* insert against the *mgtA*-deficient reference sequence. Alignment was performed using the Clustal Omega multiple sequence alignment tool. Sequence 1: pKSV7-Δ*mgtA* fragment. Sequence 2: *mgtA*-deficient reference sequence.



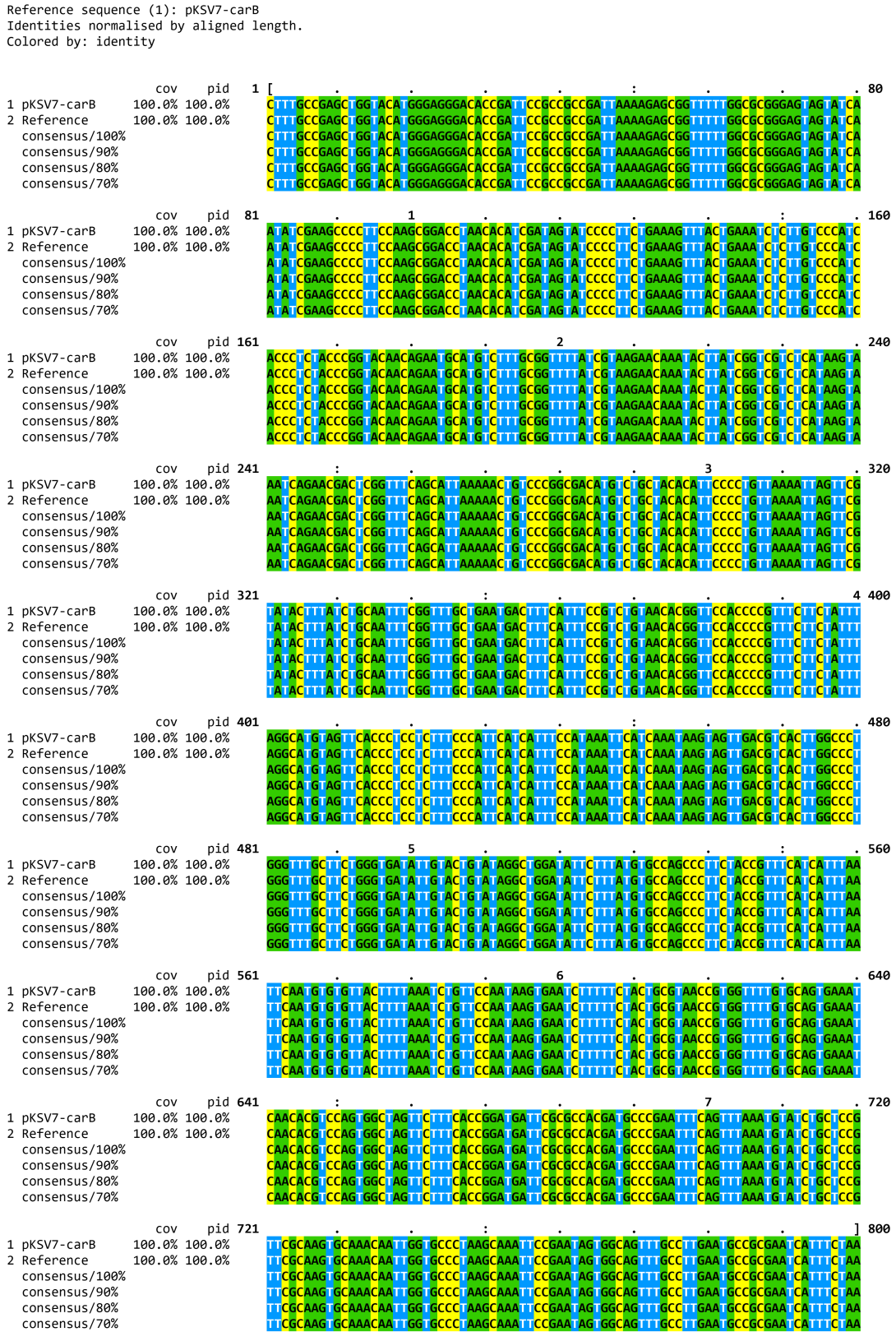
Appendix 19(II). Sequence alignment of the pKSV7-Δ*rsbU* insert against the *rsbU*-deficient reference sequence. Alignment was performed using the Clustal Omega multiple sequence alignment tool. Sequence 1: pKSV7-Δ*rsbU* fragment. Sequence 2: *rsbU*-deficient reference sequence.



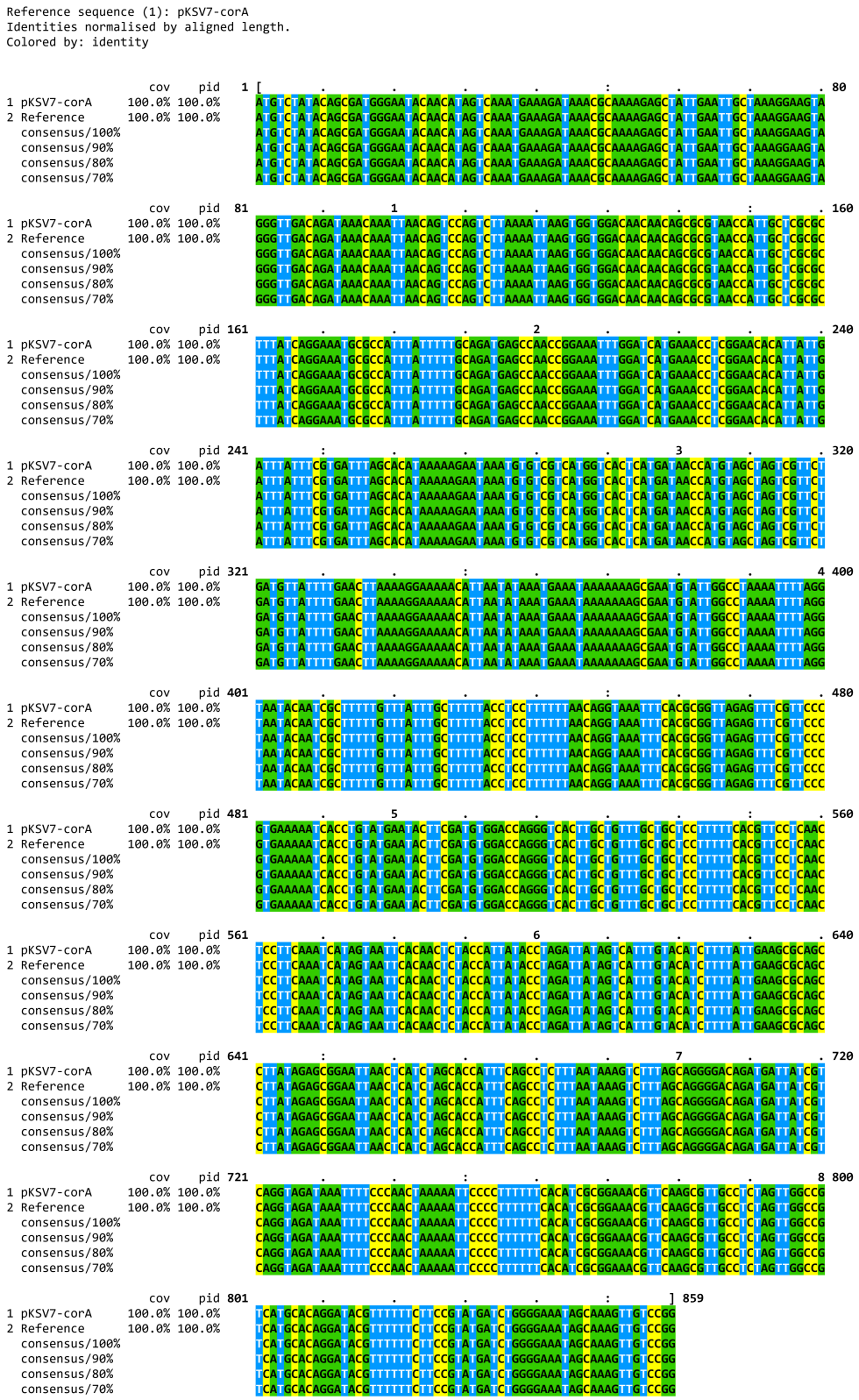
Appendix 19(III). Sequence alignment of the pKSV7-Δ*pyrD* insert against the *pyrD*-deficient reference sequence. Alignment was performed using the Clustal Omega multiple sequence alignment tool. Sequence 1: pKSV7-Δ*pyrD* fragment. Sequence 2: *pyrD*-deficient reference sequence.



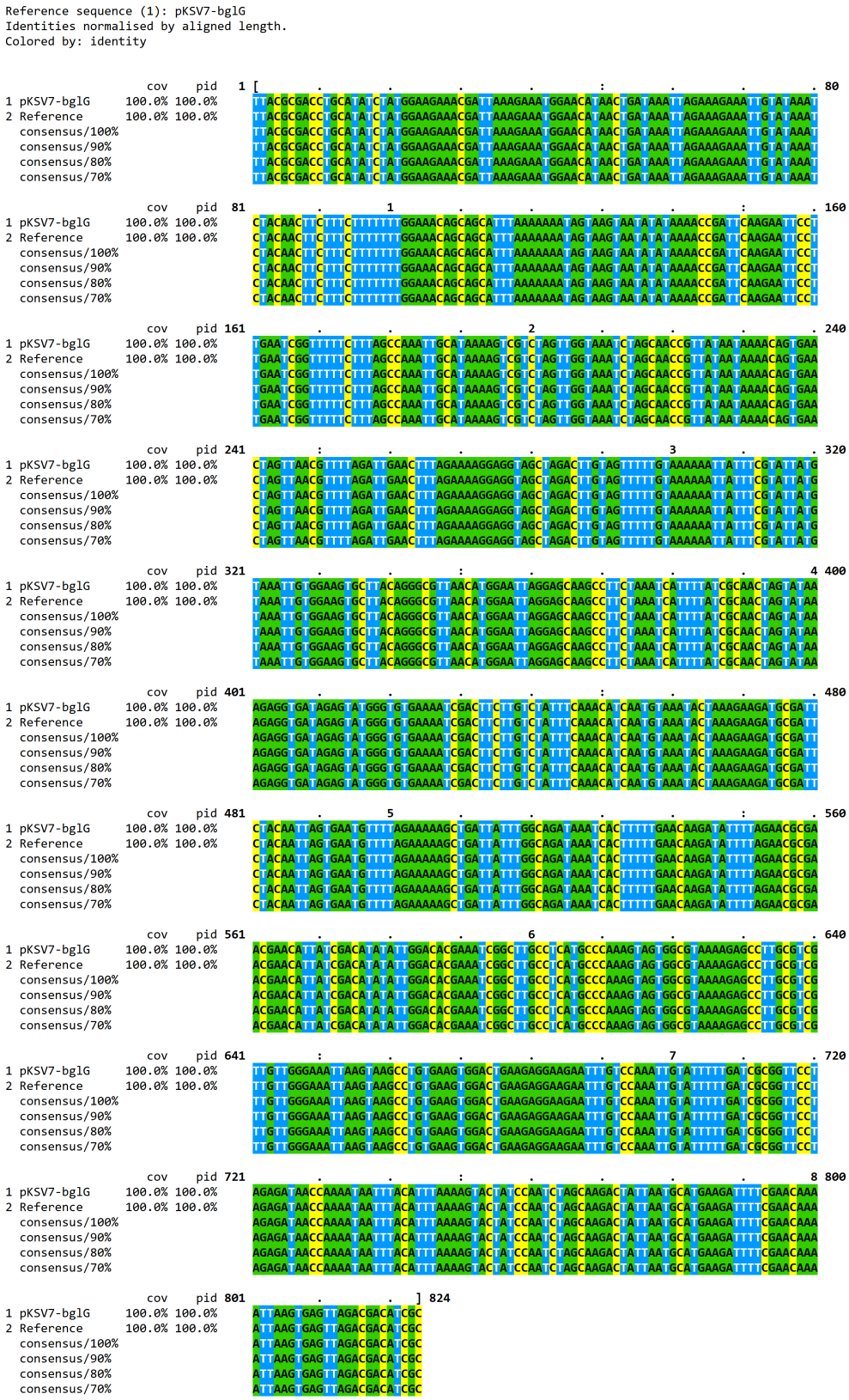
Appendix 19(IV). Sequence alignment of the pKSV7-Δ*carB* insert against the *carB*-deficient reference sequence. Alignment was performed using the Clustal Omega multiple sequence alignment tool. Sequence 1: pKSV7-Δ*carB* fragment. Sequence 2: *carB*-deficient reference sequence.



Appendix 19(V). Sequence alignment of the pKSV7-Δ*corA* insert against the *corA*-deficient reference sequence. Alignment was performed using the Clustal Omega multiple sequence alignment tool. Sequence 1: pKSV7-Δ*corA* fragment. Sequence 2: *corA*-deficient reference sequence.



Appendix 19(VI). Sequence alignment of the pKSV7-*bglG* insert against the *bglG*-deficient reference sequence. Alignment was performed using the Clustal Omega multiple sequence alignment tool. Sequence 1: pKSV7-**Δ***bglG* fragment. Sequence 2: *bglG*-deficient reference sequence.



Appendix 20(I). SNPs detected in Δ*rsbU* strain compared to the genome of the wild-type strain using Snippy.

Position	Type	Reference	Alteration	NT position	AA position	Effect	Gene	Product
172937	ins	GTTTTTTTATTTCTTTTTAAATA	GTTTTTTTTTATTTCTTTTTAAATA					
557904	snp	T	C	691/1662	231/553	missense_variant c.691A>G p.Ile231Val	*sulP*	SulP family inorganic anion transporter
1690942	snp	A	G					
1727637	snp	G	A	475/2601	159/866	missense_variant c.475G>A p.Ala159Thr	*lap*	adhesion-mediating acetaldehyde/alcohol dehydrogenase LAP
1755661	snp	A	G					
1875251	snp	C	A					
1974999	snp	A	G	1809/2628	603/875	synonymous_variant c.1809T>C p.Ala603Ala		LPXTG cell wall anchor domain-containing protein
1976022	complex	ATCC	GTCG	786/2628	261/875	synonymous_variant c.783_786delGGATinsCGAC p.263		LPXTG cell wall anchor domain-containing protein
1976031	complex	GGCG	CGCA	777/2628	258/875	synonymous_variant c.774_777delCGCCinsTGCG p.260		LPXTG cell wall anchor domain-containing protein
1976043	snp	C	G	765/2628	255/875	synonymous_variant c.765G>C p.Ala255Ala		LPXTG cell wall anchor domain-containing protein

2468341	complex	CCCA	TCCT	597/846	198/281	synonymous_variant c.594_597delTGGGinsAGGA p.200		M15 family peptidase

Appendix 20(II). SNPs detected in Δ*pyrD* strain compared to the genome of the wild-type strain using Snippy.

Position	Type	Reference	Alteration	NT position	AA position	Effect	Gene	Product
172937	ins	GTTTTTTTATTTCTTTTTAAATA	GTTTTTTTTTATTTCTTTTTAAATA					
358658	snp	T	A	69/336	23/111	missense_variant c.69T>A p.Asp23Glu		hypothetical protein
1006427	snp	T	C	944/975	315/324	missense_variant c.944A>G p.Asn315Ser		hypothetical protein
1006433	snp	T	C	938/975	313/324	missense_variant c.938A>G p.Glu313Gly		hypothetical protein
1690942	snp	A	G					
1742720	complex	AC	GT	2077/3072	692/1023	synonymous_variant c.2076_2077delGTinsAC p.694		exonuclease
1742727	complex	AATCTGTTC	CACTTGATT	2070/3072	688/1023	missense_variant c.2062_2070delGAACAGATTinsAATCAAGTG p.GluGlnIle688AsnGlnVal		exonuclease
1742742	snp	T	C	2055/3072	685/1023	synonymous_variant c.2055A>G p.Lys685Lys		exonuclease

1742753	complex	TTTCG	CTTCT	2044/3072	680/1023	missense_variant c.2040_2044delCGAAAinsAGAAG p.Thr682Ala		exonuclease
1742764	complex	GA	TC	2033/3072	678/1023	missense_variant c.2032_2033delTCinsGA p.Ser678Glu		exonuclease
1755661	snp	A	G					
1898520	snp	A	T	1377/2172	459/723	synonymous_variant c.1377T>A p.Val459Val	*bglX*	beta-glucosidase BglX
1976043	snp	C	G	765/2628	255/875	synonymous_variant c.765G>C p.Ala255Ala		LPXTG cell wall anchor domain-containing protein
1976085	del	GGCATCCGCATCCGCATCCGCATCCG	GGCATCCGCATCCGCATCCG	703/2628	233/875	conservative_inframe_deletion c.698_703delCGGATG p.Asp234_Ala235del		LPXTG cell wall anchor domain-containing protein
2468341	complex	CCCA	TCCT	597/846	198/281	synonymous_variant c.594_597delTGGGinsAGGA p.200		M15 family peptidase
3021437	snp	C	T	1245/2556	415/851	synonymous_variant c.1245C>T p.Asn415Asn	*inlJ*	internalin J
3021443	complex	TTTTGAG	CTTGTAT	1251/2556	417/851	missense_variant c.1251_1257delTTTTGAGinsCTTGTAT p.PheGlu418LeuTyr	*inlJ*	internalin J

Appendix 20(III). SNPs detected in Δ*mgtA* strain compared to the genome of the wild-type strain using Snippy.

Position	Type	Reference	Alteration	NT position	AA position	Effect	Gene	Product
427840	snp	G	A					
511848	snp	G	A					
1006433	snp	T	C	938/975	313/324	missense_variant c.938A>G p.Glu313Gly		hypothetical protein
1755661	snp	A	G					
1814925	complex	TACA	CACG	300/354	99/117	synonymous_variant c.297_300delTGTAinsCGTG p.101		Lmo1701 protein
1898520	snp	A	T	1377/2172	459/723	synonymous_variant c.1377T>A p.Val459Val	*bglX*	beta-glucosidase BglX
1974999	snp	A	G	1809/2628	603/875	synonymous_variant c.1809T>C p.Ala603Ala		LPXTG cell wall anchor domain-containing protein
1975113	snp	C	A	1695/2628	565/875	synonymous_variant c.1695G>T p.Ala565Ala		LPXTG cell wall anchor domain-containing protein

1976043	snp	C	G	765/2628	255/875	synonymous_variant c.765G>C p.Ala255Ala		LPXTG cell wall anchor domain-containing protein
1976085	del	GGCATCCGCATCCGCATCCGCATCCG	GGCATCCGCATCCGCATCCG	703/2628	233/875	conservative_inframe_deletion c.698_703delCGGATG p.Asp234_Ala235del		LPXTG cell wall anchor domain-containing protein
2571459	snp	A	G					
11848	complex	TACA	CACT	2130/2391	710/796	synonymous_variant c.2130_2133delTACAinsCACT p.712		type IV secretory system conjugative DNA transfer family protein
11863	complex	TA	AC	2145/2391	715/796	missense_variant c.2145_2146delTAinsAC p.Ile716Leu		type IV secretory system conjugative DNA transfer family protein
11869	complex	GT	AG	2151/2391	717/796	missense_variant c.2151_2152delGTinsAG p.Ser718Ala		type IV secretory system conjugative

								DNA transfer family protein

Appendix 20(IV). SNPs detected in Δ*ykoK* strain compared to the genome of the wild-type strain using Snippy.

Position	Type	Reference	Alteration	NT position	AA position	Effect	Gene	Product
172937	ins	GTTTTTTTATTTCTTTTTAAATA	GTTTTTTTTTATTTCTTTTTAAATA					
1743075	complex	CATAT	AATAC	1722/3072	573/1023	missense_variant c.1718_1722delATATGinsGTATT p.AspMet573GlyIle		exonuclease
1755661	snp	A	G					
1976022	complex	ATCC	GTCG	786/2628	261/875	synonymous_variant c.783_786delGGATinsCGAC p.263		LPXTG cell wall anchor domain-containing protein
1976031	complex	GGCG	CGCA	777/2628	258/875	synonymous_variant c.774_777delCGCCinsTGCG p.260		LPXTG cell wall anchor domain-containing protein
1976043	snp	C	G	765/2628	255/875	synonymous_variant c.765G>C p.Ala255Ala		LPXTG cell wall anchor domain-containing protein
1976085	del	GGCATCCGCATCCGCATCCGCATCCG	GGCATCCGCATCCGCATCCG	703/2628	233/875	conservative_inframe_deletion c.698_703delCGGATG p.Asp234_Ala235del		LPXTG cell wall anchor domain-containing protein
2489300	snp	T	C	35/543	12/180	missense_variant c.35A>G p.Lys12Arg		Lin2401 protein
2491168	snp	A	G	249/561	83/186	synonymous_variant c.249T>C p.Asp83Asp		DUF1642 domain-containing protein
2571459	snp	A	G					

2943274	complex	TATT	CGTA					
9399	complex	TAAA	CAAG	891/1158	297/385	synonymous_variant c.891_894delTAAAinsCAAG p.299		toprim domain-containing protein
11839	complex	AACG	GACT	2121/2391	707/796	synonymous_variant c.2121_2124delAACGinsGACT p.709		type IV secretory system conjugative DNA transfer family protein
11848	complex	TACA	CACT	2130/2391	710/796	synonymous_variant c.2130_2133delTACAinsCACT p.712		type IV secretory system conjugative DNA transfer family protein
11863	complex	TA	AC	2145/2391	715/796	missense_variant c.2145_2146delTAinsAC p.Ile716Leu		type IV secretory system conjugative DNA transfer family protein
11869	complex	GT	AG	2151/2391	717/796	missense_variant c.2151_2152delGTinsAG p.Ser718Ala		type IV secretory system conjugative DNA transfer family protein

Appendix 20(V). SNPs detected in Δ*corA* strain compared to the genome of the wild-type strain using Snippy.

Position	Type	Reference	Alteration	NT position	AA position	Effect	Gene	Product
108767	snp	C	T	458/633	153/210	missense_variant c.458C>T p.Ala153Val	*nfnB*	nitroreductase family protein
145246	complex	GGAGT	AGAGA			intragenic_variant n.145246_145250delGGAGTinsAGAGA	*rli117*	Listeria sRNA *rli117*
172937	ins	GTTTTTTTATTTCTTTTTAAATA	GTTTTTTTTTATTTCTTTTTAAATA					
100643	snp	T	C	938/975	313/324	missense_variant c.938A>G p.Glu313Gly		hypothetical protein
1690942	snp	A	G					
1755661	snp	A	G					
1974999	snp	A	G	1809/2628	603/875	synonymous_variant c.1809T>C p.Ala603Ala		LPXTG cell wall anchor domain-containing protein
1975008	snp	G	A	1800/2628	600/875	synonymous_variant c.1800C>T p.Asp600Asp		LPXTG cell wall anchor domain-containing protein
1976031	complex	GGCG	CGCA	777/2628	258/875	synonymous_variant c.774_777delCGCCinsTGCG p.260		LPXTG cell wall anchor domain-containing protein

1976043	snp	C	G	765/2628	255/875	synonymous_variant c.765G>C p.Ala255Ala		LPXTG cell wall anchor domain-containing protein
1976085	del	GGCATCCGCATCCGCATCCGCATCCG	GGCATCCGCATCCGCATCCG	703/2628	233/875	conservative_inframe_deletion c.698_703delCGGATG p.Asp234_Ala235del		LPXTG cell wall anchor domain-containing protein
2468341	complex	CCCA	TCCT	597/846	198/281	synonymous_variant c.594_597delTGGGinsAGGA p.200		M15 family peptidase
2571459	snp	A	G					
2833283	snp	A	G	1390/1398	464/465	synonymous_variant c.1390T>C p.Leu464Leu	*dgt*	deoxyguanosinetriphosphate triphosphohydrolase
2943286	complex	TAGAAAGAAAAT	CAGAAAAAT					
9399	complex	TAAA	CAAG	891/1158	297/385	synonymous_variant c.891_894delTAAAinsCAAG p.299		toprim domain-containing protein

Appendix 20(VI). SNPs detected in Δ*bglG* strain compared to the genome of the wild-type strain using Snippy.

Position	Type	Reference	Alteration	NT position	AA position	Effect	Gene	Product
172937	ins	GTTTTTTTATTTCTTTTTAAATA	GTTTTTTTTTATTTCTTTTTAAATA					
494076	snp	A	T			intragenic_variant n.494076A>T	*rliA*	Listeria sRNA *rliA*
1006433	snp	T	C	938/975	313/324	missense_variant c.938A>G p.Glu313Gly		hypothetical protein
1516380	snp	T	A	678/1668	226/555	missense_variant c.678A>T p.Arg226Ser	*rnjA*	Zn-dependent hydrolase
1524592	snp	C	T	39/1107	13/368	synonymous_variant c.39C>T p.Val13Val	*ispG*	flavodoxin-dependent (E)-4-hydroxy-3-methylbut-2-enyl-diphosphate synthase
1755661	snp	A	G					
1974998	snp	CA	CG	1809/2628	603/875	synonymous_variant c.1809T>C p.Ala603Ala		LPXTG cell wall anchor domain-containing protein
197500	snp	G	A	1800/2628	600/875	synonymous_variant		LPXTG cell wall

8						c.1800C>T p.Asp600Asp		anchor domain-containing protein
1976043	snp	C	G	765/2628	255/875	synonymous_variant c.765G>C p.Ala255Ala		LPXTG cell wall anchor domain-containing protein
1976085	del	GGCATCCGCATCCGCATCCGCATCCG	GGCATCCGCATCCGCATCCG	703/2628	233/875	conservative_inframe_deletion c.698_703delCGGATG p.Asp234_Ala235del		LPXTG cell wall anchor domain-containing protein
2489300	snp	T	C	35/543	12/180	missense_variant c.35A>G p.Lys12Arg		Lin2401 protein
2896006	ins	CTA	CATA					

Appendix 20(VII). SNPs detected in Δ*carB* strain compared to the genome of the wild-type strain using Snippy.

Position	Type	Reference	Alteration	NT position	AA position	Effect	Gene	Product
172937	ins	GTTTTTTTATTTCTTTTTAAATA	GTTTTTTTTTATTTCTTTTAAATA					
351680	snp	T	C	456/3942	152/1313	synonymous_variant c.456T>C p.Asp152Asp	lRR	Leucine-rich repeat (LRR) protein
351781	snp	T	A	557/3942	186/1313	missense_variant c.557T>A p.Phe186Tyr	lRR	Leucine-rich repeat (LRR) protein
353639	snp	C	T	2415/3942	805/1313	synonymous_variant c.2415C>T p.Tyr805Tyr	lRR	Leucine-rich repeat (LRR) protein
358167	complex	GT	AG					
358658	snp	T	A	69/336	23/111	missense_variant c.69T>A p.Asp23Glu		hypothetical protein
427840	snp	G	A					
494076	snp	A	T			intragenic_variant n.494076A>T	*rliA*	Listeria sRNA *rliA*
509634	snp	C	A	9/348	3/115	missense_variant c.9C>A p.Asn3Lys		hypothetical protein
509639	complex	TG	CA	14/348	5/115	missense_variant c.14_15delTGinsCA p.Met5Thr		hypothetical protein
50964	compl	TAA	CGG	21/348	7/115	missense_variant		hypothetical protein

6	ex					c.21_23delTAAinsCGG p.Asn8Gly		
511826	complex	TGGCGTTAGG	AAGTGTAAGC					
525905	snp	A	G					
1006433	snp	T	C	938/975	313/324	missense_variant c.938A>G p.Glu313Gly		hypothetical protein
1007188	snp	T	C	183/975	61/324	synonymous_variant c.183A>G p.Gln61Gln		hypothetical protein
1161835	snp	A	T			intragenic_variant n.1161835A>T	*rli38*	Listeria sRNA *rli38*
1315792	snp	A	C					
1690938	snp	TAGAA	TAGAG					
1743075	complex	CATAT	AATAC	1722/3072	573/1023	missense_variant c.1718_1722delATATGinsGTATT p.AspMet573GlyIle		exonuclease
1755661	snp	A	G					
1976007	ins	GGC	GGCATCCGC	798/2628	266/875	conservative_inframe_insertion c.798_799insGCGGAT p.Asp266_Ala267insAlaAsp		LPXTG cell wall anchor domain-containing protein
1976043	snp	C	G	765/2628	255/875	synonymous_variant c.765G>C p.Ala255Ala		LPXTG cell wall anchor domain-containing protein

1976085	del	GGCATCCGCATCCGCATCCGCATCCG	GGCATCCGCATCCGCATCCG	703/2628	233/875	conservative_inframe_deletion c.698_703delCGGATG p.Asp234_Ala235del		LPXTG cell wall anchor domain-containing protein
2468341	complex	CCCA	TCCT	597/846	198/281	synonymous_variant c.594_597delTGGGinsAGGA p.200		M15 family peptidase
2491168	snp	A	G	249/561	83/186	synonymous_variant c.249T>C p.Asp83Asp		DUF1642 domain-containing protein
2571459	snp	A	G					
2572308	complex	TTAC	GTAT	507/2823	169/940	synonymous_variant c.507_510delTTACinsGTAT p.171		lmo2396 family class 1 internalin
2896298	snp	C	A	99/156	33/51	synonymous_variant c.99C>A p.Pro33Pro		hypothetical protein
2943286	complex	TAGAAAGAAAAT	CAGAAAAAT					
3005036	complex	TTGC	CTGT	37/384	12/127	missense_variant c.34_37delGCAAinsACAG p.AlaIle12ThrVal		DUF1310 domain-containing protein
9399	complex	TAAA	CAAG	891/1158	297/385	synonymous_variant c.891_894delTAAAinsCAAG p.299		toprim domain-containing protein
11839	complex	AACG	GACT	2121/2391	707/796	synonymous_variant c.2121_2124delAACGinsGACT p.709		type IV secretory system conjugative DNA transfer family protein

11848	complex	TACA	CACT	2130/2391	710/796	synonymous_variant c.2130_2133delTACAinsCACT p.712		type IV secretory system conjugative DNA transfer family protein
11863	complex	TA	AC	2145/2391	715/796	missense_variant c.2145_2146delTAinsAC p.Ile716Leu		type IV secretory system conjugative DNA transfer family protein
11869	complex	GT	AG	2151/2391	717/796	missense_variant c.2151_2152delGTinsAG p.Ser718Ala		type IV secretory system conjugative DNA transfer family protein
11878	complex	AGTGGTTTTAAAT	CGTGATTCTGAAC	2160/2391	720/796	missense_variant c.2160_2172delAGTGGTTTTAAATinsCGTGATTCTGAAC p.Val722Ile		type IV secretory system conjugative DNA transfer family protein

Appendix 21. Mutations detected in natural mutants obtained through the BPM experiment. Obtained using Snippy tool by aligning short-read data of the natural mutants against the complete genome of the parental strain BL87-028.

Mutant Strain	Position	Type of mutation	Loci	Function
BL87-028-T30-No-BC-Biofilm1-3	353639	synonymous_variant c.2415C>T p.Tyr805Tyr	lRR	Leucine-rich repeat (LRR) protein
	358658	missense_variant c.69T>A p.Asp23Glu		hypothetical protein
	367355	synonymous_variant c.1038A>G p.Gly346Gly		LXG domain-containing protein
	497416	missense_variant c.835A>G p.Ser279Gly		BspA family leucine-rich repeat surface protein
	1180345	synonymous_variant c.1290_1293delCCCGinsTCCA p.432		lmo1136 family class 1 internalin
	1974999	synonymous_variant c.1809T>C p.Ala603Ala		LPXTG cell wall anchor domain-containing protein
	1975008	synonymous_variant c.1800C>T p.Asp600Asp		LPXTG cell wall anchor domain-containing protein
	1976031	synonymous_variant c.774_777delCGCCinsTGCG p.260		LPXTG cell wall anchor domain-containing protein
	1976043	synonymous_variant c.765G>C p.Ala255Ala		LPXTG cell wall anchor domain-containing protein
	1976085	disruptive_inframe_deletion c.717_722delGGATGC p.Asp240_Ala241del		LPXTG cell wall anchor domain-containing protein
	2877054	missense_variant c.2059C>A p.Leu687Ile	*mgtA*	magnesium-translocating P-type ATPase
	2879526	intragenic_variant n.2879526C>T		
BL87-028-T10-No-BC-Biofilm2-P	285134	synonymous_variant c.1134T>A p.Thr378Thr		Internalin H
	497416	missense_variant c.835A>G p.Ser279Gly		BspA family leucine-rich repeat surface protein
	1974999	synonymous_variant c.1809T>C p.Ala603Ala		LPXTG cell wall anchor domain-

				containing protein
	1976022	synonymous_variant c.783_786delGGATinsCGAC p.263		LPXTG cell wall anchor domain-containing protein
	1976031	synonymous_variant c.774_777delCGCCinsTGCG p.260		LPXTG cell wall anchor domain-containing protein
	1976043	synonymous_variant c.765G>C p.Ala255Ala		LPXTG cell wall anchor domain-containing protein
BL87-028-T30-No-BC-Biofilm1-1	353639	synonymous_variant c.2415C>T p.Tyr805Tyr	lRR	Leucine-rich repeat (LRR) protein
	497086	missense_variant c.505C>G p.Arg169Gly		BspA family leucine-rich repeat surface protein
	497416	missense_variant c.835A>G p.Ser279Gly		BspA family leucine-rich repeat surface protein
	667228	disruptive_inframe_insertion c.4595_4618dupCAAAAGATACACCAAAAGATACAC p.Pro1532_Thr1539dup		peptidoglycan bound protein
	1180345	synonymous_variant c.1290_1293delCCCGinsTCCA p.432		lmo1136 family class 1 internalin
	1605705	missense_variant c.180G>T p.Glu60Asp	*dtd*	D-aminoacyl-tRNA deacylase
	1974999	synonymous_variant c.1809T>C p.Ala603Ala		LPXTG cell wall anchor domain-containing protein
	1975008	synonymous_variant c.1800C>T p.Asp600Asp		LPXTG cell wall anchor domain-containing protein
	1975059	synonymous_variant c.1743_1749delGGATGCTinsTGACGCC p.584		LPXTG cell wall anchor domain-containing protein
	1976031	synonymous_variant c.774_777delCGCCinsTGCG p.260		LPXTG cell wall anchor domain-containing protein
	1976043	synonymous_variant c.765G>C p.Ala255Ala		LPXTG cell wall anchor domain-containing protein

	1976085	disruptive_inframe_deletion c.717_722delGGATGC p.Asp240_Ala241del		LPXTG cell wall anchor domain-containing protein
	2877054	missense_variant c.2059C>A p.Leu687Ile	*mgtA*	magnesium-translocating P-type ATPase
	2879526	intragenic_variant n.2879526C>T		
	3005036	missense_variant c.37A>G p.Ile13Val		DUF1310 domain-containing protein
	3005039	missense_variant c.34G>A p.Ala12Thr		DUF1310 domain-containing protein
BL87-028-T30-No-BC-Biofilm1-3	353639	synonymous_variant c.2415C>T p.Tyr805Tyr	lRR	Leucine-rich repeat (LRR) protein
	358658	missense_variant c.69T>A p.Asp23Glu		hypothetical protein
	367355	synonymous_variant c.1038A>G p.Gly346Gly		LXG domain-containing protein
	497416	missense_variant c.835A>G p.Ser279Gly		BspA family leucine-rich repeat surface protein
	1180345	synonymous_variant c.1290_1293delCCCGinsTCCA p.432		lmo1136 family class 1 internalin
	1974999	synonymous_variant c.1809T>C p.Ala603Ala		LPXTG cell wall anchor domain-containing protein
	1975008	synonymous_variant c.1800C>T p.Asp600Asp		LPXTG cell wall anchor domain-containing protein
	1976031	synonymous_variant c.774_777delCGCCinsTGCG p.260		LPXTG cell wall anchor domain-containing protein
	1976043	synonymous_variant c.765G>C p.Ala255Ala		LPXTG cell wall anchor domain-containing protein
	1976085	disruptive_inframe_deletion c.717_722delGGATGC p.Asp240_Ala241del		LPXTG cell wall anchor domain-containing protein
	2877054	missense_variant c.2059C>A p.Leu687Ile	*mgtA*	magnesium-translocating P-type ATPase
	2879526	intragenic_variant n.2879526C>T		

BL87-028-T30-No-BC-Biofilm3-3	497416	missense_variant c.835A>G p.Ser279Gly		BspA family leucine-rich repeat surface protein
	1184467	frameshift_variant c.1228delG p.Val410fs	*rnfC*	propanediol utilization protein
	1975008	synonymous_variant c.1800C>T p.Asp600Asp		LPXTG cell wall anchor domain-containing protein
	1976022	synonymous_variant c.783_786delGGATinsCGAC p.263		LPXTG cell wall anchor domain-containing protein
	1976031	synonymous_variant c.774_777delCGCCinsTGCG p.260		LPXTG cell wall anchor domain-containing protein
	1976043	synonymous_variant c.765G>C p.Ala255Ala		LPXTG cell wall anchor domain-containing protein
	1976085	disruptive_inframe_deletion c.717_722delGGATGC p.Asp240_Ala241del		LPXTG cell wall anchor domain-containing protein
	2443148	missense_variant c.174A>G p.Ile58Met	*pitA*	anion permease
	2626210	missense_variant c.74C>G p.Thr25Arg	*yvaK*	carboxylesterase
	2879532	intragenic_variant n.2879532T>C		

Appendix 22. Statistical significance from one-way ANOVA followed by Tukey's multiple comparison test for cell attachment assays of mutant strains involved in Mg^{2+} ion homeostasis (*ΔykoK*, *ΔmgtA*) compared to the parental strain. Conditions include 0, 1, 10, and 50 mM Mg^{2+} supplementation in 1/10 BHI. Significant pairwise comparisons are reported with corresponding p-values.

Tukey's multiple comparisons test	Mean diff.	95.00% CI of diff.	Below threshold	Summary	Adjusted P Value
dBHI *ΔykoK* vs. 1mM *ΔykoK*	0.06232	-0.1681 to 0.2927	No	ns	0.9992
dBHI *ΔykoK* vs. 10mM *ΔykoK*	-0.01443	-0.2668 to 0.2380	No	ns	>0.9999
dBHI *ΔykoK* vs. 50mM *ΔykoK*	0.2351	0.004714 to 0.4655	Yes	*	0.0408
dBHI *ΔykoK* vs. dBHI *ΔmgtA*	-0.2226	-0.4530 to 0.007782	No	ns	0.0691
dBHI *ΔykoK* vs. 1mM *ΔmgtA*	-0.02037	-0.2728 to 0.2320	No	ns	>0.9999
dBHI *ΔykoK* vs. 10mM *ΔmgtA*	0.09379	-0.1366 to 0.3242	No	ns	0.9729
dBHI *ΔykoK* vs. 50mM *ΔmgtA*	0.05353	-0.1769 to 0.2839	No	ns	0.9998
dBHI *ΔykoK* vs. dBHI WT	0.06720	-0.1632 to 0.2976	No	ns	0.9983
dBHI *ΔykoK* vs. 1mM WT	-0.1471	-0.3775 to 0.08334	No	ns	0.6207
dBHI *ΔykoK* vs. 10mM WT	-0.09856	-0.3290 to 0.1318	No	ns	0.9609
dBHI *ΔykoK* vs. 50mM WT	0.3667	0.1363 to 0.5971	Yes	****	<0.0001
1mM *ΔykoK* vs. 10mM *ΔykoK*	-0.07675	-0.3072 to 0.1537	No	ns	0.9946
1mM *ΔykoK* vs. 50mM *ΔykoK*	0.1728	-0.03328 to 0.3789	No	ns	0.2017
1mM *ΔykoK* vs. dBHI *ΔmgtA*	-0.2849	-0.4910 to -0.07886	Yes	***	0.0005
1mM *ΔykoK* vs. 1mM *ΔmgtA*	-0.08269	-0.3131 to 0.1477	No	ns	0.9899
1mM *ΔykoK* vs. 10mM *ΔmgtA*	0.03147	-0.1746 to 0.2376	No	ns	>0.9999
1mM *ΔykoK* vs. 50mM *ΔmgtA*	-0.008787	-0.2149 to 0.1973	No	ns	>0.9999
1mM *ΔykoK* vs. dBHI WT	0.004886	-0.2012 to 0.2110	No	ns	>0.9999
1mM *ΔykoK* vs. 1mM WT	-0.2094	-0.4155 to -0.003307	Yes	*	0.0426
1mM *ΔykoK* vs. 10mM WT	-0.1609	-0.3670 to 0.04520	No	ns	0.3004
1mM *ΔykoK* vs. 50mM WT	0.3044	0.09830 to 0.5105	Yes	***	0.0001
10mM *ΔykoK* vs. 50mM *ΔykoK*	0.2496	0.01915 to 0.4800	Yes	*	0.0211
10mM *ΔykoK* vs. dBHI *ΔmgtA*	-0.2082	-0.4386 to 0.02221	No	ns	0.1207
10mM *ΔykoK* vs. 1mM *ΔmgtA*	-0.005939	-0.2583 to 0.2465	No	ns	>0.9999
10mM *ΔykoK* vs. 10mM *ΔmgtA*	0.1082	-0.1222 to 0.3386	No	ns	0.9256
10mM *ΔykoK* vs. 50mM *ΔmgtA*	0.06796	-0.1624 to 0.2984	No	ns	0.9982
10mM *ΔykoK* vs. dBHI WT	0.08164	-0.1488 to 0.3120	No	ns	0.9909
10mM *ΔykoK* vs. 1mM WT	-0.1326	-0.3630 to 0.09777	No	ns	0.7602
10mM *ΔykoK* vs. 10mM WT	-0.08413	-0.3145 to 0.1463	No	ns	0.9884
10mM *ΔykoK* vs. 50mM WT	0.3811	0.1507 to 0.6115	Yes	****	<0.0001
50mM *ΔykoK* vs. dBHI *ΔmgtA*	-0.4577	-0.6638 to -0.2517	Yes	****	<0.0001
50mM *ΔykoK* vs. 1mM *ΔmgtA*	-0.2555	-0.4859 to -0.02509	Yes	*	0.0158
50mM *ΔykoK* vs. 10mM *ΔmgtA*	-0.1413	-0.3474 to 0.06475	No	ns	0.5076
50mM *ΔykoK* vs. 50mM *ΔmgtA*	-0.1816	-0.3877 to 0.02449	No	ns	0.1452
50mM *ΔykoK* vs. dBHI WT	-0.1679	-0.3740 to 0.03817	No	ns	0.2391
50mM *ΔykoK* vs. 1mM WT	-0.3822	-0.5883 to -0.1761	Yes	****	<0.0001

50mM *ΔykoK* vs. 10mM WT	-0.3337	-0.5398 to -0.1276	Yes	****	<0.0001
50mM *ΔykoK* vs. 50mM WT	0.1316	-0.07450 to 0.3377	No	ns	0.6202
dBHI *ΔmgtA* vs. 1mM *ΔmgtA*	0.2023	-0.02815 to 0.4327	No	ns	0.1491
dBHI *ΔmgtA* vs. 10mM *ΔmgtA*	0.3164	0.1103 to 0.5225	Yes	****	<0.0001
dBHI *ΔmgtA* vs. 50mM *ΔmgtA*	0.2762	0.07007 to 0.4822	Yes	***	0.0009
dBHI *ΔmgtA* vs. dBHI WT	0.2898	0.08375 to 0.4959	Yes	***	0.0003
dBHI *ΔmgtA* vs. 1mM WT	0.07555	-0.1305 to 0.2816	No	ns	0.9880
dBHI *ΔmgtA* vs. 10mM WT	0.1241	-0.08202 to 0.3301	No	ns	0.7040
dBHI *ΔmgtA* vs. 50mM WT	0.5893	0.3832 to 0.7954	Yes	****	<0.0001
1mM *ΔmgtA* vs. 10mM *ΔmgtA*	0.1142	-0.1162 to 0.3446	No	ns	0.8956
1mM *ΔmgtA* vs. 50mM *ΔmgtA*	0.07390	-0.1565 to 0.3043	No	ns	0.9961
1mM *ΔmgtA* vs. dBHI WT	0.08758	-0.1428 to 0.3180	No	ns	0.9840
1mM *ΔmgtA* vs. 1mM WT	-0.1267	-0.3571 to 0.1037	No	ns	0.8102
1mM *ΔmgtA* vs. 10mM WT	-0.07819	-0.3086 to 0.1522	No	ns	0.9937
1mM *ΔmgtA* vs. 50mM WT	0.3871	0.1567 to 0.6175	Yes	****	<0.0001
10mM *ΔmgtA* vs. 50mM *ΔmgtA*	-0.04026	-0.2463 to 0.1658	No	ns	>0.9999
10mM *ΔmgtA* vs. dBHI WT	-0.02658	-0.2327 to 0.1795	No	ns	>0.9999
10mM *ΔmgtA* vs. 1mM WT	-0.2409	-0.4469 to -0.03478	Yes	**	0.0079
10mM *ΔmgtA* vs. 10mM WT	-0.1923	-0.3984 to 0.01373	No	ns	0.0933
10mM *ΔmgtA* vs. 50mM WT	0.2729	0.06683 to 0.4790	Yes	**	0.0011
50mM *ΔmgtA* vs. dBHI WT	0.01367	-0.1924 to 0.2198	No	ns	>0.9999
50mM *ΔmgtA* vs. 1mM WT	-0.2006	-0.4067 to 0.005480	No	ns	0.0646
50mM *ΔmgtA* vs. 10mM WT	-0.1521	-0.3582 to 0.05399	No	ns	0.3880
50mM *ΔmgtA* vs. 50mM WT	0.3132	0.1071 to 0.5193	Yes	****	<0.0001
dBHI WT vs. 1mM WT	-0.2143	-0.4204 to -0.008193	Yes	*	0.0335
dBHI WT vs. 10mM WT	-0.1658	-0.3718 to 0.04032	No	ns	0.2569
dBHI WT vs. 50mM WT	0.2995	0.09342 to 0.5056	Yes	***	0.0002
1mM WT vs. 10mM WT	0.04851	-0.1576 to 0.2546	No	ns	0.9998
1mM WT vs. 50mM WT	0.5138	0.3077 to 0.7199	Yes	****	<0.0001
10mM WT vs. 50mM WT	0.4653	0.2592 to 0.6713	Yes	****	<0.0001